1.10 Multiply Bonded Compounds of Group 13 Elements

RC Fischer, Graz University of Technology, Graz, Austria

Abbreviations

Ar#	2,6-Bis[2,4,6-tri(methyl)phenyl]phenyl
Ar′	2,6-Bis[2,6-di(isopropyl)phenyl]phenyl
Ar*	2,6-Bis[2,4,6-tri(isopropyl)phenyl]phenyl
Bp	Hydridobispyrazol-1-ylborate
Bsi	Bis(trimethylsilyl)methyl
Cp	Cyclopentadienyl
Dipp	2,6-Di(isopropyl)phenyl
EPR	Electron paramagnetic resonance
HOMO	Highest occupied molecular orbital
LUMO	Lowest unoccupied molecular orbital
Mes	2,4,6-Tri(methyl)phenyl
NHC	*N*-Heterocyclic carbene
NMR	Nuclear magnetic resonance
SOMO	Singly occupied molecular orbital
Tmeda	*N*,*N*,*N*′,*N*′-tetramethylethylenediamine
Tp	Hydridotrispyrazol-1-ylborate
Trip	2,4,6-Tri(isopropyl)phenyl
UV	Ultraviolet

1.10.1 Introduction

The chemistry of homonuclear group 13 analogs of alkenes, alkynes, and related species which feature (formal) multiple bonding has rapidly advanced in recent years. Sophisticated experimental techniques and the development of either sufficiently large ligands or ligands which feature unique electronic properties provided access to compounds in unusual and otherwise highly unstable bonding situations.[1]

Despite all advances made in ligand design, the synthetic challenges encountered in low-valent group 13 chemistry greatly excel the problems associated with the synthesis of heavier group 14 and 15 element compounds. The problems encountered in low-valent boron group chemistry originate from the electron-deficient nature of the organometallic compounds, as the elements are characterized by a combination of three valence electrons but four valence orbitals.

Among the lighter triel elements, the oxidation state +III largely dominates their chemistry. However, the oxidation state +I becomes increasingly important upon descending the group and dominates the chemistry of the heaviest group 13 elements indium and thallium. Due to the fact that the energy difference between *n*s- and *n*p-valence orbitals increases with growing principal quantum number, the importance of hybridization in chemical bonding drops dramatically from boron to thallium. In other words, the s valence electrons develop an increasing degree of lone-pair character and are thus less available for chemical bonding. Strong multiple bonds are hence likely to be found in derivatives of the lighter elements, whereas the lone-pair effect dominates the bonding situation in the heavier congeners. On the other hand, especially the lighter elements are prone to three- or four-center two-electron bonding and formation of clusters and higher aggregates.

The *trans*-bent structural motif in the solid-state structures of dimetallenes REER (E = Al, Ga, In, Tl) was originally explained by orbital-based models. According to this model, each of the triels act simultaneously as a Lewis donor and as a Lewis acceptor with the consequence of *trans*-bent geometries of the molecular cores (motif D in Figure 1).[2–5] Very recent high-level calculations, however, emphasize the importance of closed-shell interactions for the heavier elements and especially for thallium (motif E in Figure 1) rather than orbital interactions. For the lighter elements the diradical bond type (motif C in Figure 1) was found to be of great significance as the highest occupied molecular orbital (HOMO) in the slipped π-bond model (B in Figure 1) is actually formally mostly antibonding with respect to metal–metal interactions and has only

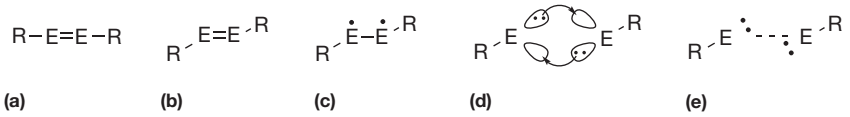

Figure 1 Multiple bonding versus lone-pair effect in group 13 element compounds REER (E = B, Al, Ga, In, Tl).

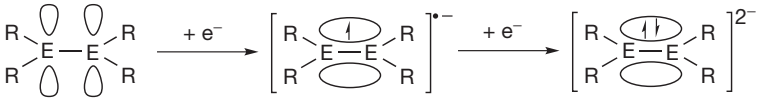

Figure 2 One- and two-electron reductions of R_2EER_2 species to yield multiple-bonded radical anions and dianions.

a minor bonding contribution from the interaction of the lone pair of the group 13 element and the opposed E–R bond of the second metal center.[6]

Synthetic strategies to overcome the drawbacks associated with the electron-deficient nature of these compounds include the utilization of sterically demanding ligands which provide enough steric protection to prevent aggregation and disproportionation of the multiple-bonded, low-valent centers. In the case of neutral group 13 compounds REER, one substituent at each of the triel centers must provide sufficient steric protection to stabilize the molecule. *m*-Terphenyl ligands proved particularly useful for the stabilization of heavier group element compounds REER, in which the lone pair at the triel center develops an increasing degree of s-character upon descending the group. As a consequence, these compounds are weakly associated and are frequently found to dissociate in solution. Bond strengths in *m*-terphenyl-based heavier group 13 element compounds REER are usually low and several examples are known to exist as monomers in the solid state. Nevertheless, owing to a combination of a lone pair and empty orbitals at the triel atom, these compounds are promising candidates with respect to their reaction chemistry with small molecules.[7,8]

Alternatively, stabilization of dimeric +1 oxidation state compounds can be accomplished by a combination of steric protection and strong electron donor properties provided by the ligands. These ligands donate electron density into the empty orbitals at the triel centers and effectively saturate their Lewis acidic character. Donation of electron density can be provided either by strong Lewis bases such as *N*-heterocyclic carbenes (NHCs) or via donor groups in the ligand periphery as for example by the nitrogen lone pairs of the imine functionalities in β-ketiminates, guanidinates, or amidinates. However, the steric demand and electronic properties of the ligands require careful control to ensure the formation of dimers rather than monomers or higher aggregates in cases where the steric demand is relatively low. β-Ketiminates, guanidinates, or amidinates were successfully applied in the syntheses of a variety of Al(I) and Ga(I) derivatives. Most of these are monomeric and are thus beyond the scope of this chapter.

Alternatively, multiple bonding in group 13 compounds can also be realized by population of empty π-orbitals which originate from bonding combinations of triel element based p-orbitals in compounds with general formula R_2EER_2.

One-electron reductions yield examples of radical anions $[R_2EER_2]^{\bullet-}$ with formal bond order 1.5, and two-electron

Figure 3 Multiple bonding in radicals R_2EER.

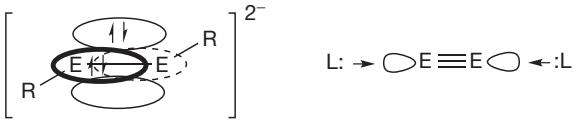

Figure 4 Molecules with formal bond orders greater than 2.

reductions lead to dianions $[R_2EER_2]^{2-}$ which are isoelectronic with alkenes (Figure 2).

Related to the radical anions $[R_2EER_2]^{\bullet-}$ are radicals with general composition $R_2EER^{\bullet}$ as these have a formal bond order of 1.5 through population of a delocalized π-type orbital with the unpaired electron (Figure 3).

Formal bond order greater than two may be realized through reduction of REER species. The dianions $[REER]^{2-}$ constitute group 13 homologs of alkynes. Finally, donation of electron density of empty orbitals of E≡E fragments by two two-electron donors leads to Lewis-base adducts of formally triple-bonded compounds L:E≡E:L (Figure 4).

1.10.2 Double-Bonded Group 13 Element Compounds

1.10.2.1 Syntheses and Structural Properties of Neutral Double-Bonded Compounds

1.10.2.1.1 Compounds with formula HEEH (E = B, Al, Ga, In)

Evaporation of boron by pulsed laser techniques followed by condensation at temperatures of 10 K in a matrix of a mixture of argon and H_2, D_2, or HD provided infrared (IR) spectroscopic data of low-molecular-weight boron hydrides. Among these, diborene, HBBH, and its respective mono- and dideuterated derivatives HBBD and DBBD were characterized and studied by means of vibrational spectroscopy and computational methods. Calculations predict that the linear triplet species HBBH is the isomer of B_2H_2 lowest in energy. In this isomer, two degenerate π-orbitals are occupied by one electron each. Experimentally found B–H stretching modes at 2690 cm^{-1} are in good agreement with theoretical results for the linear isomer.[9] Diborene, HBBH, has also been studied by

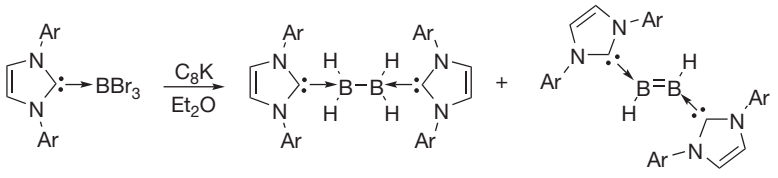

Scheme 1 *N*-Heterocyclic carbene-stabilized diborene HB=BH.

electron paramagnetic resonance (EPR) spectroscopy in neon and argon matrices at 4 K. EPR measurements revealed the triplet $X^3\Sigma_g^-$ ground state of HBBH. It is related to acetylene by removal of one electron from each of the π-type orbitals in HC≡CH and is isoelectronic to C_2. However, in sharp contrast to HBBH, C_2 has an $X^1\Sigma_g^+$ ground state. High-level calculations suggest a boron–boron distance of 1.516 Å.[10] Moreover, the existence of HBBH at low temperatures is also supported by mass spectrometric investigations.[11]

The isolation of a derivative of neutral diborene with a closed-shell ground state became feasible upon stabilization with NHCs as demonstrated by the research group of Robinson.[12] Reduction of the NHC adducts of BBr_3, L′:BBr_3, (:L′ = :C{N(C_6H_3-2,6-^{i}Pr$_2$)CH}$_2$) with potassium graphite in diethyl ether yielded a mixture of the colorless, singly bonded L′:BH_2-BH_2:L′ and the orange bis-NHC adduct of diborene, L′:BH=BH:L′ (Scheme 1)

The ^{11}B nuclear magnetic resonance (NMR) shifts of L′:BH_2–BH_2:L′ and L′:BH=BH:L′ are −31.6 and −25.3 ppm, respectively. The boron–boron distance in L′:BH=BH:L′ is 1.561(18) Å and is thus ca. 0.26 Å shorter in comparison to 1.828(4) Å in L′:BH_2–BH_2:L′. The triel atoms in the diborene complex adopt trigonal planar geometries with short distances of only about 1.543(15) Å between the boron atoms and carbons of the NHC donor molecules. This is a convincing evidence for a strong stabilizing interaction of the NHCs with the HB=BH fragment. Computational results further support its closed-shell ground state. The HOMO in L′:BH=BH:L′ is doubly occupied, with a B–B π-bonding orbital which is formed through the overlap of mainly boron 2p orbitals. Finally, a Wiberg bond index of 1.408 for L′:BH=BH:L′ strongly supports the multiple bond character of this complex. Three completely different molecular structures were found crystallographically for the slightly less crowded diborene adduct L*:BH=BH:L* (:L* = :C{N(C_6H_2-2,4,6-Me_3)CH}$_2$). In this complex, the flanking Dipp groups of the carbene ligands are replaced by slightly less bulky Mes groups. L*:BH=BH:L* adopts planar, twisted, and *trans*-bent conformations in the solid state. Among these, the *trans*-bent structure is of particular interest as it relates the planar structural motif of the diborenes and their NHC complexes to the *trans*-bent forms observed for the heavier homologs where increasing degrees of lone-pair character at the heavier triels results in increased s-orbital character of the lone pair and decreased multiple bond strength. Boron–boron double-bond distances in L*:BH=BH:L* are 1.602(5) Å for the planar, 1.582(4) Å for the twisted, and 1.679(9) Å for the *trans*-bent forms. The onset of *trans*-bending is thus accompanied by an elongation of the B–B distance and indicates a certain degree of lone-pair character at the boron centers[13] (Scheme 2).

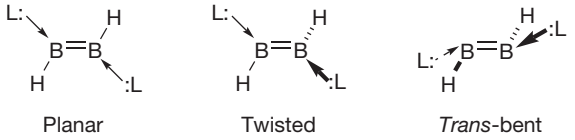

Scheme 2 Conformational differences in *N*-heterocyclic carbene-stabilized diborenes HB=BH.

A detailed account on NHC adducts of main group compounds is given in Chapter 1.16.

The heavier hydrogen-substituted homologs HGaGaH and HInInH were obtained upon irradiation of Ga or In vapors co-condensed with H_2. In these experiments, three isomers of Ga_2H_2 and two isomers of In_2H_2 were spectroscopically characterized. Thermally induced reaction of digallium with dihydrogen yields the bis(μ-hydrido)bridged isomer Ga(μ-H)$_2$Ga, which upon irradiation at 546 nm rearranges into the *trans*-bent isomer HGaGaH and the mixed oxidation state terminal dihydride $GaGaH_2$. In the case of indium, co-condensed In_2 and H_2 arrange into In(μ-H)$_2$In upon irradiation at 365 nm which can then be photochemically converted at 450 nm into *trans*-bent HInInH and monomeric InH[14,15] (Scheme 3).

In the case of aluminum, only the bis(μ-hydrido)bridged isomer was experimentally investigated to date.[16]

1.10.2.1.2 Group 13 element compounds with formula REER

Historically, first x-ray crystallographic data of dimeric compounds that follow the general formula REER and feature formal multiple bonding of group 13 elements were reported for the heaviest elements indium and thallium.

The earliest examples are all characterized by an η^5-bonding mode between ligand and metal center rather than σ-bonds between the ligand and indium or thallium atoms. Derivatives include sterically hindered cyclopentadienyl ligands,[17,18] fulvalenes,[19] or carboranes.[20]

Among these, the cyclopentadienyl-based thallium derivative is of special interest as it is known to exist in two modifications in the solid state. It is readily accessible via direct reaction of thallium (I) ethoxide with H{C_5(CH_2Ph)$_5$}.[21]

One of the two known polymorphs is the dimeric [{C_5(CH_2Ph)$_5$}Tl]$_2$ which is weakly associated and features a long Tl–Tl distance of ca. 3.63 Å. The second polymorph of [{C_5(CH_2Ph)$_5$}Tl], however, is best described as a two-dimensional, polymeric, zigzag chain with alternating –{C_5(CH_2Ph)$_5$}-Tl–{C_5(CH_2Ph)$_5$}-Tl– subunits but without direct Tl–Tl contacts[22] (Scheme 4).

The existence of two structural modifications in the solid state puts the thallium–thallium interaction in the order of magnitude of secondary Tl···Ar interactions. The analogous

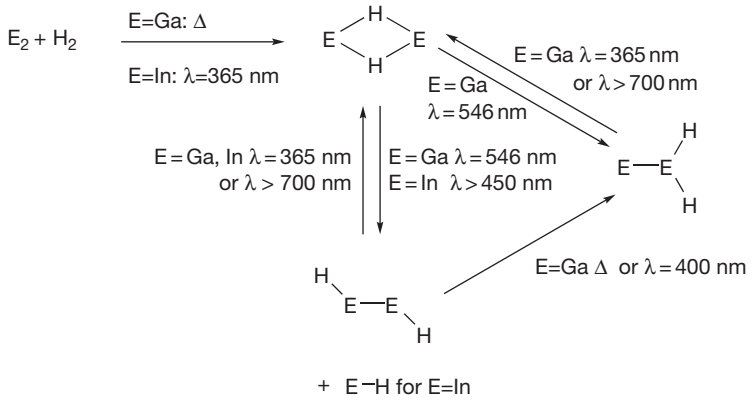

Scheme 3 Syntheses and isomerization reactions of heavier group 13 compounds HE=EH (E = Ga, In).

Scheme 4 Polymorphs of [{$C_5(CH_2Ph)_5$}Tl].

$\{C_5(CH_2Ph)_5\}^-$ derivative of indium(+I) crystallizes as dimers in which the In–In distance is 3.631 Å.[18]

Infinite chains are also the central structural motif in the solid-state structure of 1,1′,3,3′-tetra-Bu^t-5,5′-pentafulvalene dithallium. In this compound, the fulvalene dithallium subunits are weakly associated via thallium–thallium interactions with Tl–Tl distances between 3.760 and 4.625 Å.[19] A very weak thallium–thallium interaction is present in the *nido*-carborane derivative $Tl_2B_9H_9C_2Me_2$, where the closest distance between thallium atoms is 3.67 Å.[20] Other weakly associated examples with long thallium–thallium contacts include dimeric $\{Tl[Tp^{p\text{-}Tol}]\}_2$, ([$Tp^{p\text{-}Tol}$] = hydridotris(3-*para*-tolyl) pyrazol-1-yl)borate,[23] Tl–Tl = 3.86 Å), $\{Tl[Bp]\}_2$, ([Bp = hydridobis(pyrazol-1-yl)borate], Tl–Tl = 3.70 Å),[24] and {MeSi[N(Tl)^{t}Bu]$_3$}$_2$ (Tl–Tl 3.15 Å).[25] For comparison, thallium–thallium distances in some tetrameric Tl(I) compounds are 4.06 Å in $\{[TlN(SiMe_3)C_6H_3\text{-}2,6\text{-}^iPr_2]\}$,[26] 3.32–3.64 Å in {Tl[$C(SiMe_3)_3$]}$_4$,[27] or 3.64 Å in $\{Tl[Tp^{cyPr}]\}_4$ (Tp^{cyPr} = hydridotris(3-cyclopropylpyrazol-1-yl)borate).[28]

The first stable example for an organometallic compound of thallium(I) in which a monodentate ligand is bound only via a sigma bond to the metal center was provided by the *m*-terphenyl-based compound Ar′TlTlAr′ (Ar′ = 2,6-(2,6-*i*Pr$_2$-C_6H_3)$_2$-C_6H_3).

In this complex, the Ar′TlTlAr′ core adopts a *trans*-bent structure with a C–Tl–Tl angle of 122.9(4)° and a Tl–Tl distance of 3.0936(8) Å. The use of sterically less hindered ligands results in the isolation of a trimeric species ($Ar^{\#}Tl)_3$ ($Ar^{\#}$ = 2,6-(2,4,6-Me_3-C_6H_2)$_2$-C_6H_3).[29] Here, the three Tl atoms form an almost perfect isosceles triangle with two longer (3.3782(3) and 3.3590(3) Å) and one short (3.2144(3) Å) Tl–Tl distances. Coordination around the thallium atoms in the trimer is pyramidal and hence indicative of a certain degree of lone-pair character at the metal center. For instance, the sums of angles around the metal centers are 290.38(10)°, 323.15(10)°, and 337.22(10)°. In comparison to the dimeric Ar′TlTlAr′, which exhibits the shortest molecular Tl–Tl distance of 3.0936(8) Å known to date, the Tl–Tl distances in the trimer are elongated by ca. 0.22 Å on average.

Nevertheless, the thallium–thallium distances in the *m*-terphenyl based dimers and also the trimers are much shorter than the 3.46 Å found in the pure metal. Yet, these are considerably longer than the intermetallic distances found in most of the singly bonded $R_2Tl–TlR_2$ derivatives. In these, Tl–Tl distances are typically well below 3 Å, for example, 2.881(2) Å in $[(Ph^tBu_2Si)_2Tl]_2$ or 2.961(1) Å in $[(^tBu_3Si)_2Tl]_2$[30] and 2.9142(5) Å in $\{[(Me_3Si)_3Si]_2Tl\}_2$.[31] Both *m*-terphenyl-stabilized compounds were synthesized by the reaction of aryl lithium with thallium chloride at low temperatures to prevent formation of elemental thallium. In solution, these species are labile and sensitive toward light, but can be stored for extended periods in the dark at temperatures below −20 °C. The ultraviolet–visible (UV–Vis) spectra of Ar′TlTlAr′ and $(Ar^{\#}Tl)_3$, which form deep red crystals in the solid state, in hydrocarbon or aromatic solvents are almost identical and very similar to the electronic excitations observed for Ar*Tl ($Ar^{\#}$ = 2,6-(2,4,6-*i*Pr$_3$-C_6H_2)$_2$-C_6H_3) which is known to be monomeric in the solid state and believed to remain unassociated in solution.[32] Two relatively strong absorption bands around 367 and 492 nm associated with in-plane and out-of-plane n–p transitions were observed for all three compounds. Furthermore, experimental data suggest dissociation of Ar′TlTlAr′ and $(Ar^{\#}Tl)_3$ into monomers upon dissolution, although cryoscopic measurements for the heaviest group 13 Ar′EEAr′ are negatively affected by decomposition reactions. Nevertheless, both dimeric and trimeric *m*-terphenyl-based compounds react readily with $B(C_6F_5)_3$ to form 1:1 donor–acceptor complexes $ArTl \rightarrow B(C_6F_5)_3$. The Lewis acid–Lewis base complex was structurally authenticated for Ar′Tl and further evidenced by a ^{11}B NMR signal observed at −11.3 ppm. The thallium–boron distance in the $B(C_6F_5)_3$ adduct is 2.311(2) Å and is in good agreement with the sum of covalent radii. The thallium atom shows an almost perfectly linear coordination with a C–Tl–B angle of 174.358(7)°. The boron center in $ArTl \rightarrow B(C_6F_5)_3$ is strongly pyramidalized and the sum of C–B–C angles accounts for 341.03(15)°. This deviation from planarity indicates the formation of a rather strong donor–acceptor bond (**Scheme 5**).

The related indium complex Ar′InInAr′ had been obtained earlier by the reaction of Ar′Li with indium chloride in toluene.[33] Single-crystal x-ray structure analysis confirmed the *trans*-bent conformation of the C–In–In–C unit which had been computationally predicted for the heavier REER (Al–In)

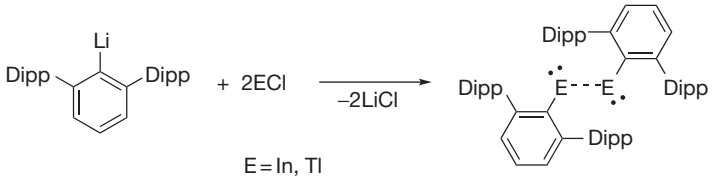

Scheme 5 Synthesis of the dimeric compounds Ar′InInAr′ and Ar′TlTlAr′.

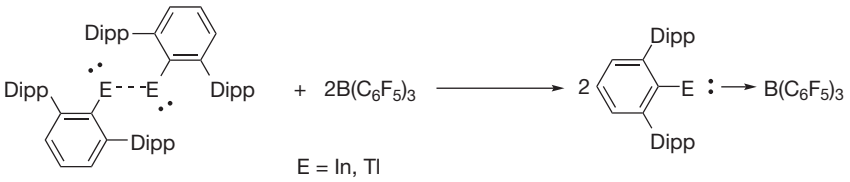

Scheme 6 Formation of BAr^F ($Ar^F = C_6F_5$) complexes of Ar′E: (E = In, Tl).

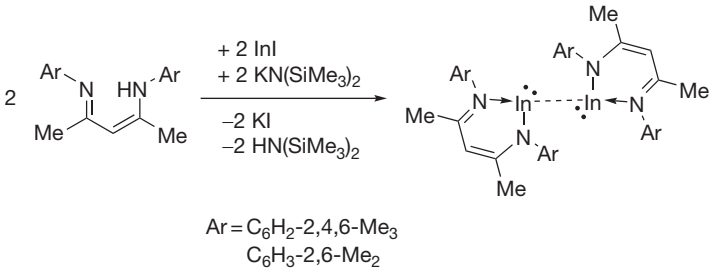

Scheme 7 Weakly associated In(I) β-diketiminates $\{In[N(Ar)C(Me)]_2CH\}_2$.

compounds.[34,35] The experimentally found indium–indium distance of 2.9786(5) Å is only ca. 0.12 Å shorter than the metal–metal distance in the respective thallium derivative and the In–In–C angle of 121.23(6)° is almost identical to the respective data of the heavier congener. The angle between the (C-*ipso*)–In–In–(C-*ipso*) unit and the central aryl ring of the *m*-terphenyl ligand is 39.3°. Consequently, the In–In 'multiple' bond in Ar′InInAr′ was shown to be very weak. For instance, it was also found to react rapidly with $B(C_6F_5)_3$ to give the 1:1 complex $Ar'In \rightarrow B(C_6F_5)_3$ (Scheme 6).

Similar to the putative 'dithallene' Ar′TlTlAr′, Ar′InInAr′ was also shown cryoscopically to dissociate into monomers in hydrocarbon solution. Further evidence for dissociation of the 'diindene' upon dissolution is gained from UV–Vis spectroscopy. UV–Vis spectra of Ar′InInAr′ in hexanes and the Ar*In complex[36] which is monomeric due to the *iso*-propyl groups in *para* position of the flanking aryl are virtually identical with two transitions associated with indium based in- and out-of-plane n–p transitions at 335 and 441 nm.

In addition to *m*-terphenyl ligands, which provide enough steric protection to stabilize compounds $(ArE)_n$, $n = 1–3$, β-ketiminates are well suited for the preparation of low-valent group 13 derivatives. These ligands stabilize the low-valent centers by a combination of steric shielding and the presence of N-donor functionalities.

Similar to the *m*-terphenyl-based indium derivatives, subtle changes in the ligand periphery of low-valent β-diketiminate indium complexes resulted in the isolation of monomeric, dimeric, or oligomeric complexes.

The β-diketiminate chelated In(I) dimer $\{In[N(C_6H_2\text{-}2,4,6\text{-}Me_3)C(Me)]_2CH\}_2$, for instance, is characterized by a remarkably long In–In distance of 3.1967(4) Å. It was isolated from the reaction of indium(I) iodide, potassium bis(trimethylsilyl) amide, and the β-imino amine $H[N(C_6H_2\text{-}2,4,6\text{-}Me_3)C(Me)]_2CH$.[37] A direct In–In contact of 3.3400(5) Å was also observed in the related, yet somewhat less crowded, complex $\{In[N(C_6H_3\text{-}2,6\text{-}Me_2)C(Me)]_2CH\}_2$.[38] Both compounds adopt a *trans*-bent conformation with respect to the coordination planes around indium in the solid state. In $\{In[N(C_6H_2\text{-}2,4,6\text{-}Me_3)_2C(Me)]_2CH\}_2$, for instance, the six-membered indium β-diketiminato subunit is almost perfectly planar and the *trans*-bending angle between this plane and the second indium center is 113.02°. Clearly, the structural motif is governed by a high degree of lone-pair character at the indium centers. Density functional theory (DFT) calculation on the model compound $\{In[N(H)C(H)]_2CH\}_2$ confirmed that the HOMO is nonbonding with respect to an indium–indium interaction and is instead composed of the In-centered lone pairs with high s-character. Degenerate HOMO-1 and HOMO-2 orbitals are essentially metal–ligand π-bonds and result from the overlap of empty In p-orbitals with N-centered lone pairs. The HOMO-3, finally, is associated with the indium–indium σ-bond and plays the central role in metal–metal bonding in this complex. As the HOMO is of nonbonding nature rather than a slipped π-bond, clearly no multiple bonding regime is operative. Calculations provided a bond dissociation energy of the model compound $\{In[N(H)C(H)]_2CH\}_2$ into two singlet indanediyl fragments: $\{In[N(H)C(H)]_2CH\}$ of only ca. 2 kcal mol^{-1} (Scheme 7).

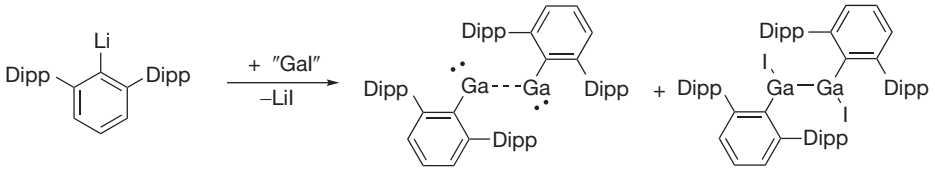

Scheme 8 Synthesis of 'digallene' Ar′GaGaAr′ and digallane Ar′Ga(X)Ga(X)Ar′ (X = iodine).

In addition to the above-mentioned dimeric compounds, variation of the aryl groups allows for the isolation of the landmark catenated indium hexamer (L)InI[In(L)]$_4$(L)InI, which shows spectroscopic properties that are consistent with σ-delocalization along the indium chain.[39]

Nevertheless, when the steric demand of the ligands was slightly augmented, such as in the symmetric β-diketiminate {[N(Dipp)C(Me)]$_2$CH}$^-$ [40,41] or in the unsymmetric {N(Dipp)C(Me)CHC(Me)N(*o*-Anis)}$^-$,[37] mononuclear complexes were isolated. Detailed diffusion ordered (DOSY) NMR spectroscopic investigations of several β-diketiminate indium compounds showed similar hydrodynamic radii and monomeric nature of all studied complexes in solution.[38]

The first example of a neutral digallium complex to follow the general formula RGaGaR was isolated when 'GaI' had been reacted with the *m*-terphenyl lithium salt Ar′Li (Ar′ = 2,6-(2,6-*i*Pr$_2$-C$_6$H$_3$)$_2$-C$_6$H$_3$) at low temperatures in toluene. The most important structural features are a Ga–Ga distance of 2.6268(7) Å, a *trans*-bending angle of 123.16(7) Å, and a perpendicular arrangement of the central aryl ring of the *m*-terphenyl ligands with respect to the (C-*ipso*)–Ga–Ga–(C-*ipso*) unit. This is in contrast to the related Tl and In compounds. In the case of Ar′TlTlAr′, a coplanar arrangement of the central rings of the *m*-terphenyl and the (C-*ipso*)–Ga–Ga–(C-*ipso*) plane was found. In the case of Ar′InInAr′, the angle of 39.3° between the central aryls and the (C-*ipso*)–In–In–(C-*ipso*) core is almost perfectly halfway between gallium and thallium (**Scheme 8**).

The synthesis of Ar′GaGaAr′ via salt elimination from Ar′Li and 'GaI' resulted in the concomitant formation and isolation of Ar′Ga(X)Ga(X)Ar′ (X = iodine).[42,43] Although Ar′Ga(X)Ga(X)Ar′ (X = iodine) is a single-bonded, trivalent Ga(II) derivative, its x-ray crystallographic structural analysis provided important structural information with respect to potential multiple bonding in Ar′GaGaAr′. In this three-coordinate Ga(II) compound, the triel centers are separated by 2.493(2) Å and are in fact about 0.14 Å closer than in the case of Ar′GaGaAr′. The Ga–Ga distance in Ar′Ga(X)Ga(X)Ar′ (X = iodine) falls well in the range of known gallium–gallium single-bond distances for which values between 2.33[44] and 2.54[45] Å have been reported. Although the Ga–Ga distance of 2.6268(7) Å in the dimeric Ga(I) species Ar′GaGaAr′ is significantly elongated with respect to Ar′Ga(X)Ga(X)Ar′ (X = iodine), the bond distance compares well with the distances found in the tetrameric, electron-deficient tetrahedral clusters (RGa)$_4$. In these, Ga–Ga distances span a range between 2.57 and 2.71 Å. Yet, these clusters were proven to dissociate in solution and an equilibrium between monomeric and tetrameric associates was established experimentally. In the gas phase, the tetramers were shown to dissociate into monomers by means of mass spectrometry and electron diffraction studies.[46,47] Hence it is not surprising that Ar′GaGaAr′

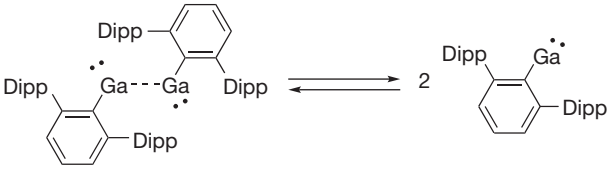

Scheme 9 Dissociation equilibrium of dimeric Ar′GaGaAr′ and monomeric Ar′Ga: in hydrocarbon solution.

sublimes similar to the tetramers at temperatures above 150 °C at a pressure of 0.05 mmHg which supports dissociation upon evaporation. UV–Vis spectra of Ar′GaGaAr′ in hydrocarbon solution display two maxima associated with gallium-related excitations at 350 and 437 nm. These have been ascribed to Ga-related n–p in-plane and out-of-plane transitions. Cryoscopic measurements support partial dissociation and the existence of a monomer/dimer equilibrium in solution for Ar′GaGaAr′ (**Scheme 9**).

The structural data and physical properties collected for Ar′GaGaAr′ substantiate the weakness of the gallium–gallium interaction and a bond order significantly less than unity.

The influence of substituents in remote ligand positions on the bonding situation in *m*-terphenyl-based gallium(I) compounds was assessed by the synthesis of a series of modified *m*-terphenyl derivatives [ArGa]$_n$ (n = 1, 2). Introduction of a *tert*-butyl substituent in *para* position of the central aromatic ring in the Ar′ ligand produced a dimeric structure with slightly shorter Ga–Ga distances. Compared to Ar′GaGaAr′, the solid-state structure of (4-Bu^{t}Ar*)GaGa(Ar*-4-Bu^t) was found disordered over three positions for which Ga–Ga distances between 2.512(7) and 2.596(4) Å were refined. Although all of the disordered parts have almost planar, *trans*-bent C–Ga–Ga–C cores in common, the C–Ga–Ga angles vary notably between 119.2(2)° and 132.4(2)°. Similarly, the gallium atoms in the dimeric, *para*-CF$_3$-substituted derivative (4-CF$_3$-Ar*)GaGa(Ar*-4-CF$_3$) are separated by 2.6031(8) Å. (Minor contributions from two further conformers together with <6% contribution put the galliums in distances of 2.61(1) and 2.569(7) Å.) Two significantly different *trans*-bending angles of 121.68(5)° and 128.53(5)°, respectively, are observed in the major component in the crystal structure of (4-CF$_3$-Ar*)GaGa(Ar*-4-CF$_3$). The bonding situation changes dramatically, however, when two *iso*-propyl groups in *meta* positions of the central ring are introduced. Owing to the steric demand of the *iso*-propyl groups attached to the central ring in the ligands, the aryl groups in 2,6-positions of the central ring are pushed forward and cause the space available for coordination of the gallium center to shrink considerably. Thus, the angle between centroids of the flanking aryls and the centroid of the central ring is reduced by ca. 10°. This is apparently just enough to

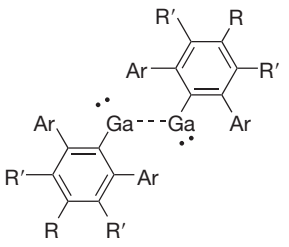

Dimeric: Ar=Dipp; R=R′=H
Ar=Trip; R=Bu^t; R′=H
Ar=Trip; R=CF_3; R′=H

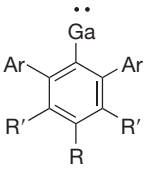

Monomeric: Ar = Trip; R=R′=H
Ar = Dipp; R=H; R′=Pr^i
Ar = Trip; R=H; R′=Pr^i

Scheme 10 Substituent modifications in *m*-terphenyl-based 'digallenes.'

increase the Ga–Ga separation in a potential dimer and to render the monomeric solid-state structures energetically favored. The solid-state structures of [C_6H-3,5-^{i}Pr$_2$-2,6-(C_6H$_3$-2,6-^{i}Pr$_2$)$_2$]Ga and [C_6H-3,5-^{i}Pr$_2$-2,6-(C_6H$_2$-2,4,6-^{i}Pr$_3$)$_2$]Ga feature strictly mono-coordinate gallium centers with Ga–C distances of ~2.03 Å. Calculations reproduced the experimentally observed bonding situation reasonably well. Bond energies of 8.1–8.9 kcal mol^{-1} for Ar′GaGaAr′, 5.3 kcal mol^{-1} for (4-^{t}BuAr*)GaGa(Ar*-4-^{t}Bu), and 5.8 kcal mol^{-1} for (4-CF_3-Ar*)GaGa(Ar*-4-CF_3) confirm a weak gallium–gallium interaction in these compounds. In contrast, computational results favor the monomeric structure for the 3,5-di-*iso*-propyl substituted derivative [C_6H-3,5-^{i}Pr$_2$-2,6-(C_6H$_2$-2,4,6-^{i}Pr$_3$)$_2$]Ga by ca. 1.7 kcal mol^{-1}. Calculations for the slightly less crowded [C_6H-3,5-^{i}Pr$_2$-2,6-(C_6H$_3$-2,6-^{i}Pr$_2$)$_2$]Ga are in favor of a dimeric structure in the gas phase which is more stable by ca. 1.4–2.9 kcal mol^{-1}. Given the weakness of the bond, packing forces may well be enough to compensate for the increase in energy and cause the experimentally observed monomeric coordination mode (Scheme 10).

The UV–Vis spectra of all *m*-terphenyl-substituted gallium (I) compounds in hydrocarbon solution feature two strong absorptions around 350 and 440 nm. According to time-dependent DFT calculations, these are associated with symmetry allowed excitations from the nonbonding HOMO lone pair with high s-orbital character at the gallium center to gallium centered out-of-plane (lowest unoccupied molecular orbital – LUMO) and in-plane (LUMO + 1) p-orbitals. In contrast, calculations predict transitions at around 450 and 810 nm in the UV–Vis spectra for the dimeric structures. The absence of the low energy transitions at around 810 nm in experimental spectra further emphasizes the importance of the monomeric structure of these Ga(I) of *m*-terphenyl-ligated Ga(I) compounds in solution.[48]

In comparison to their heavier homologs, the chemistry of neutral 'dialumene' compounds with general formula RAlAlR is by far less developed. In fact, no x-ray structural data for a 'dialuminene' have been reported to date, although compounds with formula RAlAlR were reported as reaction intermediates. The reduction of the sterically hindered organoaluminum diiodide Ar′AlI$_2$ with potassium graphite in diethyl ether yields a dark red solution, which is stable under strictly inert condition for extended periods. The formation 'dialuminene' as reaction intermediates is further substantiated by the isolation of several derivatives. These include compounds which arise from [2 + 2] or [2 + 4] cycloaddition reactions with unsaturated hydrocarbons. Removal of the solvent from reaction mixtures which contained Ar′AlAlAr′ and extraction with toluene results in the isolation of a bicyclic addition product. The formation of this intriguing species can be readily rationalized as a [2 + 4] Diels–Alder cycloaddition of toluene to a dialuminene[49] which is also supported by theoretical investigations[50] (Scheme 11).

When the reduction of Ar′AlI$_2$ with potassium graphite was carried out in toluene in the presence of 1,2-bis-trimethylsilyl acetylene, a 1,2-dialumina cyclobutene structure was obtained.[51] A related alumina cyclopropene derivative was obtained from the reduction of β-ketiminato aluminum diiodide complex I$_2$Al{C[(CMe)(NAr)]$_2$} (Ar = C_6H$_3$-2,6-^{i}Pr$_2$) with potassium in the presence of substituted alkynes RC≡CR (R = Ph, Me).[52] Reductions of *m*-terphenyl-substituted group 13 dihalides in the presence of metallocene dihalides led to the isolation of several transition metal complexes.[53–57]

Ar′AlAlAr′ was also shown to undergo two-electron reduction to yield the dianion [Ar′AlAlAr′]$^{2-}$. The latter example features potential triple bonding and is discussed in Section 1.10.5.

Finally, the existence of a series of neutral diborenes R–B=B–R (R = ^{i}Pr$_2$N,[58] *sec*-Bu$_2$N, 2,2,6,6-tetramethylpiperidyl) was verified by means of ^{11}B NMR spectroscopy, mass spectrometry, and through trapping reactions.[59] Attempts to isolate diborenes from reductions of *m*-terphenyl-substituted boron precursors have failed so far[60] (Table 1).

1.10.2.2 Reaction Chemistry of Neutral Ditrielenes REER

It was shown in the previous section that the metal–metal bond in compounds of general formula REER (E = Ga, In, Tl) is weak and that derivatives of the heavier elements gallium to thallium usually dissociate at least in part into monomers upon dissolution. As a consequence, it seems rather unlikely that the metal–metal scaffold in the complexes REER (E = Ga, In, Tl) will remain intact in the course of derivatization reactions. Nevertheless, heavier group 13 complexes of type RE: feature a combination of a lone pair of largely s-electron character and two empty orbitals with pronounced p-orbital properties. In other words, the RE: fragments combine electron-donating, Lewis-base properties with Lewis-acid properties. In this respect, they resemble the singlet Arduengo-type carbenes and are interesting candidates with respect to

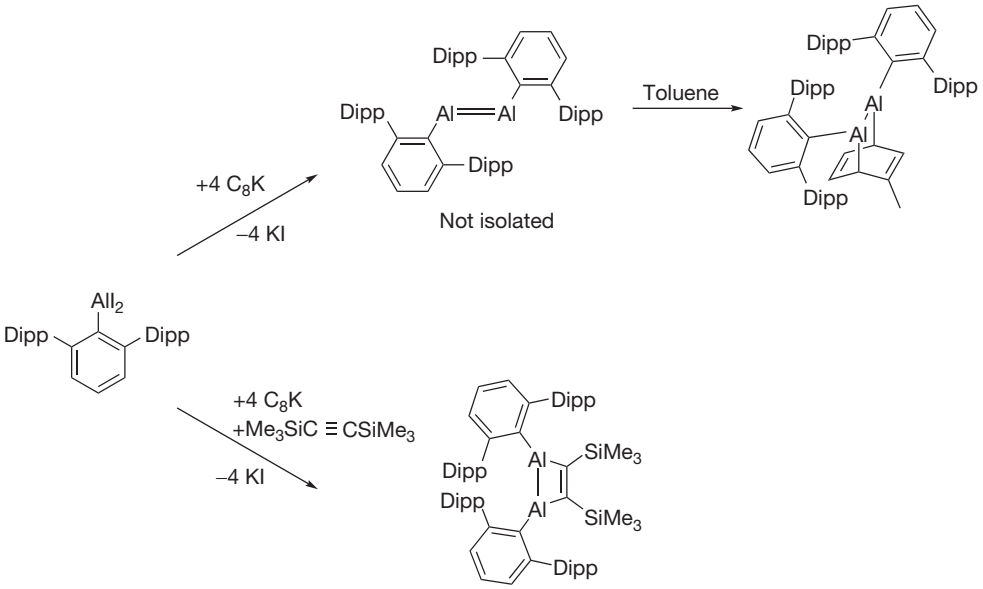

Scheme 11 Addition reactions of dialuminene Ar′AlAlAr′ with unsaturated molecules.

Table 1 Structural data and spectroscopic properties for neutral REER (E = B, Ga, In, Tl) and related species

	E–E distance (Å)	*R–E–E angle (°)*	*Ref.*
L′:BH=BH:L′ L′ = :C{N(C_6H_3-2,6-^{i}Pr$_2$)CH}$_2$	1.561(18)		[12]
L*:BH=BH:L* L* = = :C{N(C_6H_2-2,4,6-Me_2)CH}$_2$	1.582(4)–1.679(9)		[13]
Ar′GaGaAr′	2.6268(7)	123.16(7)	[42,43]
4-Bu^t-Ar*GaGaAr*-4-Bu^t	2.512(7)–2.596(4)	119.2(2)–132.4(2)	[48]
4-CF_3-Ar′GaGaAr′-4-CF_3	2.6031(8)	121.68(5)–128.53(5)	[48]
{In[N(C_6H_2-2,4,6-Me_3)C(Me)]$_2$CH}$_2$	3.1967(4)		[37]
{In[N(C_6H_3-2,6-Me_2)C(Me)]$_2$CH}$_2$	3.3400(5)		[38]
Ar′InInAr′	2.9786(5)	121.23(6)	[33]
[{C_5(CH_2Ph)$_5$}In]$_2$	3.631		[18]
Ar′TlTlAr′	3.0936(8)	122.9(4)	[29]
[{C_5(CH_2Ph)$_5$}Tl]$_2$	3.632		[21]
$Tl_2B_9H_9C_2Me_2$	3.67		[20]
{Tl[Tp$^{p\text{-Tol}}$]}$_2$	3.86		[23]
{Tl[Bp]}2	3.70		[24]
{MeSi[N(Tl)^{t}Bu]$_3$}$_2$	3.15		[25]
Cp′Tl–Cp′Tl Cp′–Cp′ = 1,1′3,3′-Bu$^t_4$-5,5′-pentafulvalene	3.76–4.625		[19]

activation of small molecules.[7,8] In contrast to the heavier congeners, the high reactivity of the aluminum derivatives RAlAlR is a result of their diradical ground state.

The putative digallene Ar′GaGaAr′ readily undergoes oxidative addition to the carbon–carbon triple bond of phenylacetylene. Even at room temperature, reaction of the green solution of the gallium(I) species Ar′GaGaAr′ with two equivalents of phenylacetylene rapidly yields the colorless 1,4-digallatacyclohexadiene derivative. This compound, in which the gallium atoms in the formal oxidation state +III, adopts a flattened chair conformation in the solid state with fold angles around 15°. In the 1,4-digallatacyclohexadiene complex, the carbon–carbon double bond distances are 1.353(2) Å, carbon–gallium separation accounts for 1.959(2) and 1.967(2) Å. Treatment of a solution of the 4π-electron 1,4-digallatacyclohexadiene with two equivalents of potassium in diethyl ether produces dark blue solutions of the respective dianionic 1,4-digallatabenzene (**Scheme 12**).

Single-crystal x-ray structure analyses confirm the dianionic nature and reveal notable structural changes upon the twofold reduction. The 6π-electron [Ar′GaCHC(Ph)]$_2^{2-}$ ring is planar with the two potassiums located above and below the centroid of the metallo-aromatic ring and complexed by the flanking aryl groups of the *m*-terphenyl substituents. The carbon–carbon distance in the ring is lengthened by ca. 0.06 Å to values of 1.408(3) and 1.418(3) Å. In contrast, the endocyclic gallium–carbon distances at 1.899(2) to 1.941(2) Å are both shorter than in the parent neutral molecule. Given the planar

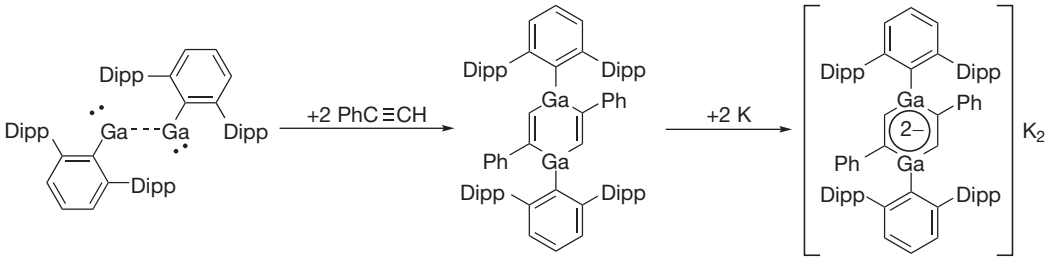

Scheme 12 Addition of phenylacetylene to 'digallene' Ar′GaGaAr′ and formation of dianionic 1,4-digallatabenzene.

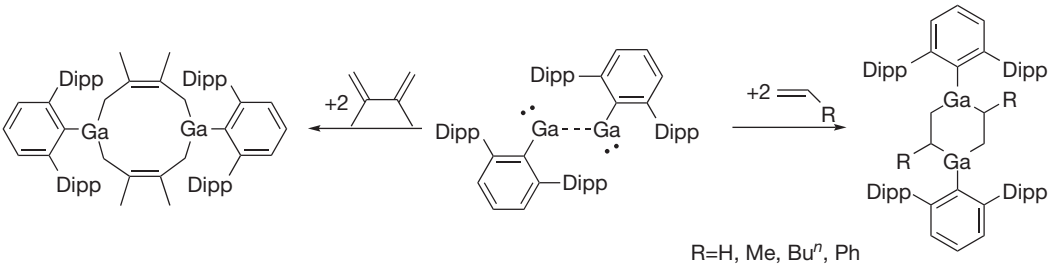

Scheme 13 Addition of terminal alkenes to 'digallene' Ar′GaGaAr′.

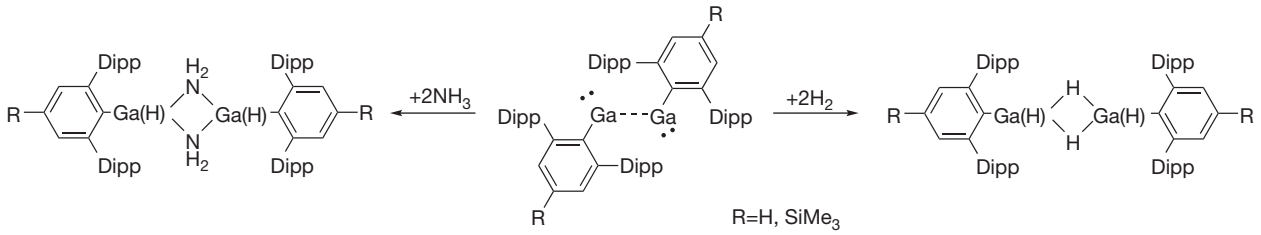

Scheme 14 Activation of dihydrogen and ammonia by digallene Ar′GaGaAr′.

structural motif, the shortening of the gallium carbon bonds and the concomitant elongation of the endocyclic carbon–carbon bonds, the formulation of $[Ar'GaCHC(Ph)]_2^{2-}$ as a delocalized 6π-electron aromatic system seems appropriate.[61]

It was also shown that the *m*-terphenyl-based digallene Ar′GaGaAr′ reacts under mild conditions with unactivated, nonconjugated olefins such as ethane, propene, 1-hexene, or styrene. In all cases, the transformations proceed under rupture of the gallium–gallium bond and the outcome of the reactions are 1,4-digallatacyclohexanes. Similarly, oxidative addition to 2,3-dimethyl-1,3-butadiene gave a 1,6-digallatacyclodecadiene derivative[42] (Scheme 13).

The mechanism of the cycloaddition reactions is currently unknown. It may proceed via a stepwise, twofold [2 + 2] cycloaddition, which is, however, symmetry-forbidden. Alternatively, the stepwise addition may involve radicals as reaction intermediates. Moreover, a reaction pathway which involves the initial dissociation of the digallene into monomers, followed by formation of a gallatacyclopropene and subsequent dimerization, is conceivable. However, no experimental evidence for the intermediate formation of a gallatacyclopropane has been observed.[62]

Probably the most significant reactions of heavier group 13 dimetallenes are activation reactions involving dihydrogen. It was shown by the group of Power that the *m*-terphenyl based, low-valent Ga(I) dimer Ar′GaGaAr′ (Ar′ = 2,6-(2,6-*i*Pr$_2$-C$_6$H$_3$)$_2$-C$_6$H$_3$) reacted upon dissolution in toluene with dihydrogen to produce the dimeric Ga(III) species $[Ar'Ga(\mu\text{-}H)H]_2$.[63] This compound features two distinctly different distances between the bridging hydrogen atoms and the gallium centers at 1.69(2) and 1.78(2) Å, respectively. The much shorter terminal gallium–hydrogen distance at 1.46(2) Å falls in the same range as in other monomeric, terminal gallium hydrides with bulky ligands such as the Ga–H distances in Mes*$_2$GaH or Ar$^{\#}_2$GaH.[64]

The activation under mild conditions (ambient temperature and hydrogen pressure of 1 bar) is remarkable as calculations suggested high activation energies of around 43 kcal mol^{-1} for the reaction between GaH and H_2 to yield GaH_3.[65–67] Interestingly, attempts to convert the respective *m*-terphenyl-substituted gallium halides into the hydrides by reaction with hydride sources such as DIBAL-H, sodium hydride, and alkali metal borohydrides were unsuccessful. Spectroscopic investigations evidenced that the complex reaction mixtures derived from these reactions did not contain $[Ar'Ga(\mu\text{-}H)H]_2$ at all (Scheme 14).

ArGaGaAr (Ar = Ar′, 4-Me$_3$Si–Ar′) also reacts directly with ammonia at ambient temperature under insertion into one of the nitrogen-hydrogen bonds in ammonia. Spectroscopic and x-ray structural analysis proved the formation of an amido-

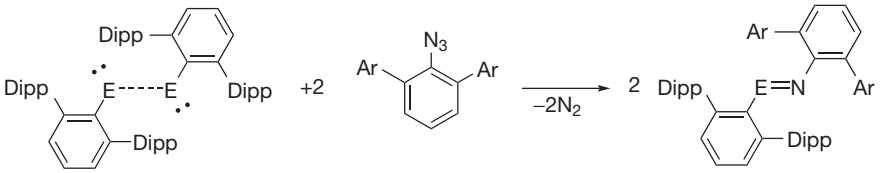

E = Ga, In; Ar = C_6H_2-2,6-Me_2-4-Bu^t

Scheme 15 Synthesis *m*-terphenyl-substituted gallium and indium imides.

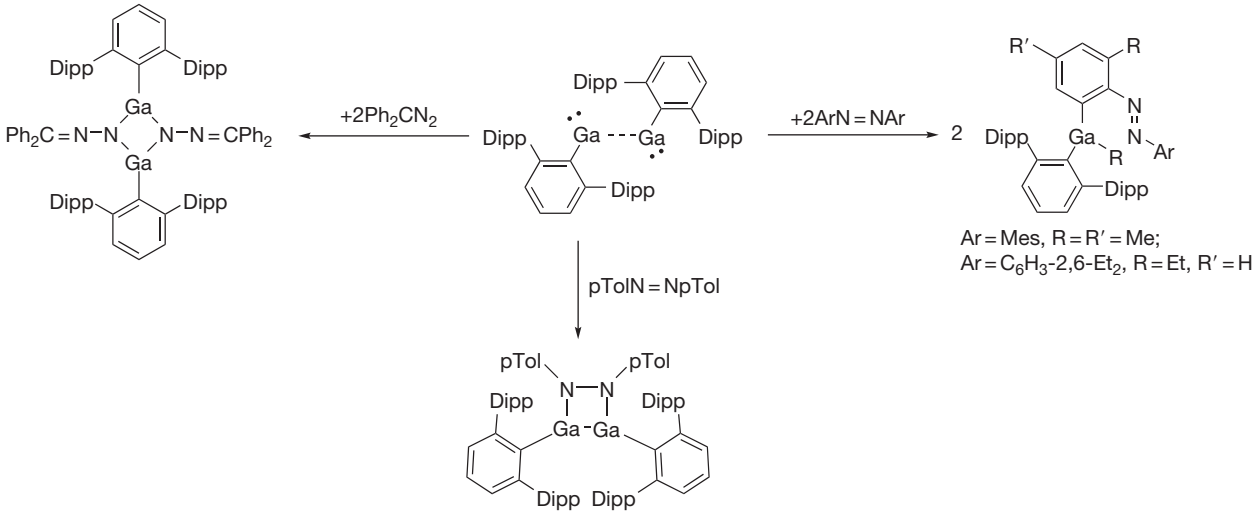

Scheme 16 Addition of unsaturated nitrogen compounds to digallene Ar′GaGaAr′.

bridged, dimeric complex with a rhombohedral, planar Ga_2N_2 core. In this, the gallium–nitrogen distances are almost identical at ca. 1.98 Å (avg.) and the gallium–nitrogen–gallium angles found, account for ca. 95° in contrast to more acute nitrogen–gallium–nitrogen angles of ca. 85°. The terminal hydrogen gallium distance of 1.54(2) Å in this species was found slightly elongated with respect to the hydrogen insertion product (*vide supra*). Earlier studies on the reaction of gallium(I) compounds with ammonia relied on much more drastic conditions. In the case of the reaction of neo-pentyl gallium(I) with ammonia at temperatures of 460°, complete decomposition of the organogallium compound was observed. The isolated reaction products included neo-pentane, dihydrogen, and gallium nitride, instead.[68]

Reaction of Ar′GaGaAr′ and Ar′InInAr′ with *m*-terphenyl azide N_3-C_6H_3-2,6-(C_6H_2-2,6-Me_2-4-Bu^t)$_2$ results in an immediate color change and the evolution of dinitrogen with concomitant formation of gallium or indium imides. Both, the gallium and the indium imides, display short E–N distances of 1.701(3) Å (E = Ga) and 1.928(3) Å (E = In) and wide angles around the triel and nitrogen atoms[69] (**Scheme 15**).

Ar′GaGaAr′ also undergoes addition reactions with the N=N unit in diazene. The outcome of these reactions, however, strongly depends on the substitution of the diazene Ar–N=N–Ar. Treatment of Ar′GaGaAr′ with dimesityl and 2,6-diethylphenyldiazene results in an insertion of Ar′Ga: into a ligand side group. Reaction with bis(*p*-tolyl)diazene proceeds under conservation of the Ga–Ga bond and yields a four-membered 1,2-Ga_2N_2 ring structure. Surprisingly, reaction of Ar′GaGaAr′ with diazoalkene Ph_2CN_2 does not lead to the evolution of dinitrogen, but yields the four-membered cyclic 1,3-Ga_2N_2 product instead. In this, the gallium atoms are bridged by Ph_2CN_2 units through their terminal nitrogen atoms[70] (**Scheme 16**).

The reaction chemistry of dithallenes Ar′TlTlAr′ is largely unexplored. Nevertheless, it readily reacts with white phosphorus to yield dithallium diaryltetraphosphabutadiendiide $Tl_2[P_4Ar_2]$ in which both thalliums are coordinated in an η-4 fashion above and below the central, planar P_4-subunit. The shortest thallium–phosphorus distances in this complex are slightly longer than 3.03 Å and the thallium–phosphorus interaction remains intact in solution as demonstrated by the observation of ^{203}Tl/^{31}P and ^{205}Tl/^{31}P coupling constants in the range of 500 Hz as well as a large ^{203}Tl/^{205}Tl coupling constant of ca. 12 000 Hz. Oxidation of $Tl_2[P_4Ar_2]$ under mild conditions with elemental iodine yields thallium(I) iodide and diaryltetraphosphabicyclobutane[71] (**Scheme 17**).

As far as reactions of group 13 dimetallenes with the group 16 elements oxygen to tellurium are concerned, reports are scarce. Both, digallenes and diindenes Ar′MMAr′, are oxidized by N_2O or elemental sulfur to yield the dimeric arylgallium and -indium oxides and sulfides, respectively.[72] In the case of thallium, no products other than Ar′H were isolated from the reaction mixtures (**Scheme 18**).

In all cases, the dimers [Ar′ME]$_2$ (M = Ga, In; E = O, S) feature three-coordinate metal centers with planar M_2E_2 core in the solid state. The oxides crystallize as almost perfectly square planar rings with M–O distances of 1.83 Å for M = Ga

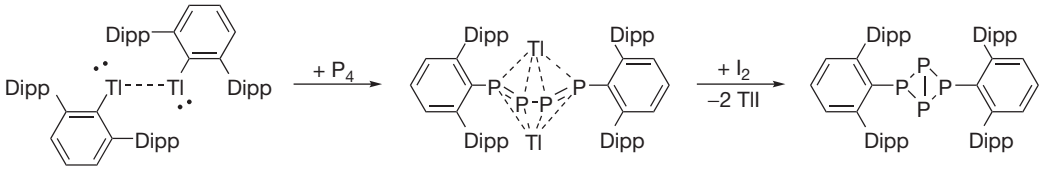

Scheme 17 Activation of white phosphorus by dithallene Ar′TlTlAr′.

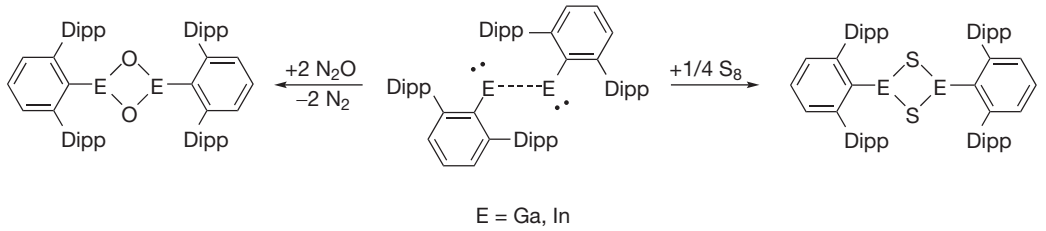

Scheme 18 Oxidation of ditrielenes Ar′EEAr′ (E = Ga, In) by nitrous oxide and elemental sulfur.

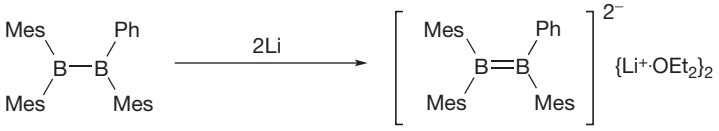

Scheme 19 Two-electron reduction of diborane $Mes_2BBMesPh$ to yield $[Mes_2BBMesPh]^{2-}$.

and 2.03 Å for M = In. In the solid state, the M_2O_2 cores adopt a perpendicular orientation with respect to the central rings of the flanking aryl groups. In the heavier chalcogenides $[Ar'MS]_2$ (M = Ga, In) the central quadrilateral deviates significantly from a square arrangement to form a rhombus in which S–M–S angles are 100.7° (M = Ga)/98.1° (M = In) and M–S–M angles account for 79.3° (M = Ga) and 81.9° (M = In).[72]

1.10.3 Syntheses and Structural Properties of Double-Bonded Dianionic Compounds $[R_2EER_2]^{2-}$

As stated in Section 1.10.1, two-electron reductions of tetraorganodiboranes result in group 13 dianions which are isoelectronic to ethenes.

In 1992, the first example of a doubly reduced diborane was reported in a groundbreaking study by the research group of Power. Treatment of $Mes_2BBMesPh$ with excess lithium in diethylether/hexane mixtures yields $[(Et_2O)Li]_2[Mes_2BBMesPh]$ as dark red crystals (Scheme 19).

Comparison of data from x-ray structural analyses of the starting material and the doubly reduced compound substantiates the formulation of $[Mes_2BBMesPh]^{2-}$ as an ethene homolog. The boron–boron distance shrinks by ca. 0.07 Å from 1.706(12) Å in neutral $Mes_2BBMesPh$ to 1.636(11) Å in the case of the dianion. The decrease in bond length in these compounds is less pronounced than in the carbon homologs where typical carbon–carbon single-bond distances are ca. 1.54 Å and double-bond distances are shorter by ca. 0.22 Å and typically account for ca. 1.32 Å. This difference is readily rationalized by considering the electronic repulsion of two vicinally oriented, negatively charged boron centers. For comparison, the boron–boron distance in the B–B singly bonded boron-centered dianion $(Me_3Si)_2C{=}B(Ar)(^-){-}B(Ar)(^-){=}C(SiMe_3)_2$, in which the two negative charges are located at the boron atoms, is 1.859(8) Å.[73] When comparing $(Me_3Si)_2C{=}B(Ar)(^-){-}B(Ar)(^-){=}C(SiMe_3)_2$ and $[Mes_2BBMesPh]^{2-}$, which both feature similar coulombic repulsion due to the negative charges, the B–B bond distance in the doubly bonded species is shortened by the same ca. 0.2 Å as observed for C–C distances in alkanes versus alkenes.[74]

The interpretation of the bonding situation in $[Mes_2BBMesPh]^{2-}$ as twofold is further corroborated by the drastic changes in the orientation of the boron coordination planes. In $Mes_2BBMesPh$, the C_2B planes are almost perpendicularly oriented with an angle of 79.1°. In $[(Et_2O)Li]_2[Mes_2BBMesPh]$, however, the C_2BBC_2 center is almost perfectly planar where the C_2B planes are twisted by only 7.3°. NMR spectroscopically, the reduction leads to a ca. 70 ppm upfield shift in ^{11}B NMR spectra from +99 ppm in $Mes_2BBMesPh$ to +24.7 ppm in $[(Et_2O)Li]_2[Mes_2BBMesPh]$.

Reduction of the diamino diaryl diborane $Ph(Me_2N)BB(NMe_2)Ph$ with elemental lithium in diethylether/THF mixtures gives the doubly reduced salt $[(Et_2O)Li]_2[Ph(Me_2N)BB(NMe_2)Ph]$. Similar to the tetraaryl-substituted diborate, the boron–boron distance contracts from 1.714(4) Å in the starting material to an average of 1.627 Å in the reduced species. It is also noteworthy that the boron–nitrogen distance increases drastically upon reduction from a value of 1.399 Å (avg.) in the neutral compound to 1.561 Å (avg.) in the dilithio salt. The N(C-*ipso*)BB(C-*ipso*)N core in $[(Et_2O)Li]_2[Ph(Me_2N)BB(NMe_2)Ph]$ is planar while the orientation of the NMe_2 groups is then perpendicular to this unit. Hence, the N–B π-interaction operative in the starting material is lost in the doubly reduced form

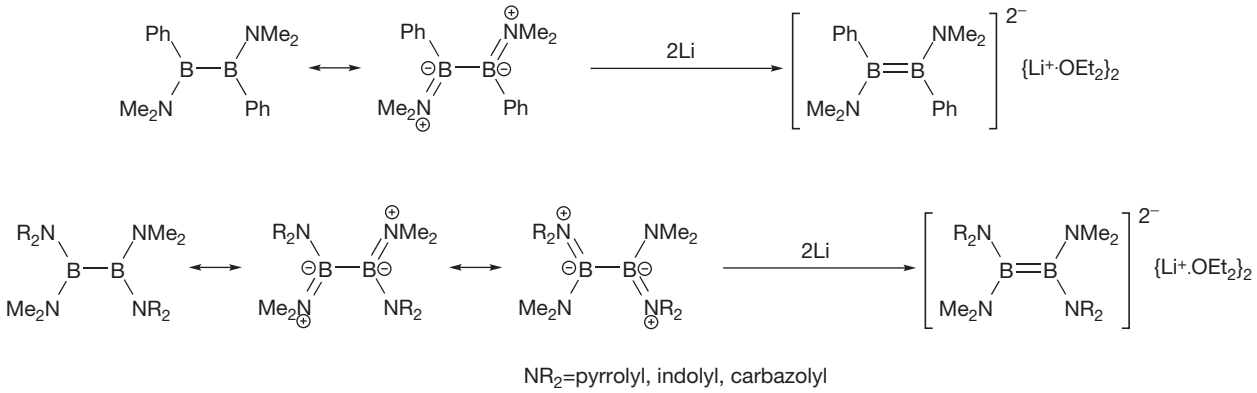

Scheme 20 Two-electron reduction of bis aminoborane $(Me_2N)PhBBPh(NMe_2)$.

at the cost of the formation of the boron–boron π-bond. ^{11}B NMR spectra display an upfield shift of ca. 16 ppm upon reduction from a shift of +49.3 ppm in $Ph(Me_2N)BB(NMe_2)Ph$ to +33 ppm in the reduced complex[75] (Scheme 20).

A series of dilithium tetraaminodiborates $[(Me_2N)(R_2N)BB(NR_2)(NMe_2)]^{2-}$ (NR_2 = pyrrolyl, indolyl, and carbazolyl) further exemplifies the shortening of the boron–boron bond upon two-electron reductions. In these dianions, the B–B bond distances decrease from 1.72 Å to values around 1.58 Å. Again, the shortening of the central B–B interaction is accompanied by very significant lengthening of the B–N bonds. In the parent neutral molecules, two distinctively different sets of B–N distances are observed. The shorter distance at ca. 1.39 Å originated from bonding to the dimethylamino group and a longer B–N separation at 1.49 Å to the aromatic substituents. This is again a strong evidence for the donation of nitrogen-based electron density into the empty orbital at each of the boron atoms. Upon reduction, however, all boron-nitrogen bonds in the dianion become almost equidistant at values slightly over 1.53 Å. Moreover, the nitrogens of the dimethyl amino substituents are pyramidalized in the reduced derivatives and the Me_2N are perpendicularly arranged with respect to the planar N_2BBN_2 unit. ^{11}B NMR shifts of the neutral diboranes were all observed around +37 ppm. Reduction causes a slight increase in chemical shielding and an upfield shift of about 4–10 ppm.[76]

A summary of bond distances, angles, and ^{11}B NMR shifts is given in Table 2.

1.10.4 Syntheses and Structural Properties of Group 13 Radicals with Multiple Bond Character

1.10.4.1 Open-Shell Boron Compounds with Bond Order Greater Than Unity

Tetraorganodiboranes, $R_2B–BR_2$, are normally unstable with respect to disproportionation. The use of sterically demanding substituents, however, provides access to examples of this class of compounds. As already exemplified, these molecules feature vacant p-orbitals at boron which are accessible for two independent one-electron reductions to yield the singly reduced radical anions $[R_2BBR_2]^{\bullet-}$ and the doubly reduced dianions $[R_2BBR_2]^{2-}$.

Population of the π-orbital which results from a combination of the p-orbitals at boron will result in a certain degree of multiple bonding with a formal bond order of 1.5 for the radical anion and 2 for the dianion (*vide supra*).

For instance, tetra-*neo*-pentyldiborane is unstable at room temperature and decomposes with a half-life of ca. 15 min in solution. Its reduction with sodium/potassium alloy in mixtures of 1,2-dimethoxyethane/THF produces the respective radical anion with $t_{1/2}$ = 20 min at 140° in solution. EPR spectroscopic investigations indicate equivalent coupling of the unpaired electron to both boron centers. A small ^{11}B hyperfine coupling constant of 0.8 G is in good agreement with population of a π-type rather than σ-type orbital.[77] Similar coupling patterns and coupling constants are also observed for the related tetra-alkyl-substituted radical anions $[Bu^t(Bu^tCH_2)BB(CH_2Bu^t)Bu^t]^{\bullet-}$ and $[Bu_t^2BBBu^t_2]^{-}$[78,79] (Scheme 21).

The related mixed alkoxy/aryl-substituted compound $\{Li(OEt_2)_2\}[Mes(MeO)BB(OMe)Mes]$ is available via stoichiometric reduction of the neutral precursor with lithium metal. In this species, the B–B distance is short at 1.636(7) Å. The boron atoms in the radical anion are about 0.09 Å closer than in the parent neutral molecule Mes(MeO)BB(OMe)Mes, where the borons are separated by 1.724(9) Å. The short B–B distance in the reduced species is accompanied by much longer B–O distances (B–O = 1.454(4) Å) in the radical anion with respect to the neutral species (B–O = 1.363(10) Å)[80] (Scheme 22).

Similar bond-shortening effects are observed for the tetraaryl compounds $Mes_2BBMesPh$ (d B–B 1.706(12) Å) and its potassium-based radical anion derivative $\{K(18\text{-crown-6})(THF)_2\}[Mes_2BB(Ph)Mes]$ (d B–B 1.649 Å).[81]

Comparison of neutral $Mes_2BBMesPh$, radical anion $[Mes_2BBMesPh]^{\bullet-}$, and dianion $[Mes_2BBMesPh]^{2-}$ is particularly interesting in the context of multiple-bonded diboron compounds as it is the only series of compounds for which x-ray crystallographic data for all three compounds are available. Both reduced compounds feature coplanar arrangements of the C_2B planes in contrast to the perpendicular orientation in the parent neutral species. B–B distances contract upon consecutive addition of electrons. The small drop in B–B distance resulting from the second reduction step is also a consequence of coulombic repulsion of the neighboring negative charges. Nevertheless, the existence of boron–boron multiple bonding is clearly evidenced by experimental facts.

Table 2 Structural and spectroscopic data for parent [REER] molecules, and radical anions $[REER]^{\bullet-}$ and dianions $[REER]^{2-}$

Compound	*E–E distance (Å)*	*E–C distances (Å)*	*Torsion angle (°)*	*UV–Vis (nm)*	*Hyperfine coupling constant to E (G)*	*^{11}B NMR shift (ppm)*	*Ref.*
Boron							
$Bu^t_2BBBu^t_2{}^{\bullet-}$					1.44		[79]
$(Bu^tCH_2)_2BB(Bu^tCH_2)_2{}^{\bullet-}$					0.8		[77]
$(Bu^tCH_2)Bu^tBBBu^t(Bu^tCH_2){}^{\bullet-}$					<0.6		[78]
Mes(MeO)BB(OMe)Mes	1.724(9)	1.572(9) (avg.) (B–C), 1.363 (10) (avg.) (B–O)	74.9			61	[80]
Mes(MeO)BB(OMe)Mes$^{\bullet-}$	1.636(7)	1.589(5) (avg.) (B–C), 1.454 (4) (avg.) (B–O)	2.5	307, 589	Not. res.		[80,86]
$Mes_2BBMesPh$	1.706(12)	1.577(11) (avg.)	79.1			+99	[74]
$Mes_2BBMesPh^{\bullet-}$	1.649(11)	1.61(2) (avg.)	6.9	630	13		[81]
$Mes_2BBMesPh^{2-}$	1.636(11)	1.637(8) avg.	7.3			+24	[74]
$Ph(Me_2N)BBPh(NMe_2)$	1.714(4)	1.399 (avg.) (B–N)	88.7	320		+49	[75]
$Ph(Me_2N)BBPh(NMe_2)^{2-}$	1.627() (avg.)	1.593(6) avg. (B–C), 1.561(5) (B–N)	0			+33	[75]
$(Me_2N)R_2NBBNR_2(NMe_2)$ NR_2 = pyrrolyl	1.718(2)	1.393(2) (avg.) (B–NMe_2), 1.488(6) avg. (B–NR_2)	73			37	[76]
$(Me_2N)R_2NBBNR_2(NMe_2)^{2-}$ NR_2 = pyrrolyl	1.59(1)	1.537(7) (B–NMe_2), 1.562(5) (B–NR_2)				27	[76]
$(Me_2N)R_2NBBNR_2(NMe_2)$ NR_2 = indolyl	1.723(4)	1.388(3) (avg.) (B–NMe_2), 1.489(3) avg. (B–NR_2)	57			37	[76]
$(Me_2N)R_2NBBNR_2(NMe_2)^{2-}$ NR_2 = indolyl	1.582(4) (avg.)	1.531(3) (avg.) (B–NMe_2), 1.562(2) avg. (B–NR_2)				28	[76]
$(Me_2N)R_2NBBNR_2(NMe_2)$ NR_2 = carbazolyl						38	[76]
$(Me_2N)R_2NBBNR_2(NMe_2)^{2-}$ NR_2 = carbazolyl	1.567(9) (avg.)	1.542(6) (avg.) (B–NMe_2), 1.569(6) avg. (B–NR_2)				29	[76]
Aluminum							
$Trip_2AlAlTrip_2$	2.647(3)	1.996(3) avg.	44.8	397, 451(sh), 742			[85]
$Trip_2AlAlTrip_2{}^{\bullet-}$	2.470(2)	2.021(1) (avg.)	1.4		10.4		[85]
$[(Me_3Si)_2CH]_2AlAl[CH(SiMe_3)_2]_2$	2.660(1)		0				[82]
$[(Me_3Si)_2CH]_2AlAl[CH(SiMe_3)_2]_2{}^{\bullet-}$	2.53(1)	2.040(5) (avg.)	0	368, 451, 551, 650 (sh)	11.1–11.9		[83,84]
$(Bu^t_3Si)AlAl(SiBu^t_3)_2{}^{\bullet}$	2.420(1)				21.8, 18.9		[90]
Gallium							
$Trip_2GaGaTrip_2$	2.515(3)	2.008(7)	43.8				[87]
$Trip_2GaGaTrip_2{}^{\bullet-}$	2.343(2)	2.038(10)	15.5	360, 900	35.4/43.9		[87]
$[(Me_3Si)_2CH]_2GaGa[CH(SiMe_3)_2]_2$	2.541(1)	1.996(5)	0				[45]
$[(Me_3Si)_2CH]_2GaGa[CH(SiMe_3)_2]_2{}^{\bullet-}$	2.401(1)	2.064(4) avg.	0	357,550	57.4/72.8 (300 K), 54.4/42.8 (200 K)		[88]
$(Bu^t_3Si)GaGa(SiBu^t_3)_2{}^{\bullet}$	2.420(1)				50/64, 32/41		[89]

1.10.4.2 Open-Shell Heavier Group 13 Compounds with Bond Order Greater Than Unity

Similar to the boron congeners, sterically hindered tetraorgano dialanes and -digallanes undergo one-electron reduction to yield stable radical anions with formal bond order of 1.5. First examples of compounds with aluminum–aluminum one-electron π-bonds were reported in two independent seminal studies in 1993 by the groups of Pörschke, Uhl, and Power. Reduction of tetrakis(bis(trimethylsilyl)methyl)dialane $Bsi_2AlAlBsi_2$[82] with lithium in diethylether in the presence of tmeda provides the black violet radical anion $\{Li(tmeda)_2\}[\{(Me_3Si)_2CH\}_2AlAl\{CH(SiMe_3)_2\}_2]$ as a solvent separated ion pair in the solid state.[83] The respective reduction products are also accessible through reaction with elemental potassium or via electron transfer from neo-pentyl lithium or trimethylsilylmethyl lithium.[84] Lithium metal reduction of tetraaryldialane $Trip_2AlAlTrip_2$ yields the dark green complex Li

$[Trip_2AlAlTrip_2]$.[85] In all these dianions, reductions cause a notable contraction of the Al–Al distance. While the Al–Al distance in $[(Me_3Si)_2CH]_2AlAl[CH(SiMe_3)_2]_2$ is 2.660(1) Å, the reduced species features a metal–metal distance of 2.53 (1) Å. The bond-shortening effect upon population of the empty π-orbital is even more pronounced in the case of the tetraaryldialane. In $Trip_2AlAlTrip_2$, for instance, the aluminum atoms are separated by 2.647(3) Å, whereas the distance in the radical anion is only 2.470(2) Å. In the latter case, the hypothesis of a single electron π-bond formed from primarily Al-based p-orbitals is further corroborated by other structural changes, which become apparent upon reduction. In the parent, neutral $Trip_2AlAlTrip_2$, the aluminum centers adopt an almost planar coordination. Yet, the coordination planes around the aluminum atoms exhibit a torsion angle of about 44.8°. In sharp contrast, all atoms of the $C_2Al–AlC_2$ core in $[Trip_2AlAlTrip_2]^{\bullet-}$ are almost coplanar with a torsion angle of only 1.4° between the C_2Al units. The EPR spectrum of $[Trip_2AlAlTrip_2]^{\bullet-}$ displays an 11-line multiplet due to symmetric coupling of the unpaired electron to two ^{27}Al nuclei (^{27}Al, I = 5/2, 100% natural abundance). Again, a small coupling constant indicative for the population of a π-orbital of 10.4 G is observed. Similar coupling constants of about 11.1–11.9 G are operative in Bsi-substituted $[(Me_3Si)_2CH]_2AlAl[CH(SiMe_3)_2]_2^{\bullet-}$[83,84] (Scheme 23).

Both, the tetraaryldigallium $Trip_2GaGaTrip_2$ and $[(Me_3Si)_2CH]GaGa[CH(SiMe_3)_2]$, were shown to undergo the same one-electron reduction chemistry as their aluminum homologs. Parent, neutral digallium compounds are available from the reaction of $Ga_2Cl_4(dioxane)_2$ with TripMgBr, and from the reaction of $Ga_2Br_4(dioxane)_2$ with $LiCH(SiMe_3)_2$, respectively.[45]

Reduction of $Trip_2GaGaTrip_2$ with lithium in diethylether in the presence of crown ether yields the radical anion $[Li(12\text{-crown-}4)_2][Trip_2GaGaTrip_2]$ as solvent separated ion pairs in the solid state. Again, reduction causes a sharp decrease of the Ga–Ga distance. While the galliums are separated by 2.515(3) Å in the neutral tetraaryl digallane, this distance decreases to 2.343(2) Å in the radical anion. As already described in the case of the tetraaryl dialane, the C_2Ga planes are strongly twisted in the parent digallane with a twist angle of 43.8°. Reduction causes a decrease of the twisting to a value of only 15.5°. In the UV–Vis spectra, two absorption maxima associated with non-aryl excitations are observed at 360 and 900 nm. EPR spectroscopy in THF solution at room temperature shows coupling of the unpaired electron to two equivalent gallium nuclei with coupling constants of approximately 35.4 and 43.9 G to the ^{69}Ga (60.4% natural abundance, I = 3/2) and ^{71}Ga (39.6% natural abundance, I = 3/2) centers.[87] Reaction of $[(Me_3Si)_2CH]GaGa[CH(SiMe_3)_2]$ with ethyl lithium in *n*-pentane/tmeda mixtures at low temperatures results in single electron transfer and formation of $[Li(tmeda)_2][(Me_3Si)_2CH]GaGa[CH(SiMe_3)_2]$. The gallium–gallium distance in the *N*,*N*′,*N*″-trimethyl triazinane complex is 2.401(1) Å and is thus ca. 0.14 Å shorter than in the parent neutral digallane. In analogy to the previously discussed aluminum analog, the gallium atoms in both, parent digallane and radical anion, feature planar coordination (sum of angles 360°). Moreover, the GaC_2 planes are strictly coplanar in the reduced derivative and almost planar with a twist angle of 8° in the neutral substance. EPR spectroscopic measurements show a strong dependence of the appearance of the spectra from temperature. At 300 K, the coupling constants are determined as 57.4 G to ^{69}Ga and 72.8 G to ^{71}Ga and are thus considerably larger than in $[Trip_2GaGaTrip_2]^{\bullet-}$. The larger coupling constant suggests a higher degree of s-character of the singly occupied molecular orbital (SOMO) in $[(Me_3Si)_2CH]GaGa[CH(SiMe_3)_2]^{\bullet-}$ compared to $[Trip_2GaGaTrip_2]^{\bullet-}$. This is ultimately a consequence of the more electron-donating properties of the $CH(SiMe_3)_2$ substituents compared to Trip groups. At 200 K, however, smaller coupling constants of 42.8 G (^{69}Ga) and 54.4 G (^{71}Ga) are observed which resemble those in $[Trip_2GaGaTrip_2]^{\bullet-}$. These EPR spectroscopic findings support the existence of a nonplanar conformation with higher s-character for the singly occupied π-orbital which is progressively populated at higher temperatures.[88] The coupling constant to the ^{29}Si atoms of 5.3 G is similar to the value observed in the related dialane radical anion (4.35 G).

The UV–Vis spectrum features two bands attributable to excitations of the gallium core at 357 and 550 nm. Among these, the band at 360 nm is also present in the parent neutral molecule and is characteristic for a Ga–Ga σ-bond.

Further examples of group 13 radicals which feature a certain degree of multiple bonding are the neutral silyl substituted

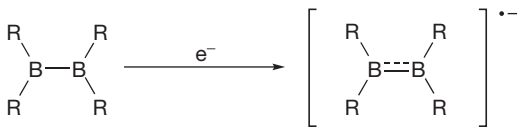

R=Bu^t, CH_2Bu^t

Scheme 21 One-electron reduction of tetra-alkyl diboranes R_2BBR_2 (R = Bu^t, CH_2Bu^t).

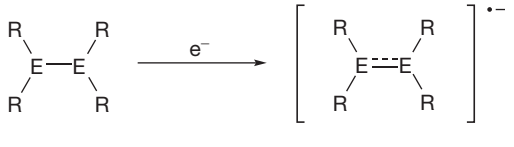

E=Al or Ga R=Trip or $CH(SiMe_3)_2$

Scheme 23 Generation of radical anions $[REER]^{\bullet-}$ by one-electron reduction of neutral [REER] (R = Trip, $CH(SiMe_3)_2$).

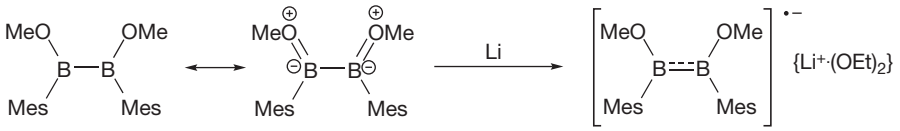

Scheme 22 One-electron reduction of Mes(MeO)BB(OMe)Mes.

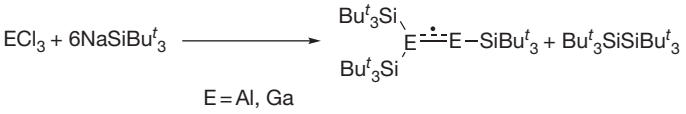

Scheme 24 Syntheses of radicals $[(Bu^t_3Si)_2EE(SiBu^t_3)]^\bullet$ (E = Al, Ga) with bond order 1.5.

radicals $[R_3SiAl(I)Al(II)(SiR_3)_2]^\bullet$ and $[R_3SiGa(I)Ga(II)(SiR_3)_2]^\bullet$ ($R_3Si = {}^tBu_3Si$).[89–91] Both compounds are accessible via reaction of the MCl_3 salts (M = Al, Ga) with excess 'supersilyl' sodium, $^tBu_3SiNa$. Concerning the mechanisms of formation of both radicals, the intermediates $(R_3Si)_2MCl$ and $(R_3Si)_2MM(SiR_3)_2$ were substantiated to play key roles. Subsequent reaction of $(R_3Si)_2MM(SiR_3)_2$ with supersilyl radical $^tBu_3Si^\bullet$ yields one equivalent of $^tBu_3SiSi^tBu_3$ and the respective group 13 radical. The x-ray structure analysis of the dark blue radical species $[R_3SiGa(I)Ga(II)(SiR_3)_2]^\bullet$ shows a planar $(R_3Si)_2Ga(II)Ga(I)$ moiety (sum of angles around the three-coordinate gallium center of 359.6°) and a linear arrangement of the divalent Ga (I) center in the $R_3SiGaGa$ subunit (SiGa(I)Ga(II) angle 170.0°). The most important finding in the context of potential multiple bonding, however, is a short Ga–Ga distance of only 2.420(1) Å. Given the planar coordination around the Ga(II) center and the linear coordination of the Ga(I), the gallium atoms are best described as sp^2 and sp hybridized, respectively. Thus, the bond order in $[R_3SiGa(I)Ga(II)(SiR_3)_2]^\bullet$ accounts for 1.5 due to a single σ-bond between the galliums in combination with a half-filled π-orbital. In the EPR spectra, two sets of hyperfine coupling constants to two distinctively different gallium centers with 50/64 and 32/41 G are observed. A slightly decreased Ga–Ga distance of 2.3797(6) Å characterizes the singly reduced, anionic species $(R_3Si)_2GaGa(SiR_3)^-$ which is accessible from $[R_3SiGa(I)Ga(II)(SiR_3)_2]$ via reduction with sodium or silyl sodiums. One-electron reduction of $[R_3SiGa(I)Ga(II)(SiR_3)_2]^\bullet$ also leads to a decrease of the $R_3SiGaGa$ angle to a value of 142.41 (4)° (Scheme 24).

The large hyperfine coupling constants in $[R_3SiGa(I)Ga(II)(SiR_3)_2]^\bullet$ are contrasted by much smaller values in the related aluminum derivative $[R_3SiAl(I)Al(II)(SiR_3)_2]^\bullet$ where values of 21.8 and 18.9 G are found. In addition to linear $[R_3SiAl(I)Al(II)(SiR_3)_2]^\bullet$, the electron-deficient cyclic radical $(R_3Si)_4Al_3$ is also obtained from thermolysis reactions of $(R_3Si)_2AlAl(SiR_3)_2$. The Al–Al distances in the dark green compound are crystallographically determined as 2.703(2), 2.737(2), and 2.776(2) Å. For comparison, the calculated aluminum–aluminum distance in $[R_3SiAl(I)Al(II)(SiR_3)_2]^\bullet$ is significantly shorter at 2.537 Å and agrees well with a formal bond order of 1.5. The related radical $[Bsi_2AlAlBsi]^\bullet$ with a hyperfine coupling constant of 1.72 G was reported by Uhl to form under photolytical conditions from $Bsi_2AlAlBsi_2$.[92]

In contrast to cyclic $(R_3Si)_4Al_3$, the respective gallium derivative $(R_3Si)_4Ga_3$ adopts an isosceles, triangular structure with two identical and rather short Ga–Ga distances of 2.5267(7) Å and a longer base of 2.879(1) Å. One-electron reduction produces the bent anion $(R_3Si)GaGa(SiR_3)_2Ga(SiR_3)^-$ with two distinctly different gallium–gallium distances at 2.494(1) and 2.569(2) Å. The shortening of a terminal gallium–gallium bond may again be interpreted in terms of a bond order greater than unity as the additional electron occupies a Ga–Ga-centered π-orbital.

Neither a respective indium nor thallium radical or radical anion has been reported to date.

A detailed account on main group radicals is given in Chapter 1.14.

1.10.5 Group 13 Element Compounds with Formal Bond Order Greater Than Two

In a seminal publication, Robinson and coworkers reported in 1997 on the reduction of $[C_6H_3\text{-}2,6\text{-}(C_6H_2\text{-}2,4,6\text{-}{}^iPr_3)]GaCl_2$ with excess sodium. x-Ray structural analysis revealed the deep red crystals isolated from the reaction mixture to be $[\{C_6H_3\text{-}2,6\text{-}(C_6H_2\text{-}2,4,6\text{-}{}^iPr_3)\}Ga]_2Na_2$, the first example of heavier group 13 alkyne analog. On account of short gallium–gallium distance of only 2.319(3) Å and the fact that $[Ar^*GaGaAr^*]^{2-}$ is isoelectronic with alkynes RC≡CR, the compound was stated to contain a gallium–gallium triple bond.[93] The sodium atoms in $[\{C_6H_3\text{-}2,6\text{-}(C_6H_2\text{-}2,4,6\text{-}{}^iPr_3)\}Ga]_2Na_2$ are complexed by the flanking tri-isopropyl phenyl groups of the *m*-terphenyl substituents and form symmetrical isosceles triangles with the gallium atoms with Na–Ga distances of ca. 3.08 Å (Scheme 25).

The interpretation of $[\{C_6H_3\text{-}2,6\text{-}(C_6H_2\text{-}2,4,6\text{-}{}^iPr_3)\}Ga]_2Na_2$ to contain a triple bond sparked immediate interest of synthetic and computational chemists and resulted in a fierce debate on the nature of the multiple bonding in this main group compound. Since its discovery, numerous theoretical approaches were undertaken to gain further insight into the nature of the bond in $[\{C_6H_3\text{-}2,6\text{-}(C_6H_2\text{-}2,4,6\text{-}{}^iPr_3)\}Ga]_2Na_2$.[34,35,94–102]

Earlier, the reduction of slightly less encumbered $[C_6H_3\text{-}2,6\text{-}(C_6H_2\text{-}2,4,6\text{-}Me_3)]GaCl_2$ under similar conditions had yielded the dianionic trimer $\{[C_6H_3\text{-}2,6\text{-}(C_6H_2\text{-}2,4,6\text{-}Me_3)]Ga\}_3Na_2$. This compound is of particular interest in the context of multiple bonding as the gallium–gallium contacts account for 2.441(1) Å. Two negative charges are delocalized over the three-membered metalloaromatic ring core in which the sum of angles around the planar gallium atoms adds up to 360°. The sodium atoms are located at a distance of ca. 3.15 Å above and below the centroid of the equilateral gallium triangle. It was thus concluded that $\{[C_6H_3\text{-}2,6\text{-}(C_6H_2\text{-}2,4,6\text{-}Me_3)]Ga\}_3Na_2$ constitutes a 2 π-electron Hückel-aromatic cyclopropenium cation homolog[103] (Scheme 26).

Slightly shorter gallium–gallium distances between 2.4187 (5) and 2.4317(5) Å were found in the respective dipotassio derivative $\{[C_6H_3\text{-}2,6\text{-}(C_6H_2\text{-}2,4,6\text{-}Me_3)]Ga\}_3K_2$. Yet, it is important to note the short distances between the alkali metals centers and the centroids of the aryl groups in 2,6-positions of the *m*-terphenyl substituents.[104] Reduction of sterically more shielded $\{C_6H_3\text{-}2,6\text{-}(C_6H_2\text{-}2,4,6\text{-}{}^iPr_3)\}GaCl_2$ with potassium rather than sodium resulted in the isolation of $[\{C_6H_3\text{-}2,6\text{-}(C_6H_2\text{-}2,4,6\text{-}{}^iPr_3)\}_2Ga_4]K_2$ which has an octahedral cluster

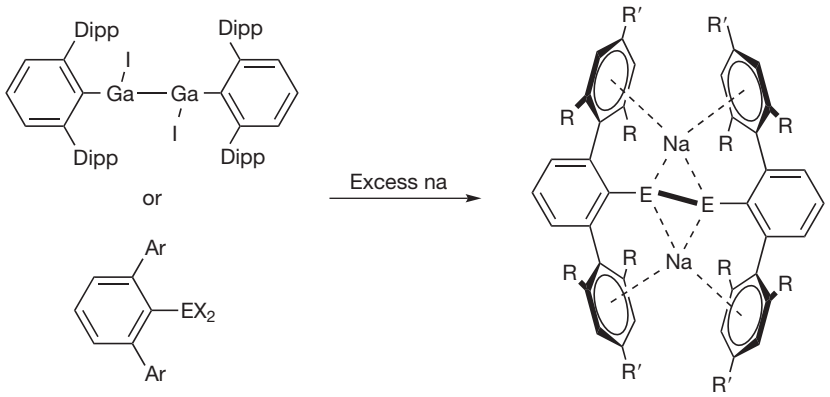

Scheme 25 Syntheses of compounds $[ArEEAr]Na_2$ which feature formal bonder order 3.

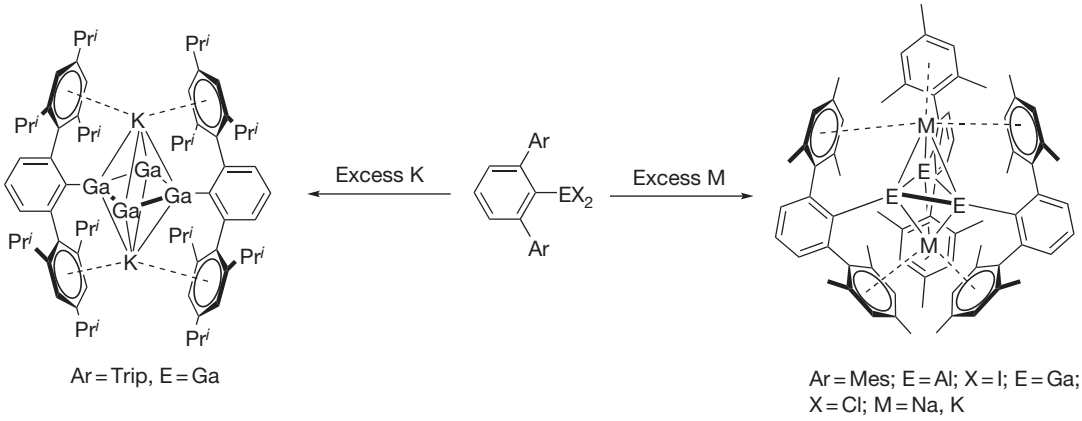

Scheme 26 Syntheses of metalloaromatic compounds $[ArE]_3M_2$ (E = Al, Ga; M = Na, K) and $[(ArGa)_2Ga_2]K_2$.

core in which the galliums form an almost perfect square which is bi-capped by the potassium atoms.[105] In all cases, the cyclic gallium derivatives exhibit two negative charges delocalized over the central triel ring.

The nature of the gallium–gallium interaction in $[\{C_6H_3\text{-}2,6\text{-}(C_6H_2\text{-}2,4,6\text{-}^iPr_3)\}Ga]_2Na_2$ was further investigated by the synthesis of the sterically slightly less hindered compounds $[\{C_6H_3\text{-}2,6\text{-}(C_6H_3\text{-}2,6\text{-}^iPr_2)\}Ga]_2Na_2$ and the related neutral complex $[\{C_6H_3\text{-}2,6\text{-}(C_6H_3\text{-}2,6\text{-}^iPr_2)\}Ga]_2$.[106] As discussed in Section 1.10.2.1.2, the solid-state structure of the neutral alkene homolog $[\{C_6H_3\text{-}2,6\text{-}(C_6H_3\text{-}2,6\text{-}^iPr_2)\}Ga]_2$ features a long Ga–Ga distance of over 2.62 Å and a *trans*-bent (C-*ipso*) GaGa(C-*ipso*) core which is indicative of a high degree of lone-pair character of the gallium atoms. Gallium–gallium bonding is weak in this compound and it is known to exist in an equilibrium of monomeric and dimeric forms in solution. The doubly reduced species $[\{C_6H_3\text{-}2,6\text{-}(C_6H_3\text{-}2,6\text{-}^iPr_2)\}Ga]_2Na_2$, however, displays very similar structural parameters with respect to the 'triple bonded' $[\{C_6H_3\text{-}2,6\text{-}(C_6H_2\text{-}2,4,6\text{-}^iPr_3)\}Ga]_2Na_2$ with Ga–Ga distances around 2.32 Å, (C-*ipso*)GaGa angles around 130°, sodium–gallium distances between 2.88 and 3.05 Å and short distances between the sodium atom and carbon atoms of the flanking aryls of around 3.0 Å. In summary, the observation of *trans*-bending in both, the neutral and the doubly reduced species, the weakness of the gallium interactions in the so-called neutral, parent 'digallenes,' and the strong interaction of the alkali metals with the *ortho*-aryl substituents of the ligands experimentally suggest a bond order of significantly less than three for the complexes $ArGaGaArM_2$. Moreover, several ArGa: compounds exist as monomers in the solid state.[48]

As far as the respective aluminum compounds are concerned, a similar picture can be drawn. The aluminum–aluminum distance of 2.428(1)Å in $[\{C_6H_3\text{-}2,6\text{-}(C_6H_3\text{-}2,6\text{-}^iPr_2)\}Al]_2Na_2$ is ca. 0.11 Å longer than the triel separation in Robinson's 'digallyne' which is presumably a consequence of the larger radius of aluminum (1.3 Å) in comparison to gallium (1.25 Å). $[Ar'AlAlAr']Na_2$ adopts a *trans*-bent structure in the solid-state ((C-*ipso*)-Al–Al angle of 131.71(7)°). In contrast to gallium, the neutral derivative Ar′AlAlAr′ is unstable in aromatic hydrocarbons and undergoes [4 + 2] cycloaddition reactions which are indicative for its high diradical character. Multiple bonding in $[\{C_6H_3\text{-}2,6\text{-}(C_6H_3\text{-}2,6\text{-}^iPr_2)\}Al]_2Na_2$ is weak with a Wiberg bond-index of 1.13. Al–Al distances in the trialuminum derivative $\{[C_6H_3\text{-}2,6\text{-}(C_6H_2\text{-}2,4,6\text{-}Me_3)]Al\}_3Na_2$, which displays the same structural motif of a planar

Table 3 Structural data for compounds $[REER]^{2-}$, $[(RE)_3]^{2-}$, and $[(RE)_2E_2]^{2-}$ (E = Al, Ga)

	E–E distance (Å)	*C–E distance (Å)*	*E–M distance (Å)*	*C–E–E angle (°)*	*Ref.*
$[Ar'AlAlAr']Na_2$	2.428(1)	2.043(2)	3.152(1)	131.71(7)	[107]
$[(Ar^{\#}Al)_3]Na_2$	2.520(1)	2.021(3)	3.285(2)	142.8(1)/157.2(1)	[107]
$[Ar^*GaGaAr^*]Na_2$	2.319(3)	2.06(2)	3.056(6)/3.085(7)	133.5(4)	[93]
$[Ar'GaGaAr']Na_2$	2.347(1)	2.059(5)		130.7(1)	[106]
$[(Ar^{\#}Ga)_3]Na_2$	2.441(1)	2.037(3)	3.229(2)	133.7(1)/166.3(1)	[103]
$[(Ar^{\#}Ga)_3]K_2$	2.4187(5)–2.4317(5)	2.040(3)–2.050(3)	3.5289(8)–3.5817(8)	143.03(10)/156.69(10)	[104]
$[(Ar^*Ga)_2Ga_2]K_2$	2.4623(4)/2.4685(3)	2.0058(19)	3.4710(6)–3.8330(6)	139.33(6)/133.44(6)	[105]

aluminum three-membered ring with sodiums above and below the central plane, are 2.520(1) Å.[107] In all these complexes, the interaction of the alkali metal centers with aryl groups plays a key role in the molecular assembly. For instance, no solvent separated ion pairs nor respective singly reduced radical anions $[ArEEAr]^{\bullet-}$ have been isolated to date (**Table 3**).

A neutral molecule with a certain degree of boron–boron triple bond character is the bis-carbonyl complex of diboron OC–B≡B–CO. It was produced by co-condensation of boron atoms with carbon monoxide in an argon matrix at 8 K and characterized by Fourier transform (FT)-IR spectroscopy of different isotopomers. DFT calculations employing broken-symmetry unrestricted wavefunctions predicted the linear triplet state in O≡C–B≡B–C≡O to be about 20.5 kcal mol^{-1} higher in energy than the linear singlet state. The molecule is best described as an excited-state diboron core which interacts with two carbonyls. The doubly degenerate HOMOs are boron–boron π-bonding orbitals which involve back-bonding from the diboron core to what are antibonding orbitals in uncomplexed carbon monoxide. The HOMO-1 orbital essentially constitutes the B–B σ-bond. In summary, singlet O≡C–B≡B–C≡O features some B–B triple bond character through the population of the HOMO-1 and degenerate HOMO orbitals. Calculations indicate a very short B–B distance of little over 1.45 Å, a value which is significantly smaller than the experimentally observed boron–boron distances known to date. Concerning the mechanism of formation, dimerization of B–CO seems more plausible than reaction of B_2 with two molecules of CO as upon thermal annealing the signal attributed to BCO had decreased while O≡C–B≡B–C≡O concomitantly formed.[108]

1.10.6 Conclusion

In summary, examples of compounds of all group 13 elements boron to thallium which feature multiple bonding or which have formal multiple bonds have been synthesized.

Most convincing experimental data for the existence of true multiple bonds are available for the lightest element boron. Isolation of the neutral bis-NHC adducts L:BH=BH:L, the singly and doubly reduced derivatives $[R_2EER_2]^{\bullet-}$, $[R_2EER_2]^{2-}$ and the formally triply bonded OC–B≡B–CO provided strong experimental evidence for the existence of true multiple bonding in these compounds. Experimental data include short B–B distances, in fact shorter than in the parent neutral molecules, and planar arrangements of the R_2BBR_2 cores in the reduced compounds in contrast to the parent molecules which frequently adopt a perpendicular arrangement of the R_2B planes. Planarity is also observed in two of the four known isomers of L:BH=BH=:L. EPR spectroscopy revealed coupling of the unpaired electron in the radical anions $[RBBR]^{\bullet-}$ to two magnetically equivalent boron atoms in symmetrical compounds and very similar hyperfine coupling constants to the borons in unsymmetrical $[Mes_2BBMesPh]^{\bullet-}$. Small hyperfine coupling constants further corroborate the nature of the SOMOs as π-orbitals which are essentially combinations of boron p-orbitals.

Multiple bonding is also operative in the singly reduced heavier group 13 compounds $[R_2EER_2]^{\bullet-}$ (E = Al, Ga; R = Trip, $CH(SiMe_3)_2$). One-electron reductions of parent dialans and digallans result in shortened E–E bonds and rearrangement of previously twisted molecules to radical anions with coplanar R_2EER_2 cores. EPR investigations clearly show delocalization of the unpaired electrons over both triel centers. Analysis of the hyperfine coupling constants show that the SOMO is in fact a delocalized π-orbital which consists of the p-orbitals at aluminum or gallium. Neither a doubly reduced derivative $[R_2EER_2]^{2-}$ nor a respective singly or doubly reduced indium or thallium compound has been isolated to date.

In contrast to reduced salts $[R_2EER_2]^{\bullet-}$ and $[R_2EER_2]^{2-}$ and the NHC-stabilized diborene L:HB=BH:L, multiple bonding in neutral, heavier group 13 compounds REER (E = Ga, In, Tl) is weak. In the case of aluminum, simultaneous population of the two π-orbitals with one electron each is responsible for the diradical nature and exceedingly high reactivity of these compounds. No structural data on dialuminene REER are currently available, although a red solid with constitution Ar'AlAlAr' was isolated from the reduction of $Ar'AlI_2$. Owing to its high reactivity which is very likely a consequence of its diradical character, only cycloaddition products have been isolated to date. Approaches to reduce the related aryl-substituted boron compounds failed, but there is some experimental evidence for the existence of amino-substituted derivatives $R_2N–B=B–NR_2$.

Heavier group 13 element derivatives REER (E = Ga, In, Tl) show an increasing tendency to exist as a monomer/dimer equilibrium in solution and to remain as monomers in the solid state. These compounds possess a combination of a lone pair and two empty orbitals which render them promising candidates with respect to coordination chemistry and activation of small molecules. Intriguing first experimental results for their reaction chemistry are provided by the activation of dihydrogen and ammonia under very mild conditions and addition to alkenes and alkynes.

Certainly the most controversial aspect in heavier group 13 multiple bonding is caused by the doubly reduced compounds

[REER]M_2. Their valence electron count puts them in relation with alkynes. Yet, significant *trans*-bending, strong interaction with alkali metal cations and the weakness of the putative multiple bonds in the neutral parent ditrielenes REER severely questions the triple bond character in these compounds. Finally, the characterization of the unusual compound OC–B≡B–CO provides an exciting perspective in the field of neutral group 13 triple bonded compounds.

References

1. (a) Rivard, E.; Power, P. P. *Inorg. Chem.* **2007**, *46*, 10047–10064; (b) Wang, Y.; Robinson, G. H. *Organometallics* **2007**, *26*, 2–11; (c) Roesky, H. W.; Kumar, S. S. *Chem. Commun.* **2005**, 4027–4038; (d) Power, P. P. *Chem. Rev.* **1999**, *99*, 3463–3504; (e) Fischer, R. C.; Power, P. P. *Chem. Rev.* **2010**, *110*, 3877–3923; (f) Wang, Y.; Robinson, G. H. *Chem. Commun.* **2009**, 5201–5213; (g) Downs, A. J.; Himmel, H.-J.; Manceron, L. *Polyhedron* **2002**, *21*, 473–488; (h) Jones, C. *Coord. Chem. Rev.* **2010**, *254*, 1273–1289; (i) Nagendran, S.; Roesky, H. W. *Organometallics* **2008**, *27*, 457–492; (j) Robinson, G. H. *Adv. Organomet. Chem.* **2004**, *47*, 283–294; (k) Brothers, P. J.; Power, P. P. *Adv. Organomet. Chem.* **1996**, *39*, 1–67; (l) Jones, C.; Stasch, A. In *The Group 13 Metals Aluminium, Gallium, Indium and Thallium-Chemical Patterns and Peculiarities*; Aldridge, A., Downs, A. J., Eds.; John Wiley and Sons, Inc.: New Jersey, USA, 2011; Chapter 5, pp 285–341, (m) Cooper, B. F. T.; MacDonald, C. L. B. In *The Group 13 Metals Aluminium, Gallium, Indium and Thallium-Chemical Patterns and Peculiarities*; Aldridge, A., Downs, A. J., Eds.; John Wiley and Sons, Inc.: New Jersey, USA, 2011; Chapter 6, pp 342–401.
2. Carter, E. A.; Goddard, W. A., III *J. Phys. Chem.* **1986**, *90*, 998–1001.
3. Malrieu, J.-P.; Trinquier, G. *J. Am. Chem. Soc.* **1989**, *111*, 5916–5921.
4. Trinquier, G.; Malrieu, J.-P. *J. Am. Chem. Soc.* **1987**, *109*, 5303–5315.
5. Treboux, G.; Barthelat, J. C. *J. Am. Chem. Soc.* **1993**, *115*, 4870–4878.
6. Moilanen, J.; Power, P. P.; Tuononen, H. M. *Inorg. Chem.* **2010**, *49*, 10992–11000.
7. Power, P. P. *Nature* **2010**, *463*, 171–177.
8. Power, P. P. *Acc. Chem. Res.* **2011**, *44*, 627–637.
9. Tague, T. J., Jr.; Andrews, L. *J. Am. Chem. Soc.* **1994**, *116*, 4970–4976.
10. Knight, L. B., Jr.; Kerr, K.; Miller, P. K.; Arrington, C. A. *J. Phys. Chem.* **1995**, *99*, 16842–16848.
11. Ruscic, B.; Mayhew, C. A.; Berkowitz, J. *J. Chem. Phys.* **1988**, *88*, 5580–5593.
12. Wang, Y.; Quillian, B.; Wei, P.; Wannere, C. S.; Xie, Y.; King, R. B.; Schaefer, H. F., III; Schleyer, P.v.R.; Robinson, G. H. *J. Am. Chem. Soc.* **2007**, *129*, 12412–12413.
13. Wang, Y.; Quillian, B.; Wei, P.; Xie, Y.; Wannere, C. S.; King, R. B.; Schaefer, H. F., III; Schleyer, P.v.R.; Robinson, G. H. *J. Am. Chem. Soc.* **2008**, *130*, 3298–3299.
14. Himmel, H.-J.; Manceron, L.; Downs, A. J.; Pullumbi, P. *Angew. Chem. Int. Ed.* **2002**, *41*, 796–799.
15. Himmel, H.-J.; Manceron, L.; Downs, A.; Pullumbi, P. *J. Am. Chem. Soc.* **2002**, *124*, 4448–4457.
16. Stephens, J. C.; Bolton, E. E.; Schaefer, H. F., III; Andrews, L. *J. Chem. Phys.* **1997**, *107*, 119–123.
17. Schumann, H.; Janiak, C.; Pickardt, J.; Börner, U. *Angew. Chem. Int. Ed Engl.* **1987**, *26*, 789–790.
18. Schumann, H.; Janiak, C.; Görlitz, F.; Loebel, J.; Dietrich, A. *J. Organomet. Chem.* **1989**, *363*, 243–251.
19. Jutzi, P.; Schnittger, J.; Hursthouse, M. B. *Chem. Ber.* **1991**, 1693–1697.
20. Jutzi, P.; Wegener, D.; Hursthouse, M. B. *Chem. Ber.* **1991**, 295–299.
21. Schumann, H.; Janiak, C.; Khani, H. *J. Organomet. Chem.* **1987**, *330*, 347–355.
22. Schumann, H.; Janiak, C.; Khan, M. A.; Zuckerman, J. J. *J. Organomet. Chem.* **1988**, *354*, 7–13.
23. Ferguson, G.; Jennings, M. C.; Lalor, F. J.; Shanahan, C. *Acta Crystallogr.* **1999**, *C47*, 2079–2082.
24. Ghosh, P.; Rheingold, A. L.; Parkin, G. *Inorg. Chem.* **1999**, *38*, 5464–5467.
25. Veith, M.; Spaniol, A.; Pöhlmann, J.; Gross, F.; Huch, V. *Chem. Ber.* **1993**, *126*, 2625–2635.
26. Waezsada, S. D.; Belgardt, T.; Noltemeyer, M.; Roesky, H. W. *Angew. Chem. Int. Ed Engl.* **1994**, *33*, 1351–1352.
27. Uhl, W.; Keimling, S. U.; Klinkhammer, K. W.; Schwarz, W. *Angew. Chem. Int. Ed Engl.* **1997**, *36*, 64–65.
28. Rheingold, A. L.; Liable-Sands, L. M.; Trofimenko, S. *Chem. Commun.* **1997**, 1691–1692.
29. Wright, R. J.; Phillips, A. D.; Hino, S.; Power, P. P. *J. Am. Chem. Soc.* **2005**, *127*, 4794–4799.
30. Wiberg, N.; Blank, T.; Amelunxen, K.; Nöth, H.; Schnöckel, H.; Baum, H.; Purath, A.; Fenske, D. *Eur. J. Inorg. Chem.* **2002**, 341–350.
31. Henkel, S.; Klinkhammer, K. W.; Schwarz, W. *Angew. Chem. Int. Ed Engl.* **1994**, *33*, 681–683.
32. Niemeyer, M.; Power, P. P. *Angew. Chem. Int. Ed Engl.* **1998**, *37*, 1277–1279.
33. Wright, R. J.; Phillips, A. D.; Hardmen, N. J.; Power, P. P. *J. Am. Chem. Soc.* **2002**, *124*, 8538–8539.
34. Allen, T.; Fink, W. H.; Power, P. P. *Dalton Trans.* **2000**, 407–412.
35. Takagi, N.; Schmidt, M. N.; Nagase, S. *Organometallics* **2001**, *20*, 1646–1651.
36. Haubrich, S. T.; Power, P. P. *J. Am. Chem. Soc.* **1998**, *120*, 2202–2203.
37. Hill, M. S.; Hitchcock, P. B.; Pongtavornpinyo, R. *Angew. Chem. Int. Ed.* **2005**, *44*, 4231–4235.
38. Hill, M. S.; Hitchcock, P. B.; Pongtavornpinyo, R. *Dalton Trans.* **2007**, 731–733.
39. Hill, M. S.; Hitchcock, P. B.; Pongtavornpinyo, R. *Science* **2006**, *311*, 1904–1907.
40. Hill, M. S.; Hitchcock, P. B. *Chem. Commun.* **2004**, 1818–1819.
41. Hill, M. S.; Hitchcock, P. B.; Pongtavornpinyo, R. *Dalton Trans.* **2005**, 273–277.
42. Hardmen, N. J.; Wright, R. J.; Phillips, A. D.; Power, P. P. *J. Am. Chem. Soc.* **2003**, *125*, 2667–2669.
43. Hardmen, N. J.; Wright, R. J.; Phillips, A. D.; Power, P. P. *Angew. Chem. Int. Ed.* **2002**, *41*, 2842–2844.
44. Brown, D. S.; Decken, A. H.; Cowley, A. H. *J. Am. Chem. Soc.* **1995**, *117*, 5421–5422.
45. Uhl, W.; Layh, M.; Hildenbrand, T. *J. Organomet. Chem.* **1989**, *364*, 289–300.
46. Haaland, A.; Martinsen, K.-G.; Volden, H. V.; Loos, D.; Schnöckel, H. *Acta Chem. Scand.* **1994**, *48*, 172–174.
47. Haaland, A.; Martinsen, K.-G.; Volden, H. V.; Kaim, W.; Waldhör, E.; Uhl, W.; Schütz, U. *Organometallics* **1996**, *15*, 1146–1150.
48. Zhu, Z.; Fischer, R. C.; Ellis, B. D.; Rivard, E.; Merrill, W. A.; Olmstead, M. M.; Power, P. P.; Guo, J. D.; Nagase, S.; Pu, L. *Chem. Eur. J.* **2009**, *15*, 5263–5272.
49. Wright, R. J.; Phillips, A. D.; Power, P. P. *J. Am. Chem. Soc.* **2003**, *125*, 10784–10785.
50. Gu, S.-Y.; Sheu, J.-H.; Su, M.-D. *Inorg. Chem.* **2007**, *46*, 2028–2034.
51. Cui, C.; Li, X.; Wang, C.; Zhang, J.; Cheng, J.; Zhu, X. *Angew. Chem. Int. Ed.* **2006**, *45*, 2245–2247.
52. Cui, C.; Köpke, S.; Herbst-Irmer, R.; Roesky, H. W.; Noltemeyer, M.; Schmidt, H.-G.; Wrackmeyer, B. *J. Am. Chem. Soc.* **2001**, *123*, 9091–9098.
53. Yang, X.-J.; Quillian, B.; Wang, Y.; Wei, P.; Robinson, G. H. *Organometallics* **2004**, *23*, 5119–5120.
54. Yang, X.-J.; Wang, Y.; Quillian, B.; Wei, P.; Chen, Z.; Schleyer, P.v.R.; Robinson, G. H. *Organometallics* **2006**, *25*, 925–929.
55. Quillian, B.; Wang, Y.; Wei, P.; Robinson, G. H. *New J. Chem.* **2008**, *32*, 774–776.
56. The chemistry of low-valent group 13 metals as ligands for electron poor main group and transition metals is reviewed in: Roesky, P. W. *Dalton Trans. 2009*, 1887–1893.
57. Su, J.; Li, X.-W.; Crittendon, C. R.; Campana, C. F.; Robinson, G. H. *Organometallics* **1997**, *16*, 4511–4513.
58. Maier, C.-J.; Pritzkow, H.; Siebert, W. *Angew. Chem. Int. Ed.* **1999**, *38*, 1666–1668.
59. Meller, A.; Maringgele, W. In *Advances in Boron Chemistry*; Siebert, W., Ed.; The Royal Society of Chemistry: Cambridge, 1997; p 224.
60. Grigsby, W. J.; Power, P. P. *J. Am. Chem. Soc.* **1996**, *118*, 7981–7988.
61. Zhu, Z.; Wang, X.; Olmstead, M. M.; Power, P. P. *Angew. Chem. Int. Ed Engl.* **2009**, *48*, 2027–2030.
62. Caputo, C. A.; Zhu, Z.; Brown, Z. D.; Fettinger, J. C.; Power, P. P. *Chem. Commun.* **2011**, *47*, 7506–7508.
63. Zhu, Z.; Wang, X.; Peng, Y.; Lei, H.; Fettinger, J. C.; Rivard, E.; Power, P. P. *Angew. Chem. Int. Ed Engl.* **2009**, *48*, 2031–2034.
64. Wehmschulte, R. J.; Ellison, J. J.; Ruhlandt-Senge, K.; Power, P. P. *Inorg. Chem.* **1994**, *33*, 6300–6306.
65. Wang, X.-F.; Andrews, L. *J. Phys. Chem. A* **2003**, *107*, 11371–11379.
66. Moc, J. *Chem. Phys. Lett.* **2004**, *395*, 38–43.
67. Moc, J. *Chem. Phys.* **2005**, *313*, 93–100.
68. Beachley, O. T., Jr.; Pazik, J. C.; Noble, J. M. *Organometallics* **1998**, *17*, 2121–2123.
69. Wright, R. J.; Phillips, A. D.; Allen, T. L.; Fink, W. H.; Power, P. P. *J. Am. Chem. Soc.* **2003**, *125*, 1694–1695.
70. Wright, R. J.; Brynda, M.; Fettinger, J. C.; Betzer, A. R.; Power, P. P. *J. Am. Chem. Soc.* **2006**, *128*, 12498–12509.

71. Fox, A. R.; Wright, R. J.; Rivard, E.; Power, P. P. *Angew. Chem. Int. Ed.* **2005**, *44*, 7729–7733.
72. Zhu, Z.; Wright, R. J.; Brown, Z. D.; Fox, A. R.; Phillips, A. D.; Richards, A. F.; Olmstead, M. M.; Power, P. P. *Organometallics* **2009**, *28*, 2512–2519.
73. Pilz, M.; Allwohn, J.; Willershausen, P.; Massa, W.; Berndt, A. *Angew. Chem. Int. Ed Engl.* **1990**, *29*, 1030–1032.
74. Moezzi, A.; Olmstead, M. M.; Power, P. P. *J. Am. Chem. Soc.* **1992**, *114*, 2715–2717.
75. Moezzi, A.; Bartlett, R. A.; Power, P. P. *Angew. Chem. Int. Ed Engl.* **1992**, *31*, 1082–1083.
76. Nöth, H.; Knizek, J.; Ponikwar, W. *Eur. J. Inorg. Chem.* **1999**, 1931–1937.
77. Klusik, H.; Berndt, A. *Angew. Chem. Int. Ed Engl.* **1981**, *20*, 870–871.
78. Berndt, A.; Klusik, H.; Schlüter, K. *J. Organomet. Chem.* **1981**, *222*, C25–C27.
79. Klusik, H.; Berndt, A. *J. Organomet. Chem.* **1982**, *232*, C21–C23.
80. Grigsby, W. J.; Power, P. P. *Chem. Commun.* **1996**, 2235–2236.
81. Grigsby, W. J.; Power, P. P. *Chem. Eur. J.* **1997**, *3*, 368–375.
82. Uhl, W. *Z. Naturforsch.* **1988**, *43b*, 1113–1118.
83. Pluta, C.; Pörschke, K.-R.; Krüger, C.; Hildenbrand, K. *Angew. Chem. Int. Ed Engl.* **1993**, *32*, 388–390.
84. Uhl, W.; Vester, A.; Kaim, W.; Poppe, J. *J. Organomet. Chem.* **1993**, *454*, 9–13.
85. Wehmschulte, R. J.; Ruhlandt-Senge, K.; Olmstead, M. M.; Hope, H.; Sturgeon, B. E.; Power, P. P. *Inorg. Chem.* **1993**, *32*, 2983–2984.
86. Moezzi, A.; Olmstead, M. M.; Bartlett, R. A.; Power, P. P. *Organometallics* **1992**, *11*, 2383–2388.
87. He, X.; Bartlett, R. A.; Olmstead, M. M.; Ruhlandt-Senge, K.; Sturgeon, B. E.; Power, P. P. *Angew. Chem. Int. Ed Engl.* **1993**, *32*, 717–719.
88. Uhl, W.; Schütz, U.; Kaim, W.; Waldhör, E. *J. Organomet. Chem.* **1995**, *501*, 79–85.
89. Wiberg, N.; Amelunxen, K.; Nöth, H.; Schwenk, H.; Kaim, W.; Klein, A.; Scheiring, T. *Angew. Chem. Int. Ed Engl.* **1997**, *36*, 1213–12135.
90. Wiberg, N.; Blank, T.; Kaim, W.; Schwederski, B.; Linti, G. *Eur. J. Inorg. Chem.* **2000**, 1475–1481.
91. Wiberg, N.; Blank, T.; Amelunxen, K.; Nöth, H.; Knizek, J.; Habereder, T.; Kaim, W.; Wanner, M. *Eur. J. Inorg. Chem.* **2001**, 1719–1727.
92. Uhl, W. *Angew. Chem. Int. Ed Engl.* **1993**, *32*, 1386–1397.
93. Su, J.; Li, X.-W.; Crittendon, R. C.; Robinson, G. H. *J. Am. Chem. Soc.* **1997**, *119*, 5471–5472.
94. Klinkhammer, K. W. *Angew. Chem. Int. Ed Engl.* **1997**, *36*, 2320–2322.
95. Cotton, F. A.; Cowley, A. H.; Feng, X. *J. Am. Chem. Soc.* **1998**, *120*, 1795–1799.
96. Xie, Y.; Grev, R. S.; Gu, J.; Schaefer, H. F., III; Schleyer, P.v.R.; Su, J.; Li, X.-W.; Robinson, G. H. *J. Am. Chem. Soc.* **1998**, *120*, 3773–3780.
97. Grützmacher, H.; Fässler, T. F. *Chem. Eur. J.* **2000**, *6*, 2317–2325.
98. Molina, J. M.; Dobado, J. A.; Heard, G. I.; Bader, R. F. W.; Sundberg, M. R. *Theor. Chem. Acc.* **2001**, *105*, 365–373.
99. Bridgeman, A. J.; Ireland, L. R. *Polyhedron* **2001**, *20*, 2841–2851.
100. Himmel, H.-J.; Schnöckel, H. *Chem. Eur. J.* **2002**, *8*, 2397–2405.
101. Chesnut, B. D. *Heteroat. Chem.* **2003**, *14*, 175–185.
102. Ponec, R.; Yuzhakov, G.; Gironés, X.; Frenking, G. *Organometallics* **2004**, *23*, 1790–1796.
103. Li, X.-W.; Pennington, W. T.; Robinson, G. H. *J. Am. Chem. Soc.* **1995**, *117*, 7578–7579.
104. Li, X.-W.; Xie, Y.; Schreiner, P. R.; Gripper, K. D.; Crittendon, R. C.; Campana, C. F.; Schaefer, H. F., III; Robinson, G. H. *Organometallics* **1996**, *15*, 3798–3803.
105. Twamley, B.; Power, P. P. *Angew. Chem. Int. Ed.* **2000**, *39*, 3500–3503.
106. Hardman, N. J.; Wright, R. J.; Phillips, A. D.; Power, P. P. *Angew. Chem. Int. Ed.* **2002**, *41*, 2842–2844.
107. Wright, R. J.; Brynda, M.; Power, P. P. *Angew. Chem. Int. Ed.* **2006**, *45*, 5953–5956.
108. Zhou, M.; Tsumori, N.; Li, Z.; Fan, K.; Andrews, L.; Xu, Q. *J. Am. Chem. Soc.* **2002**, *124*, 12936–12937.

This page intentionally left blank

1.11 Multiply Bonded Compounds of Group 14 Elements

V Ya Lee and A Sekiguchi, University of Tsukuba, Tsukuba, Ibaraki, Japan

Abbreviations

Ad	1-adamantyl
CP-MAS	Cross polarization magic angle spinning
HOMO	Highest occupied molecular orbital
LUMO	Lowest unoccupied molecular orbital
MO	Molecular orbital
NBO	Natural bond orbital
NHC	N-heterocyclic carbine
NMR	Nuclear magnetic resonance
NPA	Natural population analysis
THF	Tetrahydrofuran
UV	Ultraviolet

1.11.1 Introduction

The family of unsaturated hydrocarbons, which includes alkenes >C=C<, alkynes –C≡C–, 1,3-dienes >C=C–C=C<, and allenes >C=C=C< (and other cumulenes), constitutes one of the most fundamental classes of organic compounds, having paramount importance for the chemical industry. The multiple bonding between carbon atoms (or between carbon atom and heteroatom) is a central theme of organic chemistry, contributing to its great variety and richness.

Likewise, the analogs of unsaturated hydrocarbons, featuring multiple bonds to silicon, germanium, tin, and lead, are equally important in the chemistry of the low-coordinate organometallics of the group 14 elements. Sometimes called the 'heavy' alkenes, alkynes, 1,3-dienes, and allenes, these species are ubiquitous, initially being generated as fleeting intermediates in a vast number of chemical transformations. Although originally thought to be synthetically inaccessible (a prejudice known as the 'double-bond rule': elements with the principal quantum number equal to or greater than three cannot form multiple bonds because of the significant Pauli repulsion of the electrons in the inner shells), the analogs of alkenes $R_2E{=}ER_2$, alkynes RE≡ER, 1,3-dienes $R_2E{=}E(R){-}E(R){=}ER_2$, and allenes $R_2E{=}E{=}ER_2$ (E = Si–Pb) were finally isolated as room-temperature stable compounds stabilized by the right combination of electronic and steric effects of substituents R. As milestones of the field, one should mention the synthesis of the first stable distannene $Dsi_2Sn{=}SnDsi_2$ by Lappert in 1976,[1] disilene $Mes_2Si{=}SiMes_2$ by West in 1981,[2a] and silene $(Me_3Si)_2Si{=}C(OSiMe_3)Ad$ by Brook in 1981.[3] Despite the isoelectronic composition and formal structural similarity with organic unsaturated hydrocarbons, their heavy analogs exhibit sharply distinctive properties: synthetic approaches, structural peculiarities (double-bond nature), and reactivity.

The preparation methods leading to the stable Si, Ge, Sn, and Pb analogs of alkenes, alkynes, 1,3-dienes, and allenes, as well as their unusual structural and bonding features, are discussed in this chapter. Among the heteronuclear derivatives, only those containing a double bond between two different heavy group 14 elements are considered, whereas the combinations E=C (E = Si–Pb) and E=E′ (E = Si–Pb, E′ = group 13, 15, or 16 element) are outside the framework of this chapter. Likewise, radical, ionic, and aromatic compounds, featuring multiple bonds to the heavy group 14 elements, are not considered, nor are the aspects of the chemical reactivity of the heavy analogs of alkenes.

1.11.2 Stable Analogs of Alkenes of the Heavy Group 14 Elements

1.11.2.1 Homonuclear Derivatives

1.11.2.1.1 Disilenes >Si=Si<[4]

1.11.2.1.1.1 Synthesis

Tetramesityldisilene $Mes_2Si{=}SiMes_2$, the very first stable compound with an authenticated Si=Si double bond, was prepared by West and coworkers in 1981 by the 254 nm photolysis of the precursor $Mes_2Si(SiMe_3)_2$ via the transient silylene Mes_2Si:, dimerization of which produced the disilene $Mes_2Si{=}SiMes_2$.[2a] Since then, about 70 other room-temperature stable disilenes have been isolated and structurally characterized (excluding ionic, radical, and aromatic compounds containing Si=Si bonds, as well as compounds with conjugated Si=Si–Si=Si and cumulated Si=Si=Si bonds) (Table 1). The majority of them (57 isolable disilenes) were reported after 2000.

The general synthetic approaches leading to stable disilenes can be classified into six major methods: (1) photolysis of acyclic trisilanes (**A**); (2) photolysis of cyclotrisilanes (**B**); (3) reductive dehalogenation of 1,1-dihalosilanes (**C**); (4) reductive dehalogenation of 1,2-dihalodisilanes (**D**); (5) coupling of the stable lithium disilenides with the appropriate electrophiles (**E**); and (6) 1,2-addition across the Si≡Si triple bond of the isolable disilynes (**F**) (Scheme 1).

Method **A** was used for the preparation of the first-ever known stable disilene, $Mes_2Si{=}SiMes_2$. The cycloreversion by method **B** was mostly employed for the synthesis of tetraaryldisilenes. A great variety of alkyl-, aryl-, and silyl-substituted disilenes were synthesized by applying method **C** (28 compounds), one of the most widely used synthetic approaches for the preparation of stable disilenes. Method **D** (dehalogenation of the vicinal 1,2-dihalodisilanes), which allowed for the preparation of several alkyl-, aryl-, and silyl-substituted disilenes, is not widely used at the present time. Methods **E** and **F** were developed most recently, when lithium disilenides (starting material in **E**) and disilynes (starting material in **F**) became readily available as stable derivatives; rather unusual disilenes (17 by method E and 8 by method **F**) with a mixed substitution pattern (including heteroatom substituents), unavailable by any other synthetic approaches, were synthesized using these novel methods. Among the nontraditional methods (other methods), which can be used only for the preparation of a particular disilene, one can mention the following: reaction of the cationic $(\eta^5\text{-}Me_5C_5)Si^+{\cdot}B(C_6F_5)_4^-$ with $(Me_3Si)_2NLi$ forming disilene $(E)\text{-}(\eta^1\text{-}Me_5C_5)[(Me_3Si)_2N]Si{=}Si(\eta^1\text{-}C_5Me_5)[N(SiMe_3)_2]$; coupling of the 1,1-dilithiosilane derivatives $(R_3Si)_2SiLi_2$ ($R_3Si = SiPr^i_3$, $SiMeBu^t_2$) with dichlorosilanes Ar_2SiCl_2 (Ar = Mes, Tip) giving unsymmetrically substituted disilenes $(Pr^i_3Si)_2Si{=}SiMes_2$, $(Pr^i_3Si)_2Si{=}SiTip_2$, $(Bu^t_2MeSi)_2Si{=}SiMes_2$, and $(Bu^t_2MeSi)_2Si{=}SiTip_2$; and reduction of the *N*-heterocyclic carbene (NHC): → $SiCl_4$ complex with KC_8 forming a remarkable substituent-free NHC-supported disilene NHC: → Si = Si ← :NHC [NHC = 1,3-bis(2,6-diisopropylphenyl)-imidazol-2-ylidene], featuring a double bond between two Si atoms in the formal oxidation state of 0.

1.11.2.1.1.2 ^{29}Si NMR spectroscopy of disilenes

The origin of the diagnostic deshielding of the doubly bonded Si atoms in disilenes is well understood in terms of a highly asymmetric electronic distribution around the silicon nuclei. As was convincingly demonstrated in a comprehensive experimental/computational study,[41] disilenes showed a remarkable anisotropy of their chemical shift tensors, first of all manifested in the very strong deshielding along the *x*-axis lying in the plane of the molecule and perpendicular to the π-bond and the Si–Si bond (δ_{11}) (Figure 1). Moderate deshielding and strong shielding were found along the in-plane *y*-axis δ_{22} (along the Si–Si bond) and out-of-plane *z*-axis δ_{33} (perpendicular to the plane of the molecule) (Figure 1).

The most important deshielding along the δ_{11} vector is assigned to its strong paramagnetic contribution, stemming from the shielding current induced by the applied magnetic field. The degree of such paramagnetic contribution, which is determined by the Ramsey formula,[42] is inversely proportional to the energy difference between the interacting occupied and vacant molecular orbitals (MOs) that are mixed along the δ_{11} axis upon the application of the magnetic field. In the particular case of disilenes, these occupied and vacant MOs are σ(Si–Si) and π*(Si=Si) orbitals, respectively (for a more detailed discussion, see Ref. [41]).

Although the low-field resonances of the sp^2-Si atoms in disilenes were observed over a very wide area spanning from −47.2 to 276.3 ppm, the vast majority of them were found in the narrower range of 30.4–167.4 ppm (Table 1). The record shielding of −47.2 ppm (Si = *Si*–H), rather unusual for the doubly bonded Si atoms, was observed in the amino-substituted disilene (*E*)–R(Bu^tHN)Si=Si(H)R (R = $SiPr^i_2Dsi_2$), for which an important contribution from the charge-separated resonance form $Bu^tHN^+{=}$ Si(R)–Si^-(H)R was proposed as a result of the N lone pair – Si=Si bond π-conjugation.[35] Another, low field, extreme of 276.3 ppm (Si = $\dot{S}i$–R) was found in the NHC–disilyne complex R(NHC:→)Si=SiR [R = $SiPr^i_2Dsi_2$, NHC = $(MeCNMe)_2C$:], in which the lone-pair electrons reside on the dicoordinate Si center.[36]

The magnitudes of the ^{29}Si NMR (nuclear magnetic resonance) chemical shifts in disilenes are governed by the substitution pattern through both electronic (decrease/increase in Δ*E* (σ_{Si-Si}–$\pi^*_{Si=Si}$)) and steric (stretching/twisting of the Si=Si bond) effects. Accordingly, the doubly bonded silicon centers are the least deshielded in tetraaryldisilenes $Ar_2Si{=}SiAr_2$ (53.4–72.9 ppm); they showed a record deshielding in tetrasilyldisilenes $(R_3Si)_2Si{=}Si(SiR_3)_2$ (132.4–167.4 ppm), whereas in tetraalkyldisilenes $R_2Si{=}SiR_2$, they were observed in the intermediate region (102.5–135.9 ppm) (Table 1). The

Table 1 Crystallographic and spectral parameters of the structurally characterized disilenes.

Disilene (synthetic method)	*> Si=Si<[Å]*	*Σ(Si) [°]*	*>Si=Si<twist [°]*	*^{29}Si(Si=Si) (ppm)*	*Reference*
$Mes_2Si{=}SiMes_2$	2.143(2)	358.1	3.0		
(**A**)		358.3			
$[Mes_2Si{=}SiMes_2]{\cdot}C_7H_8$	2.160(1)	NA	12.0	63.6	[2]
(**A**)					
$[Mes_2Si{=}SiMes_2]$·thf	2.146	NA	13.0		
(**A**)					
(*E*)-Mes(Bu^t)Si=Si(Mes)Bu^t	2.143(1)	359.8	NA	90.3	[2c,d]
(**A**)					
(*E*)-Mes(Ad)Si=Si(Mes)Ad	2.138(2)	360.0	NA	87.1	[5]
(**A**)					
(*E*)-Tip(Me_3Si)Si=Si(Tip)$SiMe_3$	2.152(3)	NA	0	97.8	[6]
(**A**)					
(*E*)-Tip(Bu^t)Si=Si(Tip)Bu^t	2.157(2)	NA	0	87.4	[6]
(**A**)					
$Ar_2Si{=}SiAr_2$(Ar = 2,6-Et_2-C_6H_3)	2.140(3)	360.0	10.0	NA	[7b]
(**B**)					
$Tip_2Si{=}SiTip_2$	2.144	359.9	3.0	53.4	[8]
(**C**)					
(*E*)-Tbt(Mes)Si=Si(Tbt)Mes	2.228(3)	357.2	8.7	66.5	[9]
(**C**)		358.9			
(*Z*)-Tbt(Mes)Si=Si(Tbt)Mes	2.195(4)	358.8	14.0	NA	[9]
(**C**)		359.3			
(*E*)-Bbt(Br)Si=Si(Bbt)Br	2.2264(8)	NA	NA	79.4	[10]
(**C**)					
(*E*)-Fc(Tip)Si=Si(Fc)Tip	2.1733(15)	352.3	30.7	72.6	[11]
(**C**) [Fc = ferrocenyl]					
$Pr^i_2MeSi)_2Si{=}Si(SiMePr^i_2)_2$	2.228(2)	NA	0	144.5	[12]
(**C**)					
$(Bu^tMe_2Si)_2Si{=}Si(SiMe_2Bu^t)_2$	2.202(1)	NA	8.9	142.1	[12]
(**C**)					
$(Pr^i_3Si)_2Si{=}Si(SiPr^i_3)_2$	2.251(1)	NA	0	154.5	[12]
(**C**)					
(*E*)-$(R_3Si)(R'_3Si)Si{=}Si(SiR_3)SiR'_3$	2.196(3)	360.0	0	141.8	[13]
(**C**) [R_3Si = $SiMe_2Bu^t$,					
R'_3Si = $SiMePr^i_2$]					
(*E*)-Cl(R_3Si)Si=Si(Cl)SiR_3	2.163(4)	359.6	3.8	NA	[14]
(**C**) [R_3Si = $SiMe(SiBu^t_3)_2$]					
(*E*)-[$(R_3Si)_2MeSi$](R_3Si)Si=	2.1984(5)	359.5	29.0	103.8 (=*Si*Si_2)	[15]
$SiMe(SiR_3)$ [R_3Si = $SiMeBu^t_2$]		359.8		158.9 (=*Si*Me)	
(**C**)					
$(Bu^t_2MeSi)_2Si{=}Si(SiMeBu^t_2)_2$	2.2598(18)	359.6	54.5	155.5	[16]
(**C**)		359.7			
(*E*)-R(Bbt)Si=SiR(Bbt)					[17]
(**C**)					
R = C≡C−$SiMe_3$	2.202(2)	359.0	NA	44.6	
R = C≡C−Ph	2.1871(10)	358.5	NA	42.6	
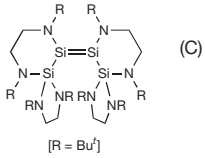 (C) [R = Bu^t]	2.2890(14)	345.6 346.6	25.1	119.5	[18]
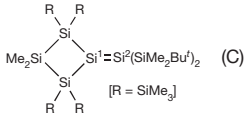 (C) [R = $SiMe_3$]	2.2061(8)	356.3/ 357.1	11.7	136.7(Si^2)/ 162.2(Si^1)	[19]

(*Continued*)

Table 1 (Continued)

Disilene (synthetic method)	*> Si=Si<[Å]*	*Σ(Si) [°]*	*>Si=Si<twist [°]*	*^{29}Si(Si=Si) (ppm)*	*Reference*
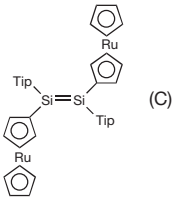 (C)	2.1851(12)	349.2	NA	70.6	[20]
(*E*)-Ar(Ph)Si=Si(Ar)Ph (**C**) 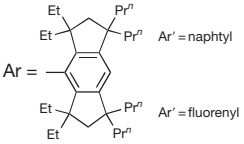	2.1556(6)	NA	0.02	NA	[21]
(*E*)-Ar(Ar′)Si=Si(Ar′)Ar (**C**) 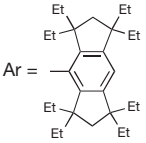	2.1623(18)/ 2.1667(12) 2.149(5)/ 2.1531(13)	357.2/ 359.7 359.8/ 359.9	NA NA	60.2/ 64.8 60.4	[22]
(*E*)-Ph(Ar)Si=Si(Ph)Ar (**C**) 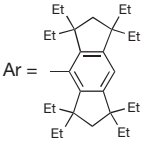	2.1593(16)	NA	3.3	63.2	[23]
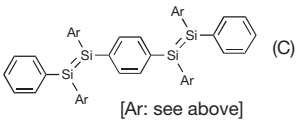 [Ar: see above]	2.156(2)	359.9/ 360.0	0.3/ 3.8	NA	[23]
(*E*)-Ph(Bu^t_3Si)Si=Si(Ph)$SiBu^t_3$ (**D**)	2.182(2)	359.5	9.0	128.0	[24a]
($Bu^tMe_2Si)_2Si$=Si($SiPr^i_3)_2$ (**D**)	2.2011(9)	360.0	28.0	142.0 152.7	[25]
($Bu^tMe_2Si)_2Si$=($SiMePr^i_2)_2$ (**D**) [2 independent molecules]	2.198(1) 2.1942(8)	360.0 360.0	9.0 11.7	132.4 156.6	[25]
(*E*)-$Me_3Si(R_3Si)Si$=Si($SiMe_3)SiR_3$ (**D**) [R_3Si = $SiPr^i_3$]	2.1967(11)	358.4	NA	147.1	[26]
Tip_2Si^1=Si^2(Tip)P(cyclohexyl)$_2$ (**E**)	2.1542(11)	359.0/ 359.5	3.5	52.5(Si^2)/ 95.4(Si^1)	[27]
Tip_2Si^1=Si^2(Tip)1 (**E**)	2.1914(9)	348.8/ 352.1	NA	76.8(Si^1)/ 51.7(Si^2)	[27]
Tip_2Si^1=Si^2($SnMe_3$)Tip (**E**)	2.1618(8)	359.3/ 359.9	NA	38.9(Si^2)/ 103.4(Si^1)	[28]
Tip_2Si^1=Si^2($SnClBu^t_2$)Tip (**E**)	2.1882(12)	355.9/ 356.8	NA	40.9(Si^2)/ 114.5(Si^1)	[28]
Tip_2Si^1=Si^2($ZrCp_2Cl$)Tip (**E**)	2.2144(7)	359.5/ 359.7	20.2	116.8(Si^1)/ 152.5 (Si^2)	[29]

Table 1 (Continued)

Disilene (synthetic method)	*> Si=Si<[Å]*	*Σ(Si) [°]*	*>Si=Si<twist [°]*	*^{29}Si(Si=Si) (ppm)*	*Reference*
$Tip_2Si^1{=}Si^2(Ph)Tip$ (**E**)	2.1754(11)	353.9/ 354.2	5.0	55.2(Si^1)/ 71.8(Si^2)	[30]
$Tip_2Si^1{=}Si^2(4\text{-}F\text{-}C_6H_4)Tip$ (**E**)	2.1468(8)	359.7/ 359.9	5.4	55.7(Si^1)/ 70.6(Si^2)	[30]
$Tip_2Si^1{=}Si^2(4\text{-}Cl\text{-}C_6H_4)Tip$ (**E**)	2.1735(4)	NA	10.8	57.3(Si^1)/ 69.3(Si^2)	[30]
$Tip_2Si^1{=}Si^2(4\text{-}Br\text{-}C_6H_4)Tip$ (**E**)	2.1707(5)	NA	10.6	57.4(Si^1)/ 69.2(Si^2)	[30]
meta-$[Tip_2Si^1{=}Si^2(Tip)]_2\text{-}C_6H_4$ (**E**)	2.189(1)	NA	10.6	54.6(Si^1)/ 72.9(Si^2)	[30]
para-$[Tip_2Si^1{=}Si^2(Tip)]_2\text{-}C_6H_4$ (**E**)	2.1674(8)	356.1/ 356.9	3.4	56.8(Si^1)/ 70.7(Si^2)	[30]

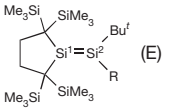

(E)

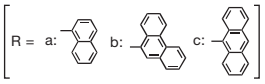

a:	2.1943(14)	352.7/ 357.8	NA	97.7(Si^2)/ 131.8(Si^1)	[31]
b:	2.209(2)	351.1/ 357.6	NA	99.6(Si^2)/ 132.4(Si^1)	[31]
c:	2.1754(12)	359.3/ 359.4	NA	85.6(Si^2)/ 123.2(Si^2)	[31]
$(Bu^t_2MeSi)_2Si^1{=}Si^2(SiMeBu^t_2)BR_2$ [R = catecholboryl] (**E**)	2.192(2)	360.0	7.1	111.7(Si^1)/ 127.3(Si^2)	[32]
(*E*)-$R(Et_2N)Si^1{=}Si^2(R)H$ [R = $SiPr^i_3Dsi_2$] (**F**)	2.1647(10)	354.9/ 358.7	NA	−39.3(Si^2)/ 170.5(Si^1)	[33]
(*E*)-$R(Ph_2N)Si^1{=}Si^2(R)H$ [R = $SiPr^i_3Dsi_2$] (**F**)	2.1790(14)	357.8	NA	66.6(Si^2)/ 136.4(Si^1)	[33]
(*E*)-$R(R'_2B)Si^1{=}Si^2(R)H$ [R = $SiPr^i_3Dsi_2$; R'_2B = catecholboryl] (**F**)	2.1634(12)	358.1/ 358.7	NA	84.3(Si^1)/ 123.4(Si^2)	[34]
(*E*)-$R(R'_2B)Si^1{=}Si^2(R)H$ [R = $SiPr^i_3Dsi_2$; R'_2B = 9-borabicyclo[3.3.1]nonan-9-yl] (**F**)	2.1838(12)	359.7/ 359.9	NA	121.7(Si^1)/ 150.5(Si^2)	[33]
(*E*)-$R(R'_2N)Si^1{=}Si^2(R)H$ [R = $SiPr^i_3Dsi_2$; R'_2N = pyrrolidyl] (**F**)	2.1596(17)	356.8/ 359.1	NA	−34.1(Si^2)/ 159.0(Si^1)	[35]
(*E*)-$R(R'_2N)Si^1{=}Si^2(R)H$ [R = $SiPr^i_3Dsi_2$; R'_2N = Bu^tNH] (**F**)	2.1949(7)	341.7/ 355.2	NA	−47.2(Si^2)/ 136.5(Si^1)	[35]
(*E*)-$R(NHC{\rightarrow})Si^1{=}Si^2{:}(R)$ [R = $SiPr^i_3Dsi_2$; NHC = $(MeCNMe)_2C{:}$] (**F**)	2.1989(6)	359.2	NA	28.7(Si^1)/ 276.3(Si^2)	[36]
(*Z*)-$R(NHC{\rightarrow})Si^1{=}Si^2{:}(\rightarrow ZnCl_2)R$ [R = $SiPr^i_3Dsi_2$; NHC = $(MeCNMe)_2C{:}$] (**F**)	2.2006(13)	355.4/ 359.7	NA	66.9(Si^1)/ 190.8(Si^2)	[36]
(*Z*)-$Tip(Tip_2HSi)Si{=}Si(SiClTip_2)Tip$ (**other methods**)	2.2149(9)	360.0/ 360.0	NA	96.0/ 102.7	[37]
(*Z*)-$Tip(Tip_2HSi)Si{=}Si(SiBrTip_2)Tip$ (**other methods**)	2.2088(10)	360.0/ 360.0	NA	95.6/ 104.1	[37]
(*E*)-$R(\eta^1\text{-}Cp^*)Si{=}Si(R)$ (η^1-Cp*) [R = $N(SiMe_3)_2$] (**other methods**)	2.1683(5)	359.1/ 359.5	4.9	NA	[38]

(*Continued*)

Table 1 (Continued)

Disilene (synthetic method)	*> Si=Si<[Å]*	*Σ(Si) [°]*	*>Si=Si<twist [°]*	*^{29}Si(Si=Si) (ppm)*	*Reference*
NHC:→S̈i=S̈i←:NHC [NHC = $(HCNAr)_2C$: [Ar = 2,6-Pr^i_2-C_6H_3] (**other methods**)	2.2294(11)	NA	NA	224.5	[39]
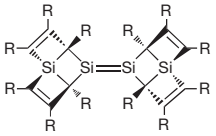 [R = Bu^t] (**other methods**)	2.2621(15)	360.0	12.1	102.5	[40a]

NA = not available.

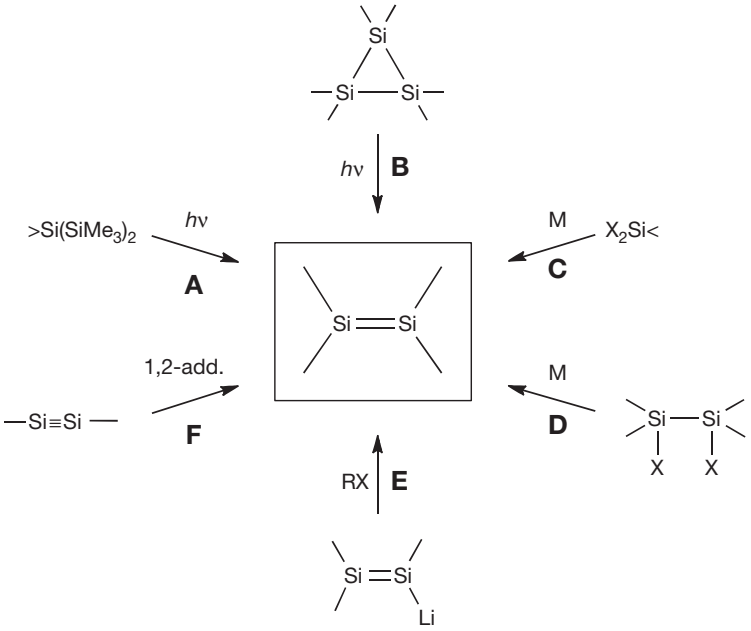

Scheme 1 Major synthetic routes to the stable disilenes >Si=Si<.

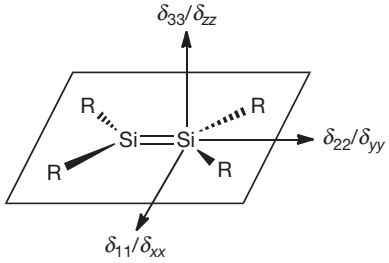

Figure 1 Directions of the principal shielding tensor components in a planar disilene $R_2Si{=}SiR_2$.

extraordinarily low-field shifted resonances of the disilenes bearing sterically demanding σ-donating silyl substituents originate from the deshielding in the δ_{11} direction. Stretching of the Si=Si bond, caused by the bulkiness of the silyl groups, and a remarkable decrease in the $\Delta E(\sigma_{Si-Si}{-}\pi^*_{Si=Si})$, caused by the raising of the σ_{Si-Si} energy level resulting from the electropositive silyl substitution, are jointly responsible for the extreme deshielding observed in tetrasilyldisilenes.

Mixed substituted disilenes (aryl(alkyl)disilenes, aryl(silyl) disilenes, and alkyl(silyl)disilenes) exhibited resonances of their doubly bonded silicon centers in the region intermediate between those of identically substituted compounds (tetraaryldisilenes/tetraalkyldisilenes, tetraaryldisilenes/tetrasilyldisilenes, and tetraalkyldisilenes/tetrasilyldisilenes).

In the particular case of disilenes $(R_3Si)_2Si = SiAr_2$ with an unsymmetrical substitution pattern, silyl-substituted sp^2-silicons were extraordinarily shielded, whereas the resonances of the aryl-substituted sp^2-silicons were found at very low fields: −0.8 and +152.3 ppm ($(Pr^i_3Si)_2Si = SiMes_2$), +14.0 and +137.2 ppm ($(Pr^i_3Si)_2Si = SiTip_2$), +8.2 and +148.6 ppm ($(Bu^t_2MeSi)_2Si = SiMes_2$), and +14.9 and +142.0 ppm ($(Bu^t_2MeSi)_2Si = SiTip_2$).[43] Such unusual NMR spectral features were explained by considering the high importance of the paramagnetic nuclear spin–electron orbit term, representing the degree of interaction with the nuclear magnetic moment and affecting the magnitude of the paramagnetic contribution and, consequently, the overall deshielding.[44]

1.11.2.1.1.3 Crystal structures of disilenes

The most fundamental structural characteristic of the doubly bonded organosilicon compounds, differentiating them from their singly bonded counterparts, is the length of the silicon–silicon bond. Although the structurally characterized Si=Si bond lengths are reported to vary rather widely from 2.138(2) to 2.2890(14) Å, the overwhelming majority of them (88%) span the narrower range of 2.14–2.22 Å with the major part (66%) fitting within the 2.14–2.19 Å range (Figure 2).

These values are comparable (albeit slightly longer because of the remarkable steric congestions) to the estimate of 2.14 Å made for the Si=Si bond on the basis of the double-bond covalent radius of 1.07 Å recently reported for the Si atom.[45] The experimental values for the Si=Si bond of 2.14–2.19 Å are also substantially shorter (6–9%) than the sum of the single-bond covalent radii for the two Si atoms of 2.32 Å[46] and the average value of the experimentally determined Si–Si single-bond lengths of 2.34 Å.

The other diagnostic features of the Si=Si bonds, principally distinguishing them from organic alkenes with planar C=C bonds, are the structural deformations, of which the *trans*-bending at sp^2-Si atoms and twisting about the Si=Si bond are the most important (for a comprehensive discussion, see leading reviews: Ref. [4]). If the twisting about the Si=Si bond is mostly attributed to the huge steric interaction between the highly sterically demanding substituents, the *trans*-bending at silicons is definitely electronic in its origin. Thus, electronegative substituents (F, OH, and NH_2) cause an increase in the singlet–triplet energy gap (ΔE_{ST}) and the extent of $\pi_{Si=Si}$–σ^*_{Si-Si} orbital mixing, resulting in a pronounced *trans*-bending at the sp^2-Si atoms, stretching and weakening the Si=Si bond. By contrast, electropositive substituents (BH_2 and SiH_3) reduce ΔE_{ST} and the degree of $\pi_{Si=Si}$–σ^*_{Si-Si} interaction, resulting in a flattening at the sp^2-Si, shortening and strengthening the Si=Si bond.

Of all structurally characterized disilenes, tetraalkyldisilenes $R_2Si{=}SiR_2$ are typically *trans*-bent and twisted when they have bulky substituents. Their structural features vary in the following range: 2.1767(6)–2.2687(7) Å (Si=Si bond length); 345.0–360.0° (sum of the bond angles around sp^2-Si indicating the degree of pyramidality); and 3.9–42.5° (twisting about Si=Si bond) (Table 1).

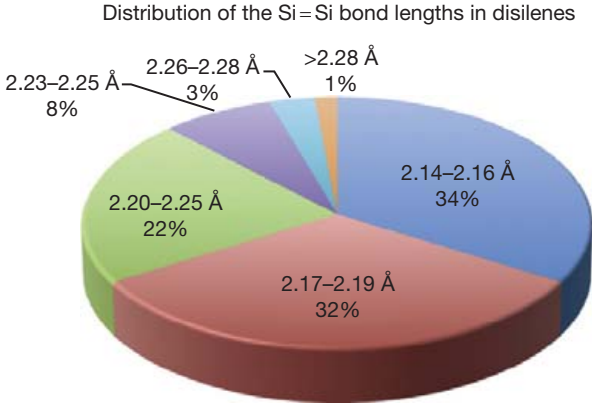

Figure 2 Distribution of the Si=Si double-bond lengths in the stable disilenes.

Tetraaryldisilenes $Ar_2Si{=}SiAr_2$ are normally less deformed than their tetraalkyl-substituted counterparts, showing the following range of structural characteristics: 2.140(3)–2.228(2) Å (bond length); 349.2–360.0° (sum of the bond angles); and 0.02–14.0° (twisting) (Table 1).

In agreement with theoretical expectations (see above), tetrasilyldisilenes $(R_3Si)_2Si{=}Si(SiR_3)_2$ are the least deformed of all known disilenes, showing nearly ideal planar geometry around the silicon centers: 356.3–360.0° (sum of the bond angles) (Table 1). However, in contrast to computational predictions, sterically congested tetrasilyldisilenes showed rather long and extremely twisted Si=Si bonds because of the extreme steric repulsion between the bulky substituents: 2.180(3)–2.2598(18) Å (bond length) and 0.0–54.5° (twisting) (Table 1). For example, in accord with its huge electropositive silyl groups, the most heavily substituted tetrasilyldisilene $(Bu^t_2MeSi)_2Si{=}Si(SiMeBu^t_2)_2$ is particularly strongly deformed with the longest Si=Si bond among tetrasilyldisilenes of 2.2598(18) Å and greatest twisting of 54.5°, being nevertheless nearly planar at the sp^2-silicons (sum of the bond angles 359.6°/359.7°).[16]

The longest known Si=Si bond of 2.2890(14) Å was reported for the unusual bis(amino)bis(silyl)disilene, which was also markedly *trans*-bent at the silicons (345.6° and 346.6°) and notably twisted (25.1°) at the Si=Si bond.[18] Both steric and electronic effects are responsible for such great structural distortions seen in this compound.

1.11.2.1.1.4 Cyclic disilenes with an endocyclic Si=Si bond

There are no universal approaches for the design of cyclic disilenes; therefore, the particular synthetic methods for each class of such derivatives (depending on the ring size) are described (Table 2).

1.11.2.1.1.4.1 Three-membered ring compounds (heavy cyclopropenes)[47] These cyclic compounds are especially interesting because of their unusual structures (combination of the highly strained three-membered ring and double bond in one molecule) and extreme reactivity (Table 2). The particular geometry of the heavy cyclopropenes, bearing electropositive σ-donating silyl groups, allows for effective $\pi_{E=E}$–σ^*_{E-Si} orbital mixing, stabilizing the highest occupied molecular orbital (HOMO)($\pi_{E=E}$) of the molecule and resulting in the remarkable relaxation of the inherent ring strain (for the π–σ* orbital interaction concept, see Ref. [48]) (Figure 3).

The first stable cyclotrisilene was prepared in 1999 by the reduction of $(Bu^tMe_2Si)_3Si{-}SiBr_2Cl$ with potassium graphite (Scheme 2).[49]

A further two stable cyclopropene analogs featuring an endocyclic Si=Si double bond, symmetrically substituted cyclotrisilene[50] and hybrid 3*H*-disilagermirene of different heavy group 14 elements,[51] were readily available by the reductive Würtz coupling of $RSiBr_3$ and R_2EX_2 (R = $SiMeBu^t_2$, E = Si/Ge, X = Cl/Br) with metallic sodium (Scheme 3).

The unprecedented alkyl-substituted heavy cyclopropene, as the nearest homolog of the above-described symmetrically substituted cyclotrisilene distinguished by only one CH_2-unit, was prepared by the thermal isomerization of trisilabicyclo[1.1.0]butane (Scheme 4).[52]

A cyclotrisilene with different substituents at the sp^3- and sp^2-Si atoms was synthesized by the coupling of $(Bu^t_2MeSi)_2SiLi_2$ and $Bu^t_3Si{-}SiBr_2{-}SiBr_2{-}SiBu^t_3$ (Scheme 5).[53]

Table 2 Crystallographic and spectral parameters of the structurally characterized cyclic disilenes.

Cyclic disilene	*>Si=Si< [Å]*	*Σ(Si)[°]*	*>Si=Si< twist [°]*	*Ring Folding [°]*	*^{29}Si NMR (Si=Si) (ppm)*	*Reference*
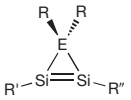						
[E = Si; R = R′ = $SiMe_2Bu^t$; R″ = SiR_3]	2.132(2)	356.7 360.0	21.4		81.9 (= *Si*-R′) 99.8 (= *Si*-R″)	[49]
[E = Si; R = R′ = R″ = $SiMeBu^t_2$]	2.138(2)	357.5 358.1	31.9		97.7	[50]
[E = Ge; R = R′ = R″ = $SiMeBu^t_{2]}$	2.146(1)	356.9 357.4	37.0		107.8	[51]
[E = Si; R = $SiMeBu^t_2$; R′ = R″ = $SiBu^t_3$]	2.1612(8)	359.8 360.0	4.8		97.4	[53]
[E = Si; R′ = R″ = $SiMe_3$; R,R = –C $(SiMe_3)_2CH_2CH_2(Me_3Si)_2C$–]	2.1428(5)	359.1 360.0	8.6		142.9	[54]
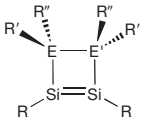						
[E = E′= Si; R = R′ = R″ = $SiMe_2Bu^t$]	2.174(4)	358.6	12.3	37.0	160.4	[55]
[E = E′ = Si; R = R′ = $SiBu^t_3$; R″ = 1]	2.257(2)	359.2 359.6	30.8	28.0	164.4	[56]
[E = E′ = Si; R= R′ = $SiBu^t_3$; R″ = H]	2.360(2)	350.4	NA	23.0	141.3	[57]
[E = E′ C; R′ = R″ = H; R = $SiMe(SiBu^t_3)_2$]	2.175(1)	359.8 360.0	NA	8.3	151.4	[58]
[E = E′ = C; R = $SiPr^iDsi_2$; R′ = Me; R″ = H]	2.1632(10)	358.1 358.4	32.2	1.0	152.1	[59]
[E = E′ = Si; R= R′ = $SiMeBu^t_2$; R″ = Br]	2.2014(9)	359.0 359.7	NA	33.7	141.4	[60]
[E = E′ = Ge; R = R′ = $SiMeBu^t_2$; R″ = Me]	2.1875(13)	355.3 357.6	NA	4.3	167.6	[61]
[E = Si, E′ = Se; R = R′ = R″ = $SiMeBu^t_2$; no substituents R′ and R″ on Se]	2.1706(12)	360.0	0.1	1.7	100.8 (=*Si*-Si) 192.1 (=*Si*-Se)	[62]
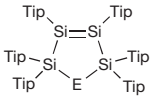	2.170(1)	358.6 359.7	26.5	NA	86.0	[63]
	2.181(1)	358.5 359.6	26.8	NA	90.3	[63]
	2.198(2)	358.6 359.3	28.2	NA	97.8	[63]
[E = S] [E = Se] [E = Te]						
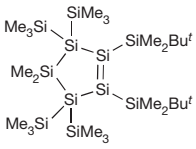	2.1926(6)	359.7/ 359.9	NA	33.4	150.2	[19]
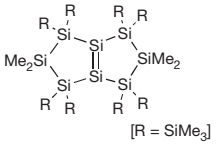 [R = $SiMe_3$]	2.180(3)	360.0	16.7	22.1	167.4	[64]
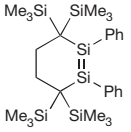	2.1595(9)	356.7/ 358.4	4.8	NA	100.9	[65]

Table 2 (Continued)

Cyclic disilene	*>Si=Si< [Å]*	*Σ(Si)[°]*	*>Si=Si< twist [°]*	*Ring Folding [°]*	*^{29}Si NMR (Si=Si) (ppm)*	*Reference*
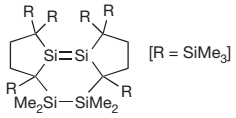 [R = $SiMe_3$]						
Trans–	2.2687(7)	345.0/ 346.0	42.5	NA	135.9	[66]
Cis–	2.1767(6)	357.7/ 359.8	3.9	NA	128.1	[66]

NA = not available.

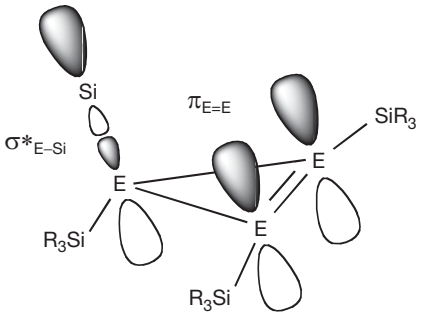

Figure 3 The stabilizing $\pi_{E=E}$–σ^*_{E-Si} orbital mixing in the heavy cyclopropenes.

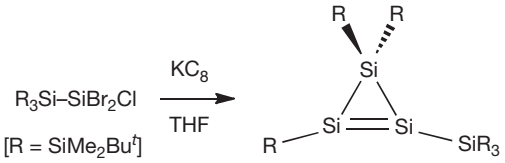

Scheme 2 Synthesis of the first stable cyclotrisilene.

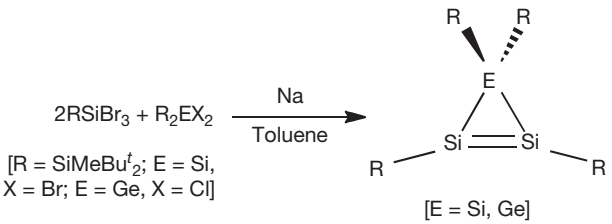

Scheme 3 Synthesis of the symmetrically substituted cyclotrisilene and hybrid 3*H*-disilagermirene.

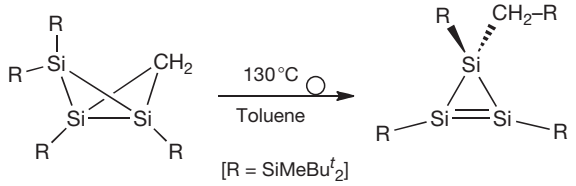

Scheme 4 Synthesis of the alkyl-substituted cyclotrisilene.

An unusual derivative, in which the cyclotrisilene fragment is a part of a spiroheptene system, was prepared by cleavage of one of the Si=Si bonds of the stable tetrasilabuta-1,3-diene followed by the intramolecular insertion of the resulting silylene into the second Si=Si bond (Scheme 6).[54]

The resonances of the sp^2-Si atoms of silyl-substituted cyclotrisilenes are observed at markedly higher fields than those of acyclic tetrasilyldisilenes: 81.9–122.8 ppm versus 132.4–167.4 ppm. This trend is in line with that in organic chemistry, where doubly bonded carbons in cyclopropene (108.7 ppm) resonate at higher fields than those in ethylene (123.5 ppm).

The Si=Si bonds in the silyl-substituted cyclotrisilenes are notably shorter than those of acyclic tetrasilyldisilenes: 2.132(2)–2.1612(8) Å versus 2.180(3)–2.2598(18) Å. However, the Si=Si bonds in cyclotrisilenes are more twisted than those in tetrasilyldisilenes with the torsion about the Si=Si bond ranging from 21.4° to 37.0°. Such remarkable twisting may result from the important steric repulsion between the eclipsing bulky silyl-substituents at the sp^2-Si atoms. As an exceptional case, the cyclotrisilene with the extraordinarily bulky Bu^t_3Si-groups at the doubly bonded silicons showed a nearly planar geometry about the Si=Si bond, with a twisting angle of only 4.8° (Scheme 5).[53]

1.11.2.1.1.4.2 Four-membered ring compounds (heavy cyclobutenes) Nine heavy cyclobutenes featuring an endocyclic Si=Si bond have been prepared to date (each by a particular synthetic method), of which eight have been structurally characterized (Table 2 and Scheme 7).

The first isolable representative, hexasilylcyclotetrasilene, was synthesized in 1996 by the coreduction of a mixture of tetrabromodisilane $RSiBr_2SiBr_2R$ and dibromosilane R_2SiBr_2 (R = $SiMeBu^t_2$) with lithium naphthalenide (Scheme 8).[55]

The first cyclic disilenes with a chalcogen atom (S, Se) incorporated into the four-membered ring were synthesized by the photochemical isomerization of 2-thia(2-selena)-1,3,4-trisilabicyclo[1.1.0]butanes (Scheme 7, H).[62] Mechanistic studies showed the symmetry-allowed [$\sigma 2s + \sigma 2s$] concerted disrotatory transformation of bicyclo[1.1.0]butane to cyclobutene as the most likely mechanistic scenario. Moreover, such chalcogen-substituted cyclic disilenes showed no signs of a significant conjugation between the Si=Si bond and S/Se lone pairs, as was determined by their structural and spectral characteristics.

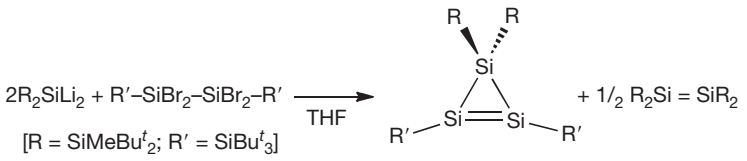

Scheme 5 Synthesis of a cyclotrisilene with different substituents at the sp^3- and sp^2-Si atoms.

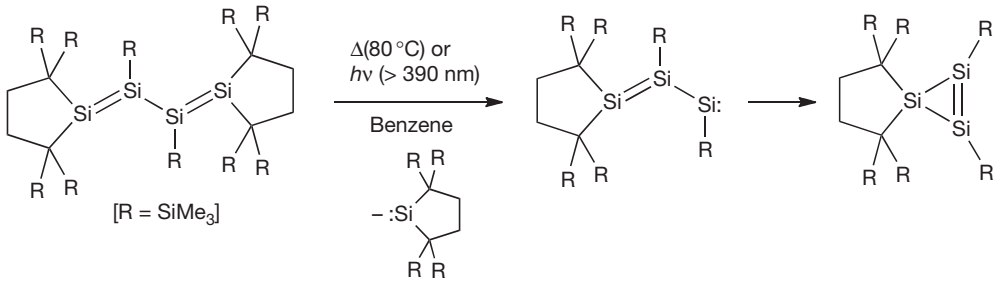

Scheme 6 Synthesis of the spirocyclic cyclotrisilene.

The resonances of the doubly bonded Si atoms of the heavy cyclobutenes were found at remarkably lower fields than those of the heavy cyclopropenes: 95.1–195.0 ppm versus 81.9–122.8 ppm. This tendency is again quite parallel to that observed in organic chemistry: deshielding of sp^2-carbons in cyclobutene (137.2 ppm) relative to those in cyclopropene (108.7 ppm). Moreover, the sp^2-silicons of cyclotetrasilenes are even more deshielded than those of acyclic tetrasilyldisilenes: 95.1–195.0 ppm versus 132.4–167.4 ppm.

The Si=Si bonds in the heavy cyclobutenes are longer than those of the heavy cyclopropenes (likewise, cyclopropenes in organic chemistry are well known to possess the shortest C=C bonds among cycloalkenes): 2.1632(10)–2.360(2) Å versus 2.132(2)–2.1612(8) Å. The extent of other structural distortions (pyramidalization at the sp^2-Si, twisting of the Si=Si bond, folding of the four-membered ring) is totally governed by the substitution pattern: 350.4–360.0° (pyramidalization); 0.1–32.2° (twisting); and 1.0–37.0° (folding).

1.11.2.1.1.4.3 Five-membered ring compounds (heavy cyclopentenes) Five stable heavy cyclopentenes (Table 2) with an endocyclic Si=Si bond have been reported to date; three of these were prepared by the [1+4]-cycloaddition of chalcogens (S, Se, and Te) to the isolable tetrasilabuta-1,3-diene derivative $Tip_2Si{=}Si(Tip){-}Si(Tip){=}SiTip_2$ (Scheme 9),[63] the cyclopentasilene by the thermal rearrangement of the cyclotetrasilane with an exocyclic Si=Si bond (Scheme 10),[19] and the fused bicyclic disilene by the reductive dehalogenation of the 1,1-dichlorocyclotetrasilane (Scheme 11).[64]

The doubly bonded silicons in the chalcogen-containing heavy cyclopentenes shown in Scheme 9 were markedly shielded (86.0–97.8 ppm),[63] compared with those of the cyclopentasilene in Scheme 10 (150.2 ppm)[19] and fused bicyclic disilene in Scheme 11 (167.4 ppm),[64] in accord with their differing substitution patterns (aryl vs. silyl substituents). The Si=Si bonds in the heavy cyclopentenes (2.170(1)–2.198(2) Å) are comparable to those in heavy cyclobutenes (2.1632(10)–2.360(2) Å), albeit longer than those in heavy cyclopropenes (2.132(2)–2.1612(8) Å). The five-membered rings are nearly planar in the chalcogen-containing heavy cyclopentenes (Scheme 9),[63] whereas in the cyclopentasilene (Scheme 10)[19] and fused bicyclic disilene (Scheme 11)[64] the rings are noticeably folded (folding angles are 33.4° and 22.1°, respectively). Although only an insignificant pyramidalization at the sp^2-Si atoms (358.6/359.3–360.0/360.0°) was observed in the heavy cyclopentenes, the twisting about the Si=Si bond was quite sizeable (16.7–28.2°).[63,64]

1.11.2.1.1.4.4 Six-membered ring compounds (heavy cyclohexenes) Three examples of six-membered ring compounds having an endocyclic Si=Si bond are represented by the cyclic disilenes prepared by the reductive cyclization of 1,1,6,6-tetrabromo-1,6-disilahexane derivatives with potassium graphite, as depicted in Schemes 12[65] and 13.[66] The sp^2-silicon resonance of the heavy cyclohexene with a mixed diaryl−dialkyl substitution pattern (Scheme 12)[65] was found at 100.9 ppm, which is between those of the tetraaryldisilenes $Ar_2Si{=}SiAr_2$ and tetraalkyldisilenes $R_2Si{=}SiR_2$. By contrast, the doubly bonded silicons in both *cis*- and *trans*-isomers of the fused tricyclic disilene (Scheme 13)[66] resonated at a lower field (128.1 and 135.9 ppm, respectively), as one can expect for a tetraalkyl-substituted disilene.

The Si=Si double bond in the heavy cyclohexene (Scheme 12)[65] of 2.1595(9) Å is slightly shorter than those in the heavy cyclobutenes (2.1632(10)–2.360(2) Å) and heavy cyclopentenes (2.170(1)–2.198(2) Å), being comparable to those in heavy cyclopropenes (2.132(2)–2.1612(8) Å). Whereas the Si=Si bond in the *cis*-isomer of the fused tricyclic disilene (Scheme 13)[66] of 2.1767(6) Å was quite normal, that of the *trans*-isomer of 2.2687(7) Å was extraordinarily stretched as a consequence of the severe strain imposed by the fused tricyclic skeleton.

The geometry around the Si=Si bond in the heavy cyclohexene (Scheme 12)[65] was almost undistorted with rather insignificant pyramidalization at the doubly bonded Si atoms (sum of the bond angles 356.7°/358.4°) and small twisting about the Si=Si bond (4.8°). However, the geometry of the Si=Si bond in the fused tricyclic disilene (Scheme 13)[66] is distinctly different in its *cis*- and *trans*-isomers: essentially planar in the *cis*-isomer (357.7/359.8° (sum of the bond angles at the sp^2-Si) and 3.9° (Si=Si twist angle)) and highly distorted in

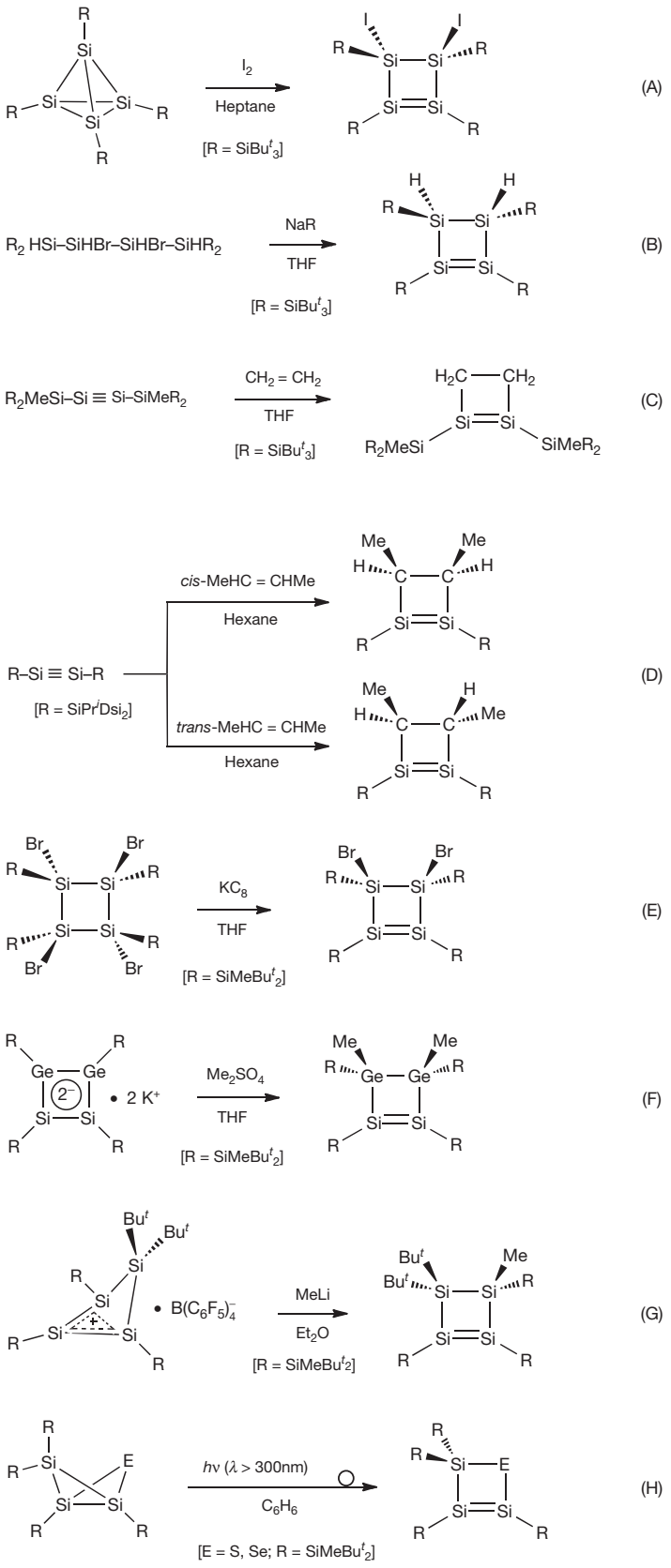

Scheme 7 Synthesis of the stable heavy cyclobutenes with an endocyclic Si=Si bond.

the *trans*-isomer (345.0/346.5° (sum of the bond angles at the sp^2-Si) and 42.5° (Si=Si twist angle)).

Accordingly, the six-membered ring in the heavy cyclohexene (**Scheme 12**)[65] adopts a conformation that is halfway between an ideal chair and an ideal half-chair, whereas the conformation of the six-membered ring in the *cis*- and *trans*-isomers of the fused tricyclic disilene (**Scheme 13**)[66] can be best described as a boat (*cis*-isomer) and a twist-boat (*trans*-isomer).

1.11.2.1.2 Digermenes >Ge=Ge<[67]

1.11.2.1.2.1 Synthesis

The first stable digermene, $Dsi_2Ge{=}GeDsi_2$, was prepared by Lappert and coworkers in 1976 (i.e., prior to the report on the first stable disilene by West[2a]) by the reaction of the stable bis(amino)germylene $[(Me_3Si)_2N]_2Ge$: with DsiLi.[68] To date, about 30 room-temperature stable digermenes have been isolated and structurally characterized (excluding ionic, radical, and aromatic derivatives containing Ge=Ge bonds, as well as compounds with conjugated and cumulated Ge=Ge bonds) (**Table 3**). Most of them (22 stable digermenes) were synthesized after 2000.

Stable acyclic digermenes are available by one of four major synthetic routes: (1) photolysis of cyclotrigermanes (**A**); (2) dimerization of germylenes (**B**); (3) reductive dehalogenation of 1,1-dichlorogermanes (**C**); and (4) 1,2-addition or cycloaddition to the isolable digermyne (**D**) (**Scheme 14**).

Photolysis of hexaarylcyclotrigermanes (method **A**) was introduced and developed as the synthetic approach for the stable tetraaryldigermenes $Ar_2Ge{=}GeAr_2$. Method **B**, used for the synthesis of the first isolable digermene $Dsi_2Ge{=}GeDsi_2$, is the most widely used procedure for accessing stable digermenes by the coupling of RLi/RMgX with $:GeX_2{\cdot}$diox complex. Reductive dehalogenation of 1,1-dichlorogermanes (method **C**), the second most popular method, allowed isolation of several digermenes bearing either aryl or silyl substituents. Method **D** represents the newest approach to the stable digermenes: 1,2-addition or cycloaddition to digermynes (or their valence isomers), which was brought into effect after the recent preparation of the latter compounds. Lappert's digermene $Dsi_2Ge{=}GeDsi_2$ (as well as some other digermenes), although stable in the solid state, is reported to be in equilibrium with the corresponding germylenes in solution $R_2Ge{=}GeR_2 \rightleftharpoons 2R_2Ge$:, confirmed by ultraviolet (UV)–visible (Vis) studies and germylene trapping reactions.

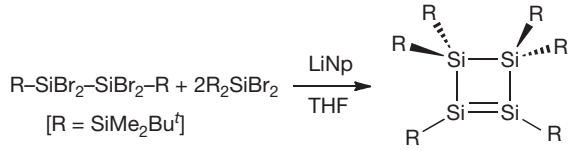

Scheme 8 Synthesis of the first stable cyclotetrasilene.

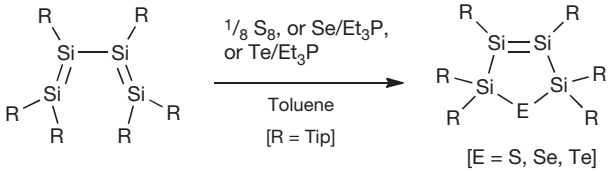

Scheme 9 Synthesis of the heavy cyclopentenes with an endocyclic Si=Si bond.

1.11.2.1.2.2 Crystal structure of digermenes

In the absence of a magnetically useful nucleus (the ^{73}Ge nucleus has a large quadrupole moment and low sensitivity resulting in a remarkable broadening of its resonance signals, greatly limiting the applicability of ^{73}Ge NMR spectroscopy), most structural information on digermenes has been obtained from their x-ray diffraction studies (**Table 3**).

The Ge=Ge double bonds, which are generally shorter than typical Ge–Ge single bonds, span a wide range of 2.213(2)–2.5087(7) Å, although the majority of them (59%) were found to fit within the narrower range of 2.30–2.39 Å (**Figure 4**). These last values are slightly longer than the 2.22 Å estimate based on the Ge atom double-bond covalent radius of 1.11 Å,[45] being nevertheless shorter than the sum of the single-bond covalent radii for the two Ge atoms of 2.42 Å.[46]

The structural deformations of digermenes are even more pronounced compared with disilenes, although the trends that determine the extent of the structural distortions are general in both cases: electronegative substituents cause appreciable *trans*-bending at the sp^2-Ge, stretching and weakening the Ge=Ge bond, whereas introduction of electropositive groups results in planarization at the sp^2-Ge, shortening and strengthening the Ge=Ge bond. Compared with Si=Si bonds, Ge=Ge bonds are usually longer, weaker, more *trans*-bent, and more twisted.

There is only one example of a tetraalkyldigermene, $Dsi_2Ge{=}GeDsi_2$, which has a Ge=Ge bond of the normal length, *trans*-bent and not twisted: 2.347(2) Å (Ge=Ge bond length);

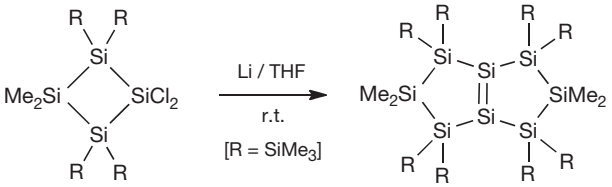

Scheme 11 Synthesis of the fused bicyclic disilene.

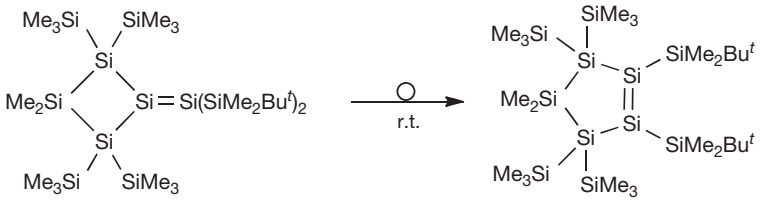

Scheme 10 Synthesis of the cyclopentasilene.

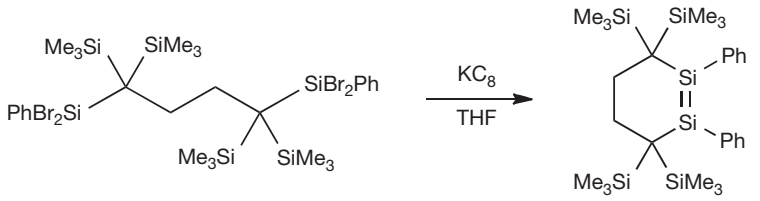

Scheme 12 Synthesis of the six-membered ring cyclic disilene.

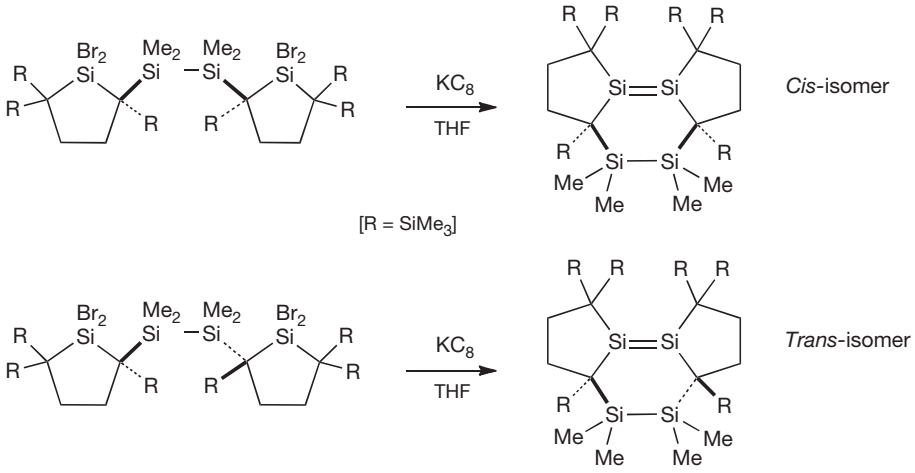

Scheme 13 Synthesis of the fused tricyclic disilene (*cis*- and *trans*-isomers).

348.5° (sum of the bond angles around sp^2-Ge indicating the degree of pyramidality); and 0.0° (twisting about Ge=Ge bond) (Table 3).[68]

Compared with the tetraalkyldigermene (see above), tetraaryldigermenes typically feature shorter and less *trans*-bent Ge=Ge bonds, which however can be twisted when substituted by bulky groups: 2.213(2)–2.416 Å (bond length); 345.5–360.0° (sum of the bond angles); and 7.0–20.4° (twisting) (Table 3).

In line with the structural trends observed in tetrasilyldisilenes, tetrasilyldigermenes are deformed rather insignificantly, featuring relatively short Ge=Ge bonds: 2.267(1)–2.298(1) Å (bond length); 357.0–359.6° (sum of the bond angles); and 0.0° (twisting) (Table 3). As a remarkable exception, one should mention tetrasilyldigermene $(Bu^t_2MeSi)_2Ge=Ge(SiMeBu^t_2)_2$, which has very bulky silyl substituents. Albeit still planar at the sp^2-germaniums (sum of the bond angles 358.8°/359.2°), this unusually colored deep-blue digermene features an extraordinarily twisted (52.8°) and stretched Ge=Ge bond of 2.346(2) Å.[82]

The record twisting of the Ge=Ge bond was reported for the digermene with a mixed bis(amino)bis(silyl)-substitution pattern – 63.0° (Table 3)[75] – whereas the longest Ge=Ge bond length was reported for the (*E*)-Bbt(Br)Ge=Ge(Bbt)Br digermene – 2.5087(7) Å.[77]

1.11.2.1.2.3 Cyclic digermenes with an endocyclic Ge=Ge bond

Eighteen organometallic compounds featuring endocyclic Ge=Ge bonds have been reported: thirteen three-membered rings, three four-membered rings, and two five-membered rings.

1.11.2.1.2.3.1 Three-membered ring compounds (heavy cyclopropenes)[47]

The first-ever reported stable cyclotrigermenes were prepared by the reaction of Bu^t_3EM (E=Si, M=Na; E=Ge, M=Li) with $GeCl_2$·diox complex (Scheme 15 and Table 4).[85]

A series of unsymmetrically substituted cyclotrigermenes was prepared by the coupling of tris(tri-*tert*-butylsilyl)cyclotrigermenylium tetrakis[3,5-bis(trifluoromethyl)phenyl]borate with the corresponding silyl-, germyl-, and aryl-alkali metal salts RM (Scheme 16 and Table 4).[86]

Treatment of tris(tri-*tert*-butylsilyl)cyclotrigermenylium tetrakis(2,3,5,6-tetrafluorophenyl)borate with potassium halides KX (X=Cl, Br, and I) resulted in the formation of halogen-substituted cyclotrigermenes (Scheme 17 and Table 4).[87]

Interaction of tetrachlorodigermane R–$GeCl_2$–$GeCl_2$–R (R=$SiMeBu^t_2$) with either 1,1-dilithiosilane R_2SiLi_2 or dilithiogermane R_2GeLi_2 was found to be another route to the three-membered ring cyclic digermenes: 1*H*-siladigermirene and cyclotrigermene (Scheme 18 and Table 4).[88] A three-membered ring dichloride A was proposed as the first reaction intermediate, undergoing a rapid Li↔Cl exchange with the second mole of R_2ELi_2 (E=Si/Ge) to give digermenoid B, which finally underwent *β*-elimination of LiCl (Scheme 18). In accord with the proposed reaction pathway, a half-equivalent of the disilene $R_2Si=SiR_2$ (or digermene $R_2G=GeR_2$) was also formed under the reaction conditions.

The nearest homologs of the above-described 1*H*-siladigermirene and cyclotrigermene, namely, alkyl-substituted heavy cyclopropenes distinguished from them by one CH_2-unit, were synthesized by the reductive dehalogenation of 1,3-dichlorocyclobutane derivatives (Scheme 19).[89] The

Table 3 Crystallographic parameters of the structurally characterized digermenes.

Digermene (sybthetic method)	*>Ge=Ge<[Å]*	*Σ(Ge) [°]*	*>Ge=Ge< twist [°]*	*Reference*
$Ar_2Ge{=}GeAr_2$ (**A**) [Ar = 2,6-Et_2-C_6H_3]	2.213(2)	358.4	10.0	[69]
$Dsi_2Ge{=}GeDsi_2$ (**B**)	2.347(2)	348.5	0.0	[68]
(*E*)-Ar(Cl)Ge=Ge(Ar)Cl (**B**) [Ar = 2,6-Mes_2-C_6H_3]	2.443(2)	333.8	NA	[70]
(*E*)-Ar(Cl)Ge=Ge(Ar)Cl (**B**) [Ar = 2,6-(2,6-Pr^i_2-C_6H_3)$_2$-C_6H_3]	2.4624(4)	327.8	NA	[71]
(*E*)-Ar(Me)Ge=Ge(Ar)Me (**B**) [Ar = 2,6-Tip_2-C_6H_3]	2.3173(3)	342.9	NA	[72]
(*E*)-Ar(Et)Ge=Ge(Ar)Et (**B**) [Ar = 2,6-Tip_2-C_6H_3]	2.47(3)	343.0	NA	[72]
(*E*)-Ar(Ph)Ge=Ge(Ar)Ph (**B**) [Ar = 2,6-Tip_2-C_6H_3]	2.3183(5)	348.4	NA	[72]
(*E*)-Ar(Cl)Ge=Ge(Ar)Cl (**B**) [Ar = 2,6-Tip_2-C_6H_3]	2.363(2)	346.6	NA	[72]
(*E*)-$Ar_2Ge{=}GeAr_2$ (**B**) [Ar = 2-Bu^t-4,5,6-Me_3-C_6H]	2.2521(8)	360.0	20.4	[73]
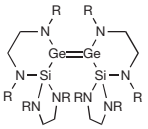 (*Z*)-isomer (B) [R = Bu^t]	2.454(2)	337.6 338.7	22.3	[74]
 (*E*) -isomer (B) [R = Bu^t, R′ = Pr^i]	2.460(1)	331.5	63.0	[75]
$Ar_2Ge{=}GeAr_2$ (**B**) [Ar = 2,5-Bu^t_2-C_6H_3]	2.3643(4)	NA	NA	[76]
(*E*)-Bbt(Br)Ge=Ge(Bbt)Br (**B**)	2.5087(7)	332.6	NA	[77]
(*E*)-R(Ar)Ge=Ge(R)Ar (**B**) [Ar = 2,6-Pr^1_2-C_6H_3)$_2$-C_6H_3] R = Me_3Si–C≡C	2.3224(4) 2.3239(3)	341.9 342.5	NA NA	[78]
R = Bu^t–C≡C (Z)-Mes(Ar)Ge=Ge(Mes)Ar (**C**) [Ar = 2,6-Pr^i_2-C_6H_3]	2.301(1)	345.5	7.0	[79]
(Pr^i_2MeSi)$_2$Ge=Ge(SiMePr^i_2)$_2$ (**C**)	2.267(1)	359.6	00	[80]
(Pr^i_3Si)$_2$Ge=Ge($SiPr^i_3$)$_2$ (**C**)	2.298(1)	357.0	0.0	[80]
(E)-Tbt(Mes)Ge=Ge(Tbt)Mes (**C**)	2.416(2)	355.3 356.6	NA	[81b]
(Bu^t_2MeSi)$_2$Ge = Ge(SiMeBu^t_2)$_2$ (**C**)	2.346 (2)	358.8 359.2	52.8	[82]
(*E*)-Ar(H)Ge = Ge(Ar)H (**D**) [Ar = 2,6-(2,6-Pr^i_2-C_6H_3)$_2$-C_6H_3]	2.3026(3)	NA	NA	[83a]
Ar·G·e=Ge(←:CNBu^t)Ar (**D**)[Ar = 2,6-(2,6-Pr^i_2-C_6H_3)$_2$-C_6H_3]	2.3432 (9)	360.0 (three-coordinate Ge)	NA	[84]

NA = not available.

reaction is believed to proceed through the intermediate formation of bicyclo[1.1.0]butane derivatives, followed by their rapid room-temperature isomerization to more stable heavy cyclopropene analogs (**Scheme 19**).

Similar to the case of cyclotrisilenes, the Ge=Ge bonds in cyclotrigermenes are slightly shorter than those of acyclic tetrasilyldigermenes: 2.239(4)–2.2743(8) Å versus 2.267(1)–2.298(1) Å (**Tables 3** and **4**). The longest Ge=Ge bonds were found in halogen-substituted cyclotrigermenes (2.2721(6)–2.2743(8) Å), which was explained by the notable $\pi_{Ge=Ge}$–σ^*_{Ge-X} orbital mixing facilitated by the electronegative halogens at the sp^3-Ge.

Typically, cyclotrigermenes showed the expected *trans*-bending at the sp^2-Ge, apart from the $(Me_3Si)_3Si$-, Br-, and I-substituted cyclotrigermenes, which showed unusual *cis*-bending at the Ge=Ge bond resulting from the electronic and steric interplay with the substituents at the sp^3-Ge.

Most cyclotrigermenes featured remarkable twisting about the Ge=Ge bond: from 8.1° to 51.0° (Table 3). Cyclotrigermene substituted with the bulky Bu^t_2MeSi groups (Scheme 18) showed a record twisting of the skeletal Ge=Ge bond in heavy cyclopropenes (59.7°).

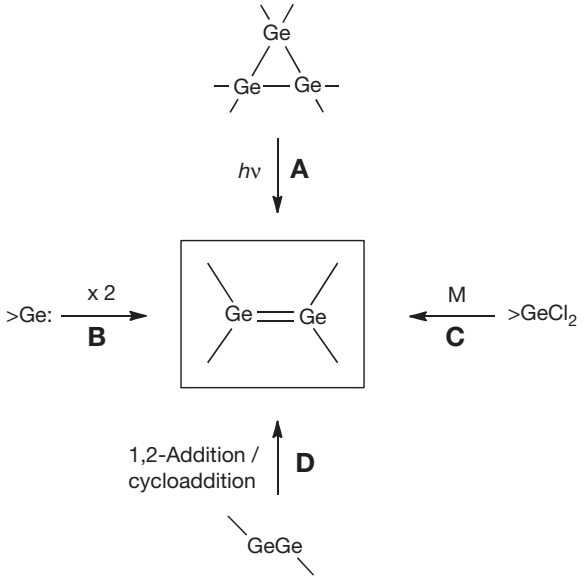

Scheme 14 Major synthetic routes to the stable digermenes >Ge=Ge<.

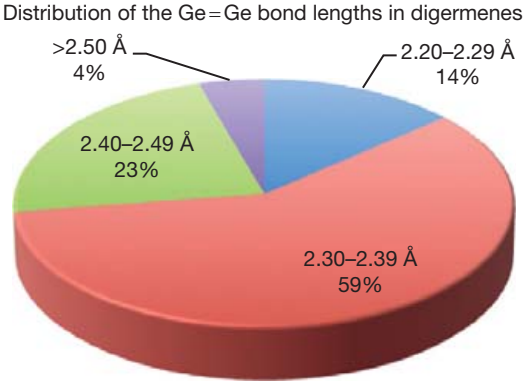

Figure 4 Distribution of the Ge=Ge double-bond lengths in the stable digermenes.

1.11.2.1.2.3.2 Four-membered ring compounds (heavy cyclobutenes) Three heavy cyclobutenes featuring an endocyclic Ge=Ge bond have been reported (Table 4).

The first four-membered ring cyclic digermene, disiladigermacyclobutene, was unexpectedly formed upon the ring expansion of either 3*H*- or 1*H*-disilagermirenes with $GeCl_2$·diox complex (Scheme 20).[90]

Overall, such a reaction represents a rather curious transformation of a Si=Si (or Si=Ge) bond of the starting disilagermirenes into a Ge=Ge bond of the final product, exemplifying a way of making a digermene from a disilene (or a silagermene). The doubly bonded germaniums in disiladigermacyclobutene are rather insignificantly pyramidalized with the sum of the bond angles around them amounting to 357.2° and 358.6° (Table 4). The Ge=Ge bond in disiladigermacyclobutene of 2.2911(4) Å is one of the longest reported for cyclic digermenes, whereas the skeletal Ge–Si bonds in the same compound are notably squeezed and the Si–Cl bonds are stretched. Such structural peculiarities can be best described by $\pi_{Ge=Ge}$–σ^*_{Si-Cl} orbital mixing, facilitated by the presence of electronegative chlorines and folding of the Ge_2Si_2-ring (28.3°) favoring such hyperconjugative interaction.

Likewise, reaction of the readily available cyclotrigermene (Scheme 18) with the $GeCl_2$·diox complex resulted in the formation of the first homonuclear heavy cyclobutene analog, tetragermacyclobutene (Scheme 21).[92]

The extent of pyramidalization at the sp^2-Ge atoms (354.4° and 356.4°) in tetragermacyclobutene is similar to that of disiladigermacyclobutene (357.2° and 358.6°), and the Ge=Ge bond of 2.2993(5) Å in the former compound is just marginally longer than 2.2911(4) Å in the latter (Table 4).

The heavy cyclobutene with an endocyclic Ge=Ge bond within the Ge_3C four-membered ring skeleton was made by a different pathway, namely, the reaction of tetragermabuta-1,3-diene Tip_2Ge=Ge(Tip)–Ge(Tip)=$GeTip_2$ with 2-methoxyphenyl isocyanide (Scheme 22).[91] For this cyclic digermene, the Ge=Ge bond distance of 2.2808(7) Å was reported, which was slightly shorter than those of the above-described disiladigermacyclobutene and tetragermacyclobutene (Table 4).

1.11.2.1.2.3.3 Five-membered ring compounds (heavy cyclopentenes) Two five-membered ring heavy cyclopentenes with skeletal Ge=Ge bonds were prepared by the [1+4]-cycloaddition reactions of chalcogens (sulfur or selenium) with the tetragermabuta-1,3-diene Tip_2Ge=Ge(Tip)–Ge(Tip)=$GeTip_2$ (Scheme 23 and Table 4).[91,93] These compounds, like their silicon counterparts (see Scheme 9), exhibited Ge=Ge bonds of 2.2841(5) and 2.2975(5) Å, which are longer than those in the cyclotrigermenes but similar to those in the cyclotetragermenes (Table 4). The pyramidalization at the sp^2-Ge atoms in the heavy cyclopentenes with an endocyclic Ge=Ge

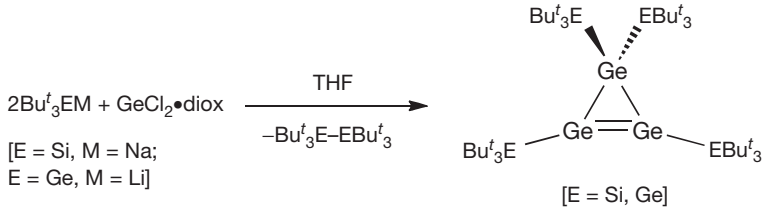

Scheme 15 Synthesis of the first isolable cyclotrigermenes.

Table 4 Crystallographic parameters of the structurally characterized cyclic digermenes.

Cyclic digermene	*>Ge=Ge< [Å]*	*∑(Ge) [°]*	*>Ge=Ge< twist [°]*	*Ring Folding [°]*	*Reference*
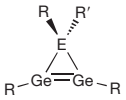					
[E = Ge; R = R′ = $SiBu^t_3$]	2.239(4)	359.9	0.0		[85]
[E = Ge; R = $SiBu^t_3$, R′ = $Si(SiMe_3)_3$]	2.264(2)	358.7 359.8	8.1		[86]
[E = Ge; R = $SiBu^t_3$, R′ = Cl]	2.2723(8)	357.2 359.3	29.7		[87]
[E = Ge; R = $SiBu^t_3$, R′ = Br]	2.2743(8)	343.7 359.4	34.9		[87]
[E = Ge; R = $SiBu^t_3$, R′ = I]	2.2721(6)	344.8 359.6	35.3		[87]
[E = Si; R = R′ = $SiMeBu^t_2$]	2.2429(6)	353.8 354.2	51.0		[88a]
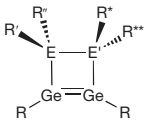					
[E = E′= Si; R = R′ = R** = $SiMeBu^t_2$; R″ = R* = Cl]	2.2911(4)	357.2 358.6	NA	28.3	[90]
[E = Ge, E′ = C; R′ = R′ = Tip; R* + R**: = N–(2-MeO-C_6H_4)]	2.2808(7)	NA	NA	NA	[91]
[E = E′= Ge; R = R′ = R** = $SiMe\ Bu^t_2$; R″ = R* = Cl]	2.2993(5)	354.4 356.4	NA	24.4 24.6	[92]
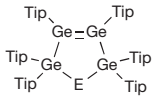					
[E = S]	2.2841(5)	348.4 351.4	NA	NA	[93]
[E = Se]	2.2975(5)	349.2 349.9	NA	NA	[91]

NA = not available.

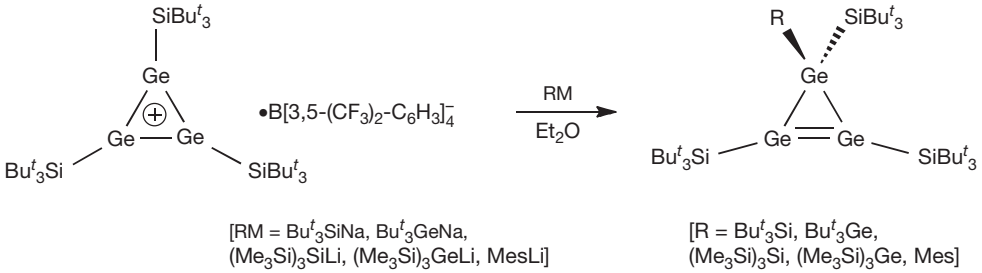

[RM = Bu^t_3SiNa, Bu^t_3GeNa, $(Me_3Si)_3SiLi$, $(Me_3Si)_3GeLi$, MesLi]

[R = Bu^t_3Si, Bu^t_3Ge, $(Me_3Si)_3Si$, $(Me_3Si)_3Ge$, Mes]

Scheme 16 Synthesis of the unsymmetrically substituted cyclotrigermenes.

bond was notable (348.4/351.4° and 349.2/349.9°), whereas the Ge_4C five-membered rings were only insignificantly folded (Table 4).

1.11.2.1.3 Distannenes >Sn=Sn< [67b,d,e]

1.11.2.1.3.1 Synthesis

Tetraalkyldistannene $Dsi_2Sn{=}SnDsi_2$ was the very first structurally characterized analog of an alkene of the heavy group 14 elements, reported by Lappert and coworkers as early as 1976.[68a,b,c,e] Distannene was synthesized by the same method as that used for the preparation of the first stable digermene (see above), namely, by the reaction of the stable bis(amino)stannylene $[(Me_3Si)_2N]_2Sn$: with DsiLi. Like the above-described digermene $Dsi_2Ge{=}GeDsi_2$, distannene $Dsi_2Sn{=}SnDsi_2$ showed a notable pyramidalization at the sp^2-Sn atoms (sum of the bond angles 342°) and nontwisted Sn=Sn bond (twist angle 0°). In the distannene, the Sn=Sn double bond of 2.764(2)Å was remarkably long, being quite comparable to typical Sn–Sn single bonds. Similar to the isostructural digermene $Dsi_2Ge{=}GeDsi_2$, distannene

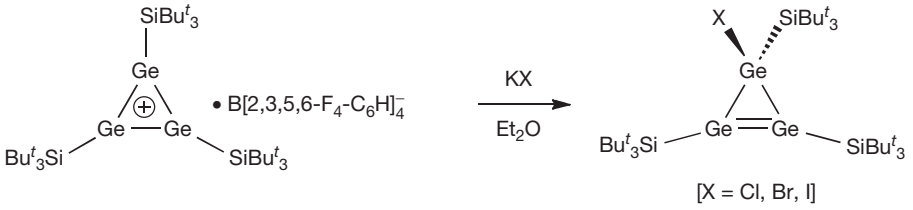

Scheme 17 Synthesis of the halogen-substituted cyclotrigermenes.

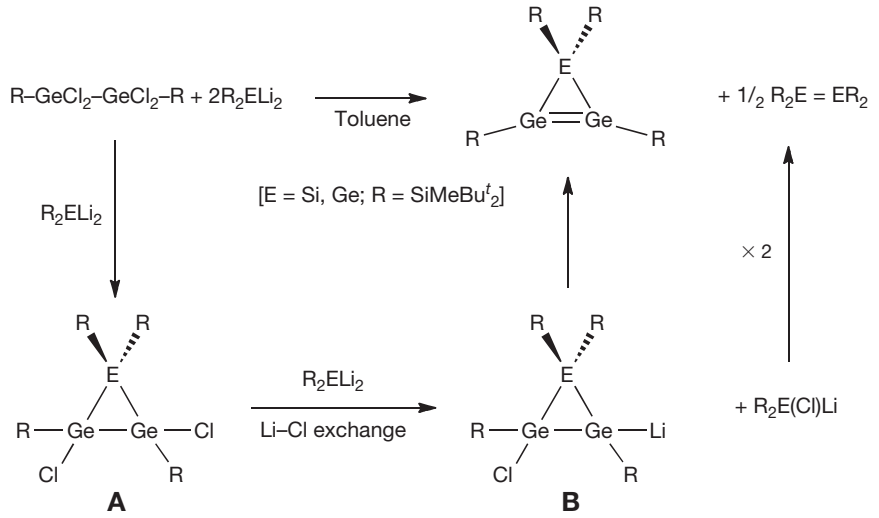

Scheme 18 Synthesis of the 1*H*-siladigermirene and cyclotrigermene.

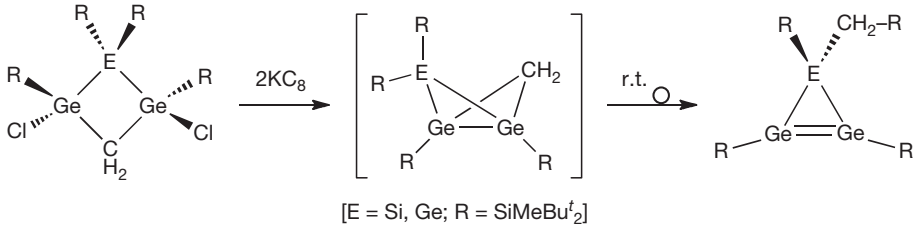

Scheme 19 Synthesis of the homologs of 1*H*-siladigermirene and cyclotrigermene.

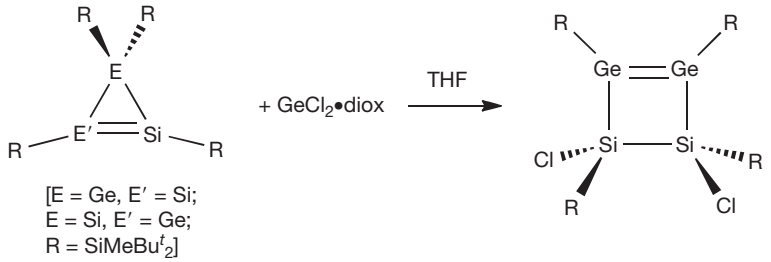

Scheme 20 Synthesis of the first four-membered ring cyclic digermene.

Dsi$_2$Sn=SnDsi$_2$ retained its structural integrity only in the solid state, whereas in solution it dissociated into a pair of stannylenes Dsi$_2$Sn:.

Since the first report on Lappert's distannene, 11 other stable distannenes (including three distannenes with an endocyclic Sn=Sn bond) have been isolated and structurally characterized (Table 5). They are available by one of three general procedures: (1) photolysis of cyclotristannanes (**A**); (2) dimerization of stannylenes (**B**); and (3) ligand redistribution between the homoleptic stannylenes R$_2$Sn: and R′$_2$Sn: to

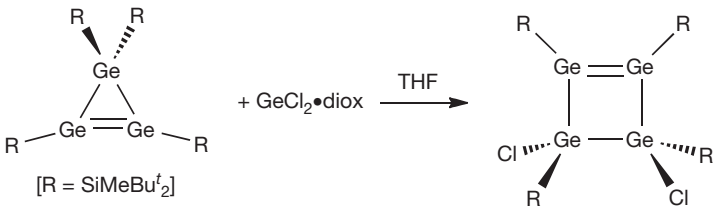

Scheme 21 Synthesis of the first tetragermacyclobutene.

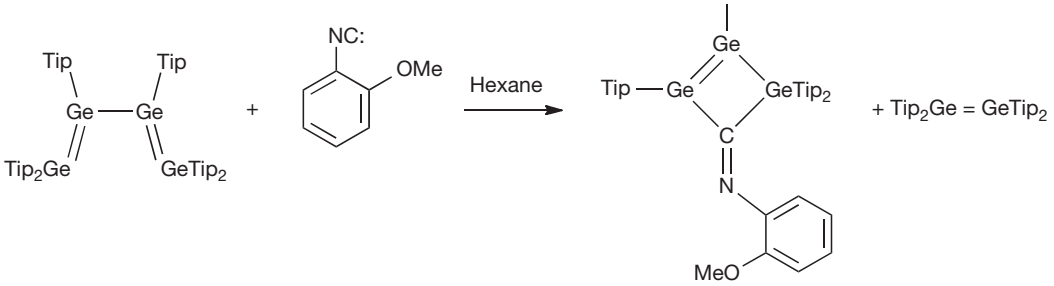

Scheme 22 Synthesis of the trigermacyclobutene featuring an endocyclic Ge=Ge bond.

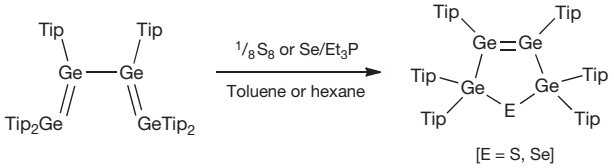

Scheme 23 Synthesis of heavy cyclopentenes with an endocyclic Ge=Ge bond.

form heteroleptic stannylenes RR′Sn:, followed by their dimerization (**C**) (Scheme 24).

As in the case of stable disilenes and digermenes, method **A** was introduced and developed for the preparation of tetraaryldistannenes, for example, $Tip_2Sn{=}SnTip_2$ by the photolysis of the hexaarylcyclotristannane *cyclo*-(Tip_6Sn_3).[94] The Sn=Sn bond in this distannene was proved to remain intact in the condensed phase, as was demonstrated by its ^{119}Sn NMR resonance observed at 427.3 ppm. By the dimerization of transient stannylenes (method **B**), several stable distannenes were prepared, including tetraaryl-, tetrasilyl-, and mixed dialkyldiaryl- and diaryldisilyldistannenes. All of these distannenes >Sn=Sn<, except for the tetrasilyldistannene ($Bu^t_2MeSi)_2Sn{=}Sn(SiMeBu^t_2)_2$, dissociate in solution into monomeric stannylenes >Sn:. Redistribution of ligands forms heteroleptic stannylenes RR′Sn:, followed by their dimerization (method **C**) was mostly employed for the synthesis of distannenes with the mixed diaryldisilyl-substitution pattern. Distannenes prepared by this method also dissociate in solution into monomeric stannylenes.

1.11.2.1.3.2 ^{119}Sn NMR spectroscopy of distannenes

^{119}Sn NMR spectroscopy is a very useful tool to elucidate the structure of distannenes in solution. From Table 5, it can be seen that the ^{119}Sn NMR resonances of the isolable acyclic distannenes in solution were observed at a very low field, well above +1000 ppm, which is in the region more typical of monomeric stannylenes than of dimeric distannenes. This observation indicates dissociation (at least partial) of the >Sn=Sn< bond of distannenes into the stannylenes >Sn:. Accordingly, all of these tin–tin doubly bonded derivatives showed solution reactivity characteristic of stannylenes but not of distannenes. Only the tetraaryldistannene $Tip_2Sn{=}SnTip_2$ was claimed to behave as a distannene with a real Sn=Sn bond (see above); however, it was not isolated as an individual compound.[94] To date, the only isolable acyclic distannene for which the presence of an authentic Sn=Sn double bond both in the solid state and in solution was reliably established is tetrasilyldistannene $(Bu^t_2MeSi)_2Sn{=}Sn(SiMeBu^t_2)_2$ made by the reaction of silyl sodium derivative $Bu^t_2MeSiNa$ with $SnCl_2$·diox complex in tetrahydrofuran (THF).[99] The tin signal was observed at 630.7 ppm, which is in the region expected for the >Sn=Sn< bond in distannenes but clearly beyond the range of stannylene >Sn: resonances. This was further corroborated by the reactivity studies of $(Bu^t_2MeSi)_2Sn{=}Sn(SiMeBu^t_2)_2$ in solution; it reacted exclusively as a distannene but not as a stannylene.

1.11.2.1.3.3 Crystal structure of distannenes

The lengths of the Sn=Sn double bond in distannenes are found in the range 2.67–2.91 Å, with the most abundant set fitting within the 2.78–2.83 Å interval (34%), values that are nearly equal to (or even longer than) those of standard Sn–Sn single bonds (Figure 5 and Table 5). Moreover, the experimental values of 2.78–2.83 Å for the Sn=Sn bond are notably greater than the sum of the Sn atoms' double-bond covalent radius of 2.60 Å,[45] being quite comparable to the sum of the single-bond covalent radii for the two Sn atoms of 2.80 Å.[46] The two double-bond extremes in distannenes are represented by the shortest (and strongest) Sn=Sn bond of 2.6683(10) Å in tetrasilyldistannene $(Bu^t_2MeSi)_2Sn{=}Sn(SiMeBu^t_2)_2$[99] and the longest bond of 2.910(1) Å in tetraaryldistannene $Ar_2Sn{=}SnAr_2$ (Ar = 2-Bu^t-4,5,6-Me$_3$C$_6$H)[96] (Table 5).

In accord with the general trends on descending group 14, distannenes manifested stronger pyramidalization at the doubly bonded Sn atoms than that of disilenes and digermenes. As expected, tetraaryl- and tetraalkyldistannenes showed

Table 5 Crystallographic and spectral parameters of the structurally characterized distannenes.

Distannene (Synthetic Method)	*>Sn=Sn< [Å]*	*Σ(Sn)[°]*	*>Sn=Sn< twist [°]*	*^{29}Sn NMR (ppm)*	*Reference*
$Dsi_2Sn{=}SnDsi_2$ (**B**)	2.764(2)	342.0	0.0	NA	[68a,b,c, e]
(*E*)-Ar(R)Sn=Sn(Ar)R (**B**) [R = CH_2(4-Bu^t-C_6H_4; Ar = 2,6-(2,6-Pr$^i_2$-C_6H_3)$_2$-C_6H_3]	2.7705(8)	329.7	NA	1205.7	[95]
$Ar_2Sn{=}SnAr_2$ (**B**) [Ar = 2-Bu^t-4,5,6,-Me_3C_6H]	2.910(1)	320.9 354.9	44.0	1401.0 (sol.) 819.0 (CP-MAS)	[96]
$[(Me_3Si)_3Si]_2Sn{=}Sn[Si(SiMe_3)_3]_2$ (**B**)	2.8247(6)	352.0	63.2	NA	[97,98b]
(*E*)-Mes[$(Me_3Si)_3Si$] Sn=Sn(Mes)[$Si(SiMe_3)_3$] (**B**)	2.7023(8)	NA	NA	NA	[98]
(Bu$^t_2$MeSi)$_2$Sn=Sn(SiMeBu$^t_2$)$_2$ (**B**)	2.6683(10)	360.0	44.6	630.7	[99]
(*E*)-R(Ar)Sn=Sn(R)Ar (**B**) [Ar = 2,6-(2,6-Pr$^i_2$-C_6H_3)$_2$-C^{6}H^3] R = $Me_3Si{-}C{\equiv}C$	2.85126 (19)	325.4	NA	381.0	[78]
(*E*)-Ar[$Me_3Si)_3$ Si]Sn=Sn(Ar)[$Si(SiMe_3)_3$] [Ar = 2,4,6-$(CF_3)_3$-C_6H_2] (**C**)	2.833(1)	337.9	NA	NA	[100]
(*E*)-Ar[$Me_3Si)_3Si$]Sn=Sn(Ar)[$Si(SiMe_3)_3$] [Ar = 2-Bu^t-4,5,6-Me_3-C_6H] (**C**)	2.7914(4)	337.4	NA	1506	[101]
Cyclic distannenes:					
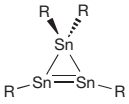 [R = $SiBu^t_3$] (2 independent molecules);	2.601 (3)/ 2.582(4)	350.8 355.8/ 359.6 360.0	NA	412.0	[102]
[R = $Si(SiMe_3)_3$]	2.575(4)	359.8 360.0	5.0	539.0	[103]
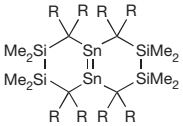 [R = $SiMe_3$] (two Sn atoms are disordered over two positions each)	2.689(5) 2.686(4)	352.2 354.0/ 352.7 353.7	27.0 28.6	544.5	[104]

Na = not available.

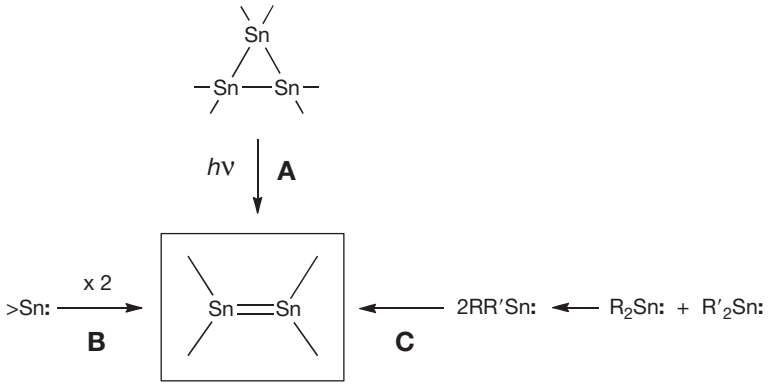

Scheme 24 Major synthetic routes to the stable distannenes >Sn=Sn<.

pyramidalization at their tin centers far greater than that of their tetrasilyl-substituted counterparts: 320.9° and 342.0° versus 360.0° (Table 5). Substitution with extraordinarily bulky substituents causes not only stretching of the Sn=Sn bond, but also its extreme twisting: from 44.0° to 63.2° (Table 5).

The above-described tetrasilyldistannene $(Bu^t_2MeSi)_2Sn{=}Sn(SiMeBu^t_2)_2$, featuring a genuine Sn=Sn double bond in the solid state and in solution, showed an unusual combination of structural characteristics caused by the presence of the very bulky electropositive silyl substituents.[99] Thus, it has a very short Sn=Sn bond of 2.6683(10) Å, which is highly twisted (44.6°) but nevertheless absolutely undistorted at the sp^2-Sn atoms (sum of the bond angles 360°) (Table 5). This unusual structural motif in distannene $(Bu^t_2MeSi)_2Sn{=}Sn(SiMeBu^t_2)_2$ (short, nonpyramidal, and highly twisted Sn=Sn bond), which has no precedent in distannene chemistry, was explained in terms of the out-of-plane interaction of the two triplet stannylenes (Scheme 25). The triplet state of bis(silyl) stannylene $(Bu^t_2MeSi)_2Sn$: might be accessible because of its relatively small singlet–triplet energy separation $\Delta E_{S-T} = 8.5$ kcal mol^{-1}, caused by the electronic effect of the σ-donating silyl-substituents and their large steric bulk.[99] Accordingly, deep-green distannene $(Bu^t_2MeSi)_2Sn{=}Sn(SiMeBu^t_2)_2$ showed a substantial red shift in its UV–Vis spectrum with $\lambda = 670$ nm (compare this value with 494 nm observed for $Tip_2Sn{=}SnTip_2$). Such a remarkable bathochromic shift in $(Bu^t_2MeSi)_2Sn{=}Sn(SiMeBu^t_2)_2$ was attributed to the extreme twisting of the Sn=Sn bond destabilizing its HOMO because of: (1) $5p_\pi$–$5p_\pi$(Sn=Sn)–σ(Sn–Si) orbital mixing and (2) reduced $5p_\pi$–$5p_\pi$ orbital overlap taking place upon twisting.

1.11.2.1.3.4 Cyclic distannenes with an endocyclic Sn=Sn bond

Only three compounds of this type have been synthesized: two three-membered rings and one six-membered ring.

The very first cyclotristannene *cyclo*-$(Bu^t_3Si)_4Sn_3$, as the tin analog of cyclopropene, was prepared by the reaction of silylsodium derivative Bu^t_3SiNa and stannylene $(Bu^tO)_2Sn$: (Scheme 26 and Table 5).[102]

Similar to the case of persilyl-substituted cyclotrisilenes (Table 2) and cyclotrigermenes (Table 4), cyclotristannene *cyclo*-$(Bu^t_3Si)_4Sn_3$ featured the shortest Sn=Sn bond among all structurally characterized distannenes of 2.601(3)/2.582 (4) Å (for two independent molecules) (Table 5).[102] However, one should be cautious when considering these Sn=Sn bond length values because of the poor x-ray crystallography refinement data ($R_1 = 0.17$). The doubly bonded Sn atoms in the cyclotristannene featured rather insignificantly distorted geometry: 350.8/355.8° and 359.6/360.0° (sum of the bond angles for the two independent molecules). In agreement with the short double bond and in contrast to most acyclic distannenes, cyclotristannene *cyclo*-$(Bu^t_3Si)_4Sn_3$ preserved its Sn=Sn bond in solution, as was manifested by the observation of the sp^2-Sn resonances at 412.0 ppm.

The second example of a stable cyclotristannene, *cyclo*-$[(Me_3Si)_3Si]_4Sn_3$, was also recently reported.[103] This novel cyclotristannene was formed upon the reaction of metastable SnBr (available by the cocondensation of Sn and HBr at 1240 °C) with $(Me_3Si)_3SiLi$ derivative. Although cyclotristannene was not isolated as an individual compound, cocrystallizing together with another product of the reaction, the metalloid cluster $Sn_{10}[Si(SiMe_3)_3]_6$, the structural parameters of the former can be discussed. The endocyclic Sn=Sn bond in the cyclotristannene *cyclo*-$[(Me_3Si)_3Si]_4Sn_3$ represents a record shortening for all distannenes (both cyclic and acyclic): 2.575 (4) Å. Such extreme shortening of the Sn=Sn bond was attributed to its planar arrangement induced by the steric bulk of the four voluminous $(Me_3Si)_3Si$-substituents. Such remarkable planarity around the Sn=Sn bond can be seen in its negligible twisting (twist angle 5°) and nonpyramidalized geometry of the doubly bonded Sn atoms (sum of the bond angles 359.8° and 360.0°). The resonance of the sp^2-Sn atoms in cyclotristannene was observed in a low-field region at 539.0 ppm, as expected.

A bicyclic distannene, in which the bridging Sn=Sn bond is embedded between the two six-membered rings, was synthesized by the reaction of the 1,4-dipotassiotetrasilane with bis(amino)stannylene $[(Me_3Si)_2N]_2Sn$: (Scheme 27).[104] The reaction is believed to proceed through the initial formation of the intermediate five-membered ring cyclic stannylene, followed by its dimerization giving distannene with an exocyclic

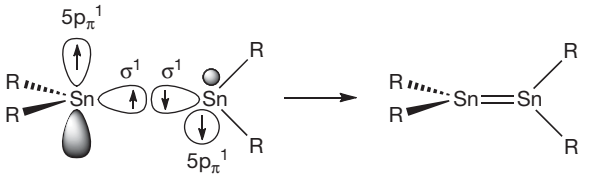

Scheme 25 Orbital interaction mode in tetrasilyldistannene $(Bu^t_2MeSi)_2Sn{=}Sn(SiMeBu^t_2)_2$: out-of-plane interaction of the two triplet stannylenes resulting in the formation of a highly twisted but not *trans*-bent Sn=Sn bond.

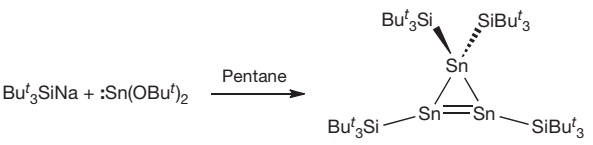

Scheme 26 Synthesis of the first isolable cyclotristannene.

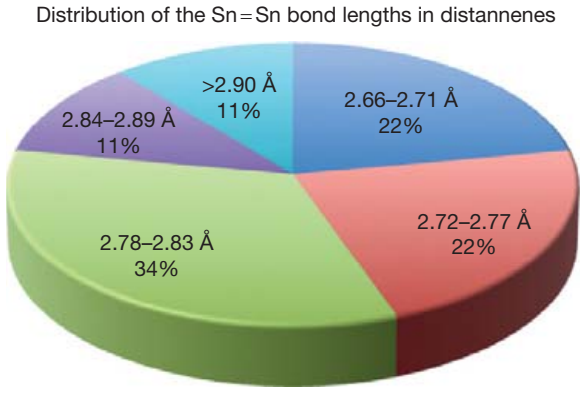

Figure 5 Distribution of the Sn=Sn double-bond lengths in the stable distannenes.

Sn=Sn bond, which finally isomerized via double 1,2-silyl migrations accompanied by ring expansion to form the final product.

This bicyclic distannene showed a low-field ^{119}Sn NMR resonance of 544.5 ppm in the region expected for the sp^2-Sn centers. Its longest wavelength UV–Vis absorption was observed at 626 nm, a value that is close to the 670 nm previously reported for the acyclic distannene $(Bu^t_2MeSi)_2Sn{=}Sn(SiMeBu^t_2)_2$. Although the crystal structure was reported for the bicyclic distannene, it should be discussed with some caution because of the low quality of its refinement data (both Sn atoms are positionally disordered over two positions in a ratio of 52:48, $R_1 = 0.12$): 2.686(4)/2.689(5) Å (Sn=Sn bond length); 352.2° and 354.0°/352.7° and 353.7° (sum of the bond angles around Sn atoms); and 27.0°/28.6° (Sn=Sn bond twist angle).

Apart from the distannenes featuring an authentic Sn=Sn bond (at least, in the solid state), there are some organotin compounds with tricoordinate tin centers, which manifest very long tin–tin separations and cannot be classified as true distannenes. Among them are compounds, which can be considered as the weakly bound stannylene dimers, zwitterionic structures $[R_2Sn:]^{\delta+}{\rightarrow}[\dot{S}nR_2']^{\delta-}$ with a single dative bond between the two greatly different stannylene units: Lewis basic electron donor and Lewis acidic electron acceptor. Moreover, given the rather shallow potential energy surface of the R_4Sn_2 derivatives, one can suggest the existence of structural isomers other than the distannenes $R_2Sn{=}SnR_2$, such as stannylstannylene, singly, doubly, and quadruply bridged structures, with some of them being recently experimentally realized (for a discussion, see Ref. [4d]).

1.11.2.1.4 Diplumbenes >Pb=Pb< [67d,e]

1.11.2.1.4.1 Synthesis

The classification of the double bond between the heavy group 14 elements based on the length of this bond becomes progressively more and more problematic descending group. For example, the lead–lead separations of 2.903–3.947 Å found between tricoordinate Pb centers, which formally can be viewed as doubly bonded, are notably longer than the standard lead–lead single bonds. Such compounds, depending on the degree of the lead–lead separation, are classified sometimes as diplumbenes with a >Pb=Pb< double bond and sometimes as plumbylene dimers with a weak association between two plumbylene monomers. However, the distinction between these two classes is very subtle, and the border between them is rather formal. In accord with the very long and weak double dative bonds between two plumbylene units in either diplumbenes or plumbylene dimers, all of them undergo easy dissociation in solution forming monomeric plumbylenes. The weakness of such donor–acceptor interaction between plumbylenes to form their dimers is due to the relativistic contraction of the lead valence s-orbital, increasing the energy gap between the s- and p-orbitals and limiting the availability of s-electrons for lead–lead bonding.

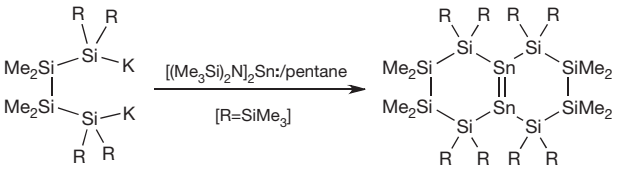

Scheme 27 Synthesis of a bicyclic distannene with an endocyclic Sn=Sn bond.

The first compound with a structurally authenticated double bond between the two tricoordinate lead atoms, tetrakis (2,4,6-triisopropylphenyl)diplumbene $Tip_2Pb{=}PbTip_2$, was prepared by the reaction between aryl Grignard reagent TipMgBr and $PbCl_2$ (Scheme 28).[105]

In accord with the general trend of progressive weakness of the double-bond descending group 14, diplumbene $Tip_2Pb{=}PbTip_2$ exhibited a lead–lead separation of 3.0515 (3) Å, which was slightly longer than that calculated for the parent $H_2Pb{=}PbH_2$, being quite comparable to (or even longer than) those of standard Pb–Pb single bonds. Accordingly, diplumbene showed remarkable pyramidalization at the doubly bonded lead atoms (sum of the bond angles 325.4°/330.1°) and moderate twisting of the Pb=Pb bond of 21.7° (Table 6).

To date, four stable compounds have been classified as diplumbenes and the other four as plumbylene dimers. These two classes of organolead derivatives, marginally distinguished by the degree of lead–lead separation, were prepared by one of two general synthetic procedures: (1) dimerization of homoleptic plumbylenes (**A**) and (2) dimerization of heteroleptic plumbylenes (**B**) (Scheme 29). No compounds featuring an endocyclic Pb=Pb double bond have been isolated to date.

Apart from the diplumbene $Tip_2Pb{=}PbTip_2$, only $MgBr_2$-stabilized plumbylene dimer $\{Mes_2Pb{\cdots}[Br{-}Mg(THF)_4{-}Br]\}_2$ has been prepared by method **A**, by the reaction of MesMgBr with $PbCl_2$. All other derivatives, either diplumbenes or plumbylene dimers featuring a greater or lesser extent of double-bond character between the two lead centers, have been synthesized by the dimerization of heteroleptic plumbylenes (method **B**).

1.11.2.1.4.2 ^{207}Pb NMR spectroscopy of diplumbenes

Because all diplumbenes or plumbylene dimers readily dissociate in solution into the monomeric plumbylenes because of the inherent weakness of the lead–lead bond (see above), they showed either no signals or very low field ^{207}Pb NMR resonances above +7000 ppm, indicative of monomeric plumbylenes >Pb: rather than dimeric diplumbenes >Pb=Pb< (Table 6).

1.11.2.1.4.3 Crystal structure of diplumbenes

Structural data have been reported for the tetraaryl-, aryl(alkyl)-, and aryl(silyl)diplumbenes and plumbylene dimers (Table 6). The lead–lead separation in these compounds spans a very broad range of more than 1 Å: from 2.9031(11) to 3.947(1) Å (from 2.9031(11) to 3.1601(6) Å (for diplumbenes) and from

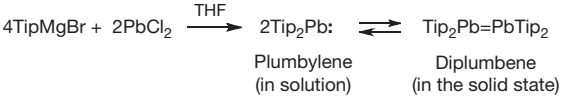

Scheme 28 Synthesis of the first stable diplumbene $Tip_2Pb{=}PbTip_2$.

Table 6 Crystallographic and spectral parameters of the structurally characterized diplumbenes.

Diplumbene or plumbylene dimer	*>Pb=Pb< [Å]*	*∑(Pb) [°]*	*>Pb=Pb< twist [°]*	*^{207}Pb NMR (ppm)*	*Reference*
$Tip_2Pb{=}Pb\ Tip_2$	3.0515(3)	325.4 330.1	21.7	NA	[105]
(*E*)-Tip[$(Me_3Si)_3Si$]Pb=Pb(Tip) [$Si(SiMe_3)_3$]	2.9899(5)	339.0	NA	NA	[106]
(*E*)-Mes[$(Me_3Si)_3Si$]Pb=Pb(Mes) [$Si(SiMe_3)_3$]	2.9031(11)	NA	NA	NA	[98]
(*E*)-Ar(Me)Pb=Pb(Ar)Me (Ar = 2,6-(2,6-$Pr^i_2C_6H_3)_2$-C_6H_3)	3.1601(6)	322.7	0.0	8738.0	[107]
(*E*)-[Ar[$(Me_3Si)_3Si$]Pb]$_2$ (Ar = 2,4,6-$(CF_3)_3$-C_6H_2) [*plumbylene dimer*]	3.537(1)	336.8	NA	NA	[100]
(*E*)-[Ar[$(Me_3Si)_3Si$]Pb]$_2$ (Ar = 2-Bu^t-4,5,6-Me_3C_6H) [*plumbylene dimer*]	3.3695(11)	NA	NA	7545.0	[108]
{Mes_2Pb[BrMg$(thf)_4$Br]}$_2$ [*plumbylene dimer*]	3.3549(6)	NA	NA	NA	[106]
[Ar(Ar')Pb]$_2$ (Ar = 2,6- (2,6-Pr^i_2-$C_6H_3)_2$-C_6H_3; Ar′ = 4-Bu^t-C_6H_4) [*plumblylene dimer*]	3.947(1)	NA	74.2	7275.0	[107]

NA = not available.

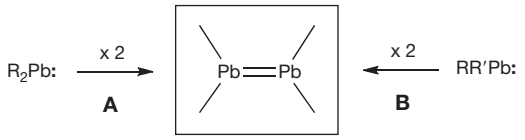

Scheme 29 Major synthetic routes to the stable diplumbenes >Pb=Pb<.

3.3549(6) to 3.947(1)Å (for plumbylene dimers)). It should be noted that all of these Pb–Pb distances are substantially longer than the usual Pb–Pb single bonds. Both diplumbenes and plumbylene dimers manifested a remarkable *trans*-bending at the lead centers: from 322.7° to 339.0°. Depending on the degree of steric interaction between substituents, diplumbenes and plumbylene dimers showed either untwisted (twist angle 0.0°) or extremely twisted (twist angle 74.2°) Pb–Pb bonds.

The recently reported valence isomers of the diplumbenes or plumbylene dimers, such as plumbylplumbylene with a single bond between the divalent and tetravalent lead centers, are not discussed in this chapter.

1.11.2.2 Heteronuclear Derivatives

1.11.2.2.1 Silagermenes >Si=Ge< [4d,109]

1.11.2.2.1.1 Synthesis

The first representatives of stable silagermenes (known also as germasilenes) were synthesized only 12 years ago. Before that, in 1991, a metastable silagermene $Mes_2Si{=}GeMes_2$ was generated by either thermolysis or low-temperature photolysis of hexamesitylsiladigermirane.[110] Formation of a tetramesitylsilagermene, which was stable only below −70 °C, was proved by low-temperature NMR and UV measurements (80.6 ppm for the sp^2-Si and 414 nm for the π–$\pi^*_{Si=Ge}$ electronic transition), as well as its quenching with methanol to form the 1,2-addition product $Mes_2(MeO)Si$–$GeMes_2H$. At room temperature, $Mes_2Si{=}GeMes_2$ underwent irreversible 1,2-Mes-migration from germanium to silicon forming silylgermylene $Mes_3Si(Mes)Ge$:, subsequently quenched with Et_3SiH to give $Mes_3Si(Mes)Ge(H)SiEt_3$ as the trapping product.

The first isolable silagermene, 1*H*-disilagermirene with an endocyclic Si=Ge bond incorporated into a three-membered ring Si_2Ge-skeleton, was synthesized in 2000 by isomerization (either photochemical or thermal) of the above-described 3*H*-disilagermirene (see Scheme 3, E=Ge) with a skeletal Si=Si bond (Scheme 30).[51]

The driving force for such an isomerization is the thermodynamic preference for the silagermene over the disilene: theoretical calculations showed ca. 2.3 kcal mol^{-1} advantage in energy of the silagermene compared with the isomeric disilene. Computations also estimated the length of the cyclic Si=Ge bond in the model H_3Si-substituted 1*H*-disilagermirene as 2.178 Å,[51] which agrees excellently with the sum of the Si and Ge atom double-bond covalent radii of 2.180 Å.[45] The doubly bonded Si atom in 1*H*-disilagermirene resonated in the diagnostic low-field region of 100.7 ppm.

Thermal isomerization of the isolable disilagermabicyclo[1.1.0]butane produced a novel 1*H*-disilagermirene as the nearest homolog of the above-described 1*H*-disilagermirene (see Scheme 30), featuring a more deshielded sp^2-Si center resonating at 126.6 ppm (Scheme 31).[111]

The first structural authentication of the Si=Ge bond was achieved in the five-membered ring 1,2-disila-3-germacyclopenta-2,4-diene prepared by the reaction of 1*H*-disilagermirene with phenylacetylene (Scheme 30).[112] The Si=Ge double bond in the 1,2-disila-3-germacyclopenta-2,4-diene was twisted by 38.6°, and its length of 2.250(1)Å was between those of typical Si=Si and Ge=Ge bonds, being notably longer than the estimates of 2.178 and 2.180 Å (see above) because of the steric hindrances caused by the bulky substituents. The doubly bonded silicon atom in the 1,2-disila-3-germacyclopenta-2,4-diene was observed in the low-field region at 124.2 ppm, as expected.

The other two examples of stable silagermenes, $(Bu^t_2MeSi)_2Si{=}GeMes_2$[113] and $(Bu^t_3Si)_2Si{=}GeMes_2$,[114] were prepared by the coupling of 1,1-dilithiosilane derivatives R_2SiLi_2 (R=$SiMeBu^t_2$, $SiBu^t_3$) with dichlorodimesitylgermane Mes_2GeCl_2. Both silagermenes exhibited unusually shielded sp^2-Si centers, observed at 22.4 and 18.7 ppm, respectively. This observation was explained by the 'push–pull' substitution pattern (electron-donating groups on Si and electron-withdrawing groups on Ge), altering the inherent $Si^{\delta+}=Ge^{\delta-}$ bond polarity to a reversed $Si^{\delta-}=Ge^{\delta+}$. This conclusion was further corroborated by the regioselectivity of MeOH addition to $(Bu^t_2MeSi)_2Si{=}GeMes_2$ to form a single regioisomer

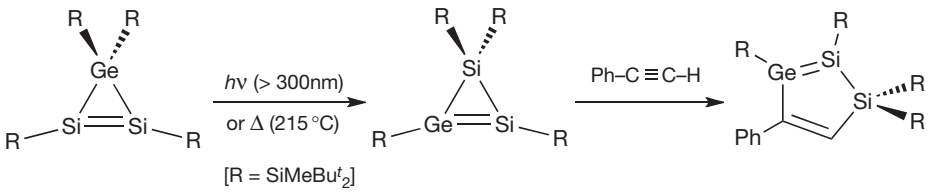

Scheme 30 Synthesis of the first stable silagermenes.

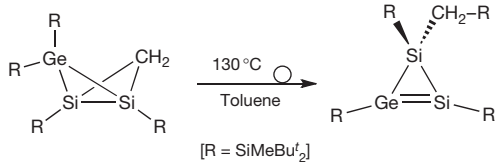

Scheme 31 Synthesis of the novel 1*H*-disilagermirene.

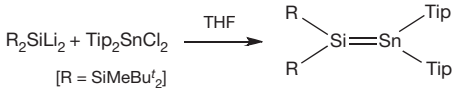

Scheme 32 Synthesis of the first silastannene.

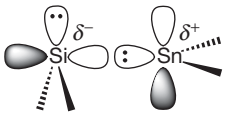

Scheme 33 Bonding interaction mode in the stable silastannene.

$(Bu^t_2MeSi)_2(H)Si–Ge(OMe)Mes_2$.[113] The Si=Ge bond in the silagermene $(Bu^t_3Si)_2Si=GeMes_2$ of 2.2769(8) Å was longer than that of the previously reported cyclic silagermene shown in Scheme 30 (2.250(1) Å), apparently because of the severe steric repulsions in the former.[114] Such important steric hindrances in $(Bu^t_3Si)_2Si=GeMes_2$ were also manifested in the notable twisting of its Si=Ge bond by 24.7°, which caused a remarkable red shift in its UV–Vis spectrum where the π–π* electronic transition was observed at 553 nm. The silagermene $(Bu^t_3Si)_2Si=GeMes_2$ undergoes thermal isomerization at 100 °C to a symmetrically substituted isomer (*E*)–[Mes$(Bu^t_3Si)Si=Ge(Mes)SiBu^t_3$].[114]

The latest example of a stable silagermene, $(Bu^tMe_2Si)_2Si=Ge(SiMe_2Bu^t)_2$, was synthesized by the reductive dehalogenation of the 1,2-dibromosilagermane $Br(Bu^tMe_2Si)_2Si–Ge(SiMe_2Bu^t)_2Br$ with sodium in toluene.[115] Because of the positional disorder between the doubly bonded Si and Ge atoms in silagermene $(Bu^tMe_2Si)_2Si=Ge(SiMe_2Bu^t)_2$, only the Si=Ge bond distance can be reliably discussed. Its value of 2.2208(4) Å is slightly shorter than those in the above-described 1,2-disila-3-germacyclopenta-2,4-diene (see Scheme 30) and $(Bu^t_3Si)_2Si=GeMes_2$ of 2.250(1)[112] and 2.2769(8) Å,[114] respectively. The geometry around the sp^2-Si and -Ge atoms in silagermene was nearly planar, and the Si=Ge double bond was insignificantly twisted by 7.5°. The isostructural digermene $(Bu^tMe_2Si)_2Ge=Ge(SiMe_2Bu^t)_2$, whose crystal data were also reported in the same paper, showed similar geometric characteristics: 2.2704(9) Å (Ge=Ge bond length), 360° (sum of the bond angles around Ge atoms), and 7.5° (Ge=Ge bond twist angle).[115] Featuring an identical silyl-substitution pattern at both Si and Ge atoms, silagermene $(Bu^tMe_2Si)_2Si=Ge(SiMe_2Bu^t)_2$ showed a highly deshielded resonance of its doubly bonded silicon center at 144.0 ppm, as expected.

Silagermenes, in which the Si=Ge bond is incorporated into an allenic fragment of the types >Si=Ge=Si< or >Ge=Si=Ge<, are discussed in Section 1.11.3.

1.11.2.2.2 Silastannenes >Si=Sn<[4d,109]

The sole example of an isolable silastannene $(Bu^t_2MeSi)_2Si=SnTip_2$ was reported in 2002, being prepared by the coupling of the 1,1-dilithiosilane derivative $(Bu^t_2MeSi)_2SiLi_2$ with the diaryldichlorostannane Tip_2SnCl_2 (Scheme 32).[116]

The silicon–tin double bond in the silastannene $(Bu^t_2MeSi)_2Si=SnTip_2$ is inversely polarized as $Si^{\delta-} = Sn^{\delta+}$ because of the 'push–pull' substitution pattern: electron donors on Si and electron acceptors on Sn (computations: −0.536 on Si and +1.400 on Sn (natural population analysis (NPA) charges of the model silastannene $(H_3Si)_2Si=SnPh_2$)). This was manifested in the remarkable deshielding of the sp^2-Sn (516.7 ppm) and shielding of the sp^2-Si (27.4 ppm). Such inversed Si=Sn bond polarization also altered the structure of the silastannene, which features a rather unusual bending pattern: the *trans*-bending at Si was unexpectedly much greater than that at Sn (26.2° vs. 9.6°), which was rationalized in terms of the nontraditional unsymmetrical donor–acceptor interaction mode (Scheme 33). Accordingly, the bending at the negatively polarized silicon part $Si^{\delta-}$ was expected to be more pronounced than that at the positively polarized tin fragment $Sn^{\delta+}$, which was indeed observed experimentally.

The Si=Sn double-bond length of 2.4188(14) Å in the silastannene $(Bu^t_2MeSi)_2Si=SnTip_2$ is intermediate between the typical values of Si=Si and Sn=Sn double bonds, being ca. 7% shorter than the standard Si–Sn single-bond length of 2.60 Å.[116] The Si=Sn bond in silastannene is notably twisted by 34.6°, demonstrating a high degree of steric interaction between the bulky substituents.

1.11.2.2.3 Germastannenes >Ge=Sn<[4d,109]

The first report on the transient germastannene $Mes_2Ge=SnTip_2$, generated by the reductive dehydrofluorination of the (fluorostannyl)germane $Mes_2(H)Ge–Sn(F)Tip_2$ with Bu^tLi, was published in 1996.[117] Because $Mes_2Ge=SnTip_2$ decomposed at room temperature to form a set of products including the three-membered ring germadistannirane *cyclo*-$(Mes_2Ge–Tip_2Sn–Tip_2Sn)$, its formulation as a germastannene was based on indirect evidence: observation of a low-field ^{119}Sn resonance at 360 ppm and trapping reactions with MeOH and PhCHO.

The first structurally authenticated germastannene $Tip_2Ge=SnTip_2$ was prepared by a simple one-pot reaction of TipMgBr, $GeCl_2$·diox complex and $SnCl_2$ (Scheme 34).[118]

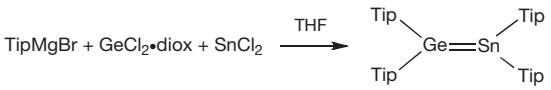

Scheme 34 Synthesis of the first structurally characterized germastannene.

The presence of the doubly bonded tin center was proved by its low-field resonance at 268.0 ppm in the ^{119}Sn NMR spectrum. The shortening of the Ge=Sn double bond of 2.5065(5) Å was ca. 4.6% compared with typical Ge–Sn single bonds, whereas the *trans*-bending at Sn was more pronounced (337.3°) than that at Ge (349.1°). Stable in the solid state, germastannene $Tip_2Ge{=}SnTip_2$ decomposed in solution forming cyclotristannane *cyclo*-$(Tip_2Sn)_3$ and digermene $Tip_2Ge{=}GeTip_2$.

By the same synthetic procedure used for the preparation of the above-described silastannene (see Scheme 32), a novel germastannene $(Bu^t_2MeSi)_2Ge{=}SnTip_2$ was synthesized by the reaction of the 1,1-dilithiogermane derivative $(Bu^t_2MeSi)_2GeLi_2$ and the diaryldichlorostannane Tip_2SnCl_2 (Scheme 35).[119] In the absence of x-ray crystallography data, this germastannene $(Bu^t_2MeSi)_2Ge{=}SnTip_2$ was identified by its diagnostic low-field ^{119}Sn NMR resonance observed at 525.1 ppm. Interestingly, upon gentle heating at 50 °C, the initially formed germastannene $(Bu^t_2MeSi)_2Ge{=}SnTip_2$ quantitatively isomerized to a novel, symmetrically substituted, germastannene (*E*)-$(Bu^t_2MeSi)TipGe{=}Sn(SiMeBu^t_2)Tip$ (Scheme 35).[119] The ^{1}H NMR kinetic studies of this isomerization gave a negative value of −12.0 cal K^{-1} mol^{-1} for the activation entropy $\Delta S^{\ddagger}$, thus suggesting a concerted isomerization mechanism implying the dyotropic 1,2-migration of the silyl and aryl groups in the starting germastannene.

$^3\Delta$-1,2,3,4-Disilagermastannetene, as the first cyclic germastannene incorporating an endocyclic Ge=Sn bond into the four-membered ring skeleton, was readily available by the ring expansion reaction of either 1*H*- or 3*H*-disilagermirenes[51] with the $SnCl_2$·diox complex (Scheme 36).[120] As expected, the sp^2-Sn center of this cyclic germastannene resonated in a characteristic low-field region at 439.3 ppm. In sharp contrast to the above-described germastannenes, $Mes_2Ge{=}SnTip_2$ and $Tip_2Ge{=}SnTip_2$, the cyclic germastannene was quite stable in the solid state and in solution without any signs of dissociation into the germylene and stannylene. The amazing thermal stability of its Ge=Sn double bond was ascribed to the cooperative effect of the σ-donating silyl substituents and to the proposed $\pi_{Ge=Sn} \rightarrow \sigma^*_{Si-Cl}$ orbital mixing resulting in a lowering of the π-energy level and overall stabilization of the HOMO.[120b]

1.11.3 Stable Analogs of 1,3-Dienes and Allenes of the Heavy Group 14 Elements

1.11.3.1 Heavy Analogs of 1,3-Dienes[121]

The first stable 1,3-diene of the heavy group 14 elements, hexakis(2,4,6-triisopropylphenyl)tetrasilabuta-1,3-diene $Tip_2Si{=}Si(Tip){-}Si(Tip){=}SiTip_2$, was synthesized in 1997 by the reaction of the tetraaryldisilene $Tip_2Si{=}SiTip_2$ with Li followed by the addition of MesBr (Scheme 37).[122] The reaction is likely to proceed through the initial generation of the disilenyllithium $Tip_2Si{=}Si(Tip)Li$, followed by its subsequent reaction with MesBr forming $Tip_2Si{=}Si(Tip)Br$, which finally coupled with the remaining $Tip_2Si{=}Si(Tip)Li$ to give tetrasilabuta-1,3-diene.

The terminal silicon atoms Si_{term} of the $Si_{term} = Si_{cent}{-}Si_{cent} = Si_{term}$ 1,3-diene system resonated at a higher field than the internal silicons Si_{cent}: 52.3 ppm versus 89.5 ppm. The particularly important issue of the conjugation between the two Si=Si units was resolved in favor of the presence of such conjugation. In solution, this was deduced from the electronic spectrum of the tetrasilabuta-1,3-diene: the longest wavelength absorption was observed at 518 nm, a value that was ca. 100 nm red-shifted in comparison with those of known tetraaryldisilenes with isolated Si=Si bonds. In the solid state, the conjugation in the tetrasilabuta-1,3-diene was demonstrated by the slight stretching of the Si=Si bonds (2.175(2) Å, which is ca. 0.03 Å longer than those of tetraaryldisilenes) and shortening of the single bond between the two sp^2-silicons = Si–Si = (2.321(2) Å, which is shorter than the standard value of 2.34 Å). The tetrasilabuta-1,3-diene featured a remarkable *s-cis* conformation with a dihedral angle between the two Si=Si units of 51.0°.

By the same synthetic procedure, a germanium analog of the above-described tetrasilabuta-1,3-diene, namely, the tetragermabuta-1,3-diene derivative $Tip_2Ge{=}Ge(Tip){-}Ge(Tip){=}GeTip_2$, was also prepared (Scheme 37, E = Ge).[123] In its crystalline form, tetragermabuta-1,3-diene also adopted an *s-cis* conformation, although the twisting between the two Ge=Ge fragments was less pronounced than that in tetrasilabuta-1,3-diene: 22.5° versus 51.0°. While the Ge=Ge double bonds in tetragermabuta-1,3-diene of 2.3568(6) and 2.3439(5) Å were longer than those of tetraaryldigermenes, the central =Ge–Ge=distance of 2.4581(5) Å was quite normal for a single bond. Although the presence of conjugation between the Ge=Ge double bonds in tetragermabuta-1,3-diene could not be deduced from its crystal structure data, it was supported by the observation of a longest wavelength absorption at 560 nm, a value that was ca. 140 nm red-shifted compared with those of tetraaryldigermenes.

Another stable tetrasilabuta-1,3-diene, *s-cis*-$(Bu^t_2MeSi)_2Si{=}Si(Mes){-}Si(Mes){=}Si(SiMeBu^t_2)_2$, was prepared by taking advantage of the synthetic utility of the 1,1-dilithiosilane reagent $(Bu^t_2MeSi)_2SiLi_2$, which was reacted with the 1,1,2,2-tetrachlorodisilane $MesCl_2Si{-}SiCl_2Mes$.[124] The doubly bonded Si atoms in $(Bu^t_2MeSi)_2Si{=}Si(Mes){-}Si(Mes){=}Si(SiMeBu^t_2)_2$ were found at 71.5 and 150.8 ppm, which is in a more deshielded area than those of $Tip_2Si{=}Si(Tip){-}Si(Tip){=}SiTip_2$. The two Si=Si bonds in $(Bu^t_2MeSi)_2Si{=}Si(Mes){-}Si(Mes){=}Si(SiMeBu^t_2)_2$ are greatly twisted, with a Si=Si–Si=Si torsional angle of 72°, which was attributed to the steric repulsion of the bulky silyl substituents. Another manifestation of the severe steric interactions was the elongation of the Si=Si bonds (2.1983(12) and 2.2003(12) Å), whereas the central = Si–Si = bond was quite normal (2.3376(11) Å). However, despite the great twisting of the buta-1,3-diene fragment, a partial conjugation in $(Bu^t_2MeSi)_2Si{=}Si(Mes){-}Si(Mes){=}Si(SiMeBu^t_2)_2$ between the two Si=Si π-bonds was still possible, as was shown by the notable bathochromic shift of ca. 100 nm for the longest UV–Vis absorption observed at 531 nm (compare with 437 nm found for the related disilene $(Bu^t_2MeSi)_2Si{=}SiMes_2$).

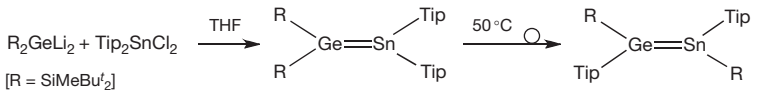

Scheme 35 Synthesis of the germastannene using 1,1-dilithiogermane precursor, and its subsequent thermal isomerization into a novel, symmetrically substituted germastannene.

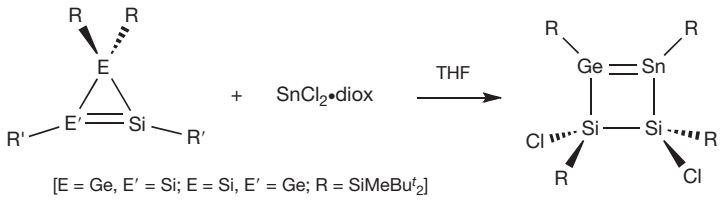

Scheme 36 Synthesis of the first cyclic germastannene.

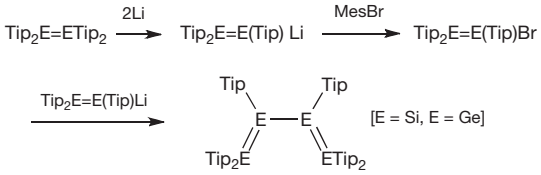

Scheme 37 Synthesis of the first stable tetrasilabuta-1,3-diene and tetragermabuta-1,3-diene.

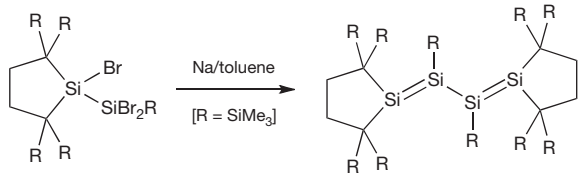

Scheme 38 Synthesis of a tetrasilabuta-1,3-diene with exocyclic Si=Si bonds.

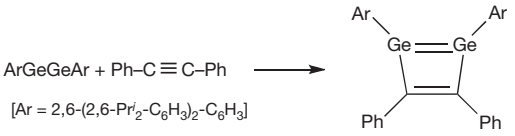

Scheme 39 Synthesis of the 1,2-digermacyclobutadiene.

A tetrasilabuta-1,3-diene, featuring two exocyclic Si=Si bonds, was synthesized by the reduction of tribromodisilane with sodium (Scheme 38).[54]

Because of the differing substitution pattern, the resonances of the central and terminal sp^2-silicons were found in highly distinctive regions: 9.3 and 210.2 ppm, respectively. In contrast to the above-described derivatives, the new tetrasilabuta-1,3-diene showed an s-*trans*-configuration of the two double bonds with a Si=Si–Si=Si torsional angle of 122.6° and Si=Si bond lengths of 2.1980(16) and 2.2168(16) Å. Similar to the previous cases, the notable red shift in the electronic spectrum of the tetrasilabuta-1,3-diene (longest absorption at 510 nm) suggested an important degree of π–π conjugation between the two Si=Si bonds. As mentioned in Section 1.11.2.1.1, both thermolysis and photolysis of the tetrasilabuta-1,3-diene with exocyclic Si=Si bonds produced the unusual spirocyclic cyclotrisilene shown in Scheme 6.[54]

In several compounds, the double bonds of the 1,3-diene unit are incorporated into cyclic systems (cyclic dienes). Thus, the above-described five-membered ring silagermene (see Section 1.11.2.2.1, Scheme 30) manifested an *s-cis*-conformation of the Si=Ge–C=C 1,3-diene unit dictated by its cyclic structure.[112] Structural trends expected for the conjugated system (stretching of the double bonds and shortening of the single bond) were not observed in the cyclic silagermene despite the planarity of the five-membered ring: the lengths of the Si=Ge (2.250(1) Å), C=C (1.343(5) Å), and Ge–C (1.972(3) Å) bonds were quite normal for such bonds. Moreover, a bathochromic shift was not observed in the UV–Vis spectrum of the five-membered ring cyclic silagermene with the Si=Ge–C=C unit compared with the 1*H*-disilagermirene with an isolated Si=Ge bond: 472 versus 467 nm. Overall, this 1,2-disila-3-germacyclopenta-2,4-diene (shown in Scheme 30) represents a cyclopentadiene system with two formally conjugated but actually isolated double bonds. This was rationalized considering the remarkable difference in the size and energy levels of the Si=Ge and C=C π-orbitals, precluding their effective conjugation.

1,2-Digermacyclobutadiene was recently prepared as the first stable cyclobutadiene derivative containing heavy group 14 elements by the [2+2]-cycloaddition of the germanium analog of an alkyne ArGeGeAr (Ar = 2,6-(2,6-Pr^i_2-C_6H_3)$_2$-C_6H_3) and diphenylacetylene (Scheme 39).[125] The cyclic carbon atoms involved in the Ge=Ge–C=C diene system resonated in the low-field region at 159.2 ppm. Although the Ge_2C_2 four-membered ring was nearly planar, the geometry at the skeletal Ge atoms was markedly pyramidal (sum of the bond angles 317.3° and 318.0°). The lengths of the endocyclic bonds in 1,2-digermacyclobutadiene are consistent with its formulation as a cyclobutadiene: C=C double bond of 1.365(7) Å, two Ge–C single bonds of 2.022(5) and 2.027(5) Å, and a 'weak' Ge=Ge double bond of 2.4708(9) Å (the last value is even greater than that of the typical Ge–Ge single bonds of 2.44 Å).

A tetrasilacyclobutadiene derivative, as the first all-heavy group 14 element-containing cyclobutadiene, was recently

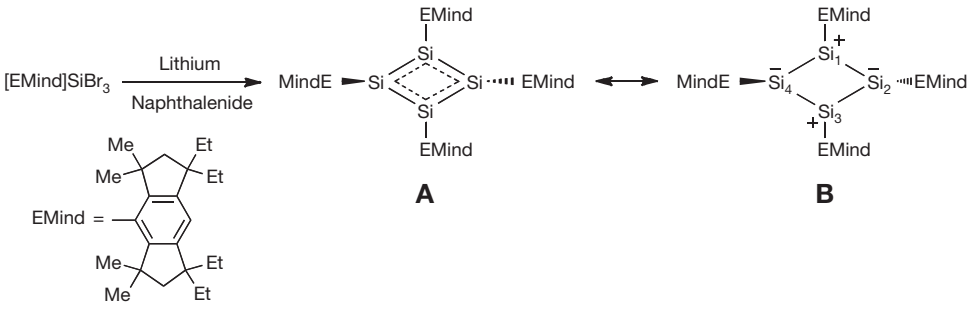

Scheme 40 Synthesis of the tetrasilacyclobutadiene.

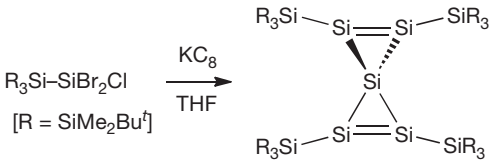

Scheme 41 Synthesis of the spiropentasiladiene.

reported, being prepared by the lithium naphthalenide reduction of the tribromosilane featuring the very bulky EMind-group (Scheme 40).[126] The Si4-ring in the tetrasilacyclobutadiene derivative is planar with the cyclic Si–Si bonds intermediate between typical Si–Si single and Si=Si double bonds (2.2877(8), 2.2671(8), 2.2846(8), and 2.2924(8) Å). The most striking structural feature of the tetrasilacyclobutadiene is the remarkably differing configuration of the skeletal silicons: whereas the geometry at the Si1 and Si3 atoms is planar (360°, sp^2-type hybridization), that of the Si2 and Si4 atoms is pyramidal (338.8° and 335.1°, sp^3-type hybridization). Such remarkable structural distortion of the Si4-ring from the expected rectangular geometry was explained in terms of the important contribution of the planar rhombic charge-separated resonance extreme **B**, in which the negative charges are located on the pyramidal Si2 and Si4 atoms and positive charges on the planar Si1 and Si3 atoms (Scheme 40). The contribution of the canonical form **B** can also be seen in the extreme chemical shift difference (>350 ppm) in the resonances of the skeletal Si atoms: −52/−50 ppm (for Si2/Si4) and 300/308 ppm (for Si1/Si3) (^{29}Si CP–MAS NMR). The NPA computations confirmed a notable charge difference in the skeleton of the tetrasilacyclobutadiene: +0.144 (for Si2) and +0.167 (for Si4) versus +0.647 (for Si1) and +0.637 (for Si3). In accord with its charge-separated structure, tetrasilacyclobutadiene exhibited neither aromaticity nor antiaromaticity, but nonaromaticity.

Overall, the polarization of the Si=Si double bonds in the tetrasilacyclobutadiene derivative results from a polar second-order Jahn–Teller distortion, counteracting the inherent cyclobutadiene antiaromaticity.

Several compounds with the two Si=Si bonds separated by more than one bond have also been reported. Among them is a remarkable spiropentasiladiene prepared by the reduction of the dibromochlorosilane $(Bu^t_2MeSi)_3Si–SiBr_2Cl$ with KC_8 (Scheme 41); the first stable cyclotrisilene was also synthesized by the same reaction (see Section 1.11.2.1.1, Scheme 2).[127]

The two cyclotrisilene units sharing a spiro-silicon are highly twisted relative to each other by 78.3°, and the cyclic Si=Si bonds are also twisted by 30.0°, whereas the doubly bonded Si atoms are only insignificantly pyramidalized (sum of the bond angles around them = 358.0° and 358.9°). The Si=Si bonds in spiropentasiladiene of 2.186(3) Å are longer than the typical double bonds in cyclotrisilenes, which was explained by the $\pi_{Si=Si}$–$\sigma^*_{Si–Si}$ orbital interaction. The longest wavelength absorption of spiropentasiladiene at 560 nm was substantially red-shifted compared with those of the known cyclotrisilenes, thus manifesting the important through-space interaction between its π- and π*-orbitals. Another indication of such notable through-space interaction in spiropentasiladiene was the considerable deshielding of its sp^2-silicons, whose resonances at 154.0 ppm were remarkably low-field-shifted compared with those of the stable cyclotrisilenes.

Several tetrasiladienes featuring two Si=Si bonds connected by a phenylene bridge, representing *m*- and *p*-bis(disilenyl)benzene derivatives, were also recently reported (their physicochemical characteristics are given in Table 1, Section 1.11.2.1.1).[23,30] In these compounds, a significant bathochromic shift of the longest wavelength absorption was observed in their electronic spectra, supporting the existence of π-conjugation between the two Si=Si bonds bridged by a phenylene unit.

1.11.3.2 Heavy Analogs of Allenes[128]

The very first stable 1-silaallene was prepared by the reduction of its precursor with Bu^tLi (Scheme 42).[129] The resonances of the Si and central allenic C atoms were observed at 48.4 and 225.7 ppm, respectively. The Si=C bond in 1-silaallene of 1.704(4) Å was short compared with the stable silenes with an isolated silicon–carbon double bond, whereas the allenic moiety Si=C=C was slightly bent with a bending angle of 173.5°.

By employing an addition–elimination reaction sequence, a series of other stable 1-silaallenes was prepared starting from the corresponding (halosilyl)acetylenes (Scheme 43).[130]

All of the new 1-silaallenes showed diagnostic signals for their sp^2-Si (13.1–58.7 ppm) and central sp^2-C (216.3–227.9 ppm) atoms. For 1-silaallene with R = Bu^t and R′ = R″ = Tip, the following structural parameters were reported: Si=C bond length of 1.693(3) Å, Si=C=C bent angle of 172.0°, essential planarity around the terminal carbon atom of the Si=C=C allene unit (359.9°), and insignificant pyramidalization at the silicon center (357.2°).

The first stable 1-germaallene was also obtained (Scheme 44) by the same procedure as that used for the preparation of the stable 1-silaallenes (see above).[131]

As expected, the central allenic carbon in the 1-germaallene was found in the very low-field region at 235.1 ppm. As in the case of 1-silaallenes, the Ge=C bond of 1.783(2) Å in the 1-germaallene is markedly shorter compared with those of the structurally characterized germenes with an isolated germanium–carbon double bond. The Ge=C=C allenic fragment in the 1-germaallene is remarkably bent with a bending angle of 159.2°, and the geometry around the Ge atom was notably pyramidal (sum of the bond angles 348.4°).

Another stable 1-germaallene, Tbt(Mes)Ge=C=CR_2 (R_2C= 9-fluorenylidene), was synthesized by either detelluration of telluragermacyclopropane with $(Me_2N)_3P$ or reductive dechlorination of (1-chlorovinyl)chlorogermane with Bu^tLi.[132] In the absence of structural data, Tbt(Mes)Ge=C=CR_2 was identified by its low-field signal at 243.6 ppm, indicative of the central carbon atom in the allenic structure.

No isolable 1-stannaallenes >Sn=C=C<, 1-plumbaallenes >Pb=C=C< or heavy allenes of the types >C=E=C<, >E=C=E′< or >E=E′=C< (E, E′ = heavy group 14 elements), have been reported to date.

Several remarkable all-heavy group 14 element-consisting allenes of the types >E=E=E< and >E=E′=E< have recently become synthetically accessible. The first one among them was the tristannaallene $(Bu^t_3Si)_2Sn{=}Sn{=}Sn(SiBu^t_3)_2$, prepared in 1999 by the straightforward reaction of bis(amino)stannylene $[(Me_3Si)_2N]_2Sn$: with Bu^t_3SiNa (Scheme 45).[102]

At room temperature, the tristannaallene gradually isomerized in solution into the more stable cyclotristannene *cyclo*-$[(Bu^t_3Si)_4Sn_3]$, which is described in Section 1.11.2.1.3 (Scheme 26), with a half-life of 9.8 h at 25 °C (first-order reaction kinetics). As expected, the terminal and central tin atoms in the tristannaallene unit Sn=Sn=Sn resonated in the low-field region at 503 and 2233 ppm, respectively. The extreme deshielding of the central Sn atom (2233 ppm), which is formally sp-hybridized, was interpreted in terms of the important contribution of the stannylene canonical forms shown in Scheme 46.

The Sn=Sn double bonds in the tristannaallene of 2.684(1) and 2.675(1) Å are notably shorter than those of the structurally characterized acyclic distannenes >Sn=Sn< (see Section 1.11.2.1.3, Table 5). As in other heavy allenes described above and in marked contrast to undistorted organic allenes, the tristannaallene unit >Sn=Sn=Sn< was considerably bent

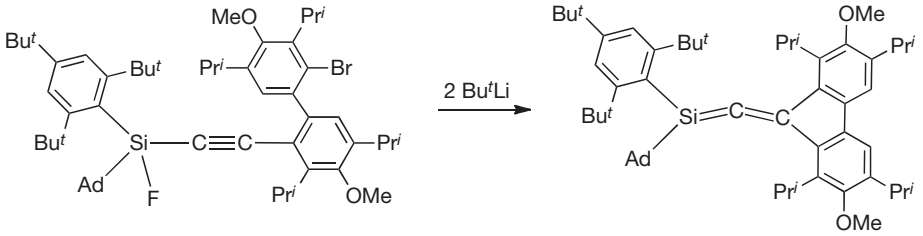

Scheme 42 Synthesis of the first stable 1-silaallene.

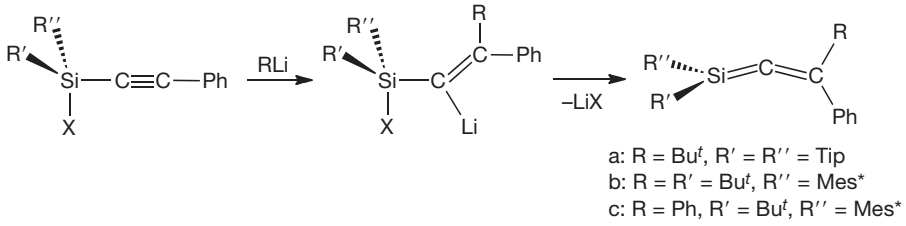

Scheme 43 Synthesis of other stable 1-silaallenes.

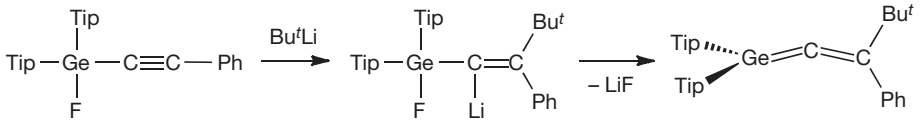

Scheme 44 Synthesis of the first stable 1-germaallene.

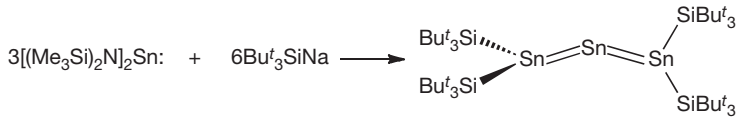

Scheme 45 Synthesis of the first tristannaallene.

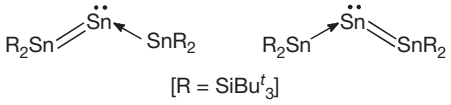

Scheme 46 Stannylene resonance extremes of the tristannaallene.

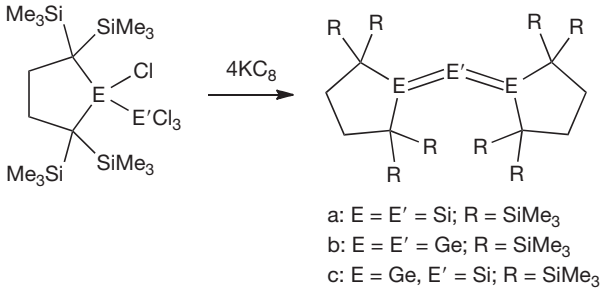

Scheme 47 Synthesis of the trisilaallene >Si=Si=Si<, trigermaallene >Ge=Ge=Ge<, and 1,3-digermasilaallene >Ge=Si=Ge< derivatives.

with a bent angle of 156.0°, which again was explained by the contribution of the stannylene resonance forms, as shown in Scheme 46. The configuration at the terminal tins was pyramidal (again, unlike organic allenes) with the sum of the bond angles being 344.3° and 346.9°.

A family of isolable heavy analogs of allenes, namely, homonuclear trisilaallene and trigermaallene, and heteronuclear 2-germadisilaallene and 1,3-digermasilaallene, was also recently reported.[133] The trisilaallene was prepared by the reductive dechlorination of the cyclic chloro(trichlorosilyl)silane with potassium graphite (Scheme 47, **a**).[133a]

The resonances of the terminal and central silicon atoms of the trisilaallene moiety were observed at 196.9 and 157.0 ppm, respectively. Structurally, trisilaallene showed the following features: (1) silicon–silicon distances of 2.177(1) and 2.188 (1)Å, which are typical for Si=Si double bonds; (2) *trans*-bending and pyramidalization at the terminal silicons (sum of the bond angles 354.1° and 354.9°); (3) highly bent Si=Si=Si skeleton (bent angle 136.5°); and (4) nearly perpendicular arrangement of the two five-membered rings. In the crystalline state of the trisilaallene >Si1=Si2=Si3<, the central allenic Si2 atom was found in four different positions at temperatures above −100 °C. These four structural isomers were nearly of the same energy (energy difference within 1 kcal · mol^{-1}), suggesting a dynamic disorder because of the rotation of the Si2 atom about the Si1–Si3 axis. The longest UV–Vis absorption of the trisilaallene at 584 nm was significantly red-shifted compared with, for example, tetramethyldisilene (350 nm), which suggests notable conjugation between the two cumulated Si=Si bonds.

Similar thermal motion of the central germanium atom of the >Si=Ge=Si< allenic system was also observed in the solid state of the 2-germadisilaallene, prepared by the coreduction of isolable cyclic silylene and $GeCl_2$·diox complex with potassium graphite (Scheme 48).[133b]

The terminal silicons in the >Si=Ge=Si< allenic fragment of 2-germadisilaallene resonated at a low field of 219.4 ppm. The Si=Ge double bonds in 2-germadisilaallene of 2.2366(7) and 2.2373(7)Å were slightly shorter than that in 1,2-disila-3-germacyclopenta-2,4-diene of 2.250(1)Å (see Section 1.11.2.2.1, Scheme 30). Similar to the above-described trisilaallene (Scheme 47, **a**), 2-germadisilaallene exhibited a bent >Si=Ge=Si< skeleton (bent angle 132.4°) and pyramidal geometry at the terminal silicon atoms (353.9° and 354.0°). A conjugation between the two Si=Ge bonds in 2-germadisilaallene was manifested in the bathochromic shift of its longest wavelength absorption observed at 599 nm.

Trigermaallene and 1,3-digermasilaallene were synthesized by the same synthetic procedure as that of trisilaallene (Scheme 47, **b** and **c**).[133c] However, unlike the above-described trisilaallene and 2-germadisilaallene, neither trigermaallene nor 1,3-digermasilaallene showed dynamic disorder in their crystal structures; accordingly the central Ge (in trigermaallene) and Si (in 1,3-digermasilaallene) atoms were found in only one of the four possible positions. This structural distinction between trisilaallene/2-germadisilaallene and trigermaallene/1,3-digermasilaallene stems from their different environments, which define the spatial position of their central allenic atoms. The >Ge=Ge=Ge< and >Ge=Si=Ge< skeletons in trigermaallene and 1,3-digermasilaallene were highly bent (122.6° and 125.7°, respectively), whereas the geometry at the terminal Ge atoms was notably pyramidal (348.5°/348.6° and 349.3°). The Ge=Ge bonds in trigermaallene of 2.321(2) and 2.330(3)Å were in the normal range, whereas the Si=Ge bonds in 1,3-digermasilaallene of 2.2694(8)Å were insignificantly longer than that of 1,2-disila-3-germacyclopenta-2,4-diene of 2.250(1)Å (see Section 1.11.2.2.1, Scheme 30). The central Si atom in the 1,3-digermasilaallene resonated at 236.6 ppm, that is, at a much lower field than that of the trisilaallene (157.0 ppm). Similarly to the above-described trisilaallene and 2-germadisilaallene, both the trigermaallene and the 1,3-digermasilaallene exhibited considerable conjugation between the Ge=Ge (in trigermaallene) and Si=Ge (in 1,3-digermasilaallene) double bonds, which can be seen in the red shift of their longest wavelength UV–Vis absorptions: 630 nm (in trigermaallene) and 612 nm (in 1,3-digermasilaallene) (note that the corresponding value for the trisilaallene is 584 nm).

The tetra(silyl)trisilaallene was prepared by the reaction of dilithiosilane derivative $(Bu^t_2MeSi)_2SiLi_2$ with $SiCl_2$–NHC complex (Scheme 49).[134] In the absence of crystallographic data, the new trisilaallene was characterized by spectroscopic techniques, computational and reactivity studies. Thus, the resonances of the terminal silicons were found at 44.6 ppm, whereas that of the central silicon was remarkably more deshielded, being observed at 418.5 ppm. The latter chemical shift was substantially lower-field-shifted compared with that of the above-described tetra(alkyl)trisilaallene[133a] (Scheme 47, **a**), 418.5 ppm versus 157.0 ppm, providing evidence for their distinctly differing structures. This was further corroborated by the fact that the bending of the allenic Si=Si=Si skeleton was notably smaller in the case of the silyl-substituted trisilaallene compared with its alkyl-substituted counterpart: 164.3° (computations of the real molecule) versus 136.5° (x-ray crystallography). As in organic allenes, the two planes defined by the three Si atoms (two substituent Si and one terminal Si to which these substituents are attached) of the tetra(silyl)trisilaallene were nearly orthogonal to each other with the dihedral angle between them being 86.6°. In accord with its peculiar substitution pattern, tetra(silyl)trisilaallene showed the Si=Si bond polarizations as $>Si^{\delta-} = Si^{\delta+} = Si^{\delta-}<$, resulting in the formation of only

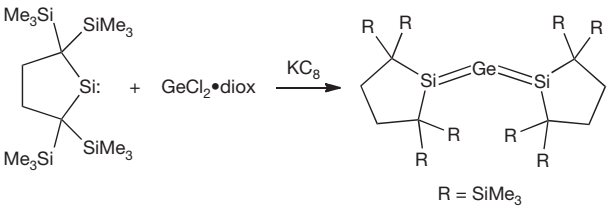

Scheme 48 Synthesis of the 2-germadisilaallene >Si=Ge=Si< derivative.

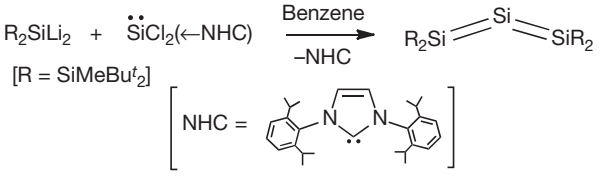

Scheme 49 Synthesis of the isolable tetra(silyl)trisilaallene.

one regioisomer $R_2Si(H)–Si(OMe)_2–Si(H)R_2$ in the reaction of the tetra(silyl)trisilaallene with methanol. Similar to the above-described case of the thermal isomerization of a tristannaallene (Scheme 45) to a cyclotristannene (Scheme 26),[102] tetra(silyl) trisilaallene also underwent rearrangement at 120 °C, forming the previously reported tetrakis(di-*tert*-butylmethylsilyl)cyclotrisilene (Scheme 3, E = Si).[134]

A couple of the bis(methanediide) derivatives of germanium and tin, whose structures can be viewed as 2-germa- and 2-stannaallenes $R_2C=E=CR_2$ (E = Ge, Sn; R = –P(Ph)$_2$ = S), have also been recently reported.[135] In these compounds, which feature certain phosphinoyl substituents R at the terminal carbons, the central E was intramolecularly supported by electron donation from the sulfur lone pairs. This expands their coordination number to four (for Ge) and six (for Sn). Such an increase in the coordination sphere of the E centers, along with the potential π-conjugation from the E=C and P=S bonds, remarkably alters the nature of the element–carbon bonds. Thus, compared with the genuine Ge=C and Sn=C double bonds in the structurally authenticated 1-germaallene (see above), germenes and stannenes, the E=C bonds are notably longer at 1.882(2) Å (for the Ge=C bond) and 2.063(2) Å (for the Sn=C bond). This suggests that the element–carbon interaction has only partial double-bond character and can be best classified as lying between a single and double bond.

1.11.4 Stable Analogs of Alkynes of the Heavy Group 14 Elements[136]

Several stable analogs of alkynes of the heavy group 14 elements of the types R–E≡E–R/R–E≡E–R′ and R–E≡E′–R′ (E, E′ = group 14 elements) have been prepared during the past decade: three disilynes RSiSiR/RSiSiR′, six digermynes (or their valence isomers) RGeGeR, twelve distannynes (or their valence isomers) RSnSnR, one valence isomer of diplumbyne RPbPbR, one silyne RSiCR′, and two germyne analogs RGeCR′. The synthetic routes to such compounds, their unusual structural features, and bonding nature are discussed below.

1.11.4.1 Disilynes RSiSiR

A relatively stable disilyne that was spectroscopically characterized, $(Bu^t_3Si)_2MeSi–Si≡Si–SiMe(SiBu^t_3)_2$, was reported in 2004, prepared by the reductive dechlorination of the 1,2-dichlorodisilene precursor (*E*)-[$(Bu^t_3Si)_2$MeSi]ClSi=Si[SiMe$(SiBu^t_3)_2$]Cl (see Section 1.11.2.1.1, Table 1) with lithium naphthalenide.[14,57,58,137] Classification of this compound as a disilyne was based on the low-field resonance of its central silicon at 91.5 ppm, high-resolution mass spectral data, and its specific reactivity toward ethylene and buta-1,3-diene to form the corresponding [2 + 2]- and [2 + 4]-cycloadducts.[58] Computational estimates for the length of the central silicon–silicon bond of 2.072 Å and a Si–Si≡Si *trans*-bent angle of 148.0° were in good agreement with the formulation of this bond as a Si≡Si triple bond.[137b] Being stable in the solid state, disilyne $(Bu^t_3Si)_2MeSi–Si≡Si–SiMe(SiBu^t_3)_2$ underwent isomerization in solution via the 1,2-migration of one of the Bu^t_3Si-groups from the substituent Si to the central Si and subsequent cyclization, forming an unsymmetrical cyclotrisilene.

The crystal structure of the first isolable disilyne $Dsi_2Pr^iSi–Si≡Si–SiPr^iDsi_2$, readily available by the reductive debromination of the 1,1,2,2-tetrabromodisilane precursor $Dsi_2Pr^iSi–SiBr_2–SiBr_2–SiPr^iDsi_2$ with potassium graphite, was reported in 2004.[138] The resonances of the triply bonded silicons in $Dsi_2Pr^iSi–Si≡Si–SiPr^iDsi_2$ were observed in the low field at 89.9 ppm. The central Si–Si bond of 2.0622(9) Å was extraordinarily short, being at least 4% shorter than typical Si=Si double bonds (2.14–2.19 Å) (see Figure 2).[138a] Moreover, in full accord with theoretical predictions, the arrangement of substituents at the triply bonded silicon atoms was *trans*-bent with a bending angle of 137.4°. Natural bond orbital (NBO) computations showed a bond order of the central Si–Si bond of 2.618 with the electron occupancy of the two $\pi_{Si≡Si}$-orbitals being 1.934 and 1.897 electrons, again in line with the Si≡Si triple-bond formulation.[138a,c] Upon *trans*-bending of the substituents at the Si≡Si bond, the degeneracy of both the HOMO and the lowest unoccupied molecular orbital (LUMO) typical of the linear alkyne structure was broken, giving rise to two nondegenerate HOMOs and LUMOs, as manifested in the observation of absorptions at 483 and 690 nm, corresponding to the π–π* electronic transitions (HOMO − 1 → LUMO/HOMO → LUMO + 1 and HOMO → LUMO).[138c]

The classification of $Dsi_2Pr^iSi–Si≡Si–SiPr^iDsi_2$ as a disilyne with a genuine Si≡Si triple bond was further supported by solid-state ^{29}Si NMR CP–MAS studies, based on the general trend of the large chemical shift anisotropy values indicative of the presence of π-bonds.[138b] As in the case of tetrasilyldisilenes (see Section 1.11.2.1.1), the deshielding of triply bonded silicon atoms in the silyl-substituted *trans*-bent

disilynes was explained in terms of the decisive role of the paramagnetic contribution.[138b,139a] The large paramagnetic contribution in bis(silyl)disilynes $R_3Si–Si{\equiv}Si–SiR_3$ stems from the mixing between the σ_{Si-Si}- and $\pi^*_{Si{\equiv}Si}$-orbitals, which in turn results from the decrease in the $\sigma–\pi^*$ energy gap because of the electropositive silyl substituents. Moreover, the increase in the *trans*-bending in disilynes reduces orbital overlap, thus raising the energy of the σ_{Si-Si}-orbital and decreasing the $\sigma–\pi^*$ energy separation, leading to an increase in the paramagnetic contribution to the chemical shielding, and finally to further deshielding of the triply bonded silicon atoms compared with those in the hypothetical linear disilyne.

Unsymmetrically substituted disilyne $Dsi_2Pr^iSi–Si{\equiv}Si–SiNpDsi_2$ (Np = CH_2Bu^t) was available by the above-described synthetic procedure, namely, by the reduction of the 1,1,2,2-tetrachlorodisilane precursor $Dsi_2Pr^iSi–SiCl_2–SiCl_2–SiNpDsi_2$ with potassium graphite.[140] This new disilyne $Dsi_2Pr^iSi–Si{\equiv}Si–SiNpDsi_2$ showed a record shortening of the central Si–Si bond, whose length was 2.0569(12) Å and characteristic *trans*-bent geometry with bending angles of 138.8° (for the Dsi_2Pr^iSi side) and 137.9° (for the Dsi_2NpSi side). Compared with the chemical shift of the central silicons in the symmetrical disilyne $Dsi_2Pr^iSi–Si{\equiv}Si–SiPr^iDsi_2$ (89.9 ppm), the unsymmetrical disilyne $Dsi_2Pr^iSi–Si{\equiv}Si–SiNpDsi_2$ showed resonances of its triply bonded Si atoms shifted to higher and lower fields: 62.6 ppm (for the triply bonded Si atom bearing the Dsi_2Pr^iSi group) and 106.3 ppm (for the triply bonded Si atom bearing the Dsi_2NpSi group). Similar to the case of the previously reported $(Bu^t_3Si)_2MeSi–Si{\equiv}Si–SiMe(SiBu^t_3)_2$, the unsymmetrical disilyne $Dsi_2Pr^iSi–Si{\equiv}Si–SiNpDsi_2$ underwent room-temperature isomerization, forming an unsymmetrically substituted cyclotrisilene via the migration of one of the Dsi groups followed by cyclization.

A disilyne with aryl substituents, Bbt–Si≡Si–Bbt {Bbt = 2,6-$[(Me_3Si)_2CH]_2$-4-$[(Me_3Si)_3C]$-C_6H_2}, was synthesized by the standard procedure: reductive debromination of 1,2-dibromodisilene (*E*)-Bbt(Br)Si=Si(Bbt)Br[10] (**Section 1.11.2.1.1**, **Table 1**) with Bu^tLi via initial lithium–bromine exchange followed by the β-elimination of LiBr from the transient disilenoid Bbt(Li)Si=Si(Bbt)Br.[10,141] Lacking the diagnostic deshielding effects of σ-donating silyl substituents because of the strong paramagnetic contribution (see **Section 1.11.2.1.1**, ^{29}Si NMR spectroscopy of disilenes), diaryldisilyne Bbt–Si≡Si–Bbt showed the resonance of its triply bonded Si atoms at a notably higher field (compared with those of the silyl-substituted disilynes; see above) at 18.7 ppm. In accord with the theoretical predictions, diaryldisilyne Bbt–Si≡Si–Bbt exhibited a slightly longer Si≡Si triple bond than that in the silyl-substituted disilynes (2.108(5) Å vs. 2.0622(9) Å and 2.0569(12) Å) with a slightly greater degree of *trans*-bending of the triple bond (133.0° (C_{Ar}–Si≡Si) vs. 137.4° and 137.9°/138.8° (Si–Si≡Si)). Comparison of the spectral and structural characteristics of isolable disilynes suggests a weaker triple-bond character of the diaryldisilyne compared with the silyl-substituted disilynes.

1.11.4.2 Digermynes RGeGeR (and Their Valence Isomers)

The first stable germanium analog of alkynes, ArGeGeAr (Ar = 2,6-$(2,6\text{-}Pr^i_2\text{-}C_6H_3)_2$-$C_6H_3$), was synthesized in 2002 by reduction of the chlorogermylene precursor Ar(Cl)Ge: with potassium.[71,142] Despite the shortening of the germanium–germanium distance in ArGeGeAr to 2.2850(6) Å, a value that was significantly shorter than standard Ge–Ge single bonds (ca. 2.44 Å) indicating its considerable multiple bond character, it was still in the range of the structurally characterized digermenes (2.21–2.51 Å, see **Section 1.11.2.1.2**). It was therefore suggested that the bonding between the two germanium atoms in ArGeGeAr is best described as a double bond with a bond order of 2 (digermene form), rather than a triple bond with a bond order of 3 (digermyne form). Accumulation of the nonbonding electron density at the Ge centers in the form of lone-pair electrons results in the significant *trans*-bending of the germanium–germanium bond of 128.7°, and accordingly, in the decrease in the Ge–Ge bond order and stretching of the bond.

Similarly, the other germanium analog of an alkyne, Ar*GeGeAr* (Ar* = 2,6-$(2,4,6\text{-}Pr^i_3\text{-}C_6H_2)_2$-$C_6H_3$), was prepared by the typical synthetic procedure: reduction of chlorogermylene Ar*(Cl)Ge: with potassium in THF; however, the crystal structure of this new digermyne was not reported.[71]

In due course, the same authors reported a family of digermynes Ar′GeGeAr′ (Ar′ = 4-Cl-2,6-$(2,6\text{-}Pr^i_2\text{-}C_6H_3)_2$-$C_6H_3$, 4-$Me_3Si$-2,6-$(2,6\text{-}Pr^i_2\text{-}C_6H_3)_2$-$C_6H_3$, and 3,5-$Pr^i_2$-2,6-$(2,4,6\text{-}Pr^i_3\text{-}C_6H_2)_2$-$C_6H_3$), modified at the *para*- or *meta*-positions of the central aryl ring of the substituents.[143] All of these digermynes were prepared by the reduction of the corresponding aryl(chloro)germylenes with potassium or potassium graphite. The digermynes displayed a planar *trans*-bent skeleton (Ge–Ge–C bond angles of 124.2–136.1°) with short Ge–Ge distances (2.2125(13)–2.3071(3) Å), consistent with the considerable germanium–germanium multiple bond character. Based on these structural data, it was argued that the bond order in the digermyne species is at least 2. The difference in the Ge–Ge bond lengths and Ge–Ge–C *trans*-bent angles in digermynes was rationalized in terms of the electronic effects of the substituents.[143] Thus, electron-donating alkyl (Pr^i) or silyl (Me_3Si) groups on the central aryl rings cause a decrease in the *trans*-bending, and consequently an increase in the bond order and a shortening of the germanium–germanium bond (Ge–Ge–C angle in °/Ge–Ge distance in Å): 136.1/2.2125(13) and 128.4/2.2438(8), respectively. Electron-withdrawing groups (Cl) have the opposite effects, namely, an increase in the *trans*-bending, decrease in the bond order, and stretching of the germanium–germanium bond (Ge–Ge–C angle in °/Ge–Ge distance in Å): 124.2/2.3071(3).

An aryl-substituted representative of the stable digermynes, BbtGeGeBbt, was prepared by the same method as its isostructural silicon analog, disilyne Bbt–Si≡Si–Bbt (see above), by the reductive debromination of 1,2-dibromodigermene (*E*)-Bbt(Br)Ge=Ge(Bbt)Br[77] (**Section 1.11.2.1.2**, **Table 3**) with potassium graphite.[144] The germanium–germanium distance in BbtGeGeBbt was shorter than that in ArGeGeAr (Ar = 2,6-$(2,6\text{-}Pr^i_2\text{-}C_6H_3)_2$-$C_6H_3$) (2.2060(8) and 2.2260(8) Å (for the two crystallographically independent molecules) vs. 2.2850(6) Å), indicative of a greater extent of triple-bond character in the former. The C_{Ar}–Ge≡Ge *trans*-bent angles in the two nonidentical molecules of BbtGeGeBbt varied over the range 123.6–138.7° (compare with the *trans*-bending of 128.7° in ArGeGeAr).

1.11.4.3 Distannynes RSnSnR (and Their Valence Isomers)

The first compound in the series of RSnSnR derivatives, featuring dicoordinate tin centers, ArSnSnAr (Ar = 2,6-(2,6-Pr^i_2-C_6H_3)$_2$-C_6H_3), was prepared in 2002 by the method previously used for the synthesis of its germanium analog, namely, by the reduction of chlorostannylene precursor Ar(Cl)Sn: with potassium.[71,145a] In the absence of ^{119}Sn NMR data, the composition of ArSnSnAr was established by x-ray diffraction analysis, which showed a highly bent C–Sn–Sn–C skeleton with the *trans*-bent angle of 125.2°, indicative of the developing lone-pair character at each tin center. The Sn–Sn distance of 2.6675(4) Å was notably shorter than the sum of the single-bond covalent radii for the two Sn atoms of 2.80 Å, being virtually identical to the value of 2.6683(10) Å found for the tetrasilyldistannene (Bu^t_2MeSi)$_2$Sn=Sn(SiMeBu^t_2)$_2$[99] (**Section 1.11.2.1.3**, **Table 5**), featuring the shortest Sn=Sn double bond among the acyclic distannenes. Accordingly, as in the case of the isostructural digermyne, the tin–tin bonding interaction in ArSnSnAr was interpreted as a double rather than a triple bond with the bond order estimated as intermediate between 1.5 and 2.0.[71]

Another stable tin analog of an alkyne, Ar*SnSnAr* (Ar* = 2,6-(2,4,6-Pr^i_3-C_6H_2)$_2$-C_6H_3), was available by the reduction of the chlorostannylene Ar*(Cl)Sn: with potassium, but this compound was not crystallographically characterized.[71]

Modification of the bulky terphenyl ligand in ArSnSnAr (Ar = 2,6-(2,6-Pr^i_2-C_6H_3)$_2$-C_6H_3) by the introduction of a Me_3Si-group at the 4-position of the central aryl ring greatly affected the structure of the resulting distannyne analog Ar′SnSnAr′ (Ar′ = 2,6-(2,6-Pr^i_2-C_6H_3)$_2$-4-Me_3Si-C_6H_2), which was prepared by the reduction of a chlorostannylene Ar′(Cl)Sn: with potassium.[145b] The tin–tin separation of 3.066(1) Å and *trans*-bent angle of 99.3° in the novel distannyne Ar′SnSnAr′ were dramatically different from those in the original distannyne ArSnSnAr, 2.6675(4) Å and 125.2°, respectively. Such extraordinary stretching of the Sn–Sn bond and narrowing of the bending angle in Ar′SnSnAr′ make it similar to the previously reported lead analog Ar*PbPbAr* (Ar* = 2,6-(2,4,6-Pr^i_3-C_6H_2)$_2$-C_6H_3),[146] for which single bonding between the two plumbylene units Ar*–$\dot{P}b$–$\dot{P}b$–Ar* was established. Likewise, the bonding between the two Ar′Sn fragments in Ar′SnSnAr′ was described as a single bond rather than a triple or even double bond.

By further modification of the terphenyl substituents at the *para*- and *meta*-positions of the central aryl rings, a series of novel distannynes Ar″SnSnAr″ (Ar″ = 4-F-2,6-(2,6-Pr^i_2-C_6H_3)$_2$-C_6H_3, 4-Cl-2,6-(2,6-Pr^i_2-C_6H_3)$_2$-C_6H_3, 4-MeO-2,6-(2,6-Pr^i_2-C_6H_3)$_2$-C_6H_3, 4-Bu^t-2,6-(2,6-Pr^i_2-C_6H_3)$_2$-C_6H_3, 4-Me_3Si-2,6-(2,6-Pr^i_2-C_6H_3)$_2$-C_6H_3, 4-Me_3Ge-2,6-(2,6-Pr^i_2-C_6H_3)$_2$-C_6H_3, 3,5-Pr^i_2-2,6-(2,6-Pr^i_2-C_6H_3)$_2$-C_6H_3, and 3,5-Pr^i_2-2,6-(2,4,6-Pr^i_3-C_6H_2)$_2$-C_6H_3) was prepared by the standard procedure: reduction of the aryl(chloro)stannylene precursors with potassium or potassium graphite.[143] These compounds displayed two distinctly different bonding modes: a multiply bonded form and a singly bonded form. A multiply bonded form (bond order between 1.5 and 2.0) is found in distannynes with the 4-Cl-, 4-MeO-, and 4-Bu^t-groups on the central aryl substituent, as manifested in their short tin–tin bonds and moderate *trans*-bent angles (Sn–Sn–C angle in °/Sn–Sn distance in Å): 121.8/2.672(2), 124.2/2.6480(12), and 124.0/2.6461(3), respectively. A singly bonded form with a long tin–tin separation and highly pronounced *trans*-bending was found in the distannyne isomers with the 4-Me_3Si- and 4-Me_3Ge-substituents at the *para*-position of the central aryl ring of the Ar″ ligand (Sn–Sn–C angle in °/Sn–Sn distance in Å): 99.1/3.0577(2) and 97.8/3.077(12), respectively. A structure intermediate between the multiply and singly bonded extremes was found in the distannyne Ar″SnSnAr″ (Ar″ = 3,5-Pr^i_2-2,6-(2,4,6-Pr^i_3-C_6H_2)$_2$-C_6H_3) with Sn–Sn distances of 2.7205(12)–2.7360(14) Å and Sn–Sn–C bond angles in the range 125.1–127.6°.[143]

Another organotin derivative Ar‴SnSnAr‴ (Ar‴ = 2,6-(Me_2NCH_2)$_2$-C_6H_3), recently prepared by reduction of the corresponding chlorostannylene derivative, was also classified as a distannyne (δ(^{119}Sn NMR) = 612 ppm).[147] However, given its very long tin–tin bond distance of 2.9712(12) Å and rather acute *trans*-bent angle of 94.3°, closely resembling those of the distannyne analog Ar′SnSnAr′ (Ar′ = 2,6-(2,6-Pr^i_2-C_6H_3)$_2$-4-Me_3Si-C_6H_2) (3.066(1) Å and 99.3°, respectively), the bonding between the two tins in Ar‴SnSnAr‴ is best described as a single bond (bond order 0.91 by NBO computations). Overall, Ar‴SnSnAr‴ represents a valence isomer of a distannyne in the form of bis(stannylene) Ar‴–$\dot{S}n$–$\dot{S}n$–Ar‴, in which the vacant *p*-orbital at each tin center is intramolecularly stabilized by nitrogen lone-pair electron donation (N → Sn) from a pair of chelating Me_2NCH_2-ligands.

1.11.4.4 Valence Isomer of Diplumbyne RPbPbR

The lead analog of an alkyne Ar*PbPbAr* (Ar* = 2,6-(2,4,6-Pr^i_3-C_6H_2)$_2$-C_6H_3), the first in the series of group 14 organometallics of the type REER (E = Si–Pb), was prepared by reduction of the corresponding bromoplumbylene Ar*(Br)Pb: with $LiAlH_4$.[146] The structural deformation of the lead–lead bond in Ar*PbPbAr* was greater than those of the above-described heavy alkyne analogs: extreme stretching of the Pb–Pb bond and an extraordinary *trans*-bending of the C_{Ar*}–Pb–Pb–C_{Ar*} skeleton. The Pb–Pb bond distance of 3.1881(1) Å was even longer than for typical lead–lead single bonds (2.844(4) Å in diplumbane Ph_3Pb–$PbPh_3$), whereas the very acute C_{Ar*}–Pb–Pb *trans*-bent angle of 94.3° (close to the right angle of 90°) was indicative of a little hybridization of the Pb valence orbitals and the presence of a lone pair at each lead center. In hybridization terms, this implies that each Pb atom in Ar*PbPbAr* used two 6p-orbitals for bonding to a substituent and the other Pb partner, whereas the remaining 6p-orbital was vacant, and the most stable 6s-orbital was occupied by a lone pair of electrons. Thus, the extreme lengthening of the Pb–Pb bond may be accounted for by the end-on overlap of p-orbitals (instead of sp^n-hybrids) to form this bond, as well as by the presence of lone pairs at the neighboring lead centers. The unusual structural features of Ar*PbPbAr* (long Pb–Pb bond, strong *trans*-bending) point to its existence in the unique form of bis(plumbylene) **B** instead of the usual linear acetylene-like diplumbyne form **A** (**Scheme 50**).

However, the preference for the nonclassical canonical structure **B** over the classical **A** was not due to the inherent weakness of the lead–lead multiple bonds in **A**, but instead should be attributed to the increased reluctance for s,p-hybridization in

heavy group 14 elements, which in the case of lead is further reinforced by relativistic effects.

1.11.4.5 Silynes RSiCR′

A single representative of the isolable silynes, base-stabilized *C*-phosphino-*Si*-amino silyne, was reported very recently, prepared by photolysis of the diazomethane derivative (Scheme 51).[148] Although the ^{13}C NMR resonance of the triply bonded carbon center in the silyne was observed at a low field of 216 ppm, the corresponding signal of its silicon partner was found in the remarkably high-field-shifted region of −89.4 ppm because of the intramolecular coordination of the phosphane ligand. The sp-type hybridization of the central carbon was demonstrated by the nearly linear geometry around it: Si–C–P bond angle of 178.2° (in contrast to the highly bent N–Si–C fragment, bent angle = 128.5°).

The Si–C bond is very short, being notably shorter than typical Si=C double bonds and in the range theoretically predicted for Si≡C triple bonds, thus indicating a substantial extent of triple bonding (Scheme 52, resonance form **B**). Although the geometry at the three-coordinate central silicon in the silyne becomes more planar compared with its diazomethane precursor (345° vs. 307°), it is still notably pyramidal because of the coordination of the phosphane ligand. The P–C bond distance in the Si≡C–P fragment of 1.682(3) Å is shorter than that in its precursor (1.844(2) Å), being between the typical values for the P=C_{sp} double (ca. 1.63 Å) and P–C_{sp} single (1.76–1.77 Å) bonds. Moreover, the geometry at both pyramidalized Si and P centers of the Si≡C–P unit is *trans*-bent, implying an interaction between the P lone pair and the π^*_{SiC}-orbital. These data suggest an important contribution from another resonance extreme A, featuring an allenic $Si^- = C = P^+$ fragment with negatively polarized silicon and positively polarized phosphorus centers (Scheme 52). Indeed, the Wiberg bond order of the Si–C bond of 1.687 is much smaller than the theoretically required 3; on the other hand, the bond order of the P–C bond of 1.219 indicates some degree of multiple bonding. The low Si–C bond order can alternatively be explained by the contribution of the other canonical form, which has a silylene–carbene character (Scheme 52, resonance form C), in accord with its reactivity toward *tert*-butylisocyanide as a carbene trapping reagent to form the corresponding keteneimine. Silyne is only stable below −30 °C in solution, isomerizing at higher temperatures into the phosphaalkene derivative via the 1,2-migration of a Pr^i_2N-group from the phosphane to the central carbon (Scheme 51).[148]

1.11.4.6 Germynes RGeCR′

Although base-stabilized *C*-phosphino-*Ge*-amino analogs of a germyne were prepared by the same procedure previously employed for the synthesis of the above-mentioned silyne (photolysis of the diazomethane derivative), their structures were distinctly different from that of its silicon analog (Scheme 53).[149]

Thus, in contrast to its silicon counterpart, which has a substantial Si≡C triple-bond character, the germyne analog

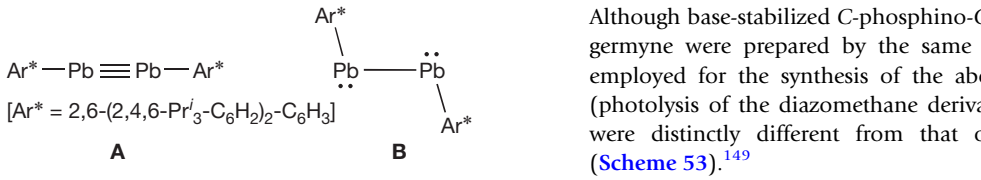

Scheme 50 Resonance structures of the diplumbyne analog Ar*PbPbAr*.

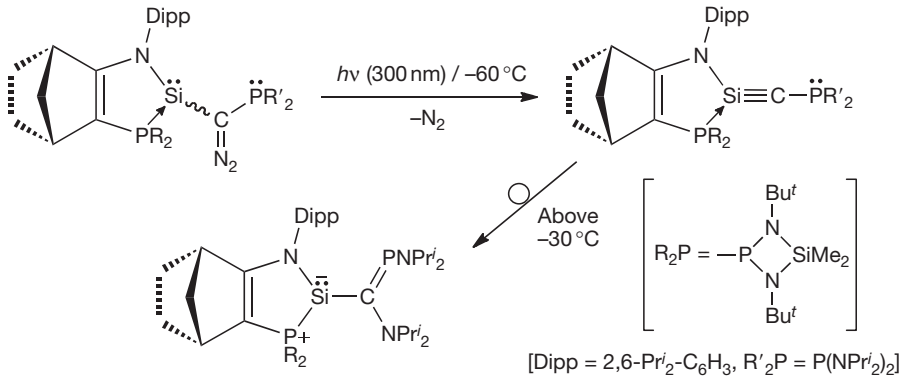

Scheme 51 Synthesis and thermal isomerization of the isolable silyne derivative.

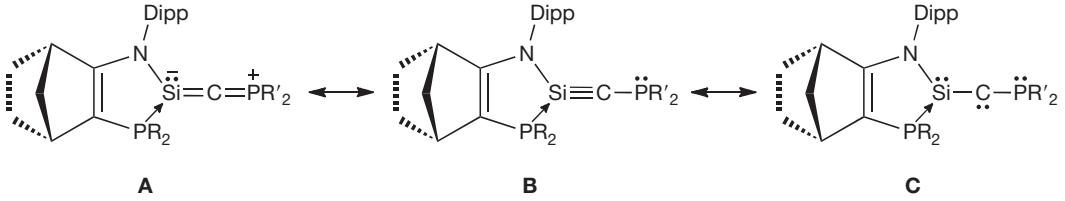

Scheme 52 Resonance structures of the isolable silyne.

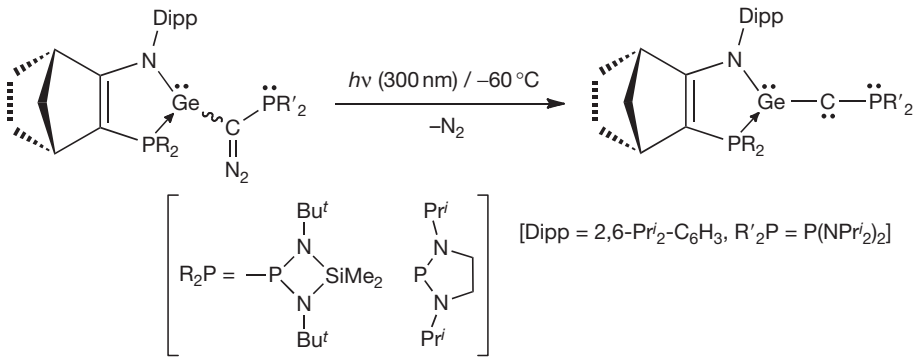

Scheme 53 Synthesis of the isolable germyne analog derivatives.

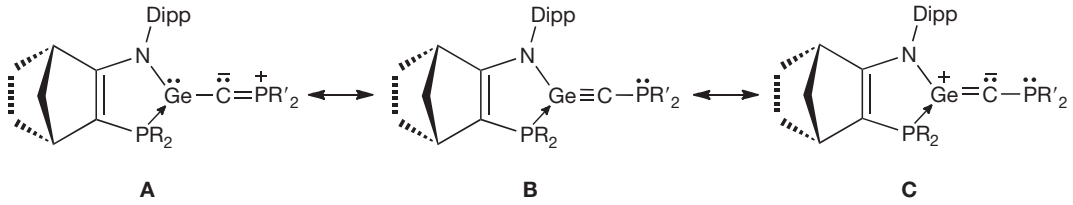

Scheme 54 Resonance structures of the isolable germyne analog derivatives.

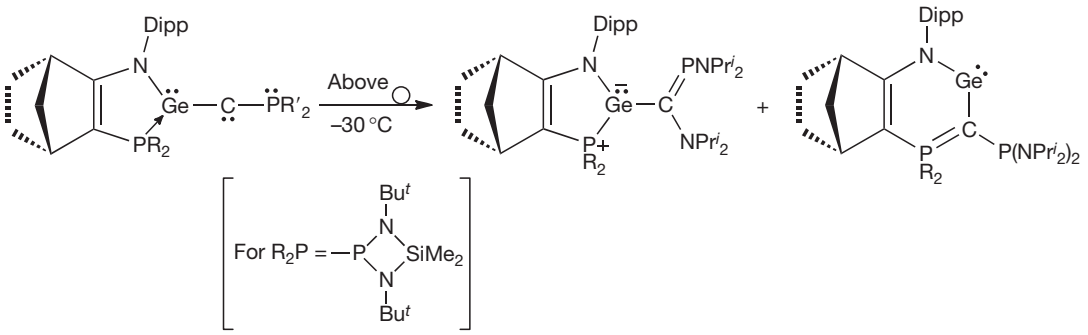

Scheme 55 Thermal isomerization of the isolable germyne analog derivative.

showed a bis(carbenoid) structure of the type–(L:→)G̈e–C̈–. This was evident from the peculiar structural features of this compound: (1) very long germanium–carbon separation of 1.887(5) Å, which is between the typical values for the Ge–Ge single and Ge=Ge double bonds, being substantially longer than the calculated Ge≡C triple-bond length of 1.73 Å; (2) trigonal–planar geometry at the Ge–C–P phosphorus atom (sum of the bond angles 359.7°); (3) extraordinarily short Ge–C–P phosphorus–carbon bond distance of 1.549(5) Å, indicative of a strong π-interaction between the phosphino substituent and the germanium–carbon fragment and being in the range of phosphinocarbenes or phosphaalkynes.

Contribution from the three resonance extremes, shown as **A**, **B**, and **C** in Scheme 54 (of which **A** is the most important contributor), can therefore be considered.

Computations showed that the singly bonded resonance structure **A** is 10 kcal mol^{-1} more favorable than the doubly bonded form **C**, whereas the triply bonded canonical form **B** is not an energy minimum of the potential energy surface. The major contribution of the bis(carbenoid) form **A** was further supported by the NBO analysis, which showed the presence of a lone pair of electrons on the germanium atom (64% s-character and 36% p-character) and on the carbon atom (2% s-character and 98% p-character), as well as a π-bond between the phosphorus and carbon atoms. Extremely high p-character of the lone pair of electrons on the C atom points to its sp-type hybridization despite the bent Ge–C–P fragment (bending angle 145.8°) (^{13}C NMR resonance of the central carbon atom at 162.4 ppm was in the region expected for a phosphinocarbene).

Like the isostructural silyne (Scheme 51), the germyne analog with the four-membered ring R_2P-fragment also undergoes isomerization at temperatures above −30 °C, giving a mixture of the phosphaalkene and cyclic six-membered ring germylene derivatives (Scheme 55).[149]

Formation of the latter involves the migration of the phosphane ligand from the Ge to the C center in the starting bis(carbenoid). By contrast, thermal isomerization of the germyne analog with the five-membered ring R_2P-fragment exclusively leads to the cyclic germylene, apparently because of the lower steric hindrances associated with the phosphane ligand migration.

1.11.5 Conclusion

The field of stable multiply bonded derivatives based on the heavy group 14 elements, which was established in the 1970–80s by the pioneering syntheses of the first distannene (1973), disilene (1981), and silene (1981), is flourishing. A variety of homo- and heteronuclear derivatives of the 'heavy' alkenes >E=E′<, 'heavy' 1,3-dienes >E′=E″–E=E<, 'heavy' allenes >E=E′=E″< and even 'heavy' alkynes –E≡E– have been prepared (and in most cases structurally characterized). In contemporary organometallic chemistry, these compounds are no longer fleeting intermediates, but readily available as preparative-scale reagents very useful for the synthesis of acyclic and cyclic derivatives unavailable by any other synthetic route. The principal structural distinctions between the 'heavy' alkenes >E=E< and their organic counterparts >C=C< (as well as between the 'heavy' alkynes –E≡E– and organic alkynes –C≡C–) are now firmly experimentally established, and the reasons behind these distinctions are well understood theoretically. The fundamental issue of the >E=E< and –E≡E– bonding natures, compared with those in the prototypical alkenes and alkynes, was comprehensively addressed in computational studies showing the principal differences in their bonding types: *classical covalent* in the planar alkenes and linear alkynes versus *nonclassical donor–acceptor* in their *trans*-bent 'heavy' analogs.

As for future prospects, one can expect developments of novel types of double bonding between the different main group elements of the types $R_2E{=}E'{-}R'$ and $R_2E{=}E''$ (E = heavy group 14 element, E′ = group 13/15 element, E″ = group 16 element). Triply bonded derivatives of the types R–E≡E′–R′ and R–E≡E″ (E, E′ = heavy group 14 elements, E″ = group 15 element), especially those lacking intramolecular stabilization by Lewis base ligands and heteroatom substituents electronically disturbing E≡E′ π-bonds through their lone-pair conjugation, are among the most prominent candidates for experimental pursuits. Apart from the purely fundamental developments, the practical utilization of 'heavy' alkenes and alkynes in the field of material science (such as their use as novel ligands for transition metal complexes) is eagerly anticipated in the near future. For related chapters in this Comprehensive, we refer to **Chapters 1.18**, **1.19**, **7.13** and **7.14**.

References

1. (a) Goldberg, D. E.; Harris, D. H.; Lappert, M. F.; Thomas, K. M. *J. Chem. Soc., Chem. Commun.* **1976**, 261; (b) Davidson, P. J.; Harris, D. H.; Lappert, M. F. *J. Chem. Soc., Dalton Trans.* **1976**, 2268.
2. (a) West, R.; Fink, M. J.; Michl, J. *Science* **1981**, *214*, 1343; (b) Fink, M. J.; Michalczyk, M. J.; Haller, K. J.; West, R.; Michl, J. *J. Chem. Soc., Chem. Commun.* **1983**, 1010; (c) West, R. *Pure Appl. Chem.* **1984**, *56*, 163; (d) Fink, M. J.; Michalczyk, M. J.; Haller, K. J.; West, R.; Michl, J. *Organometallics* **1984**, *3*, 793; (e) Shepherd, B. D.; Campana, C. F.; West, R. *Heteroatom Chem.* **1990**, *1*, 1; (f) Wind, M.; Powell, D. R.; West, R. *Organometallics* **1996**, *15*, 5772.
3. Brook, A. G.; Abdesaken, F.; Gutekunst, B.; Gutekunst, G.; Kallury, R. K. *J. Chem. Soc., Chem. Commun.* **1981**, 191.
4. Recent reviews on the stable disilenes: (a) Okazaki, R.; West, R. *Adv. Organomet. Chem.* **1996**, *39*, 231; (b) Weidenbruch, M. In *The Chemistry of Organic Silicon Compounds*. Rappoport, Z., Apeloig, Y., Eds.; Wiley: Chichester, 2001; Vol. 3, Chapter 5; (c) Kira, M.; Iwamoto, T. *Adv. Organomet. Chem.* **2006**, *54*, 73; (d) Lee, V. Ya.; Sekiguchi, A. *Organometallic Compounds of Low-Coordinate Si, Ge, Sn and Pb: From Phantom Species to Stable Compounds*. Wiley: Chichester, 2010; Chapter 5.
5. Shepherd, B. D.; Powell, D. R.; West, R. *Organometallics* **1989**, *8*, 2664.
6. Archibald, R. S.; van den Winkel, Y.; Millevolte, A. J.; Desper, J. M.; West, R. *Organometallics* **1992**, *11*, 3276.
7. (a) Masamune, S.; Hanzawa, Y.; Murakami, S.; Bally, T.; Blount, J. F. *J. Am. Chem. Soc.* **1982**, *104*, 1150; (b) Masamune, S.; Murakami, S.; Snow, J. T.; Tobita, H.; Williams, D. J. *Organometallics* **1984**, *3*, 333.
8. Watanabe, H.; Takeuchi, K.; Fukawa, N.; Kato, M.; Goto, M.; Nagai, Y. *Chem. Lett.* **1987**, 1341.
9. (a) Tokitoh, N.; Suzuki, H.; Okazaki, R.; Ogawa, K. *J. Am. Chem. Soc.* **1993**, *115*, 10428; (b) Suzuki, H.; Tokitoh, N.; Okazaki, R.; Harada, J.; Ogawa, K.; Tomoda, S.; Goto, M. *Organometallics* **1995**, *14*, 1016.
10. Sasamori, T.; Hironaka, K.; Sugiyama, Y.; Takagi, N.; Nagase, S.; Hosoi, Y.; Furukawa, Y.; Tokitoh, N. *J. Am. Chem. Soc.* **2008**, *130*, 13856.
11. Sasamori, T.; Yuasa, A.; Hosoi, Y.; Furukawa, Y.; Tokitoh, N. *Organometallics* **2008**, *27*, 3325.
12. Kira, M.; Maruyama, T.; Kabuto, C.; Ebata, K.; Sakurai, H. *Angew. Chem. Int. Ed. Engl.* **1994**, *33*, 1489.
13. Kira, M.; Ohya, S.; Iwamoto, T.; Ichinohe, M.; Kabuto, C. *Organometallics* **2000**, *19*, 1817.
14. Wiberg, N.; Niedermayer, W.; Fischer, G.; Nöth, H.; Suter, M. *Eur. J. Inorg. Chem.* **2002**, 1066.
15. Ichinohe, M.; Kinjo, R.; Sekiguchi, A. *Organometallics* **2003**, *22*, 4621.
16. Sekiguchi, A.; Inoue, S.; Ichinohe, M.; Arai, Y. *J. Am. Chem. Soc.* **2004**, *126*, 9626.
17. Sato, T.; Mizuhata, Y.; Tokitoh, N. *Chem. Commun.* **2010**, 4402.
18. Schmedake, T. A.; Haaf, M.; Apeloig, Y.; Müller, T.; Bukalov, S.; West, R. *J. Am. Chem. Soc.* **1999**, *121*, 9479.
19. Iwamoto, T.; Furiya, Y.; Kobayashi, H.; Isobe, H.; Kira, M. *Organometallics* **2010**, *29*, 1869.
20. Yuasa, A.; Sasamori, T.; Hosoi, Y.; Furukawa, Y.; Tokitoh, N. *Bull. Chem. Soc. Jpn.* **2009**, *82*, 793.
21. Matsuo, T.; Kobayashi, M.; Tamao, K. *Dalton Trans.* **2010**, *39*, 9203.
22. Kobayashi, M.; Matsuo, T.; Fukunaga, T.; Hashizume, D.; Fueno, H.; Tanaka, K.; Tamao, K. *J. Am. Chem. Soc.* **2010**, *132*, 15162.
23. Fukazawa, A.; Li, Y.; Yamaguchi, S.; Tsuji, H.; Tamao, K. *J. Am. Chem. Soc.* **2007**, *129*, 14164.
24. (a) Wiberg, N.; Niedermayer, W.; Polborn, K. *Z. Anorg. Allg. Chem.* **2002**, *628*, 1045; (b) Wiberg, N.; Niedermayer, W.; Polborn, K.; Mayer, P. *Chem. Eur. J.* **2002**, *8*, 2730.
25. Iwamoto, T.; Okita, J.; Kabuto, C.; Kira, M. *J. Organomet. Chem.* **2003**, *686*, 105.
26. Zirngast, M.; Flock, M.; Baumgartner, J.; Marschner, C. *J. Am. Chem. Soc.* **2008**, *130*, 17460.
27. Hartmann, M.; Haji-Abdi, A.; Abersfelder, K.; Haycock, P. R.; White, A. J. P.; Scheschkewitz, D. *Dalton Trans.* **2010**, *39*, 9288.
28. Abersfelder, K.; Nguyen, T.-l.; Scheschkewitz, D. *Z. Anorg. Allg. Chem.* **2009**, *635*, 2093.
29. Nguyen, T.-l.; Scheschkewitz, D. *J. Am. Chem. Soc.* **2005**, *127*, 10174.
30. (a) Bejan, I.; Scheschkewitz, D. *Angew. Chem. Int. Ed.* **2007**, *46*, 5783; (b) Jeck, J.; Bejan, I.; White, A. J. P.; Nied, D.; Breher, F.; Scheschkewitz, D. *J. Am. Chem. Soc.* **2010**, *132*, 17306.
31. Iwamoto, T.; Kobayashi, M.; Uchiyama, K.; Sasaki, S.; Nagendran, S.; Isobe, H.; Kira, M. *J. Am. Chem. Soc.* **2009**, *131*, 3156.
32. Inoue, S.; Ichinohe, M.; Sekiguchi, A. *Chem. Lett.* **2008**, *37*, 1044.
33. Takeuchi, K.; Ikoshi, M.; Ichinohe, M.; Sekiguchi, A. *J. Am. Chem. Soc.* **2010**, *132*, 930.
34. Takeuchi, K.; Ichinohe, M.; Sekiguchi, A. *Organometallics* **2011**, *30*, 2044.
35. Takeuchi, K.; Ikoshi, M.; Ichinohe, M.; Sekiguchi, A. *J. Organomet. Chem.* **2011**, *696*, 1156.
36. Yamaguchi, T.; Sekiguchi, A.; Driess, M. *J. Am. Chem. Soc.* **2010**, *132*, 14061.
37. Boomgaarden, S.; Saak, W.; Marsmann, H.; Weidenbruch, M. *Z. Anorg. Allg. Chem.* **2002**, *628*, 1745.

38. (a) Jutzi, P.; Mix, A.; Rummel, B.; Schoeller, W. W.; Neumann, B.; Stammler, H.-G. *Science* **2004**, *305*, 849; (b) Jutzi, P.; Mix, A.; Neumann, B.; Rummel, B.; Shoeller, W. W.; Stammler, H.-G.; Rozhenko, A. B. *J. Am. Chem. Soc.* **2009**, *131*, 12137.
39. Wang, Y.; Xie, Y.; Wei, P.; King, R. B.; Schaefer, H. F., III; von Schleyer, P. R.; Robinson, G. H. *Science* **2008**, *321*, 1069.
40. (a) Matsumoto, S.; Tsutsui, S.; Kwon, E.; Sakamoto, K. *Angew. Chem. Int. Ed.* **2004**, *43*, 4610; (b) Tsutsui, S.; Kwon, E.; Tanaka, H.; Matsumoto, S.; Sakamoto, K. *Organometallics* **2005**, *24*, 4629.
41. West, R.; Cavalieri, J. D.; Buffy, J. J.; Fry, C.; Zilm, K. W.; Duchamp, J. C.; Kira, M.; Iwamoto, T.; Müller, T.; Apeloig, Y. *J. Am. Chem. Soc.* **1997**, *119*, 4972.
42. Ramsey, N. F. *Phys. Rev.* **1950**, *78*, 699.
43. Ichinohe, M.; Arai, Y.; Sekiguchi, A.; Takagi, N.; Nagase, S. *Organometallics* **2001**, *20*, 4141.
44. Auer, D.; Strohmann, C.; Arbuznikov, A. V.; Kaupp, M. *Organometallics* **2003**, *22*, 2442.
45. Pyykkö, P.; Atsumi, M. *Chem. Eur. J.* **2009**, *15*, 12770.
46. Pyykkö, P.; Atsumi, M. *Chem. Eur. J.* **2009**, *15*, 186.
47. Reviews on the cyclopropene analogues of the heavy group 14 elements: (a) Lee, V. Ya.; Sekiguchi, A. In *The Chemistry of Organic Germanium, Tin and Lead Compounds*; Rappoport, Z., Ed.; Wiley: Chichester, 2002; Vol. 2, Part 1, Chapter 14; (b) Sekiguchi, A.; Lee, V. Ya. *Organosilicon Chemistry V: From Molecules to Materials*; Auner, N., Weis, J., Eds.; Wiley-VCH: Weinheim, 2003; p 92; (c) Sekiguchi, A.; Lee, V. Ya. *Chem. Rev.* **2003**, *103*, 1429.
48. (a) Göller, A.; Heydt, H.; Clark, T. *J. Org. Chem.* **1996**, *61*, 5840; (b) Naruse, Y.; Ma, J.; Inagaki, S. *Tetrahedron Lett.* **2001**, *42*, 6553.
49. (a) Iwamoto, T.; Kabuto, C.; Kira, M. *J. Am. Chem. Soc.* **1999**, *121*, 886; (b) Iwamoto, T.; Tamura, M.; Kabuto, C.; Kira, M. *Organometallics* **2003**, *22*, 2342.
50. Ichinohe, M.; Matsuno, T.; Sekiguchi, A. *Angew. Chem. Int. Ed.* **1999**, *38*, 2194.
51. Lee, V. Ya.; Ichinohe, M.; Sekiguchi, A.; Takagi, N.; Nagase, S. *J. Am. Chem. Soc.* **2000**, *122*, 9034.
52. Lee, V. Ya.; Yasuda, H.; Sekiguchi, A. *J. Am. Chem. Soc.* **2007**, *129*, 2436.
53. Ichinohe, M.; Igarashi, M.; Sanuki, K.; Sekiguchi, A. *J. Am. Chem. Soc.* **2005**, *127*, 9978.
54. Uchiyama, K.; Nagendran, S.; Ishida, S.; Iwamoto, T.; Kira, M. *J. Am. Chem. Soc.* **2007**, *129*, 10638.
55. Kira, M.; Iwamoto, T.; Kabuto, C. *J. Am. Chem. Soc.* **1996**, *118*, 10303.
56. Wiberg, N.; Auer, H.; Nöth, H.; Knizek, J.; Polborn, K. *Angew. Chem. Int. Ed.* **1998**, *37*, 2869.
57. Wiberg, N.; Niedermayer, W.; Nöth, H.; Warchhold, M. *Z. Anorg. Allg. Chem.* **2001**, *627*, 1717.
58. Wiberg, N.; Vasisht, S. K.; Fischer, G.; Mayer, P. *Z. Anorg. Allg. Chem.* **2004**, *630*, 1823.
59. Kinjo, R.; Ichinohe, M.; Sekiguchi, A.; Takagi, N.; Sumimoto, M.; Nagase, S. *J. Am. Chem. Soc.* **2007**, *129*, 7766.
60. Takanashi, K.; Lee, V. Ya.; Ichinohe, M.; Sekiguchi, A. *Angew. Chem. Int. Ed.* **2006**, *45*, 3269.
61. Lee, V. Ya.; Takanashi, K.; Matsuno, T.; Ichinohe, M.; Sekiguchi, A. *J. Am. Chem. Soc.* **2004**, *126*, 4758.
62. Lee, V. Ya.; Miyazaki, S.; Yasuda, H.; Sekiguchi, A. *J. Am. Chem. Soc.* **2008**, *130*, 2758.
63. Grybat, A.; Boomgaarden, S.; Saak, W.; Marsmann, H.; Weidenbruch, M. *Angew. Chem. Int. Ed.* **1999**, *38*, 2010.
64. Kobayashi, H.; Iwamoto, T.; Kira, M. *J. Am. Chem. Soc.* **2005**, *127*, 15376.
65. Abe, T.; Iwamoto, T.; Kira, M. *J. Am. Chem. Soc.* **2010**, *132*, 5008.
66. Tanaka, R.; Iwamoto, T.; Kira, M. *Angew. Chem. Int. Ed.* **2006**, *45*, 6371.
67. Recent reviews on the stable digermenes: (a) Escudié, J.; Couret, C.; Ranaivonjatovo, H.; Satgé, J. *Coord. Chem. Rev.* **1994**, *130*, 427; (b) Baines, K. M.; Stibbs, W. G. *Adv. Organomet. Chem.* **1996**, *39*, 275; (c) Escudié, J.; Ranaivonjatovo, H. *Adv. Organomet. Chem.* **1999**, *44*, 113; (d) Tokitoh, N.; Okazaki, R. In *The Chemistry of Organic Germanium, Tin and Lead Compounds*; Rappoport, Z., Ed.; Wiley: Chichester, 2002; Vol. 2, Part 1, Chapter 13; (e) Klinkhammer, K. W. In *The Chemistry of Organic Germanium, Tin and Lead Compounds*; Rappoport, Z., Ed.; Wiley: Chichester, 2002; Vol. 2, Part 1, Chapter 4(f) See Ref. 4d.
68. (a) Goldberg, D. E.; Harris, D. H.; Lappert, M. F.; Thomas, K. M. *J. Chem. Soc., Chem. Commun.* **1976**, 261; (b) Davidson, P. J.; Harris, D. H.; Lappert, M. F. *J. Chem. Soc., Dalton Trans.* **1976**, 2268; (c) Cotton, J. D.; Davidson, P. J.; Lappert, M. F.; Donaldson, J. D.; Silver, J. *J. Chem. Soc., Dalton Trans.* **1976**, 2286; (d) Hitchcock, P. B.; Lappert, M. F.; Miles, S. J.; Thorne, A. J. *J. Chem. Soc., Chem. Commun.* **1984**, 480; (e) Goldberg, D. E.; Hitchcock, P. B.; Lappert, M. F.; Thomas, K. M.; Thorne, A. J.; Fjeldberg, T.; Haaland, A.; Schilling, B. E. R. *J. Chem. Soc., Dalton Trans.* **1986**, 2387.
69. Snow, J. T.; Murakami, S.; Masamune, S.; Williams, D. J. *Tetrahedron Lett.* **1984**, *25*, 4191.
70. Simons, R. S.; Pu, L.; Olmstead, M. M.; Power, P. P. *Organometallics* **1997**, *16*, 1920.
71. Pu, L.; Phillips, A. D.; Richards, A. F.; Stender, M.; Simons, R. S.; Olmstead, M. M.; Power, P. P. *J. Am. Chem. Soc.* **2003**, *125*, 11626.
72. Stender, M.; Pu, L.; Power, P. P. *Organometallics* **2001**, *20*, 1820.
73. Weidenbruch, M.; Stürmann, M.; Kilian, H.; Pohl, S.; Saak, W. *Chem. Ber.* **1997**, *130*, 735.
74. Schäfer, A.; Saak, W.; Weidenbruch, M.; Marsmann, H.; Henkel, G. *Chem. Ber.* **1997**, *130*, 1733.
75. Schäfer, A.; Saak, W.; Weidenbruch, M. *Z. Anorg. Allg. Chem.* **1998**, *624*, 1405.
76. Pampuch, B.; Saak, W.; Weidenbruch, M. *J. Organomet. Chem.* **2006**, *691*, 3540.
77. Sasamori, T.; Sugiyama, Y.; Takeda, N.; Tokitoh, N. *Organometallics* **2005**, *24*, 3309.
78. Lei, H.; Fettinger, J. C.; Power, P. P. *Organometallics* **2010**, *29*, 5585.
79. Batcheller, S. A.; Tsumuraya, T.; Tempkin, O.; Davis, W. M.; Masamune, S. *J. Am. Chem. Soc.* **1990**, *112*, 9394.
80. Kira, M.; Iwamoto, T.; Maruyama, T.; Kabuto, C.; Sakurai, H. *Organometallics* **1996**, *15*, 3767.
81. (a) Kishikawa, K.; Tokitoh, N.; Okazaki, R. *Chem. Lett.* **1998**, 239; (b) Tokitoh, N.; Kishikawa, K.; Okazaki, R.; Sasamori, T.; Nakata, N.; Takeda, N. *Polyhedron* **2002**, *21*, 563.
82. Lee, V. Ya.; McNeice, K.; Ito, Y.; Sekiguchi, A. *Chem. Commun.* **2011**, 3272.
83. (a) Spikes, G. H.; Fettinger, J. C.; Power, P. P. *J. Am. Chem. Soc.* **2005**, *127*, 12232; (b) Richards, A. F.; Phillips, A. D.; Olmstead, M. M.; Power, P. P. *J. Am. Chem. Soc.* **2003**, *125*, 3204.
84. Cui, C.; Olmstead, M. M.; Fettinger, J. C.; Spikes, G. H.; Power, P. P. *J. Am. Chem. Soc.* **2005**, *127*, 17530.
85. Sekiguchi, A.; Yamazaki, H.; Kabuto, C.; Sakurai, H. *J. Am. Chem. Soc.* **1995**, *117*, 8025.
86. Sekiguchi, A.; Fukaya, N.; Ichinohe, M.; Takagi, N.; Nagase, S. *J. Am. Chem. Soc.* **1999**, *121*, 11587.
87. Sekiguchi, A.; Ishida, Y.; Fukaya, N.; Ichinohe, M.; Takagi, N.; Nagase, S. *J. Am. Chem. Soc.* **2002**, *124*, 1158.
88. (a) Lee, V. Ya.; Yasuda, H.; Ichinohe, M.; Sekiguchi, A. *Angew. Chem. Int. Ed.* **2005**, *44*, 6378; (b) Lee, V. Ya.; Yasuda, H.; Ichinohe, M.; Sekiguchi, A. *J. Organomet. Chem.* **2007**, *692*, 10.
89. Lee, V. Ya.; Yasuda, H.; Sekiguchi, A. *J. Am. Chem. Soc.* **2007**, *129*, 2436.
90. Lee, V. Ya.; Takanashi, K.; Ichinohe, M.; Sekiguchi, A. *J. Am. Chem. Soc.* **2003**, *125*, 6012.
91. Ramaker, G.; Saak, W.; Haase, D.; Weidenbruch, M. *Organometallics* **2003**, *22*, 5212.
92. Lee, V. Ya.; Ito, Y.; Yasuda, H.; Takanashi, K.; Sekiguchi, A. *J. Am. Chem. Soc.* **2011**, *133*, 5103.
93. Ramaker, G.; Schäfer, A.; Saak, W.; Weidenbruch, M. *Organometallics* **2003**, *22*, 1302.
94. Masamune, S.; Sita, L. R. *J. Am. Chem. Soc.* **1985**, *107*, 6390.
95. Stanciu, C.; Richards, A. F.; Power, P. P. *J. Am. Chem. Soc.* **2004**, *126*, 4106.
96. (a) Weidenbruch, M.; Kilian, H.; Peters, K.; von Schnering, H. G.; Marsmann, H. *Chem. Ber.* **1995**, *128*, 983; (b) Della Bona, M. A.; Cassani, M. C.; Keates, J. M.; Lawless, G. A.; Lappert, M. F.; Stürmann, M.; Weidenbruch, M. *J. Chem. Soc., Dalton Trans.* **1998**, 1187.
97. Klinkhammer, K. W.; Schwarz, W. *Angew. Chem. Int. Ed. Engl.* **1995**, *34*, 1334.
98. (a) Klett, J.; Klinkhammer, K. W.; Niemeyer, M. *Chem. Eur. J.* **1999**, *5*, 2531; (b) Klinkhammer, K. *Polyhedron* **2002**, *21*, 587.
99. (a) Fukawa, T.; Lee, V. Ya.; Nakamoto, M.; Sekiguchi, A. *J. Am. Chem. Soc.* **2004**, *126*, 11758; (b) Lee, V. Ya.; Fukawa, T.; Nakamoto, M.; Sekiguchi, A.; Tumanskii, B. L.; Karni, M.; Apeloig, Y. *J. Am. Chem. Soc.* **2006**, *128*, 11643.
100. Klinkhammer, K. W.; Fässler, T. F.; Grützmacher, H. *Angew. Chem. Int. Ed.* **1998**, *37*, 124.
101. Stürmann, M.; Saak, W.; Klinkhammer, K. W.; Weidenbruch, M. *Z. Anorg. Allg. Chem.* **1999**, *625*, 1955.
102. Wiberg, N.; Lerner, H.-W.; Vasisht, S.-K.; Wagner, S.; Karaghiosoff, K.; Nöth, H.; Ponikwar, W. *Eur. J. Inorg. Chem.* **1999**, 1211.
103. Schrenk, C.; Schnepf, A. *Chem. Commun.* **2010**, 6756.
104. Arp, H.; Baumgartner, J.; Marschner, C.; Müller, T. *J. Am. Chem. Soc.* **2011**, *133*, 5632.
105. Stürmann, M.; Saak, W.; Marsmann, H.; Weidenbruch, M. *Angew. Chem. Int. Ed.* **1999**, *38*, 187.
106. Stürmann, M.; Saak, W.; Weidenbruch, M.; Klinkhammer, K. W. *Eur. J. Inorg. Chem.* **1999**, 579.

107. Hino, S.; Olmstead, M.; Phillips, A. D.; Wright, R. J.; Power, P. P. *Inorg. Chem.* **2004**, *43*, 7346.
108. Stürmann, M.; Weidenbruch, M.; Klinkhammer, K. W.; Lissner, F.; Marsmann, H. *Organometallics* **1998**, *17*, 4425.
109. Reviews: (a)Lee, V. Ya.; Sekiguchi, A. *Organometallics* **2004**, *23*, 2822; (b) Lee, V. Ya.; Sekiguchi, A.; Escudié, J.; Ranaivonjatovo, H. *Chem. Lett.* **2010**, *39*, 312.
110. (a) Baines, K. M.; Cooke, J. A. *Organometallics* **1991**, *10*, 3419; (b) Baines, K. M.; Cooke, J. A. *Organometallics* **1992**, *11*, 3487.
111. Lee, V. Ya.; Yasuda, H.; Sekiguchi, A. *J. Am. Chem. Soc.* **2007**, *129*, 2436.
112. Lee, V. Ya.; Ichinohe, M.; Sekiguchi, A. *J. Am. Chem. Soc.* **2000**, *122*, 12604.
113. Ichinohe, M.; Arai, Y.; Sekiguchi, A.; Takagi, N.; Nagase, S. *Organometallics* **2001**, *20*, 4141.
114. Igarashi, M.; Ichinohe, M.; Sekiguchi, A. *Heteroatom Chem.* **2008**, *19*, 649.
115. Iwamoto, T.; Okita, J.; Yoshida, N.; Kira, M. *Silicon* **2010**, *2*, 209.
116. Sekiguchi, A.; Izumi, R.; Lee, V. Ya.; Ichinohe, M. *J. Am. Chem. Soc.* **2002**, *124*, 14822.
117. Chaubon, M.-A.; Escudié, J.; Ranaivonjatovo, H.; Satgé, J. *Chem. Commun.* **1996**, 2621.
118. Schäfer, A.; Saak, W.; Weidenbruch, M. *Organometallics* **2003**, *22*, 215.
119. Sekiguchi, A.; Izumi, R.; Lee, V. Ya.; Ichinohe, M. *Organometallics* **2003**, *22*, 1483.
120. (a) Lee, V. Ya.; Takanashi, K.; Ichinohe, M.; Sekiguchi, A. *J. Am. Chem. Soc.* **2003**, *125*, 6012; (b) Lee, V. Ya.; Takanashi, K.; Nakamoto, M.; Sekiguchi, A. *Russ. Chem. Bull., Int. Ed.* **2004**, *53*, 1102.
121. Reviews: (a) Willms, S.; Weidenbruch, M. In *Organosilicon Chemistry IV: From Molecules to Materials*; Auner, N., Weis, J., Eds.; Wiley-VCH: Weinheim, 2000; p 117; (b) Weidenbruch, M. *J. Organomet. Chem.* **2002**, *646*, 39; (c) Weidenbruch, M. In *Silicon Chemistry*; Jutzi, P., Schubert, U., Eds.; Wiley-VCH: Weinheim, 2003; p 100; (d) Weidenbruch, M. In *Organosilicon Chemistry V: From Molecules to Materials*; Auner, N., Weis, J., Eds.; Wiley-VCH: Weinheim, 2003; p 114.
122. Weidenbruch, M.; Willms, S.; Saak, W.; Henkel, G. *Angew. Chem. Int. Ed. Engl.* **1997**, *36*, 2503.
123. (a) Schäfer, H.; Saak, W.; Weidenbruch, M. *Angew. Chem. Int. Ed.* **2000**, *39*, 3703;(b) For the improved synthesis of tetragermabuta-1,3-diene (4 $GeCl_2$•diox + 6 TipMgBr + Mg), see: Ramaker, G.; Schäfer, A.; Saak, W.; Weidenbruch, M. *Organometallics* **2003**, *22*, 1302.
124. Ichinohe, M.; Sanuki, K.; Inoue, S.; Sekiguchi, A. *Organometallics* **2004**, *23*, 3088.
125. Cui, C.; Olmstead, M. M.; Power, P. P. *J. Am. Chem. Soc.* **2004**, *126*, 5062.
126. Suzuki, K.; Matsuo, T.; Hashizume, D.; Fueno, H.; Tanaka, K.; Tamao, K. *Science* **2011**, *331*, 1306.
127. Iwamoto, T.; Tamura, M.; Kabuto, C.; Kira, M. *Science* **2000**, *290*, 504.
128. Reviews: (a) Escudié, J.; Ranaivonjatovo, H.; Rigon, L. *Chem. Rev.* **2000**, *100*, 3639; (b) Eichler, B.; West, R. *Adv. Organomet. Chem.* **2001**, *46*, 1; (c) Escudié, J.; Ranaivonjatovo, H. *Organometallics* **2007**, *26*, 1542.
129. Miracle, G. E.; Ball, J. L.; Powell, D. R.; West, R. *J. Am. Chem. Soc.* **1993**, *115*, 11598.
130. Trommer, M.; Miracle, G. E.; Eichler, B. E.; Powell, D. R.; West, R. *Organometallics* **1997**, *16*, 5737.
131. (a) Eichler, B. E.; Powell, D. R.; West, R. *Organometallics* **1998**, *17*, 2147; (b) Eichler, B. E.; Powell, D. R.; West, R. *Organometallics* **1999**, *18*, 540.
132. Tokitoh, N.; Kishikawa, K.; Okazaki, R. *Chem. Lett.* **1998**, 811.
133. (a) Ishida, S.; Iwamoto, T.; Kabuto, C.; Kira, M. *Nature* **2003**, *421*, 725; (b) Iwamoto, T.; Abe, T.; Kabuto, C.; Kira, M. *Chem. Commun.* **2005**, 5190; (c) Iwamoto, T.; Masuda, H.; Kabuto, C.; Kira, M. *Organometallics* **2005**, *24*, 197.
134. Tanaka, H.; Inoue, S.; Ichinohe, M.; Driess, M.; Sekiguchi, A. *Organometallics* **2011**, *30*, 3475.
135. (a) Foo, C.; Lau, K.-C.; Yang, Y.-F.; So, C.-W. *Chem. Commun.* **2009**, 6816; (b) Leung, W.-P.; Chan, Y.-C.; Mak, T. C. W. *Inorg. Chem.* **2011**, *50*, 10517.
136. Reviews: (a) Power, P. P. *Chem. Commun.* **2003**, 2091; (b) Power, P. P. *Organometallics* **2007**, *26*, 4362.
137. (a) Wiberg, N. In *Organosilicon Chemistry V: From Molecules to Materials*; Auner, N., Weis, J., Eds.; Wiley-VCH: Weinheim, 2003; p 101; (b) Takagi, N.; Nagase, S. *Eur. J. Inorg. Chem.* **2002**, 2775.
138. (a) Sekiguchi, A.; Kinjo, R.; Ichinohe, M. *Science* **2004**, *305*, 1755; (b) Kravchenko, V.; Kinjo, R.; Sekiguchi, A.; Ichinohe, M.; West, R.; Balazs, Y. S.; Schmidt, A.; Karni, M.; Apeloig, Y. *J. Am. Chem. Soc.* **2006**, *128*, 14472; (c) Sekiguchi, A.; Ichinohe, M.; Kinjo, R. *Bull. Chem. Soc. Jpn.* **2006**, *79*, 825.
139. (a) Karni, M.; Apeloig, Y.; Takagi, N.; Nagase, S. *Organometallics* **2005**, *24*, 6319 see also: (b) Auer, D.; Kaupp, M.; Strohmann, C. *Organometallics* **2005**, *24*, 6331.
140. Murata, Y.; Ichinohe, M.; Sekiguchi, A. *J. Am. Chem. Soc.* **2010**, *132*, 16768.
141. Sasamori, T.; Han, J. S.; Hironaka, K.; Takagi, N.; Nagase, S.; Tokitoh, N. *Pure Appl. Chem.* **2010**, *82*, 603.
142. Stender, M.; Phillips, A. D.; Wright, R. J.; Power, P. P. *Angew. Chem. Int. Ed.* **2002**, *41*, 1785.
143. Peng, Y.; Fischer, R. C.; Merrill, W. A.; Fischer, J.; Pu, L.; Ellis, B. D.; Fettinger, J. C.; Herber, R. H.; Power, P. P. *Chem. Sci.* **2010**, *1*, 461.
144. Sugiyama, Y.; Sasamori, T.; Hosoi, Y.; Furukawa, Y.; Takagi, N.; Nagase, S.; Tokitoh, N. *J. Am. Chem. Soc.* **2006**, *128*, 1023.
145. (a) Phillips, A. D.; Wright, R. J.; Olmstead, M. M.; Power, P. P. *J. Am. Chem. Soc.* **2002**, *124*, 5930; (b) Fischer, R. C.; Pu, L.; Fettinger, J. C.; Brynda, M. A.; Power, P. P. *J. Am. Chem. Soc.* **2006**, *128*, 11366.
146. Pu, L.; Twamley, B.; Power, P. P. *J. Am. Chem. Soc.* **2000**, *122*, 3524.
147. Jambor, R.; Kasna, B.; Kirschner, K. N.; Schürmann, M.; Jurkschat, K. *Angew. Chem. Int. Ed.* **2008**, *47*, 1650.
148. Gau, D.; Kato, T.; Saffon-Merceron, N.; De Cózar, A.; Cossío, F. P.; Baceiredo, A. *Angew. Chem. Int. Ed.* **2010**, *49*, 6585.
149. Berthe, J.; Garcia, J. M.; Ocando, E.; Kato, T.; Saffon-Merceron, N.; De Cózar, A.; Cossío, F. P.; Baceiredo, A. *J. Am. Chem. Soc.* **2011**, *133*, 15930.

1.12 Multiply Bonded Compounds of Group 15 Elements

JD Protasiewicz, Case Western Reserve University, Cleveland, OH, USA

1.12.1 Introduction

1.12.1.1 Scope of the Chapter

The synthesis and study of compounds featuring multiple bonds to group 15 elements have grown immensely since the first examples appeared and now represent a rather mature research area. As such, to make this chapter manageable (if it was truly comprehensive, the topic would likely require several books' worth of text!), the following limitations in the coverage for this chapter have been imposed:

- This chapter emphasizes developments that concern compounds having heavier multiply bonded atoms of group 15 (P, As, Sb, and Bi) because the number of multiply bonded nitrogen compounds are simply too numerous to include here.
- This chapter focuses on compounds that have multiple bonds to other elements of the p-block, and, thus, excludes most compounds having transition metal group 15 multiple bonds. The field of M–E multiple bonds (largely E = P for group 15) is, again, rather large and constitutes its own area of research.[1–10]
- This chapter emphasizes compounds in which the group 15 multiple bond is not part of a ring structure. The interested reader is directed to the rather comprehensive book by Mathey[11] about such materials.
- This chapter also excludes a large number of materials having group 15 to O, C, and S multiple bonds that might be better described as ylidic or hypervalent in character.[12] This includes materials such as phosphane oxides $R_3P{=}O$, Wittig reagents $R_3P{=}CR_2$, etc., that are well known and too numerous to present full coverage here.
- The multiple-bonded compounds that are the main focus of this chapter are those having pnictogens with low coordination numbers of 1 or 2, so as to emphasize multiple bonding.[13]
- This chapter emphasizes new developments in unusual reactivity, physical properties, and applications of multiply bonded group 15 and avoids comprehensive details on the structural aspects of these compounds. The body of structural data, largely from single-crystal x-ray structure determinations, has been recently and authoritatively evaluated in a 2010 review by Fischer and Power[14] and in 1999 by Power.[15] Interested readers should consult these articles for detailed structural analyses.
- Finally, this chapter concentrates on compounds and materials that have appeared from 2000 until about 2010, highlighting compounds and applications that are newer to the field.

Between 2000 and 2010, a significant number of reviews appeared that focus on various aspects of multiply bonded group 15 compounds of interest to this chapter. To provide

Table 1 Selected review articles and books published in the past decade featuring multiply bonded group 15 compounds

Title	*Author(s)*	*Reference*
Phosphorus: The Carbon Copy	Dillon, K. B.; Mathey, F.; Nixon, J. F.	John Wiley & Sons: New York, 1998
π-Bonding and the lone pair effect in multiple bonds between heavier main group elements	Power, P. P.	*Chem. Rev.* **1999**, *99*, 3463
Some past vignettes of and future prospects for Main Group chemistry	Cowley, A. H.	*J. Organomet. Chem.* **2000**, *600*, 168
"Phospha-variations" on the themes of Staudinger and Wittig: Phosphorus analogs of Wittig reagents	Shah, S.; Protasiewicz, J. D.	*Coord. Chem. Rev.* **2000**, *210*(1), 181
Silylphosphanes: Developments in phosphorus chemistry	Fritz, G.; Scheer, P.	*Chem. Rev.* **2000**, *100*, 3341
Phosphorus 2000	Corbridge, D. E. C.	Elsevier: New York, 2000
Unusual structures of main group organometallic compounds containing *m*-terphenyl ligands	Clyburne, J. A. C.; McMullen, N.	*Coord. Chem. Rev.* **2000**, *210*, 73
Heavy allenes and cumulenes E=C=E′ and E=C=C=E′ (E = P, As, Si, Ge, Sn; E′ = C, N, P, As, O, S)	Escudie, J.; Ranaivonjatovo, H.; Rigon, L.	*Chem. Rev.* **2000**, *100*, 3639
New aspects in the chemistry of low-coordinated inter-element compounds of heavier group 15 elements	Tokitoh, N.	*J. Organomet. Chem.* **2000**, *611*, 217
Phosphaalkenes with inverse electron density	Weber, L.	*Eur. J. Inorg. Chem.* **2000**, 2425–2441
Protecting groups for stabilization of inter-element linkages	Yoshifuji, M.	*J. Organomet. Chem.* **2000**, *611*, 210
Zirconium–phosphorus chemistry: Strategies in syntheses, reactivity, catalysis, and utility	Stephan, D. W.	*Angew. Chem. Int. Ed. Engl.* **2000**, *39*, 315
Recent developments in low coordination organo-antimony and bismuth chemistry	Jones, C.	*Coord. Chem. Rev.* **2001**, *215*, 151
Phosphorus–Carbon Heterocyclic Chemistry: The Rise of a New Domain.	Mathey, F.	Pergamon: Amsterdam, 2001
Organometallic compounds containing tris(trimethylsilyl) methyl or related ligands	Eaborn, C.; Smith, J. D.	*J. Chem. Soc. Dalton Trans.* **2001**, 1541
Recent advances in the chemistry of group 14–group 16 double bond compounds	Tokitoh, N.; Okazaki, R.	*Adv. Organomet. Chem.* **2001**, *47*, 121
Comparative behaviours of phospha-alkynes and alkynes at electron-rich phosphinic metal centres	Pombeiro, A. J. L.	*J. Organomet. Chem.* **2001**, *632*, 215
Reactions of α-diketones and *o*-quinones with phosphorus compounds	Osman, F. H.; Al-Samahy, F. A.	*Chem. Rev.* **2002**, *102*, 629
Phosphanes and phosphonium salts	Allen, D. W.	*Organophosphorus Chem.* **2002**, *32*, 1–73
New synthetic opportunities using Lewis acidic phosphanes	Burford, N.; Ragogna, P. J.	*J. Chem. Soc. Dalton Trans.* **2002**, 4307
Complexes with a metal–phosphorus triple bond as versatile building blocks in coordination and organometallic chemistry	Scheer, M.; Schiffer, M.; Leiner, E.; Johnson, B. P.; Haindl, C.; Umbarkar, S.	*Phosphorus, Sulfur Silicon Relat. Elem.* **2002**, *177*, 1617
Systematic studies on homo- and heteronuclear doubly bonded compounds of heavier group 15 elements	Tokitoh, N.; Sasamori, T.; Takeda, N.; Nagase, S.	*Phosphorus, Sulfur Silicon Relat. Elem.* **2002**, *177*, 1473
Phosphinidenes	Lammertsma, K.	*Top. Curr. Chem.* **2003**, *229*, (New Aspects in Phosphorus Chemistry III), 95–119
Chemistry of phosphanylidene carbenoids	Yoshifuji, M.; Ito, S.	*Top. Curr. Chem.* **2003**, *223*, (New Aspects in Phosphorus Chemistry II), 67–89
Phospha-organic chemistry: Panorama and perspectives	Mathey, F.	*Angew. Chem. Int. Ed.* **2003**, *42*, 1578
The quest for isophosphaalkynes (isophosphocyanides) C≡P–R – still an elusive class of compounds	Weber, L.	*Eur. J. Inorg. Chem.* **2003**, *10*, 1843
Persistent and stable radicals of the heavier main group elements and related species	Power, P. P.	*Chem. Rev.* **2003**, *103*, 789
The chemistry of fluorine containing phosphaalkenes, arsaalkenes and selenocarbonyls	Grobe, J.; Le Van, D.	*J. Fluorine Chem.* **2004**, *125*, 801
Unusual geometries in main group chemistry	Bouhadir, G.; Bourissou, D.	*Chem. Soc. Rev.* **2004**, *33*, 210
Phosphasila-, phosphagerma-, and phosphaarsaallenes – P=C=E (E = Si, Ge, As) and arsa- and diarsaallenes – As=C=E (E = C, As)	Escudie, J.; Ranaivonjatovo, H.; Bouslikhane, M.; El Harouch, Y.; Baiget, L.; Cretiu Nemes, G.	*Russ. Chem. Bull.* **2004**, *53*, 1020
Low-valent organoantimony and -bismuth compounds with neopentyl and (trimethylsilyl)methyl substituents	Breunig, H. J.; Balázs, L.	*Organometallics* **2004**, *23*, 304
Expanding the analogy between P=C and C=C bonds to polymer science	Gates, D. P.	*Top. Curr. Chem.* **2005**, *250*, (New Aspects in Phosphorus Chemistry V), 107–126

(*Continued*)

Table 1 (Continued)

Title	*Author(s)*	*Reference*
Recent developments in the chemistry of metallophosphaalkenes	Weber, L.	*Coord. Chem. Rev.* **2005**, *249*, 741
Functions containing doubly bonded P, As, Sb, Bi, Si, Ge, B, or a metal	Romanenko, V. D.; Rudzevich, V. L.	*Compr. Org. Funct. Group Transform. II* **2005**, *6*, 661–711
Ketenimines and their P, As, Sb and Bi analogs	Aitken, R. A.	*Compr. Org. Funct. Group Transform. II* **2005**, *3*, 605–619
Triple-bonded heteroatom derivatives other than nitriles with another heteroatom attached to the sp carbon atom	Bergsträsser, U.	*Compr. Org. Funct. Group Transform. II* **2005**, *5*, 1081–1093
N-substituted nitriles and other hetero analogues of nitriles of the type RCZ	Escolano, C.; Vazquez, S.	*Compr. Org. Funct. Group Transform. II* **2005**, *3*, 685–704
Recent developments in the chemistry of low-coordinated organophosphorus compounds	Yoshifuji, M.	*Pure Appl. Chem.* **2005**, *77*, 2011
Organophosphorus π-conjugated materials	Baumgartner, T.; Réau, R.	*Chem. Rev.* **2006**, *106*, 4681
Terminal, anionic carbide, nitride, and phosphide transition-metal complexes as synthetic entries to low-coordinate phosphorus derivatives	Cummins, C. C.	*Angew. Chem. Int. Ed.* **2006**, *45*, 862
Some retrospectives and perspectives in main group chemistry	Cowley, A. H.	*ACS Symp. Ser.* **2006**, *917*, (Modern Aspects of Main Group Chemistry), 2–19
Phosphaalkene, phospholyl and phosphinine ligands: New tools in coordination chemistry and catalysis	Le Floch, P.	*Coord. Chem. Rev.* **2006**, *250*, 627
A niobaziridine hydride system for white phosphorus or dinitrogen activation and N- or P-atom transfer	Figueroa, J. S.; Cummins, C. C.	*Dalton Trans.* **2006**, 2161
Modern aspects of pseudohalogen chemistry: News from CN- and PN-chemistry	Brand, H.; Schulz, A.; Villinger, A.	*Z. Anorg. Allg. Chem.* **2007**, *633*, 22
Multiple bonding in heavier element compounds stabilized by bulky terphenyl ligands	Rivard, E.; Power, P. P.	*Inorg. Chem.* **2007**, *46*, 10047
Developing the chemistry of monovalent phosphorus	Mathey, F.	*Dalton Trans.* **2007**, 1861
Stable compounds containing heavier group 15 elements in the + 1 oxidation state	Ellis, B. D.; Macdonald, C. L. B.	*Coord. Chem. Rev.* **2007**, *251*, 936
Stretching bonds in main group element compounds – borderlines between biradicals and closed-shell species	Breher, F.,	*Coord. Chem. Rev.* **2007**, *251*,1007
Group 14 and 15 heteroallenes E=C=C and E=C=E′	Escudié, J.; Ranaivonjatovo, H.	*Organometallics* **2007**, *26*, 1542
Recent advances in the chemistry of phosphaalkynes: Building blocks for novel organophosphorus compounds	Lynam, J. M.	*Organomet. Chem.* **2007**, *33*, 170
Doubly bonded systems between heavier group 15 elements	Sasamori, T.; Tokitoh, N.	*Dalton Trans.* **2007**, 1395
Phospha- and arsaalkenes RE=C(NMe_2)$_2$ (E = P, as) as novel phosphinidene- and arsinidene-transfer reagents	Weber, L.	*Eur. J. Inorg. Chem.* **2007**, 4095
Diels–Alder reactions involving C=P– functionality	Bansal, R. K.; Kumawat, S. K.	*Tetrahedron.* **2008**, *64*, 10945
Doubly bonded systems between heavier group 15 elements	Sasamori, T.; Tokitoh, N.	*Dalton Trans.* **2008**, 1395
Metal-phosphido and -phosphinidene complexes in P–E bond-forming reactions	Waterman, R.	*Dalton Trans.* **2009**, 18
Unique homonuclear multiple bonding in main group compounds	Wang, Y.; Robinson, G. H.	*Chem. Commun.* **2009**, 5201
New adventures in the molecular chemistry of phosphorus	Russell, C. A.	*Angew. Chem. Int. Ed.* **2009**, *48*, 4895
Product class 2: Oxo-, thioxo-, selenoxo-, and iminophosphanes and diphosphenes	Yoshifuji, M.	*Sci. Synth.* **2009**, *42*, 37
Anionic reagents with silicon-containing double bonds	Scheschkewitz, D.	*Chem. Eur. J.* **2009**, *15*, 2476
Nucleophilic phosphinidene complexes: Access and applicability	Aktaş, H.; Slootweg, J. C.; Lammertsma, K.	*Angew. Chem. Int. Ed.* **2010**, *49*, 2102
Phospha-organic chemistry: From molecules to polymers	Bates, J. I.; Dugal-Tessier, J.; Gates, D. P.	*Dalton Trans.* **2010**, 3151
Main-group elements as transition metals	Power, P. P.	*Nature* **2010**, *463*, 171
π-Bonding and the lone pair effect in multiple bonds involving heavier main group elements: Developments in the new millennium	Fischer, R. C.; Power, P. P.	*Chem. Rev.* **2010**, *110*, 3877

the reader with ready access to these articles that deal with more specialized subcategories of multiply bonded group 15 compounds, Table 1 is presented. In addition to Table 1, there are several chapters of Comprehensive Inorganic Chemistry II that are closely aligned with topics of relevance to the reader interested in this chapter.[16–19]

1.12.1.2 Bonding

Many of the exciting developments for the p-block elements have involved multiply bonded compounds. For the group 15 elements, the general behavior and molecular geometries are somewhat akin to those of carbon-based analogs, such as alkenes or acetylenes. Thus, bonding models developed for organic compounds having π-bonds serve as a useful starting point. By contrast, multiply bonded compounds of many of the other heavier main-group elements can display greater geometric differences than their organic counterparts and require additional bonding considerations.[20–23] The key differences for the heavier group 15 elements are that (1) these elements resist undergoing hybridization and make lone pairs less available for π-donation[24] and (2) the p-orbitals for these elements are more diffuse than those of the lighter elements, so orbital overlaps are smaller, and, hence, π-bond strengths are reduced compared to organic compounds, such as ethylene. For an ethylene-type molecule, two limiting structures may be considered (Scheme 1). While the lone pair on the group 15 element (E) is poised (left) to rehybridize to form a double bond (right), most structures (excluding those of nitrogen) will typically exhibit geometries portrayed by the structure on the left.[25] The few exceptions often contain sterically demanding groups that exert steric pressures to promote planarization and/or contain electron-withdrawing groups having an empty p-orbital.

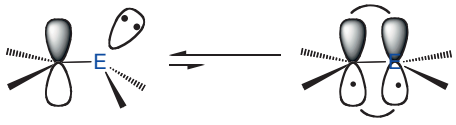

Scheme 1 Limiting structures for a double bond.

A recent illustration of this effect for a compound that could possess triple bonding is shown in Scheme 2. In this particular study, the synthesis of a compound with phosphorus–boron or arsenic–boron triple bonding was targeted.[26] While an analogous compound having nitrogen–boron triple bonding could be prepared (Scheme 2, right), attempts to prepare the P or As compounds led instead to the 4-dimethylaminopyridine (DMAP) adducts (Scheme 2, left).

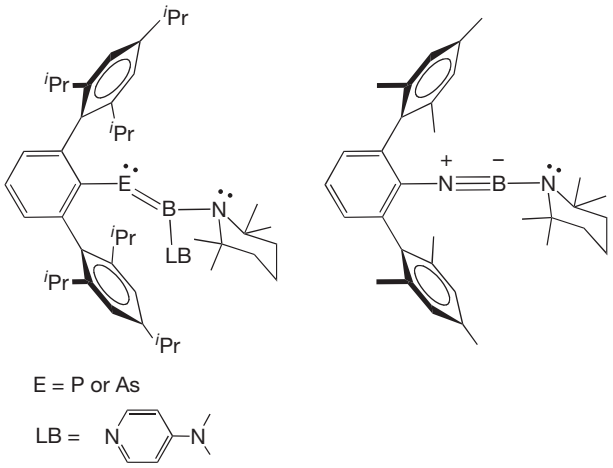

Scheme 2 Doubly and triply bonded boron-pnictogen bonds.

Because the multiple bonds in the heavier group 15 compounds are weaker and because these elements are larger, these bonds are usually more reactive and prone to various reactions that prevent their isolation, unless the compounds possess sterically demanding groups (or are bound to transition metals). Scheme 3 portrays the situation for dipnictenes,

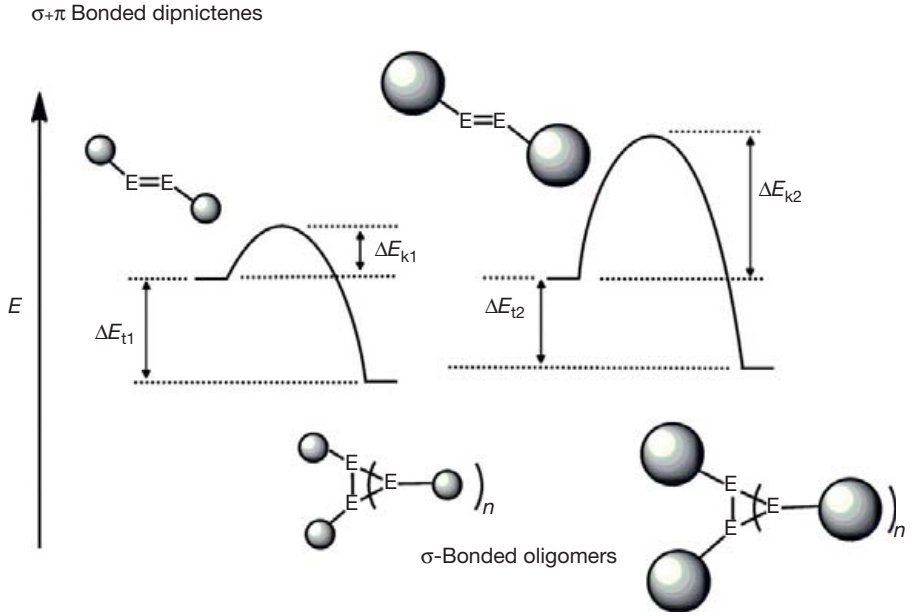

Scheme 3 Diagram illustrating kinetic stabilization provided by bulky ligands.

RE=ER. Large groups deter the reactive multiple bonds from undergoing oligomerization and/or redistribution reactions by imparting large kinetic barriers (i.e., $\Delta E_{k2} > \Delta E_{k1}$, Scheme 3), in spite of the thermodynamic preference for these systems toward a set of σ-bonds over a set of σ- and π-bonds. The presence of these 'kinetically stabilizing' groups imposes small differences in the ground-state structures, but, in certain cases, the oligomerization processes can be reversible.[27]

These large groups, however, can, at times, make it challenging to draw conclusions on structures. For example, the geometry of homonuclear doubly bonded compounds of the form RE=ER (E=P, As, Sb, Bi) displays EER angles that are significantly smaller than that expected for organic sp^2 hybridized carbon or nitrogen. Systematic structural studies where E is varied and the sterically encumbered ligand is maintained constant are rare. In one such study, a series of dipnictenes (R=*meta*-terphenyl) showed that the trend was for decreasing α from E=P to Bi (from 109.8° to 92.5°).[28] In another more limited series (R=2,4,6-tris[bis(trimethylsilyl)methyl]-phenyl), the α angle (Scheme 4) varied for E=P (106.4), As (101.4°), and for Bi (100.6°).[29–31] The subtle effects of the specific sterically demanding groups on the physical properties of the compounds should not be ignored when making comparisons.

Multiple bonds involving P, As, Sb, and Bi atoms, as mentioned above, are weaker than those involving only carbon atoms. Many of these compounds, thus, possess smaller highest occupied molecular orbital–lowest unoccupied molecular orbital (HOMO–LUMO) gaps and relatively low-lying LUMO orbitals. The LUMO orbitals are usually of π* in character and energetically at a level that often makes electrochemical reduction facile and reversible. Thus, many compounds have been studied by techniques such as cyclic voltammetry. Again, for illustration, consider dipnictenes. Diphosphenes have been subject to numerous electrochemical investigations.[32–46] In one of these studies,[39] a series of dipnictenes ArE=EAr (E=P, Sb, Bi; Ar=2,6-bis[bis(trimethylsilyl)methyl]-4-[tris(trimethylsilyl)methyl]phenyl) bearing a common bulky ligand were investigated. The results showed the following order for ease of reduction: distibene >dibismuthene>diphosphene. In concert with computational efforts on model compounds, the data suggested that, while the HOMO–LUMO gaps decreased on going from phosphorus to bismuth, the relative LUMO and HOMO energies for the dibismuthene are raised slightly compared to the distibene. This finding was attributed to possible relativistic effects of the sixth-row element bismuth and the orbitals.

The term 'multiply bonded' implies an element that is engaged in bonding to another element with a formal bond order greater than 1. In many of the multiply bonded compounds of P, As, Sb, and Bi, such as the dipnictenes mentioned above, there is little controversy in the acceptance of a multiple bond (a double bond for dipnictenes). For the convenience of this chapter, we shall emphasize compounds in which the P, As, Sb, and Bi atoms exhibit low coordination numbers of 1 or 2, where the presence of multiple bonding is fairly secure.

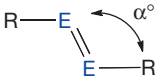

Scheme 4 Angle α about E atom in E=E bonded compound.

1.12.2 Compounds Having a Coordination Number of 1

1.12.2.1 Anionic Compounds

In 2000, red-brown crystals of a fascinating dibismuth dianion were isolated by slowly diffusing (1 month) toluene into solutions of $K_5In_2Bi_4$ and cryptand 222 in ethylenediamine (Scheme 5).[47] A related salt having cesium·NH_3·18-crown-6 cations was later isolated and structurally characterized.[48] Both of these materials feature bismuth–bismuth bond lengths indicative of double bonding. The cesium analog, however, features side-on Cs–Bi_2 bonding, whereas in the potassium salt, the Bi^{2-} unit is isolated. Unlike dioxygen, with which Bi^{2-} is formally isoelectronic, this dianion is diamagnetic.

The cyanide anion $[C{\equiv}N]^-$ is a well known and common functionality bearing a formal CN triple bond. For the heavier pnictogens, much, if not all, of the focus has been on attempts to isolate the elusive cyaphide $[C{\equiv}P]^-$ anion.[49,50] This anion is of added importance for its relationship to stable phosphaalkynes [RC≡P]. Related to cyaphide are anions of the form $[X–C{\equiv}P]^-$, where X=O, S, or NR.[51–54] In 2002, the synthesis of $[M(DME)_3][OC{\equiv}P]_2$ (M=Mg, Ca, Sr, and Ba) and the structure of $[Ca(DME)_3][OC{\equiv}P]_2$ were reported (Scheme 6).[55] The calcium derivative was the most stable of these sensitive materials.

In 2004, a rather elegant synthesis of borane-stabilized $[C{\equiv}P]^-$ and $[C{\equiv}As]^-$ anions was reported (Scheme 7).[56] Impressively, the complexes are somewhat insensitive to water in acetonitrile solution. The materials were fully characterized by spectroscopic and crystallographic methods. Interestingly, attempted metathesis of the PPh_4 cation of $[PPh_4][(CF_3)_3BC{\equiv}P]$ for potassium led to hydrolysis and the formation of $[(CF_3)_3BCH_2P(=O)(OH)]$.

In 2005, a new analog K[^{i}PrNC≡P] was prepared by desilylation of an alkylsilylamino-phosphaalkyne (Scheme 8).[57] The crystal structure of the crown ether complex K[18-C-6][^{i}PrNC≡P] afforded a C≡P bond distance of 1.603(3)Å. For this anion, two resonance structures might describe the structure (Scheme 8). The bond length and accompanying density

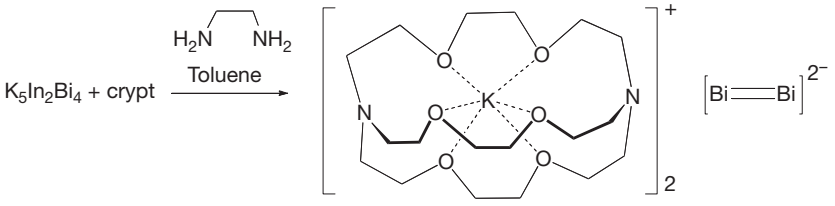

Scheme 5 Formation of doubly bonded Bi_2 dianion.

functional theory (DFT) calculations suggest that the best representation of the anion is a hybrid of the two resonance forms.

Another example of this type of anion was reported in 2010.[58] The resulting anion, when heated in dioxane for 4 weeks, yielded the isonitrile Mes*CN and products derived from the CP bond cleavage. Such facile bond cleavage lends support for contributions of a cesium phosphinidene resonance to the description of this anion (Scheme 9, far right).

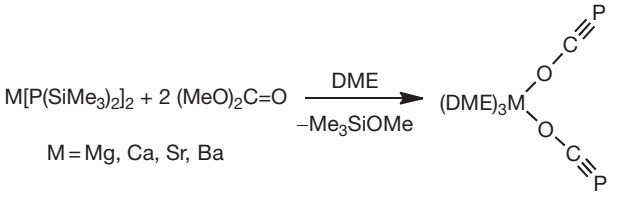

Scheme 6 Formation of metal bonded OC≡P anion.

1.12.2.2 Cationic Compounds

The interesting cation $[(Me_2N)_3PC{\equiv}P]^+$, first reported in 1991, remains the sole example of a cationic phosphaalkyne.[51] New reports, however, have appeared describing the Lewis acidity of phosphadiazonium (iminophosphenium) ions.[59] In 1988, Niecke et al. reported on the first member of this series, $[Mes^*N{\equiv}P]AlCl_4$.[60] Over the past 10 years, such cations have

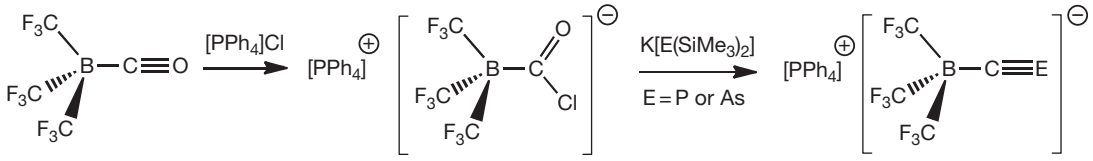

Scheme 7 Boron stabilized C≡E anions.

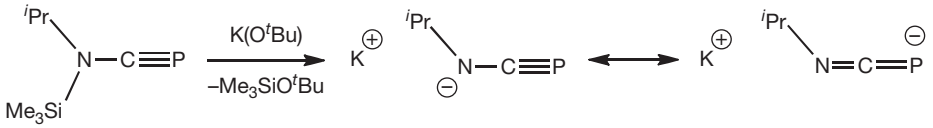

Scheme 8 Formation and resonance structures of ^{i}PrNC≡P anion.

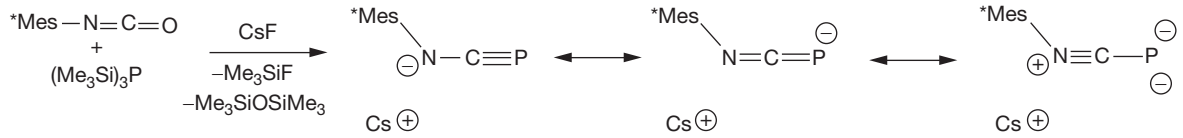

Scheme 9 Formation and resonance structures of Mes*NC≡P anion.

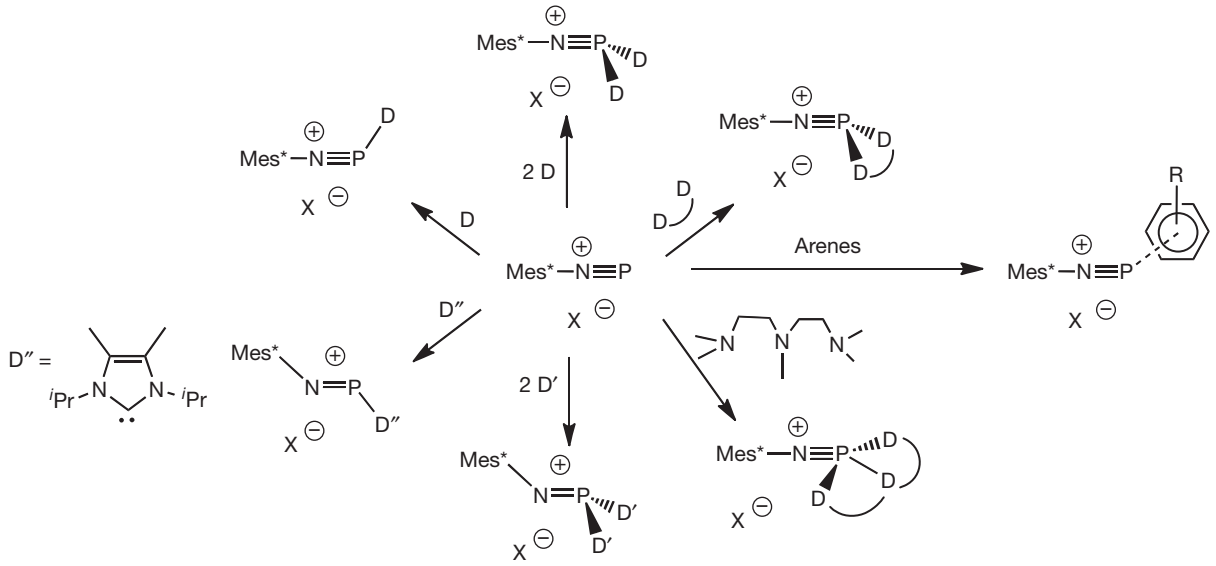

Scheme 10 Reactions of [Mes*N≡P]X with various donors.

been shown to form Lewis acid adducts with various types of donors, as summarized in Scheme 10.[61–65] The Lewis acidic phosphorus center can show interactions with the anion, and/or with one, two, or three donor atoms, as well as η^6-interactions with arenes. The types of donor atoms (D) include C, P, N, O, S, and Se atoms. For most of these adducts, the C–N–P array remains mostly linear, with two notable exceptions (D′ and D″). The coordination of $[Mes^*N{\equiv}P]^+$ with two equivalents of *p*-dimethylaminopyridine (D′ = dmap) or by an *N*-heterocyclic carbene (D″) yielded compounds whose structures were decidedly not linear at the nitrogen atom. These features, as well as the longer PN bonds, make them more akin in nature to Mes*N=PCl, which has a lower PN bond order.

1.12.2.3 Neutral Compounds

1.12.2.3.1 P_2 chemistry

As is well known, dinitrogen is a very stable molecule possessing a very strong nitrogen–nitrogen triple bond. Analogous diatomics of the group 15 heavier elements, however, are not as stable as dinitrogen and are unobservable under normal conditions. On the other hand, coordinated by one or more main-group or transition-metal centers, there are numerous examples of complexes having these reactive fragments. Interestingly, a number of these are derived by the activation of elemental phosphorus (P_4).[66–68]

There have been two recent developments that suggest that it may be possible to generate and utilize P_2 in synthetic transformations. In 2006, it was reported that P_2 could be released from a niobium complex by mild heating and subsequent products were trapped using cyclohexadiene (Scheme 11, upper path).[69] Soon afterwards, it was also reported that the products of trapping putative P_2 species could be achieved by the photolysis of solutions of P_4 in hexane at room temperature (Scheme 11, lower path).[70] These breakthroughs bode well for further advances in P_2 chemistry.[71]

1.12.2.3.2 Phosphaalkynes

Phosphaalkynes are undoubtedly the most extensively studied class of triple-bonded compounds of the group 15 elements. The oligomerization and coordination chemistry of phosphaalkynes is rich and well established.[72–77] On the other hand, isolation of the isomeric isophosphaalkynes (RP≡C) remains an unachieved goal, despite efforts to obtain such species.[78] Some of the most noteworthy developments in the past 10 years for phosphaalkynes involve (a) new modes of synthesis, (b) novel functionalized phosphaalkynes, and (c) new reactions and uses.

1.12.2.3.2.1 New developments in synthesis

The most commonly utilized route to phosphaalkynes is initiated by the reaction of either tris-trimethylsilylphosphane or LiP$(SiMe_3)_2$ with acyl chlorides bearing sterically demanding R groups, followed by treatment with base (Scheme 12).[73,76,79]

While effective, these routes depend upon silylated phosphorus precursors, and thus the search for new and atom-economical routes remain important goals. A noteworthy example was reported in 2001, whereby solutions of 'kinetically unstabilized' phosphaalkynes were generated, starting with the reaction of readily accessible and easily handled

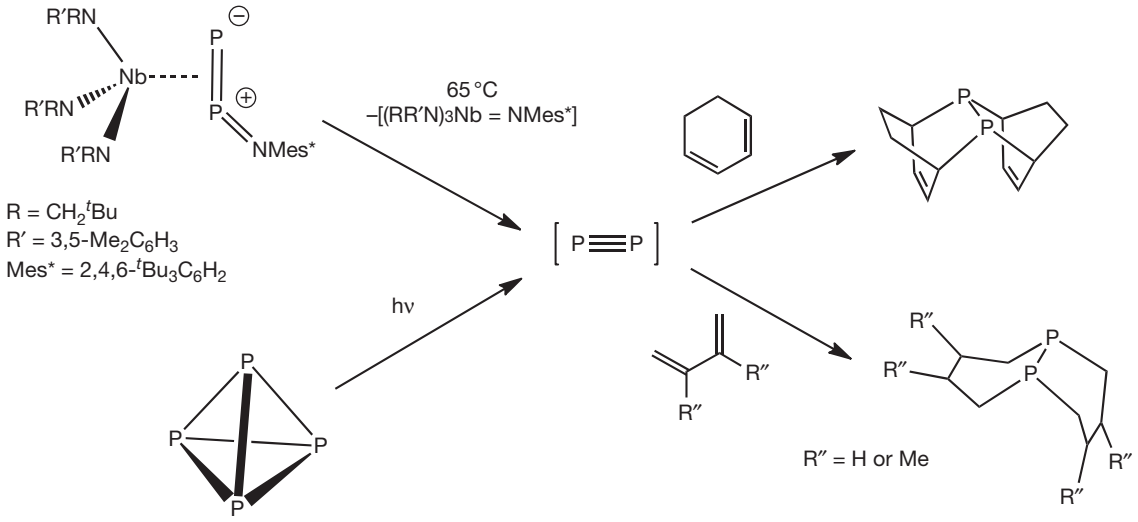

Scheme 11 Generation and trapping reactions of transient P_2 molecule.

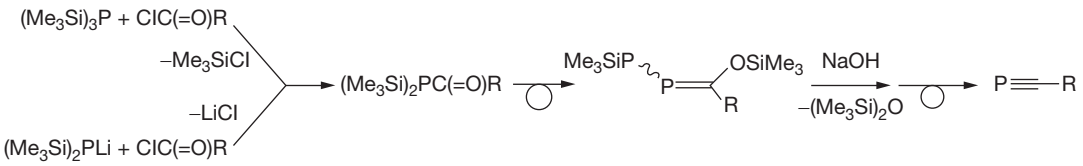

Scheme 12 Synthesis of phosphaalkynes.

α-dichlorophosphonates, which led to α-dichlorophosphanes in good to high yields via reduction with $AlHCl_2$ (Scheme 13).[80] These primary phosphanes were then converted to phosphaalkynes using 1,8-Diazabicyclo [5.4.0] undec-7-ene (DBU) to effect dehydrohalogenation. Bulb-to-bulb distillation of the reaction mixtures led to solutions of reactive phosphaalkynes that could be stored at −20 °C. The success of each synthesis was found to be dependent on the nature of the R group. For example, while $PhCH_2CH_2C{\equiv}P$ could be generated in around 60% yield, the method fails for $PhC{\equiv}P$. The solutions of phosphaalkynes showed significant stability. For example, a solution of $MeC{\equiv}P$ showed less than 10% decomposition over a 3-month period at −20 °C.

Similar reactive phosphaalkynes have been generated in the gas phase.[76,79] A recent investigation of the kinetically unstable $MeC{\equiv}P$ and $MeC{\equiv}As$ could be prepared by vacuum gas–solid reactions (VGSRs) (Scheme 14).[81] These two materials were then studied by Fourier transform ion cyclotron resonance (FTICR). One of the surprising findings of this report was that both $MeC{\equiv}P$ and $MeC{\equiv}As$ were more acidic than $HC{\equiv}P$ and $HC{\equiv}As$, respectively.

In 2004, a novel means of synthesis for phosphaalkynes was reported.[82] This route capitalizes on the reactivity of a terminal niobium phosphide to generate a niobacycle intermediate that, at modest temperatures, breaks down into a phosphaalkyne (Scheme 15, R″ = ^{t}Bu or Ad). A particularly interesting aspect of this work is that the niobium phosphide can be generated from elemental phosphorus, and that the niobium-oxo complex can be reduced to the precursor, which reacts with P_4. Thus, the process is recyclable in niobium reagent.

In 2006, another preparation of phosphaalkynes that avoids the use of silylated phosphanes was reported (Scheme 16).[83] In this development, multigram quantities of the air-stable tritylphosphaalkyne were accessed by the dehydrohalogenation of $Cl_2PCH_2Ph_3$ by 1,4-diazabicyclo[2.2.2]octane (DABCO) (Scheme 16). Interestingly, 'conventional' routes (Scheme 12) failed to yield the tritylphosphaalkyne.

1.12.2.3.2.2 Functionalized phosphaalkynes

One of the more interesting recent developments concerns the elaboration of functionalized phosphaalkynes. In 2004,

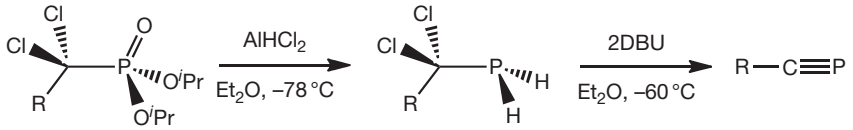

R = H, Me, Et, ^{n}Bu, $PhCH_2CH_2$, C_6H_{11}, $H_2C{=}CHCH_2$, $H_2C{=}CHCH_2CH_2$

Scheme 13 Alternative synthesis of phosphaalkynes.

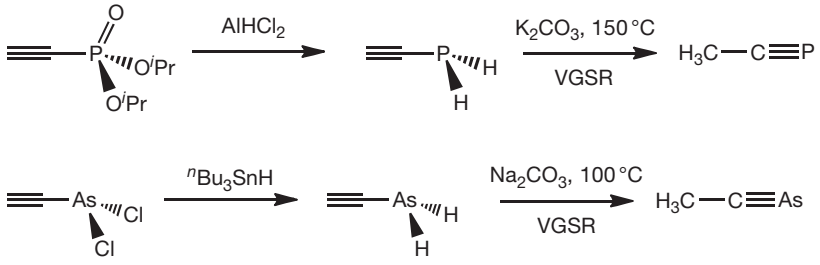

Scheme 14 Synthesis of phosphaalkynes by vacuum gas-solid reactions.

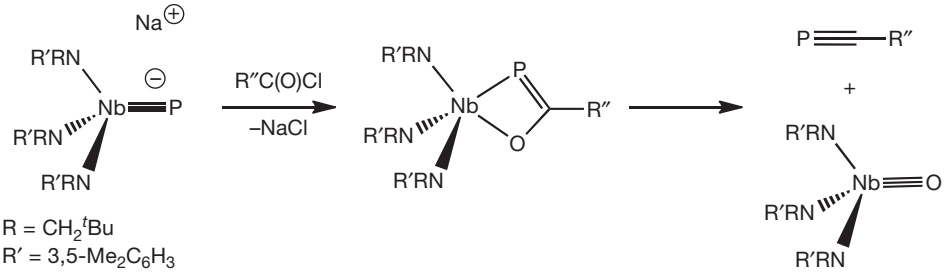

R = $CH_2{}^tBu$
R′ = 3,5-$Me_2C_6H_3$

Scheme 15 Niobium phosphide route to phosphaalkynes.

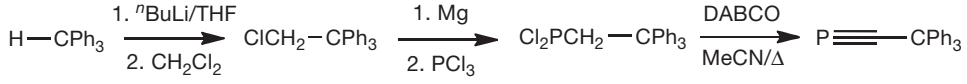

Scheme 16 Synthesis of trityl-substituted phosphaalkyne.

phosphaalkynes of the form 4-X-2,6-^{t}Bu$_2$C$_6$H$_2$C≡P, having the bulky *ortho-tert*-butyl groups, were reported (Scheme 17, left).[84] The remote substituents were varied from H, OMe, NMe$_2$, and ^{t}Bu. The impacts of the functional groups on nuclear magnetic resonance (NMR) shifts (^{31}P NMR: δ 32.1–37.2 ppm) and ultraviolet–visible (UV–vis) spectra were found to be much greater than any structural impacts.

In 2003, the first diphosphaalkyne was prepared (Scheme 17, middle), using a triptycene framework.[85] Subsequently, another less bulky analog was reported as having a bicyclo[2.2.2]octanediyl framework (Scheme 17, right).[86] Each diphosphaalkyne displays a singlet in their ^{31}P NMR, resonating at −15.7 and −60.8 ppm, respectively. These diphosphaalkynes offer opportunities as building blocks for polymers and other novel systems.[16]

1.12.2.3.2.3 Select reactions and uses

Previous investigations of phosphaalkynes have detailed their coordination chemistry and oligomerization by transition-metal complexes.[73,76,87–89] Such studies are numerous and continually growing in number. While these reactions are important and well established, a couple of novel recent developments for reactions that produce non-transition-metal-containing products merit highlighting.

A ruthenium-promoted process that converts the phosphaalkyne Ph$_3$CCP into a 1*H*-phosphaindole (Scheme 18) was reported in 2006.[83] During the overall (and complicated) process, there is activation of a CH group of a phenyl ring and a remarkable CC bond cleavage reaction. The process could also be made recyclable in ruthenium.

Click chemistry, the cycloaddition of azides with acetylenes, has been well established and is a highly efficient reaction for the production of triazoles.[90] Likewise, phosphaalkynes have also been shown to react with organic azides to afford 1,2,3,4-triazaphospholes.[91,92] More recently, this approach has been used to generate two types of stable tripodal ligands in 86–99% yield (Scheme 19).[93] Ligands of the type **A** with R = ^{t}Bu are indefinitely air stable, and reaction of this particular

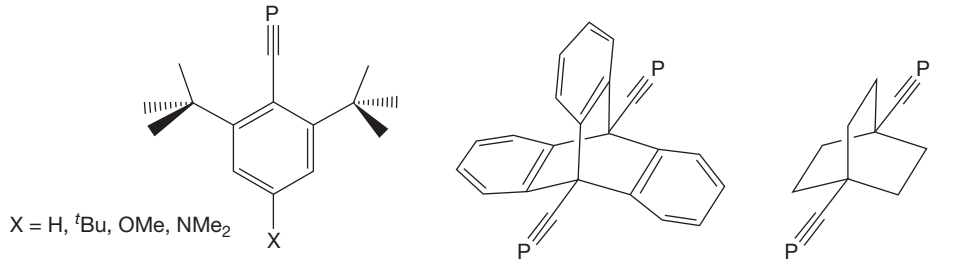

Scheme 17 Functionalized phosphaalkynes.

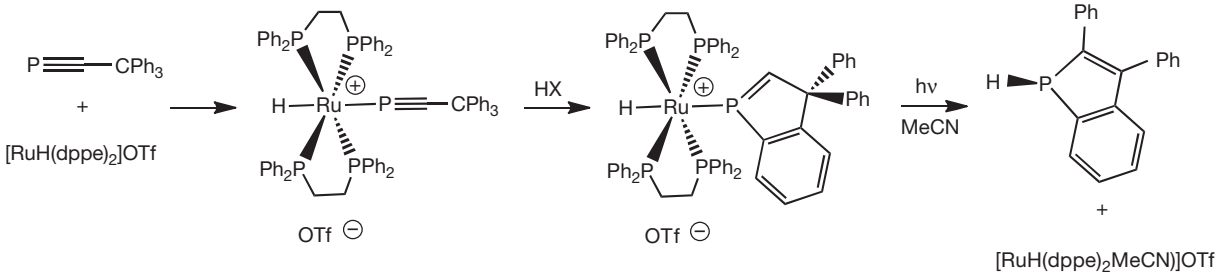

Scheme 18 Ruthenium promoted transformation of phosphaalkyne to a 1H-phosphaindole.

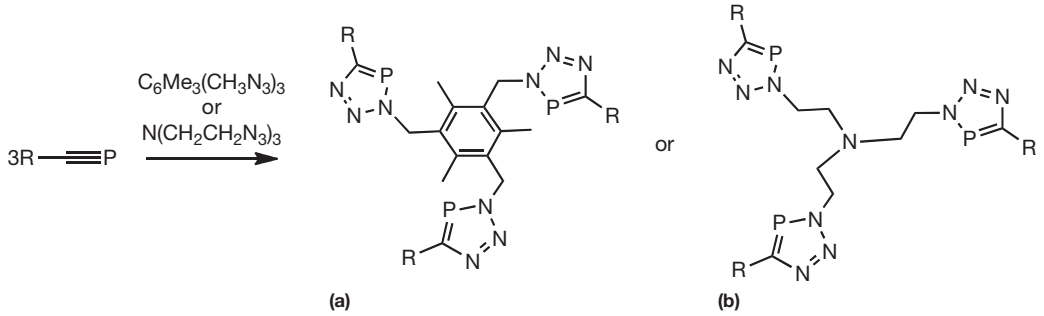

Scheme 19 Click type chemistry of phosphaalkynes.

ligand with Pt(norbornene)$_3$ yields an unusual dinuclear platinum complex.

1.12.3 Compounds Having a Coordination Number of 2

1.12.3.1 Phosphaalkenes

Phosphaalkenes, RP=CR$_2$, are one of the most extensively studied classes of low-coordinate organophosphorus compounds.[9,75,79,94,95] Arsaalkenes, RAs=CR$_2$, as well as the heavier analogs having Sb=C and Bi=C units, are much less studied.[96–101] The following areas represent developments in the chemistry of doubly bonded group 15 elements, drawing largely on the abundant chemistry of phosphorus.

1.12.3.1.1 New developments in synthesis

The rearrangement of secondary vinyl phosphanes to phosphaalkenes as a meaningful preparation of isolable phosphaalkenes having *C*-substituents was recently achieved.[102] Normally, such reactions yield equilibrium mixtures, but the use of electron-withdrawing substituent CF$_3$ drives the equilibrium to the right (Scheme 20). The tautomerization proceeds quantitatively, and isolated yields of the phosphaalkenes were as high as 89%.

While many transition-metal-based syntheses of phosphaalkenes produce η^1-phosphaalkene complexes,[9,103] the zirconium phosphido complex in Scheme 21 first inserts benzonitrile to yield an intermediate product, which undergoes isomerization to an amido complex bearing a remote phosphaalkene substituent.[104,105] The phosphaalkene product is a mixture of rapidly interconverting (on the NMR timescale) *E*- and *Z*-isomers. In the solid state, the phosphaalkene was established as the *E*-isomer by single-crystal x-ray diffraction.

1.12.3.1.2 Polarized phosphaalkenes

The differences in electronegativity between C and P (2.5 and 2.1, respectively) led to a slight polarization of the C=P functional group in the direction of C$^{\delta-}$P$^{\delta+}$.[75,79,94,95] The exact balance, of course, will also depend on the substituents present on the carbon and phosphorus atoms. Compounds where this polarization is decidedly inverted (i.e., C$^{\delta+}$P$^{\delta-}$) were first prepared almost 20 years ago, and these materials and their chemistry have been reviewed recently.[106,107] An example of how these materials can be inversely polarized by resonance effects is shown in Scheme 22.

A series of analyses of the impact of para-X-aryl substituents on the polarity of aryl-substituted phosphaalkenes has come from three independent studies. The first describes phosphaalkenes of the form Mes*P=C(H)Ar (Scheme 23A).[108] A Hammett-type analysis of 14 ^{31}P NMR shifts (δ varies from 233.0 ppm for X = NMe$_2$ to 284.6 ppm for X = NO$_2$) provided a linear correlation with σ_p. Overall, the Mes*PC(H) group acts as a weak electron donor to the attached phenyl ring. The second study examined the impact of remote substituents on the other side of the P=C array using analogs of modified Mes* ligands (Scheme 23B).[109] In this study, X varied from H, ^{t}Bu, OMe, NMe$_2$, and [NMe$_3$]$^+$ substituents, and showed ^{31}P NMR resonances (from 264.8 to 238.8 ppm) linearly varying with σ, albeit with an opposite slope for the Hammett plot. It is also worth mentioning that variations on the Mes* protecting group have also appeared where the *ortho*-position has been functionalized.[110] In other reports, compounds similar to (b) have been reported.[111,112] Compounds of the form (c) were prepared in attempts to increase the polarization of the P=C bond from both sides of the P=C unit.[113] These materials allowed for a comparison of the impact of X versus X′ substituents on properties such as electrochemical reduction, UV–vis spectroscopy, and solid-state structures. The ^{31}P NMR resonances varied from δ 240.7 to 268.4 ppm. Overall, the X′ substituent in this series had a greater impact on the physical

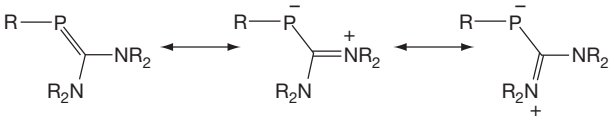

Scheme 22 Resonance structures for inversely polarized phosphaalkenes.

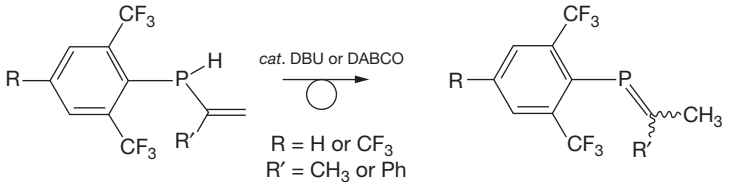

Scheme 20 Alternative synthesis of phosphaalkenes.

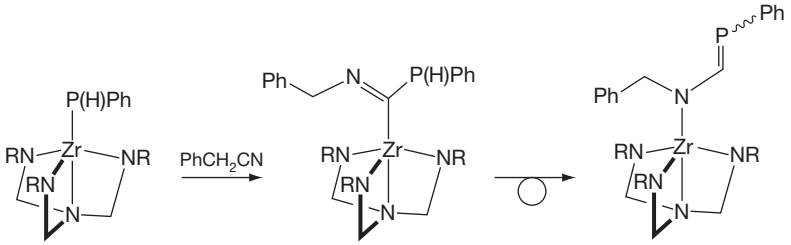

Scheme 21 Zirconium promoted synthesis of phosphaalkenes.

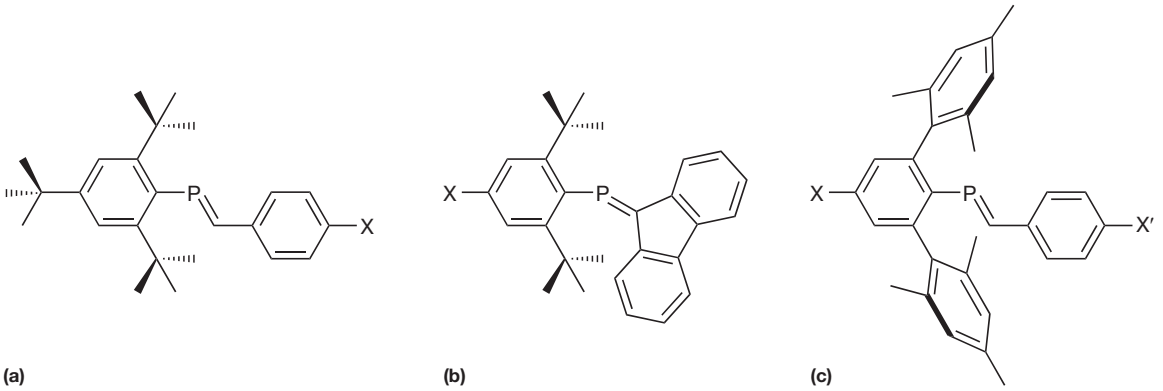

Scheme 23 Functionalized phosphaalkenes.

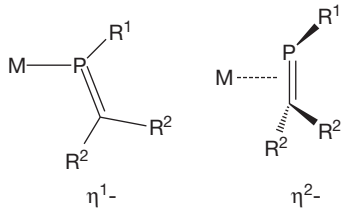

Scheme 24 Binding modes for phosphaalkenes.

properties than the X-substituent, as the X-substituted aryl group is less conjugated with the P=C bond due to the greater steric bulk of the terphenyl unit.

1.12.3.1.3 Phosphaalkenes as ligands for metals

The analogy between imines (C=N) and phosphaalkenes (C=P) would lead to the expectation that, like their nitrogen counterparts, phosphaalkenes could serve as ligands for transition-metal complexes. Indeed, there has been great recent growth in the study of phosphaalkenes as ligands.[72,114] Like olefins, phosphaalkenes can bind to metals in either η^1- or η^2-modes (Scheme 24). The former bonding mode (binding via a lone pair in phosphorus) is of more importance when used as ligands for transition-metal catalysts. Another special feature of such ligands is that the phosphaalkene unit, with its lower-lying π^*-orbitals, are good π-electron accepting groups and, thus, allow for π-backbonding from the metal center to the ligand.

The past 10 years' worth of phosphaalkene complexes are far too numerous to detail here, but three diverse representatives are shown in Scheme 25. The first example shows that phosphaalkene ligands can form elements of metal-containing conjugated polymers.[115,116] The second example illustrates that wide bite-angle-type ligands can be constructed and form interesting metal complexes.[117] This particular ligand was prepared using a 'phospha-Wittig' reagent.[118] The final example illustrates that systems having chiral centers can be used to create catalytically active complexes with promise for effecting enantioselective transformations.[119]

1.12.3.1.4 Phosphaalkene-based conjugated polymers and related materials

Comparisons have often been made between P=C bonds of phosphaalkenes and C=C bonds of olefins.[94] Less studied are analogous sets of conjugated molecules or polymers having P=C functionalities in conjugation with C=C and P=C bonds. Such materials represent a subclass of conjugated polymers and materials that incorporate phosphorus atoms.[16,120–122] The first examples of conjugated polymers having P=C functional groups in the backbone appeared in 2002.[123] The synthesis of the pale yellow polymer involved a Becker-type route to create the phosphaalkene linkages, which were determined to be a mixture of *E*- and *Z*-isomers about the P=C bonds (Scheme 26). A subsequent paper included diphosphaalkenes as model compounds for the polymer, as well as detailed analyses of the structural and optical properties of these materials.[124] In these polymers, as well as those mentioned below, steric clashes involving the substituents providing steric protection about the P=C bonds can lead to a decrease in conjugation when nonplanar structures are realized.

Another approach to integrating P=C entities into polymers utilizes phospha-Wittig reagents of the form $Me_3P{=}P{-}Ar{-}P{=}PMe_3$. The first example in 2003 generated the di-phospha-Wittig reagent *in situ* by the reduction of $Cl_2P{-}Ar{-}PCl_2$ with zinc dust in the presence of Me_3P (Scheme 27).[125] This particular all *E*-configured polymer was light orange in color. In this study, other polymers were prepared, but these were insoluble without using the organic dialdehyde-contained groups that promoted solubility (hexyloxy groups).

A more recent permutation in 2004 allowed for isolation of the di-phospha-Wittig reagent and greater flexibility in the polymerization process (Scheme 28).[126] The use of a macromonomer that has integrated sterically demanding groups at both ends, and also containing a solubility-enhancing core in the middle, allowed greater freedom to choose organic dialdehydes for this type of polymerization reaction. Consistent with the fact that these are conjugated materials, these materials absorb light of longer wavelengths and are deep orange and red-colored materials.

A series of mono-disperse oligomers having phosphaalkene units with increasing conjugation length have been reported (Scheme 29).[127] This series showed red shifts for the π–π^* electronic transitions for increasing conjugation length. Good correlations to the optical properties of phosphorus-free model compounds were observed as well.

Conjugated materials having phosphorus–carbon double bonds in π-conjugation with carbon–carbon triple bonds have been studied, appearing first in 2008.[128–130] Two examples are

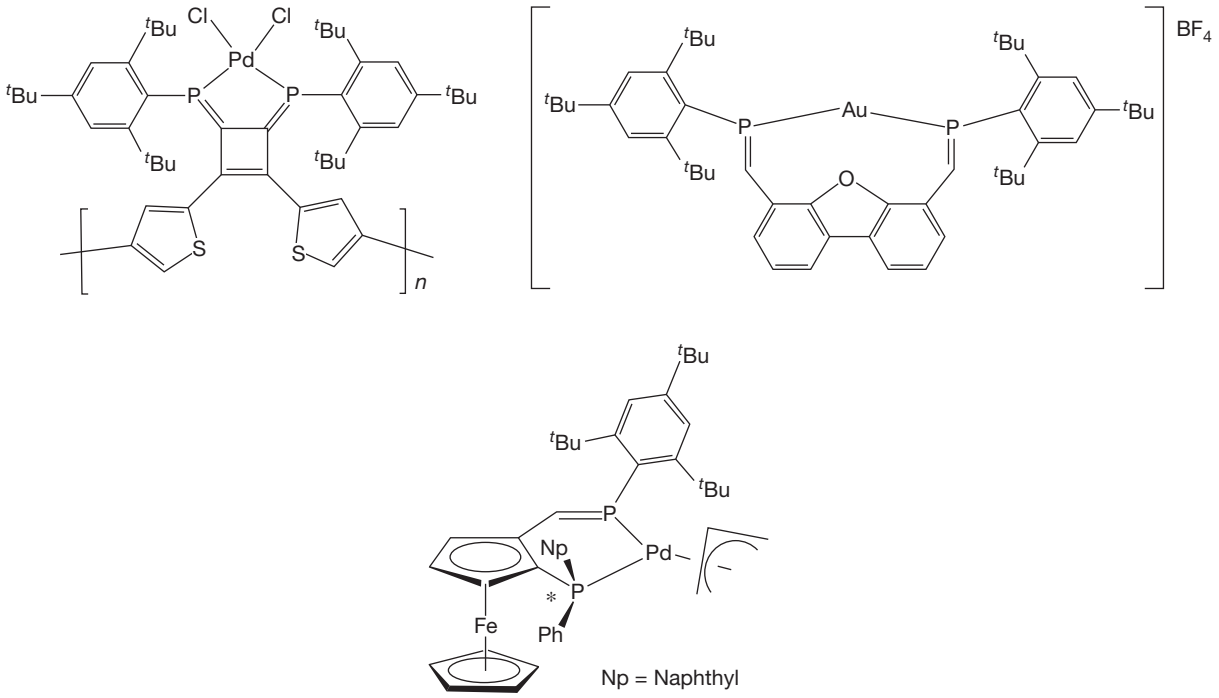

Scheme 25 Examples of phosphaalkenes as ligands for transition metals.

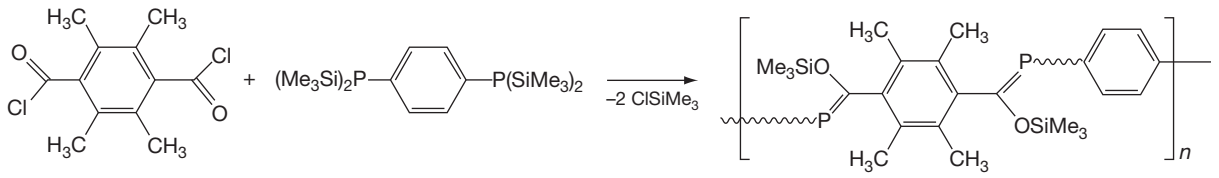

Scheme 26 First synthesis of a phosphaalkene based polymer.

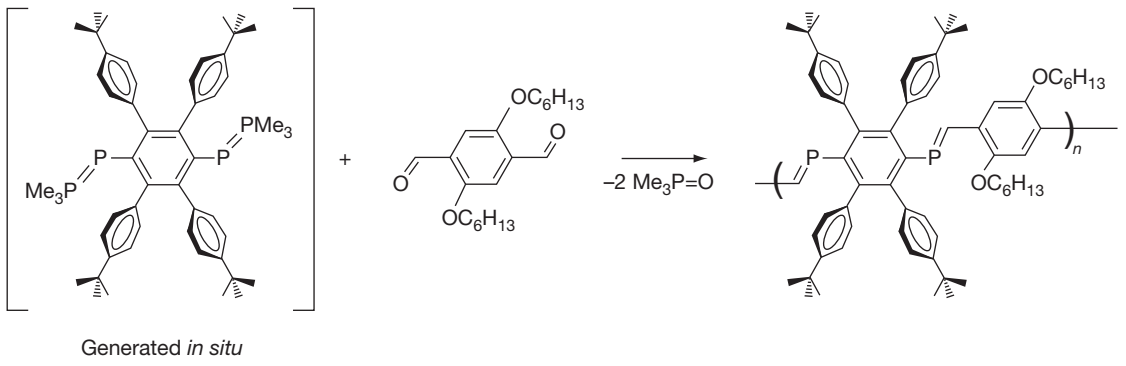

Scheme 27 Synthesis of a phosphaalkene based polymer by *phospha*-Wittig reaction.

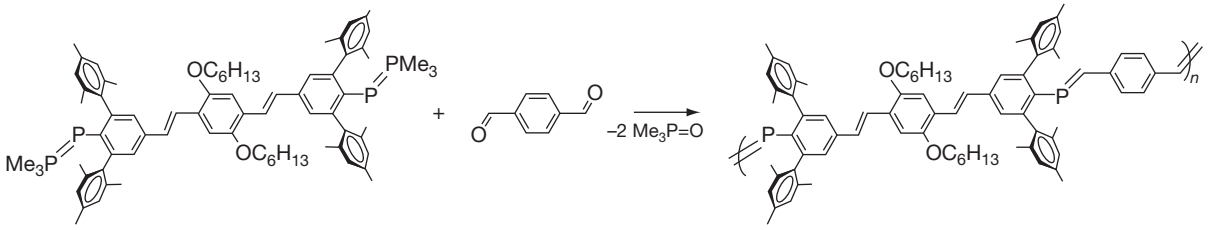

Scheme 28 Synthesis of a phosphaalkene based polymer by *phospha*-Wittig reaction.

shown in Scheme 30. Compound B is a red-colored material that shows two reduction waves for its cyclic voltammetry data. These data indicate that the two phosphaalkenes, despite having phosphorus atoms that are 18 Å apart from one another, are electronically coupled to one another.

1.12.3.1.5 Special reactivity and applications

The reaction chemistry of the P=C linkage has been reviewed previously.[9,75,79,94,95] A few newer reaction types, however, merit notice. First, the polymerization of P=C bonds to make new phosphorus-containing polymers represents a new way in which P=C bonds can mimic C=C bonds (the polymerization of which has long been an important process).[121,122] The addition polymerization of MesP=CPh_2 was reported in 2003.[131,132] Mechanistic work on the polymerization has shown that *n*-butyllithium initiates the anionic living polymerization of MesP=CPh_2.[133–135] More recently, the polymerization of P=C bonds has significantly developed to the point where sophisticated block copolymers of MesP=CPh_2 with isoprene (Scheme 31) can effect the self-assembly of gold nanostructures.[136,137]

Another recent unusual reactivity mode was seen in the reaction of the same phosphaalkene with an *N*-heterocyclic carbene that produces a hybrid phosphane–carbene (Scheme 32).[138] This is an interesting reaction, for the carbene did not react with the P=C bond to form a three-membered phosphirane ring, as might be expected for reactive carbenes. An additional interesting finding was that the final product

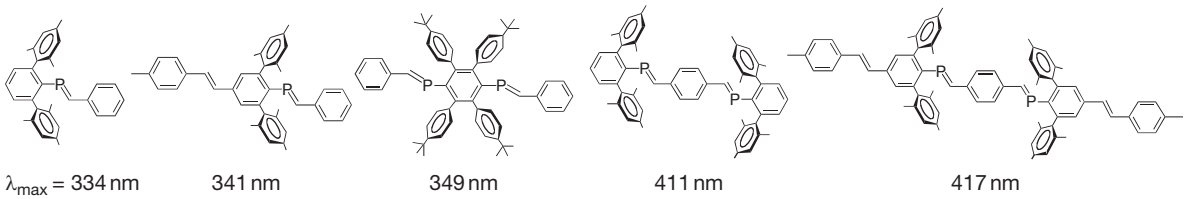

Scheme 29 λ_{max} values for series of conjugated phosphaalkenes.

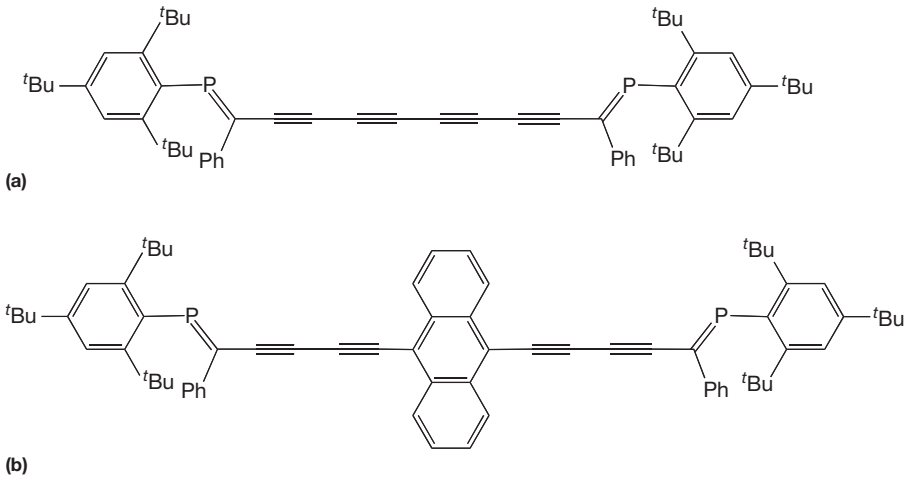

Scheme 30 Phosphaalkenes conjugated with acetylene units.

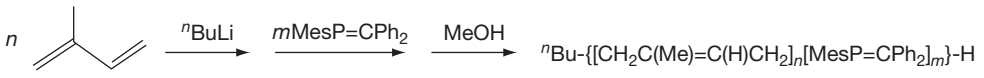

Scheme 31 Synthesis of novel phosphaalkene/alkene copolymer.

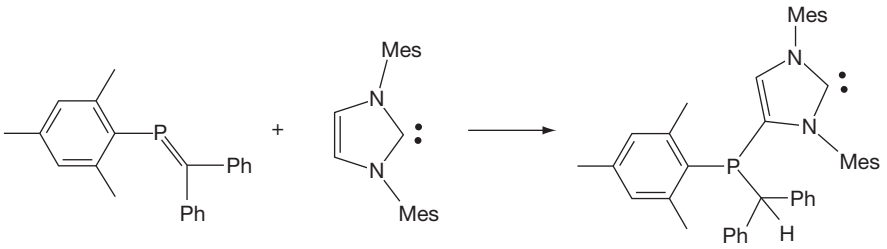

Scheme 32 Unusual reaction of *N*-heterocyclic carbene with phosphaalkene.

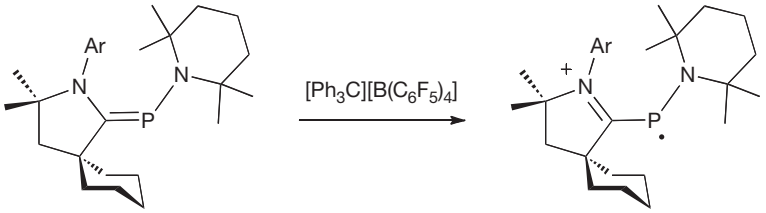

Scheme 33 Synthesis of a rare phosphorus centered radical from phosphaalkene.

could bind gold chloride fragments to the phosphorus and carbene carbon atoms.

Inversely polarized phosphaalkenes have been used as phosphinidene- and carbene-transfer reagents.[106] Their chemistry differs significantly from other phosphaalkenes. For example, some phosphaalkenes can display reversible reductive electrochemistry due to the presence of lower-lying LUMO orbitals. Recently, the electrochemical behavior of Mes*P=C$(NMe_2)_2$ and Mes*P=C(Me)(NMe_2) was examined by cyclic voltammetry.[139] Neither compound could be reduced, but both showed reversible oxidations, unlike normally polarized phosphaalkenes. The oxidation of Mes*P=C$(NMe_2)_2$ by $[Cp_2Fe]PF_6$ led to the persistent radical species [Mes*P=C$(NMe_2)_2$]PF_6.[17] In related work, it was found that a carbene-based phosphaalkene could be oxidized to a stable radical cation (Scheme 33).[140] In this particular case, single crystals of the radical could be grown and analyzed by x-ray diffraction. The resulting structure of the phosphinyl radical showed that the PC and PN bond lengths in the cation have increased and decreased, respectively, compared to the neutral phosphaalkene. The electron paramagnetic resonance (EPR) spectra of the cation were also consistent with the unpaired spin largely residing on the phosphorus atom.

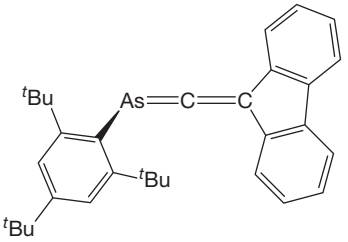

Scheme 34 An arsaallene.

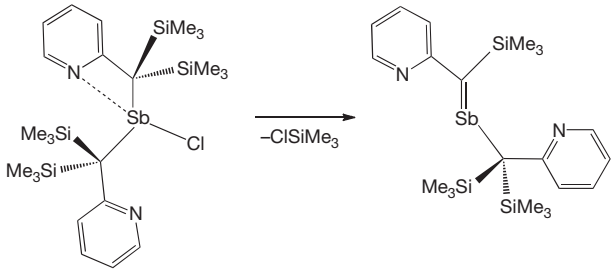

Scheme 35 Unusual stibaalkene.

1.12.3.2 Arsaalkenes and Other Related Compounds

Arsaalkenes and their heavier analogs with double bonds, while less numerous than phosphaalkenes,[96] have seen some notable recent advances. Heteroallenes of the form E=C=E′, C=E=C, and E=C=C=E′ represent an important class of doubly bonded compounds.[97,100] Recently, the first stable arsaallene below was reported (Scheme 34).[98] The single-crystal x-ray structure of this material showed definitive evidence for the heteroallene bonding within the material.

Low-coordinate chemistry of antimony and bismuth was the subject of review in 2001.[141] An interesting pyridyl-substituted stibaalkene has been isolated as a very air- and water-sensitive red oil (Scheme 35).[142] This stibaalkene is interesting, as DFT calculations predict that its thermal stability is the result of the coordination of the nitrogen atoms of both the pyridyl groups to the antimony center, as well as predict a relatively long SbC bond (2.11 Å). These calculations suggest that this material may have an SbC bond order less than that of an SbC double bond.

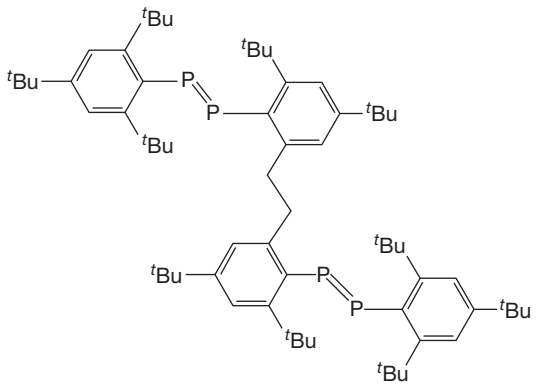

Scheme 36 A bis-diphosphene.

1.12.3.3 Diphosphenes and Other Dipnictenes

1.12.3.3.1 Compounds having more than one P=P group

This particular field of low-coordinate chemistry is fairly mature, but it remains very active. One of the more interesting areas of current activity concerns the synthesis of materials possessing two or more P=P units. The first bis-diphosphene was reported in 1996.[143] This pioneering example utilized a modified version of the Mes* ligand to enable the presence of two stable P=P units (Scheme 36).

Since then, the emphasis has centered on molecules where there is an opportunity for P=P units to be in π-conjugation with one another. The first of these appeared in 2000, where the use of a tetrarylphenyl unit allowed the preparation of a

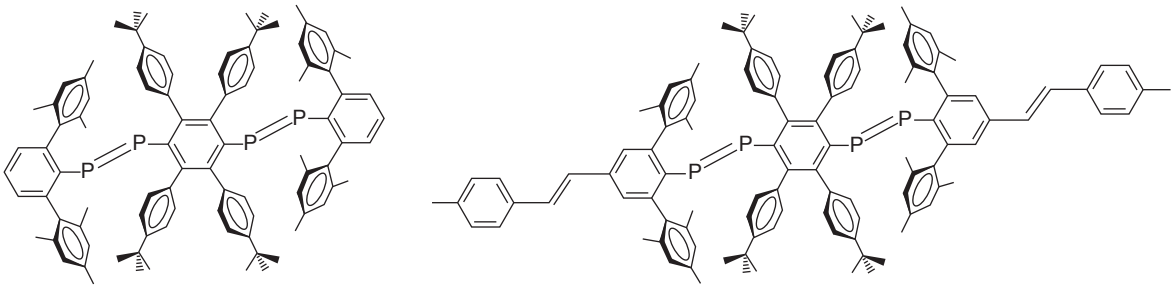

Scheme 37 Conjugated bis-diphosphenes.

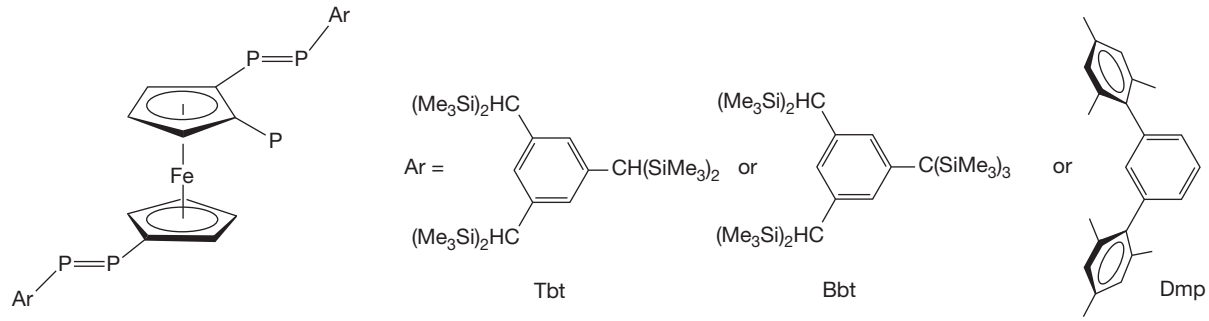

Scheme 38 Ferrocene-linked bis-diphosphenes.

para-phenylene bridged bis-diphosphene (Scheme 37, left).[144] The structure of this bis-diphosphene showed steric clashes between peripheral aromatic rings, causing significant torsional twists in the molecule and, thus, some loss of conjugation. Detailed electrochemical investigations, as well as EPR studies of the mono- and doubly reduced species, suggested that the structure of the material is redox dependent, making its behavior akin to that of a molecular switch.[37] In another study, the same authors were able to extend the conjugation length of the bis-diphosphene to produce a linear π-system that contains five phenyl rings, two vinyl groups, and two diphosphene units (Scheme 37, right).[127]

In 2006, two groups independently (one using Ar = Tbt and Dmp, and the other using Ar = Tbt and Bbt) reported bis-diphosphenes spanned by a ferrocene unit (Scheme 38).[40,41] Examination of the redox behavior of the derivatives where Ar = Tbt or Bbt was employed reveals two reversible one-electron waves separated by 0.35 V,[41] which is comparable to that found for a tetra-arylphenyl bridged species (0.34 V),[37] and, thus, these materials can be considered to have diphosphene units that are electronically coupled to one another. Subsequent studies of the ferrocenyl-bridged diphosphenes reported on the reactions with protic sources and with metal complexes.[44,145] Related biferrocenyl- and ruthenocenyl-substituted diphosphenes have also been reported.[46]

The latest examples of bis-diphosphenes feature a bridging anthracene group (Scheme 39).[146] In contrast to the above examples, the electrochemistry of these bis-diphosphenes showed single two-electron waves, suggesting that there is little electronic communication between the two diphosphene units. Anthracene-substituted diphosphenes are also of interest, as they can participate in [4+2]-cycloaddition reactions with electron-deficient olefins.[147]

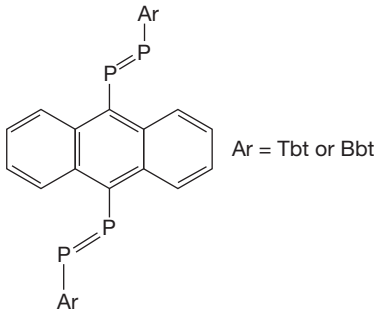

Scheme 39 Anthracene-linked bis-diphosphene.

In 2004, the first conjugated polymer having diphosphene units was reported. This polymer was prepared by either thermolysis or photolysis of a di-phospha-Wittig reagent (Scheme 40).[126] This deep-red polymer utilized the same macromonomer as mentioned in Section 1.12.3.1.1.4. Its UV–vis spectrum showed λ_{max} values of 435 and 481 nm for presumably the π–π* and n–π* transitions, respectively.

1.12.3.3.2 Functionalized diphosphenes

Other noteworthy diphosphenes bearing electronically active remote substituents are shown in Scheme 41.[35,36,109] As expected, such substituents have notable impacts on the UV–vis absorptions.

Diphosphenes and heavier dipnictenes are characterized by low-lying π* orbitals that are sufficiently low in energy that the reduction of diphosphenes is facile, and reversible in many cases. In 2006, it was reported that isolation of the resulting radical anions derived by the reduction of BbtP=PBbt and BbtSb=SbBbt was achieved.[17,42] The crystalline salt [Li(DME)$_3$][BbtSb=SbBbt] was structurally characterized and it

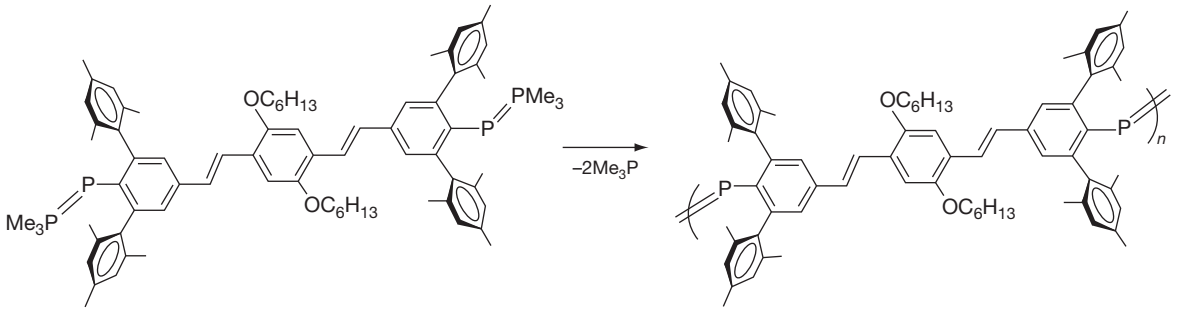

Scheme 40 Formation of a diphosphene-containing polymer from *phospha*-Wittig reagent.

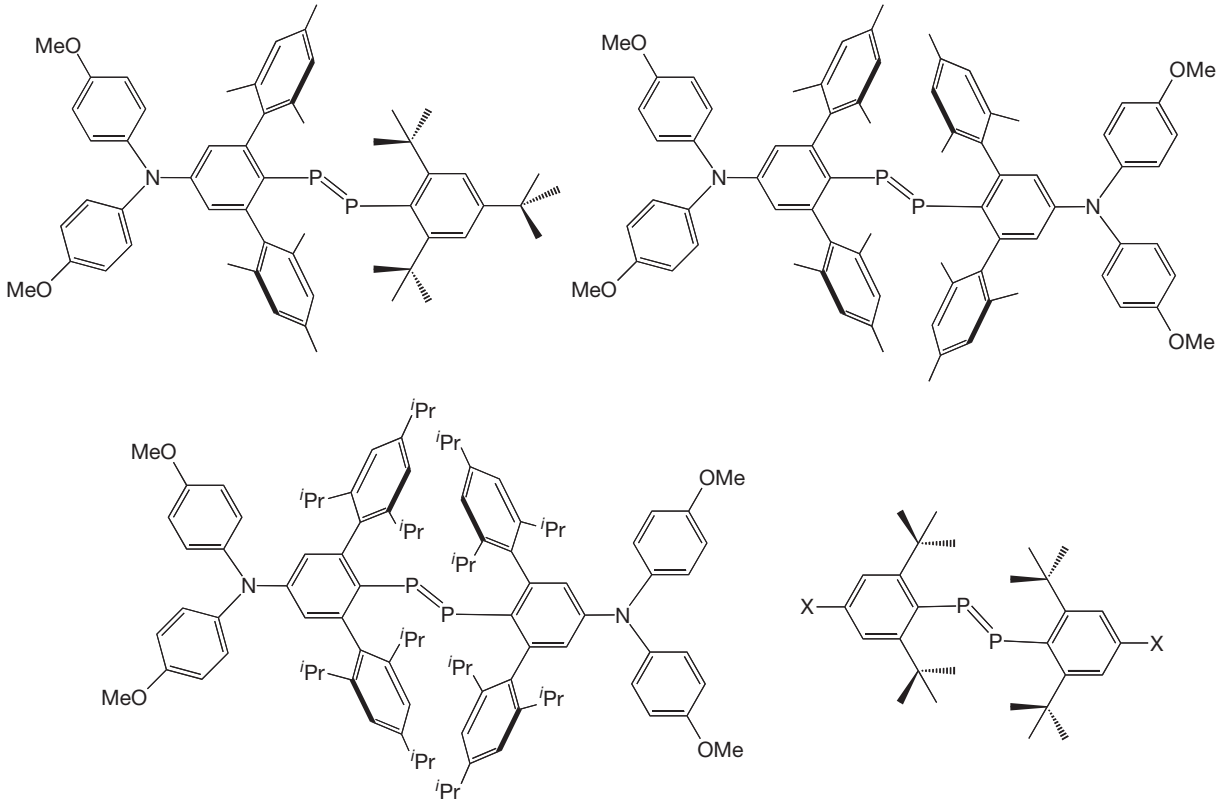

Scheme 41 Functionalized diphosphenes.

showed an SbSb bond length of 2.7511(4)Å, which is longer than that observed for the neutral parent compound (2.7037 (6)Å). Isolation of the related $[Li(DME)_3][TbtP{=}PTbt]$ was reported in 2008.[45]

1.12.3.3.3 Theoretical studies of diphosphenes

Diphosphenes have been the subject of a number of theoretical investigations prior to 2000.[148–151] Since then, other studies have continued to appear for theoretical treatments of diphosphenes.[10,23,45,149–157] All of these studies support the presence of a double bond, and that the *trans* (*E*) isomer is more stable than the *cis* (*Z*) isomer. Only a few of these reports will be discussed here.

In 2001, calculations on using DFT (B3LYP and BP86, 6-311G(d,p) basis sets) for the diphosphenes (Pn=P) and diarsenes (Pn=As) HPn=PnH, $(H_3Si)H_2CPn{=}PnCH_2(SiH_3)$, $(H_3Si)_2$ HCPn=PnCH$(SiH_3)_2$, and PhPn=PnPh were reported.[152] These efforts were made to support the analysis of the UV–PES spectra of Mes*As=AsMes* and $(Me_3Si)_3$CAs=AsC$(SiMe_3)_3$. One major finding was that there are few differences between the nature of the electronic structures of diphosphenes and diarsenes having the same substituents. Changing the ligands at the group 15 element, however, does induce significant changes in the ordering of the HOMO and HOMO(−1). In diphosphenes, these two orbitals are close in energy, and, in the case of Mes*P=PMes*, they have been assigned as the PP π molecular orbital (HOMO − 1) and *n*+ lone pair (HOMO). This study shows that the silylated alkyl groups changed the ordering to make the PP π molecular orbital as the HOMO orbital. In addition, the lone pair *n*+ orbital could be raised in energy relative to the π MO in Mes*E=EMes* due to destabilizing interactions with the phenyl ring.

The fact that attached aromatic rings could influence the ordering of the HOMO and HOMO(−1) was explored in depth by two groups in 2008 and 2009.[158–160] In these studies, the aim went well beyond just predictions of the structures, but to systematically examine the impact of rotation about the P–C_{Ar} bonds (torsional angles α_1 and α_2, Scheme 42) on the nature and ordering of molecular orbitals.

Part of the driving force to undertake the above studies was to gain an understanding of the excited states so that one could gain a greater understanding of the photochemical behavior of diphosphenes. Unlike the very significant amount of photochemistry on azobenzene,[59,161] little detailed work has been undertaken for diphosphenes. The photochemical isomerization of diphosphenes was first noted in the 1980s.[162–166] These early results found that mixtures of *E*- and *Z*-configured diphosphenes could be generated. In contrast to the photochemistry of azobenzenes, however, the photochemical behavior of diphosphenes was more complicated and depended greatly on the exact nature of the attached substituents. Photolysis of diphosphenes can also lead to the formation of cyclotetramers, or products derived from putative phosphinidene intermediates (Scheme 43). In other cases, photolysis has no impact on the diphosphene and no isomerization is observed.[160,167]

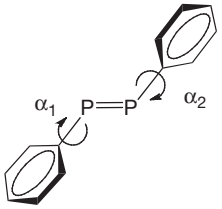

Scheme 42 Structural distortions within diaryl diphosphenes.

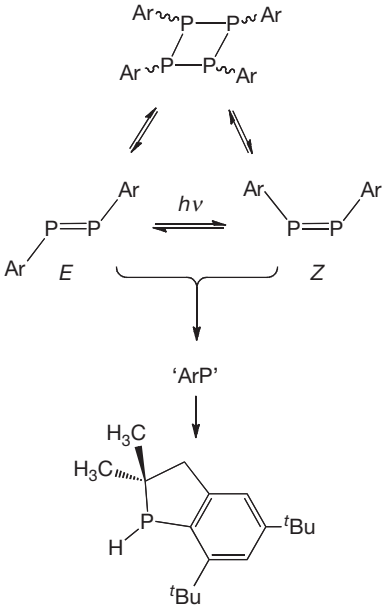

Scheme 43 Photoreactions of diphosphenes.

In order to assess these different reaction pathways and to address questions on the mechanism for the *E*–*Z* isomerization process, theoretical studies have appeared that probe photo-excited states.[158–160] These studies have led to the conclusion that the *E*–*Z* isomerization process occurs via rotation about the P=P bond, as opposed to inversion at the phosphorus center(s).

1.12.3.3.4 New syntheses of dipnictenes

New routes leading to the formation of dipnictenes have appeared in the past 10 years. In 2001, it was shown that photolysis of phospha-Wittig reagents ArP=PMe_3 could lead to diphosphenes when bulky *meta*-terphenyl ligands were used.[168] This method was used successfully in creating the first conjugated polymer having diphosphene units in the backbone (vide supra).[126] During attempts to prepare similar *arsa*-Wittig reagents of the form ArAs=PMe_3, the compounds were found to be thermally unstable and quickly produced diarsenes (Scheme 44).

Catalytic routes to new materials having group 15 multiply bonded compounds are obviously of great interest. A pair of reports details the transition-metal-catalyzed dehydrogenation of primary arsenes and stibenes (Scheme 45).[169,170] In the process leading to the diarsene, it was found that the addition of PMe_3 improved reaction yields, possibly indicating the presence of free arsenidenes via intermediary *arsa*-Wittig species.

A silyldiphosphenido complex was discovered that generates the unstable diphosphene $^{i}Pr_3SiP{=}PSi^{i}Pr_3$.[171] The diphosphene could be trapped via cycloaddition reactions to afford new cyclic products in good to excellent yields (Scheme 46). In the absence of trapping reagents, the silyldiphosphenido complex yields trimers and tetramers of the $^{i}Pr_3SiP$ phosphinidene.

Also of interest was the observation that the silyldiphosphenido complex would undergo reversible transfer of the $^{i}Pr_3SiP$ group to triphenyl phosphane to generate solutions of the new phospha-Wittig reagent $^{i}Pr_3SiP{=}PPh_3$ (Scheme 47).

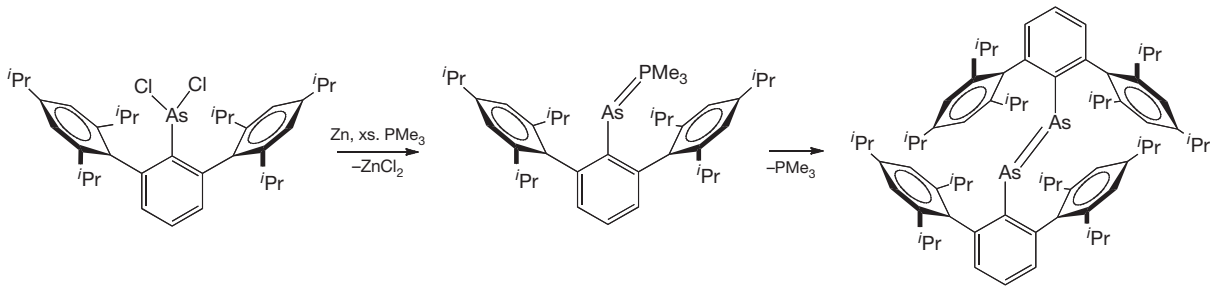

Scheme 44 Formation of an *arsa*-Wittig reagents and decomposition to diarsene.

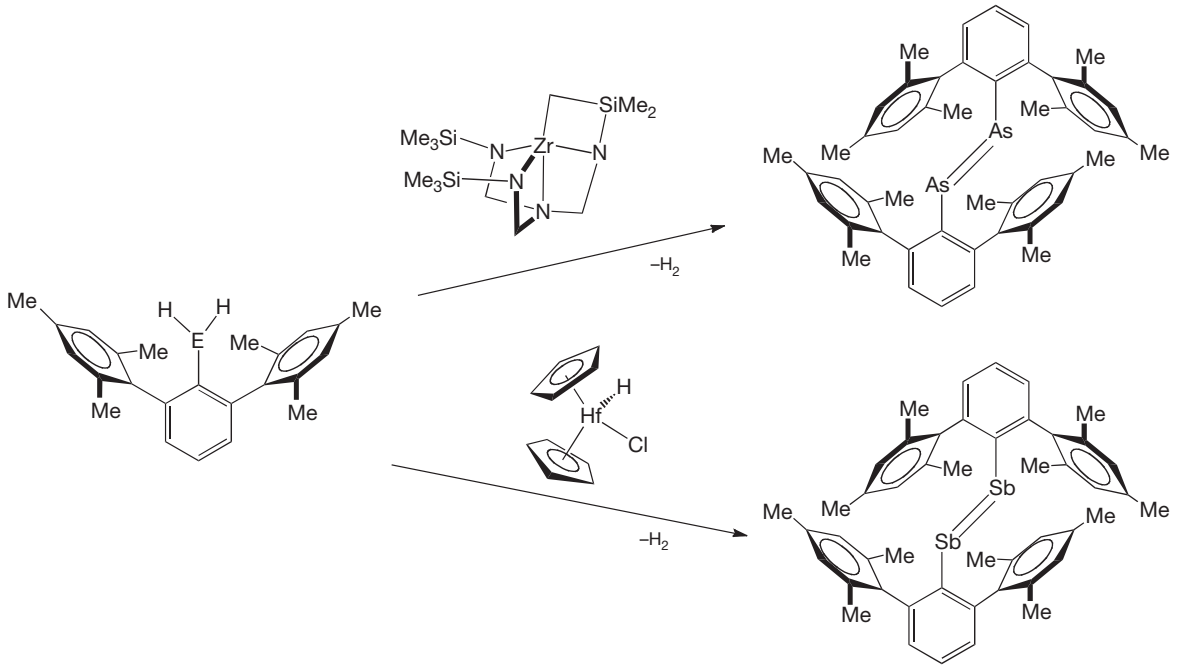

Scheme 45 Dehydrocoupling of $ArEH_2$ by transition metal complexes.

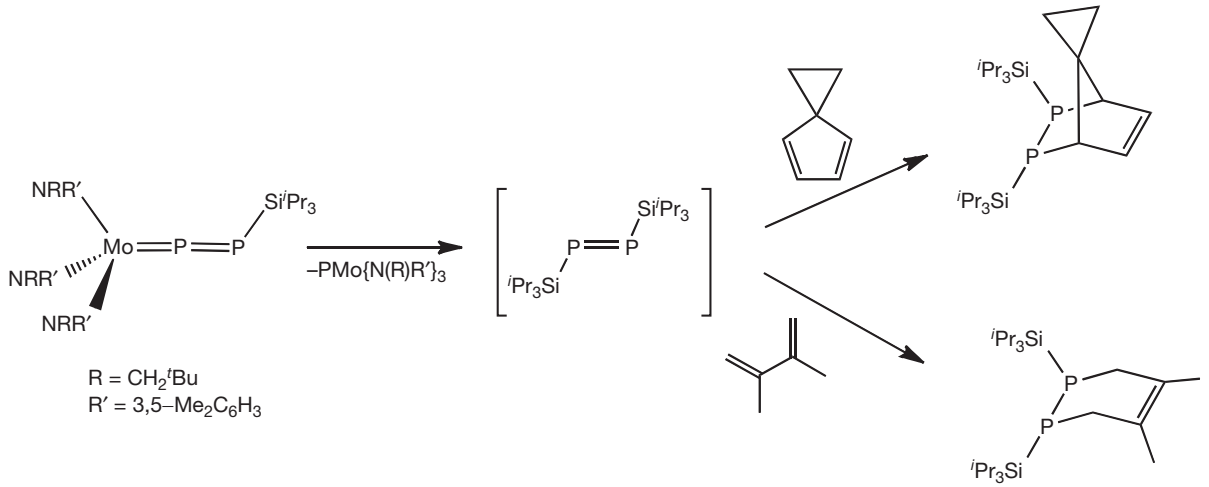

Scheme 46 Spawning and trapping of reactive diphosphene.

$$^{i}Pr_3SiPPMo\{N(R)R'\}_3 + PPh_3 \underset{}{\overset{K_{eq} = 0.7}{\rightleftharpoons}} PMo\{N(R)R'\}_3 + {}^{i}Pr_3SiP{=}PPh_3$$

Scheme 47 Equilibrium transfer of phopshinidene between molybdenum phosphide and triphenylphosphane.

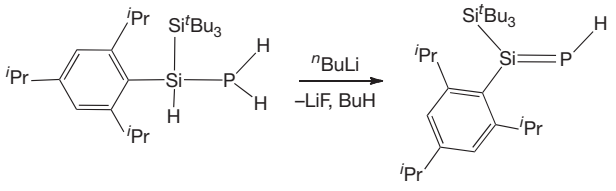

Scheme 48 Synthesis of unusual RR'Si=PH compound.

Several notable developments in doubly bonded silicon–pnictene chemistry have appeared. In 2006, the first isolable compound having a Si=PH unit appeared (Scheme 48).[172] This compound is noteworthy, for it lacks a sterically demanding group on the phosphorus atom, and it also undergoes metallation with zinc to provide a Zn–P=Si reagent.

In 2006, a material having an Si=AsH unit was isolated by the reaction of a silylene with AsH_3 (Scheme 49, Ar = 2,6-$^{i}Pr_2C_6H_3$).[173] In solution, the arsasilene complex is in equilibrium with the immediate product of direct insertion

of the silylene with AsH_3. Interestingly, the reaction of the silylene with PH_3 stops at the stage of providing the product of insertion into a single PH bond.

In 2009, the first compound bearing two Si=P units was discovered (Scheme 50, left).[174] This material utilized the Eind ligand (Scheme 50, right), which forces the two Si=P units to be coplanar with the bridging phenylene group and, thus, promotes conjugation between the two Si=P units. DFT calculations and UV–vis spectra of this material also corroborate the π-conjugation for the two Si=P units.

1.12.3.3.5 Other dipnictenes

Iminophosphanes, RP=NR′, are a well-established class of low-coordinate phosphorus compounds.[175] An example of new developments in this area involves 'push–pull' type iminophosphanes (Scheme 51).[176] The net result of experimental and computational studies shows that the polarization by the substituents is limited due to the steric interactions of the bulky aryl group inhibiting conjugation between the aromatic ring and the P=N π-system.

Iminoarsanes, RAs=NR′, are much rarer than iminophosphanes and remain few in number. One recent example is shown in Scheme 52.[177] These red to red-orange compounds are *E*-configured about the As=N bonds, which was confirmed by crystal structure analysis for $R=N(SiMe_3)_2$.

The new phosphasilene and phosphagermenes appeared in 2009 (Scheme 53, E = Si or Ge).[178] Both of these materials could be reduced by KC_8 in tetrahydrofuran (THF) to persistent radicals which displayed prominent EPR signals with strong coupling to the spin 1/2 P nucleus. Analysis of the reduction by cyclic voltammetry showed that the reversible reduction process occurs at a potential intermediate of that observed for the disilene $(^tBu_2Me)_2Si=Si(Me^tBu_2)_2$ and the diphosphene Mes*P=PMes*.

New examples of heavier dipnictenes have appeared in 2000 and 2002 (Scheme 54).[179,180] Both of these new compounds were prepared by the DBU-induced dehydrohalogenation reactions between $ArEH_2$ and $ArEBr_2$. The structure of the phosphabismuthene revealed a P=Bi bond length that was intermediate of bond lengths determined for P=P and Bi=Bi compounds. The structure of the stibabismuthene, however, was plagued by disorder of the Sb and Bi atoms, and, thus, an accurate assessment of the Sb=Bi bond length was not possible.

The stibabismuthene, while stable to room temperature, begins to disproportionate to the homonuclear distibene and dibismuthene compounds at elevated temperatures. The process was greatly accelerated under photochemical conditions (Scheme 55).

A new twist on the synthesis of dipnictenes utilizes fluorinated arsines to generate Mes*As=AsMes* and Mes*As=PMes* (Scheme 56).[181] As expected, the structure of Mes*P=AsMes* revealed an As=P bond length intermediate to E=E bond lengths found in diarsenes and diphosphenes.

1.12.4 Group 15 Multiply Bonded Compounds Derived from Carbenes and Related Species

The use of stabilized carbenes in group 15 chemistry is a rapidly emerging area of research that warrants its own section.[18] Some key developments are highlighted here, as many of the products of these reactions have potential multiple bonds to P and As atoms.[68] In 2007, it was shown that the reaction of a cyclic aminoalkyl carbene (CAAC) with elemental phosphorus (P_4) yielded a diphosphene bearing two phosphaalkene units (Scheme 57, Ar = 2,6-$^iPr_2C_6H_3$).[182]

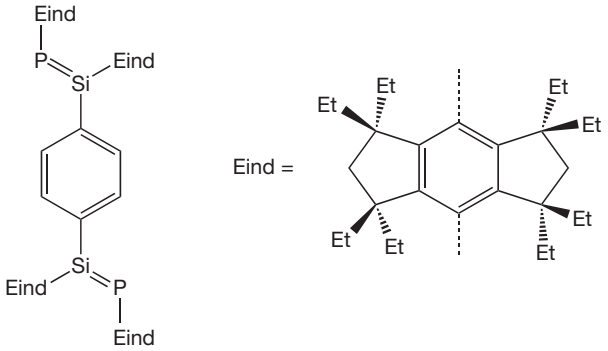

Scheme 50 Conjugation of two Si=P units across a benzene ring.

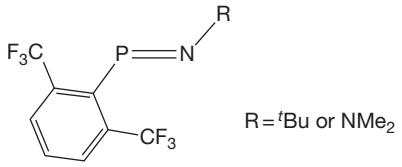

Scheme 51 A "push-pull" type of iminophosphane.

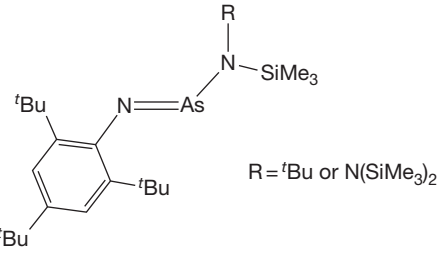

Scheme 52 An iminoarsene.

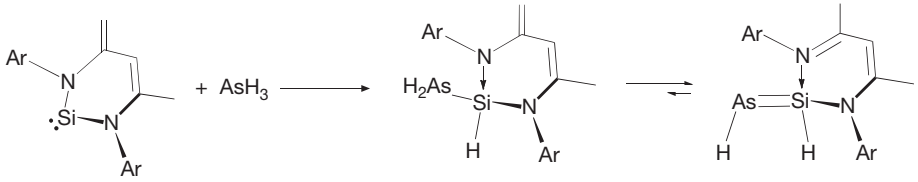

Scheme 49 Reaction of silylene with AsH_3 and formation of arsenic-silicon double bond.

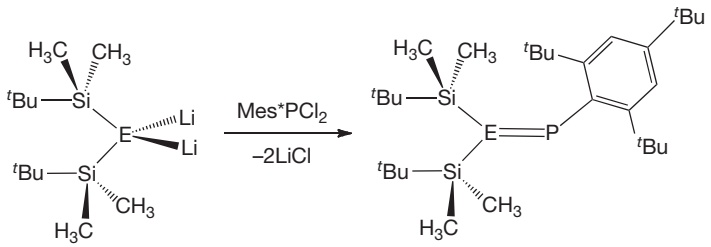

Scheme 53 Synthesis of phosphasilene (E = Si) and phosphagermene (E = Ge).

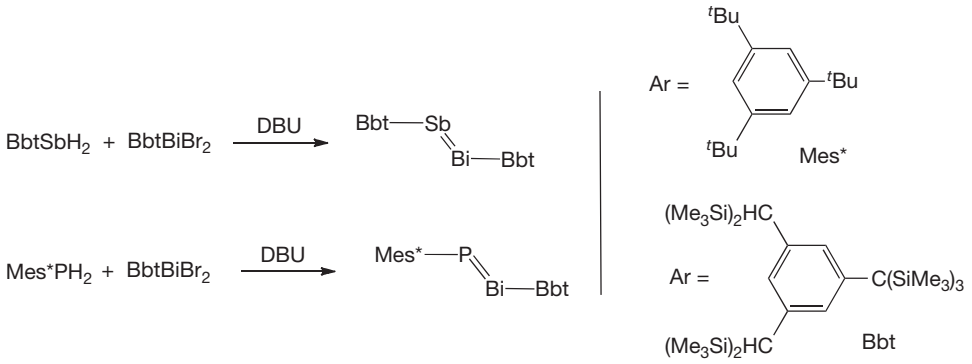

Scheme 54 Synthesis of stibabismuthene and phosphabismuthene.

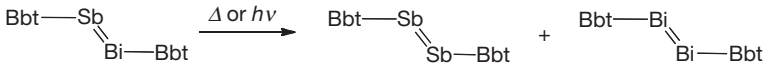

Scheme 55 Disproportionation of stibabismuthene to dibismuthene and distibene.

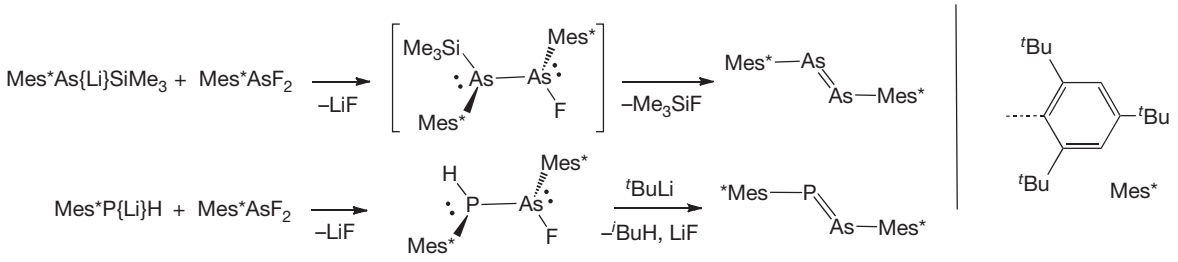

Scheme 56 Synthesis of diarsene and phosphaarsene using fluorinated precursors.

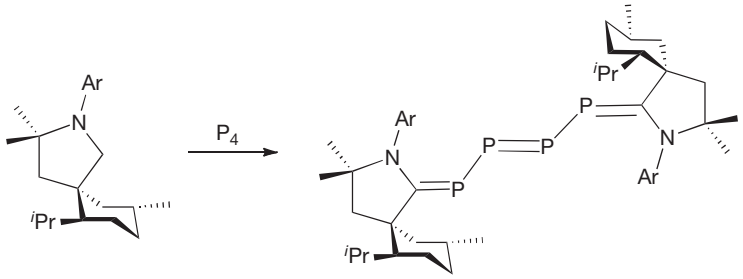

Scheme 57 Carbene activation of elemental phosphorus.

As mentioned earlier, diphosphorus (P≡P) is an extremely unstable molecule. In 2008, however, an interesting molecule possessing a diphosphorus unit sandwiched between two coordinating *N*-heterocyclic carbenes (**Scheme 58**, Ar = 2,6-$^{i}Pr_2C_6H_3$ or 2,4,6-$Me_3C_6H_2$) could be prepared by the reduction of carbene–PCl_3 adducts.[183] Two types of resonance structures were considered for these molecules, with the NHC-stabilized bis(phosphinidene) (**Scheme 58**, center) form being favored over the diphosphabutadiene form (**Scheme 58**, right).

Not long afterwards, it was found that the direct formation of carbene-stabilized diphosphorus from P_4 was possible (**Scheme 59**, Ar = 2,6-$^{i}Pr_2C_6H_3$) if a less hindered CAAC was used.[184] The favored resonance structure of this particular dicarbene-stabilized P_2 was the diphosphabutadiene. In addition, a triscarbene–P4 adduct was formed as well.

In 2010, the reaction shown in **Scheme 58** was extended to arsenic, providing a form of carbene-stabilized diarsenic (**Scheme 60**).[185]

This chemistry has also been extended to mixed diatomics. Phosphorus mononitride (P≡N) is an unstable compound that has been detected in the atmospheres of other planets and can be generated under special laboratory conditions.[186] This reactive unit can be isolated when it is bound by two CAAC ligands (**Scheme 61**).[187]

Building on these types of reports, a group 13-based NHC analog was successful in affording compounds featuring bismuth–bismuth double bonds (**Scheme 62**).[188]

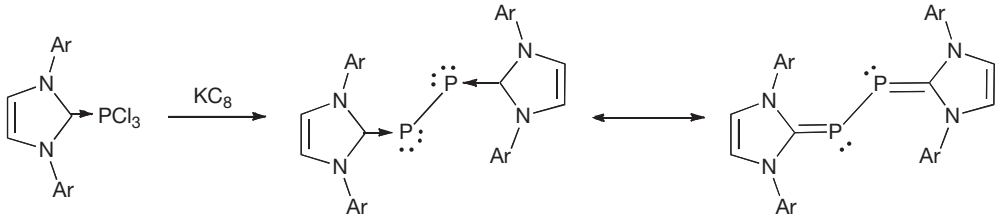

Scheme 58 Synthesis of carbene stabilized diphosphorus.

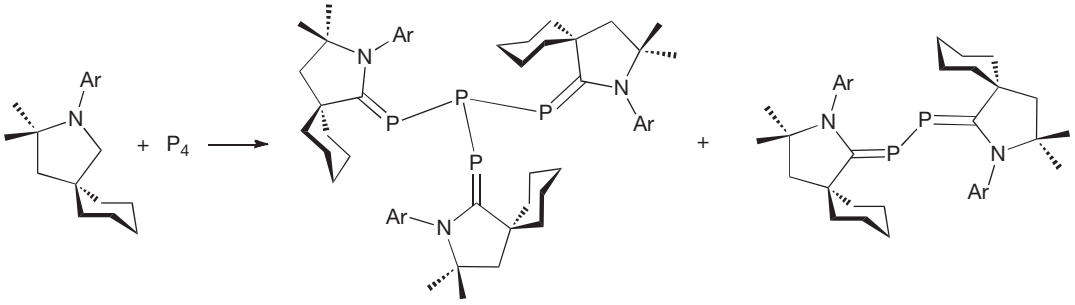

Scheme 59 Alternative route to carbene stabilized diphosphorus.

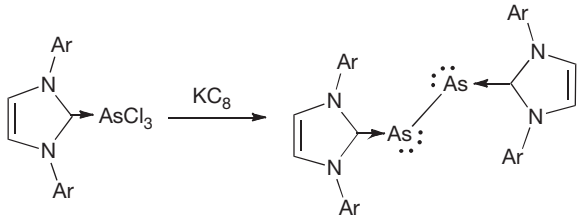

Scheme 60 Synthesis of carbene stabilized diarsenic.

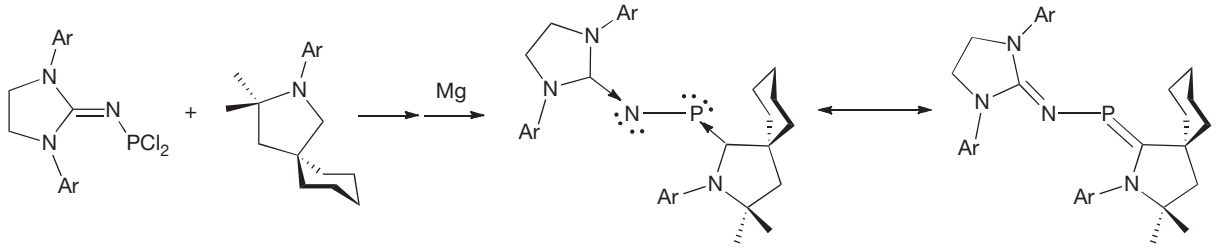

Scheme 61 Synthesis of carbene stabilized NP unit.

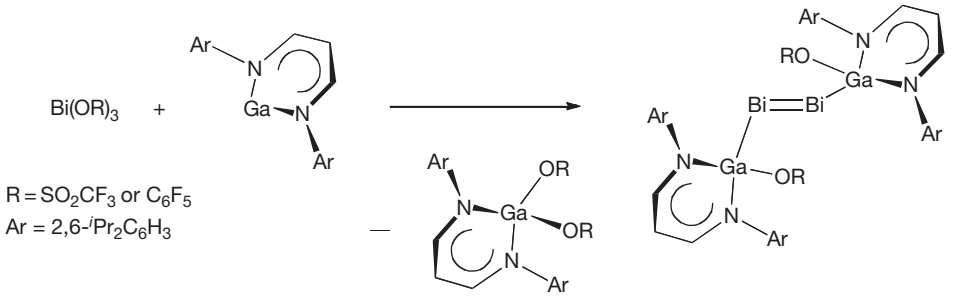

Scheme 62 Synthesis of gallium stabilized Bi═Bi bond.

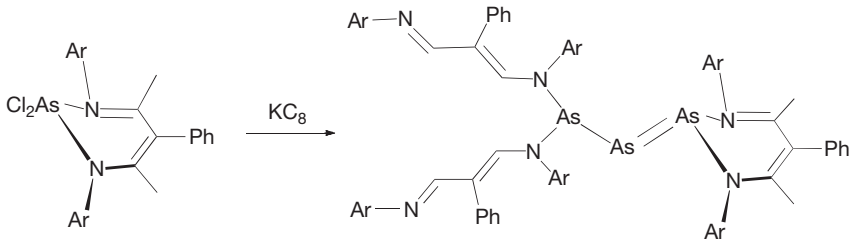

Scheme 63 Unusual formation of arsenic-arenic multiple bond.

Yet another strategy has shown that As=As multiple bonding could be supported by the use of sterically demanding guanidinato or amidinato ligands.[189,190] These examples are interesting, for the multiple bonds persist in the presence of the added base stabilization.

Another interesting material having arsenic–arsenic double bonds is shown in Scheme 63.[191]

1.12.5 Conclusion

This review covers key developments in the chemistry of multiply bonded compounds of the heavier group 15 elements phosphorus, arsenic, antimony, and bismuth published in the years 2000–2010, in particular, compounds having multiply bonded pnictogens having coordination numbers one and two. This field has grown immensely over this decade and many new types of compounds, new syntheses, and new modes of reactivity have been discovered. The next decade looks very promising not only for the discovery of other new types of multiply bonded compounds, but also for applications of these functional groups in advanced materials and in catalysis. For related chapters in this Comprehensive, we refer to Chapters 1.05, 2.05, and 2.06.

Acknowledgments

J.D.P. thanks the National Science Foundation (CHE-0748982) for support, and Michael Rectenwald (Case Western Reserve University) for his assistance with the chapter.

References

1. Cowley, A. H.; Barron, A. R. *Acc. Chem. Res.* **1988**, *21*, 81.
2. Cowley, A. H. *Acc. Chem. Res.* **1997**, *30*, 445.
3. Stephan, D. W. *Angew. Chem. Int. Ed. Engl.* **2000**, *39*, 315.
4. Mathey, F.; Huy, N. H. T.; Marinetti, A. *Helv. Chim. Acta* **2001**, *84*, 2938.
5. Lammertsma, K.; Vlaar, M. J. M. *Eur. J. Org. Chem.* **2002**, 1127.
6. Mindiola, D. J. *Acc. Chem. Res.* **2006**, *39*, 813.
7. Mathey, F. *Dalton Trans.* **2007**, 1861.
8. Aktas, H.; Slootweg, J. C.; Lammertsma, K. *Angew. Chem. Int. Ed. Engl.* **2010**, *49*, 2102.
9. Mathey, F. *Angew. Chem. Int. Ed. Engl.* **2003**, *42*, 1578.
10. Cundari, T. R. *Chem. Rev.* **2000**, *100*, 807.
11. Mathey, F. *Phosphorus–Carbon Heterocyclic Chemistry: The Rise of a New Domain*. Pergamon: Amsterdam, 2001.
12. Gilheany, D. G. *Chem. Rev.* **1994**, *94*, 1339.
13. Regitz, M., Scherer, O. J., Eds.; In *Multiple Bonds and Low Coordination in Phosphorus Chemistry*; Thieme Verlag: Stuttgart, 1990.
14. Fischer, R. C.; Power, P. P. *Chem. Rev.* **2010**, *110*, 3877.
15. Power, P. P. *Chem. Rev.* **1999**, *99*, 3463.
16. Burford, N.; Weigand, J. In *Catenated Phosphorus Compounds (including rings and cages, but not multiply bonded systems)*, Chivers, T., Ed.; Comprehensive Inorganic Chemistry II; Elsevier; Vol. 1, Chapter 1.6.
17. Chivers, T. In *Stable or Persistent (Neutral and Charged) Radicals – Groups 13–16*; Chivers, T., Ed.; Comprehensive Inorganic Chemistry II; Elsevier; Vol. 1, Chapter 1.16.
18. Rivard, E. In *NHC Adducts of MG Compounds*; Chivers, T., Ed.; Comprehensive Inorganic Chemistry II; Elsevier; Vol. 1, Chapter 1.20.
19. Baumgartner, T. In *Phosphorus-Containing Polymers;* Comprehensive Inorganic Chemistry II, Elsevier, Chapter 1.31.
20. Mahe, L.; Barthelat, J.-C. *J. Phys. Chem.* **1995**, *99*, 6819.
21. Bouhadir, G.; Bourissou, D. *Chem. Soc. Rev.* **2004**, *33*, 210.
22. Power, P. P. *J. Chem. Soc. Dalton Trans.* **1998**, 2939.
23. Landis, C. R.; Weinhold, F. *J. Am. Chem. Soc.* **2006**, *128*, 7335.
24. Kutzelnigg, W. *Angew. Chem. Int. Ed. Engl.* **1984**, *23*, 272.
25. Grant, D. J.; Dixon, D. A. *J. Phys. Chem. A* **2006**, *110*, 12955.
26. Ito, K.; Nagase, S. *Chem. Phys. Lett.* **1986**, *126*, 531.
27. Pietschnig, R.; Niecke, E. *Organometallics* **1996**, *15*, 891.

28. Twamley, B.; Sofield, C. D.; Olmstead, M. M.; Power, P. P. *J. Am. Chem. Soc.* **1999**, *121*, 3357.
29. Sasamori, T.; Takeda, N.; Tokitoh, N. *J. Phys. Org. Chem.* **2003**, *16*, 450.
30. Tokitoh, N.; Arai, Y.; Sasamori, T.; Okazaki, R.; Nagase, S.; Uekusa, H.; Ohashi, Y. *J. Am. Chem. Soc.* **1998**, *120*, 433.
31. Tokitoh, N.; Arai, Y.; Okazaki, R.; Nagase, S. *Science* **1997**, *277*, 78.
32. Culcasi, M.; Gronchi, G.; Escudié, J.; Couret, C.; Pujol, L.; Tordo, P. *J. Am. Chem. Soc.* **1986**, *108*, 3130.
33. Bard, A. J.; Cowley, A. H.; Kilduff, J. E.; Leland, J. K.; Norman, N. C.; Pakulski, M.; Heath, G. A. *J. Chem. Soc. Dalton Trans.* **1987**, 249.
34. Shah, S.; Burdette, S. C.; Swavey, S.; Urbach, F. L.; Protasiewicz, J. D. *Organometallics* **1997**, *16*, 3395.
35. Tsuji, K.; Sasaki, S.; Yoshifuji, M. *Tetrahedron Lett.* **1999**, *40*, 3203.
36. Sasaki, S.; Aoki, H.; Sutoh, K.; Hakiri, S.; Tsuji, K.; Yoshifuji, M. *Helv. Chim. Acta* **2002**, *85*, 3842.
37. Dutan, C.; Shah, S.; Smith, R. C.; Choua, S.; Berclaz, T.; Geoffroy, M.; Protasiewicz, J. D. *Inorg. Chem.* **2003**, *42*, 6241.
38. Nagahora, N.; Sasamori, T.; Takeda, N.; Tokitoh, N. *Chem. Eur. J.* **2004**, *10*, 6146.
39. Sasamori, T.; Mieda, E.; Nagahora, N.; Takeda, N.; Takagi, N.; Nagase, S.; Tokitoh, N. *Chem. Lett.* **2005**, *34*, 166.
40. Moser, C.; Nieger, M.; Pietschnig, R. *Organometallics* **2006**, *25*, 2667.
41. Nagahora, N.; Sasamori, T.; Tokitoh, N. *Chem. Lett.* **2006**, *35*, 220.
42. Sasamori, T.; Mieda, E.; Nagahora, N.; Sato, K.; Shiomi, D.; Takui, T.; Hosoi, Y.; Furukawa, Y.; Takagi, N.; Nagase, S.; Tokitoh, N. *J. Am. Chem. Soc.* **2006**, *128*, 12582.
43. Sasamori, T.; Tsurusaki, A.; Nagahora, N.; Matsuda, K.; Kanemitsu, Y.; Watanabe, Y.; Furukawa, Y.; Tokitoh, N. *Chem. Lett.* **2006**, *35*, 1382.
44. Nagahora, N.; Sasamori, T.; Watanabe, Y.; Furukawa, Y.; Tokitoh, N. *Bull. Chem. Soc. Jpn.* **2007**, *80*, 1884.
45. Nagahora, N.; Sasamori, T.; Hosoi, Y.; Furukawa, Y.; Tokitoh, N. *J. Organomet. Chem.* **2008**, *693*, 625.
46. Sasamori, T.; Hori, A.; Kaneko, Y.; Tokitoh, N. *New J. Chem.* **2010**, *34*, 1560.
47. Xu, L.; Bobev, S.; El-Bahraoui, J.; Sevov, S. C. *J. Am. Chem. Soc.* **2000**, *122*, 1838.
48. Hanauer, T.; Korber, N. *Z. Anorg. Allg. Chem.* **2004**, *630*, 2532.
49. Brand, H.; Schulz, A.; Villinger, A. *Z. Anorg. Allg. Chem.* **2007**, *633*, 22.
50. Cordaro, J. G.; Stein, D.; Ruegger, H.; Gruetzmacher, H. *Angew. Chem. Int. Ed. Engl.* **2006**, *45*, 6159.
51. Fleischer, U.; Gruetzmacher, H.; Krueger, U. *J. Chem. Soc. Chem. Commun.* **1991**, 302.
52. Becker, G.; Schwarz, W.; Seidler, N.; Westerhausen, M. *Z. Anorg. Allg. Chem.* **1992**, *612*, 72.
53. Becker, G.; Hübler, K. *Z. Anorg. Allg. Chem.* **1994**, *620*, 405.
54. Becker, G.; Heckmann, G.; Hübler, K.; Schwarz, W. *Z. Anorg. Allg. Chem.* **1995**, *621*, 34.
55. Westerhausen, M.; Schneiderbauer, S.; Piotrowski, H.; Suter, M.; Noth, H. *J. Organomet. Chem.* **2002**, *643–644*, 189.
56. Finze, M.; Bernhardt, E.; Willner, H.; Lehmann, C. W. *Angew. Chem. Int. Ed. Engl.* **2004**, *43*, 4160.
57. Becker, G.; Brombach, H.; Horner, S. T.; Niecke, E.; Schwarz, W.; Streubel, R.; Wurthwein, E.-U. *Inorg. Chem.* **2005**, *44*, 3080.
58. Ionkin, A. S.; Marshall, W. J.; Fish, B. M.; Howe, L. A. *Organometallics* **2010**, *29*, 4154.
59. Griffiths, J. *Chem. Soc. Rev.* **1972**, *1*, 481.
60. Niecke, E.; Nieger, M.; Reichert, F. *Angew. Chem. Int. Ed.* **1988**, *100*, 1781.
61. Burford, N.; Phillips, A. D.; Spinney, H. A.; Lumsden, M.; Werner-Zwanziger, U.; Ferguson, M. J.; McDonald, R. *J. Am. Chem. Soc.* **2005**, *127*, 3921.
62. Burford, N.; Spinney, H. A.; Ferguson, M. J.; McDonald, R. *Chem. Commun.* **2004**, 2696.
63. Burford, N.; Losier, P.; Phillips, A. D.; Ragogna, P. J.; Cameron, T. S. *Inorg. Chem.* **2003**, *42*, 1087.
64. Burford, N.; Cameron, T. S.; Robertson, K. N.; Phillips, A. D.; Jenkins, H. A. *Chem. Commun.* **2000**, 2087.
65. Burford, N.; Cameron, T. S.; LeBlanc, D. J.; Phillips, A. D.; Concolino, T. E.; Lam, K.-C.; Rheingold, A. L. *J. Am. Chem. Soc.* **2000**, *122*, 5413.
66. Cossairt, B. M.; Piro, N. A.; Cummins, C. C. *Chem. Rev.* **2010**, *110*, 4164.
67. Caporali, M.; Gonsalvi, L.; Rossin, A.; Peruzzini, M. *Chem. Rev.* **2010**, *110*, 4178.
68. Scheer, M.; Balázs, G.; Seitz, A. *Chem. Rev.* **2010**, *110*, 4236.
69. Piro, N. A.; Figueroa, J. S.; McKellar, J. T.; Cummins, C. C. *Science* **2006**, *313*, 1276.
70. Tofan, D.; Cummins, C. C. *Angew. Chem. Int. Ed. Engl.* **2010**, *49*, 7516.
71. Russell, C. A. *Angew. Chem. Int. Ed. Engl.* **2010**, *49*, 9572.
72. Nixon, J. F. *Chem. Rev.* **1988**, *88*, 1327.
73. Regitz, M. *Chem. Rev.* **1990**, *90*, 191.
74. Streubel, R. *Angew. Chem. Int. Ed. Engl.* **1995**, *34*, 436.
75. Appel, V. R.; Knoll, F.; Ruppert, I. *Angew. Chem. Int. Ed.* **1981**, *93*, 771.
76. Regitz, M.; Binger, P. *Angew. Chem. Int. Ed. Engl.* **1988**, *27*, 1484.
77. Lynam, J. M. *Organomet. Chem.* **2007**, *33*, 170.
78. Weber, L. *Eur. J. Inorg. Chem.* **2003**, 1843.
79. Markovski, L. N.; Romanenko, V. D. *Tetrahedron* **1989**, *45*, 6019.
80. Guillemin, J.-C.; Janati, T.; Denis, J.-M. *J. Org. Chem.* **2001**, *66*, 7864.
81. Mo, O.; Yanez, M.; Guillemin, J.-C.; Riague, E. H.; Gal, J.-F.; Maria, P.-C.; Dubin Poliart, C. *Chem. Eur. J.* **2002**, *8*, 4919.
82. Figueroa, J. S.; Cummins, C. C. *J. Am. Chem. Soc.* **2004**, *126*, 13916.
83. Cordaro, J. G.; Stein, D.; Gruetzmacher, H. *J. Am. Chem. Soc.* **2006**, *128*, 14962.
84. Toyota, K.; Kawasaki, S.; Yoshifuji, M. *J. Org. Chem.* **2004**, *69*, 5065.
85. Brym, M.; Jones, C. *Dalton Trans.* **2003**, 3665.
86. Brodkorb, F.; Brym, M.; Jones, C.; Schulten, C. *J. Organomet. Chem.* **2006**, *691*, 1025.
87. Weber, L. *Coord. Chem. Rev.* **1997**, *158*, 1.
88. Pombeiro, A. J. L. *J. Organomet. Chem.* **2001**, *632*, 215.
89. Hazari, N.; Mountford, P. *Acc. Chem. Res.* **2005**, *38*, 839.
90. Kolb, H. C.; Finn, M. G.; Sharpless, K. B. *Angew. Chem. Int. Ed. Engl.* **2001**, *40*, 2004.
91. Hermesdorf, M.; Birkel, M.; Heydt, H.; Regitz, M.; Binger, P. *Phosphorus Sulfur* **1989**, *46*, 31.
92. Roesch, W.; Facklam, T.; Regitz, M. *Tetrahedron* **1987**, *43*, 3247.
93. Choong, S. L.; Jones, C.; Stasch, A. *Dalton Trans.* **2010**, *39*, 5774.
94. Dillon, K. B.; Mathey, F.; Nixon, J. F. *Phosphorus: The Carbon Copy*. John Wiley & Sons: New York, 1998.
95. Mathey, F. *Acc. Chem. Res.* **1992**, *25*, 90.
96. Weber, L. *Chem. Ber.* **1996**, *129*, 367.
97. Escudie, J.; Ranaivonjatovo, H.; Rigon, L. *Chem. Rev.* **2000**, *100*, 3639.
98. Bouslikhane, M.; Gornitzka, H.; Ranaivonjatovo, H.; Escudie, J. *Organometallics* **2002**, *21*, 1531.
99. Escudie, J.; Ranaivonjatovo, H.; Bouslikhane, M.; El Harouch, Y.; Baiget, L.; Cretiu Nemes, G. *Russ. Chem. Bull.* **2004**, *53*, 1020.
100. Escudie, J.; Ranaivonjatovo, H. *Organometallics* **2007**, *26*, 1542.
101. Romanenko, V. D.; Rudzevich, V. L. *Compr. Org. Funct. Group Transform. II* **2005**, *6*, 661.
102. Yam, M.; Tsang, C.-W.; Gates, D. P. *Inorg. Chem.* **2004**, *43*, 3719.
103. Weber, L. *Coord. Chem. Rev.* **2005**, *249*, 741.
104. MacMillan, S. N.; Tanski, J. M.; Waterman, R. *Chem. Commun.* **2007**, 4172.
105. Waterman, R. *Dalton Trans.* **2009**, 18.
106. Weber, L. *Eur. J. Inorg. Chem.* **2000**, 2425.
107. Weber, L. *Eur. J. Inorg. Chem.* **2007**, 4095.
108. Termaten, A.; van der Sluis, M.; Bickelhaupt, F. *Eur. J. Org. Chem.* **2003**, 2049.
109. Kawasaki, S.; Nakamura, A.; Toyota, K.; Yoshifuji, M. *Bull. Chem. Soc. Jpn.* **2005**, *78*, 1110.
110. Yoshifuji, M. *J. Organomet. Chem.* **2000**, *611*, 210.
111. Toyota, K.; Kawasaki, S.; Yoshifuji, M. *Tetrahedron Lett.* **2002**, *43*, 7953.
112. Kawasaki, S.; Fujita, T.; Toyota, K.; Yoshifuji, M. *Bull. Chem. Soc. Jpn.* **2005**, *78*, 1082.
113. Gudimetla, V. B.; Ma, L.; Washington, M. P.; Payton, J. L.; Cather Simpson, M.; Protasiewicz, J. D. *Eur. J. Inorg. Chem.* **2010**, 854.
114. Le Floch, P. *Coord. Chem. Rev.* **2006**, *250*, 627.
115. Nakamura, A.; Kawasaki, S.; Toyota, K.; Yoshifuji, M. *J. Organomet. Chem.* **2007**, *692*, 70.
116. Yamada, N.; Toyota, K.; Yoshifuji, M. *Chem. Lett.* **2001**, 248.
117. Deschamps, E.; Deschamps, B.; Dormieux, J. L.; Ricard, L.; Mezailles, N.; Floch, P. L. *Dalton Trans.* **2006**, 594.
118. Shah, S.; Protasiewicz, J. D. *Coord. Chem. Rev.* **2000**, *210(1)*, 181.
119. Takita, R.; Takada, Y.; Jensen, R. S.; Okazaki, M.; Ozawa, F. *Organometallics* **2008**, *27*, 6279.
120. Baumgartner, T.; Reau, R. *Chem. Rev.* **2006**, *106*, 4681.
121. Gates, D. P. *Top. Curr. Chem.* **2005**, *250*, 107.
122. Bates, J. I.; Dugal-Tessier, J.; Gates, D. P. *Dalton Trans.* **2010**, *39*, 3151.
123. Wright, V. A.; Gates, D. P. *Angew. Chem. Int. Ed. Engl.* **2002**, *41*, 2389.
124. Wright, V. A.; Patrick, B. O.; Schneider, C.; Gates, D. P. *J. Am. Chem. Soc.* **2006**, *128*, 8836.
125. Smith, R. C.; Chen, X.; Protasiewicz, J. D. *Inorg. Chem.* **2003**, *42*, 5468.
126. Smith, R. C.; Protasiewicz, J. D. *J. Am. Chem. Soc.* **2004**, *126*, 2268.
127. Smith, R. C.; Protasiewicz, J. D. *Eur. J. Inorg. Chem.* **2004**, 998.
128. Schaefer, B.; Oberg, E.; Kritokos, M.; Ott, S. *Angew. Chem. Int. Ed. Engl.* **2008**, *47*, 8228.

129. Geng, X.-L.; Hu, Q.; Schafer, B.; Ott, S. *Org. Lett.* **2010**, *12*, 692.
130. Oeberg, E.; Schaefer, B.; Geng, X.-L.; Pettersson, J.; Hu, Q.; Kritikos, M.; Rasmussen, T.; Ott, S. *J. Org. Chem.* **2009**, *74*, 9265.
131. Tsang, C.-W.; Yam, M.; Gates, D. P. *J. Am. Chem. Soc.* **2003**, *125*, 1480.
132. Tsang, C.-W.; Baharloo, B.; Riendl, D.; Yam, M.; Gates, D. P. *Angew. Chem. Int. Ed. Engl.* **2004**, *43*, 5682.
133. Gillon, B. H.; Gates, D. P. *Chem. Commun.* **2004**, 1868.
134. Noonan, K. J. T.; Gates, D. P. *Macromolecules* **2008**, *41*, 1961.
135. Gillon, B. H.; Noonan, K. J. T.; Feldscher, B.; Wissenz, J. M.; Kam, Z. M.; Hsieh, T.; Kingsley, J. J.; Bates, J. I.; Gates, D. P. *Can. J. Chem.* **2007**, *85*, 1045.
136. Gillon, B. H.; Patrick, B. O.; Gates, D. P. *Chem. Commun.* **2008**, *18*, 2161.
137. Noonan, K. J. T.; Gillon, B. H.; Cappello, V.; Gates, D. P. *J. Am. Chem. Soc.* **2008**, *130*, 12876.
138. Bates, J. I.; Kennepohl, P.; Gates, D. P. *Angew. Chem. Int. Ed. Engl.* **2009**, *48*, 9844.
139. Rosa, P.; Gouverd, C.; Bernardinelli, G.; Berclaz, T.; Geoffroy, M. *J. Phys. Chem. A* **2003**, *107*, 4883.
140. Back, O.; Celik, M. A.; Frenking, G.; Melaimi, M.; Donnadieu, B.; Bertrand, G. *J. Am. Chem. Soc.* **2010**, *132*, 10262.
141. Jones, C. *Coord. Chem. Rev.* **2001**, *215*, 151.
142. Andrews, P. C.; McGrady, J. E.; Nichols, P. J. *Organometallics* **2004**, *23*, 446.
143. Yoshifuji, M.; Shinohara, N.; Toyota, K. *Tetrahedron Lett.* **1996**, *37*, 7815.
144. Shah, S.; Concolino, T.; Rheingold, A. L.; Protasiewicz, J. D. *Inorg. Chem.* **2000**, *39*, 3860.
145. Moser, C.; Belaj, F.; Pietschnig, R. *Chem. Eur. J.* **2009**, *15*, 12589.
146. Tsurusaki, A.; Nagahora, N.; Sasamori, T.; Matsuda, K.; Kanemitsu, Y.; Watanabe, Y.; Hosoi, Y.; Furukawa, Y.; Tokitoh, N. *Bull. Chem. Soc. Jpn.* **2010**, *83*, 456.
147. Tsurusaki, A.; Sasamori, T.; Tokitoh, N. *Organometallics* **2009**, *28*, 3604.
148. Allen, T. L.; Scheiner, A. C.; Yamaguchi, Y.; Schaefer, H. F. *J. Am. Chem. Soc.* **1986**, *108*, 7579.
149. Allen, T. L.; Scheiner, A. C.; Schaefer, H. F. *J. Phys. Chem.* **1990**, *94*, 7780.
150. Nagase, S.; Suzuki, S.; Kurakake, T. *J. Chem. Soc. Chem. Commun.* **1990**, 1724.
151. Cowley, A. H.; Decken, A.; Norman, N. C.; Krüger, C.; Lutz, F.; Jacobsen, H.; Ziegler, T. *J. Am. Chem. Soc.* **1997**, *119*, 3389.
152. Miqueu, K.; Sotiropoulos, J. M.; Pfister-Guillouzo, G.; Ranaivonjatovo, H.; Escudie, J. *J. Mol. Struct.* **2001**, *595*, 139.
153. Matus, M. H.; Nguyen, M. T.; Dixon, D. A. *J. Phys. Chem. A* **2007**, *111*, 1726.
154. Burford, N.; Ragogna, P. J. *J. Chem. Soc. Dalton Trans.* **2002**, 4307.
155. Rivard, E.; Merrill, W. A.; Fettinger, J. C.; Wolf, R.; Spikes, G. H.; Power, P. P. *Inorg. Chem.* **2007**, *46*, 2971.
156. Lein, M.; Krapp, A.; Frenking, G. *J. Am. Chem. Soc.* **2005**, *127*, 6290.
157. Lu, T.; Simmonett, A. C.; Evangelista, F. A.; Yamaguchi, Y.; Schaefer, H. F. *J. Phys. Chem. A* **2009**, *113*, 13227.
158. Amatatsu, Y. *J. Phys. Chem. A* **2008**, *112*, 8824.
159. Amatatsu, Y. *J. Phys. Chem. A* **2009**, *113*, 9667.
160. Peng, H.-L.; Payton, J. L.; Protasiewicz, J. D.; Simpson, M. C. *J. Phys. Chem. A* **2009**, *113*, 7054.
161. Tahara, T. *Adv. Multi-Photon Process. Spectrosc.* **2004**, *16*, 1.
162. Caminade, A. M.; Verrier, M.; Ades, C.; Paillous, N.; Koenig, M. *J. Chem. Soc. Chem. Commun.* **1984**, 875.
163. Yoshifuji, M.; Sato, T.; Inamoto, N. *Chem. Lett.* **1988**, 1735.
164. Yoshifuji, M.; Sato, T.; Inamoto, N. *Bull. Chem. Soc. Jpn.* **1989**, *62*, 2394.
165. Komen, C. M. D.; de Kanter, F. J. J.; Goede, S. J.; Bickelhaupt, F. *J. Chem. Soc. Perkin Trans.* **1993**, *2*, 807.
166. Yoshifuji, M.; Abe, M.; Toyota, K.; Goto, K.; Inamoto, N. *Bull. Chem. Soc. Jpn.* **1993**, *66*, 1572.
167. Tsuji, K.; Sasaki, S.; Yoshifuji, M. *Heteroat. Chem.* **1998**, *9*, 607.
168. Shah, S.; Simpson, M. C.; Smith, R. C.; Protasiewicz, J. D. *J. Am. Chem. Soc.* **2001**, *123*, 6925.
169. Roering, A. J.; Davidson, J. J.; MacMillan, S. N.; Tanski, J. M.; Waterman, R. *Dalton Trans.* **2008**, 4488.
170. Waterman, R.; Tilley, T. D. *Angew. Chem. Int. Ed. Engl.* **2006**, *45*, 2926.
171. Piro, N. A.; Cummins, C. C. *J. Am. Chem. Soc.* **2009**, *131*, 8764.
172. Driess, M.; Block, S.; Brym, M.; Gamer, M. T. *Angew. Chem. Int. Ed. Engl.* **2006**, *45*, 2293.
173. Praesang, C.; Stoelzel, M.; Inoue, S.; Meltzer, A.; Driess, M. *Angew. Chem. Int. Ed. Engl.* **2010**, *49*, 10002.
174. Li, B.; Matsuo, T.; Hashizume, D.; Fueno, H.; Tanaka, K.; Tamao, K. *J. Am. Chem. Soc.* **2009**, *131*, 13222.
175. Niecke, E.; Gudat, D. *Angew. Chem. Int. Ed. Engl.* **1991**, *103*, 217.
176. Miqueu, K.; Sotiropoulos, J.-M.; Pfister-Guillouzo, G.; Rudzevich, V. L.; Gornitzka, H.; Lavallo, V.; Romanenko, V. D. *Eur. J. Inorg. Chem.* **2004**, 2289.
177. Kruppa, C.; Nieger, M.; Ross, B.; Vath, I. *Eur. J. Inorg. Chem.* **2000**, 165.
178. Lee, V. Y.; Kawai, M.; Sekiguchi, A.; Ranaivonjatovo, H.; Escudieé, J. *Organometallics* **2009**, *28*, 4262.
179. Sasamori, T.; Takeda, N.; Tokitoh, N. *Chem. Commun.* **2000**, 1353.
180. Sasamori, T.; Takeda, N.; Fujio, M.; Kimura, M.; Nagase, S.; Tokitoh, N. *Angew. Chem. Int. Ed. Engl.* **2002**, *41*, 139.
181. Bouslikhane, M.; Gornitzka, H.; Escudie, J.; Ranaivonjatovo, H. *J. Organomet. Chem.* **2001**, *619*, 275.
182. Masuda, J. D.; Schoeller, W. W.; Donnadieu, B.; Bertrand, G. *Angew. Chem. Int. Ed. Engl.* **2007**, *46*, 7052.
183. Wang, Y.; Xie, Y.; Wei, P.; King, R. B.; Schaefer, H. F., III; Schleyer, P.v.R.; Robinson, G. H. *J. Am. Chem. Soc.* **2008**, *130*, 14970.
184. Back, O.; Kuchenbeiser, G.; Donnadieu, B.; Bertrand, G. *Angew. Chem. Int. Ed. Engl.* **2009**, *48*, 5530.
185. Abraham, M. Y.; Wang, Y.; Xie, Y.; Wei, P.; Schaefer, H. F., III; Schleyer, P.v.R.; Robinson, G. H. *Chem. Eur. J.* **2010**, *16*, 432.
186. Weber, L. *Angew. Chem. Int. Ed. Engl.* **2010**, *49*, 5829.
187. Kinjo, R.; Donnadieu, B.; Bertrand, G. *Angew. Chem. Int. Ed. Engl.* **2010**, *49*, 5930.
188. Prabusankar, G.; Gemel, C.; Parameswaran, P.; Flener, C.; Frenking, G.; Fischer, R. A. *Angew. Chem. Int. Ed. Engl.* **2009**, *48*, 5526.
189. Jones, C. *Coord. Chem. Rev.* **2010**, *254*, 1273.
190. Green, S. P.; Jones, C.; Jin, G.; Stasch, A. *Inorg. Chem.* **2006**, *46*, 8.
191. Hitchcock, P. B.; Lappert, M. F.; Li, G.; Protchenko, A. V. *Chem. Commun.* **2009**, 428.

1.13 Stable and Persistent Radicals of Group 13-17 Elements

T Chivers, University of Calgary, Calgary, AB, Canada
J Konu, University of Jyväskylä, Jyväskylä, Finland

Abbreviations

Bbt	2,6-Bis[bis(trimethylsilyl)methyl]-4-[tris(trimethylsilyl)methyl]phenyl
DFT	Density functional theory
Dipp	2,6-Di(isopropyl)phenyl
DME	Dimethoxyethane
Dpp-BIAN	1,2-Bis[2,6-di(isopropyl)phenylimino]acenaphthene
EPR	Electron paramagnetic resonance
hfcc	Hyperfine coupling constant
HOMO	Highest occupied molecular orbital
LUMO	Lowest unoccupied molecular orbital
NBO	Natural bond order
NHC	*N*-Heterocyclic carbene
PPN	Bis(triphenylphosphane)iminium
SOMO	Singly occupied molecular orbital
Tbt	2,4,6-Tris[bis(trimethylsilyl)methyl]phenyl
TEMPO	2,2,6,6-Tetramethylpiperidine-*N*-oxyl
THF	Tetrahydrofuran
TMEDA	Tetramethylethylenediamine
Tripp	2,4,6-Tri(isopropyl)phenyl
TMEDA	Tetramethylethylenediamine
UV	Ultraviolet

Symbols

a	Hyperfine splitting
g	Electron gyromagnetic ratio (or g value)
I	Nuclear spin quantum number
J	Spin–spin coupling constant
M_s	Magnetic spin quantum number

1.13.1 Introduction

Radicals are species that embody an odd (unpaired) electron. Such species, especially simple organic radicals such as $[CH_3]^\bullet$, $[C_2H_5]^\bullet$, etc., are frequently transient. However, strategies have been developed to allow the production and, in some cases, isolation of radicals containing p-block elements that may be designated as either 'stable' or 'persistent.'[1,2] Both terms can be applied to long-lived radicals. The appellation 'stable' is used to describe radicals that can be isolated and stored under an inert atmosphere for long periods, whereas the designation 'persistent' refers to radicals that have relatively long lifetimes under the conditions that they are generated. For practical purposes, these definitions imply that the solid-state structures of stable radicals can, in principle, be determined by x-ray crystallography, while the characterization of persistent radicals is limited to the application of spectroscopic methods (most commonly electron paramagnetic resonance (EPR) spectroscopy) either in solution or, infrequently, in the gas phase. Although the chemistry of stable radicals is emphasized in this chapter, persistent radicals will be included when (1) they are known to have important applications, for example, in organic synthesis or as polymerization initiators, (2) stable congeneric radicals are known for comparison, or (3) they provide important insights into the behavior or properties of a particular type of radical for which stable analogues are unknown. In addition to neutral radicals, relevant examples of charged species, that is, anion or cation radicals, are also discussed in the context of isoelectronic relationships and in cases where they enhance our understanding of the electronic structures and bonding.

With the exception of boron-containing radicals, this chapter focuses on radicals that incorporate third-row elements (i.e., Al, Si, P, S, and Cl) and their heavier congeners. Carbon-, nitrogen-, and oxygen-centered radicals are covered comprehensively in a recent book[3] and in a review that deals with stable radicals.[4] The diverse and increasingly important area of chalcogen–nitrogen (E–N) (E = S, Se) radicals is discussed in Chapter 1.14.

The principal strategy for conferring stability on boron or heavy p-block element radicals is the use of extremely bulky substituents to provide a kinetic barrier to oligomerization processes, for example, dimerization. For cyclic systems, delocalization of the unpaired electron over the entire (or part of the) ring may also contribute to stability. For heterocyclic radicals stability may also be enhanced by the presence of highly electronegative atoms. The primary interest in stable radicals of boron and heavy p-block elements has been the insights that structural studies, in conjunction with molecular orbital calculations, provide into the bonding in these paramagnetic systems. From the viewpoint of applications, the major recent advances have been in (1) the use of specific persistent radicals in organic synthesis or as polymerization initiators and (2) the incorporation of stable radicals in the design and generation of new materials with potentially useful conducting or magnetic properties (see also Chapter 1.14).

This chapter is organized sequentially according to groups 13, 14, 15, 16, and 17 in the periodic table. For group 13, the discussion commences with a consideration of boron-containing radicals, which is followed by an examination of radicals formed by the heavier group 13 elements. A similar approach is taken in the sections covering groups 14, 15, and 16 for which the discussion begins with silicon, phosphorus, and sulfur-containing radicals, respectively. Neutral radicals are presented before charged species, that is, anion or cation radicals. In the case of ring systems, paramagnetic homocycles are described prior to heterocycles. For the major types of radicals, the methods of synthesis are given along with information on their molecular and electronic structures, as revealed by x-ray structural determinations, molecular orbital calculations, and spectroscopic techniques. Where appropriate, attention is drawn to known applications or potential uses of main-group element radicals. The rapidly developing field of biradicaloids that incorporate main-group elements is covered in Chapter 1.15.

1.13.2 Group 13 Element Radicals

1.13.2.1 Boron

1.13.2.1.1 Neutral radicals

Stable boron-containing radicals have attracted interest recently for potential applications as chemical sensors or as components of extended magnetic systems.[5] Compounds with unpaired spin density on boron are also being investigated for their efficacy as polymerization initiators and as reagents in organic synthesis.

The most common examples of neutral boron-containing radicals are (1) complexes in which the $[BCl_2]^\bullet$ radical is stabilized by an *N*,*N*′-chelating ligand[6,7] and (2) adducts of the $[BH_2]^\bullet$ radical with an *N*-heterocyclic carbene (NHC)[8–10] or *N*-heteroarene.[11] Early reports provided the EPR characterization of the 2,2′-bipyridyl (bipy) complexes $[BR_2(bipy)]^\bullet$ (**1a**, R = Ph,[12] **1b**, R = NMe_2[13]) in solution (Scheme 1). More recently, black crystals of the chlorinated derivative $[BCl_2(bipy)]^\bullet$ (**1c**, R = Cl) were isolated; the radical **1c** adopts a nonbonding π-stacked structure in the solid state.[7] The related radical $[\{2\text{-}Pr^i\text{-}C_6H_4NC(Ph)\}_2BCl_2]^\bullet$ (**2**) (Scheme 1), which co-crystallizes with the diamagnetic complex $[\{2\text{-}Pr^i\text{-}C_6H_4NC(Ph)\}_2BCl]$, has been identified by EPR spectroscopy.[6] The stabilization of a neutral radical with spin density on boron by coordination to 2,2′-bipyridyl ligands is also exemplified by the 9-bora-9,10-dihydroanthracene complexes **3a** (R = Bu^t) and **3b** (R = Me) (Scheme 1), which have been characterized by EPR spectroscopy in combination with density functional theory (DFT) calculations.[14]

The strong σ-donor properties of NHCs enable these ligands to stabilize a number of otherwise highly reactive species, including diatomic main-group species and cations of electronegative elements (see Chapter 1.16).[15] This property is also evident in borane radicals of the type $[(NHC)BR_2]^\bullet$ (**4a**, R = Mes[8]; **4b**, R = H[9,10]) (Scheme 2), which may be prepared by the reduction of the corresponding cation (**4a**)[8] or by hydrogen abstraction from $(NHC)BH_3$ by *tert*-butoxy radicals (**4b**).[9,10] *N*-Heteroaryl borane radicals (e.g., $[4\text{-}(Me_2N\text{-}Py)BH_2]^\bullet$, **5**; Py = pyridyl) are readily generated as a result of the low B–H bond dissociation energies in the corresponding

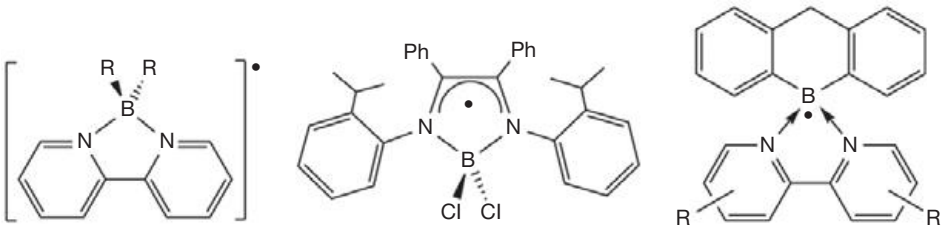

1a (R = Ph)
1b (R = NMe_2)
1c (R = Cl)

2

3a (R = Bu^t)
3b (R = Me)

Scheme 1 Cyclic boron-containing radicals.

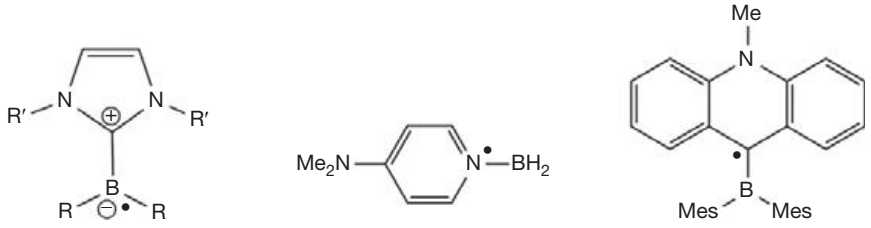

4a (R = Mes; R′ = Me)
4b (R = H; R′ = 2,6-Pr^i_2-C_6H_3)

5

6

Scheme 2 Examples of borane radicals.

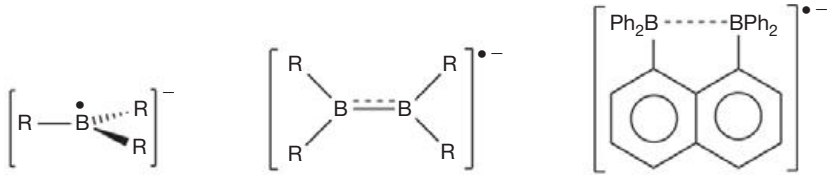

7

8

9

Scheme 3 Acyclic boron-containing radical anions.

borane adducts.[11] The boron-centered radicals **4b** rapidly abstract halogen atoms from alkyl halides.[9,10] Applications of boryl radicals of type **5** (Scheme 2) as polymerization initiators and in organic synthesis are anticipated.[11] The mesityl derivative **4a** is related to the 9-borylated acridinyl radical **6** (Scheme 2),[16] except that the one-electron B–C π-bond is polarized toward the boron atom in **4a** reflecting the poor π-accepting properties of the NHC ligand, whereas in **6** the unpaired electron is delocalized on the acridinyl moiety.

The radical anion chemistry of polyborane clusters $[B_nX_n]^{\bullet -}$ ($n = 6$, 9, 12) has been investigated extensively[5] (*vide infra*). These paramagnetic species are usually generated by one-electron oxidation of the corresponding closo dianions. By analogy, neutral radicals are expected to be formed upon oxidation of carborane monoanions in which a carbon atom replaces one of the boron atoms, for example, $[CB_{11}Me_{12}]^-$. Indeed, black crystals of the corresponding radical $[CB_{11}Me_{12}]^{\bullet}$ (deep blue in solution) have been isolated and structurally characterized.[17a] The stability of this radical is attributed to delocalization of the unpaired electron within the icosahedral cage combined with the steric protection provided by the sheath of methyl groups. The strong oxidizing power of the neutral radical $[CB_{11}Me_{12}]^{\bullet}$ is indicated by its ability to convert Ph_3N or perylene to the corresponding radical cations[17a] and by the oxidation of Me_6M_2 (M = Ge, Sn) and Me_4Pb in alkane solvents to give the salts $[Me_3M]^+[CB_{11}Me_{12}]^-$.[17b,c] The neutral radical $[CB_{11}Me_{12}]^{\bullet}$ is also involved as a methyl transfer agent in the polymerization of iso-butylene initiated by air or Bu^tOOBu^t in the presence of $Li[CB_{11}Me_{12}]$.[18]

1.13.2.1.2 Radical anions

The early work on boron-centered radicals was stimulated by the isoelectronic relationship of boron triaryl radical anions $[BR_3]^{\bullet -}$ (**7**) (Scheme 3) and the neutral carbon-centered radicals $[CR_3]^{\bullet}$ (R = aryl).[19] EPR studies of $[BPh_3]^{\bullet -}$ and its deuterated derivatives, as well as derivatives of the type

$[B(4\text{-}XC_6H_4)_3]^{\bullet-}$ (X = Cl, OMe), have revealed that the unpaired electron in **7** is located primarily at boron ($a(^{11}B) = 7.84$ G).[20] The relatively low value of the hyperfine coupling constant (hfcc) indicates that the unpaired electron density is mainly associated with the 2p orbital and that the geometry of the $[BR_3]^{\bullet-}$ radical anions is planar rather than pyramidal. This conclusion was subsequently corroborated by the crystal structure of the thermally stable, ion-separated salt, $[Li(12\text{-crown-}4)_2][BMes_3]$, which decomposes only at ~240 °C.[21] The trigonal planar boron center shows only small deviations from 120° in the C–B–C angles; the B–C bond lengths are elongated by ~0.02 Å from those observed in neutral $BMes_3$. The deep blue perfluorinated radical anion $[B(C_6F_5)_3]^{\bullet-}$, obtained by reduction of $[B(C_6F_5)_3]$ with Cp^*_2Co, has a half life of ~10 min at room temperature.[22,23] The reduction potential of $[B(C_6F_5)_3]$ is estimated to be −1.17 V versus $Cp_2Fe^{0/+}$ compared with −2.73 V for $BMes_3$.

Another example of early seminal studies on boron-centered radicals is the one-electron reduction of diboron compounds, R_2BBR_2 (R = alkyl, aryl). The resulting diborane radical anion, $[R_2BBR_2]^{\bullet-}$ (**8**) (Scheme 3), was first structurally characterized as the contact ion pair, $[Li(OEt_2)_2][MeO(Mes)BB(Mes)OMe]$, in which the Li^+ cation is bound to the anion by coordination to the methoxy oxygens.[24] The broadness of the EPR signal of this paramagnetic species precluded the determination of hfcc values. However, the solvent-separated ion-pair, $[K(18\text{-crown-}8)(THF)_2][Mes_2BB(Ph)Mes]$, which was obtained by one-electron reduction with potassium in tetrahydrofuran (THF) followed by the addition of 18-crown-6, exhibits a seven-line EPR pattern ($g = 2.0063$) with $a(^{11}B) = 13$ G due to the coupling to two boron centers (^{11}B, $I = 3/2$, 80.2%) consistent with the formation of a π-radical.[25] A π-bond order of 0.5 was indicated by comparison of the structural parameters of this radical with those of the neutral precursor, $Mes_2BB(Ph)Mes$.

The reduction of 1,8-bis(diphenylboryl)naphthalene with potassium in the presence of 18-crown-6 produces the dark purple radical anion $[1,8\text{-}(BPh_2)_2C_{10}H_6]^{\bullet-}$ (**9**) (Scheme 3), which exhibits a seven-line EPR spectrum indicating hyperfine coupling with two equivalent ^{11}B ($I = 3/2$) centers.[26] According to DFT calculations the singly occupied molecular orbital (SOMO) of **9** represents a one-electron σ-bond.

A wide variety of radical anions based on polyhedral boron frameworks $[B_nX_n]^{\bullet-}$ have been characterized, especially for $n = 6$, 9, 12.[5] The stability of octahedral hypercloso cluster anions of the type $[B_6X_6]^{\bullet-}$ is enhanced when X is an electronegative substituent, for example, X = Cl, Br, I[5]; the iodo derivative exhibits the highest stability.[27] The tricapped trigonal prismatic arrangement of cluster atoms in the dianion $[B_9Br_9]^{2-}$ is essentially maintained upon loss of an electron to form the radical anion $[B_9Br_9]^{\bullet-}$.[28–30] The icosahedral anions $[B_{12}X_{12}]^{\bullet-}$ (X = Me, OR, OH, Cl) are the most stable examples of this class of paramagnetic boron species. The permethylated derivative $[B_{12}Me_{12}]^{\bullet-}$ and the perbenzoylated analogue $[B_{12}(OBz)_{12}]^{\bullet-}$ (Bz = benzyl) are remarkably air-stable, blue or purple solids that are obtained as PPN^+ salts [PPN = N(PPh$_3$)$_2$] by one-electron oxidation of the corresponding dianions with ceric or ferric ions, respectively.[31–33] The stability of these radical anions is attributed to a combination of steric protection provided by the 12 methyl or benzoyl substituents together with electron donation to the cluster (inductive effect of the Me groups and π-donation from OBz groups, respectively).[31–33] A different approach involving the oxidative perhydroxylation of $[B_{12}H_{12}]^{2-}$ with 30% hydrogen peroxide was necessary for the synthesis of $[B_{12}(OH)_{12}]^{\bullet-}$ as the yellowish green Cs^+ salt, which can be recrystallized from water.[34] The potential for functionalizing the peripheral OH groups in this paramagnetic boron species for applications in materials science or medicine (boron neutron-capture therapy) is intriguing. The oxidation of the perchlorinated dianion $[B_{12}Cl_{12}]^{2-}$ to the dark blue radical anion $[B_{12}Cl_{12}]^{\bullet-}$ requires the strong oxidizing agent AsF_5 and the use of SO_2 as a solvent.[35] The radical anion $[B_{12}Cl_{12}]^{\bullet-}$ is itself a strong oxidizer and converts elemental sulfur to $S_8[B_{12}Cl_{12}]$, which contains the $[S_8]^{2+}$ cation.

Dicarbadecaboranes of the type 1,2-R_2-1,2-$C_2B_{10}H_{10}$ are isoelectronic with the icosahedral dodecaborane dianions $[B_{12}X_{12}]^{2-}$. The radical anion of the diphenyl derivative [1,2-Ph_2-1,2-$C_2B_{10}H_{10}]^{\bullet-}$ has been generated by electrochemical reduction and characterized in solution by a variety of spectroscopic methods.[36] DFT calculations for this $2n+3$ cluster-electron species predict a substantial lengthening of the C–C bond in the radical anion. A related radical anion with $2n+3$ cluster electrons in a 13-vertex framework [1,2-$(CH_2)_3$-1,2-$C_2B_{11}H_{11}]^{\bullet-}$ is obtained by reduction of the neutral precursor with sodium metal in THF and isolated as the $[Na(18\text{-crown-}6)(THF)_2]^+$ salt.[37] The corresponding 12-vertex radical anion with a $-CH_2CH_2CH_2-$ linker between the two cage carbon atoms cannot be prepared in this manner.[37]

The reduction chemistry of boroles is of interest in connection with the possible use of boron-containing π-conjugated molecules in optoelectronic materials. Although the 5π-electron radical anion of the parent borole has not been reported, the kinetically stabilized dibenzoborole has been reduced to the corresponding dark red, anion radical (**10**) (Scheme 4) by potassium in THF.[38] The paramagnetic species **10** was characterized by EPR spectroscopy; the spin density on boron was estimated to be 0.21. The persistent, dark purple radical anion **11** (Scheme 4) formed upon reduction of 1-ferrocenyl-2,3,4,5-tetraphenylborole has also been characterized in solution by the EPR spectrum which, in conjunction with spin density calculations, indicates delocalization within the C_4B ring.[39]

B–N analogues of polycyclic hydrocarbons are also interesting electron-acceptor molecules for materials applications. In this context, the dibenzo[*g*,*p*]chrysene analogue can be chemically reduced by $CoCp_2^*$ to the corresponding green anion radical (**12**) (Scheme 4), which has been characterized by x-ray crystallography.[40]

Boron-containing verdazyl radicals **13** (R = p-Tol, R′ = Ph; R = Ph, R′ = p-Tol) (Scheme 4) have been generated by reduction of the neutral borataverdazyl precursors with $CoCp_2$ and identified in the solid state by EPR and diffuse reflectance spectra.[41]

1.13.2.2 Aluminum, Gallium, and Indium

1.13.2.2.1 Neutral radicals: acyclic and homocyclic systems

Investigations of both acyclic and cyclic radicals involving M–M bonds (M = Al or Ga) with bulky substituents on the group 13 metal center have provided insights into the influence of the

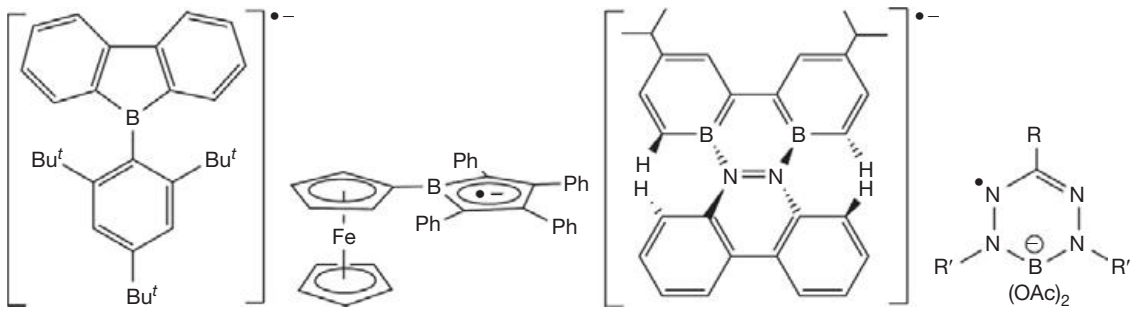

10 11 12 13

Scheme 4 Cyclic boron-containing radical anions.

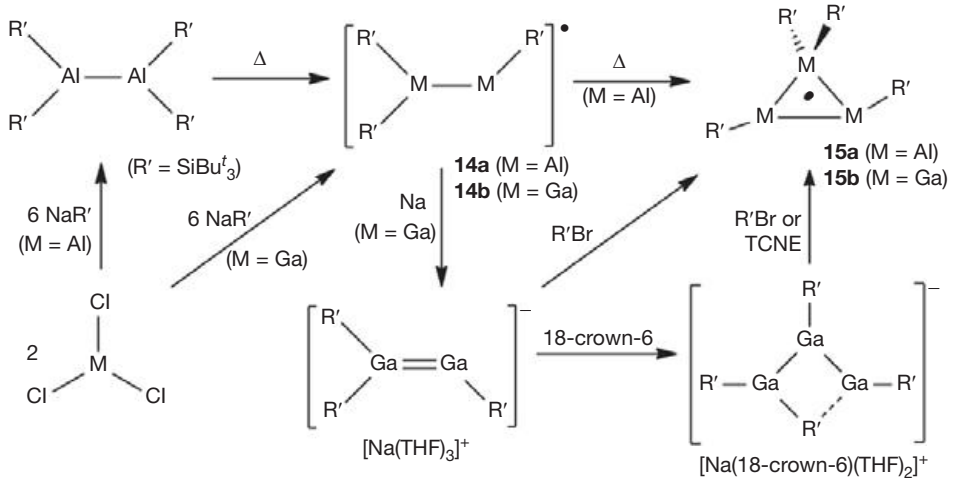

Scheme 5 Synthesis of cyclic and acyclic group 13 radicals.

metal center on relative stabilities as a result of differences in covalent radii and/or M–M bond strengths.

Thermolysis of the dimer $R'_2AlAlR'_2$ in heptane leads, via Al–Si bond cleavage, to a persistent acyclic radical, $[R'_2AlAlR']^\bullet$ (**14a**), that exists as an intermediate in the formation of the stable three-membered ring $[Al_3R'_4]^\bullet$ ($R' = SiBu^t_3$) (**15a**) (Scheme 5).[42] The isolation of black–green crystals of this homocyclic neutral radical is a cogent illustration of the ability of bulky substituents to stabilize cyclic radicals of main-group elements.

The planar, three-membered ring in **15a** forms an isosceles triangle in which two of the aluminum atoms are three-coordinate and one is four-coordinate. The Al–Al bond between the two three-coordinate metal atoms is somewhat shorter than those involving the four-coordinate Al center (2.703 vs. 2.756 Å, cf. 2.751 Å for the Al–Al single bond in $R'_2AlAlR'_2$). The poorly resolved EPR spectrum of **15a** in C_6D_{12} precludes a definitive identification of the radical present in solution. The observed hfcc values of ~3 G and two inequivalent couplings close to 13 G ($g = 2.0053$) may indicate cleavage of one of the elongated Al–Al bonds in solution leading to the acyclic radical $[R'_2Al–AlR'–AlR']^\bullet$, as suggested by DFT calculations.[42] Alternatively, the slight inequivalence of the two larger hfcc values may result from the disparity in the geometry about the two three-coordinate aluminum atoms in the solid-state structure: one of the R′Al units in **15a** is planar while the second adopts a pyramidal arrangement.

The acyclic intermediate **14a** was identified only by its EPR spectrum in solution ($a(^{27}Al) = 21.8$ and 18.9 G).[42] In contrast, the heavier gallium congener, $[R'_2GaGaR']^\bullet$ ($R' = SiBu^t_3$) (**14b**), has been isolated as blue–black crystals from the reaction between NaR′ and $GaCl_3$ in 3:1 molar ratio (Scheme 5).[43] The structure of **14b** exhibits a trigonal planar $Si_2Ga^{II}Ga^{I}$ unit and a slightly bent $Ga^{II}Ga^{I}Si$ chain (Σ ∠Ga^{II} 359.6° and ∠Ga^{II}–Ga^{I}–Si 170.3°) (the superscripts I and II refer to the formal oxidation states of the gallium centers). The gallium–gallium σ bond is formed by overlap of the sp^2- and sp-hybridized Ga atoms. The odd electron occupies a bonding π molecular orbital formed by overlap of the p_z orbitals on the two gallium atoms, resulting in a formal bond order of 1.5 for the Ga–Ga bond. The EPR spectrum of **14b** shows a 64-line signal ($g = 1.9947$) arising from coupling of the unpaired electron with the two inequivalent gallium centers (^{69}Ga, $I = 3/2$, 60.1%; ^{71}Ga, $I = 3/2$, 30.9%).[43] The two different hfcc values ($a_1(^{69/71}Ga) = 50/64$ G and $a_2(^{69/71}Ga) = 32/41$ G) could not be assigned to the two- and three-coordinate Ga atoms with certainty.

The three-membered ring $[Ga_3R'_4]^\bullet$ ($R' = SiBu^t_3$) (**15b**), the gallium analogue of **15a**, is synthesized either by oxidation of the acyclic anion $[R'_2Ga–GaR'–GaR']^-$ or by the reaction of

$[R'_2GaGaR']^-$ with R′Br (Scheme 5).[44] In contrast to the aluminum derivative **15a**, the neutral radical **15b** exhibits a Ga–Ga bond length between the two three-coordinate galliums that is ~0.35 Å longer than those involving the four-coordinate R'_2Ga unit (2.879(1) vs. 2.527(1)Å), implying the onset of Ga–Ga bond cleavage. In solution, the three-membered ring **15b** decomposes to give the EPR signal of the acyclic radical $[R'_2GaGaR']^\bullet$ (**14b**) either after prolonged standing or upon warming; the initial EPR signal arising from **15b** is not sufficiently resolved to be unambiguously analyzed.[44]

The dark crimson neutral radical $[Al(AlR_3)_2]^\bullet$ (R = N(SiMe$_2$Ph)$_2$) (**16**) is isolated in 15% yield from the reaction of a metastable solution of AlCl in toluene/diethyl ether with an equimolar amount of LiR at −78 °C.[45] The structure of the D_{3d}-symmetric Al_7 cluster is comprised of an Al atom linked symmetrically to two Al_3 rings (Figure 1). The Al–Al bonds within the three-membered rings are significantly shorter than those involving the central Al atom (2.61 vs. 2.73 Å). On the basis of detailed bonding analysis of **16** and the corresponding monoanion $[Al(AlR_3)_2]^-$ (R = N(SiMe$_3$)$_2$) (**17**), this fascinating cluster radical is referred to as a 'metalloid' system.[45]

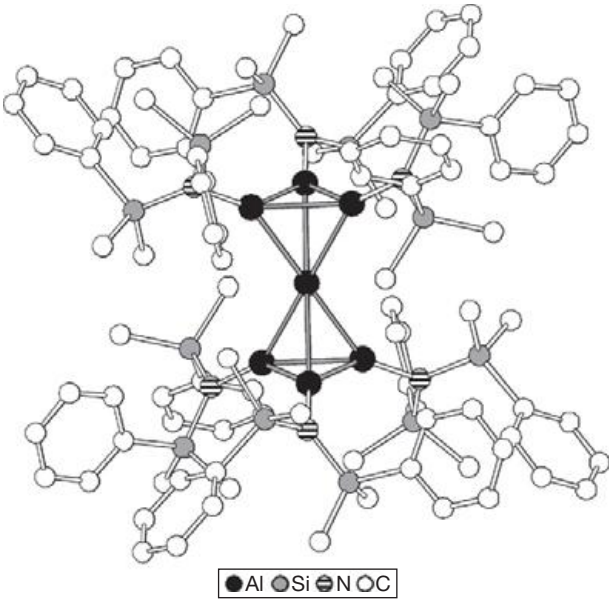

Figure 1 Crystal structure of $[Al(Al_3R_3)_2]$ (**16**, R = N(SiMe$_2$Ph)$_2$). Adapted from Yang, P.; Köppe, R.; Duan, T.; Hartig, J.; Hadiprono, G.; Pilawa, B.; Keilhauer, I.; Schnöckel, H. G. *Angew. Chem. Int. Ed.* **2007**, *46*, 3579–3583.

1.13.2.2.2 Neutral radicals: heterocyclic systems

Two classes of heterocyclic radicals involving group 13 elements have been thoroughly investigated. The first involves a series of neutral bis-boraamidinate (*bam*) radicals, $\{M[PhB(\mu\text{-}NBu^t)_2]_2\}^\bullet$ (M = B, Al, Ga, In) (**18a–d**) (Scheme 6), which are obtained by one-electron oxidation of the corresponding monoanions. The aluminum (**18b**) and gallium (**18c**) derivatives form thermally stable dark red and green crystals, respectively, which exhibit a spirocyclic arrangement of the two *bam* ligands.[46,47] The comparable *N*,*N*′-chelated bis-diazabutadiene system, $\{M[(CH)_2(\mu\text{-}NBu^t)_2]_2\}^\bullet$ (M = B, Al, Ga, In) (**19a–d**) (Scheme 6), has been studied both experimentally (**19b–c**)[48–51] and computationally (**19a–d**).[52] Although the compounds **18** and **19** are not group 13-centered radicals, these stable, spirocyclic paramagnetic compounds serve as examples of the characterization of main-group radicals containing multiple quadrupolar nuclei by EPR spectroscopy, supported by electronic structures obtained from DFT calculations.

DFT calculations of the model radicals $\{M[PhB(\mu\text{-}NMe)_2]_2\}^\bullet$ (M = B, Al, Ga, In) predict D_{2d}-symmetric geometries consistent with the observed solid-state structures of **18b** and **18c**.[46,47] The single-point calculations on the optimized geometries show that the SOMOs consist solely of nitrogen p-orbitals (Figure 2 for M = Al); they are equally delocalized over all four nitrogens as revealed by the spin densities derived from Mulliken population analysis. The EPR spectra of **18a–d** show that the central group 13 metal atom and the NBN borons have nonzero spin density values arising from polarization effects. The experimental spectra of these spirocyclic neutral radicals can therefore be simulated by assuming hyperfine interaction of the unpaired electron with four equivalent nitrogen centers, two boron atoms and the central group 13 element (^{27}Al, $I = 5/2$, 100%; ^{69}Ga, $I = 3/2$, 60.1%; ^{71}Ga, $I = 3/2$, 39.9%; ^{113}In, $I = 9/2$, 4.3%; ^{115}In, $I = 9/2$, 95.7%) (Figure 2(c) and 2(d) for M = Al). Thus, the DFT calculations and spectral simulations confirm the retention of the spirocyclic structures in solution and indicate uniform spin delocalization throughout both ligands in **18a–d**.[46,47]

The *N*,*N*′-chelated bis-diazabutadiene aluminum and gallium radicals **19b** and **19c** are prepared by co-condensation of the metal vapor with an excess of 1,4-di-*tert*-butyl-1,4-diazabutadiene.[48–51] In contrast to the bis-*bam* systems **18**, both the solid-state structures and the EPR spectra of **19b** and **19c** indicate that the unpaired electron is located on only one of the ligands with spin density contributions from two nitrogens and two hydrogen atoms in addition to a significantly smaller contribution from the group 13 center.[51] In agreement with the experimental results, distorted tetrahedral C_s (M = B)

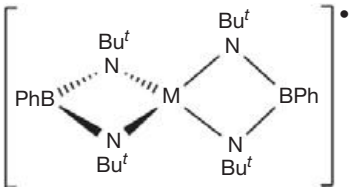

M = B (**18a**), Al (**18b**), Ga (**18c**), In (**18d**)

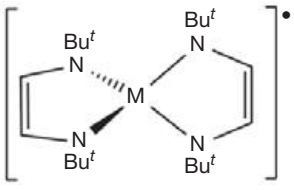

M = B (**19a**), Al (**19b**), Ga (**19c**), In (**19d**)

Scheme 6 Spirocyclic group 13 radicals.

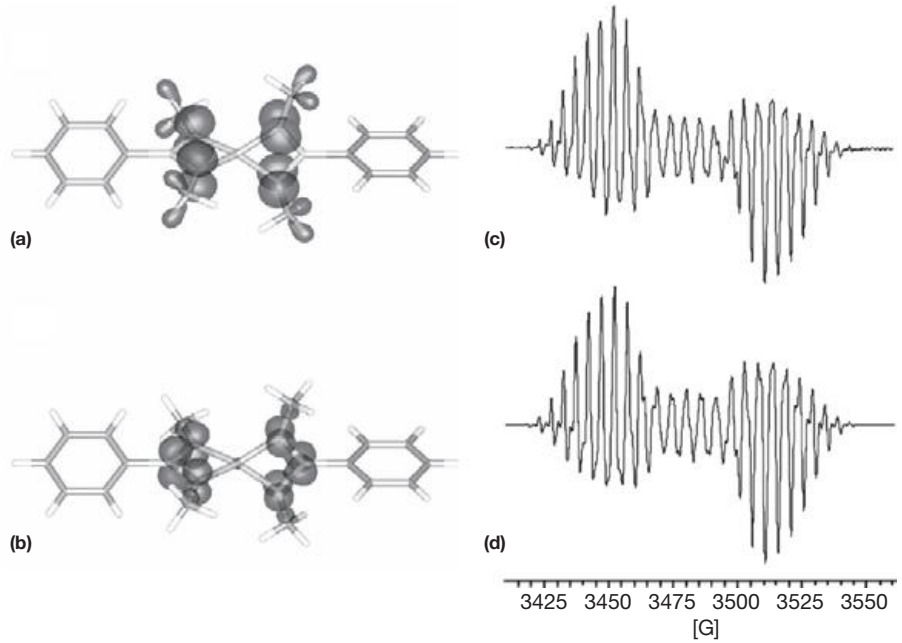

Figure 2 (a) SOMO of $\{Al[PhB(\mu\text{-}NMe)_2]_2\}^{\bullet}$ drawn at isosurface level ±0.05, (b) spin density map of $\{Al[PhB(\mu\text{-}NMe)_2]_2\}^{\bullet}$ drawn at isosurface level 0.02 (α-spin density) and –0.002 (β-spin density), (c) experimental, and (d) simulated X-band EPR spectra of a diethyl ether solution of $\{Al[PhB(\mu\text{-}NBu^t)_2]_2\}^{\bullet}$ (**18b**) at 298 K. Adapted from Chivers, T.; Eisler, D. J.; Fedorchuk, C.; Schatte, G.; Tuononen, H. M.; Boeré, R. T. *Chem. Commun.* **2005**, 3930–3931.

and C_{2v} (M = Al, Ga) symmetries with the unpaired electron localized on one ligand were also predicted by computational methods.[52] Interestingly, however, the computations indicate that the experimentally inaccessible indium radical **19d** optimizes to a pyramidal geometry (C_2 symmetry) in which the spin density is equally delocalized over both ligands similarly to the bis-*bam* compounds **18**.

Stable radicals, comprised of a four-coordinate aluminum atom in a tetraphenylporphyrin or phthalocyanin ring system, have been characterized in solution by EPR spectra and magnetic susceptibility measurements and the solid-state structures have been determined by x-ray crystallography.[53] DFT calculations indicate that the unpaired electron is delocalized throughout the ring systems.

Deep red, paramagnetic compounds containing four-coordinate aluminum **20a** (M = Al; R = Me, Et, Bu^t) (Scheme 7) are obtained by the reactions of dialkylaluminum halides R_2AlX (X = Cl, Br) with (dpp-BIAN)Na (dpp-BIAN = 1,2-bis[2,6-(diisopropylphenyl)imino]acenaphthene) in Et_2O.[54] A gallium analogue **20b** (M = Ga, R = I) is produced upon addition of (dpp-BIAN)Na to 'GaI.'[55] The stable neutral radicals **20a** and **20b** have been characterized in the solid state by x-ray crystallography. The EPR spectra indicate that the unpaired electron is primarily delocalized over the dpp-BIAN ligand, but the spin density on Al in **20a** is more than twice of that found for the related complex $[C_2H_2(NDipp)_2]AlI_2$.[56]

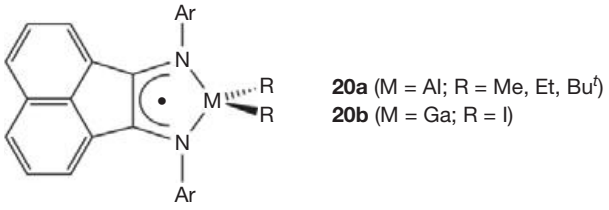

Scheme 7 Bis(imino)acenaphthene group 13 radicals.

1.13.2.2.3 Radical anions

The stabilizing effect of the sterically bulky $Bu^t_2(Me)Si$ group was also utilized in the production of trigonal planar radical anions $[MR_3]^{\bullet-}$ (M = Al (**21a**), Ga (**21b**); R = $Si(Me)Bu^t_2$) (Figure 3(a)). These odd-electron compounds are prepared by direct metallation of the neutral precursors with alkali metals (Li, Na, K), and deep red crystals of the ion-separated potassium salts were isolated by recrystallization in the presence of [2.2.2]cryptand.[57] The Si–M bond lengths (M = Al, Ga) in the nearly planar radical anions **21a**, **b** are somewhat shorter than those in the neutral congeners, suggesting that the unpaired electron predominantly occupies the $3p_z$ and $4p_z$ orbital of the central aluminum and gallium, respectively. By contrast, the prototypical pyramidal radical anions $[AlH_3]^{\bullet-}$ and $[GaH_3]^{\bullet-}$ have significant electron population in the corresponding s orbitals.[58–60] Localization of the spin density on the heavier group 13 center is also supported by the EPR spectra, which exhibit a well-resolved sextet ($a(^{27}Al)$ = 62 G, g = 2.0050) and two sets of quartets ($a(^{69}Ga)$ = 123 G, $a(^{71}Ga)$ = 157 G, g = 2.0150) for **21a** and **21b**, respectively. The relatively small hfcc values, as well as the observed crystal structures, are consistent with group 13 centered π-radicals (cf. values of 154, 420 and 534 G for $a(^{27}Al)$, $a(^{69}Ga)$ and $a(^{71}Ga)$ in $[AlH_3]^{\bullet-}$ and $[GaH_3]^{\bullet-}$, respectively).

The gallium-containing radical anion cluster, $[Ga_9R_9]^{\bullet-}$ (R = Bu^t) (**22**) (Figure 3(b)), is produced via one-electron reduction of the corresponding neutral compound with

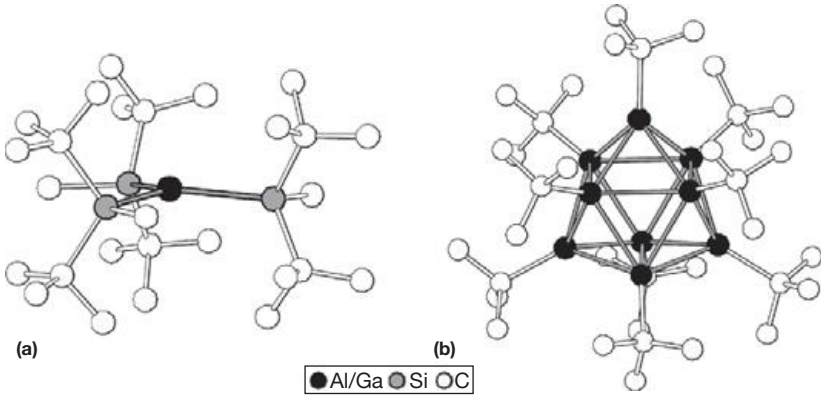

Figure 3 Crystal structures of (a) $[Al(SiMeBu^t_2)_3]^{\bullet-}$ (**21a**) and (b) $[Ga_9(Bu^t)_9]^{\bullet-}$ (**22**) radical anions. Adapted from Nakamoto, M.; Yamasaki, T.; Sekiguchi, A. *J. Am. Chem. Soc.* **2005**, *127*, 6954–6955; Uhl, W.; Cuypers, L.; Kaim, W.; Schwedersk, B.; Koch, R. *Angew. Chem. Int. Ed.* **2003**, *42*, 2422–2423.

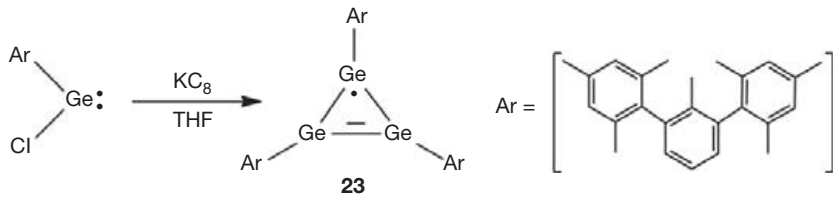

Scheme 8 Synthesis of cyclotrigermenyl radical.

Cp^*_2Co.[61] The crystal structure reveals a molecular core comprised of nine Ga atoms arranged as a tricapped trigonal prism, analogous to the boron subhalide radical anions $[B_9X_9]^{\bullet-}$ (X = Cl, Br).[29,30,62] The Ga–Ga bonds parallel to the threefold rotational axis in **22** are significantly shorter in length (by ~17 pm) than those in the neutral precursor resulting in a more regular prism. The single electron is essentially localized in the p orbitals of the Ga atoms (0.993 e^-) with the capping galliums bearing most of the negative charge (80%). Due to the numerous overlapping lines, only a poorly resolved EPR spectrum was obtained ($a(^{69/71}Ga) < 30$ G).

1.13.3 Group 14 Element Radicals

The most significant recent developments in the chemistry of stable radicals of the p-block elements have involved group 14-centered species; several recent reviews have discussed these advances in detail.[63–65] In this section, the foremost aspects of this seminal work are presented in the context of cognate organic (carbon-centered) radicals and isoelectronic group 13- and group 15-centered radicals.

1.13.3.1 Cyclic Group 14 Radicals

1.13.3.1.1 Neutral radicals

The first homocyclic, neutral group 14 radical was reported in 1997.[66] This highly protected cyclotrigermenyl, $[(2,6\text{-}Mes_2C_6H_3)Ge]_3^{\bullet}$ (**23**), is obtained as dark blue crystals by the reduction of $(2,6\text{-}Mes_2C_6H_3)GeCl$ with KC_8 in THF (Scheme 8). The disordered triangular Ge_3 core in the crystal structure of **23** is consistent with a cyclogermenyl radical (a germanium analogue of the cyclopropenyl radical) in which one of the Ge–Ge linkages shows double-bond character. The EPR spectrum of **23** displays a single resonance at $g = 2.0069$ with an hfc constant of $a(^{73}Ge) = 16$ G to one germanium nucleus (^{73}Ge, $I = 9/2$, 7.8%). The relatively low hyperfine coupling is consistent with a π radical in which the odd electron is localized on one of the planar sp^2-hybrized germanium centers.

A comparable, saturated Ge_3 triangle in the bicyclic, neutral radical **24** (Scheme 9) is obtained by one-electron oxidation of the parent anion.[67] The Ge=Ge double bond observed in **23** has been formally replaced by the bridging–H_2C–C(Me)=C(Me)–CH_2– unit in **24**. Similarly to **23**, the Ge_3 core in **24** is planar with an sp^2-hybridized germanium atom at the radical center. The EPR spectrum of **24** shows two independent sets of multiplets ($g = 2.0210$ and 2.0223) with $a_1(^{73}Ge) = 34$ G and $a_2(^{73}Ge) = 26$ G due to *endo,exo* isomerism; the small hfc constants indicate a π radical with the unpaired electron localized on the planar germanium center in solution.

An unusual example of a stable silyl radical, the red–purple cyclotetrasilenyl $[\{Bu^t_2(Me)Si\}_3\{Si(Bu^t)_2\}]^{\bullet}$ (**25**) (Scheme 9), is produced by one-electron reduction of the corresponding cation.[68] This all-silicon congener of the cyclobutenyl radical exhibits a nearly planar Si_4 ring with two Si–Si bond lengths that are intermediate between single and double bonds, while the other two Si–Si bonds are close to single bond values, thus suggesting an allylic structure. Consistently, the EPR spectrum ($g = 2.0058$) indicates additional spin density located on the terminal Si atoms of the pseudo-allyl unit with $a_1(^{29}Si) = 40.7$ G and $a_2(^{29}Si) = 37.4$ G, while the hfcc value of the central silicon is expectedly somewhat smaller ($a_3(^{29}Si) = 15.5$ G; ^{29}Si, $I = 1/2$, 4.7%).

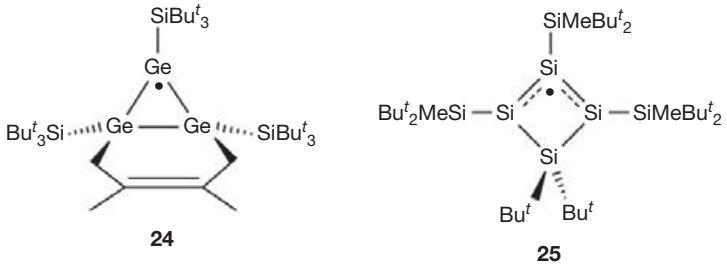

24 25

Scheme 9 Cyclic silicon and germanium-containing radicals.

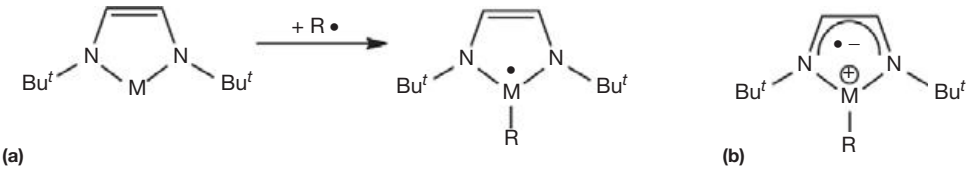

Scheme 10 (a) Reaction of *N*-heterocyclic silylenes or germylenes with radical sources (M = Si, Ge; R = TEMPO, CH_2Ph. CMe_3, $SiMe_3$, OAr, $Cr(CO)_4$, $Re(CO)_5$); (b) zwitterionic structure for the radicals produced.

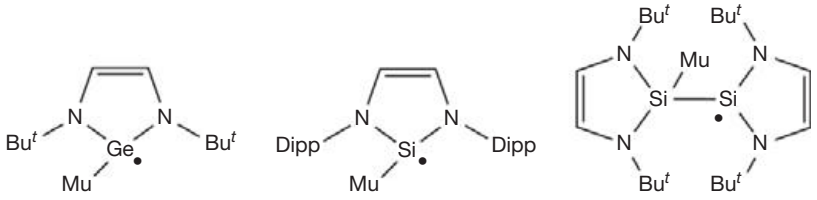

26a 26b 27

Scheme 11 Silicon and germanium radicals obtained from muonium reactions.

A number of persistent cyclic silicon- and germanium-centered radicals have been produced by the reactions of stable silylenes or germylenes with either free radicals[69,70] or muonium and characterized by EPR spectroscopy and quantum mechanical calculations.[71,72] The radical reactions involve adduct formation between *N*-heterocyclic silylenes or -germylenes and a variety of radical sources, for example, 2,2,6,6-tetramethylpiperidine-*N*-oxyl (TEMPO), benzyl, *tert*-butyl, and metal–metal-bonded radical precursors such as $(CO)_4Co–Co(CO)_4$, $(CO)_5Re–Re(CO)_5$, and $(CO)_3CpM–MCp(CO)_3$ (M = W, Mo) (see Scheme 10(a)).[69,70] The silicon-centered radicals persist at 298 K for several days and are stabilized by cyclic delocalization.[69] Surprisingly, delocalization is more extensive for Ge, indicating a strong contribution from the zwitterionic structure with a positive charge on the group 14 center (Scheme 10(b)).[70]

The outcome of the reaction of stable *N*-heterocyclic germylenes with muonium differs from that with the corresponding silylenes. The former produces the muoniated germanium-centered radical **26a**, whereas the latter gives rise to the disilanyl radical **27** via reaction of the initially formed radical with the silylene (Scheme 11).[71] However, the muoniated silicon-centered radical can be stabilized by the presence of bulky N-aryl substituents close to the silicon center as in **26b**.[72]

The neutral, monomeric germanium(I) radical [($^{t\text{Bu}}$Nacnac)Ge:]• (**28**) is obtained as a purple–red solid by reduction of the corresponding monochloride with $Na[C_{10}H_8]$.[73a] The molecular structure of **28** reveals a planar, delocalized heterocyclic core in which the Ge center is protected by two bulky Dipp groups (Figure 4). The EPR spectrum consists of a strong central signal superimposed on a decet of lines resulting from hyperfine coupling to ^{73}Ge ($I = 9/2$, 7.8%). The EPR data combined with DFT calculations indicate that **28** is a π radical in which the electron resides predominantly in the germanium $4p_\pi$ orbital.[73a] This class of radical is a likely intermediate in the formation of heavy alkyne analogues of the type RMMR (M = Ge, Sn).[73b]

1.13.3.1.2 Radical anions

The cyclic tri- and tetrasilane radical anions, $[Si\{1,2\text{-}(\mu\text{-}NCH_2Bu^t)_2C_6H_4\}]_3^{\bullet-}$ (**29**)[74a] and $[Si\{1,2\text{-}(\mu\text{-}NEt)_2C_6H_4\}]_4^{\bullet-}$ (**30**)[74b] (Scheme 12), are isolated as green crystals of ion-separated salts from the reduction of $Si[1,2\text{-}(\mu\text{-}NCH_2Bu^t)_2C_6H_4]$ and $Cl_2Si[1,2\text{-}(\mu\text{-}NEt)_2C_6H_4]$, respectively, with alkali metals in THF. The radical anions **29** and **30** exhibit planar Si_3 and Si_4 rings, comparable to those of the cyclic trigermenyl and tetrasilenyl radicals, **23** and **25**, respectively. In marked contrast to **23** and **25**, however, the EPR spectra of **29** and **30** reveal significant delocalization of the spin density over the silane rings and onto the nitrogen atoms of the *N*,*N*′-chelated $(1,2\text{-}(\mu\text{-}NR)_2C_6H_4)$ substituents (R = CH_2Bu^t, Et) as indicated by the characteristic multiplets arising from coupling to six (**29**) or eight (**30**) equivalent ^{14}N nuclei ($a(^{14}N) = 4.6$ and

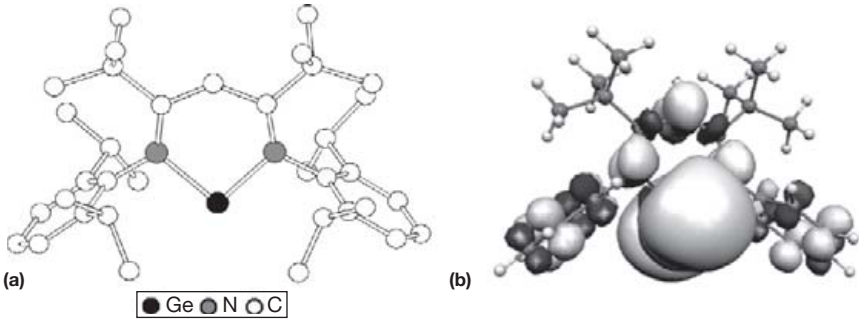

Figure 4 (a) Crystal structure and (b) SOMO of the neutral radical [($^{t\text{Bu}}$Nacnac)Ge:]$^{\bullet}$ (**28**). Adapted from (a) Woodul, W. D.; Carter, E.; Müller, R.; Richards, A. F.; Stasch, A.; Kaupp, M.; Murphy, D. M.; Driess, M.; Jones, C. *J. Am. Chem. Soc.* **2011**, *133*, 10074–10077; (b) Power, P. P. *Acc. Chem. Res*. **2011**, 44, 627–637.

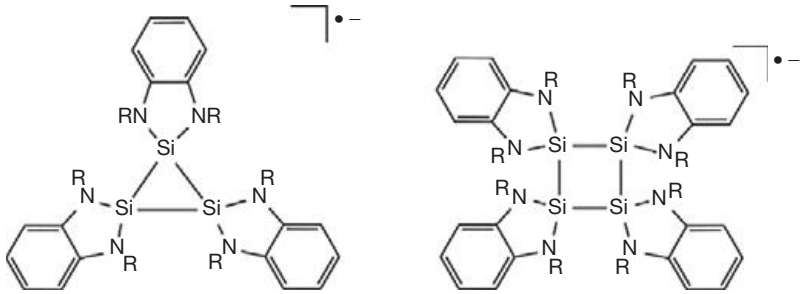

29
(R = CH_2Bu^t)

30
(R = Et)

Scheme 12 Cyclic polysilane radical anions.

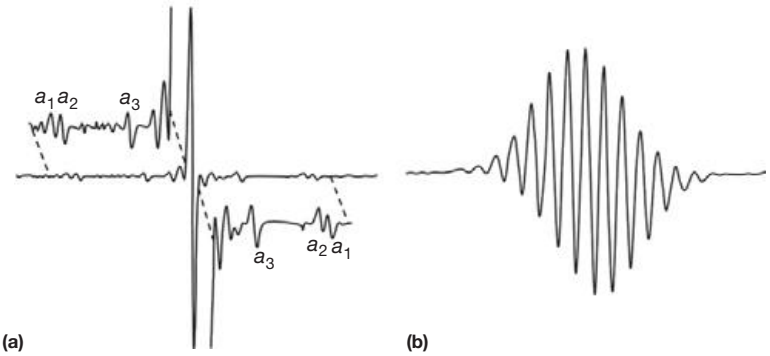

Figure 5 EPR spectrum of (a) **25** (a_1(^{29}Si) = 40.7 G, a_2(^{29}Si) = 37.4 G and a_3(^{29}Si) = 15.5 G; ^{29}Si, I = 1/2, 4.7%) and (b) **30** (a(^{14}N) = 3.5 G; ^{14}N, I = 1, 99.6%). Adapted from Sekiguchi, A.; Matsuno, T.; Ichinohe, M. *J. Am. Chem. Soc.* **2001**, *123*, 12436–12437; Gehrhus, B.; Hitchcock, P. B.; Zhang, L. *Angew. Chem. Int. Ed.* **2004**, *43*, 1124–1126.

3.5 G for **29** and **30**, respectively; ^{14}N, I = 1, 99.6%). The disparity in the distribution of the unpaired electron is clearly evident from a comparison of the EPR spectra of **25** and **30** (Figure 5). Coupling to the spin $I = 1/2$ ^{29}Si isotope with low natural abundance (4.7%) in **25** and to the spin $I = 1$ ^{14}N isotope with high natural abundance in **30** results in a substantially different appearance of the spectra.

The germanium(II) complex (dipp-BIAN)GeCl is obtained as deep red crystals from metathesis of (dipp-BIAN)Na with $GeCl_2$ in diethyl ether and has been characterized by x-ray crystallography.[75] The EPR parameters indicate that the unpaired electron is mainly ligand-localized, as is the case for analogous Al and Ga complexes (see **20a**, **b** in Scheme 7).

1.13.3.2 Acyclic Group 14 Radicals

1.13.3.2.1 Neutral radicals

The classic organic radicals involving three-coordinate carbon centers range from those with a fleeting existence, for example, the methyl radical $[CH_3]^{\bullet}$, to species that are sufficiently stable to be isolated in the solid state, for example, the perchlorinated radical $[(C_6Cl_5)_3C]^{\bullet}$. For the heavier group 14 elements, the

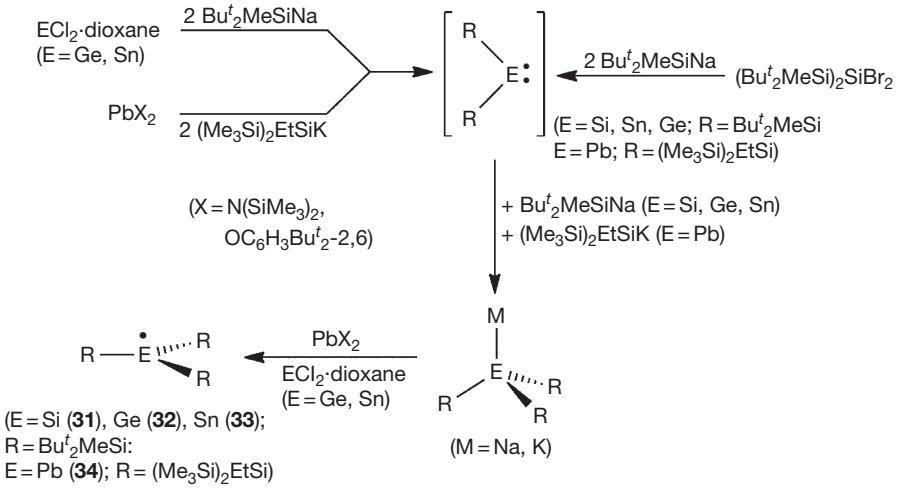

Scheme 13 Synthesis of group 14 radicals $R_3E^{\bullet}$ (E = Si, Ge, Sn, Pb).

simplest radicals $[H_3E]^{\bullet}$ (E = Si, Ge, Sn, Pb) have very short lifetimes. However, by utilizing the combination of the electronic properties and steric protection provided by very bulky silyl groups, a remarkable class of neutral radicals of the type $[R_3E]^{\bullet}$ have been isolated recently by Sekiguchi et al. (E = Si (**31**),[76] Ge (**32**),[76] Sn (**33**)[77]; R = $SiMeBu^t_2$) and by Klinkhammer et al. (E = Pb (**34**)[78,79]; R = $SiEt(SiMe_3)_2$). These stable, paramagnetic compounds are produced by a common synthetic approach in which the parent anion $[R_3E]^-$ is generated in situ and then subjected to mild, one-electron oxidation (Scheme 13).

The bright orange triarylgermyl radical $[R_3Ge]^{\bullet}$ (**35**, R = 3,5-Bu^t_2-2,6-$(EtO)_2C_6H$, Figure 6) is obtained in low yield from the addition of LiR to $GeCl_2$(dioxane).[80] The yield of **35** is greatly improved by adding LiR to a mixture of $GeCl_2$(dioxane) and the digermene $R_2Ge{=}GeR_2$.

The crystal structures of the Si, Ge, and Sn derivatives **31**–**33** show trigonal planar geometry with an sp^2-hybridized central atom, whereas the lead compound **34** displays a minor distortion toward a pyramidal arrangement (Σ ∠Pb 355°), possibly owing to the bulkier substituent ($SiEt(SiMe_3)_2$ vs. $SiMeBu^t_2$). The stability of the acyclic radicals in this series is attributed primarily to the use of sterically demanding, electropositive silyl substituents. However, additional stability is achieved in **31**–**34** by delocalization of the unpaired electron via hyperconjugation between the p_z orbital of the central group 14 atom and the σ* orbital of the Si–C(Bu^t_2) (**31**–**33**) or Si–Si(Me) (**34**) bonds. This interaction is also evident from the structural parameters, which exhibit a slight shortening in the E–Si bonds (E = Sn, Pb) compared to the anionic precursors.[77–79] Interestingly, the Si–Si bond lengths in **31** are ~0.08 Å shorter than the Al–Si bonds observed in the isoelectronic radical anion $[(Bu^t_2MeSi)_3Al]^{\bullet-}$ (**21a**), consistent with the difference in the sum of covalent radii (Si–Si 2.22 Å vs. Al–Si 2.32 Å). The structure of **35** is almost planar in the solid state (Figure 6).[80]

The solution EPR spectra of **31** and **32** show the expected patterns at $g = 2.0056$ and 2.0229 with hfcc values of $a(^{29}Si) = 58$ G and $a(^{73}Ge) = 20$ G, respectively, in addition to smaller couplings to the Si atoms of the $SiMeBu^t_2$ substituents ($a(^{29}Si) = 7.9$ and 7.3 G).[76] Only one set of satellites is observed in the EPR spectrum of **33** in solution at $g = 2.0482$ (^{117}Sn, $I = 1/2$, 7.8%; ^{119}Sn, $I = 1/2$, 8.6%) owing to the overlap of the slightly broadened signals and an average coupling constant of 329 G was reported[77] (cf. typical values of 1325–3426 G for $a(^{117/119}Sn)$ in Sn-centered σ radicals[81]). For the lead congener **34**, a broad EPR signal is observed at room temperature ($g = 2.160$), but an approximate hfc constant of $a(^{207}Pb) = 520$ G was obtained from the frozen solution (^{207}Pb, $I = 1/2$, 22.1%).[78] The EPR spectra of **31**–**34** indicate the retention of the planar geometry with sp^2-hybridized group 14 centers, and a true π-radical character for these paramagnetic species in solution. By contrast, variable-temperature EPR spectra signify a change in geometry for **35** from planar in the solid state (Figure 6) to pyramidal in solution.[80]

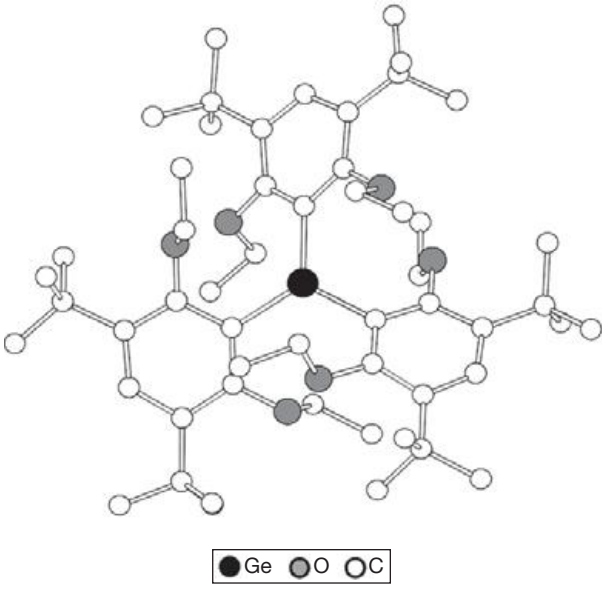

Figure 6 Crystal structure of $R_3Ge^{\bullet}$ (R = 3,5-Bu^t_2-2,6-$(EtO)_2C_6H$) (**35**). Adapted from Drist, C.; Griebel, J.; Kirmse, R.; Lönnecke, P.; Reinhold, J. *Angew. Chem. Int. Ed.* **2009**, *48*, 1962–1965.

Cyclic voltammetric studies have shown that the stable π radicals $[(Bu^t_2MeSi)_3E]^\bullet$ (E = Si, Ge, Sn; **31–33**) are more easily oxidized than reduced and that the ease of the irreversible oxidation process follows the order: Sn > Ge > Si.[82] There is a good correlation between the experimental oxidation potentials and the computed ionization energy values.

The stability of the persistent bis(silyl)-substituted σ radicals of the type $[(R_3Si)_2HE]^\bullet$ (E = C, Si, Ge) has been compared by means of EPR spectroscopy and DFT calculations. The significant difference in kinetic stability at 240 K of the persistent C-centered radicals and the short-lived Si and Ge-centered congeners is attributed to disparate decay mechanisms, that is, H abstraction for E = C and dimerization for E = Si, Ge.[83]

A one-step, high-yield synthesis of stable silyl radicals $[R_3Si–Si(SiMeBu^t_2)_2]^\bullet$ that involves the reaction of $R_3Si–SiHCl_2$ with $Bu^t_2MeSiLi$ has been developed; this potentially general approach produces orange crystals of either the new radical $[R_3Si–Si(SiMeBu^t_2)_2]^\bullet$ ($R_3Si = (Bu^t_2MeSi)_2HSi$) or the known radical ($R_3Si = SiMeBu^t_2$).[84] These radicals exhibit interesting photoreactivity; in the case of the latter species, exposure to sunlight produces the 1,2-dihydrosilane $(R_3Si)_2HSi–SiH(SiR_3)_2$ and the blue disilene $(R_3Si)_2Si=Si(SiR_3)_2$. This photoreactivity is attributed to a SOMO-1 → SOMO transition that creates a hole in the SOMO-1 orbital.

1.13.3.2.2 Radical anions and cations

By taking advantage of the relatively low-lying lowest unoccupied molecular orbital (LUMOs) and high-lying highest occupied molecular orbitals (HOMOs) of disilenes compared to those of the C=C double bond of alkenes, either one-electron oxidation of the neutral disilene, $[R_2Si=SiR_2]$ ($R = SiMeBu^t_2$), or one-electron reduction is easily achieved. Thus, the ion-separated disilene radical cation $[R_2Si=SiR_2]^{\bullet+}$ (**36**)[85] and the corresponding radical anion $[R_2Si=SiR_2]^{\bullet-}$ (**37**)[86] are formed by reactions of the neutral disilene with $[Ph_3C]^+[(C_6F_5)_4B]^-$ or Bu^tLi in THF, respectively (Scheme 14). In a similar manner, the tin-containing radical anion, $[R_2Sn=SnR_2]^{\bullet-}$ (**38a**) ($R = SiMeBu^t_2$), is produced from the neutral precursor by one-electron reduction with potassium in the presence of [2.2.2] cryptand (Scheme 14).[87]

Crystal structure determinations of the radical anions **37** and **38a** revealed one trigonal planar and one pyramidal metal center in both cases, whereas the paramagnetic cation **36** exhibits near planar geometry at both central silicon atoms. The E–E bond length in **37** (E = Si) and **38a** (E = Sn) is elongated by ~0.08 (2%) and 0.23 (9%) Å, respectively, from that observed in the neutral parent molecule, while the Si–Si bond in the radical cation **36** is intermediate in length between the distances seen in the anion **37** and the neutral precursor. These structural features suggest that the radical anions **37** and **38a** consist of an sp^3-hybridized silyl/stannyl anion and an sp^2-hybridized silyl/stannyl radical center, while the unpaired electron in the cation **36** is delocalized over the central Si–Si bond (Scheme 14). In solution, however, the EPR spectra of the paramagnetic disilene cation and anion, **36** and **37**, display virtually identical hfc constants at room temperature ($a(^{29}Si) = 23$ and 24.5 G; $g = 2.0049$ and 2.0061, respectively) that are approximately half of that observed for the structurally similar neutral silyl radical, $[(Bu^t_2MeSi)_3Si]^\bullet$ (**31**, $a(^{29}Si) = 58$ G), thus indicating delocalization of the unpaired electron in both of the charged disilene radicals. At low temperature (120 K), the delocalization in **37** is suppressed, as evinced by the increase in the hfc constant to 45 G. The tin analogue **38a**, on the other hand, exhibits a central signal ($g = 2.0517$) with two pairs of satellites ($a(^{117/119}Sn_\alpha) = 340$ G, $a(^{117/119}Sn_\beta) = 187$ G, cf. 329 G for **33**) in the solution EPR spectrum at room

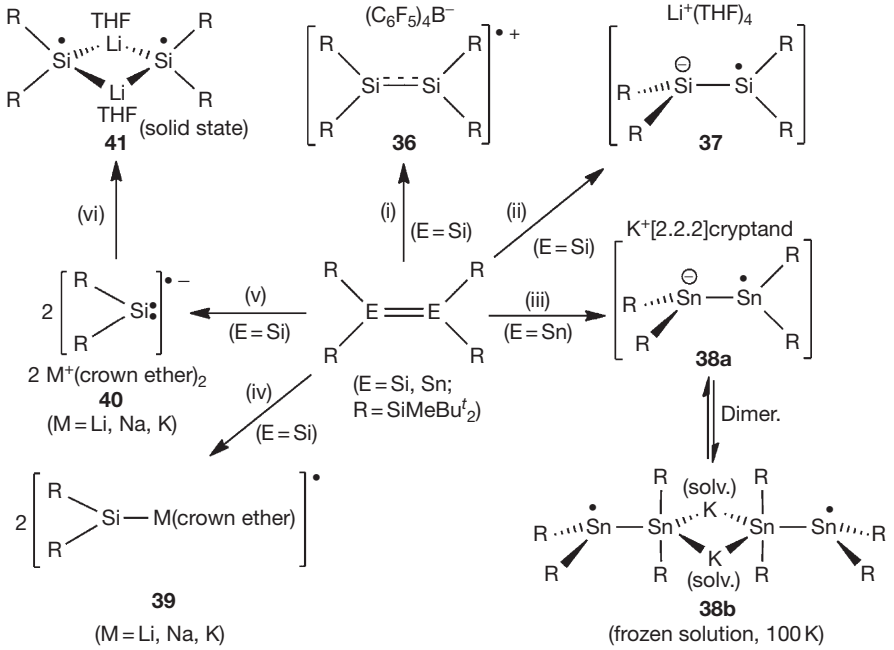

Scheme 14 Utilization of the neutral disilene and distannene, $R_2E=ER_2$ (E = Si, Sn; $R = SiMeBu^t_2$), in radical formation. (i) $[Ph_3C]^+[(C_6F_5)_4B]^-$[85]; (ii) Bu^tLi[86]; (iii) K/[2.2.2]cryptand[87,88]; (iv) 2.2 eq. M/Naphthalenide (M = Li, Na, K), 2 eq. crown ether[89,90]; (v) 2.2 eq. M/Naphthalenide (M = Li, Na, K), 4 eq. crown ether; (vi) 10 eq. LiBr, THF (M = Li).[89,90]

temperature, consistent with the localization of the single electron on one of the tin centers as was also inferred from the solid-state structure. It was suggested that the distannene radical anion **38a** aggregates to a paramagnetic triplet state dimer **38b** (Scheme 14) in glass matrix conditions (2-methyl-THF at 100 K) based on the observation of a signal corresponding to the forbidden $\Delta M_s = 2$ transition in the half-field region of the spectrum (1631 G).[88]

While the mild, one-electron reduction of the disilene $R_2Si{=}SiR_2$ ($R = SiMeBu^t_2$) affords the corresponding radical anion **37**, the use of a stronger reducing agent, M/naphthalenide (M = Li, Na, K), results in cleavage of the central Si=Si bond and formation of 'monomeric' radicals, either as contact ion-pairs $[R_2SiM(\text{crown ether})]^\bullet$ (**39**) or as ion-separated salts $[M(solv)_n]^+[R_2Si]^{\bullet-}$ (**40**) (M = Li, Na, K; solv = crown ether ($n = 2$), THF, dimethoxyethane (DME) ($n = 4$); $R = SiMeBu^t_2$), via a two-electron reduction process (Scheme 14).[89,90] The possibility of obtaining neutral radicals **39** or anionic paramagnetic species **40** (the anion radical of a silylene) was first noted when the EPR spectra of $[R_2Si]^\bullet Na(15\text{-crown-}5)_n$ were recorded in both polar (THF and DME) and nonpolar (toluene) solvents.[89] It was apparent from the EPR spectra (Figure 7) that in polar solvents the paramagnetic species exists as an ion-separated salt **40** with $a(^{29}Si_\alpha) = 29.1$ G and $a(^{29}Si_\beta) = 10.2$ G, whereas in a nonpolar solvent the coupling to the Na^+ cation was also observable for the contact ion-pair **39** ($a(^{23}Na) = 1.9$ G; ^{23}Na, $I = 3/2$, 100%). Subsequently, the controlled formation of **39** and **40**, both in solid state and in solution, was achieved by using the appropriate amount of crown ether according to the reactions (iv) and (v) in Scheme 14.[89,90]

The solvent-separated ion-pair **40** (M = Li, crown ether = 12-crown-4, Scheme 14) is converted to the contact ion-pair **39** by removal of the crown ether with LiBr. The product exists as a monomer in solution, as shown by the EPR signal with hfc constants of $a(^{29}Si_\alpha) = 34.0$ G, $a(^{29}Si_\beta) = 9.7$ G and $a(^7Li) = 1.6$ G (^7Li, $I = 3/2$, 92.5%), but dimerizes in the solid state to the diradical $[(\mu\text{-Li}{\cdot}THF)_2(SiR_2)_2]^{\bullet\bullet}$ (**41**) ($R = SiMeBu^t_2$) (Scheme 14), as proven by the x-ray crystal structure.[89,90] The diradical **41** was produced earlier by ultraviolet (UV) irradiation of the frozen hexane solution (150 K) of the gem-dilithiosilane, $[(R_2SiLi_2)(R_2HSiLi)_2]$ ($R = SiMeBu^t_2$), and its triplet state nature was determined from the EPR spectrum, which consists of a signal with four ^{29}Si sidebands arising from $\Delta M_s = 1$ transitions and a signal at half-field (1675 G) resulting from the forbidden $\Delta M_s = 2$ transition.[91]

In contrast to linear alkynes RC≡CR, the heavier group 14 congeners, RE≡ER (E = Si, Ge, Sn), assume a *trans*-bent geometry with respect to the triple bond.[92–94] Similarly to the heavy alkene analogues $R_2E{=}ER_2$ (E = Si, Sn) described above, this results in a relatively low energy level for the LUMO in the heavy alkyne compounds. By exploiting the resulting lowered potential for reduction, the disilyne radical anion, $[RSi{\equiv}SiR]^{\bullet-}$ ($R = Si(Pr^i)[CH(SiMe_3)_2]_2$) (**42**), is obtained directly from the neutral precursor by one-electron reduction with KC_8 (Scheme 15).[92] The analogous germylene and stannylene radical anions, $[RE{\equiv}ER]^{\bullet-}$ (M = Ge, R = 2,6-$Tripp_2C_6H_3$ (**43a**) or 2,6-$Dipp_2C_6H_3$ (**43b**); E = Sn, R = 2,6-$Tripp_2C_6H_3$ (**44a**) or 2,6-$Dipp_2C_6H_3$ (**44b**); Tripp = 2,4,6-$Pr^i_3C_6H_2$, Dipp = 2,6-$Pr^i_2C_6H_3$), however, are produced by the reduction of RECl (E = Ge, Sn) (Scheme 15).[93,94]

The crystal structures of the ion-separated, paramagnetic species **42**–**44** show retention of the *trans*-geometry around the central RE–ER bond.[92–94] Most significantly, the central E–E bond is markedly elongated in the radical anions (by ~0.11, 0.03, and 0.13 Å in **42**, **43b**, and **44a**, respectively) compared to the neutral molecules, even to the extent of approaching single-bond values. This extensive lengthening of the E–E bond can be explained by a structure in which both group 14 centers bear a lone pair and the unpaired electron is delocalized over the E–E p_π-orbital, thus giving a formal bond order of 1.5 (Scheme 15). In addition, narrowing of the E–E–R angles compared to the neutral, triply bonded species (by ~21°, 25°, and 31° in **42**, **43b**, and **44a**, respectively) contributes to a further elongation of the E–E distance.[94]

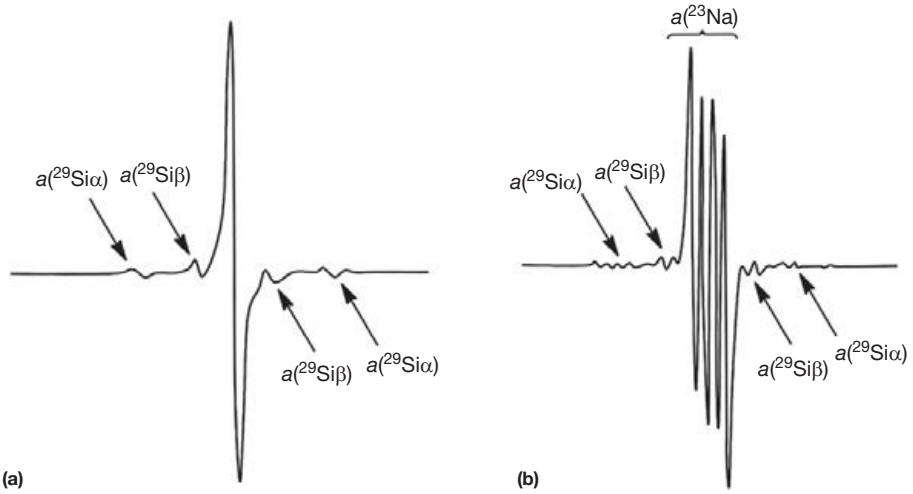

Figure 7 EPR spectrum of (a) solvent-separated ion-pair $[R_2Si]^{\bullet-}[Na^+(THF)_4]$ (**40**) in DME ($a(^{29}Si_\alpha) = 29.1$ G and $a(^{29}Si_\beta) = 10.2$ G), and (b) contact ion-pair $[R_2SiNa(15\text{-crown-}5)]^\bullet$ (**39**) in toluene ($a(^{29}Si_\alpha) = 29.1$ G, $a(^{29}Si_\beta) = 10.2$ G and $a(^{23}Na) = 1.9$ G); $g = 2.0074$, $R = SiMeBu^t_2$. Adapted from Inoue, S.; Ichinohe, M.; Sekiguchi, A. *J. Am. Chem. Soc.* **2007**, *129*, 6096–6097.

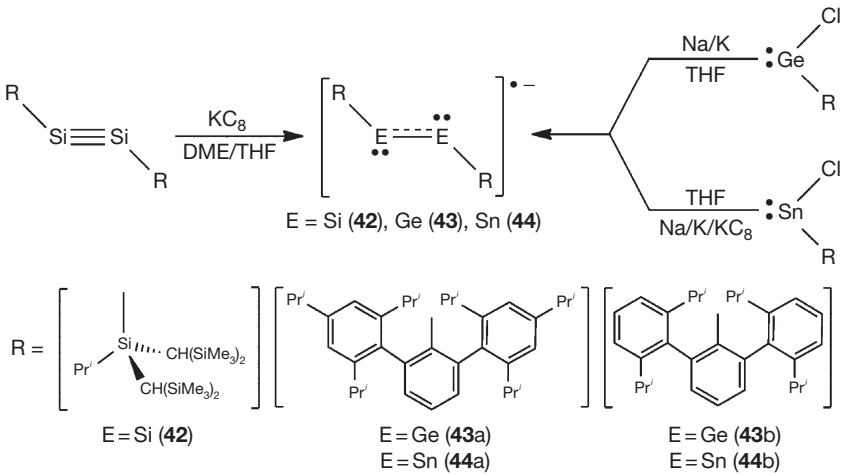

Scheme 15 Synthesis of dimetallyne radical anions.

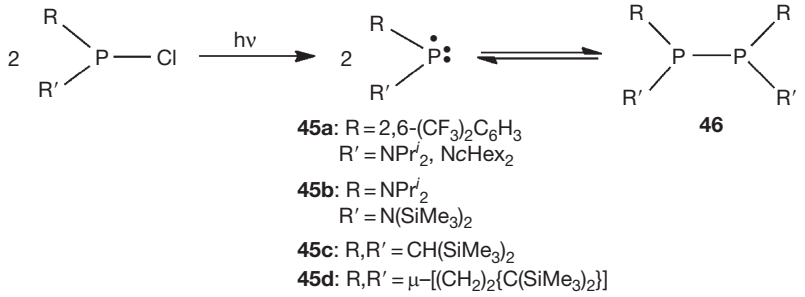

Scheme 16 Synthesis of phosphinyl radicals.

The EPR spectrum of **42** shows a triplet arising from coupling to the α-hydrogen of the *iso*-propyl groups ($a(^1H) = 2.3$ G). This triplet is accompanied by two pairs of satellites with $a(^{29}Si_\alpha) = 39.2$ G and $a(^{29}Si_\beta) = 22.4$ G. The magnitude of the hfc constants indicates the presence of a π-radical and extensive delocalization of the odd electron over the Si–Si bond and onto the substituents.[92] Consistently, relatively small hfc constants of $a(^{73}Ge) = 7.5$ G, $a(^{117}Sn) = 8.3$ G, and $a(^{119}Sn) = 8.5$ G were obtained for **43b** and **44a**, respectively,[93,94] indicative of low unpaired electron density at the germanium and tin centers, and localization of the odd electron in an orbital of π-symmetry.

The blue radical cation $\{Sn[PhB(\mu\text{-}NBu^t)_2]_2\}^{\bullet+}$ has been identified at low temperatures by EPR spectroscopy, supported by DFT calculations.[95] The thermal instability of this radical cation is reminiscent of the behavior of the isoelectronic neutral radical $\{In[PhB(\mu\text{-}NBu^t)_2]_2\}^{\bullet}$ (**18d**, Scheme 6). In contrast to the D_{2d}-symmetric indium-containing radical, however, DFT calculations predict a C_2 symmetry for $\{Sn[PhB(\mu\text{-}NBu^t)_2]_2\}^{\bullet+}$ with spin density localized on only one of the boraamidinate ligands.[95]

1.13.4 Group 15 Element Radicals

Stable radicals involving group 15 elements are restricted primarily to phosphorus-containing systems. A short review that emphasizes the diversity of both stable and persistent phosphorus radicals covers the literature up to 2004.[96]

1.13.4.1 Phosphorus

1.13.4.1.1 Neutral radicals

The simplest phosphorus-centered radicals are the two-coordinate neutral phosphinyl radicals, $[R_2P]^{\bullet}$ (**45**). Numerous derivatives of this paramagnetic species have been produced since its first discovery 45 years ago,[97] most frequently by photolysis of the appropriate chlorophosphane in the presence of an electron-rich alkene (Scheme 16).[98,99] The monomeric radicals **45** normally dimerize to the corresponding diamagnetic diphosphanes, $[R_2P]_2$ (**46**), both in the solid state and upon cooling the solutions of these odd-electron species.[100–102] Enhanced stability has been achieved, however, for example with $R = CH(SiMe_3)_2$ substituents (**45c**) resulting in derivatives that are indefinitely stable both in solution and in the gas phase.[103]

The gas-phase electron diffraction structures of **45b** ($R/R' = N(SiMe_3)_2/NPr^i_2$)[102] and **45c** ($R = R' = CH(SiMe_3)_2$)[103] reveal a V-shaped arrangement ($\angle NPN = 99.0°$ and $\angle CPC = 104.0°$, respectively) around the central phosphorus atom. Most significantly, the structure of the stable radical **45c** shows a *syn,syn* conformation for the $CH(SiMe_3)_2$ groups, in contrast to the *syn,anti* arrangement observed for the dimer **46c**. DFT calculations indicate that the disparity in the

conformations of **45c** and **46c** is a significant contributor to the remarkable stability of the monomeric radical **45c** in solution, that is, the transformation between **45c** and **46c** involves an isomerization of the substituents in addition to P–P bond cleavage. The latter process is estimated to require 95 kJ mol^{-1}, while the subsequent isomerization of the radical **45c**, to give the *syn,syn* conformation, releases an energy of 67.5 kJ mol^{-1} for each of the monomeric units, thus giving an overall exothermic process of ~40 kJ mol^{-1} for the conversion of **46c** to **45c**.[103b]

The first example of a stable dialkylphosphinyl radical **45d** was isolated recently as highly air-sensitive yellow crystals produced by reduction of the corresponding chlorophosphane with KC_8 in hexane.[104] The cyclic derivative **45d** is related to the acyclic radical **45c** via the linking of the two $C(SiMe_3)_2$ substituents through a $-CH_2-CH_2-$ bridge. Radical **45d** was shown to be monomeric in the solid state by x-ray crystallography.[104] DFT calculations show that the SOMO is an almost pure 3p orbital on the two-coordinate phosphorus atom with a small contribution from $\sigma^*(Me_3Si-C)$ orbitals, while the HOMO is a nonbonding orbital on the phosphorus atom. In solution the weak visible absorption band at 445 nm is attributed to the n(P)→3p(P) (HOMO→SOMO) transition. The spin densities on the P atom and each Si atom are 0.90 and 0.02–0.03, respectively, leading to the suggestion that **45d** is thermodynamically stabilized to some extent by 3p(P)–$\sigma^*(Me_3Si-C)$ interactions. Consistently, the EPR spectrum of **45d** in 3-methylpentane shows a doublet flanked by ^{29}Si satellites.

A vanadium-containing phosphinyl radical $[R_2P]^\bullet$ (R = NV[N(Np)Ar]$_3$; Np = neopentyl, Ar = 3,5-$Me_2C_6H_3$) (**45e**) (**Scheme 17**) that is stable both in solution and in the solid state is produced by one-electron reduction of the corresponding chlorophosphane.[105a] Similarly to the acyclic dialkylphosphinyl radicals **45b and 45c**, the solid-state structure of **45e** shows a V-shaped phosphorus center (∠NPN = 110.9°). The stability of the radical **45e** is achieved by delocalization of the unpaired electron onto the vanadium centers, which form a redox couple (IV/V). The delocalization is also evident from the EPR spectrum of **45e**. Whereas the dialkylphosphinyl radicals **45a–d** show hfc constants of 75.9–96.3 G to the central phosphorus atom (^{31}P, $I = 1/2$, 100%) with significantly smaller coupling to the substituents, the hfcc value of 42.5 G to the phosphorus atom in **45e** is substantially smaller and the coupling to the two transition-metal centers of $a(^{51}V) = 23.8$ G indicates extensive delocalization of the unpaired electron. For comparison, the hfcc values of the paramagnetic phosphinyls **45a–d** are indicative of π-radicals in which the odd electron is located predominantly in the phosphorus 3p orbital (**45a**: $a(^{31}P) = 87.0$ G, $a(^{14}N) = 5.56$ G, $6\times\ a(^{19}F) = 10.1$ G, $2\times\ a(^{1}H) = 1.0$ G[100]; **45b**: $a(^{31}P) = 75.9$ G, $a(^{14}N) = 5.95$ G[98,99]; **45c**: $a(^{31}P) = 96.3$ G, $2\times\ a(^{1}H) = 6.40$ G[98,99]; **45d**: $a(^{31}P) = 90.7$ G, ($a(^{29}Si) = 17.3$ G)).[104]

The imidazolidin-2-iminato ligand also stabilizes phosphinyl radicals as indicated by the two examples **45f** and **45g** in **Scheme 17**. The homoleptic, red compound **45f** is obtained by reduction of the corresponding cation; the heteroleptic species **45g**, a dark red solid, has also been prepared.[105b] Radical **45f** in THF solution displays a doublet [$a(^{31}P) = 78$ G] in the EPR spectrum with no observable coupling to ^{14}N. By contrast, the hybrid radical **45f** exhibits an eight-line pattern due to coupling with the ^{51}V nucleus [$a(^{51}V) = 58$ G] (^{51}V, $I = 7/2$. 99.7%) but the weak coupling (< 10 G) to ^{31}P is not resolved. Comparison of the EPR parameters for the series of phosphinyl radicals **45e–g**, in conjunction with DFT calculations, demonstrates that the vanadium-iminato ligand is more effective in delocalizing the spin density from the phosphorus nucleus.[105b]

Cyclic 7 π-electron radicals of the type $[(CH_2)_2(NR)_2P]^\bullet$ (**47**, R = Bu^t, Mes, Dipp) are generated upon warming toluene solutions of the P–P bonded dimer to 353 K as indicated by the EPR spectrum of this solution which exhibits a doublet of 1:2:3:2:1 quintets [$a(^{31}P) = 41$ G] and [$a(^{14}N) = 5.8$ G] (**Scheme 18**).[106] Couplings to P are lower and to N are higher than those in comparable acyclic phosphinyl radicals (*vide supra*) as a result of delocalization of the unpaired electron in the cyclic π-system of **47**.

The persistent diphosphanyl radical, [Mes*MePPMes*]$^\bullet$ (**48**), a close relative of the phosphinyl radicals **45**, was first observed in cyclic voltammetric studies of the diphosphene salt [Mes*MeP=PMes*][OSO_2CF_3].[107] Subsequently, **48** was produced by reduction of the corresponding cation with tetrakis

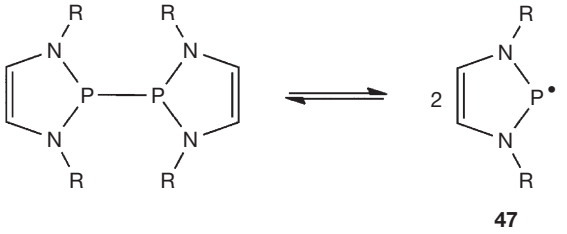

Scheme 18 Dissociation of diazaphospholene dimers into monomeric radicals **47** (R = Bu^t, Mes, Dipp).

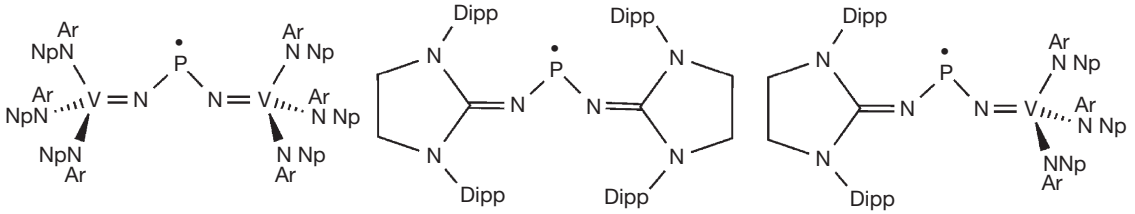

Scheme 17 Examples of stable phosphinyl radicals.

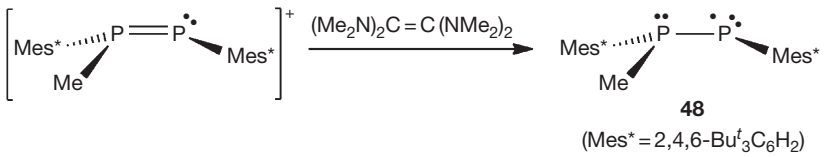

Scheme 19 Synthesis of a diphosphanyl radical.

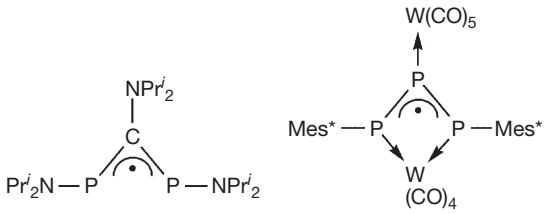

Scheme 20 A 1,3-diphosphaallyl radical and a metal complex of a triphosphaallyl radical.

(dimethylamino)ethene (Scheme 19).[108] The paramagnetic species **48** can be isolated as a solid, although magnetic measurements indicate a partial dimerization (10%) during the liquid to solid transformation; no crystal structure has been reported.[108] Slow decomposition of **48** occurs in the solid state while in solution the half-life is ~90 min.

The EPR spectrum of the diphosphanyl radical **48** shows a four-line signal consistent with coupling to two inequivalent phosphorus atoms ($a(^{31}P) = 139.3$ and 89.3 G).[108] The larger of the two hfc constants is attributed to the two-coordinate phosphorus center, which is expected to carry the major part of the spin density, and the smaller coupling is assigned to the three-coordinate phosphorus. Consistently, DFT calculations disclose a small s contribution to the SOMO (10%), while confirming that most of the spin density resides in a p orbital of the two-coordinate (74%) and three-coordinate (15%) phosphorus atoms. Since the calculations predict minimal delocalization of the unpaired electron, the stability of **48** is attributed mainly to the steric protection provided by the Mes* substituents.

Several short-lived 1,3-diphosphaallyl radicals have been suggested either as reaction intermediates or on the basis of EPR spin-trapping experiments.[109,110] The introduction of amino substituents has a powerful stabilizing effect, and the red diphosphaallyl radical $[(Pr^i_2NP)_2C(NPr^i_2)]^\bullet$ (**49**) (Scheme 20) is produced from the cyclic cation $[(Pr^i_2N)_2P(\mu_3\text{-}P)C(NPr^i_2)]^+$ either by electrolysis or by reduction with lithium metal.[111] The EPR spectrum of **49** in THF exhibits a significantly broadened five-line signal ($g = 2.0048$) with an intensity ratio of 1:3:4:3:1 that remains unchanged in the temperature range −60 to +25 °C. The spectrum can be interpreted by invoking hyperfine coupling to two equivalent phosphorus nuclei ($a(^{31}P) = 9.4$ G), two equivalent nitrogens ($a(^{14}N) = 1.5$ G), and a unique nitrogen atom ($a(^{14}N) = 9.9$ G), thus indicating significant stabilization of the radical by delocalization of the unpaired electron over a total of five atoms. The red crystals of **49** were not suitable for x-ray analysis.[111]

A black crystalline compound in which a triphosphaallyl radical is stabilized by coordination to a metal (**50**) is obtained by photolysis of the phosphinidene complex $[Cp^*P[W(CO)_5]_2]$ in the presence of Mes*P=PMes* in toluene.[112] The P–P bond lengths in **50** indicate a bond order of 1.5. The molecular orbital analysis of **50** reveals a π-allylic system that is partially resonance-stabilized by the d orbitals of both W atoms. The spin density distribution in the SOMO shows that the unpaired spin is evenly distributed over both terminal P atoms. Consistently, the EPR spectrum of **50** in hexane exhibits a doublet of triplets with $a(^{31}P) = 89.1$ G and $a(^{31}P) = 21.1$ G for the terminal and central P atoms, respectively. The radical **50** undergoes one-electron oxidation with $AgSbF_6$ to give the thermally unstable cation $\mathbf{50}^+$, while one-electron reduction with $CoCp_2$ produces the stable anion $\mathbf{50}^-$.[112]

The cyclic 1,3-diphosphacyclobuten-4-yl radical, $[(Mes^*C)_2(PBu^t)P]^\bullet$ (**51**, Mes* = 2,4,6-$Bu^t_3C_6H_2$), is isolated as deep red crystals by treatment of the phosphaalkyne Mes*C≡P with Bu^tLi followed by one-electron oxidation with iodine (Scheme 21).[113a] The structure of **51** is comprised of a nearly planar four-membered ring with trigonal planar carbon atoms, a pyramidal phosphorus atom, and a two-coordinate phosphorus atom. The bond parameters suggest a pure single bond for the P–C bonds involving the three-coordinate phosphorus atom and partial double-bond character for the other two P–C bonds. The room-temperature EPR spectrum of **51** in toluene exhibits a four-line central signal with small satellites ($g = 2.0025$), from which hfc constants of $a(^{31}P_\alpha) = 20.4$ G, $a(^{31}P_\beta) = 10.2$ G, and $a(^{13}C) = 30.2$ G were obtained. The relatively low ^{31}P hfcc values compared to those observed in phosphinyl and diphosphanyl radicals (**45** and **48**), as well as the metrical parameters, support an allylic radical in which the unpaired electron is delocalized mainly in the CPC unit (Scheme 21) cf. cyclotetrasilenyl **25** (Scheme 9). Ab initio calculations, however, predict that 80–90% of the spin density resides on the two carbon atoms. The analogous reaction with MeI instead of I_2 generates the carbon-centered biradicaloids **52** (Scheme 21) with singlet ground state owing to the conjugative interaction between the nonbonding electron pair on phosphorus and the unpaired electrons at the carbon atoms.[113b]

The phosphorus(V)-containing dianion radical $[P(NBu^t)_3(NSiMe_3)]^{2-\bullet}$ is generated, as the dilithium derivative, by one-electron oxidation of the trilithium salt of the corresponding tetrakisimidophosphate trianion $[P(NBu^t)_3(NSiMe_3)]^{3-}$ (a tetraimido analogue of orthophosphate PO_4^{3-}).[114] The formally neutral radical $\{Li_2[P(NBu^t)_3(NSiMe_3)]\}^\bullet$ exists as deep blue crystals that adopt highly distorted PN_3Li_3X cubic structures (**53a**, X=I; **53b**, X=OBu^t) in which an entrapped LiX molecule provides one edge of the cube (Scheme 22).[115] In an extremely dilute THF solution, solvation of the Li^+ counterions causes cleavage of the cubic structure to give the solvent-separated ion-pair **54**

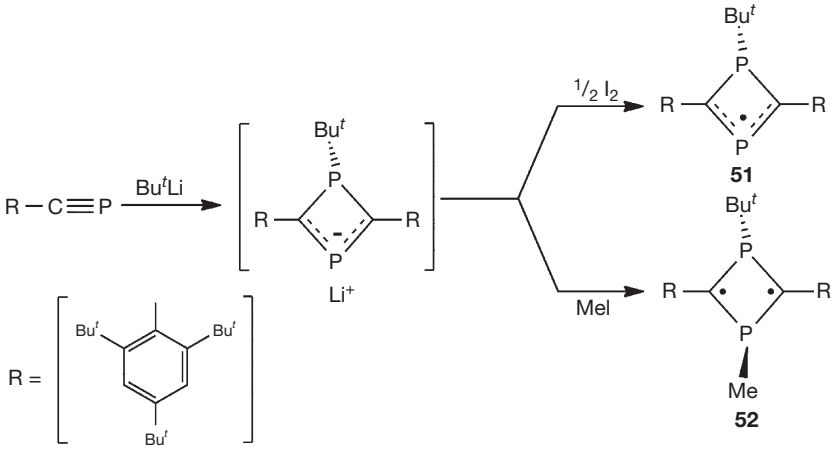

Scheme 21 Formation of the radical **51** and biradicaloid **52** from a phosphaalkyne.

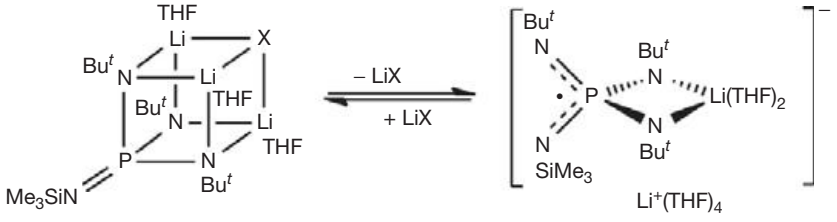

Scheme 22 Dissociation of LiX from a cubic phosphorus(V)-containing radical.

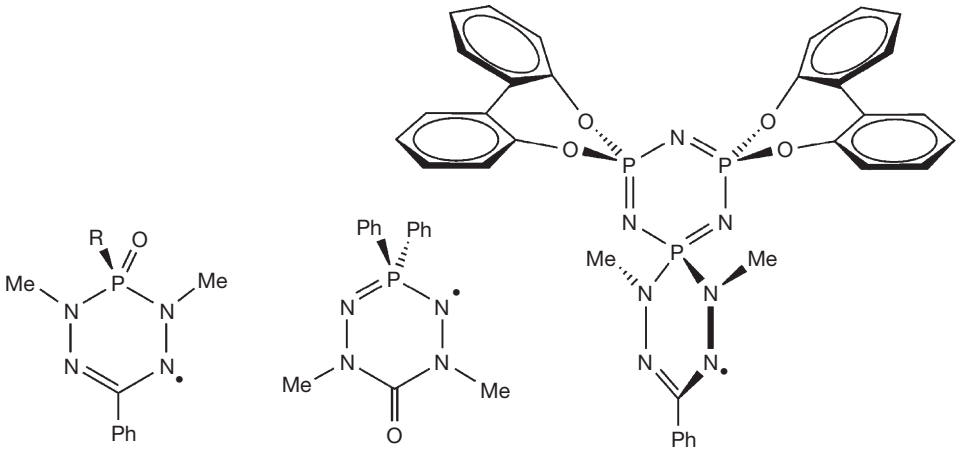

Scheme 23 Phosphorus(V)-containing verdazyl radicals.

and a molecule of $(THF)_3LiI$. The EPR spectrum of **54** displays a complicated, approximately 50-line signal ($g = 2.0063$) that is best simulated with hyperfine couplings to one phosphorus atom ($a(^{31}P) = 23.1$ G), two equivalent nitrogen centers ($a(^{14}N) = 5.38$ G), two unique nitrogen atoms ($a(^{14}N) = 7.38$ and 1.93 G), and a single lithium nucleus ($a(^{7}Li) = 0.30$ G). The relatively small ^{31}P hfc constant in **54**, compared to those in **45** and **48**, indicates a small amount of spin density located at the phosphorus center. This conclusion is supported by DFT calculations that predict a SOMO consisting predominantly of nitrogen-based 2p orbitals for **54**.[114,115]

Synthetic approaches to persistent phosphorus-containing verdazyl radicals, for example, **55**, **56**, and **57** (Scheme 23), have been developed.[116–119] These radicals decompose owing

to hydrogen transfer from the *N*-methyl groups. The EPR spectra reveal only small spin density at phosphorus [$a(^{31}P) < 5$ G]. In the phosphazene-verdazyl **57** the spin density on the phosphazene nitrogen atoms bonded to the spirocyclic phosphorus center has been attributed to a through-space, spiroconjugation mechanism.[117,118]

UV irradiation of a benzene solution of an NHC with $[\{(Pr^iO)_2(O)P\}_2Hg]$ produces the NHC-phosphoryl radical adduct **58** (Figure 8).[120] The EPR spectrum of **58** exhibits a doublet of quintets with ($a(^{31}P) = 48.7$ G) and ($a(^{14}N) = 4.7$ G. The calculated Mulliken spin density of **58** reveals a ring-centered radical with 53% of the spin density on the central C atom and 34% on the other ring atoms. The half-life of the radical **58** is estimated to be 7.1 s on the basis of a kinetic analysis of the decay of the EPR signal.[120]

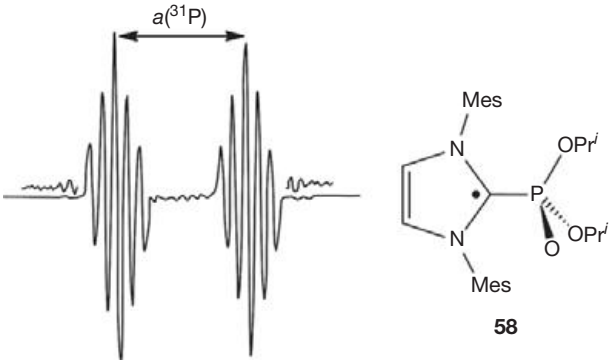

Figure 8 EPR spectrum of a benzene solution of the NHC → phosphoryl radical adduct **58** recorded at 298 K under UV irradiation. Adapted from Tumanskii, B.; Sheberla, D.; Molev, G.; Apeloig, Y. *Angew. Chem. Int. Ed.* **2007**, *46*, 7408–7411.

1.13.4.1.2 Radical cations

Sterically protected triarylphosphanes Ar_3P are produced by the in situ reactions of organocopper reagents $(ArCu)_x$ with PCl_3. Subsequent one-electron oxidation, either by bulk electrolysis or with silver(I) salts AgX ($X = [ClO_4]^-$, $[PF_6]^-$, $[SbF_6]^-$), produces persistent radical cations, $[Ar_3P]^{\bullet+}$ (Ar = Dipp, Tripp; Dipp = 2,6-$Pr^i_2C_6H_3$; Tripp = 2,4,6-$Pr^i_3C_6H_2$) (**59**) (Scheme 24).[121,122] The solution EPR spectra show a doublet with $a(^{31}P) = 239$ (**59a**) and 237 G (**59b**), thus indicating the expected pyramidal, P-centered radicals. Frozen glass EPR spectra imply a significant flattening of the molecule (small $a_\perp$ component of the hfc tensor) that brings the iso-propyl substituents in *ortho* positions closer together, thus providing more shielding for the unpaired electron and, therefore, contributing to the stability of the radical cations **59**.[122]

NHC ligands stabilize highly reactive diatomic molecules, for example, P_2[123,124] and PN[125] (see Chapter 1.16). The bis(carbene)-stabilized P_2 adduct **60** undergoes one-electron oxidation with $Ph_3C^+B(C_6F_5)_4^-$ to give the purple monocation radical $\mathbf{60}^{\bullet+}$ (Scheme 25).[124] The EPR spectrum of $\mathbf{60}^{\bullet+}$ displays a triplet of quintets due to a moderate coupling to the two equivalent P atoms [$a(^{31}P) = 42$ G] and a small coupling with two N atoms [$a(^{14}N) = 3$ G]. The EPR spectrum of the related dark red cation radical $\mathbf{61}^{\bullet+}$ (Scheme 25) also appears as a triplet [$a(^{31}P) = 44$ G], but the coupling to the four nitrogen nuclei could not be resolved.[124] The P–P bond lengths in the cation radicals $\mathbf{60}^{\bullet+}$ and $\mathbf{61}^{\bullet+}$ are significantly shorter than those in the neutral precursors as a result of the removal of one

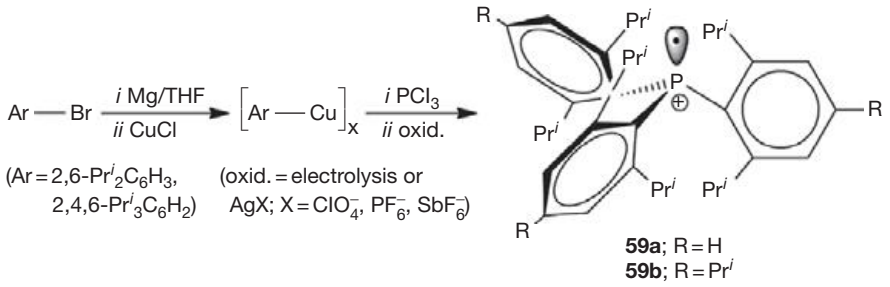

Scheme 24 Synthesis of radical cations $[Ar_3P]^{+\bullet}$.

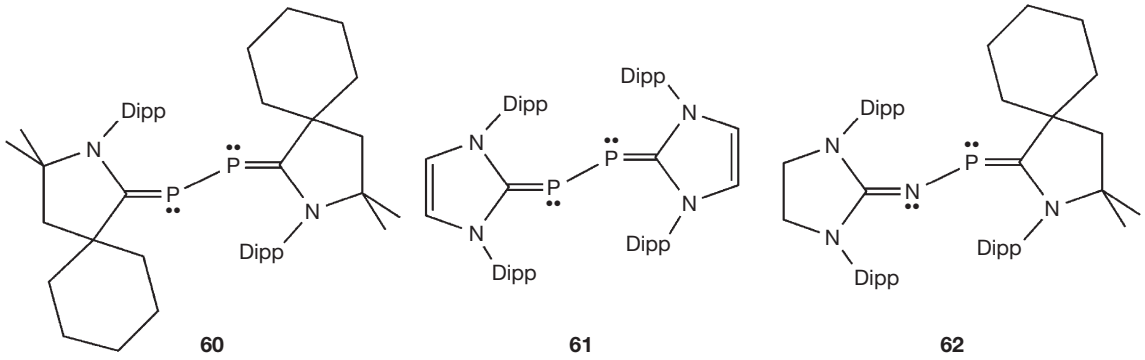

Scheme 25 Neutral precursors of the radical cations $\mathbf{60}^{\bullet+}$, $\mathbf{61}^{\bullet+}$, and $\mathbf{62}^{\bullet+}$.

electron from the doubly occupied π* orbital upon oxidation. The bis(carbene) adduct of the PN molecule **62** is also oxidized by $Ph_3C^+B(C_6F_5)_4^-$ to the dark brown cation radical **62**$^{\bullet+}$, which exhibits a doublet [$a(^{31}P) = 44$ G] in the EPR spectrum measured in fluorobenzene; coupling to the N atom of the PN unit was not observed.[125] Consistently, calculations by the natural bond order (NBO) method reveal that the spin density in **62**$^{\bullet+}$ is mainly distributed on the P atom. The P–N bond length in the cation radical **62**$^{\bullet+}$ is significantly shorter than that in the neutral precursor **62**, as expected for the removal of one electron from the doubly occupied HOMO (π* orbital) upon oxidation.

In addition to steric effects, a phosphinyl radical is stabilized by the positive charge in the cation radical **63**$^{\bullet+}$ (Scheme 26), which inhibits dimerization by electrostatic repulsion.[126] The EPR spectrum of **63**$^{\bullet+}$ shows a doublet [$a(^{31}P) = 99$ G] and some poorly resolved fine structure. The ^{31}P hfc in **63**$^{\bullet+}$ is comparable to the values of 76–96 G observed for neutral phosphinyl radicals (see Section 1.13.4.1.1). Consistently, NBO calculations confirm that the spin density in **63**$^{\bullet+}$ is primarily localized on the phosphorus atom.

The strong electron-acceptor property of pentavalent phosphorus atoms stabilizes radical cations, as exemplified by the isolation of the deep purple diphosphafulvenium monocation **64**$^{\bullet+}$ (Scheme 26), which is prepared by one-electron reduction of the corresponding dication with $CoCp_2$.[127] The structural data for **64**$^{\bullet+}$ indicate that the cyclic C=C double bond is unaffected upon reduction, whereas the exocyclic C–C bond has lost its double-bond character; consistently, the LUMO is antibonding with respect to these two carbon atoms. The solution EPR spectrum of **64**$^{\bullet+}$ at 300 K is comprised of a 1:2:1 triplet [$a(^{31}P) = 30$ G] with additional fine structure indicating hyperfine coupling with two equivalent phosphorus atoms.[127]

In contrast to monoiminophosphoranes $Ph_3P{=}NR$ (R = alkyl, aryl), bis-iminophosphoranes in which two $Ph_3P{=}N$ groups are bridged by planar π-systems, for example, ethylene or conjugated phenylenes, form persistent cation radicals upon one-electron oxidation.[128] The unpaired electron in these systems is delocalized on the two p_π N orbitals and the π-system of the bridging group with very little spin density on the phosphorus atoms.

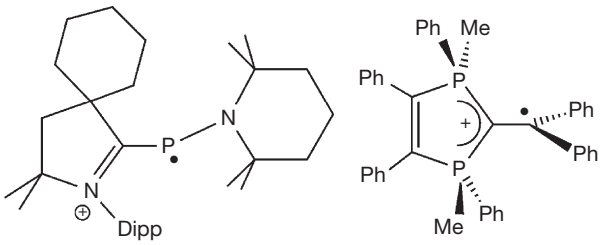

63$^{\bullet+}$ **64**$^{\bullet+}$

Scheme 26 Phosphinyl and diphosphafulvenium radical cations.

1.13.4.1.3 Radical anions

The formation of the persistent diphosphene radical anions, [RPPR]$^{\bullet-}$ (**65**), is observed in solution when the 'dimeric' contact ion pairs, $[M^+]_2[R_4P_4]^{2-}$ (M = Na, R = phenyl; M = K, R = cyclohexyl), are treated with [2.2.2]cryptand. By contrast, in the solid state, the radical anions dimerize to re-form the ion-separated salts $[R_4P_4]^{2-}$ $[(M^+)_2\{[2.2.2]\text{cryptand}\}]_2$, as established by x-ray crystallography (Scheme 27).[129] The EPR spectra of **65** exhibit a triplet arising from the coupling of the unpaired electron to two equivalent phosphorus atoms ($a(^{31}P) = 40.9$ (**65a**) and 45.2 (**65b**) G; $g = 2.0089$ and 2.0099, respectively) with additional splitting owing to spin-density distribution onto the substituents ($a(^1H) = 3.0$ and 1.4 G (**65a**) and $a(^1H) = 3.6$ G (**65b**)).

Diphosphene radical anions that are kinetically stabilized both in solution and in the solid state, **65c** (R = Bbt = 4-[$C(SiMe_3)_3$]-2,6-[$CH(SiMe_3)_2]_2C_6H_2$) and **65d** (R = Tbt = 2,4,6-[$CH(SiMe_3)_2]_3C_6H_2$), are produced by one-electron reduction of the neutral diphosphene obtained by magnesium reduction of $RPCl_2$ (Scheme 27).[130] Analogously to **65a–b**, the EPR spectra of **65c** and **65d** show a triplet with $a(^{31}P) = 48.0$ and 47.6 G ($g = 2.009$ and 2.010), respectively, indicating uniform delocalization of the spin density on both phosphorus centers. However, in contrast to **65a–b**, further delocalization onto the substituents is not observed. The Raman spectra of **65c–d** suggest significant elongation of the P–P bond compared to that in the neutral precursors by displaying a strong Raman line at ~540 cm^{-1} for the ν_{P-P} stretching vibration, cf. ~610 cm^{-1} for the P=P double bond in RP=PR (R = Bbt, Tbt) and

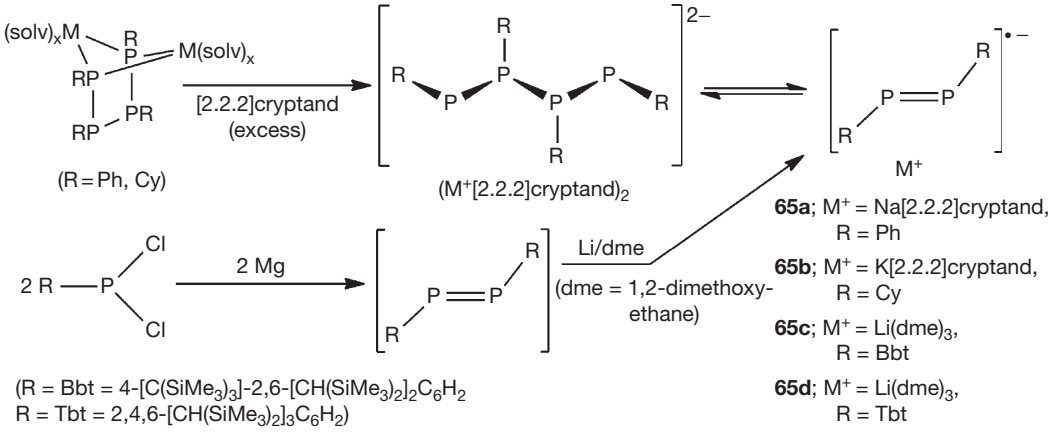

Scheme 27 Synthesis of diphosphene radical anions.

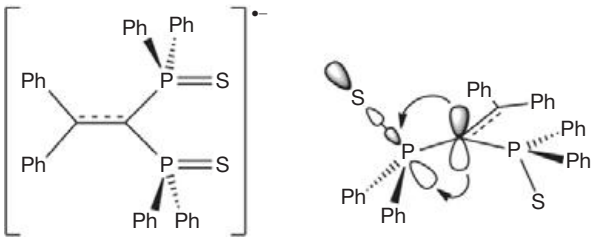

66•−

Figure 9 Negative hyperconjugation in the anion radical $[Ph_2C{=}C(PPh_2PS)_2]^{\bullet-}$ (**66**$^{\bullet-}$). Adapted from Cantat, T.; Biaso, F.; Momin, A.; Ricard, L.; Geoffroy, M.; Mézailles, N.; Le Floch, P. *Chem. Commun.* **2008**, 874–875.

530 cm^{-1} for the P–P single bond in $Ph_2P{-}PPh_2$. Elongation and, hence, weakening of the P–P bond in the radical anions **65** are consistent with DFT calculations that indicate a SOMO composed of an antibonding P–P π* orbital.[131]

The one-electron chemical or electrochemical reduction of a bis(diphosphene) in which two DippP=P units are linked by the bulky arene spacer group $-C_6(C_6H_4\text{-}4\text{-}Bu^t)_4-$ produces the corresponding anion radical.[132] The EPR spectrum of this radical is comprised of a triplet of triplets ($a(^{31}P) = 98$ and 25 G). The EPR parameters together with the results of DFT calculations indicate that the diphosphene core becomes planar upon addition of an electron and that the radical anion is best represented by quinone-like resonance structures.[132]

Pentavalent phosphorus substituents, for example, PPh_2S, are also effective in stabilizing alkene radical anions. Thus, the neutral alkene $Ph_2C{=}C(PPh_2S)_2$ is reduced by alkali metals in THF or DME to the corresponding purple radical anion **66**$^{\bullet-}$ (Figure 9), which can be isolated as the deep purple, dimeric $[K(DME)_2]^+$ salt.[133] The increase in the C–C bond length in the alkene unit by ~0.1 Å indicates a loss of double-bond character upon reduction; the SOMO in the radical anion is the π*(C=C) orbital. The EPR spectrum of the [Na(18-crown-6)]$^+$ salt of **66**$^{\bullet-}$ exhibits a 1:2:1 triplet [$a(^{31}P) = 10.3$ G] with additional fine structure resulting from interactions of the unpaired electron with the protons of the two carbon-bonded phenyl rings. Consistently, DFT calculations show that the C–C bond is strongly polarized toward this carbon atom; the resulting negative charge at the phosphorus-bonded carbon atom is stabilized by negative hyperconjugation with the σ*(P–C) and σ*(P–S) orbitals (Figure 9).

The first example of a dianion radical of a five-membered aromatic ring, the diazaphosphole derivative 3,5-Ph_2-1,2,4-C_2N_2P (**67**$^{2-\bullet}$), has been isolated as the black $[K(18\text{-crown-}6)]_2^{2+}$ salt.[134] An x-ray structural investigation revealed a triple-decker 'inverse sandwich' arrangement in which **67**$^{2-\bullet}$ is η^5-coordinated to two [K(18-crown-6)] cations. The EPR spectrum of **67**$^{2-\bullet}$ shows a doublet with a relatively small phosphorus coupling [$a(^{31}P) = 11.6$ G].

1.13.4.2 Arsenic, Antimony, and Bismuth

The chemistry of stable, arsenic-, antimony-, and bismuth-centered radicals has remained virtually unexplored. The EPR spectra of the persistent arsenic and antimony congeners of the triarylphosphane radical cation, $[Ar_3P]^{\bullet+}$ (**59**) (Scheme 24), indicate the expected pyramidal structure, but no further discussion of these species was presented.[121]

An antimony-containing congener of the diphosphene radical anion **65c**, [(Bbt)SbSb(Bbt)]$^{\bullet-}$ (**68**), is obtained from a reaction analogous to that shown for the synthesis of **65c** in Scheme 27.[131] The crystal structure of **68** reveals an elongation of ~0.05 Å in the Sb–Sb bond length (2.7511(4) Å) compared to the value of 2.7037(6) Å in the distibene [(Bbt)Sb=Sb(Bbt)], consistent with a SOMO comprised of an E–E π*-orbital as predicted for both **65** and **68** (E=P, Sb) by DFT calculations. Only a broad signal is observed in the EPR spectrum of **68** in solution ($g = 2.097$), while in the solid state a complicated spectrum is obtained due to coupling of the unpaired electron with two equivalent Sb centers each with two EPR-active isotopes (^{121}Sb, $I = 5/2$, 57.25%; ^{123}Sb, $I = 7/2$, 42.75%).[131]

The seven-atom 37-valence electron cluster $[As_7]^{2-\bullet}$ is formed in high yields as the red $[K(2,2,2\text{-crypt})]_2^{2+}$ salt from a solution of K_3As_7 in ethylenediamine and an excess of cryptand, presumably as a result of oxidation of the trianion.[135] Magnetic and EPR measurement confirm the paramagnetic nature of the radical dianion $[As_7]^{2-\bullet}$.

The synthesis of the 6π-electron anion $[1,2\text{-}C_6H_4P_2Sb]^-$ from the reaction of 1,2-$(PLi_2)_2C_6H_4$ (generated in situ in tetramethylethylenediamine (TMEDA)) with $Sb(NMe_2)_3$ in toluene is accompanied by the formation of black crystals of the $[Li(TMEDA)^+]_4$ salt of the tetranion $[1,2\text{-}(C_6H_4P_2Sb)_2]^{4-}$, which exhibits an Sb–Sb bond length that is only ~0.1 Å longer than an Sb–Sb single bond.[136] Although the tetraanion is a dimer of the 7π-electron dianion radical $[1,2\text{-}(C_6H_4P_2Sb)_2]^{2-\bullet}$, this paramagnetic species is not detectable in solution (or the solid state). DFT calculations reveal that the association into a dimer is primarily due to bonding to the Li^+ counterions.[136]

In contrast to the neutral radicals $\{M[PhB(\mu\text{-}NBu^t)_2]_2\}^{\bullet}$ (M=B, Al, Ga, In) (**18a–d**, Scheme 6), which are not group 13-centered species (see Section 1.13.2.2.2), DFT calculations for the group 15 radicals $\{M[PhB(\mu\text{-}NBu^t)_2]_2\}^{\bullet}$ (M=P, As, Sb, Bi) predict a pnictogen-centered SOMO with smaller contributions to the unpaired spin density arising from the nitrogen and boron atoms.[137] However, efforts to produce the arsenic-centered radical $\{As[PhB(\mu\text{-}NBu^t)_2]_2\}^{\bullet}$ by oxidation of the corresponding anion or reduction of the cation, either chemically or electrochemically, failed to produce an EPR-active species.

1.13.5 Group 16 Element Radicals

1.13.5.1 Sulfur

The majority of the advances in the chemistry of stable, heavy group 16 radicals in recent years are based primarily on dithiadiazolyls and related heterocyclic central nervous system (CNS)/Se radicals (see Chapter 1.14). Apart from these intriguing compounds, which show potential for the construction of novel one-dimensional metals or materials with unique magnetic properties, examples of odd-electron group 16 species within the scope of this chapter are sparse.

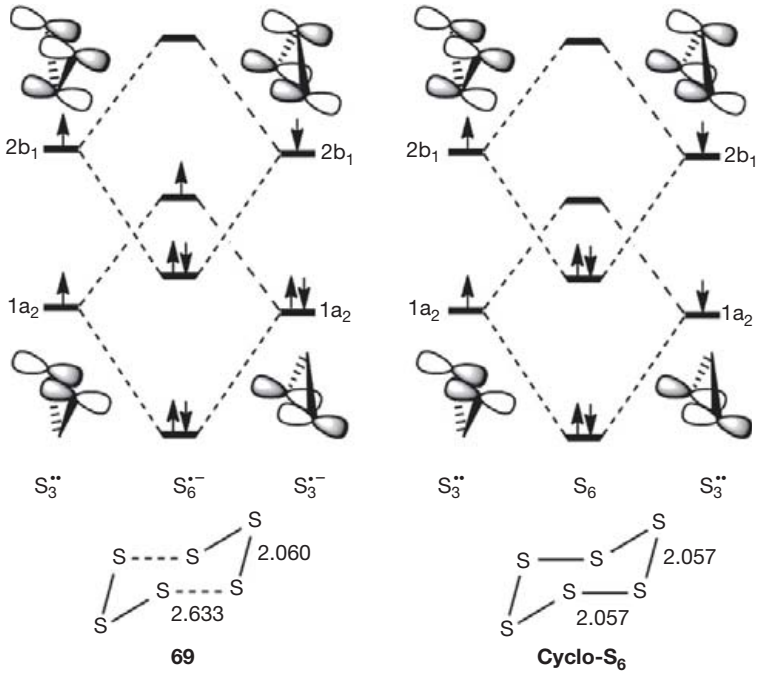

Figure 10 Orbital interaction diagram for the formation of the cyclic radical anion $[S_6]^{\bullet -}$ (**69**) and cyclo-S_6 from two S_3 units. Adapted from Neumüller, B.; Schmock, F.; Kirmse, R.; Voigt, A.; Diefenbach, A.; Bickelhaupt, F. M.; Dehnicke, K. *Angew. Chem. Int. Ed.* **2000**, *39*, 4580–4582.

The stable cyclic radical anion $[S_6]^{\bullet -}$ (**69**) is formed unexpectedly as the $[Ph_4P]^+$ salt from the reaction between $[Ph_4P]N_3$, Me_3SiN_3, and H_2S.[138] The crystal structure displays the six-membered $[S_6]^{\bullet -}$ ring in a chair conformation with two long central S–S bonds (2.633 Å) (Figure 10), thus indicating a relatively weak union of two S_3 fragments in each of which the average S–S bond length is 2.060 Å (cf. 2.057 Å in cyclo-S_6). The solid-state EPR spectrum of **69** suggests a formulation in which $[S_6]^{\bullet -}$ is comprised of the diradical $[S_3]^{\bullet\bullet}$ and the anion radical $[S_3]^{\bullet -}$. The eigenvalues for the *g*-tensor, $g_1 = 2.056$, $g_2 = 2.036$, and $g_3 = 2.003$, are consistent with those previously observed for the $[S_3]^{\bullet -}$ radical anion, the source of the blue color in ultramarine (lapis lazuli).[139] Both of these experimental observations are in agreement with the molecular orbital analysis that reveals a bonding interaction between the two S_3 fragments in **69** involving two components (Figure 10): (i) an electron-pair bond between the $2b_1$ SOMOs of both fragments and (ii) a three-electron bond between the $1a_2$ SOMO of the biradical $[S_3]^{\bullet\bullet}$ and the $1a_2$ HOMO of the $[S_3]^{\bullet -}$ radical anion. Neutral S_3 has a closed-shell ground state, but becomes a biradical after valence-excitation of an electron from $1a_2$ to $2b_1$. As a comparison, the three-electron bond in **69** is converted into a more stabilizing electron-pair bond in neutral cyclo-S_6 by the loss of the antibonding electron, thereby accounting for the disparity in the central S–S bond lengths of these two cyclic species.

The ubiquitous trisulfur radical anion $[S_3]^{\bullet -}$[140] continues to be of major interest as an important intermediate in transformations involving inorganic sulfur-containing ions. In the latest contribution it has been shown by in situ Raman spectroscopy that this paramagnetic species is the dominant stable form of sulfur in aqueous solution at high temperatures and pressures.[141] This finding has important geological implications regarding the formation of various sulfur species in hydrothermal fluids, as well as in affecting sulfur-isotope fractionation models.

1.13.5.2 Selenium and Tellurium

The simplest organochalcogeno radicals $[RE]^{\bullet}$ (E = S, Se, Te; R = alkyl, aryl) have not been isolated as stable species, presumably due to the lack of steric protection from the substituent. However, the existence of the organic tellurium-centered radicals $[RTe]^{\bullet}$ (R = Bu^n, Ph) as intermediates in the hydrotelluration reactions of alkenes and alkynes has been ascertained by spin trapping experiments.[142] The EPR spectra of the radical adducts so formed, $[(RTe)(2,6\text{-}Br_2\text{-}1\text{-}NO\text{-}3\text{-}SO_3\text{-}C_6H_2)]^{\bullet -}$ (**70**; R = Bu^n, Ph) (Scheme 28), with natural abundance tellurium (^{123}Te, $I = 1/2$, 0.9%; ^{125}Te, $I = 1/2$, 7.0%), show coupling only to the nitrogen atom and two hydrogens of the trapping agent ($a(^{14}N) = 21.6$ G; $a(^{1}H) = 0.7$ G). When isotope labeling is employed (92% ^{125}Te), a complicated spectrum is observed from which hfc constants of $a(^{14}N) = 21.6$ G, $a(^{125}Te) = 15.8$ G, $a(^{79/81}Br) = 6.95$ G, and $a(^{1}H) = 0.7$ G are obtained, thus indicating a radical with significant spin density at the tellurium center.

The first stable tellurium(III) radical cation, $[(Me_3Si)_2N]_2Te^{\bullet +}$ (**71**) (Scheme 28), was synthesized from the neutral precursor by one-electron oxidation with Ag$[AsF_6]$.[143] The crystal structure of this seminal paramagnetic species displayed a slight shortening of the Te–N bonds and elongation of the Si–N distances compared to those of the neutral precursor. Together with the observed changes in bond angles, these metrical parameters suggest enhanced back

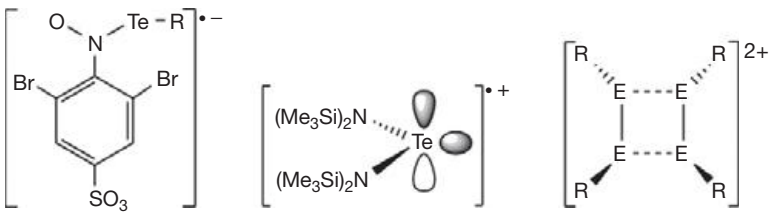

70
(R = Bu^n, Ph)

71

72
(E = Se; R = Me, Et
E = Te; R = Et, Pr, Bu^i)

Scheme 28 Tellurium-containing radical anion **70**, radical cation **71**, and the dimer of the radical cations $[RE{=}ER]^{+\bullet}$ (**72**, E = Se, Te)].

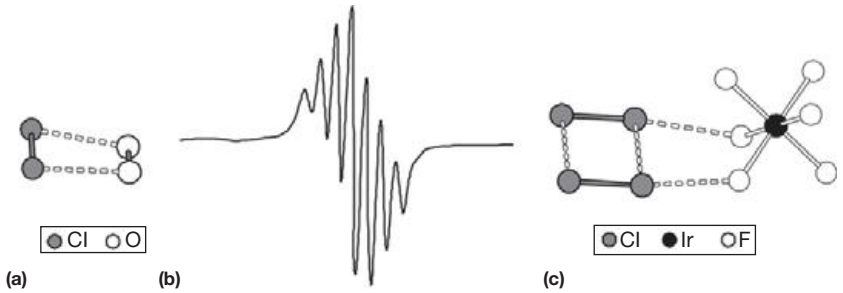

Figure 11 (a) $[Cl_2O_2]^{\bullet+}$ (**73**; anion = $[Sb_2F_{11}]^-$), (b) EPR spectrum of **73**, and (c) $[(Cl_2)_2]^+[IrF_6]^-$ (**74**·IrF_6^-). Adapted from Drews, T.; Koch, W.; Seppelt, K. *J. Am. Chem. Soc.* **1999**, *121*, 4379–4384; Seidel, S.; Seppelt, K. *Angew. Chem. Int. Ed.* **2000**, *39*, 3923–3925.

bonding of the nitrogen lone pairs to the positively charged tellurium center. Only a single, broad signal ($\Delta\omega_{1/2} = 15$ G) was observed in the EPR spectrum of **71**, indicative of a small spin density on the nitrogen atoms. These data are consistent with a tellurium-centered radical with a pair of electrons in an sp^2 orbital and the odd electron located in a p orbital (Scheme 28). Stabilization of **71** (toward dimerization) is attributed to a combination of steric protection from the substituents and electrostatic repulsion between the positively charged tellurium centers.

One-electron oxidation of dialkyl dichalcogenides, RE–ER, with $[NO]^+[OSO_2CF_3]^-$ produces the diamagnetic dications, $[(REER)_2]^{2+}$ (E = Se, R = Et, Pr, Bu^i; E = Te, R = Me, Et) (**72**) (Scheme 28), rather than the monomeric radical cations, $[RE{=}ER]^{\bullet+}$, presumably due to lack of sufficient steric protection from the substituents.[144] The chalcogen–chalcogen bond lengths in **72** are ~0.05 Å shorter than those in the neutral precursors, while the distance between the two halves of the rectangular dication is 0.6–0.7 Å longer owing to a combination of the relatively weak π*–π* interactions between two monomeric $[RE{=}ER]^{\bullet+}$ units and electrostatic repulsion between these two positively charged species (cf. formation of the I_4^{2+} cation[145–147]). DFT calculations predict that the dimerization is exothermic when solvent effects are taken into account and, consistently, no EPR signal has been observed for either the selenium or tellurium derivatives of the type **72**.[144]

1.13.6 Group 17 Element Radicals

The most common group 17 element-centered radicals are the homodiatomic dications $[E_2]^{\bullet+}$ (E = Br, I) which, as has been shown for the rectangular iodine derivative, dimerize in the solid state through π*–π* interactions to give the diamagnetic dications $[(E_2)_2]^{2+}$.[145–147] For the bromine derivative only a broad, noncharacteristic EPR signal has been observed, while the iodine congener shows no signal.[148–150]

The analogous chlorine radical cation $[Cl_2]^{\bullet+}$ has been isolated as the adduct $[Cl_2O_2]^{\bullet+}$ (**73**), which is formally a side-on π-complex of $[Cl_2]^{\bullet+}$ with dioxygen (Figure 11(a)). The source of the intriguing paramagnetic species **73** is the reaction between Cl_2 and an $[O_2]^+$ salt with either $[SbF_6]^-$ or $[Sb_2F_{11}]^-$ as the counter-ion.[66] Similar to the dimer $[I_4]^{2+}$, the structure of **73** is a planar trapezium with short bonds within the Cl_2 and O_2 units (1.909(1) and 1.207(5) Å, respectively), and a long Cl–O distance (~2.41 Å) between these two units, cf. sum of van der Waals radii for Cl and O = 3.30 Å. The Cl–Cl distance is ~0.07 Å shorter than that of Cl_2, thus indicating that most of the positive charge, and the unpaired electron, resides on the chlorine atoms. Consistently, the EPR spectrum of **73** (Figure 11(b)) shows a seven-line pattern ($g = 1.9988$) due to the coupling of the unpaired electron with two equivalent Cl centers ($a(^{35/37}Cl) = 2.23$ G; ^{35}Cl, $I = 3/2$, 75.8%; ^{37}Cl, $I = 3/2$, 24.2%).[151]

Subsequent attempts to produce the monomeric radical cation $[Cl_2]^{\bullet+}$ from the reaction between Cl_2 and IrF_6 also resulted in a dimeric product in the form of the rectangular radical cation $[(Cl_2)_2]^{\bullet+}$ (**74**) (Figure 11(c)).[152] The structure of **74** displays two short Cl–Cl bonds and two long Cl···Cl contacts (1.941(3) and 2.936(7) Å, respectively). The short chlorine–chlorine bond lengths are intermediate between those observed for Cl_2 and $[Cl_2]^{\bullet+}$, suggesting delocalization of the unpaired spin density over both units. The EPR spectrum of **74** as the $[IrF_6]^-$ salt shows only an unresolved broad

signal.[152] However, the original EPR spectroscopic study of **74** supports the uniform delocalization of the unpaired electron over all four chlorine atoms.[153]

1.13.7 Conclusion

In the past decade, a number of significant developments have occurred in the intriguing field of stable and persistent radicals, primarily through the strategy of installing extremely bulky groups on the heavy p-block element centers in order to provide kinetic stabilization of highly reactive species. For example, numerous examples of heavy group 14 analogues of classic carbon-centered radicals, as well as their isoelectronic anionic congeners from group 13, have been identified. A similar approach has also been successfully employed to generate a variety of unsaturated cyclic and acyclic (neutral and charged) phosphorus-containing radicals, most notably in the isolation of stable phosphinyl radicals involving two-coordinate phosphorus centers.

To date, the primary focus has been on the refinement of molecular design necessary for the synthesis and isolation of stable radicals and, subsequently, the elucidation of their molecular and electronic structures. With this knowledge in hand, it is likely that more attention will be given to practical applications in the future. For example, the use of stable p-block element radicals as building blocks for oligomeric or polymeric systems with unique magnetic properties represents a worthwhile synthetic challenge. While applications in materials science will probably necessitate the use of stable radicals, applications of persistent main-group element radicals in organic synthesis and as polymerization initiators are also expected to receive increasing attention.

References

1. Griller, D.; Ingold, K. U. *Acc. Chem. Res.* **1976**, *9*, 13–19.
2. Power, P. P. *Chem. Soc. Rev.* **2003**, *103*, 789–809.
3. Hicks, R. G. Ed.; In *Stable Radicals: Fundamental and Applied Aspects of Odd-Electron Compounds*; Wiley: Chichester, 2010; p 578.
4. Hicks, R. G. *Org. Biomol. Chem.* **2007**, *5*, 1321–1338.
5. Kaim, W.; Hosmane, N. S.; Zalis, S.; Maguire, J. A.; Lipscomb, W. N. *Angew. Chem. Int. Ed.* **2009**, *48*, 5082–5091.
6. Hinchcliffe, A.; Mair, F. S.; McInnes, E. J. L.; Pritchard, R. G.; Warren, J. E. *Dalton Trans.* **2008**, *2*, 222–233.
7. Mansell, S. M.; Adams, C. J.; Bramham, G.; Haddow, M. F.; Kaim, W.; Norman, N. C.; McGrady, J. E.; Russell, C. A.; Udeen, S. J. *Chem. Commun.* **2010**, *46*, 5070–5072.
8. Matsumoto, T.; Gabbai, F. *Organometallics* **2009**, *26*, 4252–4253.
9. (a) Walton, J. C.; Brahmi, M. M.; Monot, J.; Fensterbank, L.; Malacria, M.; Curran, D. P.; Lacôte, E. *J. Am. Chem. Soc.* **2011**, *133*, 10321–10330; (b) Walton, J. C.; Brahmi, M. M.; Fensterbank, L.; Lacôte, E.; Malacria, M.; Chu, Q.; Ueng, S.-H.; Soloyev, A.; Curran, D. P. *J. Am. Chem. Soc.* **2010**, *132*, 2350–2358.
10. Ueng, S.-H.; Soloyev, A.; Yuan, X.; Geib, S. J.; Fensterbank, L.; Lacôte, E.; Malacria, M.; Newcomb, M.; Walton, J. C.; Curran, D. P. *J. Am. Chem. Soc.* **2009**, *131*, 11256–11262.
11. Lalevée, J.; Blanchard, N.; Tehfe, M.-A.; Chany, A.-C.; Fouassier, J.-P. *Chem. Eur. J.* **2010**, *16*, 12920–12927.
12. Kaim, W. *Chem. Ber.* **1981**, *114*, 3789–3800.
13. Kuck, M. A.; Urry, G. *J. Am. Chem. Soc.* **1966**, *88*, 426–431.
14. Wood, T. K.; Piers, W. E.; Keay, B. A.; Parvez, M. *Chem. Commun.* **2009**, *34*, 5147–5149.
15. Chivers, T.; Konu, J. *Comment. Inorg. Chem.* **2009**, *30*, 131–176.
16. Chiu, C.-W.; Gabbai, F. *Angew. Chem. Int. Ed.* **2007**, *46*, 1723–1725.
17. (a) King, B. T.; Noll, B. C.; McKinley, A. J.; Michl, J. *J. Am. Chem. Soc.* **1996**, *118*, 10902–10903; (b) Zharov, I.; King, B. T.; Havlas, Z.; Pardi, A.; Michl, J. *J. Am. Chem. Soc.* **2000**, *122*, 10253–10254; (c) Zharov, I.; Weng, T.-C.; Orendt, A. M.; Barich, D. H.; Penner-Hahn, J.; Grant, D. M.; Havlas, Z.; Ichl, J. *J. Am. Chem. Soc.* **2004**, *126*, 12033–12046.
18. Volkis, V.; Douvris, C.; Michl, J. *J. Am. Chem. Soc.* **2011**, *133*, 7801–7809.
19. Krause, E.; Nobbe, P. *Ber. Dtsch. Chem. Ges.* **1930**, *63*, 934–942.
20. Leffler, J. E.; Watts, G. B.; Tanigaki, T.; Dolan, E.; Miller, D. S. *J. Am. Chem. Soc.* **1970**, *92*, 6825–6830.
21. Olmstead, M. M.; Power, P. P. *J. Am. Chem. Soc.* **1986**, *108*, 4235–4236.
22. Kwaan, R. J.; Harlan, C. J.; Norton, J. R. *Organometallics* **2001**, *20*, 3818–3820.
23. Cummings, S. A.; Iimura, M.; Harlan, C. J.; Kwaan, R. J.; Vu Trieu, I.; Norton, J. R.; Bridgewater, B. M.; Jäkle, F.; Sundararaman, A. *Organometallics* **2006**, *25*, 1565–1568.
24. Grigsby, W. J.; Power, P. P. *Chem. Commun.* **1996**, 2235–2236.
25. Grigsby, W. J.; Power, P. P. *Chem. Eur. J.* **1997**, *3*, 368–375.
26. Hoefelmeyer, J. D.; Gabbai, F. P. *J. Am. Chem. Soc.* **2000**, *122*, 9054–9055.
27. Lorenzen, V.; Preetz, W.; Baumann, F.; Kaim, W. *Inorg. Chem.* **1998**, *37*, 4011–4014.
28. Wong, E. H.; Kabbani, R. M. *Inorg. Chem.* **1980**, *19*, 451–455.
29. Binder, H.; Kellner, R.; Vaas, K.; Hein, M.; Baumann, F.; Wanner, M.; Winter, R.; Kaim, W.; Hönle, W.; Grin, Y.; Wedig, U.; Schultheiss, M.; Kremer, R. K.; Schnering, H. G. V.; Groeger, O.; Engelhardt, G. *Z. Anorg. Allg. Chem.* **1999**, *625*, 1059–1072.
30. Binder, H.; Kellner, R.; Vaas, K.; Hein, M.; Baumann, F.; Wanner, M.; Winter, R.; Kaim, W.; Wedig, U.; Hönle, W.; Schnering, H. G. V.; Groeger, O.; Engelhardt, G. *Z. Anorg. Allg. Chem.* **1999**, *625*, 1638–1646.
31. Peymann, T.; Knobler, C. R.; Hawthorne, M. F. *Chem. Commun.* **1999**, 2039–2040.
32. Peymann, T.; Knobler, C. R.; Khan, S. I.; Hawthorne, M. F. *Inorg. Chem.* **2001**, *40*, 1291–1294.
33. Peymann, T.; Knobler, C. R.; Khan, S. I.; Hawthorne, M. F. *Angew. Chem. Int. Ed.* **2001**, *40*, 1664–1667.
34. Van, N.; Tiritiris, I.; Winter, R. F.; Sarkar, B.; Singh, P.; Duboc, C.; Muñoz-Castro, A.; Arratia-Peréz, R.; Kaim, W.; Schleid, T. *Chem. Eur. J.* **2010**, *16*, 11242–11245.
35. Boeré, R. T.; Kacprzak, S.; Kessler, M.; Knapp, C.; Riebau, R.; Riedel, S.; Roemmele, T. L.; Rühle, M.; Scherer, H.; Weber, S. *Angew. Chem. Int. Ed.* **2011**, *50*, 549–552.
36. Fox, M. A.; Nervi, C.; Crivello, A.; Low, P. J. *Chem. Commun.* **2007**, *23*, 2372–2374.
37. Fu, X.; Chan, H.-S.; Xie, Z. *J. Am. Chem. Soc.* **2007**, *129*, 8964–8965.
38. Wakamiya, A.; Mishima, K.; Ekawa, K.; Yamaguchi, S. *Chem. Commun.* **2008**, 579–581.
39. Braunschweig, H.; Breher, F.; Chiu, H.-S.; Gamon, D.; Nied, D.; Radacki, K. *Angew. Chem. Int. Ed.* **2010**, *49*, 8975–8978.
40. Emslie, D. J. H.; Piers, W. E.; Parvez, M. *Angew. Chem. Int. Ed.* **2003**, *42*, 1252–1255.
41. Gilroy, J. B.; Ferguson, M. J.; MacDonald, R.; Patrick, B. O.; Hicks, R. G. *Chem. Commun.* **2007**, *2*, 126–128.
42. Wiberg, N.; Blank, T.; Kaim, W.; Schwederski, B.; Linti, G. *Eur. J. Inorg. Chem.* **2000**, 1475–1481.
43. Wiberg, N.; Amelunxen, K.; Nöth, H.; Schwenk, H.; Kaim, W.; Klein, A.; Scheiring, T. *Angew. Chem. Int. Ed. Engl.* **1997**, *36*, 1213–1215.
44. Wiberg, N.; Blank, T.; Amelunxen, T.; Nöth, H.; Knizek, J.; Habereder, T.; Kaim, W.; Wanner, M. *Eur. J. Inorg. Chem.* **2001**, *7*, 1719–1727.
45. Yang, P.; Köppe, R.; Duan, T.; Hartig, J.; Hadiprono, G.; Pilawa, B.; Keilhauer, I.; Schnöckel, H. G. *Angew. Chem. Int. Ed.* **2007**, *46*, 3579–3583.
46. Chivers, T.; Eisler, D. J.; Fedorchuk, C.; Schatte, G.; Tuononen, H. M.; Boeré, R. T. *Chem. Commun.* **2005**, 3930–3931.
47. Chivers, T.; Eisler, D. J.; Fedorchuk, C.; Schatte, G.; Tuononen, H. M. *Inorg. Chem.* **2006**, *45*, 2119–2132.
48. Cloke, F. G. N.; Hanson, G. R.; Henderson, M. J.; Hitchcock, P. B.; Raston, C. L. *J. Chem. Soc. Chem. Commun.* **1989**, 1002–1003.
49. Cloke, F. G. N.; Dalby, C. I.; Hanson, G. R.; Henderson, M. J.; Kennard, C. H. L.; Lamb, R. N.; Raston, C. L. *J. Chem. Soc. Chem. Commun.* **1990**, 1394–1395.
50. Cloke, F. G. N.; Dalby, C. I.; Daff, P. J.; Green, J. C. *J. Chem. Soc. Dalton Trans.* **1991**, 181–184.
51. Kaim, W.; Matheis, W. *J. Chem. Soc. Chem. Commun.* **1991**, 597–598.
52. Schoeller, W. W.; Grigoleit, S. *J. Chem. Soc. Dalton Trans.* **2002**, *3*, 405–409.
53. Cissell, J. A.; Vaid, T. P.; Rheingold, A. L. *Inorg. Chem.* **2006**, *45*, 2367–2369.

54. Schumann, H.; Hummert, M.; Lukoyanov, A. N.; Fedushkin, I. L. *Organometallics* **2005**, *24*, 3891–3896.
55. Baker, R. J.; Jones, C.; Kloth, M.; Mills, D. P. *New. J. Chem.* **2004**, *28*, 207–213.
56. Baker, R. J.; Farley, R. D.; Jones, C.; Kloth, M.; Murphy, D. M. *J. Chem. Soc. Dalton Trans.* **2002**, 3844–3850.
57. Nakamoto, M.; Yamasaki, T.; Sekiguchi, A. *J. Am. Chem. Soc.* **2005**, *127*, 6954–6955.
58. Begum, A.; Lyons, A. R.; Symons, M. C. R. *J. Chem. Soc. A* **1971**, 2290–2293.
59. Giles, J. R. M.; Roberts, B. P. *J. Chem. Soc. Chem. Commun.* **1981**, 1167–1168.
60. Brand, J. C.; Roberts, B. P. *J. Chem. Soc. Chem. Commun.* **1984**, 109–110.
61. Uhl, W.; Cuypers, L.; Kaim, W.; Schwedersk, B.; Koch, R. *Angew. Chem. Int. Ed.* **2003**, *42*, 2422–2423.
62. McKee, L. M.; Wang, Z.-X.; Schleyer, P. V. R. *J. Am. Chem. Soc.* **2000**, *122*, 4781–4793.
63. Lee, V. Y.; Sekiguchi, A. In *Reviews of Reactive Intermediate Chemistry*; Platz, M. S., Moss, R. A. Jones, M. Jr., Eds.; Wiley: New Jersey, 2007; pp 47–120.
64. Lee, V. Y.; Sekiguchi, A. *Acc. Chem. Res.* **2007**, *40*, 410–419.
65. Lee, V. Y.; Sekiguchi, A. *Eur. J. Inorg. Chem.* **2005**, 1209–1222.
66. Olmstead, M. M.; Pu, L.; Simons, R. S.; Power, P. P. *Chem. Commun.* **1997**, 1595–1596.
67. Ishida, Y.; Sekiguchi, A.; Kobayashi, K.; Nagase, S. *Organometallics* **2004**, *23*, 4891–4896.
68. Sekiguchi, A.; Matsuno, T.; Ichinohe, M. *J. Am. Chem. Soc.* **2001**, *123*, 12436–12437.
69. Tumanskii, B.; Pine, P.; Apeloig, Y.; Hill, N. J.; West, R. *J. Am. Chem. Soc.* **2004**, *126*, 7786–7787.
70. Tumanskii, B.; Pine, P.; Apeloig, Y.; Hill, N. J.; West, R. *J. Am. Chem. Soc.* **2005**, *127*, 8248–8249.
71. McCollum, B. M.; Brodovitch, J.-C.; Clyburne, J. A. C.; Mitra, A.; Percival, P. W.; Tomasik, A.; West, R. *Chem. Eur. J.* **2009**, *15*, 8409–8412.
72. Mitra, A.; Brodovitch, J.-C.; Krempner, C.; Percival, P. W.; Vyas, P.; West, R. *Angew. Chem. Int. Ed.* **2010**, *49*, 2893–2895.
73. (a) Woodul, W. D.; Carter, E.; Müller, R.; Richards, A. F.; Stasch, A.; Kaupp, M.; Murphy, D. M.; Driess, M.; Jones, C. *J. Am. Chem. Soc.* **2011**, *133*, 10074–10077; (b) Power, P. P. *Acc. Chem. Res.* **2011**, *44*(8), 627–637.
74. (a) Antolini, F.; Gehrhus, B.; Hitchcock, P. B.; Lappert, M. F. *Chem. Commun.* **2005**, *40*, 5112–5113; (b) Gehrhus, B.; Hitchcock, P. B.; Zhang, L. *Angew. Chem. Int. Ed.* **2004**, *43*, 1124–1126.
75. Fedushkin, I. L.; Khvoinova, N. M.; Baurin, A. Y.; Fukin, G. K.; Chekasov, V. K.; Bubnov, M. P. *Inorg. Chem.* **2004**, *43*, 7807–7815.
76. Sekiguchi, A.; Fukawa, T.; Nakamoto, M.; Lee, V. Ya.; Ichinohe, M. *J. Am. Chem. Soc.* **2002**, *124*, 9865–9869.
77. Sekiguchi, A.; Fukawa, T.; Lee, V. Ya.; Nakamoto, M. *J. Am. Chem. Soc.* **2003**, *125*, 9250–9251.
78. Förster, C.; Klinkhammer, K. W.; Tumanskii, B.; Krüger, H.-J.; Kelm, H. *Angew. Chem. Int. Ed.* **2007**, *46*, 1156–1159.
79. Becker, M.; Förster, C.; Franzen, C.; Hartrath, J.; Kirsten, E.; Knuth, J.; Klinkhammer, K. W.; Sharma, A.; Hinderberger, D. *Inorg. Chem.* **2008**, *47*, 9965–9978.
80. Drist, C.; Griebel, J.; Kirmse, R.; Lönnecke, P.; Reinhold, J. *Angew. Chem. Int. Ed.* **2009**, *48*, 1962–1965.
81. Iley, J. In *The Chemistry of Organic Germanium, Tin and Lead Compounds*; Patai, S., Ed.; Wiley: New York, 1995; (Chapter 5).
82. Sheberla, D.; Tumanskii, B.; Bravo-Zhivotovskii, D.; Molev, G.; Molev, V.; Lee, V. Ya.; Takanashi, K.; Sekiguchi, A.; Apeloig, Y. *Organometallics* **2010**, *29*, 5596–5606.
83. Molev, G.; Tumanskii, B.; Sheberla, D.; Botoshansky, M.; Bravo-Zhivotovskii, D.; Apeloig, Y. *J. Am. Chem. Soc.* **2009**, *131*, 11698–11700.
84. Becker, J. Y.; Lee, V. Ya.; Nakamoto, M.; Sekiguchi, A.; Chrostowska, A.; Dargelos, A. *Chem. Eur. J.* **2009**, *15*, 8480–8484.
85. Inoue, S.; Ichinohe, M.; Sekiguchi, A. *J. Am. Chem. Soc.* **2008**, *139*, 6078–6079.
86. Sekiguchi, A.; Inoue, S.; Ichinohe, M.; Arai, Y. *J. Am. Chem. Soc.* **2004**, *126*, 9626–9629.
87. Fukawa, T.; Lee, V. Ya.; Nakamoto, M.; Sekiguchi, A. *J. Am. Chem. Soc.* **2004**, *126*, 11758–11759.
88. Lee, V. Ya.; Fukawa, T.; Nakamoto, M.; Sekiguchi, A.; Tumanskii, B. L.; Kami, M.; Apeloig, Y. *J. Am. Chem. Soc.* **2006**, *128*, 11643–11651.
89. Inoue, S.; Ichinohe, M.; Sekiguchi, A. *J. Am. Chem. Soc.* **2007**, *129*, 6096–6097.
90. Inoue, S.; Ichinohe, M.; Sekiguchi, A. *Organometallics* **2008**, *27*, 1358–1360.
91. Bravo-Zhivotovskii, D.; Ruderfer, I.; Melamed, S.; Botoshansky, M.; Tumansii, B.; Apeloig, Y. *Angew. Chem. Int. Ed.* **2005**, *44*, 739–743.
92. Kinjo, R.; Ichinohe, M.; Sekiguchi, A. *J. Am. Chem. Soc.* **2007**, *129*, 26–27.
93. Olmstead, M. M.; Simons, R. S.; Power, P. P. *J. Am. Chem. Soc.* **1997**, *119*, 11705–11706.
94. Pu, L.; Phillips, A. D.; Richards, A. F.; Stender, M.; Simons, R. S.; Olmstead, M. M.; Power, P. P. *J. Am. Chem. Soc.* **2003**, *125*, 11626–11636.
95. Konu, J.; Tuononen, H. M.; Chivers, T. *Can. J. Chem.* **2009**, *87*, 461–471.
96. Armstrong, A.; Chivers, T.; Boeré, R. T. *ACS Symp. Ser.* **2005**, *917*, 66–80.
97. Schmidt, U.; Kabitzke, K.; Markau, K.; Müller, A. *Chem. Ber.* **1966**, *99*, 1497–1501.
98. Gynane, M. J. S.; Hudson, A.; Lappert, M. F.; Power, P. P. *Chem. Commun.* **1976**, 623–624.
99. Gynane, M. J. S.; Hudson, A.; Lappert, M. F.; Power, P. P. *J. Chem. Soc. Dalton Trans.* **1980**, *12*, 2428–2433.
100. Dumitrescu, A.; Rudzevich, V. L.; Romanenko, V. D.; Mari, A.; Schoeller, W. W.; Bourissou, D.; Bertrand, G. *Inorg. Chem.* **2004**, *43*, 6546–6548.
101. Bezombes, J.-P.; Hitchcock, P. B.; Lappert, M. F.; Nycz, J. E. *Dalton Trans.* **2004**, *4*, 499–501.
102. Bezombes, J.-P.; Borisenko, K. B.; Hitchcock, P. B.; Lappert, M. F.; Nycz, R. D. W. H.; Robertson, H. E. *Dalton Trans.* **2004**, *13*, 1980–1988.
103. (a) Hinchley, S. H.; Morrison, C. A.; Rankin, D. W. H.; Macdonald, C. L. B.; Wiacek, R. J.; Cowley, A. H.; Lappert, M. F.; Gundersen, G.; Clyburne, J. A. C.; Power, P. P. *Chem. Commun.* **2000**, *20*, 2045–2046; (b) Hinchley, S. H.; Morrison, C. A.; Rankin, D. W. H.; Macdonald, C. L. B.; Wiacek, R. J.; Voigt, A.; Cowley, A. H.; Lappert, M. F.; Gundersen, G.; Clyburne, J. A. C.; Power, P. P. *J. Am. Chem. Soc.* **2001**, *123*, 9045–9053.
104. Ishida, S.; Hirakawa, F.; Iwamoto, T. *J. Am. Chem. Soc.* **2011**, *133*(48), 12968–12971.
105. (a) Agarwal, P.; Piro, N. A.; Meyer, K.; Müller, P.; Cummins, C. C. *Angew. Chem. Int. Ed.* **2007**, *46*, 3111–3114; (b) Back, O.; Donnadieu, B.; von Hopffgarten, M.; Klein, S.; Tonner, R.; Frenking, G.; Bertrand, G. *Chem. Sci.* **2011**, *2*, 858–861.
106. Edge, R.; Less, R. J.; McInnes, E. J. L.; Müther, K.; Naseri, V.; Rawson, J. M.; Wright, D. S. *Chem. Commun.* **2009**, 1691–1693.
107. Loss, S.; Magistrato, A.; Cataldo, L.; Hoffmann, S.; Geoffroy, M.; Röthlisberger, U.; Grützmacher, H. *Angew. Chem. Int. Ed.* **2001**, *40*, 723–726.
108. Cataldo, H.; Dutan, C.; Mistra, S. K.; Loss, S.; Grützmacher, H.; Geoffroy, M. *Chem. Eur. J.* **2005**, *11*, 3463–3468.
109. Gouygou, M.; Tachon, C.; Koenig, M.; Dubourg, A.; Declerq, J.-P.; Jaud, J.; Etemad-Moghamad, G. *J. Org. Chem.* **1990**, *55*, 5750–5756.
110. Canac, Y.; Bourissou, D.; Baceiredo, A.; Gornitzka, H.; Schoeller, W. W.; Bertrand, G. *Science* **1998**, *279*, 2080–2082.
111. Canac, Y.; Baciердo, A.; Gigmes, D.; Schoeller, W. W.; Bertrand, G. *J. Am. Chem. Soc.* **1997**, *119*, 7579–7580.
112. Scheer, M.; Kuntz, C.; Stubenhofer, M.; Linseis, M.; Winter, R. F.; Sierka, M. *Angew. Chem. Int. Ed.* **2009**, *48*, 2600–2604.
113. (a) Ito, S.; Kikuchi, M.; Yoshifuji, M.; Arduengo, A. J., III; Konovalova, T. A.; Kispert, L. D. *Angew. Chem. Int. Ed.* **2006**, *45*, 4341–4345; (b) Sugiyama, H.; Ito, S.; Yoshifuji, M. *Angew. Chem. Int. Ed.* **2003**, *42*, 3802–3804.
114. Armstrong, A. F.; Chivers, T.; Parvez, M.; Boeré, R. T. *Angew. Chem. Int. Ed.* **2004**, *43*, 502–505.
115. Armstrong, A. F.; Chivers, T.; Tuononen, H. M.; Parvez, M.; Boeré, R. T. *Inorg. Chem.* **2005**, *44*, 7981–7991.
116. Hicks, R. G.; Hooper, R. *Inorg. Chem.* **1999**, *38*, 284–286.
117. Barclay, T. M.; Hicks, R. G.; Ichimura, A. S.; Patenaude, G. W. *Can. J. Chem.* **2002**, *80*, 1501–1506.
118. Hicks, R. G.; Öhrström, L.; Patenaude, G. W. *Inorg. Chem.* **2001**, *40*, 1865–1870.
119. Hicks, R. G. *Can. J. Chem.* **2004**, *82*, 1119–1127.
120. Tumanskii, B.; Sheberla, D.; Molev, G.; Apeloig, Y. *Angew. Chem. Int. Ed.* **2007**, *46*, 7408–7411.
121. Sasaki, S.; Sutoh, K.; Muramaki, F.; Yoshifuji, M. *J. Am. Chem. Soc.* **2002**, *124*, 14830–14831.
122. Boeré, R. T.; Bond, A. M.; Cronin, S.; Duffy, N. W.; Hazendonk, P.; Masuda, J. D.; Pollard, K.; Roemmele, T. L.; Tran, P.; Zhang, Y. *New. J. Chem.* **2008**, *32*, 214–231.
123. Wang, Y. Z.; Xie, Y. M.; Wei, P. R.; King, R. B.; Schaefer, H. F.; Schleyer, P. V. R.; Robinson, G. H. *J. Am. Chem. Soc.* **2008**, *130*, 14871–14970.
124. Back, O.; Donnadieu, B.; Parameswaran, P.; Frenking, G.; Bertrand, G. *Nat. Chem.* **2010**, *2*, 369–373.
125. Kinjo, R.; Donnadieu, B.; Bertrand, G. *Angew. Chem. Int. Ed.* **2010**, *49*, 5930–5933.
126. Back, O.; Celik, M. A.; Frenking, G.; Melaimi, M.; Donnadieu, B.; Bertrand, G. *J. Am. Chem. Soc.* **2010**, *132*, 10262–19263.
127. Biaso, F.; Cantat, T.; Mézailles, N.; Ricard, L.; Le Floch, P.; Geoffroy, M. *Angew. Chem. Int. Ed.* **2006**, *45*, 7036–7039.

128. Matni, A.; Boubbekeur, L.; Grosshans, P.; Mézailles, N.; Bernardinelli, G.; Le Floch, P.; Geoffroy, M. *Magn. Reson. Chem.* **2007**, *45*, 1011–1017.
129. Geier, J.; Harmer, J.; Grützmacher, H. *Angew. Chem. Int. Ed.* **2004**, *43*, 4093–4097.
130. Sasamori, T.; Mieda, E.; Nagahora, N.; Takeda, N.; Takagi, N.; Nagase, S.; Tokitoh, N. *Chem. Lett.* **2005**, *34*, 166–167.
131. (a) Sasamori, T.; Mieda, E.; Nagahora, N.; Sato, K.; Shiomi, D.; Takui, T.; Hosoi, Y.; Furukawa, Y.; Takagi, N.; Nagase, S.; Tokitoh, N. *J. Am. Chem. Soc.* **2006**, *128*, 12582–12588; (b) Nagahora, N.; Sasamori, T.; Hosoi, Y.; Furukawa, Y.; Tokitoh, N. *J. Organomet. Chem.* **2008**, *693*, 625–632.
132. Dutan, C.; Shah, S.; Smith, R. C.; Choua, S.; Berclaz, T.; Geoffroy, M.; Prostasiewicz, J. *Inorg. Chem.* **2003**, *42*, 6241–6251.
133. Cantat, T.; Biaso, F.; Momin, A.; Ricard, L.; Geoffroy, M.; Mézailles, N.; Le Floch, P. *Chem. Commun.* **2008**, *7*, 874–875.
134. Pi, C.; Wang, Y.; Zheng, W.; Wan, L.; Wu, H.; Weng, L.; Wu, L.; Li, Q.; Schleyer, P. V. R. *Angew. Chem. Int. Ed.* **2010**, *49*, 1842–1845.
135. Mandal, S.; Liu, R.; Reber, A. C.; Qian, M.; Saavedra, H. M.; Ke, X.; Schiffer, P.; Sen, S.; Weiss, P. S.; Khanna, S. N.; Sen, A. *Chem. Commun.* **2011**, *47*, 3126–3128.
136. Garcia, F.; Less, R. J.; Naseri, V.; McPartlin, M.; Rawson, J. M.; Wright, D. S. *Angew. Chem. Int. Ed.* **2007**, *46*, 7827–7830.
137. Konu, J.; Tuononen, H. M.; Chivers, T.; Corrente, A. M.; Boeré, R. T.; Roemmele, T. L. *Inorg. Chem.* **2008**, *47*, 3823–3831.
138. Neumüller, B.; Schmock, F.; Kirmse, R.; Voigt, A.; Diefenbach, A.; Bickelhaupt, F. M.; Dehnicke, K. *Angew. Chem. Int. Ed.* **2000**, *39*, 4580–4582.
139. Reinen, D.; Lindner, G.-G. *Chem. Soc. Rev.* **1999**, *28*, 75–84.
140. Chivers, T. *Nature* **1974**, *252*, 32–33.
141. Pokrovski, G. S.; Dubrovinsky, L. S. *Science* **2011**, *331*, 1052–1054.
142. Keppler, A. F.; Cerchiaro, G.; Augusto, O.; Miyamoto, S.; Prado, F.; Di Mascio, P.; Comasseto, J. V. *Organometallics* **2006**, *25*, 5059–5066.
143. Björgvinsson, M.; Heinze, T.; Roesky, H. W.; Pauer, F.; Stalke, D.; Sheldrick, G. M. *Angew. Chem. Int. Ed. Engl.* **1991**, *30*, 1677–1678.
144. Mueller, B.; Poleschner, H.; Seppelt, K. *Dalton Trans.* **2008**, *33*, 4424–4427.
145. Gillespie, R. J.; Kapoor, R.; Faggiani, R.; Lock, C. J. L.; Murchie, M.; Passmore, J. *J. Chem. Soc. Chem. Commun.* **1983**, 8–9.
146. Davies, C. G.; Gillespie, R. J.; Ireland, P. R.; Sowa, J. M. *Can. J. Chem.* **1974**, *52*, 2048–2052.
147. Faggiani, R.; Gillespie, R. J.; Kapoor, R.; Lock, C. J. L.; Vekris, J. E. *Inorg. Chem.* **1988**, *27*, 4350–4355.
148. Gillespie, R. J.; Passmore, J. *Adv. Inorg. Chem. Radiochem.* **1975**, *17*, 49–87.
149. Christie, K. O.; Muirhead, J. S. *J. Am. Chem. Soc.* **1969**, *91*, 7777–7778.
150. Eachus, R. S.; Sleight, T. P.; Symons, M. C. R. *Nature* **1969**, *222*, 769–770.
151. Drews, T.; Koch, W.; Seppelt, K. *J. Am. Chem. Soc.* **1999**, *121*, 4379–4384.
152. Seidel, S.; Seppelt, K. *Angew. Chem. Int. Ed.* **2000**, *39*, 3923–3925.
153. Eachus, R. S.; Symons, M. C. R. *J. Chem. Soc. Dalton Trans.* **1976**, 431–434.

This page intentionally left blank

1.14 Chalcogen–Nitrogen Radicals

RT Boeré and TL Roemmele, University of Lethbridge, Lethbridge, AB, Canada

Glossary

B3LYP A hybrid density functional theory method incorporating Becke 3-parameter pxchange and Lee, Yang, and Parr correlation terms; RB3LYP designates a restricted and UB3LYP an unrestricted calculation for closed and open shell species, respectively.

CCSD and CCSD(T) A 'coupled cluster' *ab initio* quantum electronic structure calculation that includes singles and doubles fully, and another variant that includes triples noniteratively. These are computationally expensive, very high accuracy methods and can be coupled with a variety of sophisticated basis sets such as Pople basis sets like 6-311++G(3df,3pd) or Dunning quadrupole correlation-consistent basis sets like cc-pVQZ.

hfac Hexafluoroacetylacetonate, a popular uni-negative chelating ligand for metal coordination compounds.

HOMO Highest occupied molecular orbital.

MP2 Møller–Plesset perturbation theory refers to a correlation-consistent approach to quantum electronic structure calculations.

1.14.1 Introduction and Survey

Compounds between nitrogen and the chalcogens, especially oxygen, sulfur, and selenium, are among the richest sources of open-shell species outside the transition metals and lanthanides. Only carbon compounds can compare for the range of known stable radicals.[1] The longest known examples are the gases NO$^\bullet$ (nitrogen monoxide) and $NO_2^\bullet$ (nitrogen dioxide). Even the highly reactive radical $NO_3^\bullet$ was already detected spectroscopically in 1880. NO$^\bullet$ is reactive in air with rapid oxidation to $NO_2^\bullet$ but has a vast chemistry in reducing media; in recent years, it has been discovered to have an intrinsic, beneficial role in biology as well as a harmful role in carcinogenesis; a whole branch of life sciences has grown up around nitrogen monoxide. The corresponding NS$^\bullet$ and $NS_2^\bullet$ are too reactive to isolate except in low-temperature matrices because of a much stronger tendency toward catenation. Just as elemental oxygen exists as O_2 while sulfur is the ring compound S_8, NO$^\bullet$ is a stable diatomic molecule but NS$^\bullet$ oligomerizes to diamagnetic species. Recent work has drawn attention to the importance of the monomer NS$^\bullet$ in the chemical transformation of binary and heterothiazyl compounds. The discovery of molecules such as NO$^\bullet$ and NS$^\bullet$ in interstellar dust clouds and even in comet tails has created a strong impetus for their further study in the laboratory. This chapter focuses on a systematic treatment of the fundamental types of chalcogen–nitrogen radicals, including their tendencies toward dimerization or oligomerization. Coverage is primarily of results published in the decade 2000–2011 but older literature will be cited wherever deemed necessary for comprehension or comprehensiveness.

1.14.1.1 Why Are There So Many Chalcogen–Nitrogen Radicals?

The unique position of nitrogen in the periodic system is ultimately the source of the many open-shell nitrogen compounds. As the central element in the p-block, nitrogen has the highest range of accessible oxidation states (from +5 to −3) as illustrated in Figure 1 and a number of these oxidation states are open-shell species (green-shaded boxes). In aqueous acid, the relative oxidizing strength of nitrogen–oxygen compounds is almost identical from HNO_3 to N_2 (as indicated by the constancy in the slopes of the *NV*/oxidation-state lines in Figure 1) which helps explain the facile interchange reactions between, in particular, the nitrogen oxides. Figure 1 also draws attention to the many direct sulfur analogs to nitrogen oxide radicals (yellow-shaded boxes) most of which also have selenide and telluride analogs. However, the chemical behavior is often quite different with the heavier chalcogens. Hydrazinyl radicals (purple-shaded box, Figure 1) are not considered in this article.

Figure 2 presents the electronegativity data for these elements. Just as the so-called 'diagonal relationship' has featured heavily in rationalizing the similarity of low-coordinate phosphorus and carbon, there is also a diagonal relationship connecting nitrogen and sulfur. Thus, using Allred–Rochow values for sake of argument, oxygen is more electronegative than nitrogen, but sulfur is less electronegative. Note that as a consequence of the scandide contraction, selenium and sulfur have very similar electronegativities as well as other properties, so that N, Se chemistry is expected to be very similar to N,S. In other words, such diagonal relationships do not apply to the fourth period elements. Another consequence of electronegativity is the reversal of polarity for N–O versus N–S bonds. One common consequence of this is that many scientists insist on calling the binary nitrogen sulfides, selenides, and tellurides instead sulfur, selenium, and tellurium nitrides, although this contravenes the International Union of Pure and Applied Chemistry nomenclature rules. Here for the sake of emphasizing the group relationships as well as for conforming to the naming rules, we will not adopt this convention. Nevertheless, the chemical consequences of this reversal of polarity will be highlighted as they come up. The chemistry of nitrogen is, of course, also significantly different from that of higher period elements, which explains the far lower frequency of open-shell compounds involving the heavy pnictogens (see Chapter 1.13).

It has been argued that in (unsaturated) thiazyl linkages, that is, –N=S•–, the effect of hyper-conjugative polarization of the π-electrons tends to even out the effective electronegativity difference between sulfur and nitrogen, so that the chemistry of catenated N,S compounds is subject to smaller effective dipoles than expected.[2] Following Streitweiser, the polarity of this bond is then better reflected by the Mulliken–Jaffé p-orbital electronegativities (Figure 2).[3] In any π-bond between dissimilar elements, the bonding π-orbital is always polarized toward the more electronegative center, while the antibonding π*-orbital has larger coefficients for the less electronegative element. Factoring in the orbital occupancies, both schemes result in a net transfer of π-charge from S to N but the degree is smaller using the p-orbital electronegativities. Consequently, the effective electronegativity difference between sulfur and nitrogen is smaller than expected in thiazyl linkages.

1.14.1.2 Physical Properties of Chalcogen–Nitrogen Radicals

Table 1 compiles molecular and thermodynamic constants for the most important examples of the binary open-shell species. It is often stated that nitrogen sulfide and selenide bonds are 'unstable'. It should be recognized, however, that all the binary nitrogen chalcogenides including the oxides are endothalpic and endoergous with respect to decomposition to the elements. (Moreover, while the bond energies show a steady decrease with heavier chalcogen, even NTe• has an appreciable bond energy of 220 kJ mol^{-1}.) Thus, kinetic properties will also be very important in determining the distribution of possible species and their relative reactivity. There are often several isomers to consider and for the binary compounds, high reactivity is the norm. The incorporation of heteroelements such as

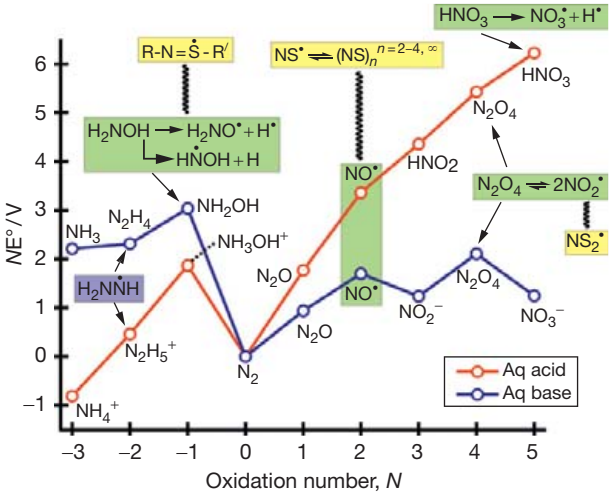

Figure 1 A Frost diagram for nitrogen in 1 M aqueous acid (red line) and 1 M aqueous base (blue line). Green-shaded boxes indicate associated free-radical species for the oxides of nitrogen; isovalent sulfides of nitrogen are in yellow-shaded boxes. Potential data taken from Shriver, D. F.; Atkins, P. W. *Inorganic Chemistry*, 3rd ed.; W. H. Freeman and Company: New York, 1999.

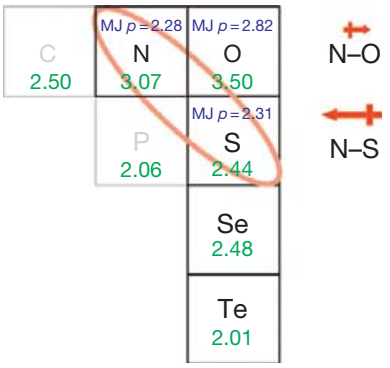

Figure 2 The so-called 'diagonal relationship' for nitrogen and the chalcogens. Numbers in green text are Allred–Rochow electronegativities; the Mulliken–Jaffé valence p-orbital electronegativity values (on the Pauling scale) are shown in blue.

Table 1 Physical properties of the most important nitrogen chalcogenide radicals

Property	*NO*	*NO_2*	*NS*	*NS_2*	*NSe*	*NSe_2*	*NTe*	*NTe_2*
mp, K	109.64[a]	261.90[a]	–	–	–	–	–	–
bp, K	121.4[a]	294.25[a]	–	–	–	–	–	–
$\triangle_{fusion}H^{\circ}$, kJ·mol^{-1}	2.300[a]	14.652[a]	–	–	–	–	–	–
$\triangle_{vaporization}H^{\circ}$, kJ·mol^{-1}	13.776[a]	38.116[a]	–	–	–	–	–	–
$\triangle_f H^{\circ}$, kJ·mol^{-1}	+90.24[a]	+33.32[a]	+283.4(2)[g]	–	–	–	–	–
$\triangle_f G^{\circ}$, kJ·mol^{-1}	+86.57[a]	+17.506[a]	+217.2(2)[g]	–	–	–	–	–
S° 273, J/deg	+207.5/273 K[a]	+240.5/273 K[a]	+222.093/ 298K[g]	–	–	–	–	–
B.D.E.	627.6[a]	465.6[a]	463±24[g]	–	370 Cal[n]	–	220 Cal[n]	–
d(*N*–*E*), Å	1.1517[b]	1.197[e]	1.4938(2)[h]	1.553 Cal[j]	1.6634 Cal[b]	1.715 Cal[p]	1.897 Cal[n]	1.911 Cal[q]
∠*E*–*N*–*E*°	–	134.3[e]	–	152.3 Cal[j]	–	146(5) Cal[p]	–	143.7 Cal[q]
ν(*N*–*E*), cm^{-1}	1877[a]		1204.089[i]	1225.2[m]	944.5422[o]	1019[p]	783.5, 790.3[q]	973.5[q]
Mag. mom, BM	1.82[a]	1.72[e]		Variable, see Bohle[8]	1.718[o]		–	–
$A_{iso}(^{14}N)$, mT	0.794[c]	5.37[f]	0.765[j]	2.11 Cal[j]	–	–	–	–
A_{iso}(E), mT	–	–		0.56 Cal[j]	–	–	–	–
$\triangle H$ 1st I.E., eV	9.25(2)[a]	11[a]	9.85±0.28[k]	7.82 Cal[b]	8.7 Cal[b]		7.2 Cal[b]	
$\triangle H$ 1st E.A., eV	0.024 0.016 Cal[b]	4.0	1.194(11)[k]; 1.047 Cal[b]	1.60[b]	1.352 Cal[b]	–	–	–
D.M., *D*	+0.16 0.18 Cal[b]	+0.39[e]	−1.86(3)[l] −1.73 Cal[b]	–	1.99 Cal[b]	–	–	–
Spin–orbit CC, cm^{-1}	119.82[d]	–	223[b]	–	891.89[o]	–	–	–
Bond order	2.5	1.5	2.5	1.5	2.5	1.5	2.5	1.5
Color	Colorless	Red	–	–	–	–	–	–

Standard deviation errors are given within parentheses modifying the last digit: 2.34(8) means 2.34 ± 0.08. Data are experimental values unless marked 'Cal' = calculated.

Ref: [a]Butler, A. R.; Nicholson, R. *Life, Death and Nitric Oxide*; Cambridge: Royal Society of Chemistry, 2003.

[b]Kalcher, J. *Phys. Chem. Chem. Phys.* **2002**, *4*, 3311–3317.

[c]Miller, R. J.; Feller, D. *J. Phys. Chem.* **1994**, *98*, 10375.

[d]Atkins, P.; Friedman, R. *Molecular Quantum Mechanics* 4th Ed., Oxford, 2005, pp 383.

[e]Bohle, D. S. In Hicks, R. G., Ed. *Stable Radicals: Fundamentals and Applied Aspects of Odd-Electron Compounds*, Wiley, 2010, pp. 147–171.

[f]Adrian, F. J. *J. Chem. Phys.* **1962**, *36*, 1692–1693.

[g]Lodders, K. J. Phys. Chem. Ref. Data **2003**, *333*, 357–367.

[h]Huber, K.P.; Herzberg, G. *Constants of Diatomic Molecules*, vol. IV., Van Nostrand Reinhold, New York, 1979.

[i]Matsumura, K. Kawaguchi, K.; Nagai, K.; Yamada, C.; Hirota, E. *J. Mol. Spectrosc.* **1980**, *84*, 68–73.

[j]Boeré, R. T.; Tuononen, H. M.; Chivers, T.; Roemmele, T. L. *J. Organomet. Chem.* **2007**, *692*, 2683–2696.

[k]Burnett, S. M.; Feigerle, C. S.; Stevens, A. E.; Lineberger, W. C. *J.Phys.Chem.* **1982**, *86*, 4486.

[l] Byfleet, C. R.; Carrington, A.; Russell, D. K. *Mol. Phys.* **1971**, *20*, 271–277.

[m]Hassanzadeh, P.; Andrews, L. *J. Am. Chem. Soc.* **1992**, *114*, 83–91.

[n]Rekhis, M.; Ouamerali, O.; Joubert, L.; Tognetti, V.; Adamo, C. *THEOCHEM* **2008**, *863*, 79–83.

[o]Brown, J. M.; Uehara, H. *J. Chem. Phys.* **1987**, *87*, 880–884.

[p]Andrews, L.; Hassanzadeh, P.; Lanzisera, D. V.; Brason, G. D. *J. Phys. Chem.* **1996**, *100*, 16667–16673.

[q]Sundarajan, K.; Sankaran, K.; Kavitha, V. *J. Mol. Struct.* **2008**, *876*, 240–249.

carbon or phosphorus, which induce kinetic stability, enormously extends the range of isolable species, especially for nitrogen sulfides and selenides. For this reason, the number of stable free radicals among such heteroelement species is much greater than for binary compounds, so extensive that herein we can only indicate the major classes with a focus on their relationship to the binary radicals.

1.14.1.3 Further Reading

Very thorough coverage of both nitrogen oxygen and sulfur chemistry can be found in Greenwood and Earnshaw.[4] Useful and quite up-to-date articles on nitrogen oxides (both inorganic and bioinorganic), sulfur nitrogen compounds, and articles on selenium and tellurium chemistry that include the nitrogen chemistry are found in the 2005 edition of the *Encyclopedia of Inorganic Chemistry*.[5] The chemistry of the oxides of nitrogen is described in standard textbooks and collective volumes including the first edition of *Comprehensive Inorganic Chemistry*.[6] Nitrogen oxide radicals feature prominently in the famous text book *The Organic Chemistry of Nitrogen* by Sidgwick[7] and in the book chapter by Bohle.[8] The modern organic chemistry of NO$^{\bullet}$ has recently been comprehensively reviewed.[9] For nitrogen chalcogenides, the comprehensive but now dated book by Heal can still be recommended,[10] as can insightful reviews by Gleiter,[11] Chivers,[12] and Oakley[2] and the recent book by Chivers.[13] Electron paramagnetic resonance (EPR) data for nitrogen chalcogenides up to 1990 were

reviewed by Preston and Sutcliffe,[14] and electrochemistry data up to 2000 have been compiled.[15] Metal complexes of S,N compounds have recently been reviewed by Preuss.[16] Banister and later Rawson have each published reviews on the superconducting polymer $(SN)_x$.[17,18] Several chapters in the book by Hicks deal with nitrogen oxide, nitroxide, and nitrogen sulfide radicals.[1]

1.14.2 Nitrogen Oxide Radicals

There are both diamagnetic and paramagnetic oxides of nitrogen, and the three primal open-shell species $NO^{\bullet}$, $NO_2^{\bullet}$, and $NO_3^{\bullet}$ continue to attract great attention. The first two of these are extremely common and are routinely prepared by beginning students as part of their laboratory practicums; $NO_3^{\bullet}$, by contrast, is a transient species sensitive to light but is considered one of the most reactive constituents of nighttime urban smog. These monomers and their various association products (**Figure 3**) act as coupled reservoirs in the complex equilibria that regulate the family of nitrogen oxides in the atmosphere.[19] Their role in atmospheric pollution at low elevation as well as their effect on the ozone balance in the troposphere and stratosphere has been recognized.[20,21] The fact that the oxides of nitrogen have the lowest ionization energies among the abundant components of the atmosphere contributes to their importance.[22] The direct combination of N_2 and O_2 requires high temperatures and a catalyst, including internal combustion engines, where the production of smog-producing 'NO_x' depends on the engine design and operating conditions. Serious health effects of smog have, in turn, required emission controls on modern combustion engine vehicles, including exhaust gas recirculation, the open particulate matter after treatment system usually combined with an oxidation catalyst which increases the ratio of $NO_2^{\bullet}$ to $NO^{\bullet}$, and a selective catalytic reduction system in order to reduce NO_x. SCR is an after-treatment method that requires an urea-based additive, AdBlue.[23]

1.14.2.1 Nitrogen Monoxide ($NO^{\bullet}$) and Its Dimer $(NO)_2$

Nitrogen monoxide, commonly known as nitric oxide, was first described by the Belgian chemist Jan Baptist van Helmont in 1620 from pouring nitric acid over metal filings.[24] However, its identity was established by Priestley who first recognized it as a distinct compound.[25] It is best prepared in the laboratory by reaction of ferrous ion with nitrite in aqueous solution under protection from air since the reaction with oxygen to $NO_2^{\bullet}$ is spontaneous.[26] Nitrogen monoxide constitutes the simplest radical that exists at room temperature (RT) as a neat substance.[9] It forms an integral part of interstellar molecular clouds in star-forming regions and is a trace component of several planetary atmospheres.[27–29] The lower atmosphere of Mars, for instance, contains 1.7 ppb of $NO^{\bullet}$. Concentrations of 5.5 ± 1.5 ppb of $NO^{\bullet}$ were detected in altitudes of 60 km above Venus' surface.[30–33]

1.14.2.1.1 The anomalous electronic structure of $NO^{\bullet}$ and EPR spectroscopy

The molecular orbital (MO) description of $NO^{\bullet}$ is shown schematically in **Figure 4** and is closely related to those of the diatomic 'parents' N_2 and O_2. Electronically, $NO^{\bullet}$ most closely resembles O_2 with which it has in common a partly occupied, degenerate, π^* orbital, for example, by the manner in which both coordinate to many transition-metal ions. The magnetic moment μ of $NO^{\bullet}$ is much smaller than that predicted from the

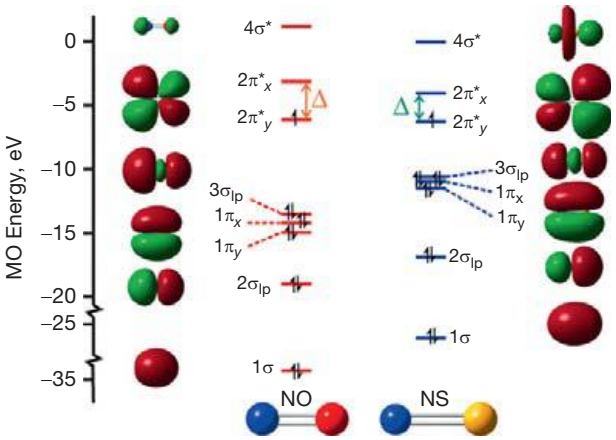

Figure 4 Valence molecular orbital diagrams for $NO^{\bullet}$ and $NS^{\bullet}$ based on UB3LYP/6-311++(2df,2p) calculations. Note the breaks in the energy scale and that the unrestricted calculation separates the degeneracy of $2\pi^*$ (by Δ).

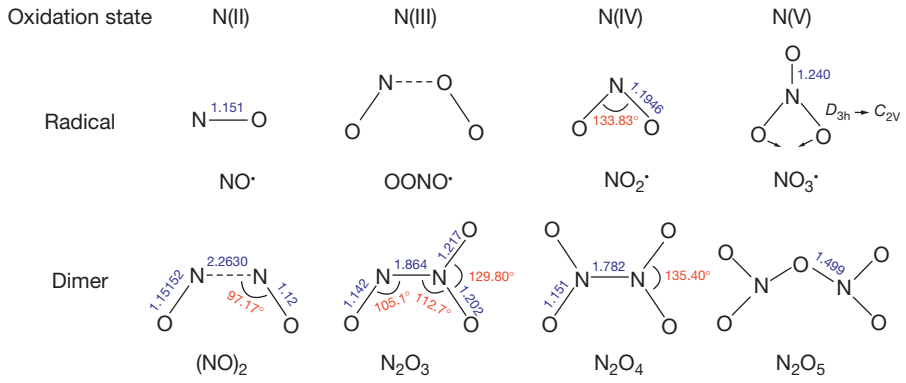

Figure 3 Geometries of neutral nitrogen oxide radicals and their dimers compiled from experiment and high-level quantum calculations (distances in Å and bond angles in degrees).

valence $(1\sigma)^2(2\sigma_{lp})^2(3\sigma_{lp})^2(1\pi)^4(2\pi^*)^1$ configuration of the $X\ ^2\Pi$ ground state; it varies from 1.55 Bohr-magneton (BM) at 120 K to 1.85 BM at 300 K.[8] The electronic and magnetic behavior of NO$^\bullet$ reflects Hund's 'case (a)' in which (1) the electron orbital angular momentum is strongly pinned to the internuclear axis by the Coulombic field of the nuclei and (2) the spin angular momentum is aligned with the orbital angular momentum by spin–orbit coupling. When mediated by molecular rotation, this results in a component $\Omega\hbar$ of the total angular momentum parallel to the axis which is related to the orbital and spin angular momenta by $\Omega = \Lambda + \Sigma$ (**Figure 5(a)**). For the $^2\Pi$ state of NO$^\bullet$, where $\Lambda = \pm 1$ and $\Sigma = \pm 1/2$ Ω is therefore equal to either $\pm 1/2$ or $\pm 3/2$; of these the latter is found to be 121 cm^{-1} higher in total energy.[34] The ground $^2\Pi_{1/2}$ state is approximately diamagnetic ($g_J \approx 0$) due to cancellation of Λ and Σ contributions to Ω, but at RT the intensely paramagnetic $^2\Pi_{3/2}$ electronic state is thermally populated ($kT \approx 200$ cm^{-1}) and a number of rotational states are occupied. Only the lowest rotational state is observable with EPR instruments operating in the most common frequency range (X-band) because g_J becomes extremely small for the higher levels. It is often incorrectly stated that the EPR spectrum of NO$^\bullet$ is unobservable, whereas in fact the strong spectrum shown in **Figure 5 (b)** is taken from an undergraduate experiment (!) developed by Whitaker using a standard research-grade spectrometer and a conventional TE_{102} cavity resonator (note that the magnetic field must be at least 0.9 T).[35] For those unfamiliar with EPR spectroscopy in the gas phase, it is important to emphasize that the large gas-phase $A_{gas}(^{14}N)$ hyperfine splitting of 2.705(9) mT cannot be directly compared to the isotropic Fermi contact couplings measured in condensed phases; however, by making use of the Frisch and Foley magnetic hyperfine structure parameters *a–d*,[36] the equivalent Fermi term $A_{iso}(^{14}N) = 0.794$ mT can be extracted from the gas-phase value.[37] The calculated value at the UB3LYP/6-311++(2df,2p) level of theory, $A_{iso}(^{14}N) = 0.50$ mT, is in reasonable agreement with this value. In more specialized EPR experiments, it is advantageous to use a cylindrical TM_{011} resonator and to operate at lower frequency. For an example where both the $J = 3/2$ and 5/2 rotational levels were observed in the L-band frequency range (approximately one-third of the X-band frequency), the reader is directed to the paper by Brown.[36] For a detailed explanation of the peculiarities of small-molecule gas-phase EPR spectroscopy, the excellent treatment in Chapter 7 of the classic text by Weil, Bolton, and Wertz is highly recommended[38] (see **Chapter 9.13**).

(i) EPR spectroscopy of NO$^\bullet$ on surfaces
When NO$^\bullet$ is adsorbed to a surface ('L' in **Figure 5(c)**), an EPR signal may be observed due to (1) quenching of the orbital angular momentum by the electric field of the adsorption site which transforms $^2\Pi_{1/2}$ into a pure spin state and (2) lifting of the degeneracy of the $2\pi^*$ orbitals with the result that the energy splitting Δ (**Figure 4**) controls the *g* value of the adsorbed NO$^\bullet$ at close to the free-electron value (2.002). In fact, NO$^\bullet$ is one of the most important probes for surfaces of MO_x (M = Mg, Zn, Ti, Al, Sn, and Ce) and zeolites as interpreted through (anisotropic) EPR spectra which display intense signals with large *g*- and *A*-value anisotropies.[39] These workers also monitored the effect of concentration which shows a decrease in signal intensity above 2×10^{19} molecules g^{-1} attributed to formation of diamagnetic dimers $(NO)_2$ (see **Section 1.14.2.1.2**). A detailed and informative review of the use of surface-localized inorganic radicals to probe surfaces has recently been published.[40]

(ii) EPR spectroscopy of NO$^\bullet$ in liquids and 'spin trapping'
The situation that pertains in the liquid phase is different from both the gas- and solid-adsorbed cases. The large *g*-value anisotropy combined with the random tumbling of the molecules contributes to a very powerful relaxation mechanism for the electron spin resulting in complete collapse of the signal. Reliable EPR data for NO$^\bullet$ in solution have never been reported and even inert gas matrices have insufficient grip on the almost-spherical radicals to quench the orbital angular momentum.[41] Attempts to freeze out molecular motion in donor solvents also fail, likely due in this case to the formation of diamagnetic $(NO)_2$ upon cooling. Detection of NO$^\bullet$ in solution, therefore, entirely depends on the use of suitable spin traps (a spin trap is a species that interacts with a free radical to produce a secondary radical favorable for EPR detection under the applicable environmental conditions). It turns out that coordination to a metal ion has a similar effect to that observed in surface probes (see **Section 1.14.2.1.4**). Perhaps the most important assay for NO$^\bullet$ in solution and in biological samples for several decades has made use of

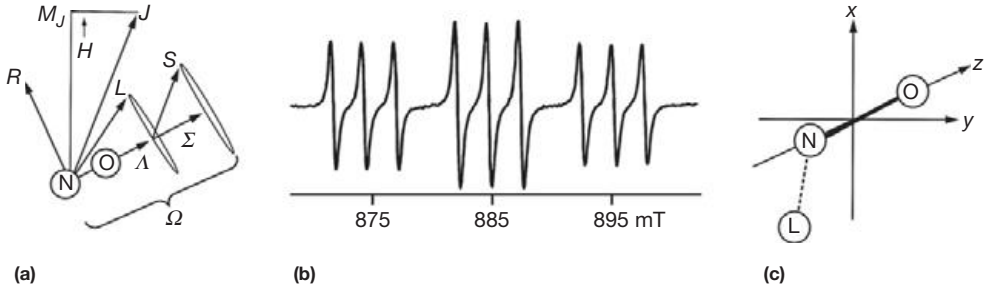

Figure 5 (a) Vector diagram showing the orbital (Λ) and spin (Σ) contributions to the magnetic moment of NO$^\bullet$ as drawn for the $^2\Pi_{3/2}$ state; in the $^2\Pi_{1/2}$ state, the vector Σ points in the opposing direction. (b) A gas-phase X-band EPR spectrum taken of $\leq$1 mbar NO$^\bullet$ at 298 K. The center of the spectrum is at 885 mT ($g_J = 4/5 = 0.77$). The three 1:1:1 triplets are due to ^{14}N hyperfine splitting $A(^{14}N) = 2.705(9)$ mT but have slightly uneven line spacing due to electron–quadrupole coupling from the $I = 1$ nucleus; the larger 3:4:3 intensity triplet is due to the (field dependent) $3/2 \rightarrow 1/2$, $1/2 \rightarrow -1/2$, $-1/2 \rightarrow -3/2$ second-order Zeeman interaction mediated by rotational coupling. (c) Orientation of a surface-adsorbed NO$^\bullet$ radical. Adapted from Whittaker, J. W. *J. Chem. Educ.* **1991**, *68*, 421–423, copyright (1991) American Chemical Society.

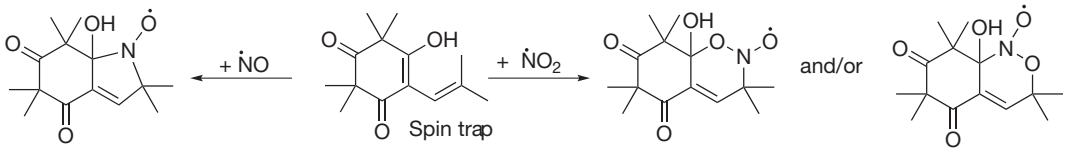

Scheme 1 5-Hydroxy-2,2,6,6-tetramethyl-4-(2-methylprop-1-en-yl)cyclohex-4-ene-1,3-dione, a new cheletropic spin trap for NO• and NO^{2}• detection.[43]

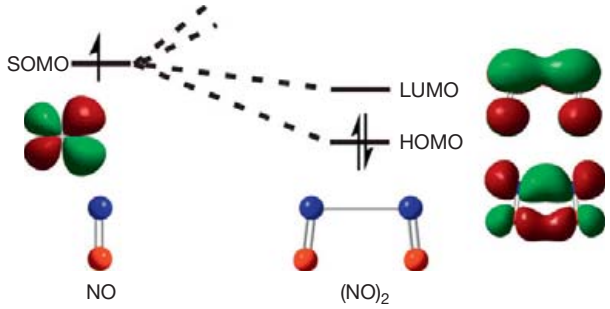

Figure 6 The mode of dimerization in $(NO)_2$ involving so-called 'diffuse π^*–π^*' bonding, a modality which has been found to be ubiquitous among nitrogen–chalcogen-free radicals and becomes a dominant factor when E = S, Se. Adapted from Zhao, Y. L.; Bartberger, M. D.; Goto, K.; Shimada, K.; Kawashima, T.; Houk, K. N. *J. Am. Chem. Soc.* **2005**, *127*, 7964–7965, copyright (2010) American Chemical Society.

the dithiocarbamate complex $[Fe(S_2CNEt_2)_2]$; like NO•,[42] this complex, on its own, is EPR silent but the adduct $[Fe(S_2CNEt_2)_2(NO)^{\bullet}]$ displays a characteristic triplet EPR signal with $g = 2.035–2.040$ and $A(^{14}N) = 1.26$ mT.[42] However, not all samples are suitable for this assay and alternatives have been proposed, including a recently reported organic chelotropic trap suitable for spin trapping of both NO• and $NO_2^{\bullet}$ (Scheme 1).[43]

1.14.2.1.2 Oligomerization of NO•: the cis(ONNO) dimer

NO• forms a weakly bound dimer, *cis*-ONNO, which is close to rectangular in shape but, by most structure determination methods, is shown to have a larger OO than NN separation (Figure 3).[44–46] The 'bond' consists of a diffuse side-on overlap between a $2\pi^*_x$ singly occupied molecular orbital (SOMO) from each contributing monomer (Figure 6); the bond energy in the gas phase is only 8.5(5) kJ mol^{-1} which is consistent with the extremely long N...N separation, and yet this is sufficient to induce spin pairing such that $(NO)_2$ is diamagnetic in all phases.[47] In this dimer, the bond order within the monomers is only marginally affected by the interaction. Furthermore, the concomitant side-on π-overlap of the $2\pi^*_y$ lowest unoccupied molecular orbitals (LUMOs) is also weakly favorable but this level remains unoccupied in the dimer. $(NO)_2$ remains a very challenging species to describe due to the open-shell electronic structure of NO• monomer.[19,22,46,47] While it is tempting to neglect such an obviously weak interaction, there is in fact strong evidence that the formation of $(NO)_2$, despite the very low value of $K^{298} = 6.6 \times 10^{-5}$ atm^{-1}, is a major factor in the chemical behavior of nitric oxide, including the all-important atmospheric chemistry of NO_x (see Section 1.14.2.3.3). Both inter- and intramolecular diffuse π^*–π^* bonding is a constant theme in the chemistry of the nitrogen chalcogenides and is much stronger for the heavier chalcogens.

1.14.2.1.3 NO• in living cells

The 1998 Nobel Prize in Medicine was awarded to Furchgott,[48] Ignaro,[49] and Murad for their discoveries concerning 'nitric oxide as a signaling molecule in the cardiovascular system' (Figure 7). NO• is thus responsible for vascular smooth muscle relaxation, vindicating the early proponents of its biological role and explaining the active agent in various therapies such as the use of nitroglycerin (which had been in use to treat angina pectoris since 1878 without it being recognized as a source of NO• within cells). In addition, this extremely oxygen-sensitive free radical can act as a cytotoxic mediator of the immune system and as a neurotransmitter in the central nervous system.[50,51] Current interest in the biology of NO• remains intense, one evidence of which is the appearance of a dedicated journal, *Nitric Oxide: Biology and Chemistry* which achieved a 2011 impact factor of 3.384. The biosynthetic source of NO• is from the oxygenation of arginine (a substituted guanidine) to citrulline (a substituted urea) catalyzed by the heme protein nitric oxide synthetase (See Figure 8, which also shows alternate sources and consumption of NO• in living cells.)[8]

Sulfur, in the form of cysteine, is involved in biological NO• chemistry. *S*-Nitrosylation is the covalent attachment of NO• to the sulfur moiety of a cysteine, which provides an additional signaling pathway in addition to the direct diffusional passage of NO• between cells.[52] The modified cysteine residue of *S*-nitrosohemoglobin was previously identified as a distorted *S*-nitrosothiol (RSNO) or an *S*-hydroxyamino radical (RSN•OH) but now there is evidence that a thionitroxide (RSNHO•, *S*-aminyloxyl radical) is likely the observed species; an oxidation reaction converts this species to RSNO (Scheme 2).[53–55] Despite this close association of thiols and NO•, there is as yet no evidence for the involvement of nitrogen sulfide radicals (Section 1.14.3.1) in biological systems.

1.14.2.1.4 NO• and transition metals: nitrosyl complexes

The transition-metal chemistry of the nitrosyl ligand has seen a tremendous revival since the discovery of nitric oxide as an essential biological molecule.[56] The relevant coordination chemistry has been thoroughly reviewed and the importance of the redox activity of NO• in solution was stressed.[57] Other recent reviews deal with infrared (IR) spectroscopy and density functional theory (DFT) calculations of NO• complexes,[58] photoinduced linkage isomerism,[59] coordination and organometallic chemistry,[60] nitrogen nuclear magnetic resonance (NMR) spectroscopy,[61] the solid-state structures of metalloporphyrin nitrosyls,[62] and mechanisms of reductive nitrosylation in copper and iron systems.[63] An EPR study of the nitroprusside trianion $[(NC)_5Fe(NO)]^{3-}$ provides support for NO• as a ligand in the radical state,[64] and linkage isomerism in the same complex has been studied by transient IR spectroscopy.[65]

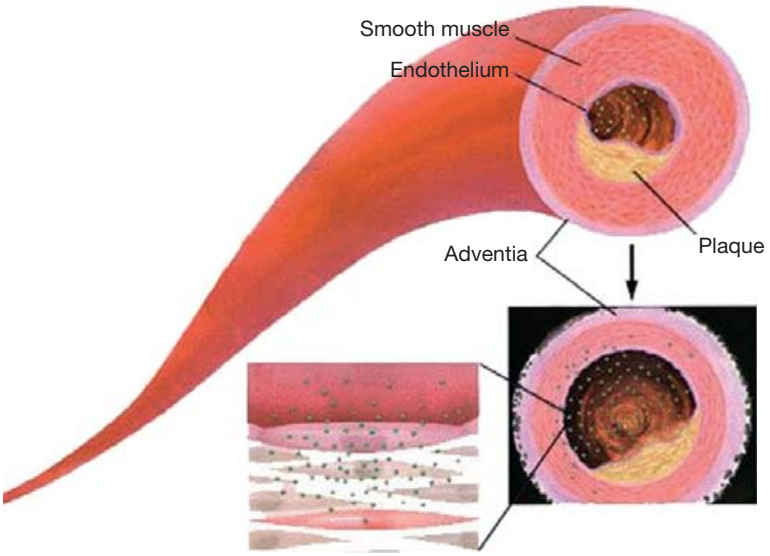

Figure 7 The clinical use of nitroglycerine to treat angina pectoris emulates the endogenous release of NO• as a signaling agent to relax (expand) small blood vessels. Adapted from "The Nobel Prize in Physiology or Medicine 1998". Nobelprize.org. Accessed 18 Oct 2011; http://www.nobelprize.org/nobel_prizes/medicine/laureates/1998/.

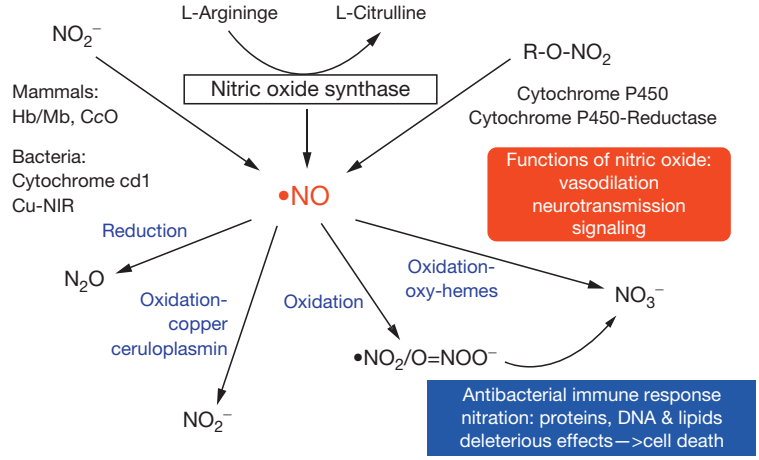

Figure 8 Schematic illustration of currently recognized pathways for production and consumption of NO• in biological systems. Reprinted from Schopfer, M. P.; Wang, J.; Karlin, K. D. *Inorg. Chem.* **2010**, *49*, 6267–6282, copyright (2010) American Chemical Society.

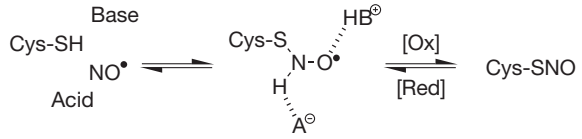

Scheme 2 S-Nitrosylation of cysteine.[53–55]

The noninnocence of NO• in nitrosyl ruthenium complexes has been stressed.[66] While there are many ways to synthesize nitrosyl complexes, the reaction of a metal nitride complex with an oxygen source is important because this method can be extended to heavier chalcogens (see **Sections 1.14.3.1.6** and **1.14.4.1.3**).[67] A similar reaction has been reported for an unusual square planar ruthenium complex [$(N(SiMe_2CH_2P^tBu_2)_2)$RuN].[68] The first insertion reactions of NO• into lanthanide–carbon bonds has recently been reported[69] and $[H(CH_3)_4C_5]_3$UNO is the first f-element nitrosyl complex.[70]

1.14.2.2 Nitrogen Dioxide (NO_2•) and Its Dimer (N_2O_4)

NO_2• has been known since the 1770s from the work of Priestley and others and it is spontaneously formed when nitric oxide reacts with oxygen or air.[25] It is an intensely colored red-brown gas which is corrosive and highly toxic. Although it can be purchased in cylinders, it is best prepared just before use for laboratory work by the thermal decomposition of ultrapure lead nitrate, thus avoiding mixtures caused by disproportionation reactions.

1.14.2.2.1 Electronic structure of $NO_2^•$ and EPR spectroscopy

$NO_2^•$ is a 17-electron radical with a gently bent structure (Figure 3) and its shape is a consequence of Walsh bending caused by partial occupancy of the π_3 MO of the 16-electron linear system (e.g., the CO_2 electronic structure). It has an $\tilde{X}^2A_1$ electronic ground state with a well-defined paramagnetism represented by the $S = 1/2$ spin state with $\mu = 1.72$ BM at RT. Unlike $NO^•$, $NO_2^•$ is a σ-radical and the unpaired electron is concentrated 50% on N and 25% on each O atom (the $4a_1$ SOMO, see Figure 10). The EPR spectrum has been detected in the gas phase but it is extremely complex due to coupling of the electron spin to the molecular rotation of the asymmetric top molecule; at a pressure of 0.03 mbar well over 200 lines have been observed.[71] Pressure broadening above 1 mbar results in partial collapse of the rotational fine structure resulting in the expected 1:1:1 triplet with an apparent $A(^{14}N) = 5.09$ mT.[72] The rotationally coupled spectrum is further complicated by centrifugal distortion in the rotational motion at higher rotational states; a computer fitting of data taken from EPR and laser magnetic resonance has resulted in improved fits to more than 50 molecular parameters.[73] The corrected value from this analysis for $A(^{14}N) = 147.3(7)$ MHz which, while not directly comparable to the coupling in mT because of uncertainty in the g value, is in good agreement with 144.4 MHz from a UB3LYP/6-311G++(2df) calculation. $NO_2^•$ in an argon matrix at 4.2 K has an axial EPR spectrum with $g_{||} = 1.9920(5)$, $g_\perp = 2.0033(5)$, and $A_{iso}(^{14}N) = 5.34$ mT.[72] An extensive re-investigation of solution-phase EPR spectra of $NO_2^•$ concluded that only broad lines (50–120 mT wide) with g-values ranging from 1.999 to 2.176 are obtained in a range of solvents from water to hexane at 290 K to the limit of detectability; at lower temperatures, the samples become diamagnetic due to formation of N_2O_4. The naively expected 1:1:1 triplet signals which are often reported for $NO_2^•$ in organic solvents are actually due to nitroxide-type radicals resulting from reaction of $NO_2^•$ (or perhaps $NO^•$ as a trace contaminant) with the solvent or solvent impurities.[74] EPR has been used to determine the dissociation equilibrium constant of N_2O_4 by measurements of $NO_2^•$.[75] Spin trapping of $NO_2^•$ in solution can lead to adducts with sharper and hence more easily detectable spectra (Scheme 1; see Chapter 9.13).[43]

A compilation of EPR parameters for $NO_2^•$ radicals trapped on surfaces and in noble-gas matrices is available.[76] In their recent comprehensive review, Chiesa et al. point out that the high reactivity of $NO_2^•$ limits its use as a surface probe except in the case of relatively inert oxides or Vycor glass.[40] However, where it can be used, the bent shape (asymmetric top) and high spin density on N render this molecule particularly interesting for probing surface dynamics (Figure 9).

1.14.2.2.2 Oligomerization of $NO_2^•$ – the D_{2h} dimer N_2O_4

Dinitrogen tetroxide is used extensively as a reagent in organic synthesis (nitration reactions among others). Another important commercial use is as the oxidant in hypergolic rocket engines (that is, where mixing with fuels such as methylhydrazine leads to spontaneous combustion). Its structure (Figure 3), which is well known in the gas phase from electron-diffraction measurements as well as by X-ray diffraction from crystals, poses some intriguing questions.[76,77] The electronic structure of N_2O_4 remains an area of active investigation (Figure 10) and the odd features of the structure: the very long (1.78 Å compared to 1.47 Å in N_2H_4) and weak (57.3 kJ mol^{-1}) N···N bond and the preference for co-planarity in the absence of π bonding continue to challenge theory.[78] There is general agreement that: (1) the two $NO_2^•$ components have essentially the structure of free NO_2, (2) the D_{2d} (twist) structure of N_2O_4 is a transition state (maximum) in the rotational barrier, and (3) there is no barrier to dissociation of N_2O_4 into its constituents.[19,79–81] Natural bond orbital analysis has shown that the high barriers to rotation in both O_2NNO_2 and $ONNO_2$ arise principally from a combination of *cis* O–O interactions and hyperconjugation.[80] Delocalization of electrons from n_{2p} lone pairs of the O atoms into the central σ_{NN}^* antibond modulates the strength of the 1,4 interactions, stabilizing the planar forms of these molecules slightly relative to the twisted ones. Collectively, these are more important than π-bonding (Chapters 9.01 and 9.03).

1.14.2.3 Further Oxidation of NO_x

1.14.2.3.1 The peroxynitrite radical OONO• and the mechanism for oxidation of NO•

In addition to its self-dimerization to $(NO)_2$, $NO^•$ is now known to form adducts in the gas phase with many small molecules, including CO_2, Ne, Ar, H_2, HF, C_2H_4, and C_2H_2.[7] Of particular importance is the possibility of forming adducts with O_2, specifically the open-shell doublet $OONO^•$, the role of which in the oxidation of nitric oxide to nitrogen dioxide remains controversial. In high-level *ab initio* multireference CASSCF and CI studies the $OONO^•$ radical was predicted to be unbound,[82] while neutralization–reionization mass spectrometry studies support

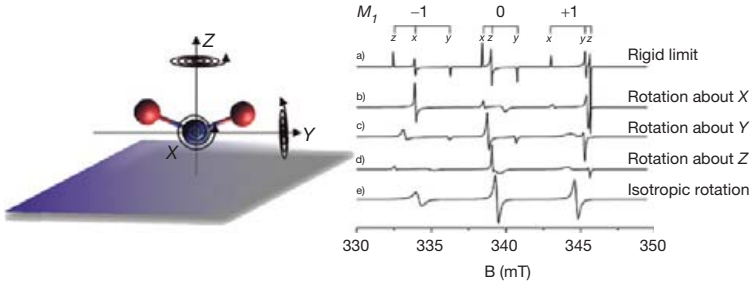

Figure 9 A symmetric top molecule such as $NO_2^•$ provides a very sensitive surface probe because the EPR spectra are very distinct for different modes of rotation. Reprinted from Chiesa, M.; Giamello, E.; Che, M. *Chem. Rev.* **2010**, *110*, 1320–1347, copyright (2010) American Chemical Society.

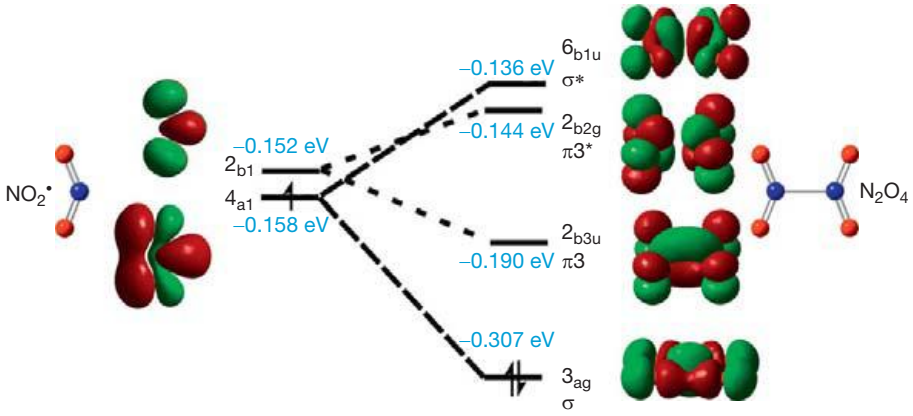

Figure 10 Partial MO level diagram for the dimerization of $NO_2^{\bullet}$ based on UB3LYP/6-311++(2df,2p) calculations. The π-bonding MO $2b_{3u}$ appears to be a good bonding orbital, yet addition of two more electrons to fill this level actually leads to separation into two NO_2^- ions.

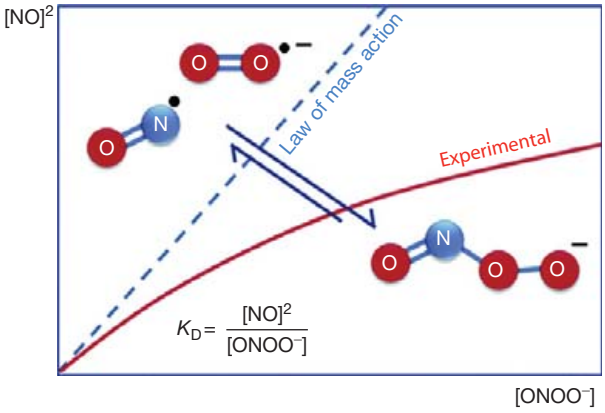

Figure 11 The deviation of the rate law for the reaction between nitric oxide and superoxide is attributed to a diffusion-controlled distance-dependent reaction rate constant ($k_f^{310K} \geq 7.5 \times 10^9\ M^{-1}\ s^{-1}$). Reprinted from Botti, H.; Moller, M. N.; Steinmann, D.; Nauser, T.; Koppenol, W. H.; Denicola, A.; Radi, R. *J. Phys. Chem. B* **2010**, *114*, 16584–16593, copyright (2010) American Chemical Society.

its existence.[83] A gas-phase EPR study has concluded that $OONO^{\bullet}$ ($g = 2.014$) is an intermediate ($t_{1/2} = 0.1$ s) in the autooxidation of $NO^{\bullet}$.[84] These workers also isolated a red substance ($\lambda_{max} = 500$ nm) from the reaction at high concentration of nitric oxide and oxygen in 2-methylbutane at 113 K which they assign to ONOONO, that is, from further reaction of the peroxynitrite radical with a second equivalent of $NO^{\bullet}$. The EPR spectrum of $OONO^{\bullet}$ was previously detected in a frozen H_2SO_4 matrix and is axial with $g_{||} = 2.048$, $g_{\perp} = 2.003$, and $A(^{14}N) = 0.35$ mT.[85] A recent matrix study employing the co-deposition of $Ne/NO^{\bullet}$ and Ne/O_2 discovered strong, structured charge-transfer bands with a $\lambda_{max} = 275$ nm attributed to transfer of an electron from $NO^{\bullet}$ to O_2 in a weak van der Waals complex between the two.[86] A very thorough matrix IR study supports the two-step mechanism for the autooxidation of $NO^{\bullet}$ first proposed by McKee.[87,88] The thermochemistry of all species involved in atmospheric interconversion of the various nitrogen oxides has been investigated using high-level computational methods.[19] Two detailed computational studies at the complete active space (CAS) level of theory have investigated this mechanism. These workers found that a balanced treatment of both dynamic and static electron correlation is necessary for the correct energy estimation for intermediates; when this is taken into account, it provides strong support for the two-step mechanism of $NO^{\bullet}$ oxidation.[89,90]

1.14.2.3.2 The peroxynitrite ion and $OONO^{\bullet}$ in solution

A related species that is of intense current interest to the biological role of $NO^{\bullet}$ is the peroxynitrite ion $OONO^-$ which is formed by the fast spin-allowed reaction between nitric oxide and superoxide anion radical: $NO^{\bullet} + O_2^{\bullet -} \rightarrow OONO^-$. Recent work has shown that this reaction depends on [$OONO^-$], thus contradicting the law of mass action (Figure 11).[91] A fascinating voltammetric experiment using microelectrodes in a human tissue cell (fibroblast) has resulted in measurement of the electrical signature for the oxidation of peroxynitrite with $E^0 = +0.27$ versus SCE; the lifetime of the electrogenerated $OONO^{\bullet}$ radical was determined as $t_{1/2} \approx 0.1$ s.[92] This discovery has since become the basis of several assays for the detection of $OONO^-$.[93]

1.14.2.3.3 Nitrogen trioxide ($NO_3^{\bullet}$)

The transient trigonal radical $NO_3^{\bullet}$ (Figure 3) was first detected spectroscopically around 1880[94] but was correctly identified in the 1930s[95]; it remains one of the most complicated molecules known to chemical physics.[95] Like the other nitrogen oxides, it is a free radical and the open-shell electronic structure leads to similar complexities. For example, the basic trigonal geometry is subject to a pseudo-Jahn–Teller distortion even in the ground $\tilde{A}^2\ A'_2$ electronic state resulting from remarkably strong vibronic coupling to excited states that have a distorted geometry, thereby converting the D_{3h} to a planar C_{2v} geometry. The question of the true geometry of the ground state has yet to be resolved but this reflects a fundamental property: the adiabatic potential energy surface of the electronic ground state is extremely flat with respect to the e' vibrational mode of distortion. The absorption spectrum (Figure 12(b)) shows very strong vibrational coupling because excitation involves an oxygen nonbonding p-electron being promoted to a strongly N–O σ* level, ($\tilde{B}^2E' \leftarrow \tilde{X}^2A_{2'}$ transition). There is intense interest in this, the most transient of the

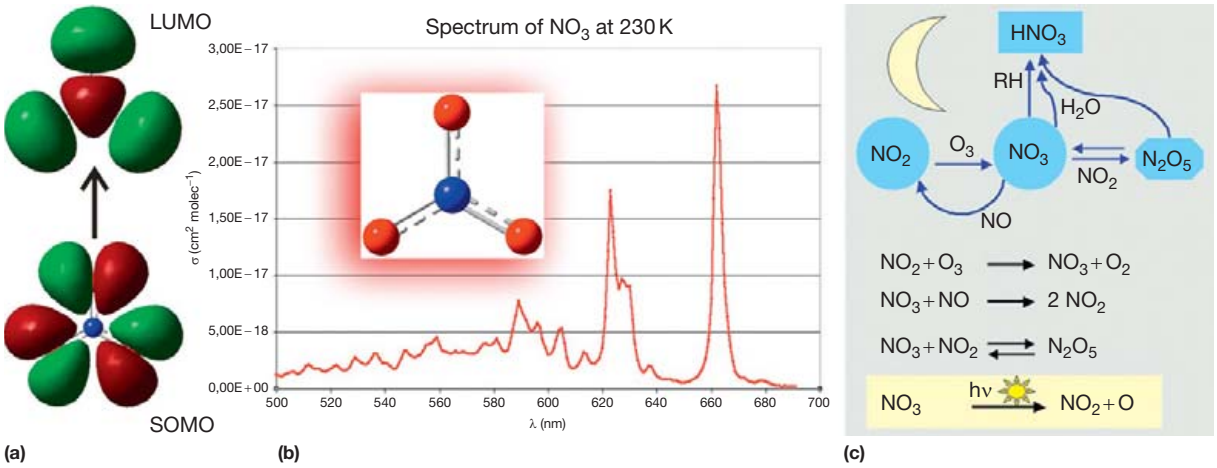

Figure 12 (a) SOMO and LUMO of $NO_3^{\bullet}$. (b) Its gas-phase electronic absorption spectrum at 230 K in the visible wavelength range. The spectrum is strongly temperature dependent and there is extensive vibronic fine structure as is also the case for the spectrum of $NO_2^{\bullet}$. Adapted from Chesnut, D. B.; Crumbliss, A. L. *Chem. Phys.* **2005**, *315*, 53–58, copyright (2005) American Chemical Society. (c) The involvement of $NO_3^{\bullet}$ in atmospheric NO_x cycling as a function of day and night. From: http://www.atmosphere.mpg.de/enid/24z.html.

nitrogen oxide radicals, because it is thought to be the dominant oxidant in the troposphere at nighttime where it is formed chiefly by the reaction of $NO_2^{\bullet}$ with ozone, whereas during daylight hours $NO_3^{\bullet}$ is destroyed by sunlight.[96] Thus, there is constant diurnal cycling involving $NO_3^{\bullet}$ as shown schematically in **Figure 12(c)**. An excellent treatment of $NO_3^{\bullet}$ can be found in the book by Wayne.[97] The EPR spectrum of $NO_3^{\bullet}$ was determined in a frozen matrix at 88 K and found to be planar with true axial symmetry having the following computed parameters: $g_{||} = 2.0041(3)$, $g_{\perp} = 2.0207(3)$, and $\sigma(1/2\ \Delta H_{pp}) = 5.16$ Oe.[98] It has also been detected in a number of crystalline environments but the spectra show greater distortion and a range of $A(^{14}N)$ values (0.17–0.37 mT)[41] (see **Chapters 9.13** and **9.04**).

The formation and subsequent decomposition of $NO_3^{\bullet}$ in a neon matrix containing mixtures of $NO^{\bullet}$ and O_2 have been reported and a dispute over the correct assignment of some fundamental vibrations settled.[86,99] The role of ionization reactions in atmospheric chemistry led to the observation of both $NO_3^{\bullet}$ and NO_3^{+} from the ionization of NO_x and O_3 mixtures.[83,100] Gas-phase reactivity of $NO_3^{\bullet}$ with organic molecules is important to explore the role of volatile organic compounds in urban smog; thus, the reaction of $NO_3^{\bullet}$ with ethene has been investigated.[101] Reactions between $NO_3^{\bullet}$ and fluorinated alkenes may be relevant to reactivity of hydrochlorofluorocarbons in the stratosphere.[102] An extensive investigation of the electronic structure and optical spectrum of $NO_3^{\bullet}$ has recently been reported.[95,103,104] This work includes a determination of the cavity ring-down spectrum of $NO_3^{\bullet}$ which has been used in an aircraft-based spectrometer designed to measure $NO_3^{\bullet}$ levels in the atmosphere.[105] A differential optical absorption spectroscopy method had been developed for simultaneous tropospheric detection of $NO_3^{\bullet}$, $NO_2^{\bullet}$, and O_3.[106]

1.14.2.4 Reduced NO_x Radicals: $NO_2^{2\bullet-}$ and $NO_3^{2\bullet-}$

The radical dianion $NO_2^{2\bullet-}$ is the supposed monomer of the yellow solid formed from the reduction of nitrite salts with sodium in liquid ammonia,[107] and its production from γ-irradiation of dilute nitrite ions dispersed in KCl crystals has been asserted.[41] No new information is available for this species, but theoretical consideration has been given to its doubly protonated form, the neutral dihydroxyaminyl radical, HON-$^{\bullet}$OH which may be an intermediate in rocket fuel combustion.[108] More is known about $NO_3^{2\bullet-}$ radicals, which are similarly formed by γ-radiolysis of certain ionic nitrate salts.[41] A detailed investigation of the dependence of radical formation on the type and crystal symmetry of the nitrate lattices has been undertaken, wherein it was demonstrated that $NO_3^{2\bullet-}$ is sometimes formed but $NO_3^{\bullet}$ or $OONO^{\bullet}$ may also be produced.[109] Lattice sites with symmetries that fit best for the different structures of these products seem to enhance their formation. $NO_3^{2\bullet-}$ has an extra electron compared to NO_3^{-} which induces pyramidalization to C_{3v} geometry. Interestingly, it has been shown by EPR spectroscopy that $NO_3^{2\bullet-}$ can form from the interaction of $NO^{\bullet}$ with highly purified CaO surfaces in the absence of radiation.[110] Recent studies have also focused on solution-phase generation of $NO_3^{2\bullet-}$. Under photoionization of alkaline solutions of phenols that contain high nitrate concentration, electron transfer from $ArO^{\bullet}$ to NO_3^{-} produces $NO_3^{2\bullet-}$ as detected by Fourier transform EPR spectroscopy.[111] Two studies have focused on the γ irradiation of aqueous nitrate solutions because of the dominant role such solutions play in nuclear waste management. The redox potential for the $NO_3^{-}/NO_3^{2\bullet-}$ couple has been estimated to be $E^{\circ} \approx -1.1$ V versus normal hydrogen electrode (NHE).[112] The role of nitrate ions in the decomposition of water under γ-radiolysis involves $NO_3^{2\bullet-}$.[113] The strongly reducing $NO_3^{2\bullet-}$ radical can persist in solution for no more than 20 μs before it is converted to $NO_2^{\bullet}$.

1.14.2.5 The Heterodimers N_2O_3 and N_2O_5

The heterodimer between $NO^{\bullet}$ and $NO_2^{\bullet}$ is the planar N–N-bonded species N_2O_3, the structure of which has been established by low-temperature X-ray crystallography

(Figure 3).[114] Bonding in this species is considered to be similar to the two homodimers, that is, the π* orbital of $NO^{\bullet}$ interacts with the σ_N SOMO of $NO_2^{\bullet}$. This compound is diamagnetic but has a deep blue color due to a low-energy electronic transition. The frequent attribution of blue color to condensates of $NO^{\bullet}$ or $NO_2^{\bullet}$ is probably due to its presence. Similarly, N_2O_5 is the N–O–N bridged dimer between $NO_2^{\bullet}$ and $NO_3^{\bullet}$ and is the direct anhydride of nitric acid. The formation of both these dimers has been investigated by high-level computational methods with a specific focus on their thermodynamic properties.[19] The barrier to rotation in N_2O_3 was found to have a similar origin as that in N_2O_4, namely a combination of 1,4-oxygen–oxygen interactions and hyperconjugation, by a detailed computational investigation.[80] These dimers are intimately involved in the cycle of reactions that produce NO_x compounds and act as coupled reservoirs for their reactive radical constituents in the complex equilibria that regulate the family of nitrogen oxides in the atmosphere.

1.14.2.6 Derivatives of Hydroxylamine: Aminoxyls and *N*-Hydroxyaminyls

Two different kinds of radicals, aminoxyl $H_2NO^{\bullet}$, and the *N*-hydroxyaminyls *cis*-$HNO^{\bullet}H$ and *trans*-$HNO^{\bullet}H$, are derived by abstraction of hydrogen from either the oxygen or nitrogen atoms of hydroxylamine (Scheme 3). They are reactive short-lived species and the structure of aminoxyl has been determined from its microwave rotational spectrum.[115] It was shown to be planar with a short N–O bond length of 1.280(4) Å. The $H_2NO^{\bullet}$ radical is an important intermediate in the atmospheric oxidation of ammonia, which is one of the key sources of NO_x along with sources from fossil fuel and biomass burning.[116,117] Early atmospheric oxidation studies of NH_3 found that, after the initial reaction of $OH^{\bullet}$ radicals with NH_3, the resulting byproduct of the oxidation is HNO_3[118] (see Chapter 7.17). Dixon et al. have produced accurate thermodynamic data for these species for the first time.[119] Coupled-cluster calculations through noniterative triple excitations were used to compute optimized structures, atomization energies at 0 K, and heats of formation at 0 and 298 K for $H_2NO^{\bullet}$ and *trans*-$HNOH^{\bullet}$. The reaction system produced by 193 nm flash photolysis of a mixture of NH_3 and $NO_2^{\bullet}$ has been investigated experimentally and modeled.[120] The accepted belief that only two channels are of significance for the reaction between $NH_2^{\bullet}$ and $NO_2^{\bullet}$, producing (a) N_2O and H_2O and (b) $H_2NO^{\bullet}$ and $NO^{\bullet}$, was confirmed. In recent experiments, in which solid H_2 or D_2 containing $NO^{\bullet}$ held near 3 K was irradiated with vacuum–ultraviolet (UV) light from a synchrotron, new absorption lines at 1241.7, 1063.6, and 726.2 cm^{-1} were detected. These have been assigned by DFT methods in conjunction with deuterium shifts to three vibrational modes of the *N*-hyroxyaminyl *trans*-$HNO^{\bullet}H$. The calculations also show that the most stable isomer is $H_2NO^{\bullet}$ but that *cis*-$HNO^{\bullet}H$ is 61 and *trans*-$HNO^{\bullet}H$ is only 44.5 kJ mol^{-1} higher in energy.[121]

1.14.3 Nitrogen Sulfide Radicals

The same inherent arithmetic propensity for forming free radicals occurs with nitrogen sulfides as for nitrogen oxides, but there are important differences between the second- and the higher-period chalcogens, including reversed polarity of the N–E bond and enhanced tendency for catenation. Thus, not only 'dimers' but also trimers and tetramers have a much more extensive chemistry than the parent radical $NS^{\bullet}$.[122] The formal dimer of $NS_2^{\bullet}$, S_2NNS_2, does not exist whereas the six-membered ring compound cyclo-4,6-N_2S_4 does (Section 1.14.3.4.3). When heteroatoms are introduced (principally carbon, pentavalent phosphorus, or transition metals), a huge diversity of often quite stable nitrogen sulfide radicals have been synthesized which possess a surprisingly wide range of materials properties, including low-activation semiconductors, metallic conductors, borderline magnetic behavior, and both canted and true ferromagnetism.[123] General references to this area of study are provided in Section 1.14.1.3.

1.14.3.1 Nitrogen Monosulfide ($NS^{\bullet}$), Its Oligomers (N_2S_2, $N_3S_3^{\bullet}$, N_4S_4), and the Polymer $(NS)_x$

Nitrogen monosulfide, a transient gas-phase species, is the direct sulfur analog to nitrogen monoxide and was identified from its electronic spectrum in 1932.[124] The past decade has seen a continuation of intense interest in this species in the literature, although the sheer number of citations is much lower than for $NO^{\bullet}$ in view of the lack of a known biological role for $NS^{\bullet}$. Far less is known about the chemistry of $NS^{\bullet}$ than $NO^{\bullet}$ because it cannot be isolated as a liquid or solid and, even in the vapor phase, has only been prepared at very low pressures or trapped in dilute low-temperature matrices. While often characterized as an unstable radical, a comparison of the physical properties in Table 1 suggests otherwise: the bond dissociation energy is around 463 kJ mol^{-1}, which is appreciable although admittedly smaller than 627.6 kJ mol^{-1} for $NO^{\bullet}$. The inability to isolate bulk $NS^{\bullet}$ is therefore more correctly attributed to its high reactivity. When $NS^{\bullet}$ is produced, oligomerization leads to many isolable species (Scheme 4). Indeed, the range and importance of $NS^{\bullet}$ oligomers is much more extensive than that of $NO^{\bullet}$ for which the weak dimer *cis*-ONNO is the only important species (see Section 1.14.2.1.2). The chemically most important oligomer is undoubtedly N_4S_4 while thiazyl polymer $(NS)_x$ is extremely significant because it exhibits both metallic- and, below 4.2 K, super-conductivity; it is chemically interesting in that it can be vaporized to a variety of $NS^{\bullet}$ oligomers, including $N_3S_3^{\bullet}$, and the high polymer is reformed upon condensation.

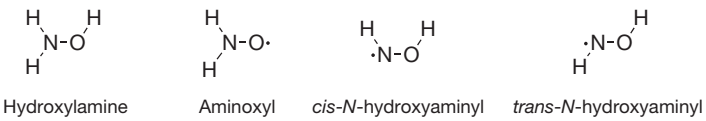

Scheme 3 Derivatives of hydroxylamine.

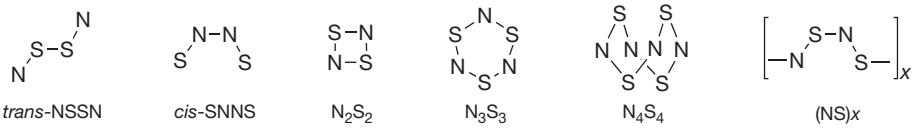

Scheme 4 Oligomers of nitrogen monosulfide.

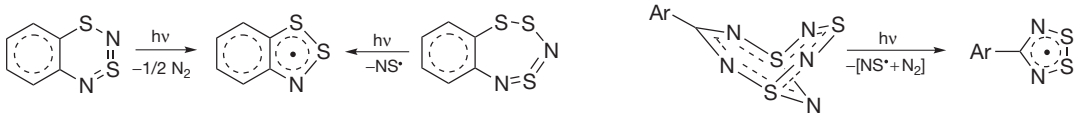

Scheme 5 Photochemical production of NS$^{\bullet}$ in condensed media.

1.14.3.1.1 The electronic structure of NS$^{\bullet}$

An MO diagram for NS$^{\bullet}$ is provided in Figure 4. Like NO$^{\bullet}$, NS$^{\bullet}$ in its $X\ ^2\Pi_{1/2}$ electronic ground state has a very small magnetic moment because of opposing spin and orbital angular momenta. The calculated S–N bond length of NS$^{\bullet}$ in this state is 1.501 Å at the UB3LYP/(aug)cc-pVTZ level of theory, which may be compared to the experimental value of 1.4938(2) Å from gas-phase spectroscopy.[125] A value of 1.5021 Å was obtained by CCSD(T)/cc-pVQZ calculations.[126] The bond distance in $[NS]^+$ has been established to be 1.440(5) Å by gas-phase photoelectron spectroscopy.[127] The longer bond in the neutral radical is consistent with occupancy of the $2\pi^*$ orbital by a single electron, reducing the formal bond order to 2.5 from 3.0 in the monocation. Note that the Fermi-contact hyperfine interaction to the ^{14}N nucleus in NS$^{\bullet}$ is only 4% smaller than that in NO$^{\bullet}$, in support of the notion that NS$^{\bullet}$ is only marginally polarized with respect to the π-electronic system. However, the dipole moment of NS$^{\bullet}$ at −1.83(3) *D* is much larger than in the almost nonpolar NO$^{\bullet}$. Thus, it is not surprising that NS$^{\bullet}$ converts to N_2S_2 and N_4S_4 in an alternating N to S pattern, whereas NO$^{\bullet}$ prefers the symmetrical dimer $(NO)_2$ (see Section 1.14.2.1.2).

1.14.3.1.2 Spectroscopic properties of NS$^{\bullet}$

The EPR spectrum of the thermally accessible excited $X\ ^2\Pi_{3/2}$ state (223 cm^{-1} above $X\ ^2\Pi_{1/2}$) has been detected in the gas phase and the $A_{gas}(^{14}N)$ nuclear hyperfine constant was determined to be 2.056(8) mT in an X-band spectrum where the second-order Zeeman interaction was ∼22 mT (see Section 1.14.2.1.1 and Figure 5).[128] Using the Frosch and Foley magnetic hyperfine structure parameters *a*–*d*, the Fermi contact interaction term $A_{iso}(^{14}N) = 0.765$ mT can be determined from the experimental data,[37] which can be directly compared to a high-level DFT calculated value $A_{calc}(^{14}N) = 0.65$ mT.[129] All claims in the literature to have detected an EPR spectrum for NS$^{\bullet}$ in solution or in the solid state are in error.[14,129] Just as for NO$^{\bullet}$, the incomplete quenching of the orbital angular momentum and extreme *g*-anisotropy between the rotationally coupled and rotationally quenched states will contribute, respectively, to extremely efficient relaxation and massively broadened lines. Since NS$^{\bullet}$ is a leading candidate for involvement in the well-documented rearrangements of nitrogen sulfide rings and cages induced by both redox and nucleophilic reactions, the EPR silence of this radical in condensed phases is a significant limitation. The very recent discovery that $[Fe(S_2CNEt_2)_2]$ can act as a solution-phase spin trap for NS$^{\bullet}$ is therefore of great significance (see Section 1.14.3.1.6). The rotational spectrum of NS$^{\bullet}$ is of importance to astrophysics for its extra-terrestrial detection (see Section 1.14.3.1.4 and Chapter 9.13).[130]

1.14.3.1.3 Preparation and reactivity of NS$^{\bullet}$

In the earliest work, NS$^{\bullet}$ was produced in flow systems from atomic nitrogen and H_2S or S_2Cl_2,[131] by microwave discharge of NSCl, direct reaction of atomic nitrogen with S_2(g), or photolysis of HNS_7[127] using helium as a diluent gas. The yield of product was found to be strongly affected by the copious production of black $(NS)_x$.[127] Uehara showed that co-discharging of N_2 and SCl_2 using a microwave source produced much stronger signals for NS$^{\bullet}$.[128] A significant improvement on these early studies uses low-pressure discharges of just elemental nitrogen and sulfur, followed by trapping in argon matrices at low temperature.[132] The observed products in these cold argon matrices include NS$^{\bullet}$, NNS, SNS$^{\bullet}$, and NSS$^{\bullet}$. Under conditions of high sulfur content in the discharge, the open-shell adduct SSNS$^{\bullet}$ was identified. Under conditions where both NS$^{\bullet}$ and SNS$^{\bullet}$ are co-deposited in the matrix, signals identified as coming from the asymmetric dimer $SNNS_2$ were observed. Another 'clean' way to produce NS$^{\bullet}$, albeit initially in excited electronic states, is by two-photon photolysis of N_4S_4 at 248 or 222 nm (see Section 1.14.3.1.9).[133] Evidence has also been obtained for photochemical production of NS$^{\bullet}$ in condensed media during photolysis of several nitrogen sulfide heteroelement rings and cages (Scheme 5).[134–138]

An attempt was made to produce NS$^{\bullet}$ in solution by electrolysis of $[NS][SbF_6]$ but the solvent system that was selected in order to solubilize the salt (a mixture of trifluoroacetic anhydride and trifluoroacetic acid containing $[^nBu_4N^+][BF_4^-]$ as electrolyte) was unfavorable.[139] Indeed, EPR signals attributable to $N_2S_3^{+\bullet}$, a well-known product when nitrogen sulfides are dissolved in strong acids, were detected even before electrolysis commenced.[14,129] By cyclic voltammetry, a chemically irreversible process was observed with a half-height potential of +0.76 V at a platinum electrode versus SCE. No follow-up experiment was undertaken to identify end-products voltammetrically.[139]

Not much is known about specific reactivity of NS$^{\bullet}$ with many species, although the first-ever direct kinetic measurements on this radical have shown that, in the gas phase, it does not react with NO$^{\bullet}$ or O_2 but that it reacts rapidly with $NO_2^{\bullet}$

with no activation barrier.[140] The final products of the (multistep) reaction are N_2 and SO_2. There is also strong indirect evidence that $NS^\bullet$ reacts with itself and evidently leads to N_2S_2, N_4S_4, and the high polymer $(NS)_x$ under a variety of conditions and in the presence of several possible catalysts.

1.14.3.1.4 Astrophysical significance of $NS^\bullet$

Nitrogen monosulfide was first identified in astronomical sources in the giant molecular cloud SGR B2 with an estimated column density of 10^{14} cm^{-2}.[141] The only other detected sulfur molecule of comparable concentration was SO. $NS^\bullet$ has since been observed in a wide variety of sources including dense interstellar clouds in regions of massive star formation, for example, in the dark clouds TMC-1 and L134N with column densities of ~8 and ~3 × 10^{12} cm^{-2}.[142] A number of sulfur species (SO, SO_2, OCS, CS, H_2S, H_2CS, and $NS^\bullet$) have been detected in massive young stars by submillimeter wave spectroscopy.[143] $NS^\bullet$ was recently detected by rotational spectroscopy in the coma of the comet Hale-Bopp and its rate of production was found to be at least a few hundredth of a percent compared to water and with a total column density of 6.8 × 10^{12} cm^{-2}.[144] The half-life of $NS^\bullet$ was found to be between 5000 and 10^5 s with an expectation that it would be destroyed by solar photoionization. In order to clarify issues raised by the Halle-Bopp discovery, CCSD(T)/6-311++G (3df,3pd) calculations were used to study the formation of ^2NS from different reactions paths. The only energetically favorable and spin-allowed reaction path these workers could find is the reaction $^1NH + {}^2SH \rightarrow {}^2NS + H_2$ for which $H^\circ = -154$ kJ mol^{-1}.[145] High concentrations of $NS^\bullet$ were also discovered in an extragalactic source, the nucleus of the starburst galaxy NGC 253, and its high abundance was attributed to shock chemistry.[146]

1.14.3.1.5 $NS^\bullet$ in combustion chemistry and electrical insulator stability

$NS^\bullet$ has been detected in sulfur-containing flames using laser-induced fluorescence.[147,148] It is thought that the $NS^\bullet$ radical plays an important role in the interaction between nitrogen and sulfur species in flames and can thereby affect the NO_x content of exhaust gases. Wendt et al. first suggested the reaction: $^2NS + {}^1O \rightarrow {}^1SO + {}^2N$ as a primary cause of increased N_2 generation in a sulfur doped flame.[149] Other reactions, such as $^2NS + {}^2NO \rightarrow {}^1N_2 + {}^1SO$ and $^2NS + {}^2N \rightarrow {}^1N_2 + {}^1S$, have been included in model calculations to explain the effect of sulfur on flame composition. Currently, there is increasing interest in the decomposition of SF_6 in the presence of nitrogen during circuit breaker arc plasmas.[126] For such reactions, the neutral species NF, $NS^\bullet$, S_2, and F_2 as well as their monovalent ions need to be considered and some unknown or poorly characterized parameters of these species were studied at the CCSD(T) computational level. Discharges of SF_6 with N_2, O_2, and N_2/O_2 mixtures have been studied experimentally using IR matrix isolation spectroscopy.[150]

1.14.3.1.6 $NS^\bullet$ and transition metals: thionitrosyl complexes and spin trapping of $NS^\bullet$

The coordination of $NS^\bullet$ to transition metals parallels closely the behavior of $NO^\bullet$.[151] About 40 crystal structures have now been reported in which $NS^\bullet$ is coordinated via nitrogen to transition metals in a range of different oxidation states.[129] The N–S bond distances in these complexes are reported to range from 1.591[152] to 1.383 Å.[153] Just as for nitrosyl, there are two fundamental ways to make thionitrosyl complexes. The first uses one of several sources containing an NS unit (but never $NS^\bullet$ itself unlike the case for $NO^\bullet$); for example, an Re–NS complex was reported from dehalogenation of an Re–NSCl complex.[154] The second approach is both more elegant and versatile and involves building the N–E unit at the metal center from a preexisting metal nitride. This has been the most reported method during the past decade; examples include osmium nitrides reacting with Ph_3PS,[155] Li_2S,[156] S_2Cl_2,[157] or sodium thiosulfate.[158] Similar approaches have been shown to work for rhenium.[157,159] Typical ν(NS) stretching frequencies range from ~1065 cm^{-1} for low-valent to 1390 cm^{-1} for high-valent metal complexes,[151] values which clearly bracket the 1204 cm^{-1} of the gas-phase radical (Table 1).

In an important recent series of papers, the novel $S = 1/2$ thionitrosyl complexes $[Cr(NS)(CN)_5]^{3-}$, $[Cr(NS)(dimethylsulfoxide)_5]^{2+}$, $[Cr(NS)(dimethylsulfoxide)_5]^{2+}$, and $[Cr(NS)(H_2O)_5]^{2+}$ have been prepared and investigated by EPR spectroscopy and their electronic structures compared to related NO and NSe complexes.[160–162] Most significantly, the related $[Cr(NS)(CH_3CN)_5]^{2+}$ has been shown to release $NS^\bullet$ upon flash or continuous photolysis, and the $NS^\bullet$ could be trapped by the classical nitric oxide spin trap $[Fe(S_2CNEt_2)_2]$ (Scheme 6).[42] This represents the first example of well-characterized chemical reactivity of $NS^\bullet$ in solution. Moreover, it shows that the iron dithiocarbamate complex can function as a suitable spin trap for nitrogen monosulfide exactly as it does for $NO^\bullet$. By careful comparison of the behavior of the nitrogen monoxide and nitrogen monosulfide systems, this study found evidence for partial consumption of $NS^\bullet$ during the chromium to iron transfer reaction, which was attributed to $NS^\bullet$ oligomerization processes.[42]

1.14.3.1.7 N_2S_2, the dimer of $NS^\bullet$

Scheme 4 shows three of the possible isomers of the dimer of $NS^\bullet$; it has been shown in an exhaustive DFT computational study that no fewer than 10 minima and 10 saddle points exist for the lowest singlet electronic state of species with empirical formula 'N_2S_2' as well as 11 minima and 13 saddle points for the lowest triplet state.[163] All of these are higher in energy compared to N_2 and S_2 in the gas phase. The $^1A_1$ state of *cis*-SNNS is the direct sulfur analog to $(NO)_2$ while ^1A_g *trans*-NSSN is the only gas-phase species accessible by direct dimerization of $NS^\bullet$ monomers. If to this picture is added the trimeric $N_3S_3^\bullet$ (for which both linear and the cyclic form shown in Scheme 4 have been claimed), the internally associated cage structure

$$Cr(CH_3CN)_5(NS)^{2+} + Fe(S_2CNEt_2)_2 + CH_3CN \xrightarrow{h\nu} Cr(CH_3CN)_6^{2+} + Fe(S_2CNEt_2)_2(NS)$$

Scheme 6 Transfer of $NS^\bullet$ between Cr(II) and Fe(II) complexes in solution.

of N_4S_4, and the complex behavior of $(NS)_x$ which forms by solid-state polymerization of cyclo-N_2S_2, then the immense complexity of the energy hypersurface for NS• and its oligomers becomes apparent.

One species which accompanied the deposition of NS• in matrix isolation experiments using N* and S* from discharges, but which disappeared upon annealing the sample (heating to below the evaporation point of the matrix), was proposed to be the chain dimer *trans*-NSSN (**Figure 13**, see also **Section 1.14.3.1.7**).[132] The calculated structure of this species has a long central S–S bond and a barrier to dissociation of only 50 kJ mol^{-1}.[163] Interestingly, under their conditions, the reaction of atomic nitrogen and sulfur does not lead to cyclo-N_2S_2, whereas this species was observed along with N_4S_4 when the feedstock for the matrix deposition was a heated sample of $(NS)_x$.[132]

The standard way to make cyclo-N_2S_2 is by thermal cracking of N_4S_4 in the gas phase over heated silver metal.[13] A rare example of chemical synthesis of cyclo-N_2S_2 was reported from $[NS][AsF_6]$ and CsN_3, but under the reaction conditions the only isolable product is the polymer $(NS)_x$.[164] The well-known polymerization of N_2S_2 to $(NS)_x$ has potential as a forensic tool for developing latent fingerprints.[165] Formal insertion of transition metals into one of the N–S bonds leads to a large number of metalla-1,3,2,4-dithiadiazole complexes.[151] Interest in this field continues apace with reports on Cp*M(NSNS), M = Co, Rh, and Ir,[166] $Cp_2TiNi(NSNS)_2$[167] and CpCo(NSNS).[168]

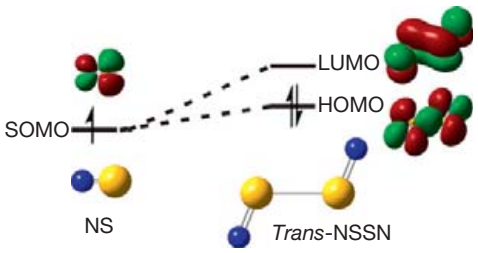

Figure 13 Dimerization of NS• to give ^1A_g *trans*-NSSN from a B3LYP/6-311++G(2df) calculation. Note the increase in MO energies on adduct formation; the triplet state is by contrast stabilized, but expected to be more reactive; for details, see Hassanzadeh et al.[132]

1.14.3.1.8 N_3S_3•, the open-shell trimer of NS•

The neutral 9π-electron ring radical N_3S_3• is an elusive member of the family of binary nitrogen sulfide radicals.[169–171] It has been detected by photoelectron spectroscopy in vapors produced from $[SN]_x$ polymer,[172,173] but has never been reliably characterized in condensed phases.[174] The geometry calculated at the UB3LYP/(aug)cc-pVTZ level (**Figure 14(a)**)[129] supports a planar structure such as in the crystallographically characterized diamagnetic 10π-electron anion $S_3N_3^-$ (for which average dimensions of S–N = 1.607(21) Å; ∠SNS = 123.8(10)°; ∠NSN = 116.1(9)°) but shows that the radical is mildly distorted toward C_{2v} symmetry through a Jahn–Teller effect.[175] Note that, although the geometrical distortions predicted for N_3S_3• are quite small (**Figure 14(a)**), the effects these changes have on the calculated isotropic hfc constants are very significant, with a factor of 3 difference in coupling to the two kinds of ^{14}N nuclei; **Figure 14(b)** shows the effect on simulated EPR spectra for the extreme scenarios of fully static and rapidly averaged $A(^{14}N)$ values. Earlier attempts by Fritz and Bruchhaus to generate N_3S_3• by *in situ* electrolytic oxidation of [PPN][S_3N_3] in CH_2Cl_2 solution containing [$^nBu_4N$][BF_4] electrolyte[139] at RT and more recent exhaustive attempts at temperatures down to −60 °C failed to detect any EPR signals for this species even though voltammetric evidence for finite concentrations of N_3S_3• was strong.[175] Possible reasons for failure to detect the EPR signal include exchange broadening (that the temperatures investigated fall within a broad coalescence region of the two extremes in **Figure 14(b)**) or that rapid (and reversible) dimerization occurs such as to the DFT-calculated structure $[N_3S_3]_2$ shown in **Figure 14(c)**. Note that radical-monomer/diamagnetic-dimer equilibria are known for many nitrogen sulfide hetero-radicals (see **Section 1.14.5**), but these usually show strong EPR signals for radicals resulting even from small degrees of dissociation. Alternatively, a dimer such as $[N_3S_3]_2$ may disproportionate irreversibly to

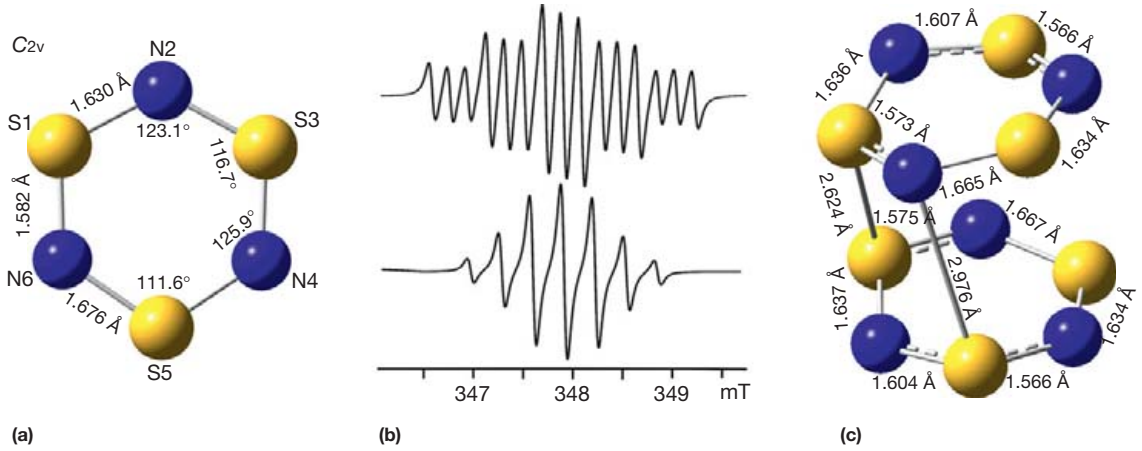

Figure 14 (a) Calculated geometry. Adapted from Boeré, R. T.; Tuononen, H. M.; Chivers, T.; Roemmele, T. L. *J. Organomet. Chem.* **2007**, *692*, 2683–2696, copyright (2007) Elsevier. (b) predicted isotropic EPR spectra with static and averaged hfc values, and (c) PBE1PBE/(aug)cc-pVTZ calculated π*–π* dimer geometry for N_3S_3•. Adapted from Boeré, R. T.; Chivers, T.; Roemmele, T. L.; Tuononen, H. M. *Inorg. Chem.* **2009**, *48*, 7294–7306, copyright (2009) American Chemical Society.

(diamagnetic) N_4S_4 and N_2S_2. *In situ* EPR-electrochemistry was able to demonstrate the rapid formation of N_4S_4 under conditions where $[N_3S_3]^-$ was oxidatively electrolyzed. The best kinetic model developed for the interconversion of N_4S_4 and $N_3S_3^\bullet$ in solution proposed a steady-state $NS^\bullet$ concentration ~20% that of bulk $N_3S_3^-$ and a half-life in solution for $N_3S_3^\bullet$ of 0.2–0.8 s.[175]

The ground-state wave function of neutral $N_3S_3^\bullet$ has been determined to be multideterminantal by [3,3]-CAS calculations supported by further work at the MP2 and CCSD level. The CI vector coefficients indicate that the ground-state wave function is a linear combination of five Slater determinants, which form two configurations as shown schematically in Figure 15. Thus, $N_3S_3^\bullet$ fits into current interest in triradicals with an open-shell doublet ground state. Since the ground-state wave function is dominated by the closed-shell doublet configuration, it is not a true triradical species but can be best viewed as a 'triradicaloid'.[175,176]

1.14.3.1.9 N_4S_4, the tetramer of $NS^\bullet$

The chemically most important $NS^\bullet$ oligomer is undoubtedly N_4S_4 which may be prepared in bulk by a variety of methods, including the original condensation of ammonia with S_2Cl_2 in inert solvents.[177] This is the most important starting material for thiazyl chemistry and also a common product or byproduct even though it is an endoergic species; the latter property is demonstrated by its tendency to detonate with friction or heating. N_4S_4 forms a highly puckered eight-atom ring with the cage-like structure shown in Figure 16 (left) as a result of intramolecular π^*–π^* interactions.[13] In an elegant study of the photochemistry of N_4S_4 dispersed in Ar matrices at 12 K, reversible wavelength-dependent transformations were observed (Figure 16).[178] Irradiation at 254 nm (the band maximum of N_4S_4) produces a boat-shaped eight-membered cyclic isomer and a six-membered N_3S_3 ring with a pendant SN group. Further irradiation with 313 nm light converted both to a fourth species assigned to N_3S_3 with a pendant NS group, while at wavelengths above 405 nm the ground-state structure was reformed.

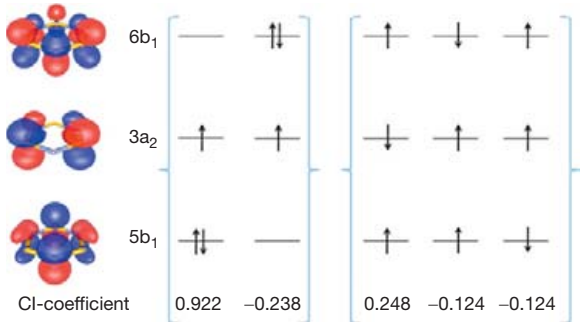

Figure 15 Frontier MO surfaces and leading configurations in the wave function of $N_3S_3^\bullet$. Reprinted from Boeré, R. T.; Chivers, T.; Roemmele, T. L.; Tuononen, H. M. *Inorg. Chem.* **2009**, *48*, 7294-7306, copyright (2009) American Chemical Society.

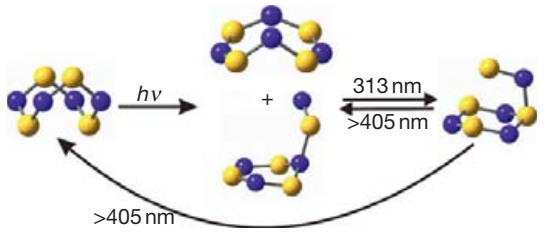

Figure 16 Structure of N_4S_4 (left) and reversible rearrangements during photolysis at 12 K. Adapted from Pritchina, E. A.; Gritsan, N. P.; Zibarev, A. V.; Bally, T. *Inorg. Chem.* **2009**, *48*, 4075-4082, copyright (2009) American Chemical Society.

These fascinating transformations in low-temperature matrices may be compared to gas-phase photolysis. The facile emission from gaseous N_4S_4 irradiated by two-photon 248 nm excitation extends from the UV (~200 nm) into the green (~550 nm) and comprises two distinct band systems (Figure 17).[133] The broader and more extensive double-headed system was identified as $NS^\bullet$ ($B^2\ \Pi_{1/2,3/2} \rightarrow X^2\ \Pi_{1/2,3/2}$) and shows the characteristic 1/2–3/2 spin–orbit components. A second much sharper band system is visible in the 200–330 nm region and is attributed to $NS^\bullet$ ($H^2\ \Pi_{1/2} \rightarrow X^2\ \Pi_{1/2}$). The initial byproduct of photolysis, supposedly a chain isomer of $N_3S_3^\bullet$, is predicted to absorb a single photon to produce more $NS^\bullet$ and N_2S_2.[133] The result is to produce, after the facile emissions decay away, a relatively high concentration of vibronically excited electronic ground-state $NS^\bullet$ molecules. The overall efficiency of conversion of absorbed photons by N_4S_4 into $NS^\bullet$ ($B^2\ \Pi_{1/2,3/2}$) was determined to be 2.6(7)%. This discovery lends support to the notion of a commonality among photoexcitation, chemical or electrochemical reduction, and reaction with nucleophiles: each is expected to populate the LUMO of S_4N_4 (see Section 1.14.3.4.4) which is σ^*(S···S) and π^*(S–N). Follow-on reactions that either flatten the ring (opening the transannular S···S 'bond'), or contract the ring via a 1,3-nitrogen shift reaction, are therefore to be expected.

1.14.3.1.10 $(NS)_x$, a high polymer of $NS^\bullet$

$(NS)_x$, considered the first polymeric metal, was most recently reviewed in 1997[18] and 1998,[17] and Heeger and MacDiarmid, along with Shirakawa, received the Nobel Prize in Chemistry in 2000 for their discovery of conducting polymers including $(NS)_x$.[179] Despite over three decades of work by physical chemists, physicists, and theoreticians, the electronic structure of $(NS)_x$ is still not fully understood and has recently been reinvestigated.[180–184] The main unresolved issues are: (1) Why is $(NS)_x$ a metallic polymer and superconductor at low temperatures? (2) What causes the suppression of the Peierls transition normally observed in single-chain thiazyl compounds? The amazing behavior whereby this polymer evaporates to small fragments, including $N_3S_3^\bullet$ (see Section 1.14.3.1.8), on heating in a high vacuum but on cooling condenses back to a high polymer represents remarkable reactivity that clearly involves nitrogen sulfide radicals. The presence of radicals in the solid-state polymerization of N_2S_2 has received a great deal of attention. Blue-black N_2S_2 crystals give a free-radical signal ($g = 2.005$) which initially increases and then decreases with time as polymerization proceeds.[185] EPR measurements of the radical concentration in polymerizing microcrystalline thin films of N_2S_2 at ambient temperature showed that the radicals decayed in about 12 h, indicating the end of the reaction[186] (see Chapter 1.26).

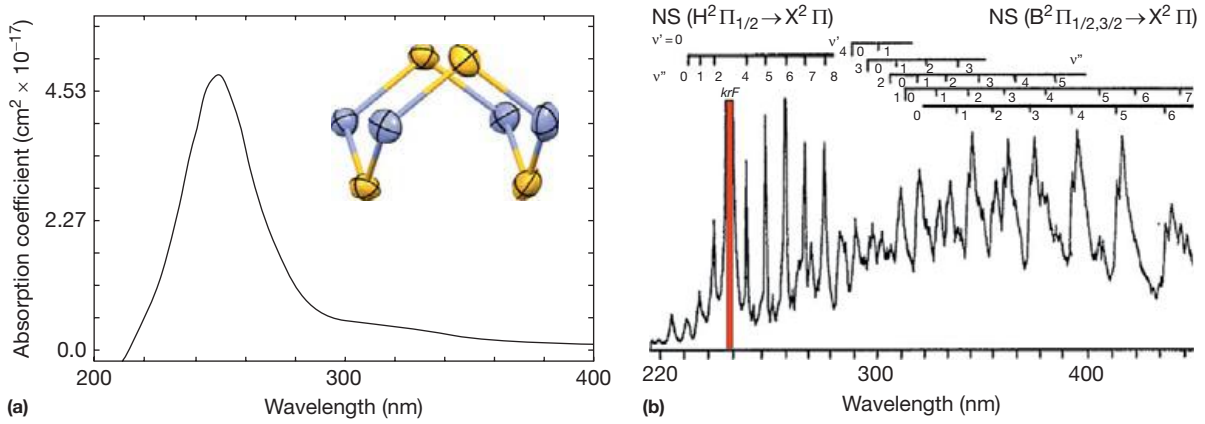

Figure 17 (a) UV–visible absorption spectrum of N_4S_4 (3×10^{-3} M in CH_3CN). (b) Emission spectrum produced from NS$^\bullet$ with 248 nm excitation of N_4S_4. The broad band near 248 nm (colored red) is due to the KrF laser spike. Adapted from Ongstad, A. P.; Lawconnell, R. I.; Henshaw, T. L. *J. Chem. Phys.* **1992**, *97*, 1053–1064, copyright (1992) American Chemical Society.

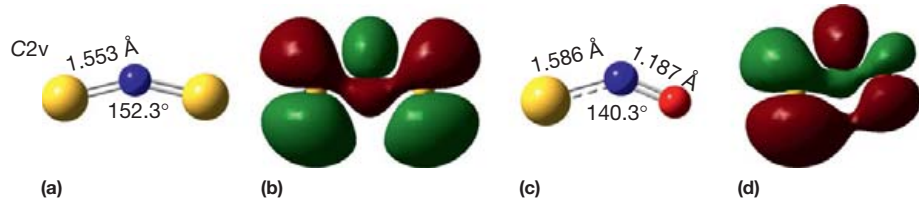

Figure 18 (a) The geometry and (b) SOMO isosurface of SNS$^\bullet$. Adapted from Boeré, R. T.; Tuononen, H. M.; Chivers, T.; Roemmele, T. L. *J. Organomet. Chem.* **2007**, *692*, 2683–2696, copyright (2007) Elsevier. (c) The geometry and (d) SOMO isosurface of 2*A*′ ONS$^\bullet$ from a UB3LYP/6-311+G* calculation.

1.14.3.2 Other Neutral Nitrogen Sulfide Radicals: SNS$^\bullet$ and $^\bullet NS_7$

1.14.3.2.1 SNS$^\bullet$, the sulfur analog of $NO_2^\bullet$, its possible dimers, and ONS$^\bullet$

SNS$^\bullet$ has been prepared in the gas phase by mass spectrometry through ion-recombination techniques from the monocation which was itself generated from the novel starting material [1,2,5]thiadiazolo[3,4-*c*][1,2,5]thiadiazole (see Section 1.14.5.2.8).[187] In an earlier investigation, it was prepared by matrix isolation from an argon gas discharge of sulfur and nitrogen; significantly by this route, both the linear asymmetric isomer NSS$^\bullet$ and the symmetric SNS$^\bullet$ isomer were obtained and unambiguously identified from vibrational spectroscopy.[132,188] Upon irradiation ($\lambda = 400$–245 nm), NSS$^\bullet$ ($^2A'$) isomerized irreversibly to the more stable SNS$^\bullet$ ($^2A_1$) in agreement with calculations that the latter is 80.3 kJ mol^{-1} more stable.[189] The importance of the matrix isolation technique for many of the fundamental nitrogen chalcogenides will be obvious to readers of this article; a thorough review of the method and its achievements has recently been published.[190]

Calculations performed at the UB3LYP/(aug)cc-pVTZ level of theory indicate a bent structure for the SNS$^\bullet$ radical in its $^2A_1$ ground state, with a bond angle of 152.3° and an S–N bond distance of 1.553 Å (Figure 18(a))[129] which is in excellent agreement with results from large basis-set orbital methods.[163] Calculations have shown it to be a rather floppy molecule; the classical barrier energy to linearity is estimated to be only 8–12 kJ mol^{-1}. The SOMO from this calculation is shown in Figure 18(b), indicating similarity in topology to the SOMO of $NO_2^\bullet$ except that the contribution of the nitrogen p-orbital is much smaller (compare Figure 10). It is fully consistent with population of a lone-pair-type orbital at N with a single electron in the linear geometry of the well-characterized $[S{=}N{=}S]^+$ cation (d(SN) = 1.46–1.49 Å).[191] The latest calculations also report isotropic hfc constants of $A(^{14}N) = 2.11$ mT and $A(^{33}S) = 0.56$ mT, respectively. The latter reflects the small sulfur atomic s-component to the total spin density as a consequence of the almost pure p-contribution by S to the SOMO (Figure 18(b)); for comparison, $A(^{14}N) = 5.34$ mT in $NO_2^\bullet$ (see Section 1.14.2.2.1). The EPR spectrum of SNS$^\bullet$ is expected to be notoriously featureless: a single 1:1:1 triplet; consequently, there have been several claims in the literature for this species but none fit well with the DFT calculated values.[129]

SNS$^\bullet$ ought to be accessible from chemical or electrochemical reduction of the cation $[SNS]^+$, first reported by Gillespie.[192] An unconfirmed and preliminary study by cyclic voltammetry claims +0.72 (CH_3CN) or +0.76 (SO_2) V versus SCE for the reduction of SNS^+ from its AsF_6^- salt.[191] On a preparative scale, reduction of $[SNS][AsF_6]$ with sodium dithionite ($Na_2S_2O_4$) results in the (known) AsF_6^- salt of the $N_2S_3^{+\bullet}$ radical cation (see Section 1.14.3.3.1). The mechanism of this reaction is not known but it can be hypothesized that (highly reactive) SNS$^\bullet$ (or NS$^\bullet$ from its breakdown) is trapped by excess SNS^+. This reaction has no analog in nitrogen oxide chemistry where reduction of ONO^+ salts leads cleanly to the production of $NO_2^\bullet$.[191] Some insight into this result may be

obtained by considering that the main reactivity of ONO^+, nitration via electrophilic aromatic substitution, produces bonds to the central nitrogen atom, whereas all known reactivity of SNS^+ occurs at the terminal sulfur atoms.[191] Of special interest is that reaction of SNS^+ with N_3^- yields $(NS)_x$ polymer, the first known chemical synthesis other than ring-opening polymerization of N_2S_2 (see Section 1.14.3.1.7) This contrast in reactivity can be directly related to the differing topologies of the ENE^+ LUMO, which is N-centered for E=O and S-centered for E=S. New results in this area include the publication of a high-yield synthesis of the SO_2-soluble salt [SNS][SbF_6][193] and the CH_2Cl_2-soluble [SNS][$Al(OC(CF_3)_3)_4$].[194] These may be excellent reagents for re-investigation of SNS^+ electrochemistry.

Chesnut calculated an S_2NNS_2 dimer analogous to dinitrogen tetroxide and conclude that the bound state is 7.1 kJ mol^{-1} higher in energy than two $SNS^\bullet$ radicals (Scheme 7).[79] A dimer of $SNS^\bullet$ was reported along with the monomer by matrix isolation of a sulfur and nitrogen discharge and identified as the cyclo-3,6-N_2S_4 molecule (Scheme 7).[132] Early DFT calculations claimed that the 3,6-isomer is 54–73 kJ mol^{-1} higher in energy than crystalline dark red cyclo-4,6-N_2S_4, which can be made in bulk from S_2Cl_2 and NH_4OH in CS_2 and has been well characterized by crystallography and spectroscopy (Section 1.14.3.4.4).[195] These two cyclic dimers therefore differ fundamentally from N_2O_4 and the observed dimerization reflects the different topology (S vs. N centered) of the SOMOs of $SNS^\bullet$ and $NO_2^\bullet$.

Finally, there are several reports on the mixed oxide/sulfide $ONS^\bullet$.[196–199] Calculations at the B3LYP/6-311+G* level of theory predict that the ground electronic state is the bent form $2A'$ $ONS^\bullet$ (dNO = 1.186, dNS = 2.613; Figure 18(c)).[200] The SOMO (Figure 18(d)) can be viewed as a hybrid of those of $SNS^\bullet$ and $NO_2^\bullet$ (compare Figure 10). There are no reports in the literature on the fate of $ONS^\bullet$ if the matrix is warmed or any indication of what other chemistry this species may undergo.

1.14.3.2.2 The cyclic neutral radical $^\bullet NS_7$

The cyclic geometry expected for the neutral $^\bullet NS_7$ radical and the expectation of considerable spin density on N suggest at least a geometric relationship to that of $SNS^\bullet$. However, at the electronic level $^\bullet NS_7$ is actually related to the (unknown) $NS_2^{2\bullet-}$ with two extra electrons and thus isoelectronic with $NO_2^{2\bullet-}$ (see Section 1.14.2.4). An EPR spectrum purported to belong to this radical formed by γ-irradiation of HNS_7 powders and crystals was reported many years ago[201] and the signal appears to be stable in the powder form for a considerable time at 77 K. The trace of the hfc tensor measured from these solids gives an estimated isotropic splitting of ~2.6 mT, in reasonable agreement with 1.90 mT recently calculated by DFT methods.[129] By analogy to the formation of thioaminyl radicals from RN(H)SR′ (see Section 1.14.5.1.4), solution-phase oxidation of the parent compound should be attempted to try and verify this result. This has a better chance of succeeding than by using the thermally unstable anion. The geometry calculated for $^\bullet NS_7$ at the UB3LYP/(aug)cc-pVTZ level predicts a bond angle of 139.6° at nitrogen (Figure 19(a)). This value is smaller than the 152.3° obtained for neutral $SNS^\bullet$, suggesting that the smaller angle in the cyclic system may be caused by ring strain from the 'bridging' S_5 chain. An analysis of the SOMO (Figure 19(b)) reveals that, unlike $SNS^\bullet$ in which in-plane orbitals are involved, the unpaired spin density is concentrated in p-orbitals that are perpendicular to the SNS plane. Indeed, in $^\bullet NS_7$ the in-plane orbitals that correspond to the SOMO of $SNS^\bullet$ are involved in bonding of the SNS unit to the S_5 fragment. All the calculated hfc constants for $^\bullet NS_7$ are smaller than those in $SNS^\bullet$, but in approximately similar ratios. The chemical reaction of S_8^{2+} salts with azide ion, N_3^-, leads to the isolation of salts of SNS^+ and not the expected NS_7^+.[191] However, the reaction of *cyclo*-S_8 with azide ion in hexamethylphosphoramide gives HNS_7 in reasonable yields.[202]

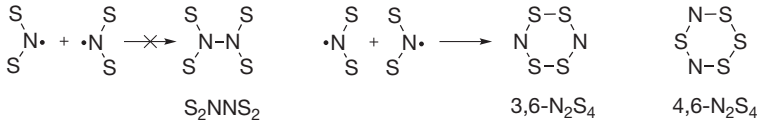

Scheme 7 Dimerization of $SNS^\bullet$.

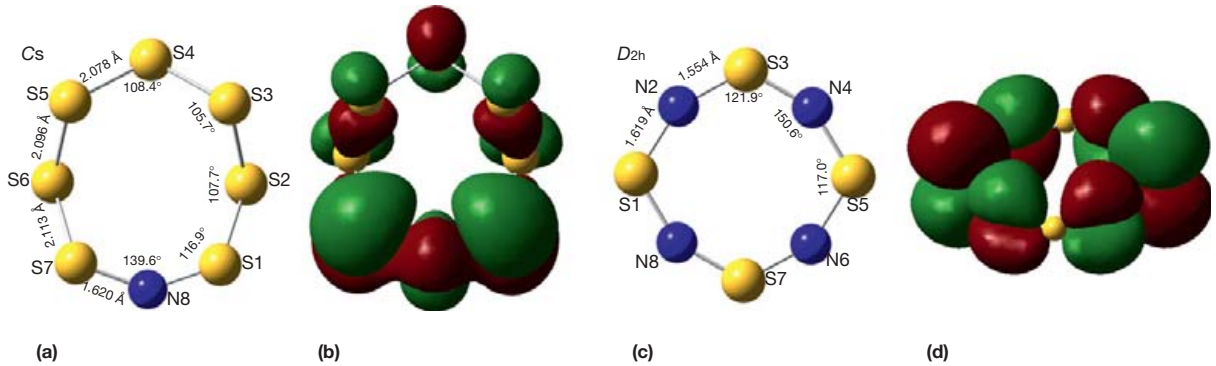

Figure 19 (a) Geometry-optimized structure and (b) SOMO isosurface calculated for the $^\bullet NS_7$ radical. (c) Geometry-optimized structure and (d) SOMO isosurface of $N_4S_4^{+\bullet}$. Adapted from Boeré, R. T.; Tuononen, H. M.; Chivers, T.; Roemmele, T. L. *J. Organomet. Chem.* **2007**, *692*, 2683–2696, copyright (2007) Elsevier.

1.14.3.3 Cationic Nitrogen Sulfide Radicals ($N_2S_3^{+\bullet}$, $N_2S_2^{+\bullet}$, and $N_4S_4^{+\bullet}$)

1.14.3.3.1 The cyclic $N_2S_3^{+\bullet}$ cation radical

The thermodynamically stable cation radical cyclo-3,5-$N_2S_3^{+\bullet}$ (structure and atom numbering in Figure 20(a)), a rigorously planar cyclic π-radical, is by far the best-characterized binary nitrogen sulfide radical and has been intensively investigated in part because of the false assignment of its EPR spectrum to several other species over the years. For example, the 'five-line' ^{14}N spectrum obtained from solutions of both N_4S_4 and N_2S_2 in concentrated aqueous acid was eventually identified as belonging to $N_2S_3^{+\bullet}$ through ^{15}N and ^{33}S isotope enrichment studies carried out in the early 1980s.[203] It has been made by the direct oxidation of N_4S_4 using the powerful, if unusual, oxidants Te_6^{4+} or S_8^{2+}(204) and more simply from N_4S_4 and AsF_5 in SO_2 solution.[205] The orbital-symmetry-allowed formation (and dissociation) of the unstable dication $N_2S_3^{2+}$ from the known ions NS^+ and SNS^+ has been demonstrated on a theoretical basis. By contrast, occupancy of the $2a_1$ π* orbital with a single electron in $N_2S_3^{+\bullet}$ renders the ring stable against such a dissociation; this is a rare example in nitrogen sulfide chemistry where a 7π electron system is found to be more thermodynamically stable than a Hückel 6π state; the high cation charge of the latter may be a contributing factor.[206]

A calculated geometry at the UB3LYP/(aug)cc-pVTZ level of theory is provided in Figure 20(a) and the π*-SOMO isosurface is shown (Figure 20(b)) indicating that the majority of the spin density is located on the $S_{1,2}$ and $N_{3,5}$ atoms. There are in fact a number of known crystal structures containing $N_2S_3^{+\bullet}$, but in all such structures it is found as the antarafacially linked dimer via side-on π*–π* contacts of ~3.0 Å (Figure 20(c) and 20(d)),[208–212] a bonding interaction which may affect the in-plane S–N bond distances somewhat. Hence, for this species, computation is the only way to get the precise structure of the monomeric radical cation. A full assignment of the hfc and *g* tensors was reported by Preston, Sutcliffe, and their coworkers from solid-state experiments in which the radical is doped in a diamagnetic crystal host or measured in frozen solutions (Table 2)[203,207,213] (see Chapter 9.13). The other cyclic isomer, 4,5-$N_2S_3^{+\bullet}$, has the two nitrogen atoms adjacent; there is no evidence for the existence of such a species. No new experimental results have been reported in the past decade for this important nitrogen sulfide free radical; however, an extremely rich chemistry has developed for whole families of related neutral radicals in which one or more S^+ or N is isoelectronically replaced by a planar R–C group (see Section 1.14.5.2).

1.14.3.3.2 The cyclic $N_2S_2^{+\bullet}$ cation radical

Early claims in the literature for the formation of the 1,3-$N_2S_2^{+\bullet}$ cation radical from the dissolution of either N_2S_2 or N_4S_4 in acidic media[214,215] have been convincingly reassigned to the characteristic $I = 1$ quintet with $A(^{14}N) = 0.32$ mT of the thermodynamically stable $N_2S_3^{+\bullet}$ cation radical (see Section 1.14.3.3.1).[216] The solution electrochemistry of cyclo-1,3-N_2S_2 has been reinvestigated in detail in CH_3CN, CH_2Cl_2, and tetrahydrofuran solutions but failed to detect an oxidation process that can be reliably assigned to the formation of the cation radical.[217] Indeed, the process previously reported as the 0/+1 redox couple was observed to occur with $E_m^0 = -0.30$, -0.35, and -0.34 versus $Fc^{0/+}$ in these three solvents. However, this was shown unequivocally to

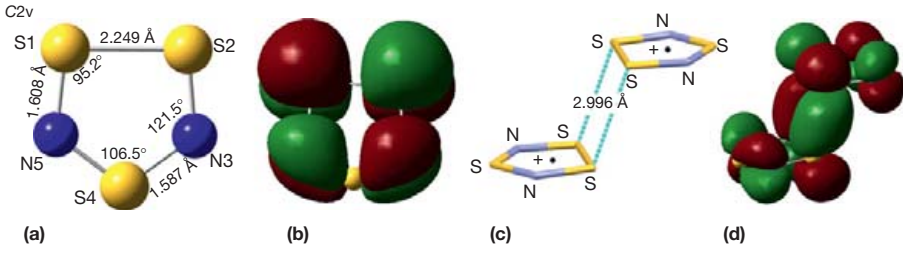

Figure 20 (a) Calculated structure for an isolated $N_2S_3^{+\bullet}$ cation radical in the gas phase and (b) π*-SOMO isosurface. Adapted in part from Boeré, R. T.; Tuononen, H. M.; Chivers, T.; Roemmele, T. L. *J. Organomet. Chem.* **2007**, *692*, 2683–2696, copyright (2007) Elsevier. (c) Antarafacial dimerization in crystal lattices and (d) strong in-phase π*–π* SOMO interactions, based on B3LYP/6-311++G(2df) calculations.

Table 2 Anisotropic and isotropic EPR parameters for the paradigmatic 3,5-$N_2S_3^{+\bullet}$ radical[a]

	g	$A(^{14}N_{3,5})$ (mT)	$A(^{15}N_{3,5})$ (mT)	$A(^{33}S_{1,2})$ (mT)	$A(^{33}S_4)$ (mT)
xx	2.0013	0.918	1.285	3.784	0.893
yy	2.0062	~0	~0	~0	~0
zz	2.0250	~0	~0	−0.882	~0
Average	2.0108	0.306	0.428	0.967	0.298
Isotropic	2.01112(1)	0.319(1)	0.446(3)	0.861(7)	0.297(4)
Calculated[b]		0.32		0.78	−0.29
Calculated[c]		0.36		0.56	−0.34

[a]Fairhurst, S. A.; Johnson, K. M.; Sutcliffe, L. H.; Preston, K. F.; Banister, A. J.; Hauptman, Z. V.; Passmore, J. *J. Chem. Soc., Dalton Trans.* 1986, 1465–1472.
[b]Gassmann, J.; Fabian, J. *Magn. Reson. Chem.* 1996, *34*, 913–920
[c]Boeré, R. T.; Tuononen, H. M.; Chivers, T.; Roemmele, T. L. *J. Organomet. Chem.* 2007, *692*, 2683–2696.

belong to the $N_3S_3^{-/0}$ redox couple, the origin of which is due to rapid reaction of cyclo-1,3-$N_2S_2^{\bullet-}$ with neutral cyclo-1,3-N_2S_2 to form $N_4S_4^{\bullet-}$; the latter is known to decompose rapidly to $N_3S_3^-$ under similar conditions.[175]

1.14.3.3.3 The cyclic $N_4S_4^{+\bullet}$ cation radical

This cation radical, 2,4,6,8-$N_4S_4^{+\bullet}$ (structure and atom numbering in Figure 19(c)), is the postulated intermediate for the AsF_5 oxidation of N_4S_4 that leads via elimination of NSN to $N_2S_3^{+\bullet}$,[205] but its presence in these reactions has not been proved. The only reported EPR spectrum of $N_4S_4^{+\bullet}$ is a ~4.5 mT broad, featureless, signal generated in frozen $CFCl_3$ solution many years ago using γ-irradiation.[218] The average g value of this spectrum is 2.004, and the lack of resolved ^{14}N hfc was interpreted by the authors to indicate it to be a π*-radical with a planar structure. The planar structure was confirmed by recent DFT calculations at the UB3LYP/(aug)cc-pVTZ level of theory with the geometry and SOMO isosurface shown in Figure 19(d). This study provided calculated isotropic hfc values for $[S_4N_4]^{+\bullet}$ of $A(^{14}N) = 0.32$, $A(^{33}S_{1,5}) = 0.78$, and $A(^{33}S_{3,7}) = -0.39$ mT, thus quite similar to those found for $N_2S_3^{+\bullet}$.[129] All claims for the solution-phase detection of cation radicals from, for example, dissolution of N_4S_4 in strong acids have been reinterpreted as being due to formation of $N_2S_3^{+\bullet}$ (see Section 1.14.3.3.1). In a recent thorough reinvestigation of the solution electrochemistry of N_4S_4 in CH_3CN and CH_2Cl_2 solutions, no oxidation process was detected out to the solvent limit so long as scans are first taken in the anodic direction (Section 1.14.3.4.4).[175]

1.14.3.4 Anionic Nitrogen Sulfide Radicals ($NSN^{\bullet-}$, $N_2S_2^{\bullet-}$, $N_2S_4^{\bullet-}$, $N_4S_4^{\bullet-}$, and $N_5S_4^{2\bullet-}$)

1.14.3.4.1 The $NSN^{\bullet-}$ anion radical

The experimental EPR claims for the $NSN^{\bullet-}$ radical are quite diverse. It was first postulated as the species formed when N_2S_2 is reduced with metallic potassium in dimethoxyethane.[214] A very similar spectrum is obtained when $N_5S_4^{\bullet-}$ is cathodically reduced in CH_2Cl_2 solution at RT within an EPR electrolysis cell.[219] A similar EPR spectrum was obtained from hydrolysis of dilute solutions of $[PhCN_3S_2]_2$ in CH_2Cl_2 in air,[220] and as a byproduct of oxidative electrolysis of $N_3S_3^-$ in CH_2Cl_2 solution.[175] In all of these measurements, the two equivalent ^{14}N nuclei display A_N ~0.50–0.52 mT, in reasonable agreement with the UB3LYP/(aug)cc-pVTZ calculated value of 0.40 mT.[129] The calculated geometry of this bent anion radical is shown in Figure 21(a); it may be compared to the geometry of $[NSN]^{2-}$ which has only recently been crystallographically characterized, with S–N = 1.484(3)Å and ∠NSN = 129.9(2)°.[221] The increased size of the bond angle in the anion radical is consistent with one fewer 'lone-pair-like' electron than in the dianion. The SOMO (Figure 21(b)) is an in-plane a_2-symmetric orbital dominated by N p and S s atomic orbitals, that is, an MO that bears a topological resemblance to the SOMO of $[SNS]^{\bullet}$, except that the S and N atoms are transposed. Thus, for $NSN^{\bullet-}$, it is the ^{33}S nucleus that has the larger calculated hfc constant of 3.08 mT, while the two ^{14}N nuclei have quite small calculated hfc constants (0.40 mT) indicative of small s-orbital coefficients for N. It is interesting in this context that Chivers and Hojo reported that the exhaustive controlled potential electrolysis of S_4N_4 at –2.8 V versus Ag/Ag^+ eventually produces $[NSN]^{2-}$ quantitatively.[222] However, voltammetry conducted on the resulting solution in which the $[NSN]^{2-/\bullet-}$ redox couple might have been observed was not reported.

1.14.3.4.2 The $N_2S_2^{\bullet-}$ anion radical and protonated $N_2S_2H^{\bullet}$

The DFT calculated gas-phase geometry and isotropic hfc values for this anion radical concluded that it adopts a D_{2h} geometry quite similar to that of the parent neutral compound but with calculated bond lengths 0.064 Å longer than in the neutral molecule, consistent with single-electron population of the π* SOMO (Figure 22(a) and 22(b)). An exhaustive solution electrochemistry study of N_2S_2 in CH_3CN, CH_2Cl_2, and tetrahydrofuran containing electrolyte has been undertaken.[217] Cathodic scans indicate a rich reductive voltammetry with an irreversible first reduction occurring respectively at −1.40, −1.37, and −1.29 V versus $Fc^{0/+}$ in the three solvents. Upon further cathodic scanning, the CV shows continuous current flow, with a second irreversible peak occurring at −2.18, −2.20, and −2.25 V in the same solvents. Reversal of the scan direction after traversing either the first or the second cathodic processes shows a strong quasi-reversible oxidation process that is readily identified as being due to the $N_3S_3^{-/0}$ redox couple. These results have been interpreted and kinetically modeled in terms of the rapid dimerization reaction between $N_2S_2^{\bullet-}$ and excess N_2S_2 to form $N_4S_4^{\bullet-}$ in solution (see Section 1.14.3.4.4). No EPR signal could be detected from $N_2S_2^{\bullet-}$ due to its very short lifetime; however, protonation

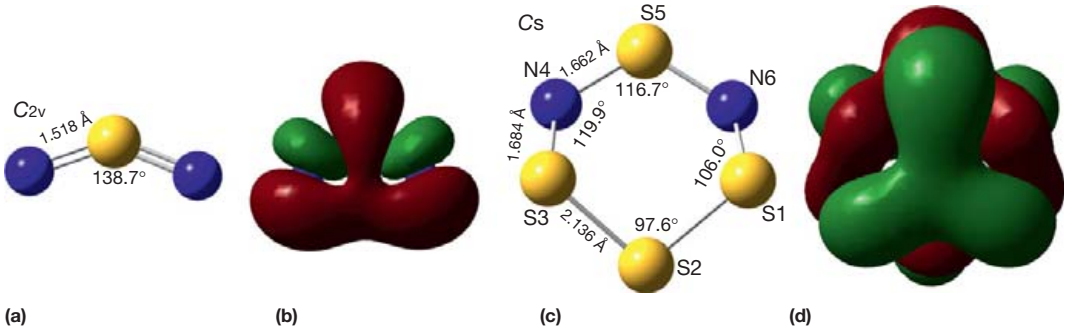

Figure 21 (a) UB3LYP/(aug)cc-pVTZ calculated geometry and (b) SOMO orbital isosurface for $NSN^{\bullet-}$. (c) UB3LYP/(aug)cc-pVTZ computed gas-phase structure and (d) SOMO isosurface for 4,6-$N_2S_4^{\bullet-}$. Adapted in part from Boeré, R. T.; Tuononen, H. M.; Chivers, T.; Roemmele, T. L. *J. Organomet. Chem.* **2007**, *692*, 2683–2696, copyright (2007) Elsevier.

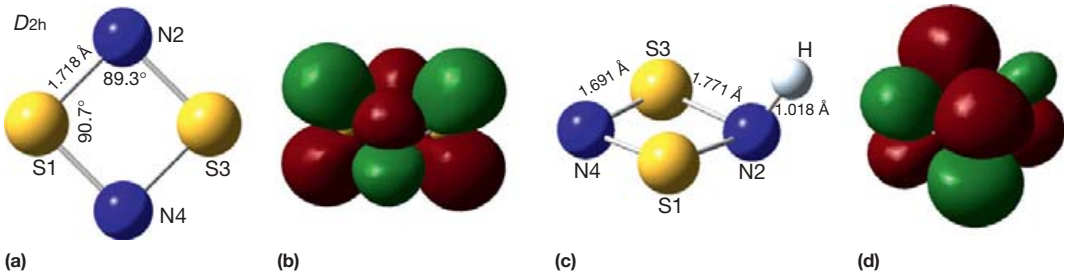

Figure 22 (a) UB3LYP/(aug)cc-pVTZ calculated structure and (b) SOMO isosurface for $N_2S_2^{\bullet-}$. Adapted from Boeré, R. T.; Tuononen, H. M.; Chivers, T.; Roemmele, T. L. *J. Organomet. Chem.* **2007**, *692*, 2683–2696, copyright (2007) Elsevier. (c) UB3LYP/(aug)cc-pVTZ geometry-optimized structure and (d) SOMO isosurface of the protonated radical $N_2S_2H^{\bullet}$. Taken in part from Roemmele, T. L.; Konu, J.; Boeré, R. T.; Chivers, T. *Inorg. Chem.* **2009**, *48*, 9454–9462, copyright (2009) American Chemical Society. Dr. H. M. Tuononen, University of Jyväskylä, Finland is acknowledged for the DFT calculation on $N_2S_2H^{\bullet}$.

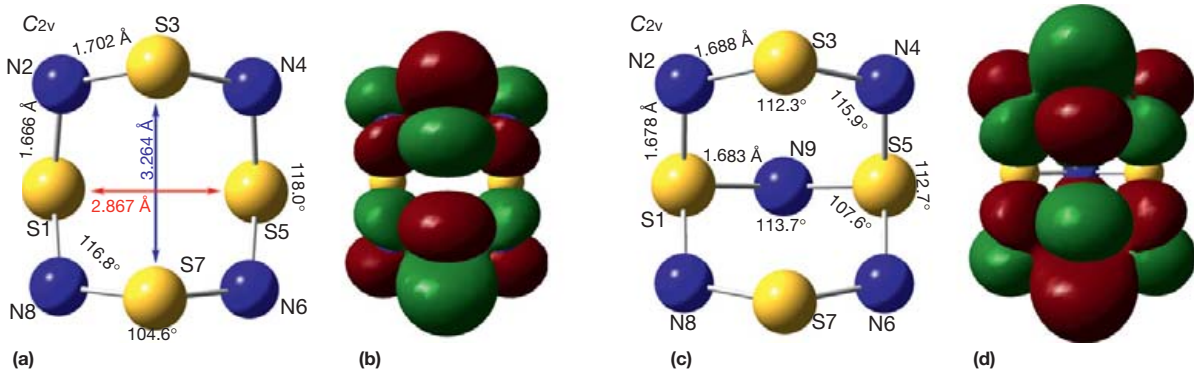

Figure 23 (a) Computed C_{2v} UB3LYP/(aug)cc-pVTZ gas-phase geometry and (b) SOMO isosurface for $N_4S_4^{\bullet-}$. (c) UB3LYP/(aug)cc-pVTZ gas-phase geometry and (d) SOMO isosurface for $N_5S_4^{2\bullet-}$. Adapted from Boeré, R. T.; Tuononen, H. M.; Chivers, T.; Roemmele, T. L. *J. Organomet. Chem.* **2007**, *692*, 2683–2696, copyright (2007) Elsevier.

from adventitious or deliberately introduced moisture or acid produced strong solution-phase EPR signals attributed to $N_2S_2H^{\bullet}$ (Figure 22(c)): $A(^{14}N_1 = 1.12)$; $A(^{14}N_2 = 0.65)$; $A(^1H = 0.60\ mT)$; and $g = 2.0136(1)$ at −20 °C in CH_3CN. This radical has an estimated half-life in solution of 7(1) s at −70 °C.[217] Consistent with the mechanism established by electrochemistry, a variety of chemical reducing agents was found to reduce N_2S_2 to salts of $N_3S_3^-$ quantitatively.

1.14.3.4.3 The $N_2S_4^{\bullet-}$ anion radical

The reduction of neutral 4,6-N_2S_4 (Section 1.14.3.2.1) by polarography and rotating-disk-electrode voltammetry was investigated some time ago showing that the initial reduction product, presumably the radical anion 4,6-$N_2S_4^{\bullet-}$ (structure and numbering in Figure 21(c)), is unstable with respect to disproportionation to other binary sulfur–nitrogen anions.[223] The overall reaction at a platinum rotated-disk electrode corresponds to $9\ N_2S_4 + 10\ e^- \rightarrow 6\ NS_4^- + 4\ N_3S_3^-$. The two ultimate products were detected by UV–vis spectroscopy of the electrolyzed solutions. More recently, the UB3LYP/(aug)cc-pVTZ computed gas-phase structure and isotropic hfc constants for the putative 4,6-$N_2S_4^{\bullet-}$ anion radical have been reported.[129] The SOMO (Figure 21(d)) is a pseudo-π* orbital that is antibonding over the N=S=N portion of the molecules, and the computed bond distances reflect bond lengthening in this region compared to crystal structures of the neutral compound.

1.14.3.4.4 The $N_4S_4^{\bullet-}$ anion radical

The anion radical $N_4S_4^{\bullet-}$ is the next-best characterized nitrogen sulfide free radical after $N_2S_3^{+\bullet}$; whereas the latter is a thermodynamically stable planar π-radical, $N_4S_4^{\bullet-}$ is a cage-shaped, reactive, short-lived intermediate (half-life = 50 s at −21.6 °C) that has been identified through *in situ* electrolysis at low temperatures.[175,224,225] The gas-phase structure was recently computed at the UB3LYP/(aug)cc-pVTZ level of theory along with calculated isotropic hfc values (Figure 23(a)).[129] The expected Jahn–Teller distortion of the D_{2d} structure of the neutral N_4S_4 cage leads to a symmetry-lowered C_{2v} geometry in which all four nitrogen atoms remain equivalent but the two pairs of sulfur atoms are no longer equivalent as a consequence of population of the transannular-antibonding SOMO (Figure 23(b)). This is reflected in the calculated hfc values: $A(^{14}N) = +0.08$, $A(^{33}S_{1,5}) = -0.65$, and $A(^{33}S_{3,7}) = +0.97$ mT.

EPR spectra from $N_4S_4^{\bullet-}$ detected in an *in situ* EPR-electrochemistry cell at subambient temperatures have been reported for each isotopic species $^{14}N_4{}^{32}S_4^{\bullet-}$, $^{15}N_4{}^{32}S_4^{\bullet-}$, and $^{14}N_4{}^{33}S_4^{\bullet-}$ as part of a detailed re-investigation of the voltammetry of N_4S_4 in a variety of common solvent/electrolyte systems.[175] The measured hfc values at −20 °C in CH_2Cl_2 solution are: $A(^{14}N) = 0.1175$, $A(^{15}N) = 0.1535$, and $A(^{33}S_{1\text{-}7}) = 0.20$ mT; $g = 2.0008(1)$. These data are consistent with a rapid exchange process between the two degenerate C_{2v} structures of the anion radical at −20 °C resulting in averaging of the

$A(^{33}S)$ hfc values (the calculated average due to the opposite signs of the two values comes to 0.32 mT). In this study, the average agreement between calculated and measured hfc values was only 30%, which was attributed to the sensitivity of the hfc values to the precise geometry adopted in solution by such a nonplanar, nonrigid species. The ^{14}N hfc values were found to be small relative to the spectral linewidths (~0.06 mT) resulting in a very characteristic EPR signature for $^{14}N_4{}^{32}S_4{}^{\bullet-}$. Based on detailed digital simulations of the cyclic voltammetric data (Figure 24(a)) and stoichiometry established from rotated-disk voltammetry as well as bulk electrolysis, this work proposed a detailed mechanism for the rearrangement of the activated $N_4S_4{}^{\bullet-}$ anion radical through a well-attested 1,3-nitrogen shift reaction followed by expulsion of $NS^{\bullet}$, the latter rapidly oligomerizing to fresh N_4S_4 (Figure 24(b)). An Arrhenius activation energy for the first-order decay of $N_4S_4{}^{\bullet-}$ was measured as 62(2) kJ mol^{-1} in reasonable agreement with earlier results.[225] There is an obvious similarity here to the proposed mechanism for photolysis of N_4S_4 in a noble gas matrix (see Section 1.14.3.1.9 and Figure 16).

1.14.3.4.5 The $N_5S_4{}^{2\bullet-}$ dianion radical

The neutral radical $N_5S_4{}^{\bullet}$ is unknown, but the radical dianion $N_5S_4{}^{2\bullet-}$ was reported to be a short-lived species at low temperature by *in situ* EPR-electrochemical reduction of $[^nBu_4N][N_5S_4]$ in CH_2Cl_2 solution at –40 °C.[219] Recent UB3LYP/(aug)cc-pVTZ calculations predicted the geometry shown in Figure 23(c), which is quite similar to that of the well-characterized parent anion $N_5S_4{}^-$, except for the marked increase in the size of the transannular $S_3...S_7$ distance from 2.71 to 3.34 Å. The calculated isotropic hfc values at this level of theory were reported as: $A(^{14}N_{1\text{-}4}) = 0.10$, $A(^{14}N_5) = -0.10$, $A(^{33}S_{1,2}) = -0.30$, and $A(^{33}S_{3,4}) = 1.05$ mT.[129] The experimental EPR spectrum for this species is quite characteristic with $A(^{14}N_{1\text{-}4}) = 0.175$ and $A(^{14}N_5) = 0.05$ mT, fully consistent with greater spin density on the four equal equatorial nitrogen nuclei and less on the unique bridging nitrogen (Figure 23(d)). The smaller coupling is only slightly larger than the experimental linewidth of 0.04 mT. Neither the lifetime nor the *g* value of this dianion radical has been reported.[219] When electrolysis was conducted at higher temperatures, $N_5S_4{}^{2\bullet-}$ was not detected and instead complex mixtures of EPR signals were observed including one attributed to $NSN^{\bullet-}$ (see Section 1.14.3.4.1).

1.14.4 Nitrogen Selenide and Telluride Radicals

It is often asserted that the bond energies in nitrogen selenides and tellurides are significantly lower than in the sulfides to rationalize the much smaller scope for their chemistry. Certainly, it must be acknowledged that N_4Se_4 is viciously explosive and extremely touch-sensitive and should only be made using extreme caution. It has been shown to have a similar structure to that of N_4S_4 but the tellurium analog is not known; instead, there are different structural types with formulas such as N_8Te_6. The standard heat of formation ΔH°_f for $N_4S_4(s)$ obtained from measurements of the heat of decomposition is +460(8) kJ mol^{-1}, for which the average N–S bond energy in N_4S_4 is 307.5(41) kJ mol^{-1}, and thus higher than the average N–S single bond energy of ~188 kJ mol^{-1}. The corresponding values for N_4Se_4 are +618(25), 247(42), and ~167 kJ mol^{-1}, respectively.[226] This suggests that inherently weak bonds can be only part of the picture; lack of kinetic stability as well as unexpectedly low volatility may also be contributing factors. It has been shown that unsaturated N–Se and N–Te bonds are strongly associated by dipole–dipole contacts to neighboring molecules in solid lattices.[227] Considerable progress has been made in recent years for both nitrogen selenide[228] and nitrogen telluride chemistry.[229] However, very little is as yet known about free radicals.

1.14.4.1 Nitrogen Monoselenide ($NSe^{\bullet}$), Nitrogen Diselenide ($SeNSe^{\bullet}$), and Their Oligomers

1.14.4.1.1 Nitrogen monoselenide ($NSe^{\bullet}$)

The $NSe^{\bullet}$ radical has been known for a long time as a transient species that can be formed in the gas phase and detected

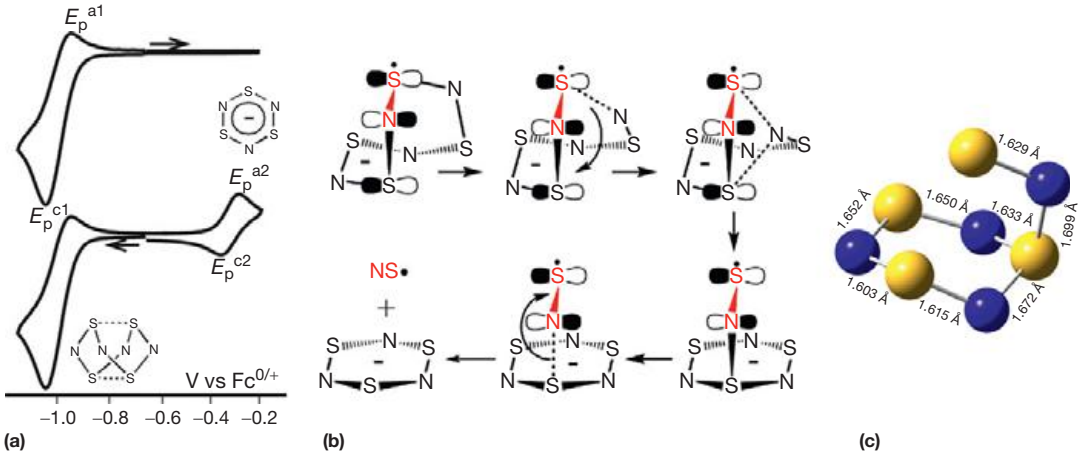

Figure 24 (a) Representative cyclic voltammograms showing the interrelationship of $N_4S_4{}^{\bullet-}$ and $N_3S_3{}^-$; scanning anodically first detects nothing at −0.3 V versus $Fc^{0/+}$, but after scanning cathodically through the $N_4S_4{}^{-/0}$ couple a strong wave is observed for the $N_3S_3{}^{-/0}$ redox couple. (b) Proposed mechanism for 1,3-nitrogen shifts in the anion radical followed by elimination of $NS^{\bullet}$ (compare Figure 16). (c) The PBE1PBE/(aug)cc-pVTZ geometry optimized structure including bond lengths of the intermediate [*cyclo*-N_3S_3–N=S]$^{\bullet-}$ from which $NS^{\bullet}$ is expelled. Adapted from Boeré, R. T.; Chivers, T.; Roemmele, T. L.; Tuononen, H. M. *Inorg. Chem.* **2009**, *48*, 7294–7306, copyright (2009) American Chemical Society.

by electronic spectroscopy.[230–233] Brown determined the vibrational–rotational spectrum using laser magnetic resonance (because it is a paramagnetic molecule).[233] The vibrational band origin for $N^{80}Se^{\bullet}$ is determined to be 944.54216 (9) cm^{-1}. It has the same $X\,^2\Pi_{1/2}$–$X\,^2\Pi_{3/2}$ anomaly as $NO^{\bullet}$ and $NS^{\bullet}$ but the spin–orbit coupling term of $\tilde{A} = 891.89132(11)$ cm^{-1} is much larger than for the lighter exemplars; moreover, it is very close to the fundamental vibrational level for $X\,^2\Pi_{1/2}$ so that there is considerable mixing between the v+1 rotational lines of $X\,^2\Pi_{1/2}$ and the v=0 rotational lines of the $X\,^2\Pi_{3/2}$ levels (the effect of this on rotational spectroscopy is termed an 'anomalous Λ doubling' of the rotational progressions). Thus, in every way, $NSe^{\bullet}$ behaves as a direct analog to $NS^{\bullet}$ although there are no reports as yet regarding its detection in interstellar dust or comets. This lack of astrochemical significance perhaps explains the far fewer studies in the literature compared to $NS^{\bullet}$. Andrews was able to prepare $NSe^{\bullet}$, $SeNSe^{\bullet}$, and NSe_2^{+} species by condensing the effluent from an argon/nitrogen/selenium microwave discharge onto a 12 K substrate and identify them by IR spectroscopy using isotopic substitution.[234,235] Key physical parameters measured or calculated for $NSe^{\bullet}$ are compiled in Table 1.

1.14.4.1.2 Oligomers of nitrogen monoselenide ($NSe^{\bullet}$): $SeSeNSe^{\bullet}$, N_4Se_4, and $Se_2N_4S_2$

The matrix work of Andrews also provided the first evidence for direct synthesis of an oligomer of $NSe^{\bullet}$, namely NSeNSe, and the open-shell adducts *cis*- and *trans*-$SeSeNSe^{\bullet}$.[234,235] No comprehensive evaluation of the potential energy surface for oligomers of $NSe^{\bullet}$ has been undertaken of the kind that has been reported for $NS^{\bullet}$.[163] The most important oligomer is N_4Se_4; a chemical synthesis from the condensation reaction between $SeCl_4$ or $SeBr_4$ and liquid ammonia has been known for a long time.[236] The crystal structure shows the same D_{2d} cage structure for the molecule as in N_4S_4.[237] The N–N distance is 2.82, Se–Se 2.97 Å. The transannular Se–Se contact from diffuse π*–π* interactions is 2.76 Å, the mean value of the Se–N bond length is 1.80 Å, the ∠N–Se–N 103° and ∠Se–N–Se 111°. The careful reaction of $SeCl_4$ and $Me_3SiNSNSiMe_3$ in CS_2 at −70 °C yields 1,5-$Se_2N_4S_2$ (numbered as in Figure 23(a)), a mixed oligomer of $NS^{\bullet}$ and $NSe^{\bullet}$, isostructural with N_4S_4.[238]

1.14.4.1.3 $NSe^{\bullet}$ and transition metals: selenonitrosyl complexes

The first and only example of a selenonitrosyl complex was reported in 1998 by the method of reacting elemental selenium with an osmium nitride complex.[239] The ν(NSe) stretching band in the complex was found at 1156 cm^{-1}, a much higher frequency than gas-phase $NSe^{\bullet}$ (Table 1) and is suggestive of NSe^{+} character in the complex. The ^{15}N NMR spectrum has a chemical shift of +65.6 relative to nitromethane and shows one-bond N–Se coupling of 140(6) Hz. The structures and properties of the whole series $CpCr(CO)_2NE$ (E = O, S, Se, and Te) were investigated, albeit using probably inadequate semi-empirical methods.[240] It was shown that the Cr–N bond order increases steadily with the higher chalcogenides, while the N–E bond orders are calculated to decrease from 1.47 for $NO^{\bullet}$ to only 0.76 for $NTe^{\bullet}$. High-quality DFT calculations have been undertaken for $[Cr(NSe)(H_2O)_5]^{2+}$ along with the nitrido, nitrosyl, and thionitrosyl analogs. The σ-donating ability was found to be in the order $N^{3-} >> NO^{\bullet} < NS^{\bullet} \approx NSe^{\bullet}$, whereas the π-accepting order is $NO^{\bullet} > NS^{\bullet} \approx NSe^{\bullet}$.[160]

1.14.4.1.4 Nitrogen diselenide ($SeNSe^{\bullet}$) and $ONSe^{\bullet}$

Matrix studies of nitrogen selenides produced the first evidence for $SeNSe^{\bullet}$, the direct analog to $NO_2^{\bullet}$ and $SNS^{\bullet}$, and IR spectroscopy supported the expected bent structure with ∠SeNSe = 146(5)°.[234,235] These experiments also provide evidence for the existence of a second isomer, that is, $SeSeN^{\bullet}$, which, like the sulfur analog $SSN^{\bullet}$, is a higher-energy species than the symmetric isomer (from DFT calculations). Mixed radicals were also detected such as $ONSe^{\bullet}$ with the source of oxygen being the quartz walls of the reactor and with a fundamental vibration at 1570 cm^{-1} in the argon matrix at 12 K. There are no reports on bona fide oligomers of $SeNSe^{\bullet}$ in the literature.

1.14.4.2 Cationic Nitrogen Selenide Radicals $N_2S_xSe_y^{+\bullet}$ (x+y=3)

Many, but not all, mixed S/Se derivatives of trithiadiazolyl, the most stable and best-characterized nitrogen sulfide radical, have been prepared as shown in Scheme 8.

The preparation of $N_2SeS_2^{+\bullet}$ (Scheme 8) from $NS^{+}AsF_6^{-}$ and Se is consistent with the intermediate formation in solution of $SeNS^{+}$ which then undergoes a concerted cycloaddition reaction with more NS^{+}.[241] Note that these reactions always produce mixtures of mono- and dications, the latter are important species but not the focus of this article. The reaction of $[(Me_3Si)_2N]_2S$ with a 2:1 mixture of $SeCl_4$ and Se_2Cl_2 affords $[(N_2Se_2S)Cl]_2$ and the product was identified by vibrational spectroscopy.[236] In a manner analogous to the production of $N_2S_3^{+\bullet}$ by oxidation of N_4S_4 with S_8^{2+}, $N_2Se_2S^{+\bullet}$ (Scheme 8) was also prepared as its π-dimer in solid lattices by oxidation of N_4S_4 with Se_4^{2+}.[242] $N_2Se_3^{+\bullet}$ (Scheme 8) was prepared by the direct oxidation of N_4Se_4 in SO_2 with AsF_5.[243] This all-selenium species was also found among several nitrogen selenide cations produced by laser ablation of elemental Se in the presence of N_2 followed by supersonic expansion.[244] It is much more thermodynamically stable than N_4Se_4 and can be heated in solution and in the solid state without decomposition. It has the typical antarafacial dimeric structure for this type of species in the solid state (Figure 20(c)).

The reaction between the well-known sulfur transfer agent $[(Me_3Si)_2N]_2S$ with an equimolar amount of $SeCl_4$ in dioxane at 50 °C affords $[(N_2Se_2S)Cl]_2$ in excellent yield.[245] This reaction, depending on conditions, can also produce 1,5-$Se_2N_4S_2$ (CS_2, −70 °C). Maaninen *et al.* believe that this is because the neutral N_4E_4 is an intermediate on the way to making the $N_2E_3^{+\bullet}$ radical. A strong EPR signal was observed for a powdered sample of $[(N_2Se_2S)Cl]_2$ with $A(^{14}N) = 1.298$ mT and $g = 2.0143$ at RT indicating the presence of radical impurities among the dimers in the solid state, but insufficient solubility prevented measurement of solution-phase spectra. This, the most recent paper on the subject, suggests that the

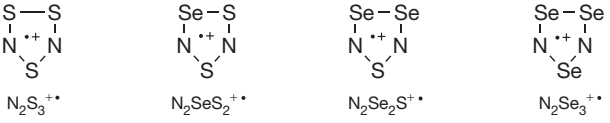

Scheme 8 Cationic nitrogen selenide radicals $N2S_xSe_y^{+\bullet}$.

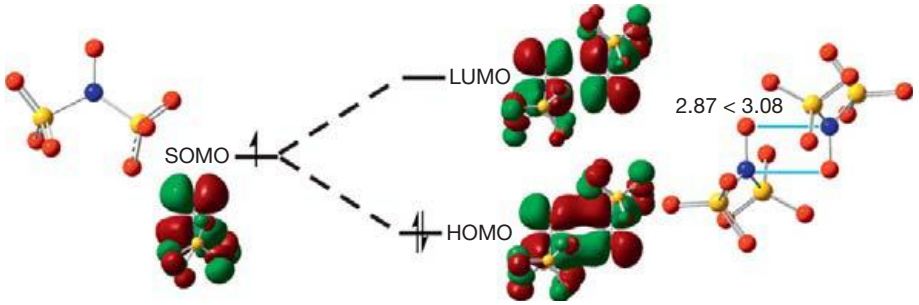

Figure 25 A diffuse π*–π* dimer between two Fremy's anions which unlike $(NO)_2$ has a head-to-tail orientation. The O to N contact distance of 2.87 Å is ~7% less than the sum of their van der Waals' radii. Based on B3LYP/6-311++G(2df) calculations using anion coordinates from Howie, R. A.; Glasser, L. S. D.; Moser, W. *J. Chem. Soc. A* **1968**, 3043–3047.

Table 3 Average interatomic distances (Å) & bond orders for $N_2E_3^{+\bullet}$ dimers, and EPR data (mT) for the radicals

	$N_2S_3^{+\bullet}$		$4\text{-}N_2S_2Se^{+\bullet}$		$1,2\text{-}N_2SSe_2^{+\bullet}$[a]		$1,2\text{-}N_2SSe_2^{+\bullet}$[b]		$N_2Se_3^{+\bullet}$	
	dist(A)	*bond order*	*dist(A)*	*bond order*	*dist(A)*	*bond order*	*dist(A)*	*bond order*	*dist(A)*	*bond order*
S-S	2.13	0.74								
Se-S			2.27	0.82						
Se-Se					2.35	0.91	2.35	0.85	2.40	0.82
N=S=N	1.56	1.85	1.57	1.79	1.56	1.85	1.56	1.85		
N=Se=N									1.71	1.85
N-S	1.63	1.48	1.68	1.25						
N-Se			1.73	1.73	1.76	1.42	1.80	1.25	1.76	1.57
S···S	2.92	0.06								
Se···S			3.11	0.05						
Se···Se					3.14	0.07	3.07	0.08	3.14	0.07
g iso	2.0111		2.0262		2.0472				2.043	
$A(^{14}N)$ av	0.306		0.267		0.2427				0.30	
$A(^{77}Se)$			10.							

Structural data from Maaninen et al.[245] EPR data from Awere et al.[243,246]
[a]AsF_6– salt.
[b]Cl– salt.

application of the latest methodologies and reagents could really open up this field of study and perhaps lead to novel applications of nitrogen selenide radicals. Just as is the case for $N_2S_3^{+\bullet}$, there is an extensive chemistry of heterocyclic nitrogen selenide species by replacement of S^+/Se^+ or N with an RC^+ group (see Section 1.14.3.3.1). Replacement of further N or S atoms with organic groups affords thiaselenazolyls and diselenazolyls (see Section 1.14.5.2) (Table 3).

1.14.4.3 Nitrogen Monotelluride (NTe•) and Nitrogen Ditelluride (TeNTe•)

The formula NTe was originally assigned to a highly explosive yellow solid obtained from the reaction of $TeBr_4$ with liquid NH_3,[247] but later work indicates that the correct stoichiometry is closer to N_3Te_4.[248] The use of tris(trimethylsilyl)amine, expected to be a milder and more controllable reagent than ammonia, affords a rhombic dodecahedral cluster of composition $Te_6N_8{\cdot}4TeCl_4{\cdot}4THF$. However, no radicals have been reported from these or other nitrogen telluride clusters.[249] Interest in NTe• and TeNTe• is less driven by astrophysics; there is just one recent report which includes NTe• in a study estimating the Kronecker product periodic system of diatomics by statistical methods for the purpose of establishing radiative transfer models for earth and interstellar atmospheres.[250] Rather, interest derives from the fact that tellurium is a reactive fission product from nuclear reactors.[251] Laser ablation of elemental Te was conducted in the presence of nitrogen and the effluent condensed in a low-temperature Ar matrix. Fourier transfer infrared (FTIR) spectroscopy detected the presence of both NTe• and TeNTe•. For the former, split features were detected at 790.3 and 783.5 cm^{-1} similar to those observed for NSe•. For TeNTe•, DFT calculations predict three bands at 150.2, 377.6, and 887.5 cm^{-1}. An intense experimental feature was observed at 973.5 cm^{-1} which was assigned to this species with the typical bent structure of an ENE• radical. A fundamental vibration attributed to ONTe• was also observed at 1575.7 cm^{-1} analogous to the formation of ONS• and ONSe• (see Sections 1.14.3.2.1 and 1.14.4.1.1). The bond distances in NTe• and NTe^+ as well as the ionization energies and fundamental stretching frequencies have been determined by a wide range of quantum and DFT calculations.[252] Key molecular parameters are compiled in Table 1.

1.14.4.3.1 NTe• and transition metals: telluronitrosyl complexes

The method used successfully to prepare an osmium NSe• complex failed with elemental tellurium.[239] The failure could

be due to lack of a suitable tellurium transfer reagent. A reaction of exactly this type was recently reported in which elemental tellurium was added to a ruthenium carbide complex resulting in a tellurocarbonyl complex.[253]

1.14.5 Chalcogen–Nitrogen Hetero-Radicals (Including Organic Derivatives)

For nitrogen oxide radicals, there are only three major types of organic or other hetero-substituted derivatives: the aminoxyls, $R_2NO^{\bullet}$ (better known as nitroxides), the isomeric *N*-alkoxyaminyls, $RN^{\bullet}OR'$, as well as iminoxyls, $R_2C{=}NO^{\bullet}$, derivatives of the imine functional group which are outside the scope of this chapter.[254] By contrast, hetero-substituted nitrogen radicals containing chalcogens beyond the second period form a large and diverse field of stable linear and cyclic free radicals. The most abundant examples involve the isoelectronic replacement of Se^{+}/S^{+} or N by an unsaturated R–C, R_2P^{V}, or R_2As^{V} moiety. As for aminoxyls, a multiplicity of examples is possible merely by changing the 'R' group substituents and this leads to such a wealth of detail that an exhaustive account is beyond the space available here. However, the main paradigmatic forms will be mentioned briefly and readers looking for greater depth can confidently be directed to the superb book chapter by Hicks.[123] The latter work also provides a useful roadmap to the extensive materials properties and applications of stable hetero-thiazyl radicals. Another review which is focused on stable heterocyclic radicals is also worth consulting.[256] The importance of the magnetic properties of some hetero-radicals in this class has been highlighted.[257]

1.14.5.1 Hetero-Radicals Derived from Hydroxylamine

1.14.5.1.1 Aminoxyl radicals (nitroxides)

Among the oxygen derivatives, aminoxyls (Scheme 9) represent by far the majority and there is a vast literature for this class; over 1500 crystal structures of aminoxyls or aminoxyl-derivatives are known and over 8000 citations have been reported in the past decade. An excellent summary has recently been published.[258] Several book-length treatments are available, the most recent by Likhtenshtein.[259] Aminoxyls are exceptionally stable. They have four electrons less than $NO^{\bullet}$, resulting in a $(\sigma)^2(\pi)^1$ configuration with a bond order of 1.5 (d(N–O) = 1.25 to 1.30 Å) and bond energies of typically ~400 kJ mol^{-1}. The spin density is very evenly distributed between O and N. When the 'R' groups are reasonably bulky as in the famous 2,2,6,6-tetramethylpiperidyl-1-oxide (TEMPO), the radicals often crystallize unassociated or with very weak contacts through the oxygen atoms. However, aminoxyls which lack sterically shielding side groups normally dimerize in the solid state as π*–π* dimers (in contrast to the sulfur analog, Section 1.14.5.1.3). For example, in crystalline Fremy's salts (the sodium or potassium salts of $[(O_3S)_2NO^{\bullet}]^{2-}$), the two $NO^{\bullet}$ groups align sideways head to tail (Figure 25), unlike *cis*-ONNO. A geometrically similar dimerization of two $R_2NO^{\bullet}$ groups occurs on the rim of a calixarene.[260] Fremy's salts are suitable probes for studying rotational diffusion by EPR spectroscopy in RT ionic liquids to probe their fluid behavior.[261]

1.14.5.1.2 N-Alkoxyaminyl radicals

N-alkoxyaminyl radicals (Scheme 9) are much less well known than their branched cousins, although approximately ten crystal structures have been reported for this class. First discovered in 1967[262] and structurally characterized in 2001, this radical has found use as a spin trap.[263] Recently, Tanaka *et al.* have performed a series of DFT calculations to establish the best parameters for predicting both the g values and the $A(^{14}N)$ values for aminoxyls and alkoxyaminyls.[264] *N*-Alkoxyaminyls seem to have somewhat smaller A(N) and g values than similarly substituted aminoxyls, which seems to be due to significantly greater delocalization of the spin onto the *N*-aryl group than is typical for aminoxyls.[265]

1.14.5.1.3 Aminothiyl radicals, $R_2NS^{\bullet}$ (thionitroxides)

The structure of H_2NSH, the sulfur analog of hydroxylamine, has been determined by microwave spectroscopy, indicating that *cis* and *trans* conformers have very similar energies with NS bond distances of 1.705 and 1.719 Å, respectively.[266] There is only fleeting evidence for existence of $H_2NS^{\bullet}$, but organic derivatives $R_2NS^{\bullet}$, dialkylaminothiyl radicals (Scheme 9), are known from the photolysis or thermolysis of their weak disulfide-linked dimers (Figure 26(a)).[255,267] Twenty-one crystal structures of such dimers have been reported in the Cambridge Structural Database (CSD) (2011 version). The TEMPO analog bis(2,2,6,6-tetramethylpiperidyl-1) (TEMPS, Figure 26(b)) disulfide[268] is a source of the radical for coordination chemistry and for thermo-reversible hemolytic-cleavage type linkages for covalent adaptable polymer networks (CANs).[269]

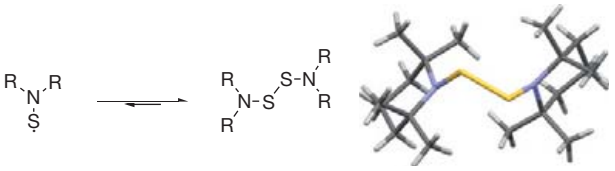

Figure 26 (a) Aminothiyl disulfide equilibria favor the dimers. (b) Representation of the molecular structure of one independent molecule found in the crystal structure of the dimer of TEMPS. From Hursthouse, M. B.; Coles, S. J.; Bricklebank, N., private communication, 2003, in the Cambridge Structural Database version 5.32, 2011.

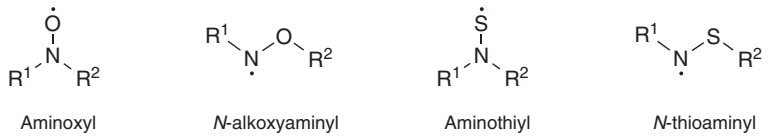

Scheme 9 Hetero-radicals derived from hydroxylamine.

1.14.5.1.4 N-Thioaminyl (RN•SR′) and dithioaminyl radicals (RNS•NR′)

There is an extensive chemistry of RN•SR′ radicals (Scheme 9) which has been developed almost exclusively by the research group of Miura. Fourteen crystal structures of thioaminyls are known, none of which show the disulfide-type coupling of the aminothiyls and all but one of which contain essentially isolated radical units in the solid lattices.[270–274] There is one example which crystallizes as a radical dimer through π*–π* interactions with d(S···N) = 3.266(3) Å.[275] Two structures have also been reported in which 4-pyridyl-substituted thioaminyls are coordinated to metal complexes.[276] A number of heterocyclic thioaminyl radicals have also been reported.[277] Dithioaminyl radicals RNS•NR′ are also known.

1.14.5.2 Hetero-Radicals Derived from 1,3-$N_2E_3^{+\bullet}$

It is noteworthy that the most extensive set of nitrogen chalcogenide hetero-radicals are derivatives of the best-characterized and most stable binary radicals of sulfur and selenium (see Sections 1.14.3.3.1 and 1.14.4.2). Of special importance are the four neutral ring species shown in Scheme 10 which are isoelectronic with the parent radical by virtue or replacement of S^+ (or Se^+) by 'RC' and which can often exist in three oxidation states, as 6π mono-cation, 7π radical, and 8π mono-anion with varying degrees of stability.

1.14.5.2.1 1,2,3,5-Dithiadiazolyl radicals and selenium analogs

Replacement of the unique sulfur atom in 3,5-$N_2S_3^{+\bullet}$ by RC leads to a large family of 1,2,3,5-dithiadiazolyls (1,2-dtda, Scheme 11) which were first reported in 1980 with R = Ph.[278] The chemistry of this compound class was comprehensively reviewed in 1995,[279] as was the extensive electrochemical data including selenium analogs in 2000.[15] A detailed review of the crystal engineering of the various supramolecular synthons for 1,2-dtdas, both interacting among themselves (Figure 27) and with other donor atoms which are normally incorporated on or in the 'R' groups belonging to the 'RC' moieties, has appeared.[280] The impressive diversity observed in such intermolecular interactions seems to be the origin of the properties of the crystalline solids which include semiconductivity and, most famously, spin-canted ferromagnetism in rare examples where the dimerization in the solid state is overcome by intermolecular interactions. Around 35 citations in the literature during the past decade show that interest in this radical type remains strong. It is gratifying to see that the general focus has moved on from basic chemistry and properties to numerous application-oriented studies in materials science.

In solutions of de-oxygenated aprotic solvents and in the gas phase, the dimers dissociate to thermally stable free radicals. The isotropic EPR spectra consist of characteristic 1:2:3:2:1 pentets from coupling to two equivalent nitrogen nuclei; A (^{14}N) ≈ 0.5 mT values are highly conserved as a consequence of a π* SOMO that is nodal at the ring C atom; g values of

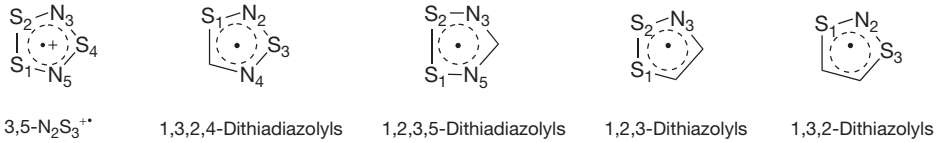

Scheme 10 Hetero-radicals derived from 1,3-$N_2E_3^{+\bullet}$.

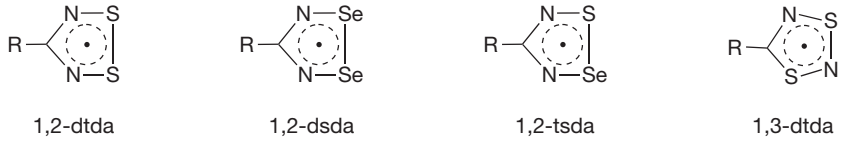

Scheme 11 1,2,3,5-Dithiadiazolyl radicals and selenium analogs.

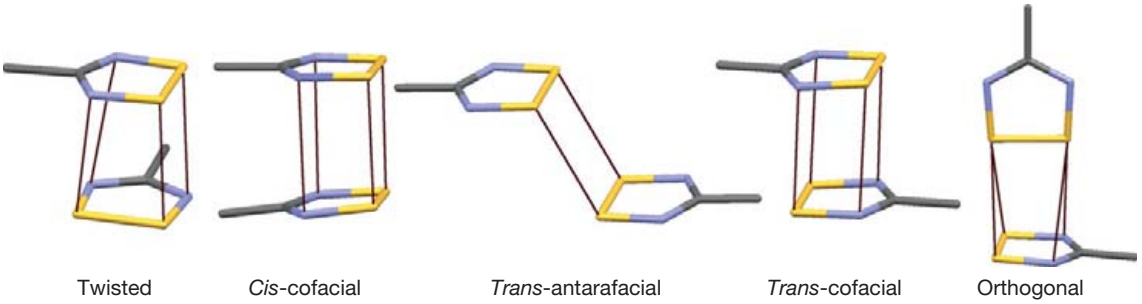

Figure 27 The known configurations for self-association of 1,2,3,5-dithiadiazolyls in solid-state lattices using fragments from real examples reported in the CSD, version 5.32, 2011.[280]

2.011 are typical, but increase to ~2.038 in 1,2,3,5-diselenadiazolyls (1,2-dsda, Scheme 11) which is attributed to higher spin–orbit coupling involving the heavier chalcogen; the latter also have such broad lines that the nitrogen hfc pattern is obscured.[281] Hyperfine coupling to both nitrogen and selenium could be resolved in a frozen glass for $PhCN_2Se_2$, from which the isotropic equivalent values were extracted as $A_{av}(^{14}N) = 0.567$ and $A_{av}(^{77}Se) = 1.20$ mT.[282] Extraction of unpaired spin density from the coupling constants indicates that replacement of S by Se increases the spin density on the chalcogen, consistent with a stronger SeSe dimer interaction and much lower solubility. A mixed 1-thia-2-selena-3,5-diazolyl (1,2-tsda, Scheme 11) has been reported but has not been prepared as a pure material separate from dithia- or diselenadiazoyl.[283]

Recent reports on monomeric 1,2-dtda include the magnetic properties of bulky 2,4,6-tris-(trifluoromethyl)phenyl[284] and *ortho*-chlorophenyl substituted radicals,[285] two studies where the 'R' group is a simple halogen,[286,287] the effect on magnetism and low melting temperature when 'R' is a long fluorous tail,[288] and several studies on the origin of the famous spin-canted ferromagnetism of some of the polymorphs that form when 'R' is 4-XC_6F_4 (X = CN, NO_2).[289–293] A study of other multifluoro aryl derivatives has appeared;[294] it has been shown that crystalline thin films of 1,2-dtda can be deposited on surfaces of highly oriented pyrolytic graphite;[295] the incorporation of 1,2-dtda into mesogenic phases has been attempted;[296] and it has been shown that 1,2-dtda is a product of the thermolysis of sulfur nitrogen cage compounds of type RCN_5S_3.[297]

1.14.5.2.2 1,3,2,4-Dithiadiazolyl radicals

The isomeric 1,3,2,4-dithiazolyls (1,3-dtda, Scheme 11) were first reported in 1985 and are exclusively produced by a general, quantitative, symmetry-allowed cycloaddition reaction between SNS^+ salts (see Section 1.14.3.2.1) and organic nitriles followed by reduction.[298] Considerably less chemistry has been reported for this isomer than for the 1,2-analog in part because while the 6π cations are stable, the 7π radicals undergo photo- and thermally initiated rearrangements whereby the 1,3-isomers convert into the 1,2-isomers.[191,299] Solution electrochemistry shows quasi-reversible behavior for the one-electron reduction from the 6π cation to the 7π radical for most exemplars of this group.[15] The redox potentials for this process for numerous pairs bearing identical substituents show that the 1,3-dtda will be 0.27 V more easily oxidized than the 1,2-isomer (the 1,3-isomer therefore is expected to have a lower first IE, which is borne out by MO calculations). The EPR spectra are dominated by a single large $A(^{14}N) \approx 1.1$ mT to the nitrogen of the NSN moiety on which the π* SOMO is centered; the $A(^{14}N)$ values for the nitrogen atom adjacent to the central ring are typically much smaller, ~0.05–0.06 mT. The smaller ionization energy in the 1,3-isomer can then be rationalized by a major interaction of the SOMO electron with only one rather than two of the more electronegative nitrogen atoms. A recent study demonstrates facile cycloaddition of SNS^+ to several polynitriles, but reduction to radicals was not attempted for these exemplars.[300] Selenium analogs of these 1,3-dtda have not been reported.

1.14.5.2.3 Bis-dithiadiazolyl radicals and selenium analogs

Bis-dithiadiazolyl diradicals spaced by a benzene ring (Scheme 12; $n = 1$) have been prepared and crystallographically characterized with two 1,2-,[301–305] and two 1,3-dtda groups, examples of which have been fully purified with crystal structures. A recent example of such a study contains the first report of a material that contains a bis-dtda radical cation dimer.[306] An example with a substituted biphenyl spacer (Scheme 12(a), n=2) has been structurally characterized.[307] Three 1,2-dta radicals have been combined to one benzene ring to make a triradical.[308] Heterocyclic spacers (furan, thiophene, and triazine) have also been successfully employed.[309–311] Selenium analogs of some of these bridged 1,2-dtda radicals have also been prepared.[301–303] For the mixed 1,2-/1,3-dtda spaced by benzene (Scheme 12(c), $n = 1$), only the diamagnetic dication is structurally characterized.[312] The disjoint diradical 4,4′-bis (1,2,3,5-dithiadiazolyl) (Scheme 12(a), $n = 0$) [313] has been the object of intensive interest, including its use to efficiently harvest an alternating photocurrent[314] and a detailed spectroscopic study of the electronic structures of thin films of this material.[315] The bis-1,3-dtda without a spacer (Scheme 12(b), $n = 0$) has been prepared and purified, its paramagnetism has been shown to increase upon grinding of the solid[316] and the mixed biradical with one 1,2- and one 1,3-dtda ring (Scheme 12(c), n = 0) has been crystallographically characterized.[317]

1.14.5.2.4 1,2,3-Dithiazolyl radicals and selenium analogs

1,2,3-Dithiazolyl radicals (1,2,3-dta, Scheme 13) have been known for a very long time, especially the benzo-fused compounds known as 'Hertz radicals'. Synthetic entry into this system is extremely diverse and thankfully has been recently reviewed,[318] while their structural, physical, and spectroscopic properties have been critically assessed.[319] Like most nitrogen sulfide free radicals, 1,2,3-dta are quite sensitive to molecular oxygen; it is rare that the fate of the reaction is actually known but in one study the product was shown to be a substituted *N*, *N*′-disulfinyl-2,2′-diaminodiphenyl disulfide.[320] A combined pulse EPR and electron nuclear double-resonance spectroscopic study has shown that the spin-density distribution was

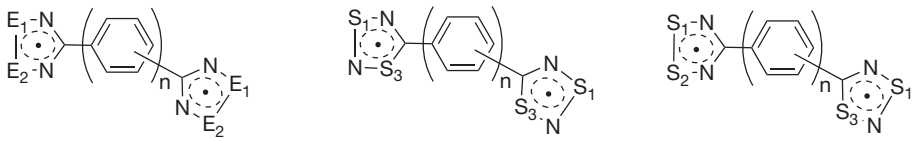

(a) E = S, Se; n = 0, 1, 2 (b) n = 0, 1 (c) n = 0, 1

Scheme 12 *Bis*-dithiadiazolyl radicals and selenium analogs.

nearly the same for 1,2,3-dta and possible thiaselenazolyl isomers (1,2,3-sta; 1,2,3-dsa; Scheme 13).[321] Fused naphthalene 1,2,3-dta derivatives have been prepared with all possible combinations of sulfur and selenium.[322] A highly delocalized 1,2,3-dta radical is formed when it is fused to a thiadiazole–pyrazine ring.[323] A relatively rare example of a well-characterized 1,2,3-dta radical that is not fused to an aromatic ring is $(Cl_2C_3NS)(ClC_2NS_2)$, an isothiazolyl-substituted 1,2,3-dta radical which has evenly spaced, slipped π-stacks but is found to be a Mott insulator.[324] Attempts to prepare 1,2,3-dta analogs containing tellurium in place of sulfur were successful for some 6π cations but not for the 7π radicals.[325,326]

1.14.5.2.5 1,3,2-Dithiazolyl radicals and selenium analogs

The synthesis and structures of 1,3,2-dithiazolyl (1,3,2-dta, Scheme 13) have been critically assessed,[319] while physical and spectroscopic properties, including materials applications, have been emphasized.[327] The cycloaddition of SNS^+ salts (see Section 1.14.3.2) to alkynes represents a particularly elegant entry into this ring system. As with the 1,2,3-isomer, these rings are most commonly fused to an aromatic ring but very stable examples with strongly electron withdrawing groups (CF_3, CN) exist as monocycles.[328,329] The parent 1,3,2-benzodithiazolyl adopts a *trans*-antarafacial geometry in the solid state through diffuse π*–π* bonding but the melt is paramagnetic from monomeric radicals.[330] Much interest is still being shown in the structural and magnetic properties of solids containing related fused-ring dta's, where the aromatic group may be a 2,3-substituted thiophenyl,[331] 2,3-substituted pyridine,[332] or 4-trifloromethylpyridine,[285] a benzothiadiazole group,[333] or a pyrazinothiadiazole.[334] Both the unpaired spin distribution in the radicals and the redox potentials for oxidation and reduction are strongly affected by the different substituents. A primary focus is on the magnetic properties of these species in the solid state as some examples show significant bistability.[335] It has now been shown that cycloaddition of SNS^+ works also for benzo-[336,337] and naphthoquinones,[338] which potentially open up many new ways to derivatize this ring system. Methods have been developed for calculating the hyperfine coupling and *g* tensors in this class using DFT and configuration interaction.[339]

1.14.5.2.6 Bis-1,2,3-dithiazolyl radicals and selenium analogs

There has been a long fascination with thiazyl radicals where two groups are fused to a common linker (most commonly an aromatic ring such as benzene or, occasionally, naphthalene, but also C–C or N–N bonds have been employed).[340] Bis-1,2,3-dta's have a high propensity for forming closed-shell quinoidal ground states (Scheme 14(a)),[341,342] and the radical cations of this latter class have also been investigated for molecular conductivity as charge-transfer species. In order to obtain the benefits of electron delocalization in a neutral species, the research group of Oakley has pioneered the use of odd-electron bridging groups in place of benzene. This was achieved most commonly with an alkylated bridging pyridyl group which introduces a positive charge into the system and upon one-electron reduction affords a neutral species with a zwitterionic ground state resulting in 'a molecule like sodium' (Scheme 14(c)).[343] The first examples were reported in 2000[344] and show full spin delocalization among the two functional groups resulting in a low on-site Coulombic barrier U to charge transfer in the solid state.[345,346] A variety of examples have been prepared with changing substituents on the bridging carbon and nitrogen,[347,348] selective replacement of sulfur by selenium,[349–352] and use of a bridging 1,4-pyrazine group in place of pyridine.[353,354] The Oakley group has focused extensively on structure property relationships, including systematic substitution of each S by Se[349,352,355,356] and the effect of pressure on the band structure.[357,358] Recently, ferromagnetic ordering has been discovered in this class of compounds, also affected by the applied pressure.[359–362] The role of multicenter bonding in controlling such magnetic interactions is strongly indicated by structural studies (Figure 28) and has also been investigated computationally.[355]

Scheme 13 1,2,3-Dithiazolyl radicals and selenium analogs.

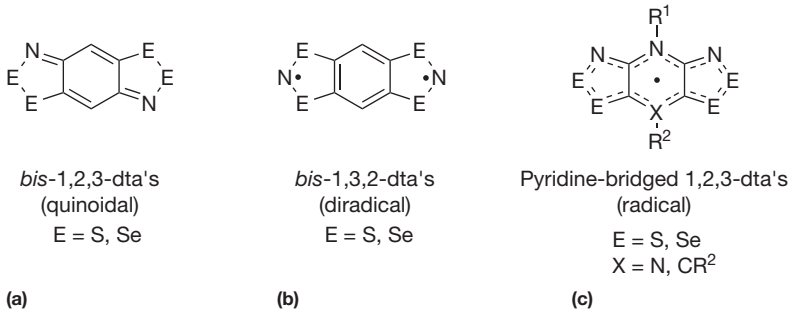

Scheme 14 *Bis*-1,2,3-dithiazolyl radicals and selenium analogs.

1.14.5.2.7 Bis-1,3,2-dithiazolyl radicals and selenium analogs

Bis-1,3,2-dta's tend to give biradicals (Scheme 14(b)) unlike the 1,2,3-analogs (Section 1.14.5.2.6). The first full structural characterization of the diradical benzo-1,2:4,5-bis(1,3,2-dithiazolyl) was reported in 1997[363] and was shown to have a very low first ionization energy. Structural and magnetic studies have been reported for a number of salts of the radical monocation of the same species.[364–370]

1.14.5.2.8 1,2,5-Thiadiazolyl anions and related radicals

The 1,2,5-thiadiazole ring system is very well known in organic chemistry.[15] Structural types include monocycles (stabilized by electron withdrawing groups, Scheme 15(a)), benzofused examples which are by far the best known and readily made from *ortho*-diphenylenes (Scheme 15(b)), and the back-to-back fused [1,2,5]thiadiazolo[3,4-*c*][1,2,5]thiadiazole (Scheme 15(c)). All members of this class of compound can be electrochemically reduced to radical anions which are normally persistent. Recently, a number of studies have reported on the isolation and structural characterization of the radical monoanions as salts with a range of counter-ions: K^+(18-crown-6),[320] Na^+(15-crown-5),[371] Li^+(12-crown-4),[371] Cp_2Co^+,[372] $[C(NMe_2)_2]_2^+$,[373] and bis(pentamethyl)cyclopentadienylchromium.[374] The related [1,2,5]selenadiazolo[3,4-*c*][1,2,5]thiadiazolyl radical anion has been isolated with K^+(18-crown-6).[375] The benzo-2,1,3-thiadiazolyl radical anion has been crystallized with $K(thf)^+$[376] and the hydrolysis of this salt has been fully characterized.[377] Recent studies report on the reduction of 3,4-dicyano-1,2,5-thiadiazole and the related selenadiazole[378] and on the electrochemical reduction and EPR characterization of a large number of monocylic and benzofused fluorinated thia- and selenadiazoles.[379] Several salts of the radical anion of 1,2,5-thiadiazolo-naphthoquinone have also been reported.[380]

A different approach to generating radicals from the diamagnetic 1,2,5-chalcogenadiazole (E = S, Se, and Te) ring system involves alkylation of one of the nitrogen atoms with methyl triflate, followed by reduction of the monocations (Scheme 15(d)).[325,326] The resulting neutral radicals have been investigated by electrochemistry, EPR spectroscopy, and crystallography of the triflate salts; an EPR signal was not observed when E = Te which is attributed to very strong intermolecular association with the heaviest chalcogen.[227]

1.14.5.3 Hetero-Radicals Related to $N_3S_3^\bullet$ and Selenium Analogs

The second-largest group of hetero-radicals are 7π six-membered ring compounds that are formally derived from the 9π $N_3S_3^\bullet$ radical (see Section 1.14.3.1.9) by replacement of two 'S' units by 'RC' (with two fewer electrons, so not an isoelectronic series). Some selenium analogs have also been reported. The much lower diversity of extant isomers, derivative types, and number of reported examples compared to five-membered ring radicals is striking. What makes this series particularly interesting, however, is that R_2P^V analogs are known, whereas none have been reported for the five-membered ring radicals.

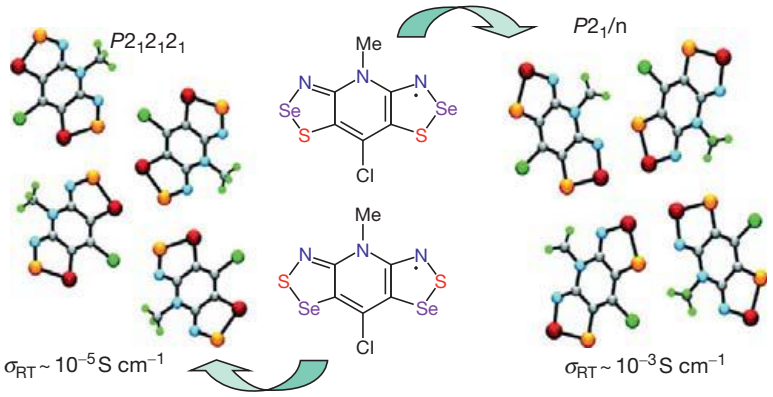

Figure 28 Structural differences in the lattice observed for two isomeric bis(thiaselenazolyls), which induce stronger intermolecular Se···Se' contacts for the isomer that crystallizes in $P2_1/n$, result in a two orders of magnitude difference in conductivity of the putative neutral radical conductors at ambient pressure. Reprinted from Leitch, A. A.; Yu, X. Y.; Winter, S. M.; Secco, R. A.; Dube, P. A.; Oakley, R. T. *J. Am. Chem. Soc.* **2009**, *131*, 7112–7125, copyright (2009) American Chemical Society.

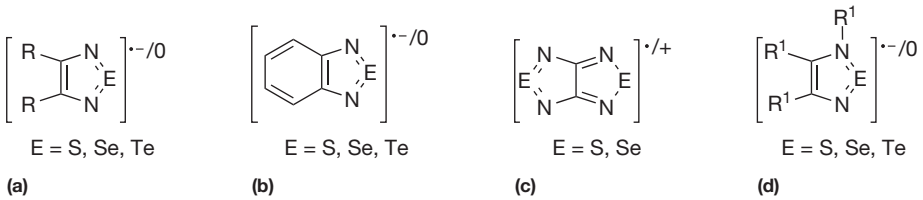

Scheme 15 1,2,5-Thiadiazolyl anions and related radicals.

1.14.5.3.1 Thiatriazinyl and selenatriazinyl radicals

Radicals are obtained for the 1,2,4,6-thiatriazinyl ring system (Scheme 16) when the chalcogen is two-coordinate; typically they are made by the reduction of E–Cl compounds.[381–383] Updated EPR spectroscopic data have been reported for a number of symmetrically di-substituted thiatriazinyl radicals.[384] Recently, a general synthetic route to 3-trifluoromethyl-5-aryl-1λ^3-1,2,4,6-thiatriazinyl radicals was developed.[385] Several radicals were crystallographically characterized and exist in the solid state as diffuse π^*–π^* co-facial dimers linked by S···S contacts. The voltammetric behavior is indicative of monomer–dimer equilibria in solution (Figure 29). A single report appeared some time ago on the 3,5-diphenyl-1,2,4,6-selenatriazinyl which is notably less soluble than the sulfur analog.[386] In contrast to the well-characterized exemplars of the 1,2,4,6-isomer, only a single report has appeared for 3,6-diphenyl-1,2,4,5-thiatriazinyl for which only a solution-phase EPR spectrum is available.[387]

1.14.5.3.2 Phospha- and diphospha-1,2,4,6-thiatriazinyl and selenatriazinyl radicals

The Oakley group has reported Ph_2P^V analogs to 1,2,4,6-thiatriazinyl radicals such as $Ph_4P_2N_3S^{\bullet}$[388] and $Ph_2P(PhC)N_3S^{\bullet}$ (Scheme 16).[389] Both show extensive hyperfine coupling to the ^{31}P nuclei in addition to the usual nitrogen hfc, resulting in highly characteristic signals. The corresponding selenatriazinyls have also been prepared and characterized; whereas the sulfur radicals associate in the solid state by SS contacts, the selenium radical shows intermolecular NSe bonding and structural features of a cation–anion pair.[390]

1.14.5.3.3 1,2,4-Thiadiazinyl radicals

Benzo-fused 1,2,4-thiadiazinyls (Scheme 16) have been shown to be persistent radicals and some examples, notably with fluorinated benzo rings, have been isolated and structurally characterized as well as studied by voltammetry and EPR spectroscopy.[391,392] Their incorporation into liquid crystals has also received attention.[393] Several delocalized bis-1,2,4-thiadiazinyls have been prepared by the Oakley group using a similar approach to the successful strategy employed for bis-1,2,3-dithiazolyls (Section 1.14.5.2.7) using an alkylated pyridine group as the bridging fused ring in place of benzene.[394] These afford, by reduction, neutral radicals that are fully delocalized over both heterocyclic rings; however, the conductivity within the crystalline solid was disappointingly low and no further work on this system has been reported.

1.14.6 Metal Coordination by Chalcogen–Nitrogen Hetero-Radicals

The coordination behavior of many types of chalcogen–nitrogen hetero-radicals has been actively investigated. A special focus of this area has been in the design of high-spin coordination complexes.[395] This field has been thoroughly described in a recent review.[16]

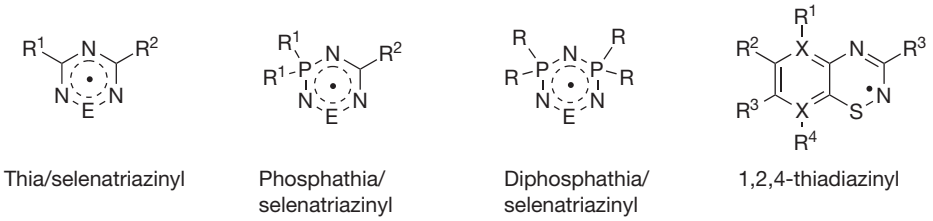

Scheme 16 Thiatriazinyl, selenatriazinyl, and thiadiazinyl radicals.

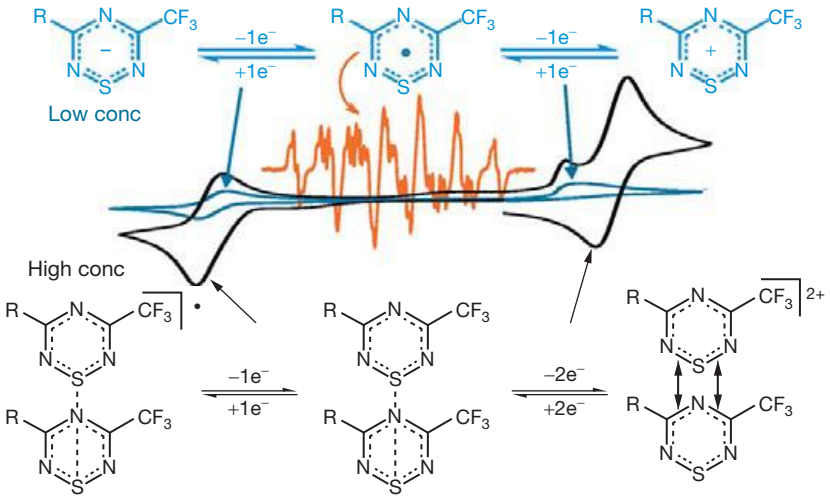

Figure 29 Voltammetry and EPR spectroscopy of a 3-trifluoromethyl-5-aryl-1λ^3-1,2,4,6-thiatriazinyl radical are indicative of monomer-dimer equilibria in solution. Reprinted from Boeré, R. T.; Roemmele, T. L.; Yu, X. *Inorg. Chem.* 2011, *50*, 5123–5136, copyright (2011) American Chemical Society.

1.14.6.1 Direct Coordination of Hetero-Radicals to Metals

The early work largely concerned the reactivity of 1,2,3,5-dithiadiazolyls (Section 1.14.5.2.1) with low-valent transition metals resulting in both paramagnetic and diamagnetic products from oxidative addition; this has been thoroughly reviewed.[396] When 1,3,5-trithia-2,4,6-triazapentalenyl coordinates to $Cu(hfac)_2$, one ring attaches via the dithiazole nitrogen atom, while the other uses one of the thiadiazole nitrogens.[397] An extensive chemistry occurs when 1,3,2-benzodithiazolyl (Section 1.14.5.2.5) is mixed with metal complexes. With cobalt bis-maleonitrildithiolate, π-coordination occurs between the heterocyclic ring and the cobalt ion[398,399]; with the corresponding nickel(II) complex, the dta interacts with the remote nitrile groups via short NS interactions[400]; with copper, an almost perfect one-dimensional magnetic material forms[401]; while with $Ni(dmit)_2$, a multiband molecular conductor is obtained.[402] This diverse behavior has been reviewed.[403] The first π-coordination complexes to be recognized between 1,2,3,5-dithiadiazolyls and transition metals involve $CpCr(CO)_2^{\bullet}$ moieties[404–406]; consequently, the adducts are diamagnetic. However, they can be electrochemically reduced and the resulting radical anions characterized by simultaneous electrochemistry electron paramagnetic resonance (SEEPR) spectroscopy (Figure 30(a)). Similarly, a number of 1,2,4,6-thiatriazinyls (Section 1.14.5.3.1) have been found to coordinate bidentate (Figure 30(b)) to $CpCr(CO)_2^{\bullet}$ or monodentate (Figure 30(c)) to $CpCr(CO)_3^{\bullet}$.[407]

1.14.6.2 Complexes with Ancillary Hetero-Radicals

N-(4-Pyridylthio)-4-ethoxycarbonyl-2,6-bis(4-chlorophenyl) phenylaminyl and related radicals with a pendant pyridyl group have been coordinated to $M(hfac)_2$ (M = Cu, Mn).[276] More robust coordination is achieved with 1,2,3,5-dithiadiazolyls (Section 1.14.5.2.1) modified to bear a 2-pyridyl group attached to the ring backbone.[408] Coordination of this kind of ligand to $M(hfac)_2$ has been reported for Co^{2+},[408] Ni^{2+} (Figure 31(a)), Fe^{3+},[409] Mn,[2+] and Cu^{2+}.[410] More complex ligands have been devised with pyrimidyl groups, which are capable of bridging two $M(hfac)_2$ units, and benzoxazole groups attached to the ring backbone.[411] Secondary donors on the pyridyl group have been employed in attempts to modify crystal packing.[412] A characteristic of this class of metal complexes is that the ligands retain their full open-shell character; in several examples, the magnetic

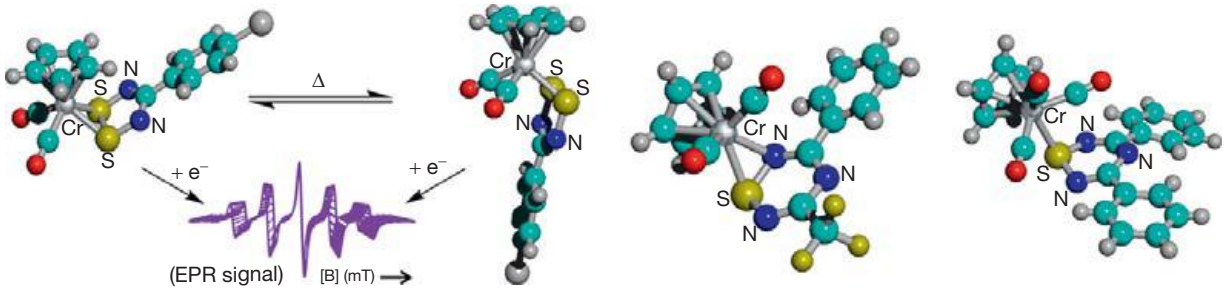

Figure 30 (a) Bidentate coordination of 4-aryl-dithiadiazolys to $CpCr(CO)_2$. (b) Bidentate coordination of an asymmetric thiatriazinyl to $CpCr(CO)_2$. (c) Monodentate coordination of symmetrical thiatriazinyl to $CpCr(CO)_3$. Part (a) refers to the whole ensemble of two isomers, the double arrow, and the signal at the LHS, (b) the molecule just past the middle of the line, and (c) the molecule at the RHS. Adapted in part from Lau, H. F.; Ang, P. C. Y.; Ng, V. W. L.; Kuan, S. L.; Goh, L. Y.; Borisov, A. S.; Hazendonk, P.; Roemmele, T. L.; Boeré, R. T.; Webster, R. D. *Inorg. Chem.* **2008**, *47*, 632-644, copyright (2008) American Chemical Society.

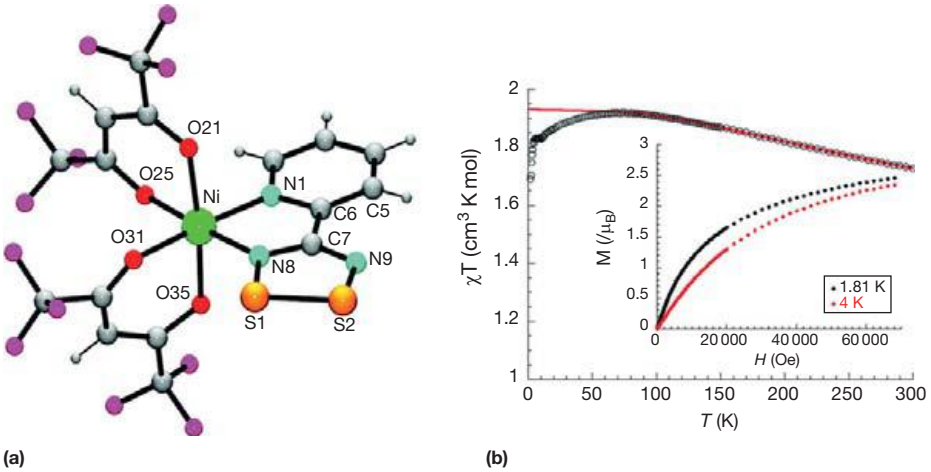

Figure 31 (a) Structure of Ni(1,1,1,5,5,5-hexafluoroacetylacetonato)$_2$(4-(2′-pyridyl)-1,2,3,5-dithiadiazolyl) in the crystal lattice and (b) magnetic susceptibility of the crystalline material: outer plot is χT versus T at an applied field of 1000 Oe; inner plot is M versus H at 1.81 and 4 K. Reprinted from Hearns, N. G. R.; Fatila, E. M.; Clerac, R.; Jennings, M.; Preuss, K. E. *Inorg. Chem.* **2008**, *47*, 10330–10341, copyright (2008) American Chemical Society.

coupling between the metal ion and paramagnetic ligand was readily obtained from solid-state magnetic measurements (Figure 31(b)).

1.14.7 Conclusion

The nitrogen compounds of the chalcogens continue to be among the most prolific sources for free radicals amenable to study by a variety of methods ranging from IR spectroscopy of low-temperature matrix-isolated species to bulk synthesis with single-crystal X-ray structure determinations to confirm their structures. There is still much to learn even about the simplest binary compounds and the demonstrated presence of such molecules in stardust speaks to their intrinsic importance to the history of the universe. Here on earth, extensive variety is afforded when ancillary substitution is possible. Thus, there are myriads of organic aminoxyls and *N*-alkoxyaminyls which have a wide range of applications. Similarly, when –N=S$^{\bullet}$– or –N=Se$^{\bullet}$– linkages are incorporated into hetero-rings and cages, the possibilities become endless. Many fascinating properties and new applications are eagerly anticipated.

References

1. Hicks, R. G. *Stable Radicals: Fundamentals and Applied Aspects of Odd-Electron Compounds*; Wiley: New York, 2010.
2. Oakley, R. T. *Prog. Inorg. Chem.* **1988**, *36*, 299–391.
3. Streitweiser, A., Jr. *Molecular Orbital Theory for Organic Chemistry*. Wiley: New York, 1961.
4. Greenwood, N. N.; Earnshaw, A. *Chemistry of the Elements*, 2nd ed.; Butterworth-Heinemann: Oxford, UK, 1997.
5. King, R. B. *Encyclopedia of Inorganic Chemistry*, 2nd ed.; Wiley: New York, 2005.
6. Jones, K. *In Comprehensive Inorganic Chemistry;* Bailar, J. C., Ed.; Pergamon Press Oxford, 1973; Vol. 2, pp 147–388.
7. Sidgwick, N. V. *The Organic Chemistry of Nitrogen*; Clarendon Press: Oxford, 1966.
8. Bohle, D. S. In *Stable Radicals: Fundamentals and Applied Aspects of Odd-Electron Compounds*; Hicks, R. G., Ed.; Wiley: New York, 2010; pp 147–171.
9. Hartung, J. *Chem. Rev.* **2009**, *109*, 4500–4517.
10. Heal, H. G. *The Inorganic Heterocyclic Chemistry of Sulfur Nitrogen and Phosphorus*. Academic Press: London, 1980.
11. Gleiter, R. *Angew. Chem. Int. Ed Engl.* **1981**, *20*, 444–452.
12. Chivers, T. *Acc. Chem. Res.* **1984**, *17*, 166–171.
13. Chivers, T. *A Guide to Chalcogen-Nitrogen Chemistry*; World Scientific: Singapore, 2005.
14. Preston, K. F.; Sutcliffe, L. H. *Magn. Reson. Chem.* **1990**, *28*, 189–204.
15. Boeré, R. T.; Roemmele, T. L. *Coord. Chem. Rev.* **2000**, *210*, 369–445.
16. Preuss, K. E. *Dalton Trans.* **2007**, 2357–2369.
17. Banister, A. J.; Gorrell, I. B. *Adv. Mater.* **1998**, *10*, 1415–1429.
18. Rawson, J. M.; Longridge, J. J. *Chem. Soc. Rev.* **1997**, *26*, 53–61.
19. Glendening, E. D.; Halpern, A. M. *J. Chem. Phys.* **2007**, *127*, 164307.
20. Anderson, J. G. *Annu. Rev. Phys. Chem.* **1987**, *38*, 489–520.
21. Wennberg, P. O.; Cohen, R. C.; Stimpfle, R. M.; Koplow, J. P.; Anderson, J. G.; Salawitch, R. J.; Fahey, D. W.; Woodbridge, E. L.; Keim, E. R.; Gao, R. S.; Webster, C. R.; May, R. D.; Toohey, D. W.; Avallone, L. M.; Proffitt, M. H.; Loewenstein, M.; Podolske, J. R.; Chan, K. R.; Wofsy, S. C. *Science* **1994**, *266*, 398–404.
22. Urban, B.; Strobel, A.; Bondybey, V. E. *J. Chem. Phys.* **1999**, *111*, 8939–8949.
23. Trautwein, W.-P. DGMK Research Report 616-1, Hamburg, 2003.
24. Lancaster, J. R.; Giles, G. I. *In Encyclopedia of Inorganic Chemistry;* King, R. B., Ed.; Wiley New York, 2005; Vol. 6, pp 3601–3621.
25. Priestley, J.; Hey, W. *Philos. Trans.* **1772**, *62*, 147–264.
26. Blanchard, A. A. *Inorg. Synth.* **1946**, *2*, 126–128.
27. Taylor, S. D.; Morata, O.; Williams, D. A. *Astron. Astrophys.* **1998**, *336*, 309–314.
28. Gerin, M.; Viala, Y.; Pauzat, F.; Ellinger, Y. *Astron. Astrophys.* **1992**, *266*, 463–478.
29. Ziurys, L. M.; McGonagle, D.; Minh, Y.; Irvine, W. M. *Astrophys. J.* **1991**, *373*, 535–542.
30. Krasnopolsky, V. A. *Icarus* **2006**, *182*, 80–91.
31. Bertaux, J. L.; Leblanc, F.; Perrier, S. V.; Quemerais, E.; Korablev, O.; Dimarellis, E.; Reberac, A.; Forget, F.; Simon, P. C.; Stern, S. A.; Sandel, B.; Team, S. *Science* **2005**, *307*, 566–569.
32. Bertaux, J. L.; Leblanc, F.; Witasse, O.; Quemerais, E.; Lilensten, J.; Stern, S. A.; Sandel, B.; Korablev, O. *Nature* **2005**, *435*, 790–794.
33. Yung, Y. L.; DeMore, W. B. *Photochemistry of Planetary Atmospheres*. Oxford University Press: Oxford, 1999.
34. Atkins, P. W.; Friedman, R. *Molecular Quantum Mechanics*, 4th ed.; Oxford University Press: Oxford/Toronto, 2005.
35. Whittaker, J. W. *J. Chem. Educ.* **1991**, *68*, 421–423.
36. Brown, R. L.; Radford, H. E. *Phys. Rev.* **1966**, *147*, 6–12.
37. Miller, R. J.; Feller, D. *J. Phys. Chem.* **1994**, *98*, 10375.
38. Weil, J. A.; Bolton, J. R.; Wertz, J. E. *Electron Paramagnetic Resonance*, 2nd ed.; Wiley: New York, 1994.
39. Volodin, A.; Biglino, D.; Itagaki, Y.; Shiotani, M.; Lund, A. *Chem. Phys. Lett.* **2000**, *327*, 165–170.
40. Chiesa, M.; Giamello, E.; Che, M. *Chem. Rev.* **2010**, *110*, 1320–1347.
41. Atkins, P. W.; Symons, M. C. R. *The Structure of Inorganic Radicals: An Application of Electron Spin Resonance to the Study of Molecular Structure*; Elsevier: Amsterdam/New York, 1967.
42. Dethlefsen, J. W.; Hedegard, E. D.; Rimmer, R. D.; Ford, P. C.; Dossing, A. *Inorg. Chem.* **2009**, *48*, 231–238.
43. Lauricella, R.; Triquigneaux, M.; Andre-Barres, C.; Charles, L.; Tuccio, B. *Chem. Commun.* **2010**, *46*, 3675–3677.
44. East, A. L. L. *J. Chem. Phys.* **1998**, *109*, 2185–2193.
45. East, A. L. L.; McKellar, A. R. W.; Watson, J. K. G. *J. Chem. Phys.* **1998**, *109*, 4378–4383.
46. East, A. L. L.; Watson, J. K. G. *J. Chem. Phys.* **1999**, *110*, 6099–6102.
47. Pajón-Suarez, P.; Rubayo-Soneira, J.; Hernandez-Lamoneda, R. *J. Phys. Chem. A* **2011**, *115*, 2892–2899.
48. Furchgott, R. F. In *Vasodilation: Vascular Smooth Muscle, Peptides, Autonomic Nerves and Endothelium*; Vanhoutte, P. M., Ed.; Raven: New York, 1988; pp 401–414.
49. Ignarro, L. J.; Buga, G. M.; Wood, K. S.; Byrns, R. E.; Chaudhuri, G. *Proc. Natl. Acad. Sci. USA* **1987**, *84*, 9265–9269.
50. Palmer, R. M. J.; Ferrige, A. G.; Moncada, S. *Nature* **1987**, *327*, 524–526.
51. Collier, J.; Vallance, P. *Trends Pharmacol. Sci.* **1989**, *10*, 427–431.
52. Matsumoto, A.; Gow, A. J. *Nitric Oxide* **2011**, *25*, 102–107.
53. Adam, C.; García-Rio, L.; Leis, J. R. *Org. Biomol. Chem.* **2004**, *2*, 1181–1185.
54. Gaston, B.; Singel, D.; Doctor, A.; Stamler, J. S. *Am. J. Respir. Crit. Care Med.* **2006**, *173*, 1186–1193.
55. Zhao, Y. L.; Houk, K. N. *J. Am. Chem. Soc.* **2006**, *128*, 1422–1423.
56. Schopfer, M. P.; Wang, J.; Karlin, K. D. *Inorg. Chem.* **2010**, *49*, 6267–6282.
57. McCleverty, J. A. *Chem. Rev.* **2004**, *104*, 403–418.
58. Andrews, L.; Citra, A. *Chem. Rev.* **2002**, *102*, 885–911.
59. Coppens, P.; Novozhilova, I.; Kovalevsky, A. *Chem. Rev.* **2002**, *102*, 861–883.
60. Hayton, T. W.; Legzdins, P.; Sharp, W. B. *Chem. Rev.* **2002**, *102*, 935–991.
61. Mason, J.; Larkworthy, L. F.; Moore, E. A. *Chem. Rev.* **2002**, *102*, 913–934.
62. Wyllie, G. R. A.; Scheidt, W. R. *Chem. Rev.* **2002**, *102*, 1067–1089.
63. Ford, P. C.; Fernandez, B. O.; Lim, M. D. *Chem. Rev.* **2005**, *105*, 2439–2455.
64. Wanner, M.; Scheiring, T.; Kaim, W.; Slep, L. D.; Baraldo, L. M.; Olabe, J. A.; Zalis, S.; Baerends, E. J. *Inorg. Chem.* **2001**, *40*, 5704–5707.
65. Lynch, M. S.; Cheng, M.; Van Kuiken, B. E.; Khalil, M. *J. Am. Chem. Soc.* **2011**, *133*, 5255–5262.
66. Lahiri, K. L.; Kaim, W. *Dalton Trans.* **2010**, *39*, 4471–4478.
67. McCarthy, M. R.; Crevier, T. J.; Bennett, B.; Dehestani, A.; Mayer, J. M. *J. Am. Chem. Soc.* **2000**, *122*, 12391–12392.
68. Pap, J. S.; Snyder, J. L.; Piccoli, P. M. B.; Berry, J. F. *Inorg. Chem.* **2009**, *48*, 9846–9852.
69. Casely, I. J.; Suh, Y.; Ziller, J. W.; Evans, W. J. *Organometallics* **2010**, *29*, 5209–5214.
70. Siladke, N. A.; Fang, M.; Furche, F.; Long, J. R.; Evans, W. J. *J. Am. Chem. Soc.* **2012**, *134*(2), 1243–1249. http://dx.doi.org/10.1021/ja2096128.
71. Schaafsma, T. J. *Chem. Phys. Lett.* **1967**, *1*, 16–18.
72. Adrian, F. J. *J. Chem. Phys.* **1962**, *36*, 1692–1693.
73. Liu, Y. Y.; Liu, X. Y.; Liu, H. P.; Guo, Y. Q. J. *Mol. Spec.* **2000**, *202*, 306–308.
74. Mendiara, S. N.; Sagedahl, A.; Perissinotti, L. J. *Appl. Magn. Reson.* **2001**, *20*, 275–287.
75. Mendiara, S. N.; Perissinotti, L. J. *Appl. Magn. Reson.* **2003**, *25*, 323–346.

76. Borisenko, K. B.; Kolonits, M.; Rozsondai, B.; Hargittai, I. J. *Mol. Struct.* **1997**, *413*, 121–131.
77. Tsirelson, V. G.; Shishkina, A. V.; Stash, A. I.; Parsons, S. *Acta Crystallogr.* **2009**, *B65*, 647–658.
78. Ahlrichs, R.; Keil, F. *J. Am. Chem. Soc.* **1974**, *96*, 7615–7620.
79. Chesnut, D. B.; Crumbliss, A. L. *J. Chem. Phys.* **2005**, *315*, 53–58.
80. Halpern, A. M.; Glendening, E. D. *J. Chem. Phys.* **2007**, *126*, 154305.
81. Liu, R. F.; Zhou, X. F. *J. Phys. Chem.* **1993**, *97*, 4413–4415.
82. Eisfeld, W.; Morokuma, K. *J. Chem. Phys.* **2003**, *119*, 4682–4688.
83. Cacace, F.; de Petris, G.; Rosi, M.; Troiani, A. *Chem. Eur. J.* **2002**, *8*, 5684–5693.
84. Galliker, B.; Kissner, R.; Nauser, T.; Koppenol, W. H. *Chem. Eur. J.* **2009**, *15*, 6161–6168.
85. Frears, E.; Nazhat, N.; Blake, D.; Symons, M. *Free Radic. Res.* **1997**, *27*, 31–35.
86. Beckers, H.; Willner, H.; Jacox, M. E. *Chemphyschem* **2009**, *10*, 706–710.
87. Beckers, H.; Zeng, X. Q.; Willner, H. *Chem. Eur. J.* **2010**, *16*, 1506–1520.
88. McKee, M. L. *J. Am. Chem. Soc.* **1995**, *117*, 1629–1637.
89. Gadzhiev, O. B.; Ignatov, S. K.; Razuvaev, A. G.; Masunov, A. E. *J. Phys. Chem. A* **2009**, *113*, 9092–9101.
90. Gadzhiev, O. B.; Ignatov, S. K.; Gangopadhyay, S.; Masunov, A. E.; Petrov, A. I. J. *Chem. Theory Comput.* **2011**, *7*, 2021–2024.
91. Botti, H.; Moller, M. N.; Steinmann, D.; Nauser, T.; Koppenol, W. H.; Denicola, A.; Radi, R. *J. Phys. Chem. B* **2010**, *114*, 16584–16593.
92. Amatore, C.; Arbault, S.; Bruce, D.; de Oliveira, P.; Erard, M.; Vuillaume, M. *Chem. Eur. J.* **2001**, *7*, 4171–4179.
93. Quinton, D.; Griveau, S.; Bedioui, F. *Electrochem. Commun.* **2010**, *12*, 1446–1449.
94. Chappuis, J. *Ann. l'ecole Norm. Sup.* **1882**, *11*, 159–162.
95. Stanton, J. F. *Mol. Phys.* **2009**, *107*, 1059–1075.
96. Peiró-García, J.; Nebot-Gil, I. J. *Comput. Chem.* **2003**, *24*, 1657–1663.
97. Wayne, E. P. *The Nitrate Radical: Physics, Chemistry and the Atmosphere.* Commission of the European Communities/European Union: Brussels, 1990.
98. Martin, T. W.; Swift, L. L. *J. Chem. Phys.* **1970**, *52*, 2138–2143.
99. Jacox, M. E.; Thompson, W. E. *J. Chem. Phys.* **2008**, *129*, 204306.
100. Ndome, H.; Hochlaf, M. *J. Chem. Phys.* **2009**, *130*, 204301.
101. Nguyen, T. L.; Park, J.; Lee, K.; Song, K.; Barker, J. R. *J. Phys. Chem. A* **2011**, *115*, 4894–4901.
102. Papadimitriou, V. C.; Lazarou, Y. G.; Talukdar, R. K.; Burkholder, J. B. *J. Phys. Chem. A* **2011**, *115*, 167–181.
103. Stanton, J. F.; Okumura, M. *Phys. Chem. Chem. Phys.* **2009**, *11*, 4742–4744.
104. Stanton, J. F. *J. Chem. Phys.* **2007**, *126*, 134309.
105. Kennedy, O. J.; Ouyang, B.; Langridge, J. M.; Daniels, M. J. S.; Bauguitte, S.; Freshwater, R.; McLeod, M. W.; Ironmonger, C.; Sendall, J.; Norris, O.; Nightingale, R.; Ball, S. M.; Jones, R. L. *Atmos. Meas. Tech.* **2011**, *4*, 1759–1776.
106. McLaren, R.; Wojtal, P.; Majonis, D.; McCourt, J.; Halla, J. D.; Brook, J. *Atmos. Chem. Phys.* **2010**, *10*, 4187–4206.
107. Clark, H. C.; Horsfield, A.; Symons, M. C. R. *J. Chem. Soc.* **1961**, 7–11.
108. Hsu, C.-C.; Lin, M. C.; Mebel, A. M.; Melius, C. F. *J. Chem. Phys. A* **1997**, *101*, 60–66.
109. Bannov, S. I.; Nevostruev, V. A. *Radiat. Phys. Chem.* **2003**, *68*, 917–924.
110. Paganini, M. C.; Chiesa, M.; Dolci, F.; Martino, P.; Giamello, E. *J. Phys. Chem. B* **2006**, *110*, 11918–11923.
111. Bussandri, A.; van Willigen, H. *J. Phys. Chem. A* **2001**, *105*, 4669–4675.
112. Cook, A. R.; Dimitrijevic, N.; Dreyfus, B. W.; Meisel, D.; Curtiss, L. A.; Camaioni, D. M. *J. Phys. Chem. A* **2001**, *105*, 3658–3666.
113. Yakabuskie, P. A.; Joseph, J. M.; Stuart, C. R.; Wren, J. C. *J. Phys. Chem. A* **2011**, *115*, 4270–4278.
114. Simon, A.; Horakh, J.; Obermeyer, A.; Borrmann, H. *Angew. Chem. Int. Ed Engl.* **1992**, *31*, 301–303.
115. Mikami, H.; Saito, S.; Yamamoto, S. *J. Chem. Phys.* **1991**, *94*, 3415–3422.
116. Logan, J. A. *J. Geophys. Res. C: Oceans Atmos.* **1983**, *88*, 785–807.
117. Lee, D. S.; Kohler, I.; Grobler, E.; Rohrer, F.; Sausen, R.; GallardoKlenner, L.; Olivier, J. G. J.; Dentener, F. J.; Bouwman, A. F. *Atmos. Environ.* **1997**, *31*, 1735–1749.
118. Graedel, T. E. *J. Geophys. Res. C: Oceans Atmos.* **1977**, *82*, 5917–5922.
119. Dixon, D. A.; Francisco, J. S.; Alexeev, Y. *J. Phys. Chem. A* **2006**, *110*, 185–191.
120. Sun, F.; DeSain, J. D.; Scott, G.; Hung, P. Y.; Thompson, R. I.; Glass, G. P.; Curl, R. F. *J. Phys. Chem. A* **2001**, *105*, 6121–6128.
121. Wu, Y. J.; Lin, M. Y.; Hsu, S. C.; Cheng, B. M. *Chemphyschem* **2009**, *10*, 901–904.
122. Greenwood, N. N. *J. Chem. Soc. Dalton Trans.* **2001**, 2055–2066.
123. Hicks, R. G. In *Stable Radicals: Fundamentals and Applied Aspects of Odd-Electron Compounds*; Hicks, R. G., Ed.; Wiley: New York, 2010; pp 317–380.
124. Fowler, A.; Bakker, C. J. *Proc. R. Soc. London Ser. A* **1932**, *136*, 28–36.
125. Huber, K. P.; Herzberg, G. *Constants of Diatomic Molecules*; Van Nostrand Reinhold: New York, 1979; Vol. IV.
126. Czernek, J.; Zivny, O. *J. Chem. Phys.* **2004**, *303*, 137–142.
127. Dyke, J. M.; Morris, A.; Trickle, I. R. *J. Chem. Soc., Faraday Trans. 2* **1977**, *73*, 147–151.
128. Uehara, H.; Morino, Y. *Mol. Phys.* **1969**, *17*, 239–248.
129. Boeré, R. T.; Tuononen, H. M.; Chivers, T.; Roemmele, T. L. J. *Organomet. Chem.* **2007**, *692*, 2683–2696.
130. Barrow, R. F.; Downie, A. R.; Laird, R. K. *Proc. Phys. Soc. London Sect. A* **1952**, *65*, 70–71.
131. Carrington, A.; Howard, B. J.; Levy, D. H.; Robertson, J. C. *Mol. Phys.* **1968**, *15*, 187–200.
132. Hassanzadeh, P.; Andrews, L. *J. Am. Chem. Soc.* **1992**, *114*, 83–91.
133. Ongstad, A. P.; Lawconnell, R. I.; Henshaw, T. L. *J. Chem. Phys.* **1992**, *97*, 1053–1064.
134. Vlasyuk, I. V.; Bagryansky, V. A.; Gritsan, N. P.; Molin, Yu.N.; Makarov, A. Yu.; Gatilov, Yu.V.; Scherbukhin, V. V.; Zibarev, A. V. *Phys. Chem. Chem. Phys.* **2001**, *3*, 409–415.
135. Shuvaev, K. V.; Bagryansky, V. A.; Gritsan, N. P.; Makarov, A. Yu.; Molin, Yu.N.; Zibarev, A. V. *Mendeleev Commun.* **2003**, *13*, 178–179.
136. Gritsan, N. P.; Shuvaev, K. V.; Kim, S. N.; Knapp, C.; Mews, R.; Bagryansky, V. A.; Zibarev, A. V. *Mendeleev Commun.* **2007**, *17*, 204–206.
137. Gritsan, N. P.; Pritchina, E. A.; Bally, T.; Makarov, A. Yu.; Zibarev, A. V. *J. Phys. Chem. A* **2007**, *111*, 817–824.
138. Gritsan, N. P.; Kim, S. N.; Makarov, A. Yu.; Chesnokov, E. N.; Zibarev, A. V. *Photochem. Photobiol. Sci.* **2006**, *5*, 95–101.
139. Fritz, H. P.; Bruchhaus, R.; Mews, R.; Hofs, H. U. *Z. Anorg. Allg. Chem.* **1985**, *525*, 214–220.
140. Blitz, M. A.; McKee, K. W.; Pilling, M. J.; Vincent, M. A.; Hillier, I. H. *J. Phys. Chem. A* **2002**, *106*, 8406–8410.
141. Gottlieb, C. A.; Ball, J. A.; Gottlieb, E. W.; Lada, C. J.; Penfield, H. *Astrophys. J.* **1975**, *200*, L147–L149.
142. McGonagle, D.; Irvine, W. M.; Ohishi, M. *Astrophys. J.* **1994**, *422*, 621–625.
143. van der Tak, F. F. S.; Boonman, A. M. S.; Braakman, R.; van Dishoeck, E. F. *Astron. Astrophys.* **2003**, *412*, 133–145.
144. Irvine, W. M.; Senay, M.; Lovell, A. J.; Matthews, H. E.; McGonagle, D.; Meier, R. *Icarus* **2000**, *143*, 412–414.
145. Pereira, P. S. S.; Macedo, L. G. M.; Pimentel, A. S. *J. Phys. Chem. A* **2010**, *114*, 509–515.
146. Martín, S.; Mauersberger, R.; Martín-Pintado, J.; García-Burillo, S.; Henkel, C. *Astron. Astrophys.* **2003**, *411*, L465–L468.
147. Jeffries, J. B.; Crosley, D. R. *J. Chem. Phys.* **1987**, *86*, 6839–6846.
148. Jeffries, J. B.; Crosley, D. R.; Smith, G. P. *J. Phys. Chem.* **1989**, *93*, 1082–1090.
149. Wendt, J. O. L.; Wootan, E. C.; Corley, T. L. *Combust. Flame* **1983**, *49*, 261–274.
150. Schriver, A.; Schriver-Mazzuoli, L. *Asian J. Spectr.* **2001**, *5*, 1–10.
151. Chivers, T.; Edelmann, F. *Polyhedron* **1986**, *5*, 1661–1699.
152. Hursthouse, M. B.; Motevalli, M. *J. Chem. Soc. Dalton Trans.* **1979**, 1362–1366.
153. Vollmer, B.; Wocadlo, S.; Massa, W.; Dehnicke, K. *Z. Anorg. Allg. Chem.* **1996**, *622*, 1306–1310.
154. Dietrich, A.; Neumuller, B.; Dehnicke, K. *Z. Anorg. Allg. Chem.* **2000**, *626*, 1268–1270.
155. Huynh, M. H. V.; White, P. S.; Meyer, T. J. *Inorg. Chem.* **2000**, *39*, 2825–2830.
156. Leung, C. F.; Yiu, D. T. Y.; Wong, W. T.; Peng, S. M.; Lau, T. C. *Inorg. Chim. Acta* **2009**, *362*, 3576–3582.
157. Reinel, M.; Hocher, T.; Abram, U.; Kirmse, R. *Z. Anorg. Allg. Chem.* **2003**, *629*, 853–861.
158. Wu, A.; Dehestani, A.; Saganic, E.; Crevier, T. J.; Kaminsky, W.; Cohen, D. E.; Mayer, J. M. *Inorg. Chim. Acta* **2006**, *359*, 2842–2849.
159. Yi, X.-Y.; Lam, T. C. H.; Sau, Y.-K.; Zhang, Q.-F.; Williams, I. D.; Leung, W.-H. *Inorg. Chem.* **2007**, *46*, 7193–7198.
160. Dethlefsen, J. R.; Dossing, A.; Hedegard, E. D. *Inorg. Chem.* **2010**, *49*, 8769–8778.
161. Dethlefsen, J. W.; Dossing, A.; Kadziola, A. *Inorg. Chim. Acta* **2009**, *362*, 1585–1590.
162. Dethlefsen, J. W.; Dossing, A. *Inorg. Chim. Acta* **2009**, *362*, 259–262.
163. Mawhinney, R. C.; Goddard, J. D. *Inorg. Chem.* **2003**, *42*, 6323–6337.
164. Klapotke, T. M.; Schulz, A. *Polyhedron* **1996**, *15*, 4387–4390.
165. King, R. S. P.; Kelly, P. F.; Dann, S. E.; Mortimer, R. J. *Chem. Commun.* **2007**, 4812–4814.
166. Matuska, V.; Tersago, K.; Kilian, P.; Van Alsenoy, C.; Blockhuys, F.; Slawin, A. M. Z.; Woollins, J. D. *Eur. J. Inorg. Chem.* **2009**, 4483–4490.

167. Edelmann, F. T.; Blaurock, S.; Lorenz, V.; Chivers, T. *Z. Anorg. Allg. Chem.* **2008**, *634*, 413–415.
168. Droogenbroeck, J. V.; Van Alsenoy, C.; Aucott, S. M.; Woollins, J. D.; Hunter, A. D.; Blockhuys, F. *Organometallics* **2005**, *24*, 1004–1011.
169. Chivers, T.; Rao, M. N. S. *Can. J. Chem.* **1983**, *61*, 1957–1962.
170. Chivers, T.; Cordes, A. W.; Oakley, R. T.; Pennington, W. T. *Inorg. Chem.* **1983**, *22*, 2429–2435.
171. Zhu, J. K.; Gimarc, B. M. *Inorg. Chem.* **1983**, *22*, 1996–1999.
172. Lau, W. M.; Westwood, N. P. C.; Palmer, M. H. *J. Chem. Soc., Chem. Commun.* **1985**, 752–753.
173. Lau, W. M.; Westwood, N. P. C.; Palmer, M. H. *J. Am. Chem. Soc.* **1986**, *108*, 3229–3237.
174. Love, P.; Myer, G.; Kao, H. I.; Labes, M. M.; Junker, W. R.; Elbaum, C. *Ann. N. Y. Acad. Sci.* **1978**, *313*, 745–757.
175. Boere, R. T.; Chivers, T.; Roemmele, T. L.; Tuononen, H. M. *Inorg. Chem.* **2009**, *48*, 7294–7306.
176. Boeré, R. T.; Tuononen, H. M. Unpublished results.
177. Gregory, W. J. *Pharm. Chim.* **1835**, *21*, 315.
178. Pritchina, E. A.; Gritsan, N. P.; Zibarev, A. V.; Bally, T. *Inorg. Chem.* **2009**, *48*, 4075–4082.
179. Heeger, A. J. *J. Phys. Chem. B* **2001**, *105*, 8475–8491.
180. Remacle, F.; Levine, R. D. *Faraday Discuss.* **2006**, *131*, 45–67.
181. Mawhinney, R. C.; Goddard, J. D. *J. Mol. Struct. (THEOCHEM)* **2008**, *856*, 16–29.
182. Larsson, S. *Faraday Discuss.* **2006**, *131*, 69–77.
183. McCreery, R. L.; Viswanathan, U.; Kalakodimi, R. P.; Nowak, A. M. *Faraday Discuss.* **2006**, *131*, 33–43.
184. Modelli, A.; Venuti, M.; Scagnolari, F.; Contento, M.; Jones, D. *J. Phys. Chem. A* **2001**, *105*, 219–226.
185. Cohen, M. J.; Garito, A. F.; Heeger, A. J.; Macdiarmid, A. G.; Mikulski, C. M.; Saran, M. S.; Kleppinger, J. *J. Am. Chem. Soc.* **1976**, *98*, 3844–3848.
186. Muller, H.; Svensson, S. O.; Birch, J.; Kvick, A. *Inorg. Chem.* **1997**, *36*, 1488–1494.
187. Nguyen, M. T.; Flammang, R.; Goldberg, N.; Schwarz, H. *Chem. Phys. Lett.* **1995**, *236*, 201–205.
188. Brown, R. D.; Elmes, P. S.; McNaughton, D. J. *Mol. Spec.* **1990**, *140*, 390–400.
189. Yamaguchi, Y.; Xie, Y. M.; Grev, R. S.; Schaefer, H. F. *J. Chem. Phys.* **1990**, *92*, 3683–3687.
190. Himmel, H. M.; Downs, A. J.; Greene, T. M. *Chem. Rev.* **2002**, *102*, 4191–4241.
191. Parsons, S.; Passmore, J. *Acc. Chem. Res.* **1994**, *27*, 101–108.
192. Faggiani, R.; Gillespie, R. J.; Lock, C. J. L.; Tyrer, J. D. *Inorg. Chem.* **1978**, *17*, 2975–2978.
193. Cameron, T. S.; Mailman, A.; Passmore, J.; Shuvaev, K. V. *Inorg. Chem.* **2005**, *44*, 6524–6528.
194. Knapp, C.; Mailman, A.; Nikiforov, G. B.; Passmore, J. *J. Flourine Chem.* **2006**, *127*, 916–919.
195. Chivers, T.; Codding, P. W.; Laidlaw, W. G.; Liblong, S. W.; Oakley, R. T.; Trsic, M. *J. Am. Chem. Soc.* **1983**, *105*, 1186–1192.
196. Tchir, P. O.; Spratley, R. D. *Can. J. Chem.* **1975**, *53*, 2311–2317.
197. Tchir, P. O.; Spratley, R. D. *Can. J. Chem.* **1975**, *53*, 2318–2330.
198. Hawkins, M.; Downs, A. J. *J. Phys. Chem.* **1984**, *88*, 3042–3047.
199. Andrews, L.; Hassanzadeh, P.; Brabson, G. D.; Citra, A.; Neurock, M. *J. Phys. Chem.* **1996**, *100*, 8273–8279.
200. Sun, L. X.; Bu, Y. X.; Yan, S. H. *Chem. Phys. Lett.* **2003**, *370*, 616–624.
201. Machmer, P.; McNeil, D. A. C.; Symons, M. C. R. *Trans. Faraday Soc.* **1970**, *66*, 1309–1311.
202. Bojes, J.; Chivers, T. *J. Chem. Soc. Dalton Trans.* **1975**, 1715–1717.
203. Fairhurst, S. A.; Preston, K. F.; Sutcliffe, L. H. *Can. J. Chem.* **1984**, *62*, 1124–1126.
204. Gillespie, R. J.; Kent, J. P.; Sawyer, J. F. *Inorg. Chem.* **1981**, *20*, 3784–3799.
205. Gillespie, R. J.; Ireland, P. R.; Vekris, J. E. *Can. J. Chem.* **1975**, *53*, 3147–3152.
206. Gimarc, B. M.; Warren, D. S. *Inorg. Chem.* **1991**, *30*, 3276–3280.
207. Fairhurst, S. A.; Johnson, K. M.; Sutcliffe, L. H.; Preston, K. F.; Banister, A. J.; Hauptman, Z. V.; Passmore, J. *J. Chem. Soc. Dalton Trans.* **1986**, 1465–1472.
208. Gassmann, J.; Fabian, J. *Magn. Reson. Chem.* **1996**, *34*, 913–920.
209. Bojes, J.; Chivers, T.; Laidlaw, W. G.; Trsic, M. *J. Am. Chem. Soc.* **1979**, *101*, 4517–4522.
210. Jones, R.; Kelly, P. F.; Williams, D. J.; Woollins, J. D. *Polyhedron* **1987**, *6*, 1541–1545.
211. Jagg, P. N.; Kelly, P. F.; Rzepa, H. S.; Williams, D. J.; Woollins, J. D.; Wylie, W. *J. Chem. Soc., Chem. Commun* **1991**, 942–944.
212. Banister, A. J.; Hansford, M. I.; Hauptman, Z. V.; Luke, A. W.; Wait, S. T.; Clegg, W.; Jorgensen, K. A. *J. Chem. Soc. Dalton Trans.* **1990**, 2793–2802.
213. Fairhurst, S. A.; Hulmelowe, A.; Johnson, K. M.; Sutcliffe, L. H.; Passmore, J.; Schriver, M. J. *Magn. Reson. Chem.* **1985**, *23*, 828–831.
214. Chapman, D.; Massey, A. G. *Trans. Faraday Soc.* **1962**, *58*, 1291–1298.
215. McNeil, D. A. C.; Murray, M.; Symons, M. C. R. *J. Chem. Soc. A* **1967**, 1019–1021.
216. Preston, K. F.; Charland, J. P.; Sutcliffe, L. H. *Can. J. Chem.* **1988**, *66*, 1299–1303.
217. Roemmele, T. L.; Konu, J.; Boeré, R. T.; Chivers, T. *Inorg. Chem.* **2009**, *48*, 9454–9462.
218. Chandra, H.; Rao, D. N. R.; Symons, M. C. R. *J. Chem. Soc. Dalton Trans.* **1987**, 729–732.
219. Fritz, H. P.; Bruchhaus, R. *Electrochim. Acta* **1984**, *29*, 947–950.
220. Boeré, R. T.; French, C. L.; Oakley, R. T.; Cordes, A. W.; Privett, J. A. J.; Craig, S. L.; Graham, J. B. *J. Am. Chem. Soc.* **1985**, *107*, 7710–7717.
221. Borrmann, T.; Lork, E.; Mews, R.; Shakirov, M. M.; Zibarev, A. V. *Eur. J. Inorg. Chem.* **2004**, 2452–2458.
222. Chivers, T.; Hojo, M. *Inorg. Chem.* **1984**, *23*, 1526–1530.
223. Chivers, T.; Hojo, M. *Inorg. Chem.* **1984**, *23*, 2738–2742.
224. Meinzer, R. A.; Pratt, D. W.; Myers, R. J. *J. Am. Chem. Soc.* **1969**, *91*, 6623–6625.
225. Williford, J.; Vanreet, R. E.; Eastman, M. P.; Prater, K. B. *J. Electrochem. Soc.* **1973**, *120*, 1498–1501.
226. Barker, C. K.; Cordes, A. W.; Margrave, J. L. *J. Phys. Chem.* **1965**, *69*, 334–335.
227. Cozzolino, A. F.; Elder, P. J. W.; Vargas-Baca, I. *Coord. Chem. Rev.* **2011**, *255*, 1426–1438.
228. Atwood, D. A. *In Encyclopedia of Inorganic Chemistry;* King, R. B., Ed.; Wiley New York, 2005; Vol. 8, pp 4948–4955.
229. Hammerl, A.; Klapötke, T. M. *In Encyclopedia of Inorganic Chemistry;* King, R. B., Ed.; Wiley New York, 2005; Vol. 6, pp 3559–3600.
230. Subbaram, K. V.; Rao, D. R. *Chem. Phys. Lett.* **1970**, *4*, 653–655.
231. Harding, L.; Jones, W. E.; Yee, K. K.; Jenouvri, A.; Daumont, D.; Pascat, B.; Guenebau, H. *Can. J. Phys.* **1971**, *49*, 2033–2051.
232. Jenouvrier, A.; Pascat, B.; Lefebvre-Brion, H. J. *Mol. Spec.* **1973**, *45*, 46–54.
233. Brown, J. M.; Uehara, H. *J. Chem. Phys.* **1987**, *87*, 880–884.
234. Andrews, L.; Hassanzadeh, P. *J. Chem. Soc., Chem. Commun.* **1994**, 1523–1524.
235. Andrews, L.; Hassanzadeh, P.; Lanzisera, D. V.; Brabson, G. D. *J. Phys. Chem.* **1996**, *100*, 16667–16673.
236. Wolmershäuser, G.; Brulet, C. R.; Street, G. B. *Inorg. Chem.* **1978**, *17*, 3586–3589.
237. Bärnighausen, H.; von Volkmann, T.; Jander, J. *Angew. Chem. Int. Ed.* **1965**, *4*, 72–73.
238. Maaninen, A.; Laitinen, R. S.; Chivers, T.; Pakkanen, T. A. *Inorg. Chem.* **1999**, *38*, 3450–3454.
239. Crevier, T. J.; Lovell, S.; Mayer, J. M.; Rheingold, A. L.; Guzei, I. A. *J. Am. Chem. Soc.* **1998**, *120*, 6607–6608.
240. Teague, C. M.; O'Brien, T. A.; O'Brien, J. F. *J. Coord. Chem.* **2002**, *55*, 627–631.
241. Awere, E. G.; Brooks, W. V. F.; Passmore, J.; White, P. S.; Sun, X. P.; Cameron, T. S. *J. Chem. Soc. Dalton Trans.* **1993**, 2439–2449.
242. Gillespie, R. J.; Kent, J. P.; Sawyer, J. F. *Inorg. Chem.* **1981**, *20*, 4053–4060.
243. Awere, E. G.; Passmore, J.; White, P. S.; Klapotke, T. *J. Chem. Soc., Chem. Commun.* **1989**, 1415–1417.
244. Liu, H.; Yang, X.; Lin, Z.; Loy, M. M. T.; Yang, S. *Chem. Eur. J.* **2001**, *7*, 652–656.
245. Maaninen, A.; Konu, J.; Laitinen, R. S.; Chivers, T.; Schatte, G.; Pietikainen, J.; Ahlgren, M. *Inorg. Chem.* **2001**, *40*, 3539–3543.
246. Awere, E.; Passmore, J.; Preston, K. F.; Sutcliffe, L. H. *Can. J. Chem.* **1988**, *66*, 1776–1780.
247. Metzner, R. *Ann. Chim. Phys.* **1898**, *15*, 250.
248. Schmitz-DuMont, O.; Ross, B. *Angew. Chem. Int. Ed Engl.* **1967**, *6*, 1071.
249. Massa, W.; Lau, C.; Möhlen, M.; Neumüller, B.; Dehnicke, K. *Angew. Chem. Int. Ed.* **1998**, *37*, 2840–2842.
250. Hefferlin, R. J. *Quant. Spectrosc. Radiat. Transfer* **2010**, *111*, 71–77.
251. Sundararajan, K.; Sankaran, K.; Kavitha, V. J. *Mol. Struct.* **2008**, *876*, 240–249.
252. Rekhis, M.; Ouamerali, O.; Joubert, L.; Tognetti, V.; Adamo, C. *J. Mol. Struct. (THEOCHEM)* **2008**, *863*, 79–83.
253. Mutoh, Y.; Kozono, N.; Araki, M.; Tsuchida, N.; Takano, K.; Ishii, Y. *Organometallics* **2010**, *29*, 519–522.
254. Ingold, K. U. In *Stable Radicals: Fundamentals and Applied Aspects of Odd-Electron Compounds*; Hicks, R. G., Ed.; Wiley: New York, 2010; pp 231–244.
255. Maillard, B.; Ingold, K. U. *J. Am. Chem. Soc.* **1976**, *98*, 520–523.
256. Rakitin, O. A. *Russ. Chem. Rev.* **2011**, *80*, 647–659.
257. Miller, J. S. *Chem. Soc. Rev.* **2011**, *40*, 3266–3296.

258. Karoui, H.; Moigne, F. L.; Ouari, O.; Tordo, P. In *Stable Radicals: Fundamentals and Applied Aspects of Odd-Electron Compounds*; Hicks, R. G., Ed.; Wiley: New York, 2010; pp 173–229.
259. Likhtenshtein, G.; Yamauchi, J.; Nakatsuji, S.; Smirnov, A. I.; Tamura, R. *Nitroxides: Applications in Chemistry, Biomedicine and Materials Science*. Wiley-VCH: Weinheim, 2008.
260. Rajca, A.; Pink, M.; Rojsajjakul, T.; Lu, K.; Wang, H.; Rajca, S. *J. Am. Chem. Soc.* **2003**, *125*, 8534–8538.
261. Miyake, Y.; Akai, N.; Kawai, A.; Shibuya, K. *J. Phys. Chem. A* **2011**, *115*, 6347–6356.
262. Balaban, A. T.; Frangopol, P. T.; Frangopol, M.; Negoita, N. *Tetrahedron* **1967**, *23*, 4661–4676.
263. Terabe, S.; Konaka, R. *J. Am. Chem. Soc.* **1971**, *93*, 4306–4307.
264. Tanaka, A.; Nakashima, K. *Magn. Reson. Chem.* **2011**, *49*, 603–610.
265. Miura, Y.; Tomimura, T. *Chem. Commun.* **2001**, 627–628.
266. Lovas, F. J.; Suenram, R. D.; Stevens, W. J. J. *Mol. Spec.* **1983**, *100*, 316–331.
267. Danen, W. C.; Newkirk, D. D. *J. Am. Chem. Soc.* **1976**, *98*, 516–520.
268. Jaitner, P.; Jager, K.; Dorfer, A.; Schwarzhans, K.-E. *J. Organomet. Chem.* **2001**, *621*, 173–176.
269. Kloxin, C. J.; Scott, T. F.; Adzima, B. J.; Bowman, C. N. *Macromolecules* **2010**, *43*, 2643–2653.
270. Miura, Y.; Tanaka, A.; Hirotsu, K. *J. Org. Chem.* **1991**, *56*, 6638–6643.
271. Miura, Y.; Tanaka, A. *J. Org. Chem.* **1991**, *56*, 3950–3954.
272. Miura, Y.; Kurokawa, S.; Nakatsuji, M.; Ando, K.; Teki, Y. *J. Org. Chem.* **1998**, *63*, 8295–8303.
273. Miura, Y.; Oyama, Y.; Teki, Y. *J. Org. Chem.* **2003**, *68*, 1225–1234.
274. Miura, Y.; Nakamura, S.; Teki, Y. *J. Org. Chem.* **2003**, *68*, 8244–8247.
275. Miura, Y.; Tomimura, T.; Teki, Y. *J. Org. Chem.* **2000**, *65*, 7889–7895.
276. Miura, Y.; Kato, I.; Teki, Y. *Dalton Trans.* **2006**, 961–966.
277. Kaszynski, P. *Molecules* **2004**, *9*, 716–724.
278. Vegas, A.; Perezsalazar, A.; Banister, A. J.; Hey, R. G. *J. Chem. Soc. Dalton Trans.* **1980**, 1812–1815.
279. Rawson, J. M.; Banister, A. J.; Lavender, I. In *Advances in Heterocyclic Chemistry*; Academic Press: New York, 1995; Vol. 62, pp 137–247.
280. Haynes, D. A. *CrystEngComm* **2011**, *13*, 4793–4805.
281. Boeré, R. T.; Moock, K. H.; Parvez, M. *Z. Anorg. Allg. Chem.* **1994**, *620*, 1589–1598.
282. Rawson, J. M.; Banister, A. J.; May, I. *Magn. Reson. Chem.* **1994**, *32*, 487–491.
283. Less, R. J.; Rawson, J. M.; Jones, M. *Polyhedron* **2001**, *20*, 523–526.
284. Alberola, A.; Clarke, C. S.; Haynes, D. A.; Pascu, S. I.; Rawson, J. M. *Chem. Commun.* **2005**, 4726–4728.
285. Alberola, A.; Carter, E.; Constantinides, C. P.; Eisler, D. J.; Murphy, D. M.; Rawson, J. M. *Chem. Commun.* **2011**, *47*, 2532–2534.
286. Bond, A. D.; Griffiths, J.; Rawson, J. M.; Hulliger, J. *Chem. Commun.* **2001**, 2488–2489.
287. Knapp, C.; Lork, E.; Gupta, K.; Mews, R. *Z. Anorg. Allg. Chem.* **2005**, *631*, 1640–1644.
288. Shuvaev, K. V.; Decken, A.; Grein, F.; Abedin, T. S. M.; Thompson, L. K.; Passmore, J. *Dalton Trans.* **2008**, 4029–4037.
289. Luzon, J.; Campo, J.; Palacio, F.; McIntyre, G. J.; Goeta, A. E.; Pask, C. M.; Rawson, J. M. *Polyhedron* **2003**, *22*, 2301–2305.
290. Luzon, J.; Campo, J.; Palacio, F.; McIntyre, G. J.; Goeta, A. E.; Ressouche, E.; Pask, C. M.; Rawson, J. M. *Phys. B Condens. Matter* **2003**, *335*, 1–5.
291. Farley, R. D.; Feeder, N.; Less, R. J.; Luzon, J.; Oliete, P.; Palacio, F.; Pask, C. M.; Paulsen, C.; Rawson, J. M. *Phosphorus. Sulfur Silicon Relat. Elem.* **2004**, *179*, 975–976.
292. Deumal, M.; LeRoux, S.; Rawson, J. M.; Robb, M. A.; Novoa, J. J. *Polyhedron* **2007**, *26*, 1949–1958.
293. Deumal, M.; Rawson, J. M.; Goeta, A. E.; Howard, J. A. K.; Copley, R. C. B.; Robb, M. A.; Novoa, J. J. *Chem. Eur. J.* **2010**, *16*, 2741–2750.
294. Clarke, C. S.; Haynes, D. A.; Smith, J. N. B.; Batsanov, A. S.; Howard, J. A. K.; Pascu, S. I.; Rawson, J. M. *CrystEngComm* **2010**, *12*, 172–185.
295. Caro, J.; Fraxedas, J.; Santiso, J.; Figueras, A.; Rawson, J. M.; Smith, J. N. B.; Antorrena, G.; Palacio, F. *Thin Solid Films* **1999**, *352*, 102–106.
296. Rawson, J. M.; Clarke, C. S.; Bruce, D. W. *Magn. Reson. Chem.* **2009**, *47*, 3–8.
297. Gritsan, N. P.; Shuvaev, K. V.; Kim, S. N.; Knapp, C.; Mews, R.; Bagryansky, V. A.; Zibarev, A. V. *Mendeleev Commun.* **2007**, *17*, 204–206.
298. MacLean, G. K.; Passmore, J.; Rao, M. N. S.; Schriver, M. J.; White, P. S.; Bethell, D.; Pilkington, R. S.; Sutcliffe, L. H. *J. Chem. Soc. Dalton Trans.* **1985**, 1405–1416.
299. Burford, N.; Passmore, J.; Schriver, M. J. *J. Chem. Soc., Chem. Commun.* **1986**, 140–142.
300. Decken, A.; Jenkins, H. D. B.; Mailmn, A.; Passmore, J.; Shuvaev, K. V. *Inorg. Chim. Acta* **2008**, *361*, 521–539.
301. Andrews, M. P.; Cordes, A. W.; Douglass, D. C.; Fleming, R. M.; Glarum, S. H.; Haddon, R. C.; Marsh, P.; Oakley, R. T.; Palstra, T. T. M.; Schneemeyer, L. F.; Trucks, G. W.; Tycko, R.; Waszczak, J. V.; Young, K. M.; Zimmerman, N. M. *J. Am. Chem. Soc.* **1991**, *113*, 3559–3568.
302. Cordes, A. W.; Haddon, R. C.; Oakley, R. T.; Schneemeyer, L. F.; Waszczak, J. V.; Young, K. M.; Zimmerman, N. M. *J. Am. Chem. Soc.* **1991**, *113*, 582–588.
303. Cordes, A. W.; Haddon, R. C.; Hicks, R. G.; Kennepohl, D. K.; Oakley, R. T.; Palstra, T. T. M.; Schneemeyer, L. F.; Scott, S. R.; Waszczak, J. V. *Chem. Mater.* **1993**, *5*, 820–825.
304. Beekman, R. A.; Boeré, R. T.; Moock, K. H.; Parvez, M. *Can. J. Chem.* **1998**, *76*, 85–93.
305. Banister, A. J.; Rawson, J. M.; Clegg, W.; Birkby, S. L. *J. Chem. Soc. Dalton Trans.* **1991**, 1099–1104.
306. Britten, J. F.; Cordes, A. W.; Haddon, R. C.; Itkis, M. E.; Oakley, R. T.; Reed, R. W.; Robertson, C. M. *CrystEngComm* **2002**, 205–207.
307. Barclay, T. M.; Cordes, A. W.; George, N. A.; Haddon, R. C.; Itkis, M. E.; Oakley, R. T. *Chem. Commun.* **1999**, 2269–2270.
308. Cordes, A. W.; Haddon, R. C.; Hicks, R. G.; Oakley, R. T.; Palstra, T. T. M.; Schneemeyer, L. F.; Waszczak, J. V. *J. Am. Chem. Soc.* **1992**, *114*, 5000–5004.
309. Cordes, A. W.; Chamchoumis, C. M.; Hicks, R. G.; Oakley, R. T.; Young, K. M.; Haddon, R. C. *Can. J. Chem.* **1992**, *70*, 919–925.
310. Cordes, A. W.; Haddon, R. C.; Hicks, R. G.; Kennepohl, D. K.; Oakley, R. T.; Schneemeyer, L. F.; Waszczak, J. V. *Inorg. Chem.* **1993**, *32*, 1554–1558.
311. Cordes, A. W.; Haddon, R. C.; MacKinnon, C. D.; Oakley, R. T.; Patenaude, G. W.; Reed, R. W.; Rietveld, T.; Vajda, K. E. *Inorg. Chem.* **1996**, *35*, 7626–7632.
312. Banister, A. J.; Lavender, I.; Rawson, J. M.; Clegg, W.; Tanner, B. K.; Whitehead, R. J. *J. Chem. Soc. Dalton Trans.* **1993**, 1421–1429.
313. Bryan, C. D.; Cordes, A. W.; Goddard, J. D.; Haddon, R. C.; Hicks, R. G.; MacKinnon, C. D.; Mawhinney, R. C.; Oakley, R. T.; Palstra, T. T. M.; Perel, A. S. *J. Am. Chem. Soc.* **1996**, *118*, 330–338.
314. Hu, L. G.; Iwasaki, A.; Suizu, R.; Yoshikawa, H.; Awaga, K.; Ito, H. *Chem. Phys. Lett.* **2010**, *484*, 177–180.
315. Kanai, K.; Yoshida, H.; Noda, Y.; Iwasaki, A.; Suizu, R.; Tsutumi, J.; Imabayashi, H.; Ouchi, Y.; Sato, N.; Seki, K.; Awaga, K. *Phys. Chem. Chem. Phys.* **2009**, *11*, 11432–11436.
316. Antorrena, G.; Brownridge, S.; Cameron, T. S.; Palacio, F.; Parsons, S.; Passmore, J.; Thompson, L. K.; Zarlaida, F. *Can. J. Chem.* **2002**, *80*, 1568–1583.
317. Decken, A.; Cameron, T. S.; Passmore, J.; Rautiainen, J. M.; Reed, R. W.; Shuvaev, K. V.; Thompson, L. K. *Inorg. Chem.* **2007**, *46*, 7436–7457.
318. Konstantinova, L. S.; Rakitin, O. A. *Russ. Chem. Rev.* **2008**, *77*, 521–546.
319. Rawson, J. M.; McManus, G. D. *Coord. Chem. Rev.* **1999**, *189*, 135–168.
320. Makarov, A. Y.; Kim, S. N.; Gritsan, N. P.; Bagryanskaya, I. Y.; Gatilov, Y. V.; Zibarev, A. V. *Mendeleev Commun.* **2005**, 14–17.
321. Pivtsov, A. V.; Kulik, L. V.; Makarov, A. Y.; Blockhuys, F. *Phys. Chem. Chem. Phys.* **2011**, *13*, 3873–3880.
322. Oakley, R. T.; Reed, R. W.; Robertson, C. M.; Richardson, J. F. *Inorg. Chem.* **2005**, *44*, 1837–1845.
323. Barclay, T. M.; Cordes, A. W.; Haddon, R. C.; Itkis, M. E.; Oakley, R. T.; Reed, R. W.; Zhang, H. *J. Am. Chem. Soc.* **1999**, *121*, 969–976.
324. Beer, L.; Cordes, A. W.; Haddon, R. C.; Itkis, M. E.; Oakley, R. T.; Reed, R. W.; Robertson, C. M. *Chem. Commun.* **2002**, 1872–1873.
325. Risto, M.; Assoud, A.; Winter, S. M.; Oilunkaniemi, R.; Laitinen, R. S.; Oakley, R. T. *Inorg. Chem.* **2008**, *47*, 10100–10109.
326. Risto, M.; Reed, R. W.; Robertson, C. M.; Oilunkaniemi, R.; Laitinen, R. S.; Oakley, R. T. *Chem. Commun.* **2008**, 3278–3280.
327. Rawson, J. M.; Alberola, A.; Whalley, A. J. *Mater. Chem.* **2006**, *16*, 2560–2565.
328. Brownridge, S.; Du, H. B.; Fairhurst, S. A.; Haddon, R. C.; Oberhammer, H.; Parsons, S.; Passmore, J.; Schriver, M. J.; Sutcliffe, L. H.; Westwood, N. P. C. *J. Chem. Soc. Dalton Trans.* **2000**, 3365–3382.
329. Wolmershäuser, G.; Kraft, G. *Chem. Ber.* **1990**, *113*, 881–885.
330. Awere, E. G.; Burford, N.; Haddon, R. C.; Parsons, S.; Passmore, J.; Waszczak, J. V.; White, P. S. *Inorg. Chem.* **1990**, *29*, 4821–4830.
331. Alberola, A.; Farley, R. D.; Humphrey, S. M.; McManus, G. D.; Murphy, D. M.; Rawson, J. M. *Dalton Trans.* **2005**, 3838–3845.
332. Alberola, A.; Clements, O. P.; Collis, R. J.; Cubbitt, L.; Grant, C. M.; Less, R. J.; Oakley, R. T.; Rawson, J. M.; Reed, R. W.; Robertson, C. M. *Cryst. Growth Des.* **2008**, *8*, 155–161.
333. Brusso, J. L.; Clements, O. P.; Haddon, R. C.; Itkis, M. E.; Leitch, A. A.; Oakley, R. T.; Reed, R. W.; Richardson, J. F. *J. Am. Chem. Soc.* **2004**, *126*, 8256–8265.

334. Barclay, T. M.; Cordes, A. W.; George, N. A.; Haddon, R. C.; Itkis, M. E.; Mashuta, M. S.; Oakley, R. T.; Patenaude, G. W.; Reed, R. W.; Richardson, J. F.; Zhang, H. *J. Am. Chem. Soc.* **1998**, *120*, 352–360.
335. Brusso, J. L.; Clements, O. P.; Haddon, R. C.; Itkis, M. E.; Leitch, A. A.; Oakley, R. T.; Reed, R. W.; Richardson, J. F. *J. Am. Chem. Soc.* **2004**, *126*, 14692–14693.
336. Decken, A.; Mailman, A.; Mattar, S. M.; Passmore, J. *Chem. Commun.* **2005**, 2366–2368.
337. Decken, A.; Mailman, A.; Passmore, J. *Chem. Commun.* **2009**, 6077–6079.
338. Decken, A.; Mailman, A.; Passmore, J.; Rautiainen, J. M.; Schererb, W.; Scheidtb, E.-W. *Dalton Trans.* **2011**, *40*, 868–879.
339. Mattar, S. M.; Durelle, J. *Magn. Reson. Chem.* **2010**, *48*, S122–S131.
340. Barclay, T. M.; Beer, L.; Cordes, A. W.; Oakley, R. T.; Preuss, K. E.; Reed, R. W.; Taylor, N. J. *Inorg. Chem.* **2001**, *40*, 2709–2714.
341. Barclay, T. M.; Cordes, A. W.; Goddard, J. D.; Mawhinney, R. C.; Oakley, R. T.; Preuss, K. E.; Reed, R. W. *J. Am. Chem. Soc.* **1997**, *119*, 12136–12141.
342. Barclay, T. M.; Cordes, A. W.; Oakley, R. T.; Preuss, K. E.; Reed, R. W. *Chem. Mater.* **1999**, *11*, 164–169.
343. Cordes, A. W.; Haddon, R.; Oakley, R. *Phosphorus. Sulfur Silicon Relat. Elem.* **2004**, *179*, 673–684.
344. Beer, L.; Oakley, R. T.; Mingie, J. R.; Preuss, K. E.; Taylor, N. J.; Cordes, A. W. *J. Am. Chem. Soc.* **2000**, *122*, 7602–7603.
345. Beer, L.; Brusso, J. L.; Cordes, A. W.; Godde, E.; Haddon, R. C.; Itkis, M. E.; Oakley, R. T.; Reed, R. W. *Chem. Commun.* **2002**, 2562–2563.
346. Beer, L.; Brusso, J. L.; Cordes, A. W.; Haddon, R. C.; Itkis, M. E.; Kirschbaum, K.; MacGregor, D. S.; Oakley, R. T.; Pinkerton, A. A.; Reed, R. W. *J. Am. Chem. Soc.* **2002**, *124*, 9498–9509.
347. Beer, L.; Britten, J. F.; Brusso, J. L.; Cordes, A. W.; Haddon, R. C.; Itkis, M. E.; MacGregor, D. S.; Oakley, R. T.; Reed, R. W.; Robertson, C. M. *J. Am. Chem. Soc.* **2003**, *125*, 14394–14403.
348. Beer, L.; Britten, J. F.; Clements, O. P.; Haddon, R. C.; Itkis, M. E.; Matkovich, K. M.; Oakley, R. T. *Chem. Mater.* **2004**, *16*, 1564–1572.
349. Beer, L.; Brusso, J. L.; Haddon, R. C.; Itkis, M. E.; Oakley, R. T.; Reed, R. W.; Richardson, J. F.; Secco, R. A.; Yu, X. Y. *Chem. Commun.* **2005**, 5745–5747.
350. Brusso, J. L.; Derakhshan, S.; Itkis, M. E.; Kleinke, H.; Haddon, R. C.; Oakley, R. T.; Reed, R. W.; Richardson, J. F.; Robertson, C. M.; Thompson, L. K. *Inorg. Chem.* **2006**, *45*, 10958–10966.
351. Brusso, J. L.; Cvrkalj, K.; Leitch, A. A.; Oakley, R. T.; Reed, R. W.; Robertson, C. M. *J. Am. Chem. Soc.* **2006**, *128*, 15080–15081.
352. Leitch, A. A.; Yu, X. Y.; Robertson, C. M.; Secco, R. A.; Tse, J. S.; Oakley, R. T. *Inorg. Chem.* **2009**, *48*, 9874–9882.
353. Leitch, A. A.; McKenzie, C. E.; Oakley, R. T.; Reed, R. W.; Richardson, J. F.; Sawyer, L. D. *Chem. Commun.* **2006**, 1088–1090.
354. Leitch, A. A.; Reed, R. W.; Robertson, C. M.; Britten, J. F.; Yu, X. Y.; Secco, R. A.; Oakley, R. T. *J. Am. Chem. Soc.* **2007**, *129*, 7903–7914.
355. Leitch, A. A.; Yu, X. Y.; Winter, S. M.; Secco, R. A.; Dube, P. A.; Oakley, R. T. *J. Am. Chem. Soc.* **2009**, *131*, 7112–7125.
356. Winter, S.; Datta, S.; Hill, S.; Oakley, R. T. *J. Am. Chem. Soc.* **2011**, *133*, 8126–8129.
357. Tse, J. S.; Leitch, A. A.; Yu, X. Y.; Bao, X. Z.; Zhang, S. J.; Liu, Q. Q.; Jin, C. Q.; Secco, R. A.; Desgreniers, S.; Ohishi, Y.; Oakley, R. T. *J. Am. Chem. Soc.* **2010**, *132*, 4876–4886.
358. Leitch, A. A.; Lekin, K.; Winter, S. M.; Downie, L. E.; Tsuruda, H.; Tse, J. S.; Mito, M.; Desgreniers, S.; Dube, P. A.; Zhang, S. J.; Liu, Q. Q.; Jin, C. Q.; Ohishi, Y.; Oakley, R. T. *J. Am. Chem. Soc.* **2011**, *133*, 6051–6060.
359. Robertson, C. M.; Leitch, A. A.; Cvrkalj, K.; Myles, D. J. T.; Reed, R. W.; Dube, P. A.; Oakley, R. T. *J. Am. Chem. Soc.* **2008**, *130*, 14791–14801.
360. Robertson, C. M.; Leitch, A. A.; Cvrkalj, K.; Reed, R. W.; Myles, D. J. T.; Dube, P. A.; Oakley, R. T. *J. Am. Chem. Soc.* **2008**, *130*, 8414–8425.
361. Mito, M.; Komorida, Y.; Tsuruda, H.; Tse, J. S.; Desgreniers, S.; Ohishi, Y.; Leitch, A. A.; Cvrkalj, K.; Robertson, C. M.; Oakley, R. T. *J. Am. Chem. Soc.* **2009**, *131*, 16012–16013.
362. Lekin, K.; Winter, S. M.; Downie, L. E.; Bao, X. Z.; Tse, J. S.; Desgreniers, S.; Secco, R. A.; Dube, P. A.; Oakley, R. T. *J. Am. Chem. Soc.* **2010**, *132*, 16212–16224.
363. Barclay, T. M.; Cordes, A. W.; delaat, R. H.; Goddard, J. D.; Haddon, R. C.; Jeter, D. Y.; Mawhinney, R. C.; Oakley, R. T.; Palstra, T. T. M.; Patenaude, G. W.; Reed, R. W.; Westwood, N. P. C. *J. Am. Chem. Soc.* **1997**, *119*, 2633–2641.
364. Shimizu, K.; Gotohda, T.; Matsushita, T.; Wada, N.; Fujita, W.; Awaga, K.; Saiga, Y.; Hirashima, D. S. *Phys. Rev. B* **2006**, *74*, 172413–172416.
365. Fujita, W.; Awaga, K.; Takahashi, M.; Takeda, M.; Yamazaki, T. *Chem. Phys. Lett.* **2002**, *362*, 97–102.
366. Fujita, W.; Awaga, K. *Chem. Phys. Lett.* **2004**, *393*, 150–152.
367. Fujita, W.; Awaga, K.; Kondo, R.; Kagoshima, S. *J. Am. Chem. Soc.* **2006**, *128*, 6016–6017.
368. Fujita, W.; Kikuchi, K.; Awaga, K. *Angew. Chem. Int. Ed Engl.* **2008**, *47*, 9480–9483.
369. Fujita, W.; Kikuchi, K. *Chem. Asian J.* **2009**, *4*, 400–405.
370. Fujita, W.; Takahashi, K.; Kobayashi, H. *Cryst. Growth Des.* **2011**, *11*, 575–582.
371. Ikorskii, V. N.; Irtegova, I. G.; Lork, E.; Makarov, A. Y.; Mews, R.; Ovcharenko, V. I.; Zibarev, A. V. *Eur. J. Inorg. Chem.* **2006**, 3061–3067.
372. Konchenko, S. N.; Gritsan, N. P.; Lonchakov, A. V.; Irtegova, I. G.; Mews, R.; Ovcharenko, V. I.; Radius, U.; Zibarev, A. V. *Eur. J. Inorg. Chem.* **2008**, 3833–3838.
373. Gritsan, N. P.; Lonchakov, A. V.; Lork, E.; Mews, R.; Pritchina, E. A.; Zibarev, A. V. *Eur. J. Inorg. Chem.* **2008**, 1994–1998.
374. Semenov, N. A.; Pushkarevsky, N. A.; Lonchakov, A. V.; Bogomyakov, A. S.; Pritchina, E. A.; Suturina, E. A.; Gritsan, N. P.; Konchenko, S. N.; Mews, R.; Ovcharenko, V. I.; Zibarev, A. V. *Inorg. Chem.* **2010**, *49*, 7558–7564.
375. Bagryanskaya, I. Y.; Gatilov, Y. V.; Gritsan, N. P.; Ikorskii, V. N.; Irtegova, I. G.; Lonchakov, A. V.; Lork, E.; Mews, R.; Ovcharenko, V. I.; Semenov, N. A.; Vasilieva, N. V.; Zibarev, A. V. *Eur. J. Inorg. Chem.* **2007**, 4751–4761.
376. Konchenko, S. N.; Gritsan, N. P.; Lonchakov, A. V.; Radius, U.; Zibarev, A. V. *Mendeleev Commun.* **2009**, *19*, 7–9.
377. Lork, E.; Mews, R.; Zibarev, A. V. *Mendeleev Commun.* **2009**, *19*, 147–148.
378. Suturina, E. A.; Semenov, N. A.; Lonchakov, A. V.; Bagryanskaya, I. Y.; Gatilov, Y. V.; Irtegova, I. G.; Vasilieva, N. V.; Lork, E.; Mews, R.; Gritsan, N. P.; Zibarev, A. V. *J. Phys. Chem. A* **2011**, *115*, 4851–4860.
379. Vasilieva, N. V.; Irtegova, I. G.; Gritsan, N. P.; Lonchakov, A. V.; Makarov, A. Y.; Shundrin, L. A.; Zibarev, A. V. J. *Phys. Org. Chem.* **2010**, *23*, 536–543.
380. Morgan, I. S.; Jennings, M.; Vindigni, A.; Clérac, R.; Preuss, K. E. *Cryst. Growth Des.* **2011**, *11*, 2520–2527.
381. Cordes, A. W.; Hayes, P. J.; Josephy, P. D.; Koenig, H.; Oakley, R. T.; Pennington, W. T. *J. Chem. Soc., Chem. Commun.* **1984**, 1021–1022.
382. Hayes, P. J.; Oakley, R. T.; Cordes, A. W.; Pennington, W. T. *J. Am. Chem. Soc.* **1985**, *107*, 1346–1351.
383. Boeré, R. T.; Cordes, A. W.; Hayes, P. J.; Oakley, R. T.; Reed, R. W.; Pennington, W. T. *Inorg. Chem.* **1986**, *25*, 2445–2450.
384. Boeré, R. T.; Roemmele, T. L. *Phosphorus. Sulfur Silicon Relat. Elem.* **2004**, *179*, 875–882.
385. Boeré, R. T.; Roemmele, T. L.; Yu, X. *Inorg. Chem.* **2011**, *50*, 5123–5136.
386. Oakley, R. T.; Reed, R. W.; Cordes, A. W.; Craig, S. L.; Graham, J. B. *J. Am. Chem. Soc.* **1987**, *109*, 7745–7749.
387. Farrar, J. M.; Patel, M. K.; Kaszynski, P.; Young, V. G. *J. Org. Chem.* **2000**, *65*, 931–940.
388. Oakley, R. T. *J. Chem. Soc., Chem. Commun.* **1986**, 596–597.
389. Cordes, A. W.; Koenig, H.; Oakley, R. T. *J. Chem. Soc., Chem. Commun.* **1989**, 710–712.
390. Bestari, K.; Cordes, A. W.; Oakley, R. T.; Young, K. M. *J. Am. Chem. Soc.* **1990**, *112*, 2249–2255.
391. Zienkiewicz, J.; Kaszynski, P.; Young, V. G. *J. Org. Chem.* **2004**, *69*, 2551–2561.
392. Zienkiewicz, J.; Kaszynski, P.; Young, V. G., Jr. *J. Org. Chem.* **2004**, *69*, 7525–7536.
393. Zienkiewicz, J.; Fryszkowska, A.; Zienkiewicz, K.; Guo, F. L.; Kaszynski, P.; Januszko, A.; Jones, D. *J. Org. Chem.* **2007**, *72*, 3510–3520.
394. Leitch, A. A.; Oakley, R. T.; Reed, R. W.; Thompson, L. K. *Inorg. Chem.* **2007**, *46*, 6261–6270.
395. Lemaire, M. T. *Pure Appl. Chem.* **2011**, *83*, 141–149.
396. Banister, A. J.; May, I.; Rawson, J. M.; Smith, J. N. B. J. *Organomet. Chem.* **1998**, *550*, 241–253.
397. Fujita, W.; Awaga, K. *J. Am. Chem. Soc.* **2001**, *123*, 3601–3602.
398. Kepenekian, M.; Le Guennic, B.; Awaga, K.; Robert, V. *Phys. Chem. Chem. Phys.* **2009**, *11*, 6066–6071.
399. Umezono, Y.; Fujita, W.; Awaga, K. *J. Am. Chem. Soc.* **2006**, *128*, 1084–1085.
400. Umezono, Y.; Fujita, W.; Awaga, K. *Chem. Phys. Lett.* **2005**, *409*, 139–143.
401. Staniland, S. S.; Fujita, W.; Umezono, Y.; Awaga, K.; Camp, P. J.; Clark, S. J.; Robertson, N. *Inorg. Chem.* **2005**, *44*, 546–551.
402. Staniland, S. S.; Fujita, W.; Umezono, Y.; Awaga, K.; Clark, S. J.; Cui, H. B.; Kobayashi, H.; Robertson, N. *Chem. Commun.* **2005**, 3204–3206.
403. Awaga, K.; Umezono, Y.; Fujita, W.; Yoshikawa, H.; Cui, H. B.; Kobayashi, H.; Staniland, S. S.; Robertson, N. *Inorg. Chim. Acta* **2008**, *361*, 3761–3770.

404. Boeré, R. T.; Goh, L.-Y.; Ang, C. Y.; Kuan, S. L.; Lau, H. F.; Lin Ng, V. W.; Roemmele, T. L.; Seagrave, S. D. J. *Organomet. Chem.* **2007**, *692*, 2697–2704.
405. Lau, H. F.; Ng, V. W. L.; Koh, L. L.; Tan, G. K.; Goh, L. Y.; Roemmele, T. L.; Seagrave, S. D.; Boeré, R. T. *Angew. Chem. Int. Ed.* **2006**, *45*, 4498–4501.
406. Lau, H. F.; Ang, P. C. Y.; Ng, V. W. L.; Kuan, S. L.; Goh, L. Y.; Borisov, A. S.; Hazendonk, P.; Roemmele, T. L.; Boeré, R. T.; Webster, R. D. *Inorg. Chem.* **2008**, *47*, 632–644.
407. Ang, C. Y.; Boeré, R. T.; Goh, L. Y.; Koh, L. L.; Kuan, S. L.; Tan, G. K.; Yu, X. *Chem. Commun.* **2006**, 4735–4737.
408. Hearns, N. G. R.; Preuss, K. E.; Richardson, J. F.; Bin-Salamon, S. *J. Am. Chem. Soc.* **2004**, *126*, 9942–9943.
409. Hearns, N. G. R.; Fatila, E. M.; Clerac, R.; Jennings, M.; Preuss, K. E. *Inorg. Chem.* **2008**, *47*, 10330–10341.
410. Britten, J.; Hearns, N. G. R.; Preuss, K. E.; Richardson, J. F.; Bin-Salamon, S. *Inorg. Chem.* **2007**, *46*, 3934–3945.
411. Fatila, E. M.; Goodreid, J.; Clerac, R.; Jennings, M.; Assoud, J.; Preuss, K. E. *Chem. Commun.* **2010**, *46*, 6569–6571.
412. Hearns, N. G. R.; Clérac, R.; Jennings, M.; Preuss, K. E. *Dalton Trans.* **2009**, 3193–3203.

This page intentionally left blank

1.15 Main Group Biradicaloids

S González-Gallardo and F Breher, Karlsruhe Institute of Technology (KIT), Karlsruhe, Germany

Abbreviations

AIM	Atoms-in-molecules
B3LYP	Becke, three-parameter, Lee–Yang–Parr
Bbt	2,6-Bis[bis(trimethylsilyl)methyl]-4-[tris (trimethylsilyl)methyl]phenyl
bcp	Bond-critical point
CAS	Complete active space
CASSCF	Complete active space self-consistent field
CP-MAS	Cross-polarization-magic angle spinning
CV	Cyclic voltammetry
Dep	2,6-$Et_2C_6H_3$
DFT	Density functional theory
dme	Dimethoxyethane
Dmp	2,6-$Me_2C_6H_3$
E_D	Delocalization energy
EELS	Electron energy loss spectroscopy
EPR	Electron paramagnetic resonance
Fc	Ferrocenyl
HOMO	Highest occupied molecular orbital
LANL2DZ	Los Alamos National Laboratory 2-double-ζ
LB	Long bond
LDA	Lithium diisopropylamide
LUMO	Lowest unoccupied molecular orbital
MCSCF	Multi-configurational self-consistent field
Mes*	2,4,6-$tBu_3C_6H_2$
MO	Molecular orbital
NICS	Nucleus-independent chemical shift
NMR	Nuclear magnetic resonance
NOE	Nuclear Overhauser effect
PES	Potential energy surface
PP	Perfect pairing
PQ	Perfect quadruples
RAS-2SF	Restricted active space double spin flip
RI-DFT	Resolution of the identity density functional theory
SB	Short bond
SOMO	Singly occupied molecular orbital
TD-DFT	Time-dependent density functional theory
temp	2,2,6,6-$Me_4C_5H_6N$
TEMPO	(2,2,6,6-Tetramethylpiperidin-1-yl)oxyl
TMEDA	Tetramethylethylenediamine
TZVP	Triple zeta valence polarization
UV/Vis	Ultraviolet/visible spectroscopy
VB	Valence bond
ZPE	Zero point energy

1.15.1 Introduction

The landmark paper of Gomberg on the stable free triphenylmethyl radical[1] initiated numerous investigations on molecules containing one (or more) unpaired electrons. Several kinds of persistent and stable radicals[2] have been described ever since, and several more general classes of (poly)radicals have been developed in recent times. As stated recently, "much of the current interest in stable radicals probably arises [...] from the fundamental structure and bonding issues that naturally arise with this class of compounds".[3] However, apart from these fundamentally important questions, many applications of stable radicals have been reported or envisaged.[4] In particular, the development of new materials with technologically relevant properties, such as magnetism or conductivity, is in the current focus of interest.[5,6] A very appealing idea in this

context is to use stable radicals as both a charge carrier and a magnetic coupler.[7]

Most often, light carbon-based or heteroatom radicals have been studied. Investigations on heavier main group radicals are fewer in number, although the last few decades witnessed spectacular discoveries in the chemistry of the heavier main group elements.[8,9] The design of novel synthetic strategies, particularly the use of very bulky substituents, has led to the isolation of a wide range of compounds, including main group radicals. This area has been reviewed recently.[10,11]

Among others, one important development in the late 1980s and 1990s was the synthesis of a wide range of novel singlet biradicaloids,[12] that is, closed-shell molecules whose common feature is the incorporation of main group elements, such as boron, nitrogen, silicon, phosphorus, or sulfur, in their structures and which can be regarded as stable, isolable analogs of organic biradicals.[13] The latter consist of two unpaired electrons in two, almost degenerate, nonbonding molecular orbitals (MOs). Depending on several factors, the molecules can form either a singlet (S) or a triplet (T) spin state.[14] Most prominent localized biradicals with two well-defined radical substructures are, for instance, cyclobutane-1,3-diyls (**Scheme 1**). The orbital interaction diagram of the latter illustrates that 'through-space' and 'through-bond' interactions lead to an almost degenerate orbital set to be occupied by two electrons. For cyclobutane-1,3-diyls, both spin states (S vs. T) are very close in energy (1.7 kcal mol^{-1}). Although the triplet state could be observed by electron paramagnetic resonance (EPR) spectroscopy, singlet

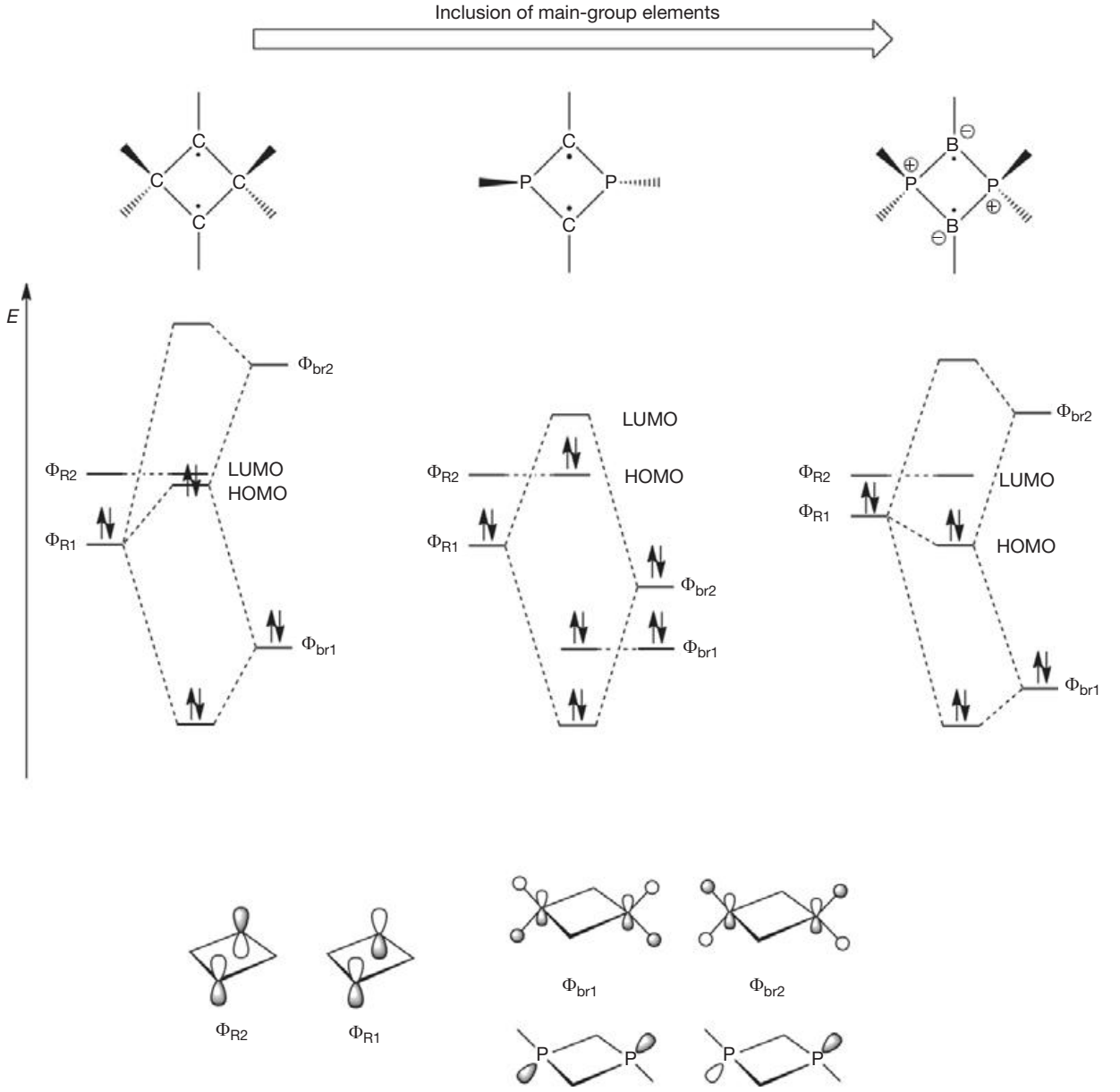

Scheme 1 Schematic orbital interaction diagrams for three selected biradical(oid)s: Cyclobutan-1,3-diyls (left), P_2C_2 (middle), and P_2B_2 heterocycles (right). Φ_{R1} and Φ_{R2} are general representations of the π-orbitals carrying the two electrons ($CR^{\bullet}$ and $BR^{\bullet-}$); Φ_{br1} and Φ_{br2} are those for the bridging entities. The energy scale (vertical axis) is only qualitative.

cyclobutane-1,3-diyls were predicted as extremely short-lived transition states for the ring inversion of bicyclo[1.1.0]butanes ($\Delta E = \sim$40–50 kcal mol^{-1}). However, if some or all the carbon atoms in the skeletons of the organic biradicals are replaced by main group elements, stable analogs of the organic biradicals can be isolated in certain cases, which in turn possess less biradical and more closed-shell characteristics.[15] A qualitative MO picture of this increased stability and decreased biradical character is given in Scheme 1. The atom substitutions result in singlet ground states, larger highest occupied molecular orbital–lowest unoccupied molecular orbital (HOMO–LUMO) gaps, larger differences between the spin states (ΔE_{S-T}), and lower LUMO occupation numbers. All these factors unavoidably diminish their biradical character and, in fact, all biradicaloids isolated so far are (formally, at least) closed-shell species.[16] However, there is no clear threshold to determine whether a molecule belongs to a certain class.

Although many questions have to be answered, it appears that the 'recent work indicates that future investigations of such species have the potential to lead to interesting advancements in (1) the creation of new materials with novel properties, and (2) unusual reactivity involving main group compounds.'[9] More specifically, it has recently been stated that "catenation of singlet biradicals, *via* appropriate linkers, is predicted to lead to antiferromagnetic low-spin polymers, in which the half-filled electron bands would confer the capability for metallic conduction without doping."[17]

In this chapter, we focus on synthetically accessible main group biradicaloids, in which both radical sites are located in close spatial proximity. To this end, the main emphasis will be on the chemistry of neutral species and, in particular, on small rings and cages containing elements of the groups 13, 14, and 15. The chapters are arranged in such a way that the historical development is reflected. For that reason, all developments on four-membered P_2C_2 heterocycles are described in the first part, after which we focus on related B_2P_2 systems. The final section addresses early findings and most recent developments on small rings and clusters comprising group 14 elements.

For the major types of biradicaloids, the methods of synthesis are illustrated alongside supporting information on their electronic properties and molecular structures. For space limitation reasons, catenated systems in which two radical units such as verdazyl, aminyl, nitroxide, nitronyl nitroxides, or thiazyls are bridged by an appropriate linker are not discussed here. Chalcogen–nitrogen rings and cages are also not considered here, since this area is covered by another chapter in this book and some key reviews.[18] This fact is particularly emphasized, since it has been recently suggested that the weak transannular S–S bonds in certain sulfur–nitrogen ring systems, for example, S_4N_4 and 1,5-$R_4P_2N_4S_2$,[19] might also be a potential source of biradical character.[20]

1.15.2 Biradicaloids of Four-Membered P_2C_2 Heterocycles

1.15.2.1 Syntheses of 1,3-Diphosphacyclobutane-2,4-Diyls

As mentioned in Section 1.15.1, the presence of heteroatoms aids in the stabilization of the otherwise elusive biradicaloid species. In this regard, cyclobutane-1,3-diyl analogs containing heavy main group elements have attracted considerable interest. Already in 1995, Niecke and coworkers reported the synthesis of several four-membered P_2C_2 heterocycles consisting of the 1,3-diphosphacyclobutane-2,4-diyl scaffold, $(RP)_2(CCl)_2$ (**2-I**), where R is a bulky substituent such as Mes* (**2-1**) (Mes* = 2,4,6-tBu$_3$C$_6$H$_2$) or temp (**2-2**) (temp = 2,2,6,6-Me$_4$C$_5$H$_6$N). In general, these species are accessible from the reaction of *C*-dichloro phosphaalkenes with *n*BuLi at low temperatures (Scheme 2).[21,22]

In 2003, Yoshifuji and coworkers reported on a novel synthetic strategy for a high-yield access to a different class of 1,3-diphosphacyclobutane-2,4-diyls. Ring systems of the general formula $(R^1R^2P)_2(CMes^*)_2$ (**2-III**, Mes* = 2,4,6-tBu$_3$C$_6$H$_2$) are accessible from the sterically protected phosphaalkyne **2-3** and a sequential addition of nucleophilic and electrophilic reagents (R^1Li and R^2X in Scheme 2).[23] In contrast to the heterocycles **2-I**, these derivatives feature bulky Mes* ligands on the carbon instead of the phosphorus atoms, which render them stable even in air. This elegant method enables various kinds of nucleophiles and electrophiles to be employed in the reaction, in order to obtain a wide range of 1,3-diphosphacyclobutane-2,4-diyls. Commonly, *t*BuLi is used to prepare the intermediate **2-II** (Scheme 2), but other nucleophiles such as lithium diisopropylamide (LDA) are also appropriate.[24] The second P atom can be substituted by salt metathesis using simple alkyl halides (R^2X) as well as other functionalized chloro derivatives.[25]

The ultraviolet/visible spectroscopy (UV/Vis) absorption of **2-4** at 612 nm (cf. 478 nm for **2-1**) clearly indicates that the energy splitting between the lowest energy and first excited singlet states is small.[21] Based on these data, an increased biradical character may be anticipated. Variations of the substituents on the P atoms in **2-III** lead to shifts in the UV/Vis absorption (Table 1).[26] A bathochromic shift, which might correspond to a smaller HOMO–LUMO gap, has been associated with the presence of electron-withdrawing groups such as benzoyl or SR. For instance, calculations at the Becke, three-parameter, Lee–Yang–Parr (B3LYP)/6-311+G(d,p) level on the model compounds $(MeR^2P)_2(CMe)_2$ have indeed revealed a smaller HOMO–LUMO gap (2.37 eV) for **2-5** (R^2 = SPh) as compared to **2-6** ($R^2 = CH_2Ph$) (2.54 eV).[27] However, an electronegative C_3F_7 group in **2-11** does not cause a red shift, which might indicate unique σ-electron-withdrawing and π-electron-donating effects of the fluorine atoms.[26]

Very recently, the nuclear magnetic resonance (NMR) spectroscopy of compound **2-4** was revisited.[28] By performing various ^{1}H and ^{31}P coupled and decoupled experiments, it was established that while the *t*Bu-substituted phosphorus atom interacts quite strongly with the protons in its *t*Bu moiety ($^3J_{PH} = 14$ Hz) and the methyl protons bonded to the Me-substituted phosphorus center ($^4J_{PH} = 6$ Hz), the latter does not interact with any protons. The nuclear Overhauser effect (NOE) experiments suggest that the orientation of the phosphorus lone pairs has a significant influence on the magnetic environment of the molecule, causing the differentiation of the signals corresponding to the *t*Bu ($\delta = 1.63$ and 1.61 ppm) and aromatic protons ($\delta = 7.40$ and 7.21 ppm) on both sides of the Mes* group.

The central ring skeleton of the Niecke-type P_2C_2 heterocycles **2-I** is planar, featuring (weakly) pyramidalized coordination spheres at both the carbon and the phosphorus centers.[21] The reasonably high inversion barrier at phosphorus impedes the formation of a planar 6π-conjugated heterocycle. As a consequence, the LUMO occupation number of 0.4 e$^-$ as

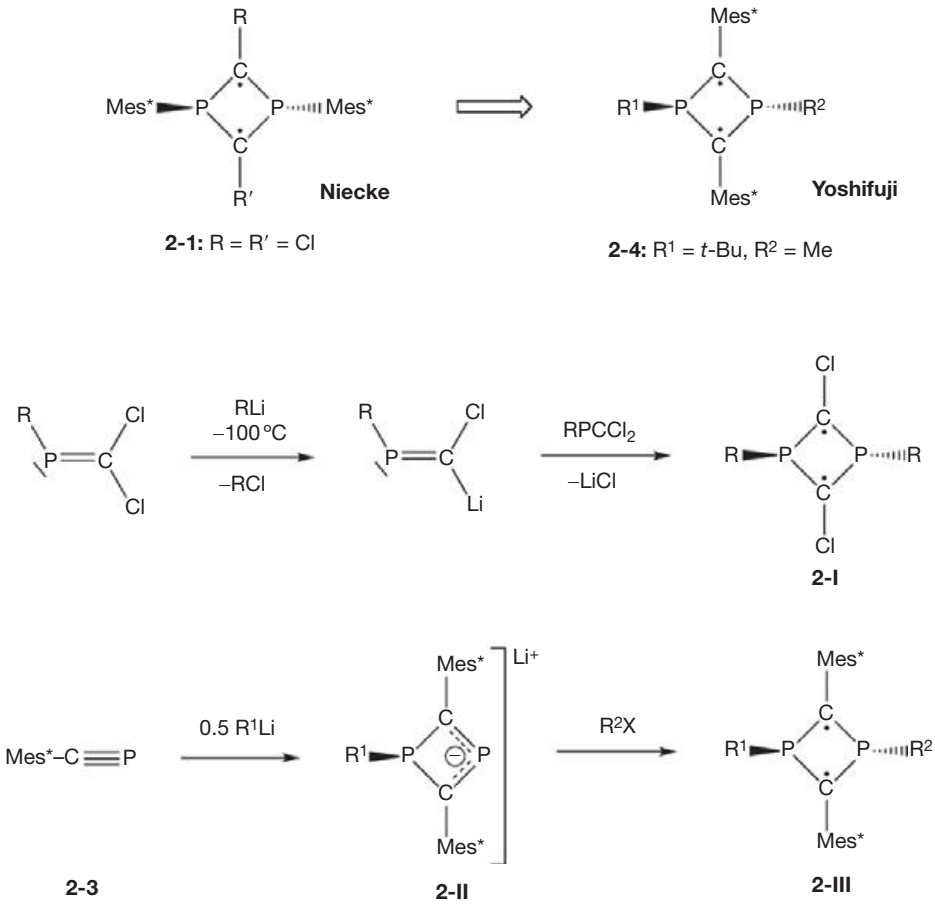

Scheme 2 Synthesis of 1,3-diphosphacyclobutane-2,4-diyls of the general structure **2-I** and **2-III**; Mes* = 2,4,6-tBu$_3$C$_6$H$_2$.

Table 1 UV/Vis data of (tBuR^{2}P)$_2$(CMes*)$_2$ compounds (**2-4**, **2-7**–**2-13**)

Compound	R^2	λ_{max} ($\varepsilon \times 10^{-3}$) ($nm^{-1}$)
2-4	Me	612
2-7	tBu	574
2-8	CH_2Ph	610
2-9	C(O)Ph	664
2-10	$C_{18}H_{37}$	606
2-11	C_3F_7	587
2-12	SMe	640
2-13	S(p-Tol)	643

well as the small singlet–triplet energy gap ($-\Delta E_{S-T}$) of 6.2 kcal mol^{-1} (CAS(14,12)/6-31g(d,p))[29] suggested considerable biradicaloid character. On the other hand, the environment at the P atoms is less pyramidal than in common phosphanes, which indicates some degree of π-donation from the P lone pairs to the carbon radical centers. The stabilization of the singlet state can be explained by a conjugative interaction of the unpaired electrons at the C atoms with the nonbonding electron pairs at the P atoms. The electronic ground state may be approximated by the resonance structures **2-A** and **2-B** shown in Scheme 3. Diphosphacyclobutane-2,4-diyls of this type may therefore be described as weak π-conjugated biradicaloids. Scheme 3 also shows the schematic MO diagram calculated for the parent system (PH)$_2$(CH)$_2$ (see also Scheme 1).[21]

In contrast, the structures of the Yoshifuji-type derivatives (**2-III**) feature carbon atoms in a planar environment, while both phosphorus centers are pyramidalized (Σ(P1) = 341°, Σ(P2) = 319° (**2-4**)[23]; Σ(P1) = 344.2°, Σ(P2) = 317.9° (**2-8**)[30]; Σ(P1) = 350.7°, Σ(P2) = 310.9° (**2-11**)[26]; Σ(P1) = 346.9°, Σ(P2) = 313.0° (**2-13**)).[27] Considering the distance between both carbon atoms for all these biradicaloids, it can be concluded that no bond between them is present (C1···C2 > 250 pm).

The biradicaloid character of the unsymmetrical derivatives **2-III** has been critically argued because the P_2C_2 four-membered rings display two different sets of phosphorus carbon bond lengths, which could be ascribed to the presence of P–C single and (partial) P=C double bonds (e.g., **2-4**: P1–C1 170 pm, P1–C2 172 pm, P2–C1 177 pm, and P2–C2 179 pm).[23] In order to address this point, the symmetrical derivatives **2-7** ($R^1 = R^2 = t$Bu), **2-14** (Me), **2-15** (sBu), and **2-16** (nBu) were isolated. The X-ray structure analysis on single crystals of **2-14** revealed P–C bond lengths of ~175 pm, which are comparable with those observed for the Niecke-type biradicals **2-I**. Furthermore, ^{31}P NMR and UV/Vis spectroscopic

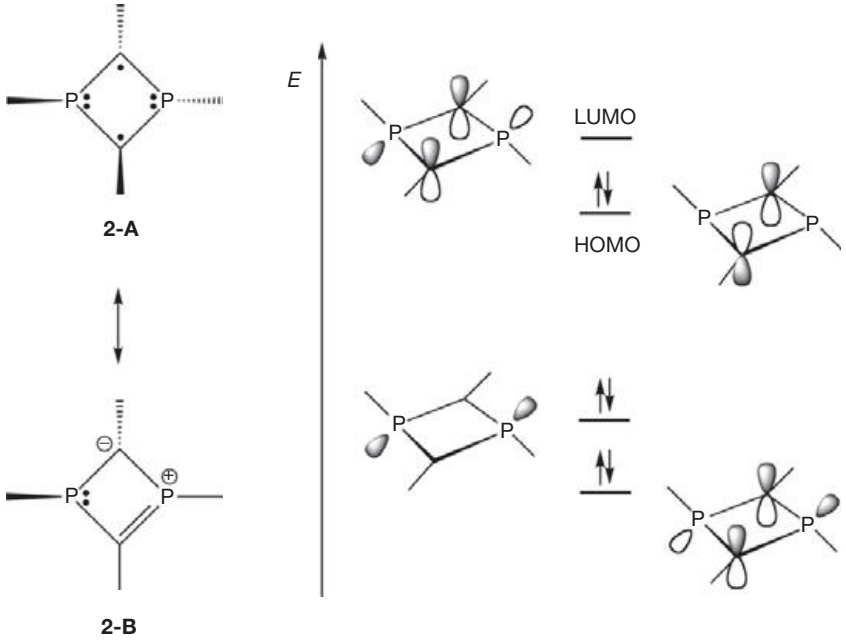

Scheme 3 Resonance structures **2-A** and **2-B** (left) and schematic molecular orbital diagram (right, qualitative energy scale).

data suggest no significant difference in the biradical character of both symmetrical and unsymmetrical species.[26,31]

In order to obtain compounds that would exhibit novel electronic and magnetic properties, the catenation of biradical units into oligomeric and polymeric structures has attracted considerable interest in recent years (cf. section 1.15.1). The 1,3-diphosphacyclobutane-2,4-diyls **2-III** constitute promising species for the development of electronic and magnetic materials due to their high stability and easy handling. Therefore, the catenation of two and three biradical units by using nonconjugative 1,2-, 1,3-, and 1,4-dimethylene- and 1,3,5-trimethylenebenzene spacers was investigated (Scheme 4). The use of such spacers has allowed the observation of weak, through-space interactions between biradical units.[31–33]

While the isolation of bis(biradicaloids) derived from the reaction of the cyclic phosphallyl anion **2-II** with 1,3- and 1,4-bis(halomethyl)benzenes proceeded easily in a one-step reaction, the formation of the 1,2-disubstituted derivatives was not so straightforward, probably due to steric congestion. For the formation of the bulkier *t*Bu-substituted derivative **2-25**, utilization of the chelating diamine tetramethylethylenediamine (TMEDA) to increase the nucleophilicity of the phosphallyl moiety, along with a slow addition of the 1,2-bis(bromomethyl)benzene, was essential to avoid the formation of the product of partial substitution, which does not react readily with a second equivalent of **2-II**. In contrast, the formation of the *s*Bu-substituted derivative **2-26** was achieved in a two-step reaction as shown in Scheme 4. The key role played by the *P*-substituents is reflected in the surprisingly different stability of these polyradicaloids. While the *t*Bu-substituted compounds are stable for months, the less sterically hindered *s*Bu analogs decompose within a few days when handled in air at room temperature.[31,33]

A close analysis of the ^{31}P NMR data of the bis(biradicaloids) **2-17**–**2-20**, **2-25**, and **2-26** suggests that the geometry around the phosphorus centers remains undistorted if compared to their corresponding monomeric counterparts **2-8** and **2-28**. On the other hand, the analogous signals for the tris(biradicaloid) species **2-23** and **2-24** are considerably influenced ($\Delta\delta^{31}P(1) = 5.4$ ppm, $\Delta\delta^{31}P(2) = -1.3$ ppm (**2-23**); $\Delta\delta^{31}P(1) = 9.5$ ppm, $\Delta\delta^{31}P(2) = -3.6$ ppm (**2-24**)), suggesting that, due to steric factors, the phosphorus centers might exhibit slightly less pyramidalized geometries. This effect is also reflected by the observed $^{2}J_{PP}$ coupling constants as well as in the absorption maxima in the UV/Vis spectra. For the latter, a slight bathochromic shift was observed owing to the presence of two or three biradicaloid units in the molecule (Table 2). When the effect of the less bulky *s*Bu substituent is analyzed, a more pronounced pyramidalization of the phosphorus centers can be proposed: the ^{31}P NMR resonances are found at lower frequencies as compared to those observed for the corresponding *t*Bu derivatives. Furthermore, the larger $^{2}J_{PP}$ constants suggest a stronger interaction between phosphorus atoms within the *s*Bu-substituted biradicaloid units (Table 2).

Cyclovoltammetric analyses of the redox properties of these species showed stepwise electron releases, consistent with the number of biradical units present in the molecule. The first oxidation potentials ($E^{0}_{1/2}(1)$, Table 3) for all catenated structures nicely correspond to the value determined for the related monomer, indicating a quite small alteration of the HOMO energy levels upon catenation. The smaller electron-donating properties of the *s*Bu group cause these derivatives to possess anodically shifted oxidation potentials as compared to those observed for the *t*Bu analogs. Although the effects are very small, conceivably enhanced nonconjugative interactions between biradical units are reflected by the larger separation between the first and second redox potentials of the

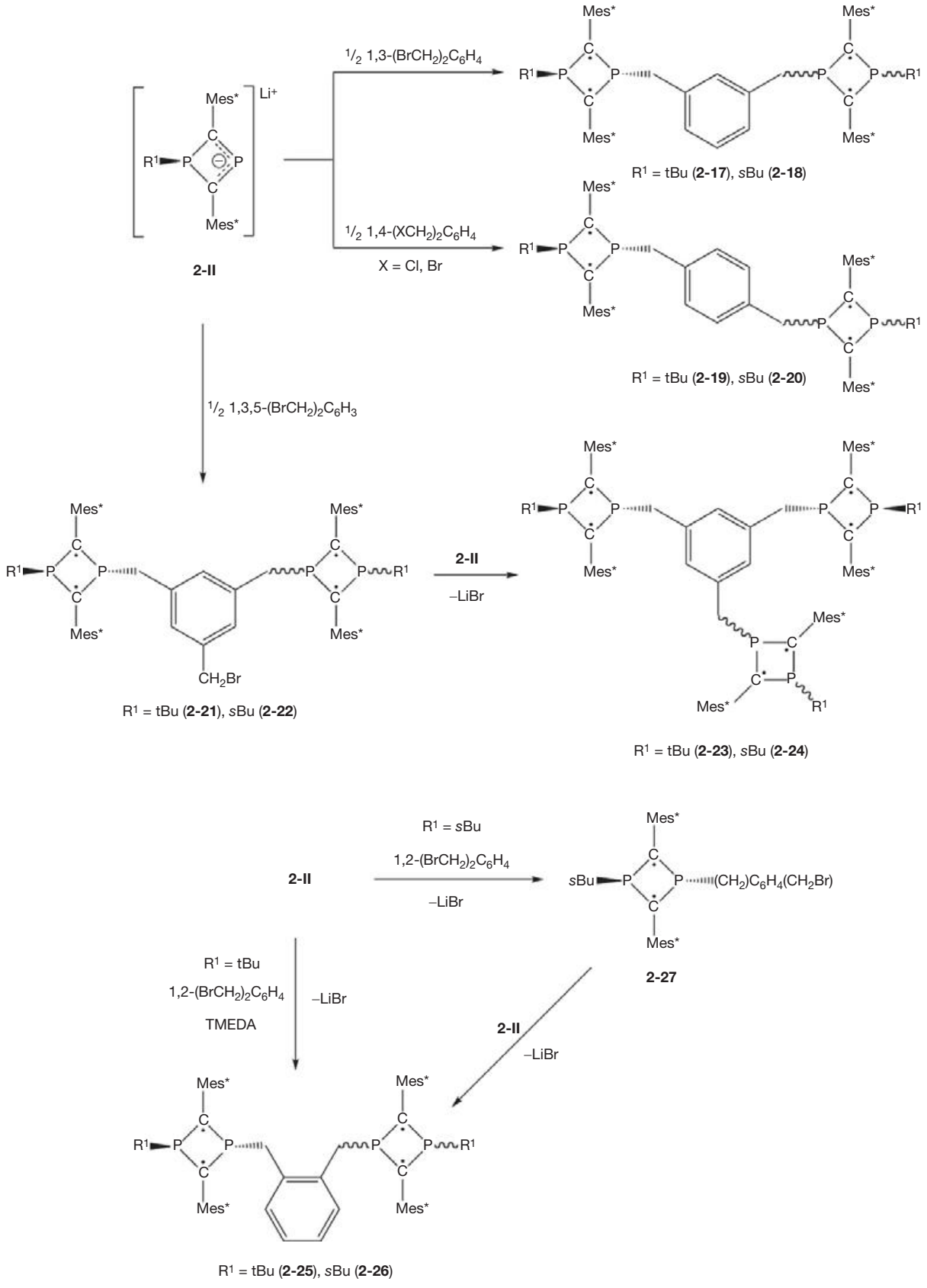

Scheme 4 Catenation of 1,3-diphosphacyclobutane-2,4-diyls; Mes* = 2,4,6-*t*Bu$_3$C$_6$H$_2$.

Table 2 Spectroscopic data for monomeric **2-8** and **2-28**, and oligo(biradicaloids) **2-17**–**2-20**, **2-23**–**2-26**

Substitution	*tBu*				*sBu*			
	$\delta^{31}P$ *(ppm)*		$^2J_{PP}$ *(Hz)*	λ_{max} *(nm)*	$\delta^{31}P$ *(ppm)*		$^2J_{PP}$ *(Hz)*	λ_{max} *(nm)*
Mono	58.1	0.6	334.8	610	26.6	1.5	379.1	606
1,2-	54.9	−0.8	337.8	614	27.2	0.3	374.4	–
1,3-	57.7	1.0	335.2	616	27.7	1.3	377.9	610
1,4-	–	–	–	–	25.8	2.1	380.2	608
1,3,5-	63.5	−0.7	327.2	626	36.1	−2.1	365.6	620

Table 3 (Quasi)-reversible redox potentials $E^0_{1/2}$ for oligo(biradicals) versus Fc/Fc^+

Substitution	*tBu*			*sBu*		
	$E^0_{1/2}(1)$	$E^0_{1/2}(2)$	$E^0_{1/2}(3)$	$E^0_{1/2}(1)$	$E^0_{1/2}(2)$	$E^0_{1/2}(3)$
Mono	+0.38			+0.44		
1,2-	+0.35	+0.50		–	–	
1,3-	+0.35	+0.48		+0.45	+0.53	
1,4-	–	–	–	+0.47	+0.56	
1,3,5-	+0.31	+0.45	+0.52	+0.43	+0.59	–

*t*Bu-substituted bis-(biradical) **2-17** ($\Delta E^0_{1/2}(1,2) = 0.13$ V, cf. 0.08 V for **2-18**). Since this separation remains unaffected by the type of the benzyl spacer, it was suggested that no significant difference in the magnitude of intramolecular interaction is caused by π-conjugation. On the other hand, when the third oxidation potential $E^0_{1/2}(3)$ of **2-23** is considered, a reduced interaction is observed, as suggested by the smaller difference with the corresponding second oxidation potential ($\Delta E^0_{1/2}(2,3) = 0.07$ V).

So far, it has only been possible to determine the solid-state structure of **2-17** (Figure 1).[32] Despite the low quality of the crystal structure data, it was shown that each P_2C_2 unit within the molecule retains the structural features of the known monomeric derivatives. Quite surprisingly, the heterocycles are orientated in a *syn*-type conformation in the solid state, regardless of the steric congestion. In order to shed some more light on the structural features of these bridged species, quantum chemical calculations (B3LYP/6-31G(d)) were performed on the model compounds **2-IVa** (R = R^1 = Me) and **2-IVb** (R = Mes*, R^1 = *t*Bu; Table 4). These calculations revealed that the *anti*-conformation is only slightly more stable than the *syn*-form for all bis(biradicals) (Table 4). Moreover, the energetic difference between *syn*- and *anti*-conformations is related to both the type of benzyl-spacer and the steric bulk of the substituents. While the *syn*/*anti*-difference decreases with increasing separation between P_2C_2 units, it increases with higher steric bulk of the substituents. It has been proposed that through-space interactions between the heterocycles in **2-17** or crystal packing forces might be responsible for overcoming the very small energy barrier. For the tris(biradicals), alternate and cone-type structures were considered for the model compounds **2-Va** (Me) and **2-Vb** (R = Mes*; Table 4). As expected, the calculations revealed in both cases the alternate structure to be more stable.[33]

1.15.2.2 Reactivity of 1,3-Diphosphacyclobutane-2,4-Diyls

Since the pioneering work of Niecke concerning 1,3-diphosphacyclobutane-2,4-diyls, and thanks to the extraordinary stability and simple accessibility of some derivatives, the reactivity of these compounds has been extensively explored. The 'simplest' reaction these species may undergo is the bond formation between the two radical sites to furnish bicyclo[1.1.0]butane derivatives, in which it was found that the substituents on both the carbon and phosphorus atoms play a decisive role.

The Cl substituents in **2-1** can be exchanged to $SiMe_3$ and H to give **2-29** (red compound), featuring both trigonal planar C environments and a planar P_2C_2 ring structure.[34] Although **2-29** is thermally very stable (up to 150 °C), it undergoes an almost quantitative ring-closing reaction to **2-29a** under photolytic conditions (Scheme 5). The X-ray crystal structure analysis of the yellow single crystals of **2-29a** unambiguously confirmed the formation of a bicyclic, butterfly-like 2,4-diphosphabicyclo[1.1.0]butane. The photolytically allowed ring-closing reaction can be easily rationalized by recalling the symmetry of the frontier orbitals depicted in Scheme 3.

In contrast, the use of sterically more demanding substituents on both carbon atoms (R = R′ = $SiMe_3$ (**2-30**), Scheme 5) suppresses the formation of the butterfly structure (**2-30a**), since the ring closure would result in (large) steric interactions of the two substituent groups in close spatial contact. This behavior was first observed for the Niecke-type biradical **2-30**, but can also explain why the Yoshifuji-type derivatives **2-III** do not undergo a photochemical isomerization (Mes* on C). However, the bis(trimethylsilyl)-substituted compound **2-30** undergoes a fragmentation reaction under photochemical conditions: one P–Mes* bond is cleaved under formation of supermesityl (Mes*•) and phosphaallyl (**2-31**) radicals.[35]

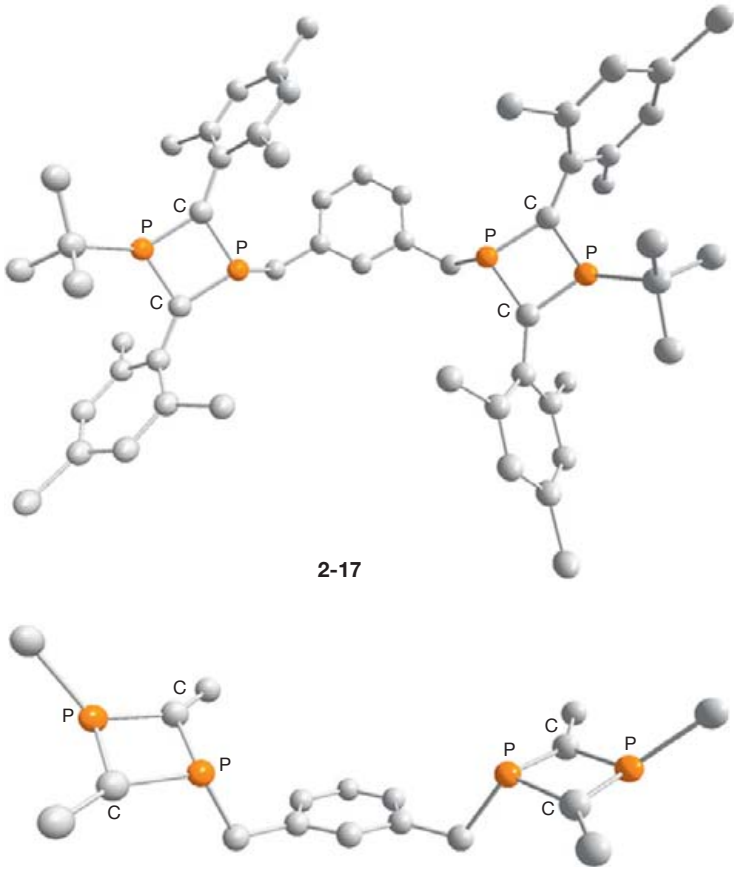

Figure 1 Molecular structure of bis(biradical) **2-17** (top). Mes* and *i*Pr groups are omitted to show the *syn*-conformation of the biradical units (bottom).

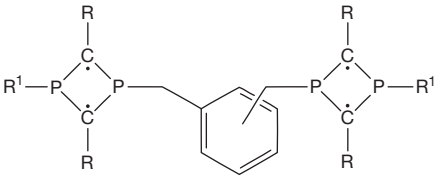

$R = R^1 = Me$ **(2-IVa)**
$R = 2,6\text{-}t\text{Bu}_2C_6H_3$, $R^1 = t\text{Bu}$ **(2-IVb)**

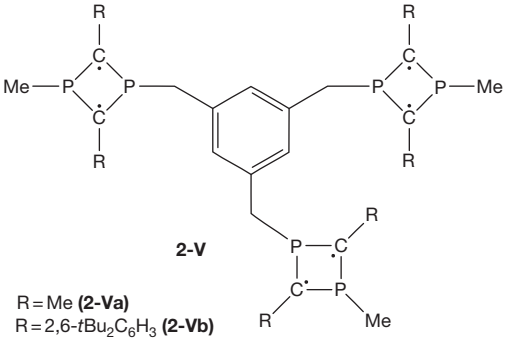

R = Me **(2-Va)**
$R = 2,6\text{-}t\text{Bu}_2C_6H_3$ **(2-Vb)**

Table 4 Calculated energy difference (kcal mol^{-1}) between *anti*- and *syn*-conformations of the biradical units for **2-IV** and alternate and cone-type configurations for **2-V** (B3LYP/6-31G(d))

Substitution	***2-IVa*** *(kcal mol^{-1})*	***2-IVb*** *(kcal mol^{-1})*
1,2-	1.88	5.98
1,3-	0.13	3.93
1,4-	0.03	–
1,3,5-	0.38 (**2-Va**)	2.05 (**2-Vb**)

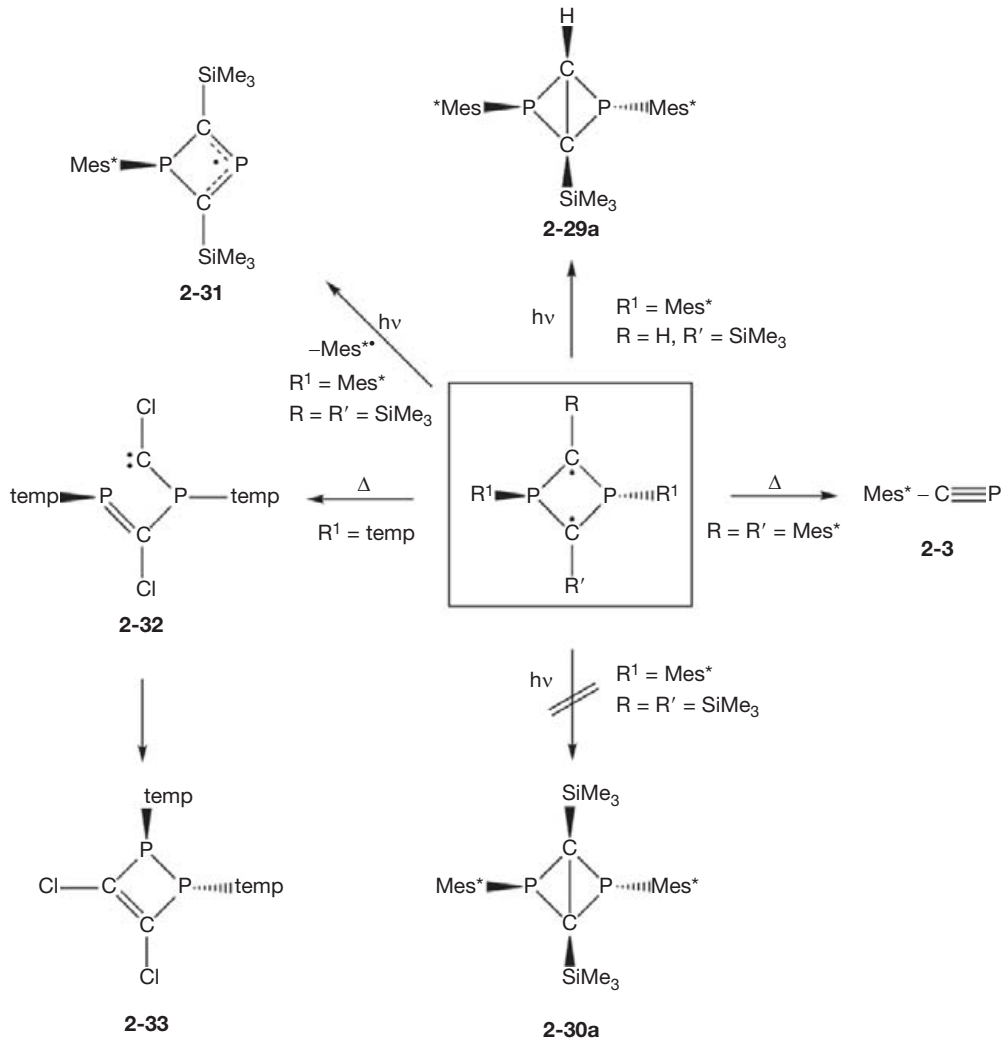

Scheme 5 Photochemically and thermally induced transformations of 1,3-diphosphacyclo-butane-2,4-diyls.

This contrasts with the observations that derivatives **2-III** do not react under the same conditions, but decompose to the starting material **2-3** and unidentified byproducts upon thermolysis. The *P*-amino derivative **2-2** (R^1 = temp, Scheme 5) is unstable at room temperature and isomerizes rapidly and quantitatively in solution, and slowly in the solid state, to 1,2-dihydrodiphosphete **2-33**. Quantum chemical calculations at the multiconfigurational self-consistent field (MCSCF) (10,10)/6-31G(d) level revealed that the isomerization is a two-step process (**2-2** → **2-32** → **2-33**) involving a singlet phosphanylcarbene (**2-32**) as intermediate.[22]

In addition to photochemically and thermally induced transformations, the general reactivity of 1,3-diphosphacyclo-butane-2,4-diyls has also been investigated. Scheme 6 summarizes and compares the most important findings.

The cleavage of the P–C_{aryl} bond in **2-30** under photochemical conditions suggested that an aniomesolytic fragmentation under reducing conditions would be possible. As expected, the reaction of **2-30** with two equivalents of Li or K afforded the dianions **2-34** (M = Li) and **2-35** (M = K) in high yield.[36] The X-ray crystal structure analysis of **2-35** revealed a monomeric ion pair featuring a D_{2h}-symmetric P_2C_2 heterocycle with both lithium cations located above and below, each solvated by additional dimethoxy ethane (dme) molecules. The exocyclic Si–C bond lengths of 181.9 pm are somewhat shorter than observed in silyl-substituted cyclobutadiene dianions,[38] which can be attributed to p(C) → σ*(Si–C) back donation of electron density (negative hyperconjugation). Based on a nucleus-independent chemical shift (NICS)(0) value[37] of −7.0 ppm (B3LYP/6-311+G**//B3LYP/6-31+G*), the aromaticity of the 1,3-diphosphacyclobutadien-diides $[P_2(CSiMe_3)_2]^{2-}$ (**2-34**, **2-35**) was found to be comparable to the analogous carbon systems, $[(CSiMe_3)_4]^{2-}$ (−9.2 ppm; up to −23.7 ppm for the dilithiated species $Li_2C_4R_4$ (R = H, Me, *t*Bu)).[38,39] Further calculations revealed that upon reduction of $(ArP)_2(CSiMe_3)_2$ (Ar = 2,6-$tBu_2C_6H_3$) (**2-36**), the radical anion **[2-37]**$^{\bullet-}$ is generated, which is 29 kcal mol^{-1} more stable. The latter shows a particularly elongated, and thus weakened, P–Ar bond of 194 pm. The anticipated aniomesolytic fragmentation, that is, the process **[2-37]**$^{\bullet-}$ → **2-38** + Ar$^{\bullet}$, occurs in a second step furnishing the cyclic anion **2-38** (Scheme 6), which is 21.1 kcal mol^{-1} more stable than the intermediate **[2-37]**$^{\bullet-}$.

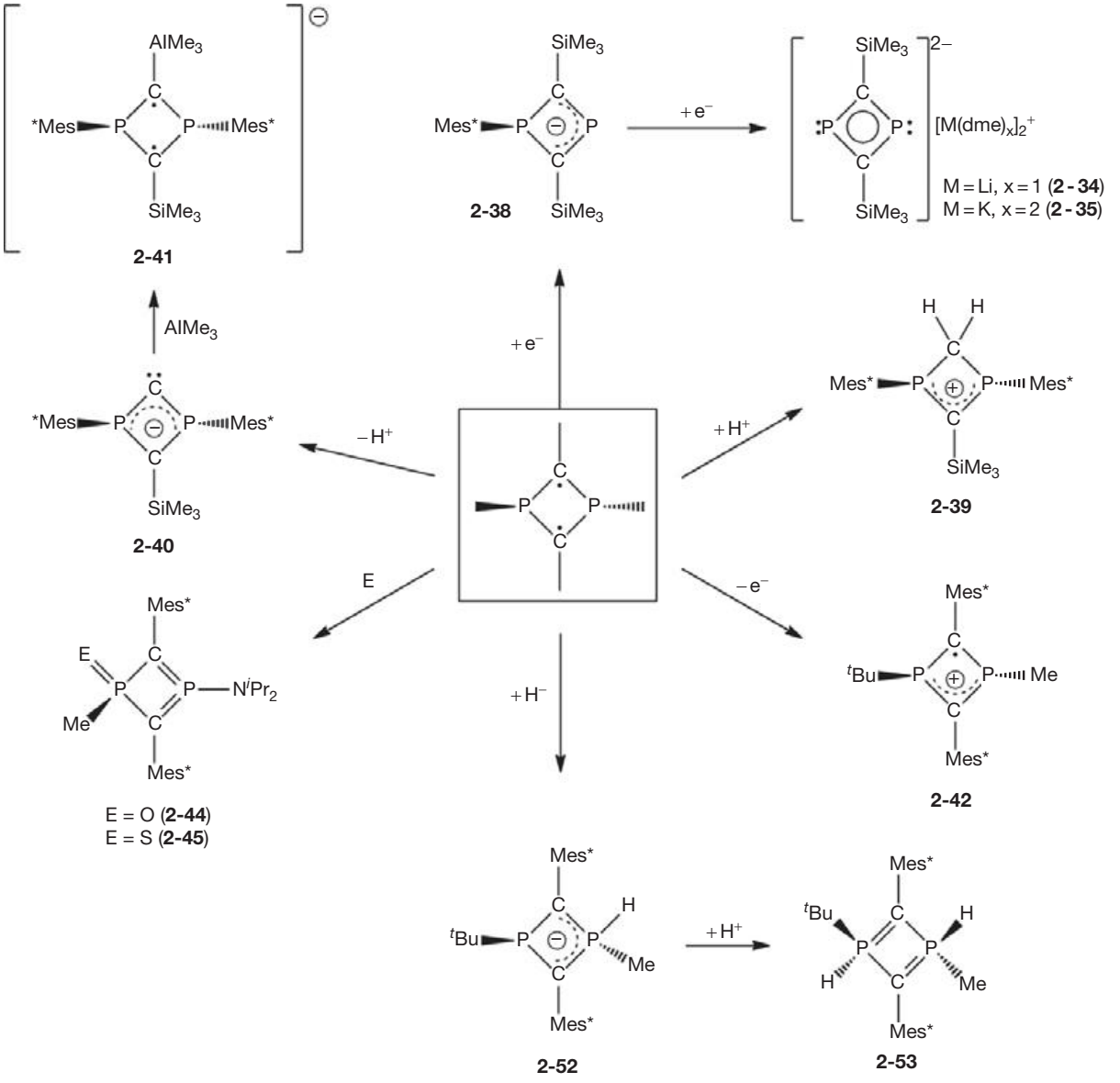

Scheme 6 Reactivity of 1,3-diphosphacyclobutane-2,4-diyls.

The 1,3-diphosphacyclobutane-2,4-diyls **2-I** also turned out to be valuable precursor compounds for the synthesis of new and otherwise unknown molecules. The unusual[40] bis(phosphanyl)carbocation **2-39** (Scheme 6) is straightforwardly accessible by protonation of **2-29** with one equivalent of triflic acid (HOTf).[41] The X-ray structure analysis as well as NMR spectroscopic investigations revealed only a slight alteration of the central P_2C_2 ring geometry suggesting a delocalization of the positive charge in an allyl-type system. The LUMO is located at the $SiMe_3$-substituted C atom and features a considerable contribution of the lone pairs at the pyramidal P atoms. Quantum chemical calculations (B3LYP/6-31+G*) predicted an overall stabilization of ~132 kcal mol^{-1} with respect to the nondelocalized carbocation.

In addition to protolysis, the 1,3-diphosphacyclobutane-2,4-diyls are readily deprotonated by LDA. The unprecedented, anionic carbene **2-40** can be reacted with the Lewis acid $AlMe_3$ to give the adduct **2-41** (Scheme 6).[42] The X-ray crystal structure analysis of **2-41** showed that the central P_2C_2 ring is planar and the noncarbene C-atom slightly pyramidalized. *Ab initio* calculations predicted both carbon atoms to be negatively charged. The 1,3-diphosphacyclobutane-2,4-diyl-2-ylidenide **2-40** can be described as a cyclic, anionic bis(phosphanyl) carbene,[43] which is stabilized by π-electron density of the carbanionic C-atom. The singlet–triplet energy gap of the carbene was calculated to amount to 7.4 kcal mol^{-1}.

Electrochemical investigations using cyclic voltammetry (CV) showed that the biradicaloids can be readily and reversibly oxidized, which suggests that stable radical cations might be formed upon chemical oxidation. By using $[N(4\text{-}BrC_6H_4)_3]^+[SbCl_6]^-$ ('magic blue') as a one-electron oxidizing agent, cationic **2-42** was formed (Scheme 6).[44] Oxidation of **2-43** by irradiation in the presence of (2,2,6,6-tetramethylpiperidin-1-yl)oxyl (TEMPO) led to the monoxide **2-44**, which was characterized

by ^{31}P NMR spectroscopy ($\delta = 121.8$, 25.4 ppm; $^{2}J_{PP} = 183.2$ Hz), while the reaction with elemental sulfur gave the corresponding sulfide **2-45** ($\delta = 101.7$, 45.7 ppm; $^{2}J_{PP} = 194.2$ Hz).[24,26]

Incorporation of functional groups in the four-membered ring of Yoshifuji's 1,3-diphosphacyclobutane-2,4-diyls proved to be simple, thanks to the versatility of their synthetic preparation. Therefore, the properties of the P_2C_2 ring can be easily tuned, enabling the investigation of a variety of reactions, including oxidation, reduction, protonation, ring-opening, and ring-expansion reactions, which are advantageous for the formation of novel heterocyclic structures. For instance, the presence of carbonyl or amino groups as substituents on the P_2C_2 ring activates them to undergo ring-opening, valence isomerization, and ring-expansion reactions to afford novel organophosphorus compounds. A selection is presented in Scheme 7.

The unstable derivative **2-43** ($R^1 = N{i}Pr_2$, $R^2 = Me$, Scheme 7) undergoes decomposition even at low temperature, probably due to the instability of the P–N bond. Its hydrolysis affords a mixture of products from which **2-46** and **2-47** could be identified. It is likely that compounds **2-46** and **2-47** correspond to the product of a ring-opening reaction of a 1-hydroxy-1λ^5,3λ^3-diphosphacyclobutene intermediate, followed by rearrangement and de-aromatization of the Mes* substituent. Derivative **2-48** ($R^1 = N{i}Pr_2$, $R^2 = PhC(O)$, Scheme 7), although not isolated, has been shown to undergo isomerization to the six-membered ring 2*H*-[1,2,4]oxadiphosphinine **2-49**. Upon heating, **2-49** in turn undergoes an Arbuzov-type rearrangement to afford 1-oxo-1H-[1,3]diphosphole **2-51** (Scheme 7). The latter is analogous to **2-50**, which is formed upon heating derivative **2-9**.

The study of the reaction of a wide range of 1,3-diphosphacyclobutane-2,4-diyls **2-III** with hydride has shown a substituent dependence.[45] The reaction of alkyl-substituted derivatives leads to the corresponding cyclic anions **2-VI** featuring a P–H bond.[46] With resonance-stabilized substituents present, an elimination reaction takes place, affording the corresponding cyclic phosphaallyl anions **2-II** (Scheme 8). For instance, treating **2-4** with $LiAlH_4$ affords the cyclic anion **2-52**, whose protonation subsequently leads to the corresponding di-λ^5-phosphacyclobutadiene **2-53** with a diylidic structure and two P–H entities. On the other hand, phosphaallyl anions **2-II** have been quenched with methyl iodide to form the corresponding derivative **2-III′**, where only the R^2 substituent has been exchanged for a Me group.

In the former case, for the formation of the cyclic anion **2-52**, the hydride selectively attacks the sterically less-hindered, Me-substituted phosphorus atom, which corresponds to addition to the LUMO of the singlet 1,3-diphosphacyclobutane-2,4-diyl **2-4**. The cyclic anion **2-52** was characterized by ^{31}P NMR spectroscopy, where the signal at $\delta = -37.1$ ppm exhibits a large $^{1}J_{PH}$ coupling constant of 322.1 Hz, confirming the presence of a P–H moiety. The signal assigned to the second phosphorus is found at 143.8 ppm and exhibits a $^{2}J_{PP}$ constant of 49.3 Hz, which is considerably smaller than that observed for **2-4**. Protonation of **2-52** with methanol proceeded regioselectively on the remaining trivalent phosphorus atom (Scheme 8). The diylidic character of **2-53** is reflected in its ^{13}C NMR spectra: the sp^2 carbon atoms within the four-membered ring exhibit a considerably different chemical shift ($\delta = 12.6$ ppm) as compared to those observed for **2-4** ($\delta = 111.3$ ppm). The regioselectivity of this transformation has been attributed solely to steric encumbrance.

Following a different reaction path, phosphaallyl anions **2-II** are formed from **2-III** when a hydride attacks the primary carbon

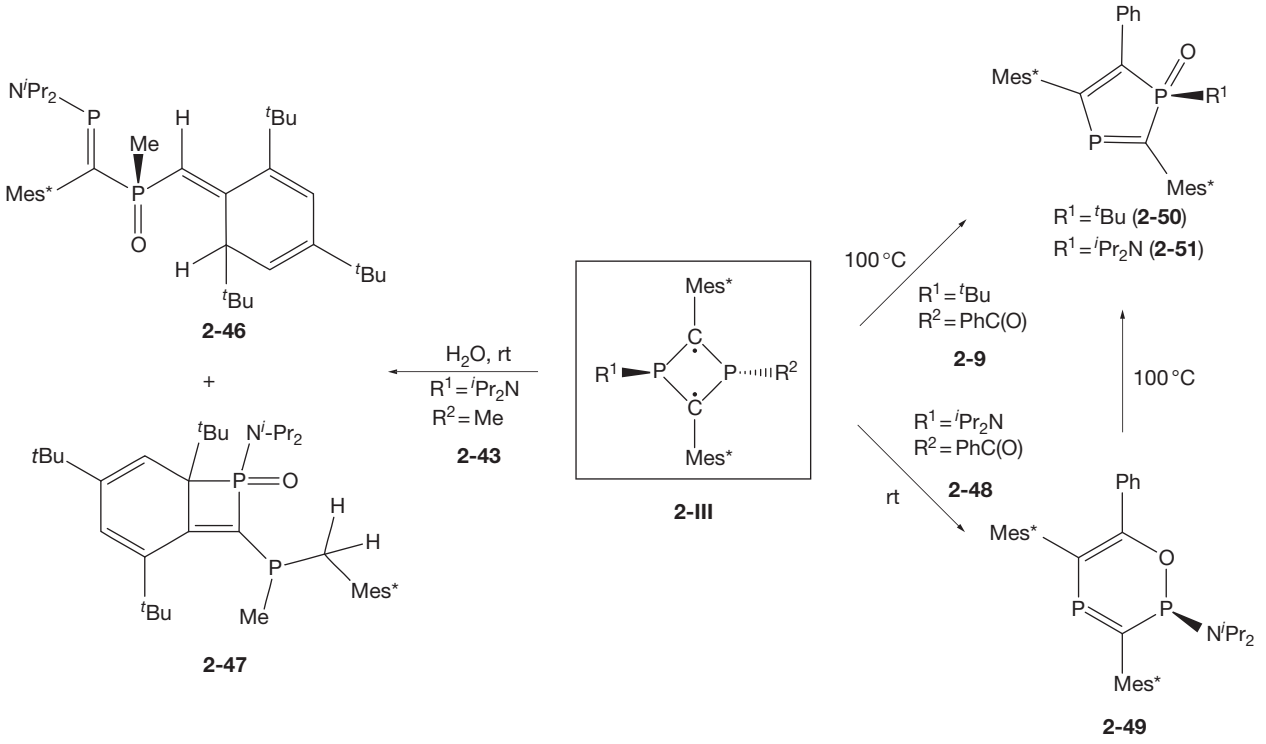

Scheme 7 Ring-expansion reactions of 1,3-diphosphacyclobutane-2,4-diyls.

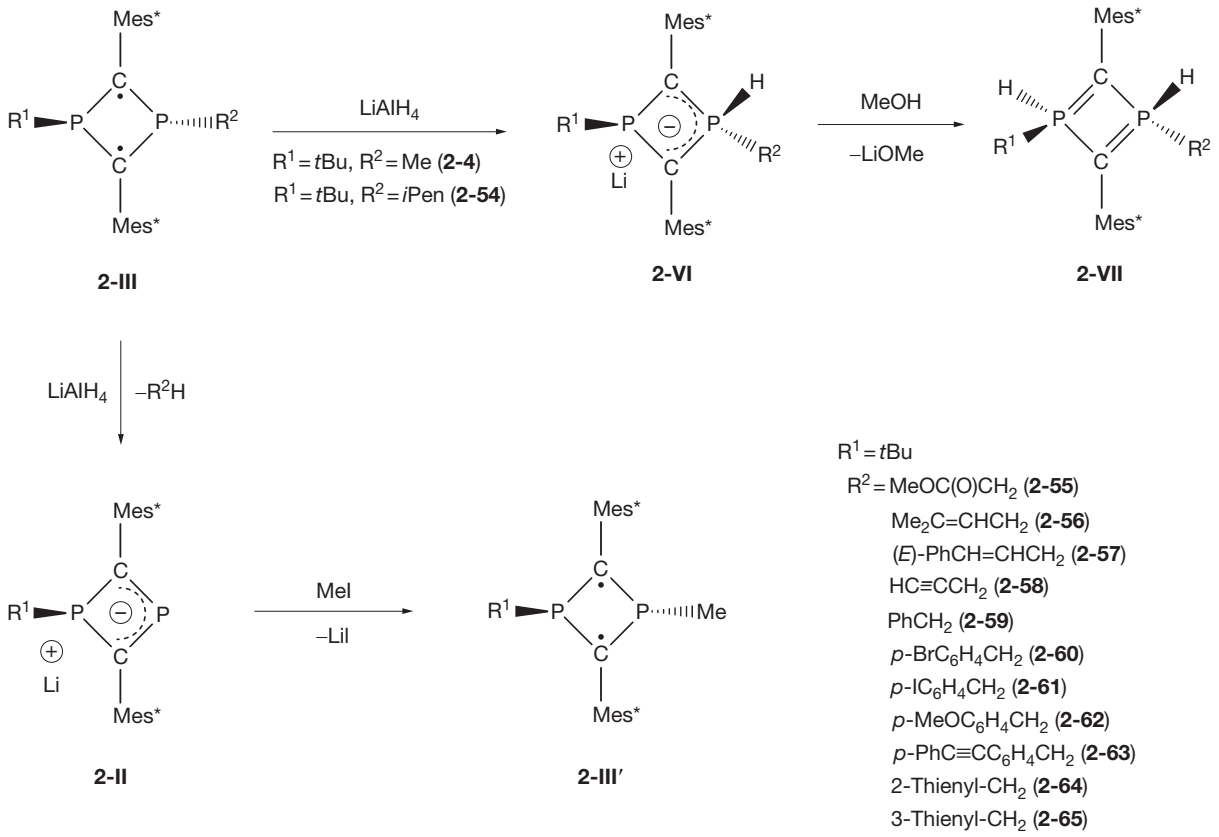

Scheme 8 Substituent-dependent reactions of **2-III** with hydrides.

atom of a resonance-stabilized substituent R^2 in an S_N2 fashion, leading to elimination of R^2H. ^{31}P NMR spectroscopy has been useful to easily identify the anions **2-II** ($\delta = 269.0$, 87.6 ppm, $^2J_{PP} = 86.8$ Hz), since they are intermediates in the synthesis of **2-III**. Although further studies are necessary to fully understand the mechanism of these reactions, it is worth noting that apparently a combination of hydride anion and an alkali metal is essential for the formation of the cyclic anions involved in both reaction paths.

1.15.3 Biradicaloids of Four-Membered B_2P_2 Heterocycles

1.15.3.1 Syntheses of B_2P_2 Biradicals

Boron-centered singlet biradicaloids have become a new class of compounds of high interest since the breakthrough discovery of Bertrand et al. in 2002.[47] They succeeded in synthesizing and characterizing the 1,3-dibora-2,4-diphosphoniocyclobutane-1,3-diyl (**3-1**). The $(RP)_2(CR)_2$ motif of the 1,3-diphosphacyclobutane-2,4-diyls (cf. section 1.15.2) was replaced by the isoelectronic $(R^2P)_2(BR)_2$ unit, both containing 22 valence electrons for R = H. This had two important consequences for the stability and favorability of the open, biradical(oid) form: (1) the contribution of the resonance structure **3-B** (Scheme 3) to the electronic ground state is largely diminished because the P lone pair of 1,3-diphosphacyclobutane-2,4-diyls has been transformed into a P–C σ-bond in the P_2B_2 biradicaloids and (2) the heterocycle in **3-1** is expanded because of the intrinsically longer P–B bonds (~190 pm vs. ~175 pm for P–C in **2-III**). Note that contrary to **2-III** the symmetry of the HOMO of **3-1** (cf. Scheme 11) allows for a transannular B···B π-interaction.

The B_2P_2 heterocycle **3-1** was synthesized in 68% yield from 1,2-di-*t*Bu-1,2-dichlorodiborane and two equivalents of lithium diisopropylphosphide (Scheme 9). Other derivatives, which are discussed in detail below, have been synthesized by using the reductive coupling approach. Compound **3-1** was found to be extremely air-sensitive, but thermally very stable. The X-ray crystal structure analysis of **3-1** revealed a planar B_2P_2 ring consisting of a transannular B···B distance of 257 pm (Scheme 9). The sterically demanding *i*Pr substituents attached to the P atoms can be comfortably accommodated in the planar form. As expected, **3-1** is EPR silent in solution and the solid state (singlet ground state). Quantum chemical calculations predicted the singlet state of **3-1** to be 17.2 kcal mol^{-1} lower in energy than the corresponding triplet state, demonstrating a coupling between the two radical sites by through-bond and through-space B–B interactions.

The involvement of transient 2,3-diborata-1,4-diphosphoniabuta-1,3-dienes in the mechanism of formation of 1,3-diborata-2,4-diphosphoniabicyclo[1.1.0]butanes and 1,3-diborata-2,4-diphosphoniacyclobutane-1,3-diyls has been proposed since the first reports on B_2P_2 systems (Scheme 10).[17] However, it was only recently that a careful tuning of the steric bulk of the substituents on the P and B atoms led to a deeper

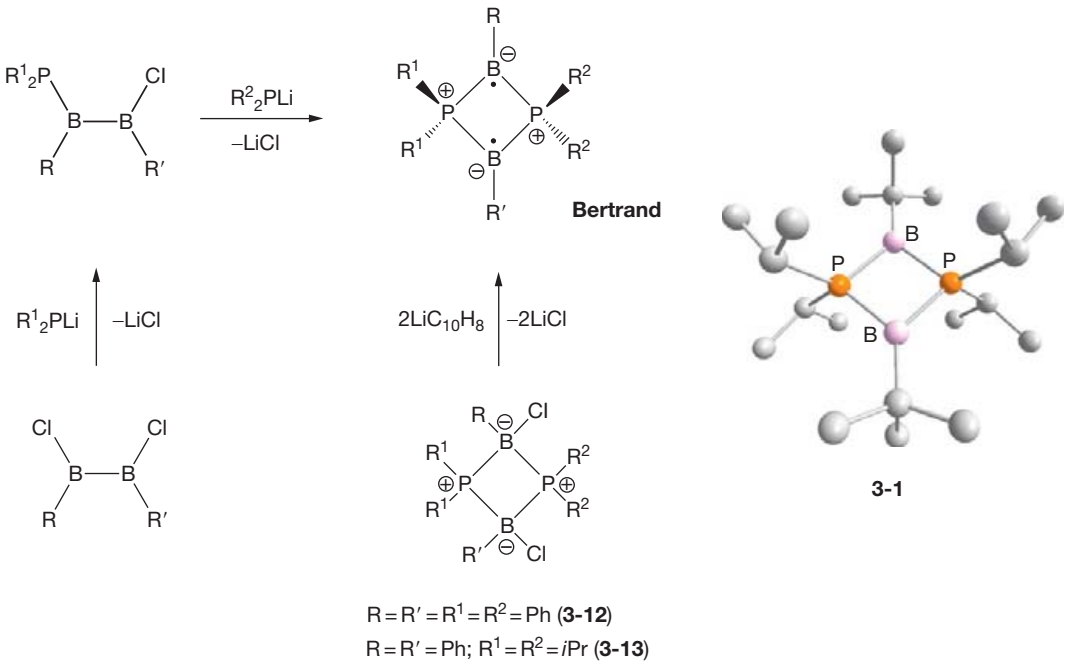

Scheme 9 Synthesis of B_2P_2 biradicals (left); molecular structure of **3-1** (right).

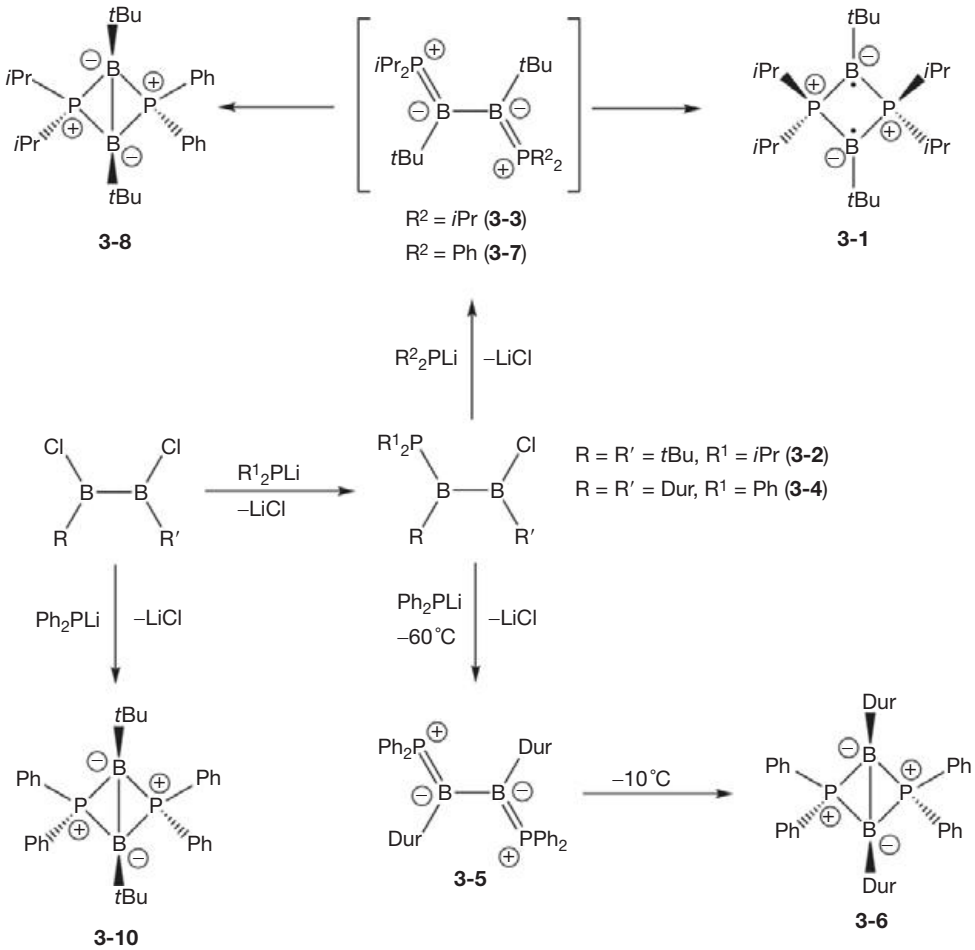

Scheme 10 Effects of the substituents on B and P atoms: the involvement of 2,3-diborata-1,4-diphosphoniabuta-1,3-dienes in the mechanism of formation of 1,3-diborata-2,4-diphosphoniabicyclo[1.1.0]butanes and 1,3-diborata-2,4-diphosphonia-cyclobutane-1,3-diyls; Dur = 2,3,5,6-tetramethylphenyl.

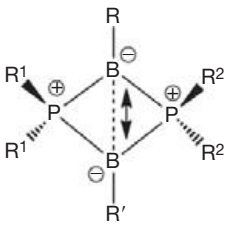

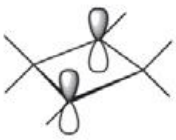

	R	R′	Yield	B–B (pm)	τ (°)
3-1	*i*Pr	*t*Bu	68%	257	180
3-9	*i*Pr	Dur	72%	224	130
3-10	Ph	*t*Bu	71%	199	118
3-11	Et	Dur	58%	189	115
3-12	Ph	Ph	47%	183	114

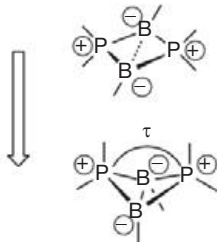

Scheme 11 Derivatives **3-1** and **3-9**–**3-12** featuring variable B–B separations (pm) (double-sided arrow) and interflap angles τ(°); schematic representation of the HOMO of **3-1**.

understanding of the reaction mechanism for the formation of these species. The principles are outlined in Scheme 10.[48] The isolation of the putative intermediate was not possible when 1,2-di-*t*Bu-1,2-dichlorodiborane was employed in the reaction with $LiPPh_2$. However, when the duryl-substituted derivative was used (Dur = 2,3,5,6-tetramethylphenyl), it was possible to isolate the corresponding 2,3-diborata-1,4-diphosphoniabuta-1,3-diene **3-5** (Scheme 10). Furthermore, its thermal isomerization into the corresponding bicyclic derivative **3-6** was observed. ^{11}B and ^{31}P NMR spectra at −60 °C gave strong evidence of the formation of **3-5**, since only one signal was observed for both nuclei ($\delta(^{11}B) =$ 76 ppm; $\delta(^{31}P) = 12$ ppm), suggesting a symmetrical structure of the low-temperature product. When the temperature was raised to −10 °C, these signals were replaced by the resonances belonging to the bicyclic derivative **3-6** ($\delta(^{11}B) = -13$ ppm; $\delta(^{31}P) = -51$ ppm). Interestingly, this thermal rearrangement is opposite to that observed for the parent hydrocarbon, where the butadiene derivative is the most favored isomer. Upon irradiation, **3-6** shows interesting rearrangement processes, which are discussed in more detail in the section below.

In order to shed some light on the theoretically predicted biradicaloid character (see below) and the general reactivity of B_2P_2 heterocycles of this type, Bertrand and coworkers performed several investigations. As shown in Scheme 11, the symmetry of the HOMO allows a thermal disrotatorial ring closure (in contrast to the P_2C_2 biradicaloids discussed in section 1.15.2). Therefore, the variation of the P and B substituents was expected to strongly influence the ground-state structure, for example, the open biradicaloid form versus the bicyclic structure of the B_2P_2 heterocycle. Indeed, Bertrand and coworkers were able to adjust the B···B distance in a way that any conformation on the internal reaction profile for the bicyclo[1.1.0]butane inversion could be isolated (Scheme 11).[49]

Compounds **3-9**–**3-11** were prepared as described for **3-1**. Derivative **3-12** was synthesized by treating the 1,3-dichloro-1,3-diborata-2,4-diphosphoniocyclobutane precursor with two equivalents of lithium naphthalenide ($Li^+C_{10}H_8^{\bullet -}$, Scheme 9). All compounds are accessible in moderate to good yield as very air-sensitive, but thermally stable solids (melting points ∼200 ± 20 °C). The crystal structures for all derivatives nicely showed that the central B_2P_2 entities adopt very different structures depending on the substituents attached to P or B. The most folded structure (interflap angle $\tau = 114°$), featuring the shortest B–B distance of 183 pm, was obtained for hexaphenyl derivative **3-12**. T-dependent NMR spectroscopic studies revealed that compounds **3-9**–**3-12** invert rapidly at room temperature (butterfly movement). For **3-11**, the inversion barrier was estimated to amount to ca. 8.5 kcal mol^{-1}.

Besides this 'static approach' that makes use of different substituents in order to favor either the planar or the bicyclic structure, it was also reported that both isomers can co-exist in solution.[50] The solid-state structure of the *B*-phenyl-substituted derivative $(BPh)_2(iPr_2P)_2$ (**3-13**, Scheme 12) is similar to **3-1**, featuring a square-planar P_2B_2 heterocycle with the phenyl rings almost co-planar to the central B_2P_2 moiety. T-dependent ^{31}P NMR and UV/Vis investigations clearly showed an interconversion ($\Delta G^{\neq}_{143K} = 6.6 \pm 1.8$ kcal mol^{-1}) between the open form **3-13** and the corresponding bicyclic isomer **3-13a**, with the latter being favored at higher temperature. Both structures essentially co-exist in solution, as shown by ^{31}P NMR spectroscopy at −145 °C ($\delta = 4.0$ ppm (**3-13**) and $\delta = -32.2$, −41.8 ppm; two conformers of **3-13a** as supported by calculations). The order of stability of the bond-stretch isomers[70] **3-13** and **3-13a** appears to be strongly entropy driven. The isomer **3-13** with the co-planar phenyl groups has fewer degrees of freedom than the bicyclic form **3-13a**. The B–B σ-bond in **3-13a** is broken at lower temperature in opposition to the bond-formation process, which is entropically favored (Scheme 12).

Before entering a further discussion on the chemistry of these interesting species, it is instructive to concisely summarize some theoretical results. Shortly after Bertrand and

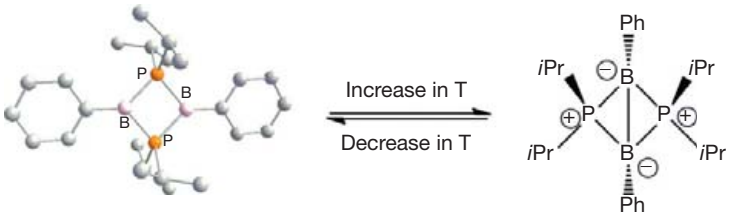

3-13 **3-13a**

Scheme 12 Temperature-dependent interconversion between a planar biradicaloid structure **3-13** (d_{exp}(B···B) = 257 pm) and the corresponding bicyclic isomer (**3-13a**, d_{calc}(B–B) = 186 pm); molecular structure of **3-13**.

Table 5 LUMO occupation numbers and ΔE_{S-T} values for some calculated model compounds of the general formula $(PR'_2)_2(BR)_2$. Details concerning the level of theory can be found in the literature citations

R	*R′*	*LUMO occ. no [e⁻]*	*−ΔE$_{S-T}$ (kcal mol^{-1})*	*Ref.*
H	H	0.221	27.3	52,53
		0.233	25.8	56
		n.a.	15.8[a]	51
		0.21	18.7	55
		n.a.	17.2	49
H	Me	0.21	20.1	55
H	*i*Pr	0.20	20.7	55
H	SiH_3	0.39	5.8	55
*t*Bu	H	n.a.[b]	30.4	56
*t*Bu	Me	n.a.[b]	29.4	56
*t*Bu	Et	n.a.[b]	27.9	56
*t*Bu	$SiMe_3$	0.30	8.7	55
SiH_3	H	n.a.[b]	18.4	56
*t*Bu	*i*Pr	0.169	33.7	52,53
		n.a.[b]	28.4	56
		0.19	23.4	55

[a]The authors supplied several values for various levels of theory. The MCSCF values with zero-point vibrational correction are given here. The reader is referred to the cited literature for detailed information.

[b]Although no LUMO occupation numbers were given, the authors supplied the number of effectively unpaired electrons from CAS(2,2)/6-31G* computations. For comparison, these values are not given. The reader is referred to the cited literature for detailed information.

Table 6 LUMO occupation numbers and ΔE_{S-T} values for some calculated heteroatom-substituted model compounds of the general formula $(X)_2(BR)_2$. Details concerning the level of theory can be found in the literature citations

R	*X*	*LUMO occ. no [e⁻]*	*−ΔE$_{S-T}$ (kcal mol^{-1})*	*Ref.*
H	NH_2	0.437	13.1	52,53
H	NH_2	n.a.	7.6[a]	51
H	AsH_2	n.a.	17.0[a]	51
H	SH	0.316	n.a.	52,53
H	OH	0.533	n.a.	52,53

[a]The authors supplied values for various levels of theory. The MCSCF values with ZPE correction are given here. The reader is referred to the cited literature for detailed information.

coworkers published their milestone paper on **3-1**, the groups of Schoeller,[51] Head-Gordon,[52–54] Cramer,[55] and Hu[56] independently reported numerous quantum chemical calculations, whose specific details fall by far out of the scope of this chapter. Selected results such as calculated geometries, singlet–triplet splittings (ΔE_{S-T}), and LUMO occupation numbers (if available) are compiled in the Tables 5 and 6. It is worth noting that Cramer et al. suggested an alternative bonding picture for B_2P_2 heterocycles such as **3-1**. They described the orbital mixing as equivalent to an aromatic π-system. Also in this picture, the HOMO is dominated by a cross-ring B–B π-bonding interaction, while the LUMO is B–B π*-antibonding.

As can be seen from the LUMO occupation numbers and the ΔE_{S-T} values given in the Tables 5 and 6, the biradicaloid character of the 1,3-dibora-2,4-diphosphoniocyclobutane-1,3-diyls is not very large; certainly less than most other organic biradicals but more than normal closed-shell molecules. The origin of the comparably low biradicaloid character was attributed to transannular through-space interactions between the two boron atoms as well as through-bond neighboring group interactions. Upon modifying the ring constituents, the originally small gap between HOMO and LUMO for 'classical' organic singlet biradicals such as cyclobutanediyls is increased by stabilizing the HOMO. The basic principles have already been discussed in the Introduction. Nevertheless, due to the strong influence of neighboring groups (constituents or substituents) several derivatives were calculated, expecting substantial changes of the overall electronic structure in dependence of the ligands employed. Indeed, as briefly mentioned by Head-Gordon et al., substitution of isopropyl with the more electropositive $SiMe_3$ groups at phosphorus should increase the LUMO occupation number to 0.30 e^- (instead of 0.17 e^- for **3-1**). Cramer et al. calculated for this alkyl to silyl replacement a substantial decrease of the singlet–triplet gap ($(\Delta E_{S-T}$ $(t\text{BuB})_2[(Me_3Si)_2P]_2) = -8.7$ kcal mol^{-1}, cf. $(\Delta E_{S-T}$ $(t\text{BuB})_2(i\text{Pr}_2\text{P})_2) = -23.4$ kcal mol^{-1}). In addition, time-dependent density functional theory (TD-DFT) calculations at the B3LYP/6-311+G(d,p) level predicted a UV/Vis absorption of $\lambda = 704$ nm, that is at much longer wavelength than found for **3-1** ($\lambda_{max} = 446$ nm). Most revealingly, the ring geometry changes substantially upon silyl substitution. In particular, the transannular boron–boron distance was predicted to be considerably shorter. Hence, perhaps contrary to an initial guess, the biradicaloid character is 'increased' for the species with 'minimum' transannular B···B distance, that is, between the centers formally assigned as carrying the unpaired spins in the simple biradicaloid resonance picture. The same

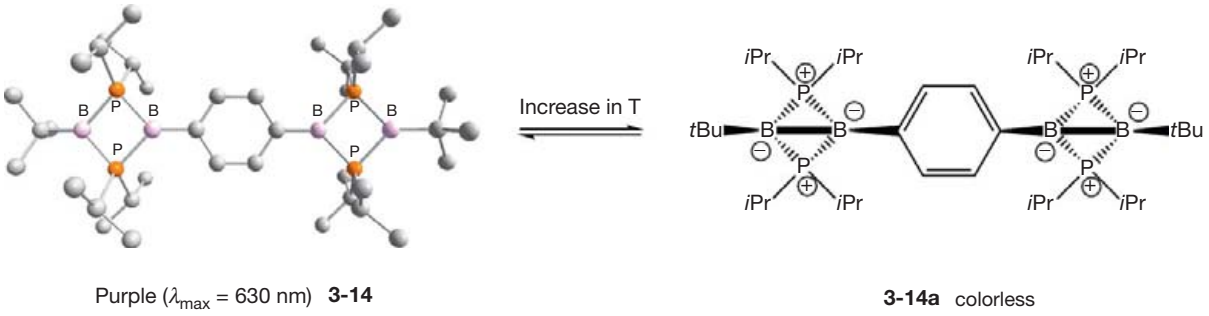

Purple (λ_{max} = 630 nm) **3-14** **3-14a** colorless

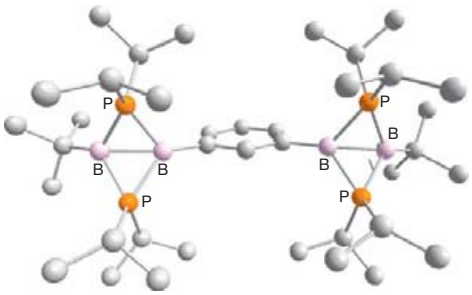

3-15

Scheme 13 Equilibrium between the *para*-phenylene-bridged, planar tetraradicaloid **3-14** and its bis(bicyclic) form **3-14a**; molecular structures of **3-14** and **3-15**.

conclusion was drawn by Head-Gordon and coworkers. They found the closely related nitrogen derivative $(HB)_2(H_2N)_2$ to have a larger biradicaloid character with a shorter B–B distance of 203.8 pm (cf. 260 pm for $(HB)_2(H_2P)_2$). In principle, this was confirmed by Schoeller et al. by performing a close analysis of the hetero-substituted $(HB)_2(H_2X)_2$ systems ($XH_2 = NH_2$, PH_2, and AsH_2). Their calculations predicted for the nitrogen derivative a much smaller singlet–triplet energy gap. Furthermore, electronegative substituents should increase ΔE_{S-T}, which is in line with the prediction that electropositive *P*-silyl substituents should increase the biradical character. In addition, Hu et al. found a singlet–triplet energy gap of $\Delta E_{S-T} = -18.4$ kcal mol^{-1} for *B*-silyl-substituted systems (CAS(2,2)/6-31G*). Overall, it seems clear that the electronic interactions with neighboring groups (or substituents) markedly control the extent of biradicaloid character.

The formation and properties of catenated singlet biradicals have been investigated, in particular in view of applications as antiferromagnetic low-spin polymers.[57] To this end, *para*-phenyl bridged tetraradicaloid **3-14** has been synthesized featuring a bis(planar) structure in the solid state (Scheme 13).[58]

NMR and UV/Vis investigations in solution revealed the deep purple, open structure **3-14** to predominate at low temperature, whereas at room temperature the bis(bicyclic) system **3-14a** is the major product. Interestingly, since the energy difference between the planar form and the bicyclic isomer of substituted B_2P_2 derivatives only amounts to a few kcal mol^{-1}, no dynamic behavior was observed for the *meta*-phenylene-bridged derivative (**3-15**). The latter shows the bis(bicyclic) structure in the solid state. This was confirmed by quantum chemical calculations, which predicted the *para*-tetraradicaloid **3-14** to be 2.2 kcal mol^{-1} more stable than the *meta*-tetraradicaloid **3-15**. The energy benefit for the ring closure of **3-14** (16.8 kcal mol^{-1}) is 2.1 kcal mol^{-1} smaller than for **3-15**.

To explain the differences between the *para*-phenylene and *meta*-phenylene-bridged tetraradicaloids, a weak 'communication' mechanism between both biradical sites was postulated, considering that the *para*-phenylene linker favors the biradicaloid form. To further explore this hypothesis, the bicyclo[1.1.0]butane **3-16** has been synthesized (Scheme 14).[59] Compound **3-16** is related to **3-14** and **3-15** by formally removing the second B_2P_2 ring. Since no suitable single crystals of **3-16** for X-ray analysis could be obtained, the naphtyl-substituted derivative **3-17** was isolated (Scheme 14). Its solid-state structure showed that the preferred conformation is the bicyclo[1.1.0]butane structure, which *a priori* supports the hypothesis that the presence of a second B_2P_2 moiety in the *para*-position of the phenylene linker is needed to favor the bis(biradicaloid) form. On the other hand, this effect may solely be due to the σ-donor properties of the second electron-rich B_2P_2 unit, and does not necessarily involve a communication between them. The essential point is that the phenylene linker must be coplanar to the boron–phosphorus heterocycles. To shed some more light on this hypothesis, a steric restriction was introduced by substituting the *ortho*-positions of the linker with one (**3-18**) or two (**3-19**) methyl groups (Scheme 14). When one methyl substituent is introduced to the linker, one of the B_2P_2 units in **3-18** can be coplanar with the phenylene linker, while the other cannot. Therefore, no communication of the biradical units can take place, but the σ-donor effect of the second B_2P_2 moiety can be tested. In this case, **3-18** also adopts a bicyclo[1.1.0]butane structure, which strongly suggests that

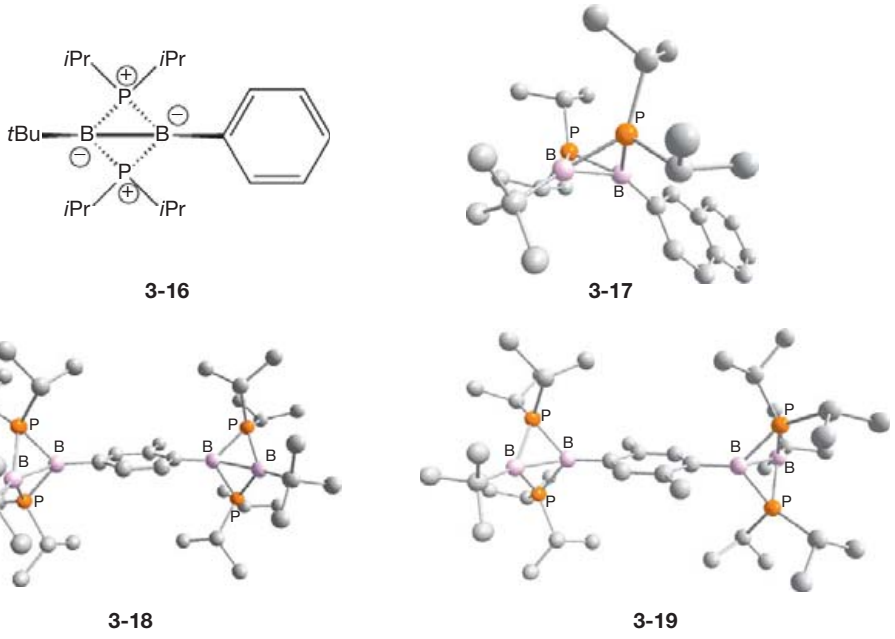

Scheme 14 Schematic drawing of **3-16** and molecular structures of compounds **3-17**–**3-19**.

communication between the two biradicaloid units through the coplanar *para*-phenylene ring is essential for the formation of the tetraradicaloid form. Furthermore, the 2,5-dimethyl-substituted derivative **3-19** adopts a bis(bicyclo[1.1.0]butane) structure, which shows that the σ-donor effect of the second heterocycle is not enough to favor the formation of the planar bis(biradical) form.

In order to shed some light on the most relevant aspects of the nature of these molecules, including geometries, energies, and the communication between biradicaloid substructures, a very recent theoretical study has approached these tetraradicaloid molecules from various electronic structure perspectives.[60] In general, this study supports the hypothesis that the communication between B_2P_2 units is favored for the *para* isomer,[58,59] although it is rather weak. A structural analysis of both planar and bicyclic conformations of compounds **3-1**, **3-14**, **3-15**, and **3-16** and their hydrogen-substituted analogs **3-1H**, **3-14H**, **3-15H**, and **3-16H**, was performed. Regarding the relative stability of the different isomers it was shown that for both the alkyl and H-substituted molecules the planar isomers are destabilized with respect to the corresponding bicyclic forms. However, the energy difference between both isomers is significantly smaller for the alkyl-substituted **3-14**, with a difference of only 0.1 kcal mol^{-1}, which is in very good agreement with the experimentally observed equilibrium in solution (Scheme 13). Thus, this result further supports the argument that substituents on the phosphorus and boron atoms are of critical importance on the relative stability of the planar versus bicyclic geometry, as previously discussed.[17] Furthermore, electronic structure calculations have confirmed the ground state to be a singlet ($S=0$).

Similar to the experimental approach of Bertrand and coworkers,[59] this theoretical study was also based on the assumption that coplanarity of the B_2P_2 units and the phenylene linker is required for the communication between the two biradical fragments. Calculations were performed in order to determine

Table 7 Computed effective unpaired electrons

	3-14H	*3-15H*	*3-14*	*3-15*
PP[a]	0.77	0.77	0.75	0.76
PP[b]	0.90	0.92	0.87	0.91
CASSCF	0.79	0.77	0.77	0.76
RAS-2SF	0.89	0.88	0.88	0.88

[a]Two pairs.
[b]Five pairs.

the importance of π-delocalization on the stabilization of the planar *para* isomer. The energetic cost of twisting the phenyl ring by 90° with (1) and without (2) the second B_2P_2 unit in *para* position has been compared. The delocalization energy (E_D) was defined as the energy difference between the two cases mentioned above ($E_D = E_{twist}^{(a)} - 2E_{twist}^{(b)}$). This value should give in turn an estimate of the communication between the two biradical sites *via* the π-system. This analysis showed that the delocalization energy (E_D) for **3-14H** (1.6 kcal mol^{-1}) coincides with the total energy difference between the *para* and *meta* isomers (1.8 kcal mol^{-1}), thus indicating that the communication through the π-system is indeed the main driving force for the stabilization of the *para* planar isomer. However, when the fully substituted system was analyzed, E_D accounts for only one-third of the energy difference between both isomers, suggesting that there are other electronic and steric factors involved in the stabilization of the planar *para* form.

Orbital occupation numbers were computed by perfect pairing (PP), complete active space self-consistent field (CASSCF), and restricted active space double spin-flip (RAS-2SF) methods. Calculations employing the Head-Gordon expression[61] revealed that the radical character of **3-14H** and **3-15H** is quite low, since less than one unpaired electron is present in the planar molecules (Table 7). Furthermore, it was

shown that alkyl substitution does not significantly modify the orbital occupation numbers. It was surmised that the surprising stability of the tetraradicaloid species can be rationalized in terms of their moderate radical character.

Although the number of unpaired electrons is almost identical for the *para* and *meta* isomers, their electron distribution in the corresponding frontier orbitals is different. Consequently, the *para* isomer shows a clear preference for the π-bonding interactions between the two molecular ends, while such interactions through the phenylene linker are hardly distinguishable for the *meta* isomer. Furthermore, in order to decide whether **3-14** and **3-15** can be considered as tetraradicaloids, their extent of open-shell singlet character has been assessed, considering that both species exhibit singlet ground states. For a system featuring four unpaired electrons, an open-shell singlet can be obtained by coupling two singlet or two triplet units. The combination of two singlets can be interpreted as communication between two singlet biradical sites, while the combination of two triplets would correspond to the excitation of the two biradical units. This difference could help to discern between two extreme situations: two interacting biradicals (two sets of two strongly correlated electrons) and a true tetraradical (four strongly correlated electrons). The t_4 couple cluster amplitude, computed by the perfect quadruples (PQ) extension of PP, defines the weight corresponding to the simultaneous excitation of four electrons and can be correlated to the tetraradical character. The magnitude of the t_4 amplitude from the doubly occupied HOMO − 1 and HOMO to the LUMO and LUMO + 1 indicated a small interaction between the two B_2P_2 units, and both methods used (CASSCF and RAS-2SF) predicted the coupling to be larger for the **3-14H** *para* isomer. This result was expected to be fully transferable for the *i*Pr- and *t*Bu-substituted derivatives.

The low-lying excited states of the tetraradical systems were analyzed in order to characterize them, in a way similar to that used to characterize biradicals, based on their singlet–triplet splitting. RAS-2SF methods have been used to compute the singlet ground state and the low-lying singlet, three triplets, and the quintet state for **3-14**/**3-14H** and **3-15**/**3-15H**. Only small differences were found between the excitation energies for the alkyl- and H-substituted molecules, where the introduction of the alkyl substituents leads to a slight reduction (0.4–1.2 kcal mol^{-1}) of the excitation energies (Table 8).

The computed vertical excitation energies for the *para* (**3-14**/**3-14H**) and *meta* (**3-15**/**3-15H**) P_2B_2 dimers have been rationalized by taking into account only the magnetic couplings due to the interaction between nearest neighbors. To this end, the short-range interaction (σ) between the boron atoms in the same B_2P_2 unit and a long-range interaction (λ) through the phenylene ring were analyzed. While the σ interaction relates to the singlet–triplet gap of the B_2P_2 core, the magnitude of λ is a direct measure of the communication between both cores. In the case where two noninteracting B_2P_2 units and an antiferromagnetic interaction ($\sigma < 0$) are considered, the most stable state has singlet spin multiplicity, with two triplet states at σ and three higher states (singlet, triplet, and quintet) at 2σ energy separations. When the long-range interaction is considered, the degenerate states split in accordance to the sign of λ. Hence, the larger the communication between biradicaloid sites, the larger the separation between the states. The magnitude of σ was found to be more than 3 times larger than λ for the *para* isomers **3-14**/**3-14H** and almost 20 times larger for the *meta* isomers **3-15**/**3-15H**. In both cases, this result indicates the interaction of two singlet subunits, rather than two triplet moieties. Hence, it was reasonably concluded that σ is responsible for having a singlet ground state (as the small t_4 amplitudes already suggested). On the other hand, λ indicated antiferro- and ferromagnetic couplings for the *para*- and *meta*-phenylene linkers, respectively, and its magnitude is more than two times larger for the *para* isomer.

Table 8 Vertical excitation energies (kcal mol^{-1}) of **3-14H**/**3-14** and **3-15H**/**3-15** low-lying singlet, triplet, and quintet states computed by RAS-2SF/6-31G(d)

	sym	***3-14H***	***3-14***	*sym*	***3-15H***	***3-15***
S_1	$^1A_{1g}$	42.4	41.1	$^1A_1$	49.1	47.9
T_1	$^3B_{3u}$	21.0	20.5	$^3A_1$	23.4	23.0
T_2	$^3A_{1g}$	25.1	24.7	$^3B_1$	24.1	23.6
T_3	$^3B_{3u}$	45.7	44.6	$^3B_1$	48.6	47.5
Q_1	$^5A_{1g}$	50.5	49.4	$^5A_1$	47.6	46.5

In an effort to further expand the number of stable B_2P_2 biradicals, Bertrand and coworkers investigated theoretically (CAS(10,10)/6-311++g**) the nature of the parent system $(H_2BPH)_2$ (**3-20**), in which the roles played by the phosphorus and boron moieties are inverted (Scheme 15).[62] The results suggested that the occupation of both the HOMO and the LUMO in this system is very close to 1, and therefore would exhibit a considerably enhanced biradicaloid character. However, these calculations also suggest that the four-membered planar biradical derivative is not the most favored isomer, but it should be possible to isolate the corresponding bicyclo[1.1.0]butanes, which readily form by ring closure.

In order to isolate such compounds, 1,2-dipotassium-1,2-dialkyldiphosphanes were treated with two equivalents of a chlorodi(alkyl)borane, leading to 1,2-diboryl-1,2-diphosphanes **3-21**–**3-23**, whose valence isomerization would afford the desired biradicaloid derivatives (Scheme 15). The steric bulk of the substituents is a determining factor in the formation of the 1,2-diboryl-1,2-diphosphanes, as demonstrated by the isolation of **3-24**. The latter exhibits a three-membered-ring, when bulky *t*Bu substituents were present. By decreasing the size of the substituents it was possible to isolate 1,2-diboryl-1,2-diphosphanes **3-21**–**3-23** as extremely air-sensitive compounds.

Interestingly, along the series **3-21** → **3-22** → **3-23**, the P–B distances are lengthened and a pyramidalization of the phosphorus centers is observed as well. Both observations suggest a decreasing interaction between the phosphorus and boron in the α position, so that they should be more nucleophilic and electrophilic, respectively. Thus, the desired 1,3-interactions, which would lead to the formation of the corresponding 2,4-diborata-1,3-diphosphonio-[1.1.0]bicyclobutanes and its biradical valence isomers, was expected to be favored. However, all attempts to thermally or photochemically induce the desired rearrangements were unsuccessful. By further decreasing the size of the substituents, the 2,4-diborata-1,3-diphosphonio[1.1.0]bicyclobutane **3-25** was isolated, which exhibits a *cis* butterfly structure, with bridging phosphorus atoms ($\delta(^{31}P) = -106$ ppm) and tetracoordinated boron centers

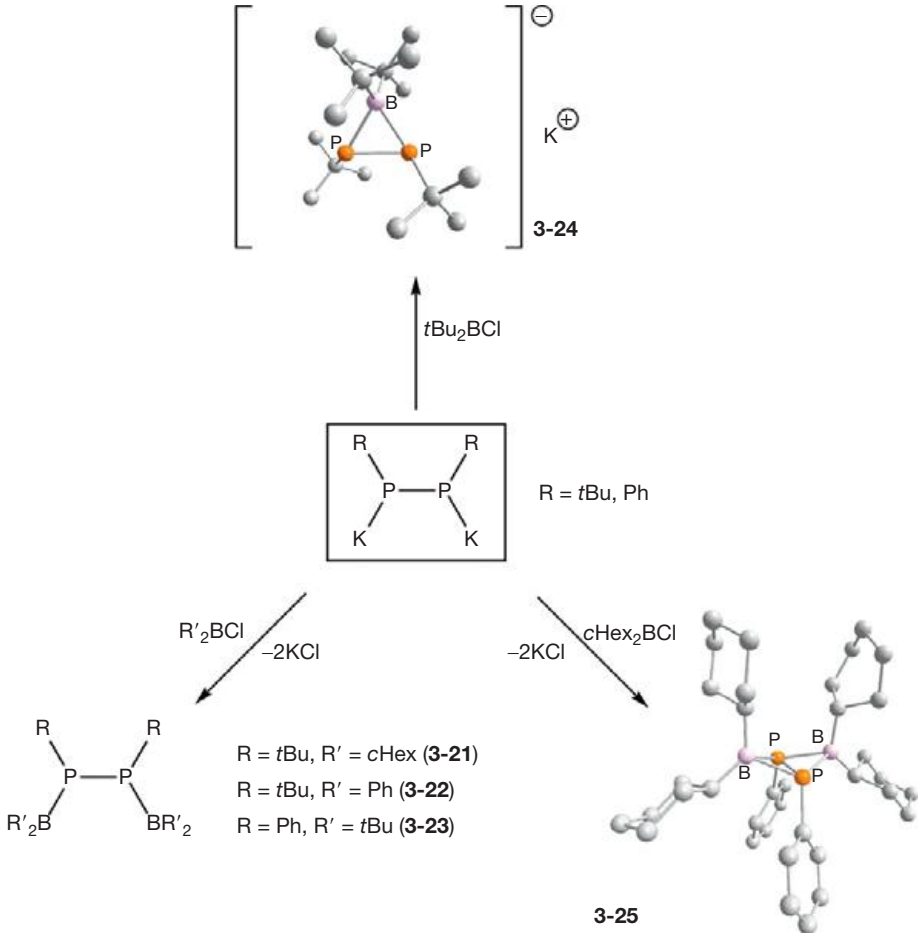

Scheme 15 Syntheses of 1,2-diboryl-1,2-diphosphanes **3-21**–**3-23**, the three-membered-ring **3-24**, and the 2,4-diborata-1,3-diphosphonio-[1.1.0] bicyclobutane **3-25**. Molecular structures are given for the products.

($\delta(^{11}B) = 37$ ppm). Analysis of the ^{13}C NMR spectra at low temperature allowed the determination of a free energy of activation for the inversion of this bicyclo[1.1.0]butane of 11.6 kcal mol^{-1}. This low value suggests that **3-25** might behave as a biradical under thermal or photochemical excitation. Despite the fact that **3-25** undergoes a fragmentation into a phosphinodiborane **3-26** and phenylphosphinidene upon irradiation with UV light, evidence of its biradical behavior was obtained by the spontaneous formation of a mixture of the *cis* and *trans* isomers of the four-membered heterocycle **3-27**, upon reaction with two equivalents of Bu_3SnH at room temperature (Scheme 16).

1.15.3.2 Reactivity of B_2P_2 Biradicals

In certain cases, B_2P_2 biradicals tend to isomerize. It was shown that under photolytic conditions, the 1,3-diborata-2,4-diphosphoniabicyclo[1.1.0]butanes **3-6** and **3-8** undergo ring-opening reactions accompanied by a 1,2-shift, which afford cyclobutenes **3-28** and **3-29**, respectively (Scheme 17).[48] The four-membered ring **3-28** could only be characterized at low temperature, since it rapidly rearranges into the acyclic derivative **3-30**. The latter consists of an allylic 2π-electron structure, with the internal phosphorus atom in a planar coordination environment and the terminal P-center in a pyramidal one. The analogous compound **3-29** is formed quantitatively at room temperature as a single regioisomer, in which the 1,2-migration selectively involves a phenyl ring rather than an isopropyl group (Scheme 17). Compound **3-29** comprises a planar four-membered ring, whose short P2–B1 bond length of 1.795 (8) Å and planar environment around P2 indicate the presence of a $P^+ = B^-$ double bond as shown for **3-28** in Scheme 17.

The chemical behavior of **3-1** has been extensively studied. Scheme 18 summarizes and compares the most relevant findings.[63,64] Compound **3-1** readily reacts with mild oxidizing reagents such as chloroform yielding *cis*-**3-31** and *trans*-**3-31** in a ratio of 3:1. The B_2P_2 heterocycle remains perfectly planar for *trans*-**3-31** and is only slightly folded for *cis*-**3-31**. Through-space and through-bond B···B interactions are cancelled and the P–B bonds are significantly elongated to 205–207 pm (cf. 189 pm for **3-1**).

Typical reagents for radical-type reactivity such as Me_3SnH can be readily added to **3-1**. The *trans*-1,3-adduct **3-32** was isolated in 73% yield featuring two signals in the ^{11}B NMR spectrum ($\delta = -3.8$ and -10 ppm). As the *trans* geometry was unambiguously confirmed by single-crystal X-ray structure analysis, it is likely that a stepwise rather than a concerted mechanism is favorable for this reaction. The treatment of

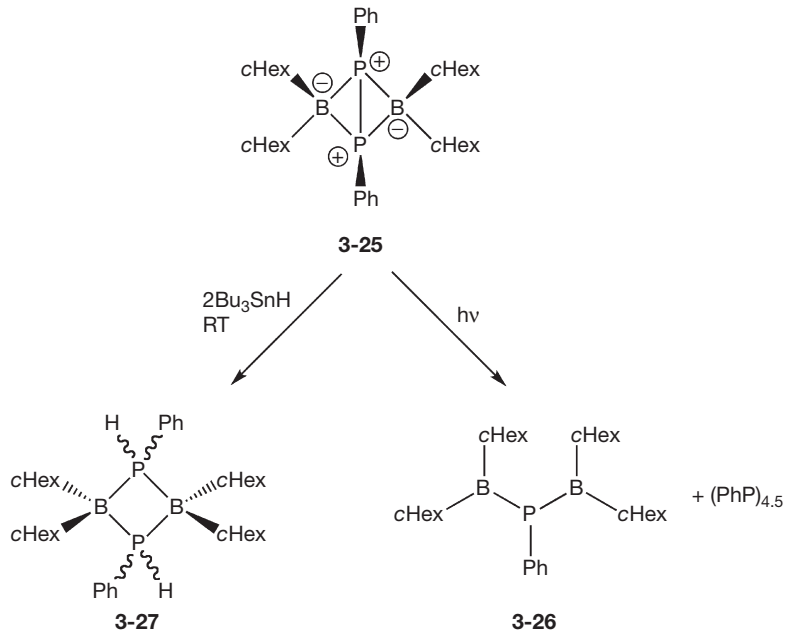

Scheme 16 Compound **3-25** undergoes a fragmentation into a phosphinodiborane **3-26** and phenylphosphinidene upon irradiation (hν); the reaction of **3-25** with two equivalents of Bu_3SnH furnishes *cis* and *trans* isomers of the four-membered heterocycle **3-27**.

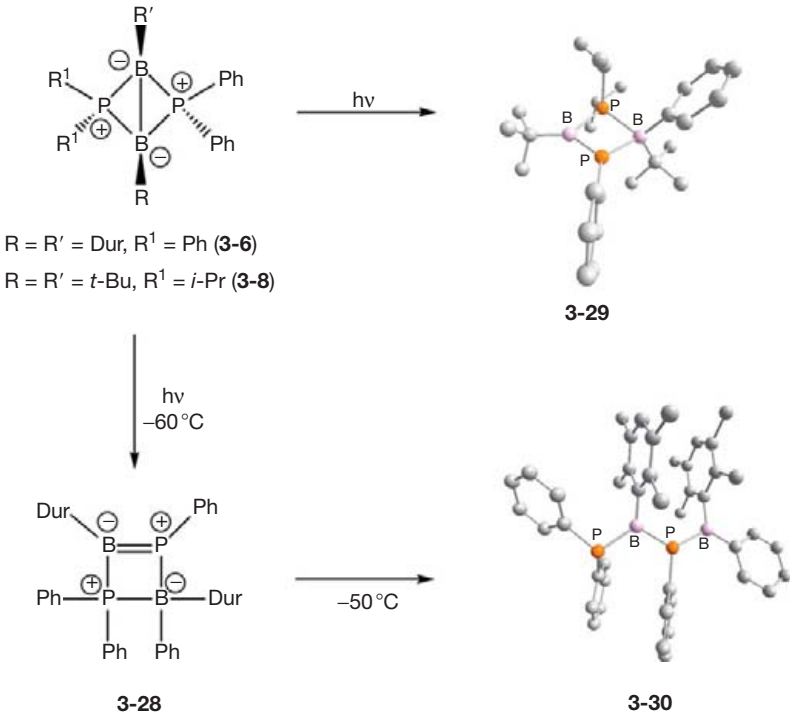

Scheme 17 Photochemical isomerizations of **3-6** and **3-8**. Molecular structures are given for the products.

3-1 with $BrCCl_3$ afforded further evidence for its radical-type behavior. Besides small amounts of the *trans*-1,3-dibromo adduct, a novel *B*-spirocyclic compound (**3-33**) was isolated (Scheme 18). The B_2P_2 four-membered ring structure remains intact; one B atom is attached to a Br substituent and the second is incorporated in the BC_2 ring. Although the detailed mechanism for the formation of **3-33** is not known, a stepwise reaction was anticipated: (1) $Br^{\bullet}$ abstraction from $BrCCl_3$ to afford the radical pair $[1Br]^{\bullet}[CCl_3]^{\bullet}$ and (2) H atom transfer from one *t*Bu substituent to give **3-33** and $HCCl_3$.

Furthermore, it was shown that both elemental selenium and diphenyl diselenide (PhSeSePh) cleanly react with **3-1** to furnish in 70% isolated yield an asterane-like structure (**3-34**, Scheme 18).[63] Compound **3-1** also reacts readily with

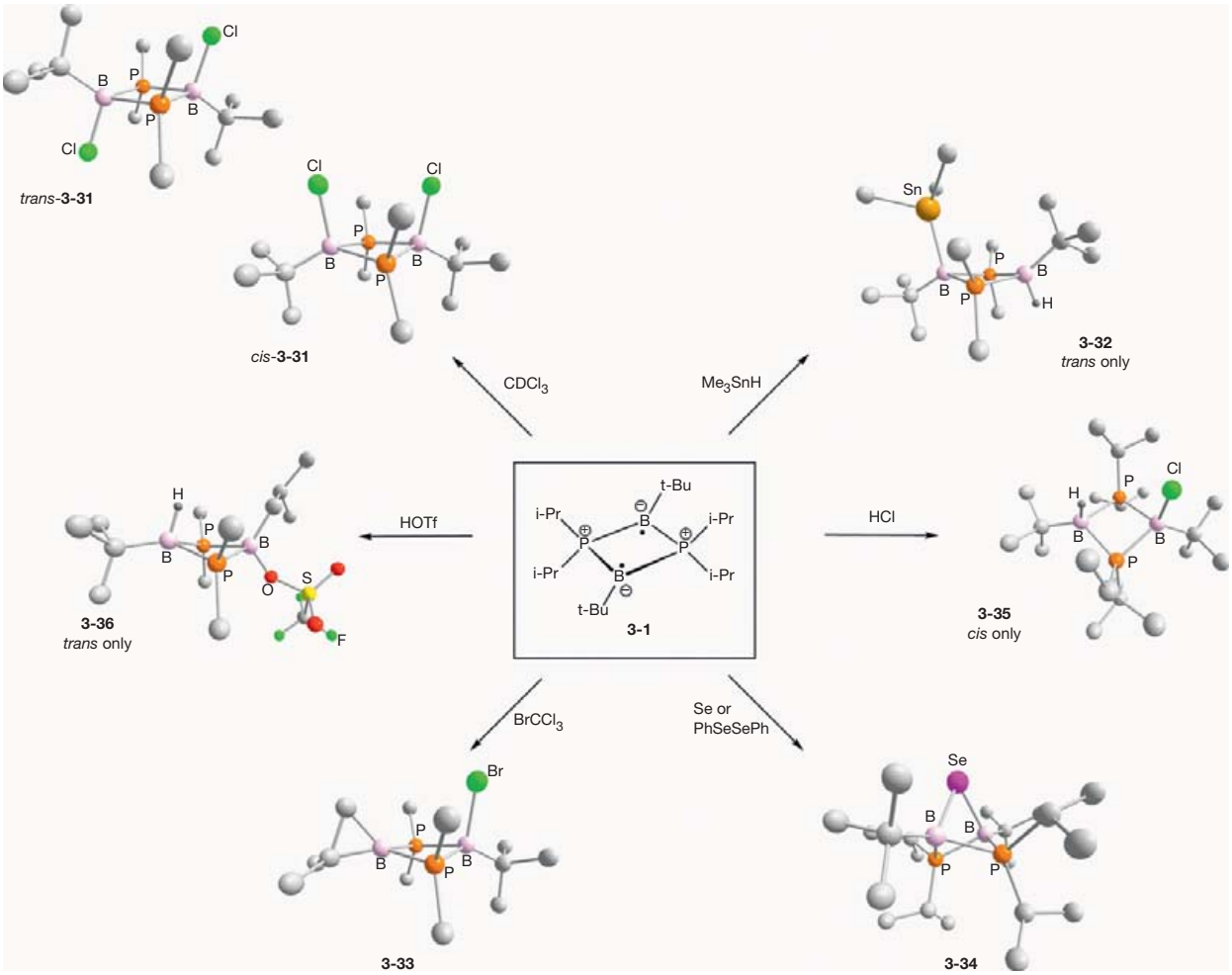

Scheme 18 Reactivity of the 1,3-dibora-2,4-diphosphoniocyclobutane-1,3-diyl (**3-1**). Molecular structures are given for the products.

HX ($X^- = Cl^-$, OTf^-; with $OTf^- = [O_3SCF_3]^-$ = triflate) at low temperatures.[64] ^{11}B NMR spectra indicate the presence of two nonequivalent, anionic, tetracoordinate boron centers (**3-35**: $\delta = 5.6, -15.0$ ppm; **3-36**: $\delta = 6.2, -17.9$ ppm), one of which is bonded to a proton, as indicated by the observed broad signals in the ^1H NMR spectra. When the unsymmetrically substituted compound **3-16** was reacted with HCl and HOTf, the formation of the analogous addition products was observed, as corroborated by their ^{11}B NMR spectra (**3-37**: $\delta = 6.7, -18.4$ ppm; **3-38**: $\delta = 4.9, -18.3$ ppm) (Scheme 19). Close analysis of the conformation of these products strongly suggested that steric factors rather than electronic properties of the boron centers determine the regio- and stereoselectivity of the addition reactions. In particular, the formation of derivative **3-36** proceeds with an unusual *t*Bu to *i*Bu isomerization, which, according to DFT calculations, involves a carbocationic σ-borane adduct as a key intermediate.

When silver salts AgX (X = Cl, OTf) are used as oxidizing agents for the starting material **3-13**, the bis(chloride) and bis(triflate) salts **3-39** and **3-40** are formed.[65] The reactions proceed readily at room temperature, as visually indicated by the discoloring of the reaction mixture and the formation of a silver mirror. Determination of the solid-state structure of the bis(triflate) adduct **3-40** showed that the B_2P_2 core is only slightly deviated from planarity and that the two covalently bound OTf groups are in *trans* relationship. As expected, both the P–B (**3-13**: 189 pm, **3-40**: 202–205 pm) and the B–B (**3-13**: 257 pm, **3-40**: 288 pm) distances are longer in the product. CV studies revealed an electrochemically irreversible oxidation process centered at $E^0_{1/2} = -0.41$ V (vs. Fc/Fc^+). DFT calculations showed that, upon removal of one electron, the 1,3-diborata-2,4-diphosphonio-cyclobutane-1,3-diyl moiety retains its planar geometry, but the B–B and P–B bonds are significantly lengthened, as should be expected for the decreased through-space and through-bond interactions between both boron centers. The singly occupied molecular orbital (SOMO) of the hypothetical radical cation $[\mathbf{3\text{-}13}]^{\bullet+}$ (Scheme 20) is very similar to the HOMO of **3-13**, and has been formally associated with a one-electron B–B π-bonding interaction.

1.15.3.3 Isoelectronic Al_2P_2 Systems

During their studies on subvalent aluminum compounds, Schnöckel, Klopper, and coworkers have recently investigated in a combined theoretical and experimental study four-membered heterocycles of the general formula Al_2R_4, which

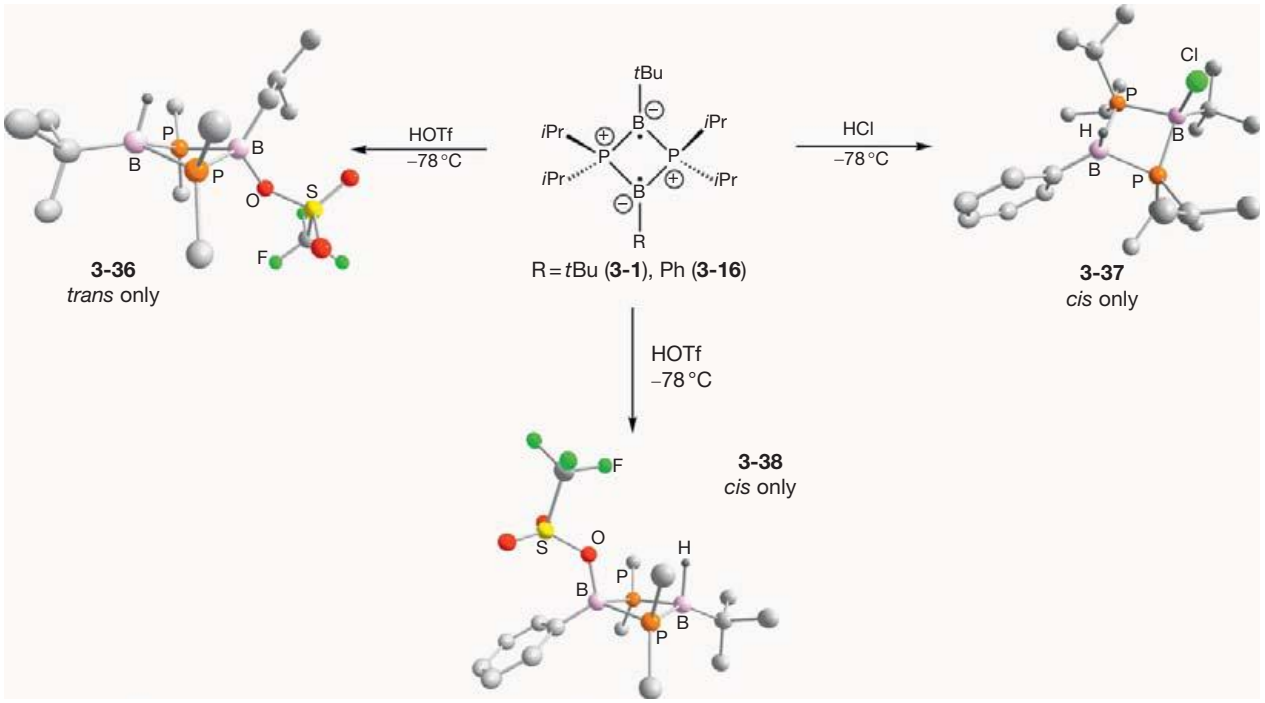

Scheme 19 Reactivities of 1,3-dibora-2,4-diphosphoniocyclobutane-1,3-diyls toward protic reagents (left). Note the *t*Bu to *i*Bu isomerization in **3-36** ($OTf^- = [O_3SCF_3]^- =$ triflate). Molecular structures are given for the products.

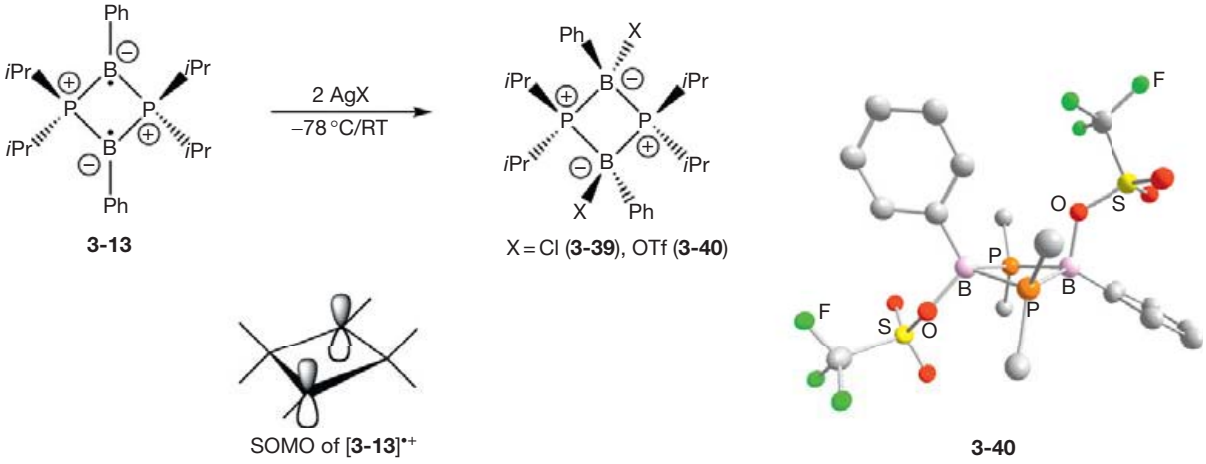

Scheme 20 Oxidation reactions of **3-13** yielding the bis(chloride) and bis(triflate) salts **3-39** and **3-40**. DFT calculated SOMO of the hypothetical radical cation $[\mathbf{3\text{-}13}]^{\bullet+}$ (left). Molecular structure of compound **3-40**. *i*Pr groups have been omitted for clarity (right).

are isoelectronic to the 1,3-dibora-2,4-diphosphoniocyclobutane-1,3-diyls (cf. **3-1**).[66] Both the planar (**3-41**) and the bicyclic (**3-41a**) form of $[Al_2(PtBu_2)_4]$ have been obtained from the reaction of AlX (X = Cl, Br) solutions with $LiPtBu_2$ (Figure 2). Both can be viewed as intermediates of the formation of Al–Al σ-bonds starting from $\{AlR^2\}$ units. It was found that differences in the reaction conditions determine which of both isomers is obtained. Most revealingly, very different Al–Al distances have been observed for **3-41** (350.8 pm) and **3-41a** (258.7 pm) by X-ray crystallographic studies on green and yellow single crystals, respectively. In addition to extensive experimental investigations, detailed quantum chemical calculations have been performed. Highly energetic $[AlR^2]^\bullet$ species should dimerize under formation of the triplet biradical intermediate $[RAl(\mu\text{-}R^2)AlR]$ (**3-41**) with a long Al···Al separation ($d(Al\cdots Al)_{calc.} = 346.2$ pm) with the unpaired electron residing in Al-centered, p-type SOMOs. These triplet molecules **3-41** can formally undergo a spin-flip procedure (singlet state of **3-41**, $d(Al\cdots Al)_{calc.} = 305.1$ pm) and a subsequent ring-closing reaction leads to bicyclic molecule $[RAlR^2AlR]$ (**3-41a**, $d(Al\cdots Al)_{calc.} = 261.8$ pm) as thermodynamically stable species (σ-bond formation). The quantum chemical predictions have

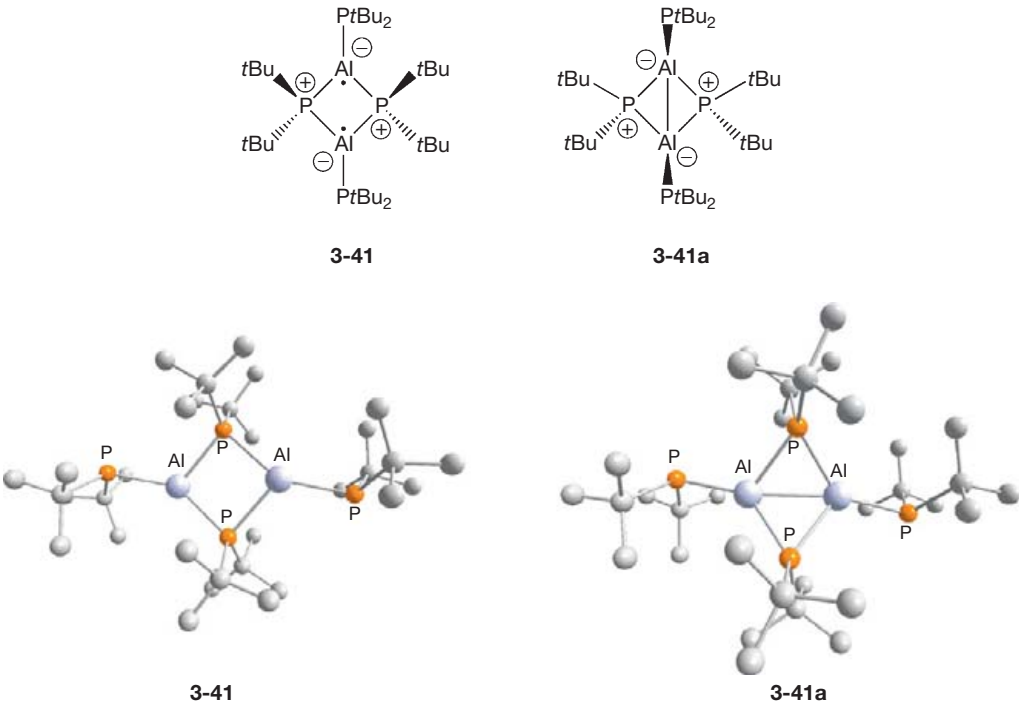

Figure 2 Molecular structures of biradicaloid **3-41** (left) and bicyclic **3-41a**.

been supported by a complex reaction mechanism, considering known intermediates that have been structurally characterized in the Schnöckel group. It was concluded that both isomers originate from the reaction of AlX and AlX_3 species in donor-rich solutions. At low donor (L) concentration, $[Al_2X_4L_2]$ affords the bicyclic species **3-41a**, while at high donor concentration the biradicaloid molecule **3-41** is obtained via $[Al_5X_7L_5]$. Although the triplet state of **3-41** could not be confirmed by EPR studies due to high reactivity and sensitivity of this species, several findings support a triplet assignment. For instance, the observed green color of crystals of **3-41** (yellow for **4-31a**) was confirmed by the TD-DFT calculations. A close analysis of the X-ray structure data revealed **3-41** to form a columnar packing in the solid state. Obviously, the sterically demanding $PtBu_2$ substituents prevent any intermolecular interaction between individual $[Al_2(PtBu_2)_4]$ molecules (e.g., formation of dimers as observed for other derivatives) and only permit weak intermolecular interactions within the columns. It was also suggested that upon formation of **3-41** this reactive species is immediately stabilized by the crystallization process and that this process seems to circumvent a spin-flip and the thermodynamically favored formation of **3-41a**. As emphasized by the authors, 'this unprecedented discovery was only possible owing to the particularly mild reaction conditions present in metastable AlX/AlR solutions'.[66,106]

In this context, it is also important to mention that for a gallium compound reported by Uhl and coworkers, that is $(Me_3Si)_3CGa(H)(\mu\text{-}PPh_2)_2Ga(H)C(SiMe_3)_3$ (**3-42a**), the Ga–H bond formation was attributed to hydrogen abstraction from the solvent by radical intermediates.[67] Hence, it may be possible that the conceivable biradicaloid $(Me_3Si)_3CGa(\mu\text{-}PPh_2)_2GaC(SiMe_3)_3$ (**3-42**) has been formed in the reaction of the diiodo-substituted digallane(4), $(Me_3Si)_3CGa(I)\text{-}Ga(I)C(SiMe_3)_3$, with $LiPPh_2$.

1.15.4 Group 14 Element Systems

1.15.4.1 Bicyclo[1.1.0]butanes E_4R_6 and Related Compounds

Strained, bicyclic structures of group 14 element compounds have been subject of increased interest, because they were identified as suitable candidates for the synthesis of stable biradicaloids. For the heavier congeners of bicyclo[1.1.0]butanes,[68] several quantum chemical calculations[69] predicted the phenomenon of bond-stretch isomerism. For such systems, two distinct minima on the potential energy surface (PES) exist, which mainly differ by the length of one bond. The general topic of bond-stretch isomerism has been addressed by several review articles.[70]

For both isomers, the central bond (E_b–E_b) is formed from almost pure p-orbitals (Scheme 21). For the long-bond (LB) isomer **4-LB** they are slightly polarized by s-orbital contribution furnishing a less effective orbital overlap and consequently a weak E–E bond (inverse σ-bond). The unpolarized p-orbitals of the short-bond (SB) isomer **4-SB** form an E–E bond with slightly larger π-character, although the individual orbitals are rotated by about 40° from the ideal alignment (cf. ~30° for **4-SB**). Comprehensive calculations by Koch et al. for the SB and LB tetrasilabicyclo[1.1.0]butanes (Si_4R_6, with R = H, Me, Ph, 2,6-dimethylphenyl)[71] revealed that the relative energies of **4-LB** and **4-SB** strongly depend on the substituent R due to a competition between ring strain[72] and steric effects. Small groups R favor the formation of **4-LB** (larger angle Φ) while steric repulsion (larger angle Θ) provides the same isomer to be unstable for bulkier aryl substituents. Hence, 'true' bond-stretch isomerism can only be discussed for selected ligands of suitable size because both isomers **4-SB** and **4-LB** do not coexist for very small and for sterically demanding substituents.

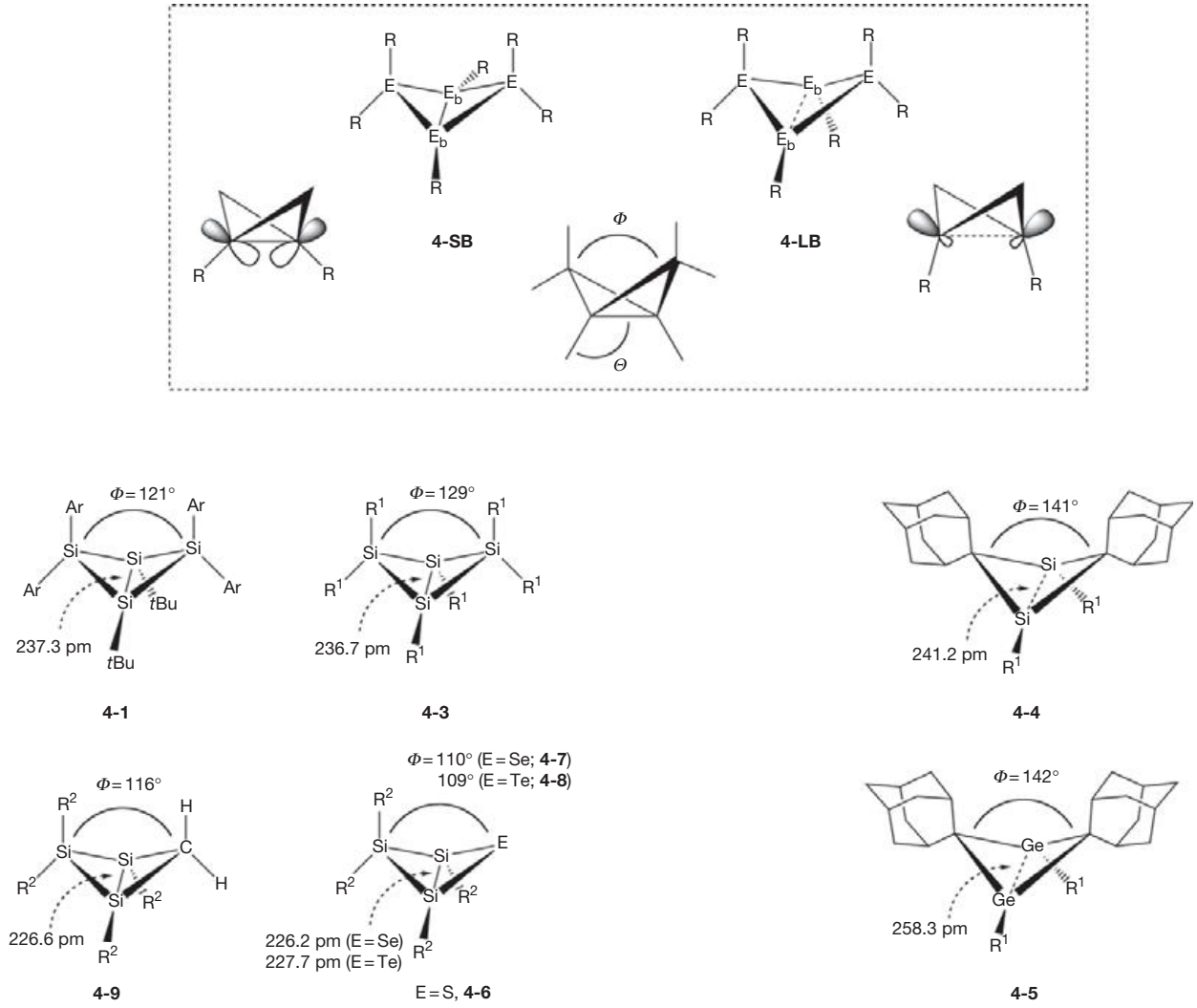

Scheme 21 Bicyclo[1.1.0]butane derivatives containing group 14 elements; the angles Φ and Θ within these scaffolds. Ar = 2,6-$Et_2C_6H_3$; R^1 = Si*t*BuMe$_2$, R^2 = Si*t*Bu$_2$Me.

In contrast, the germanium bicyclic structure is more flexible than the corresponding silicon isomer.[73] The difference in strain energy between four-membered and three-membered rings, which decides the preferred geometry for small groups R, is much more pronounced for the germanium rings compared to their silicon counterparts. Hence, the LB structure **4-LB** is clearly favored over **4-SB**. For the calculated germanium analogs, Ge_4R_6, **4-SB** revealed to be no minimum on the PES, indicating that apparently only the LB isomer exists. Atoms-in-molecules (AIM) calculations on the LB germanium and silicon isomers showed no bond-critical point (bcp; a saddle point in the total electron density indicating the existence of a bond between two atoms in a molecule)[74] between the bridgehead atoms and only one ring critical point. Therefore, the structure can be described as a singlet biradicaloid confirming Schleyer's original description from 1987 for the model compound Si_4H_6.[69a]

Although the quantum chemical calculations predicted such interesting phenomena for some isomers of the E_4R_6 PES,[75] synthetically accessible and structurally characterized tetrasilabicyclo[1.1.0]butanes are very rare (Scheme 21). The sterically encumbered derivative **4-1** reported by Masamune[76] has a normal Si_b–Si_b bond length of 237.3 pm and an interflap angle Φ of 121°, suggesting its classification as SB isomer **4-SB**. However, the physical and chemical properties of **4-1** indicate the energetically close relationship to the biradicaloid form. Crystals of **4-1** are thermochromic and the ring-inversion barrier for **4-1** was estimated by NMR methods to be low ($E_a \approx 15$ kcal mol^{-1}). Furthermore, the central Si_b–Si_b bond is very reactive since degassed water or Cl_2 is readily added furnishing the corresponding cyclotetrasilane products. Wiberg et al. also reported the synthesis of the isomeric bicyclo[1.1.0]tetrasilanes, but without a detailed analysis of their molecular structures.[77]

The silyl-substituted derivative **4-3**, which was generated by photolysis from the tetrasilacyclobutene derivative **4-2**, has been published by Kira and coworkers.[78] In the photostationary state at 288 K, 91% conversion was reached, as determined by UV/Vis spectroscopy. Compound **4-3** was initially characterized by ^{1}H NMR spectroscopy and by product analysis of its

hydrolysis. At that time, no further spectroscopic data such as ^{29}Si or ^{13}C NMR spectra could obtained because **4-3** thermally rearranges quantitatively to the cyclobutene in the dark ($k_{288} = 5.67 \times 10^{-5}$ s^{-1}). Both the thermal and photochemical isomerizations were confirmed using substituent-labeling experiments to proceed *via* 1,2-silyl-migration rather than skeletal isomerization.[79] In a recent study, Iwamoto, Kira et al. achieved the isolation of **4-3** at low temperature *via* an alternative synthetic route (Wurtz-type coupling reaction of 1,3-dibromocyclotetrasilane with potassium graphite) and characterized its unique structural features in the solid state and in solution.[80] The cyclotetrasilane **4-3** was found to adopt the SB structure (**4-SB**) due to the steric effects of bulky *t*Bu-Me$_2$Si groups at the bridgehead silicon atoms (d(Si$_b$–Si$_b$) = 236.7 pm; interflap angle $\Phi = 129.25°$). The ^{29}Si resonances for the ring silicon nuclei of **4-3** appearing at −145.1 ppm (Si$_b$) and −90.6 ppm (bridge Si atoms) suggest that **4-3** adopts the SB structure also in solution. Kinetic NMR studies revealed **4-3** to undergo a facile ring flipping in solution. The $\Delta G^{\ddagger}$ of this dynamic process was estimated to be 14.3 kcal mol^{-1} at 333 K (cf. 15 kcal mol^{-1} for **4-1**). As mentioned by Kira in a footnote,[80] a planar bicyclotetrasilane, hexa-*tert*-butylbicyclo[1.1.0]tetrasilane, has been isolated.[81] The skeletal structure of this cyclotetrasilane-1,3-diyl is similar to that assigned as the transition state for the flipping of **4-3**. To the best of our knowledge, however, no further data have been reported yet for this species.[82]

Recently, Kira et al. were also able to isolate a compound (**4-4**)[83] featuring a long central Si$_b$–Si$_b$ bond of 241.2 pm, which is considerably longer than Si–Si bonds of known disiliranes (227–233 pm). The 1,3-disilabicyclo[1.1.0]butane **4-4** was obtained as air- and moisture-sensitive bright-yellow crystals in 70% isolated yield by using a formal double sila-Peterson reaction. X-ray crystal structure analysis, quantum chemical calculations, as well as ^{13}C and ^{29}Si NMR spectroscopic investigation predicted this LB isomer to be stable in the solid state and in solution. Interestingly, **4-4** shows no ring-flipping tendency as evidenced by ^{13}C NMR spectroscopy. A distinct band maximum at 420 nm in the UV/Vis spectrum could be assigned to a $\sigma \rightarrow \sigma^*$ transition of the Si$_b$–Si$_b$ bond. The biradicaloid behavior of the Si–Si bond in **4-4** was confirmed by its reactions with alkyl halides, phenylacetylene, and ketones.[84] The analogous germanium compound, 1,3-digermabicyclo[1.1.0]butane **4-5**, was synthesized and characterized as LB isomer consisting of a long Ge$_b$–Ge$_b$ distance of 258.3 pm and a UV/Vis absorption maximum at 440 nm.[85]

Structurally related 1,2,3-trisilabicyclo[1.1.0]butanes consisting of a bicyclic Si$_3$E core structure (E = S, Se, Te, **Scheme 21**) have been reported recently by Sekiguchi and coworkers.[86] They have employed a novel approach for the preparation of these scaffolds by using [1 + 2] cycloaddition reactions of a chalcogen E (S, Se, Te) to the Si=Si bond of a cyclotrisilene. Thus, 2-thia-, 2-selena-, and 2-tellura-1,3,4-trisilabicyclo[1.1.0]butanes **4-6**–**4-8** were prepared in good yields isolated in the form of yellow–orange crystals. The compounds exhibit folded structures in solution and the solid state. The interflap angles in both **4-7** and **4-8** are acute ($\Phi = 110.34°$ and 109.4°). The short bridging Si–Si bonds of 226.2 and 227.7 pm are close to the upper limit of the Si=Si double-bond range and much shorter as compared to those observed for the other bicyclo[1.1.0]butane derivatives discussed so far. Interestingly, the bicyclo[1.1.0]butanes **4-6** and **4-7** were transformed into cyclobutene species upon photochemical irradiation.

A similarly short bridging Si–Si bond (226.64 pm) has been reported by Sekiguchi for the trisilabicyclo[1.1.0]butane **4-9**, also consisting of a butterfly-type skeleton (**Scheme 21**).[87] The authors stated that "in the framework of the well-established in bicyclo[1.1.0]butane chemistry 'short- and long-bond isomers' concept, one should definitely recognize **4-9** as the 'very short bond isomer,' representing an opposite extreme to 1,3-disilabicyclo[1.1.0]butane with the very long bridging Si–Si bond" (cf. **4-4**).

Closely related dimetalla derivatives featuring considerably long central carbon–carbon bonds[88] were reported for the 2,4-disilabicyclo[1.1.0]butane **4-10** ($d_{C-C} = 178.1$ pm)[89] and the disilabenzvalene **4-11** ($d_{C-C} = 168.0$ pm).[90] Furthermore, West and Driess[91] reported on 1,3-diphospha-2,4-disilabicyclo[1.1.0]butanes (**4-12**) and the corresponding As compounds **4-13** (**Scheme 22**). Both group 15 element bicycles contain unusually long P–P and As–As bonds. The P$_2$Si$_2$ butterfly-like compounds of the type **4-12** also tend to undergo a ring inversion *via* an unusual silanediyl fragmentation in the transition state. However, the ring-inversion barrier for the model compound (H$_2$Si)$_2$P$_2$ was predicted to be relatively high (51.0 kcal mol^{-1} (MP2)).[92] Based on calculated orbital occupation numbers (CAS-MCSCF/6-31G*) and singlet–triplet gaps ($\Delta E_{S-T} = -88.4$ kcal mol^{-1}) it was suggested that the biradical character of these molecules is fairly low. The elongation of the P–P bond was attributed to ring strain and coulomb repulsion between the two P atoms.

1.15.4.2 Heavy [1.1.1]Propellanes of Group 14

By analogy to these [1.1.0]bicyclobutanes, the central bond between the bridgehead atoms of heavy [1.1.1]propellanes of group 14 is significantly elongated. [1.1.1]Propellane molecules (International Union of Pure and Applied Chemistry

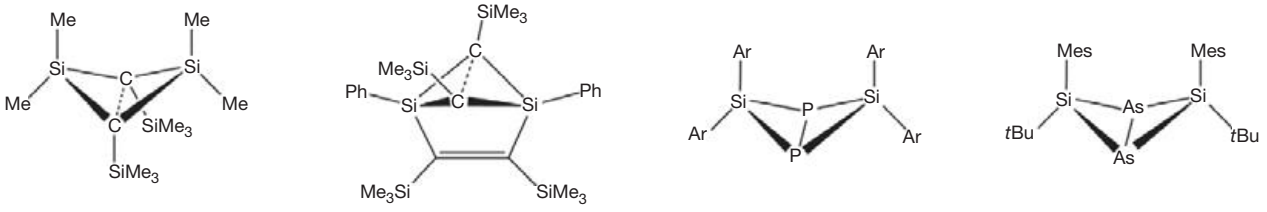

4-10 **4-11** **4-12** **4-13**

Scheme 22 Related bicyclobutanes consisting of long central carbon–carbon bonds (**4-10** and **4-11**); 1,3-diphospha- (**4-12**) and 1,3-diarsa-2,4-disilabicyclo[1.1.0]butanes (**4-13**) with unusually long E–E bonds; Ar = 2,4,6-Me$_3$C$_6$H$_2$ (Mes) or 2,4,6-*i*Pr$_3$C$_6$H$_2$ (Tip).

(IUPAC) nomenclature: tricyclo[1.1.1.$0^{1,3}$]pentane) intrigue chemists for a number of reasons, not at least because their core structures resemble the 'eponymous macroscopic propellers.'[93] The intrinsic [1.1.1] scaffolds of these five-atom clusters belong to the so-called 'nonclassical' structures, showing inverted tetrahedral bridgehead atoms (umbrella-like configuration,[94] i.e., all substituents point in the same hemisphere of space).[95] In particular, the question about the interaction between the bridgehead atoms in propellanes has been extensively discussed in the literature.[96] All efforts are mainly directed toward the clarification of fundamental aspects of the nature of the interaction between the inverted bridgehead atoms.

Even the well-known all-carbon propellanes, C_5R_6,[97] have attracted renewed interest, from both experimentalists and theoreticians. The bond strength of the all-carbon [1.1.1]propellane was estimated to be ~60 kcal mol^{-1}.[98] Natural bond orbital analysis predicted the occupancy for the central bonding orbital to be 1.83 (0.15 for the antibonding orbital), indicative of some biradicaloid character.[99] Detailed information about electronically excited states of the parent carbon propellane has been obtained by electron energy loss spectroscopy (EELS).[100] The first excited singlet is located at 7.26 eV and corresponds roughly to an HOMO–LUMO excitation. The equilibrium geometry of the excited singlet state is similar to that of the ground state. However, the equilibrium geometry is very different for the lowest triplet state, observed by EELS at 4.70 eV (peak maximum). The central C–C bond is greatly stretched in the excited triplet state. Experimental investigations on the electron density in an all-carbon [1.1.1]propellane derivative as well quantum chemical calculations performed by Luger and co-workers revealed the existence of a bonding path between both bridgehead carbon atoms.[101] The authors found significant electron density at the bcp from which a bond order of 0.71 was deduced. However, the corresponding experimentally observed Laplacian at the bcp is positive (even larger than the calculated one)[102] suggesting that a central C–C bond does indeed exist, but not of usual covalent type.[103] A valence bond (VB) study by Shaik, Hiberty, and coworkers also found the existence of a so-called charge-shift bond, in which the resonance energy between covalent and ionic forms plays a major role.[104]

Heavy analogs of all-carbon propellanes, for example, group 14 clusters of the general formula E_5R_6 (E = Si, Ge, Sn), have continuously attracted considerable interest in the last few decades, not at least because they are often fundamentally different from their carbon counterparts and have remained a challenge for both experimentalists and theoreticians for a long time.[105] These molecules have frequently been described as singlet biradicaloids due to their considerably stretched bond between the 'naked'[106] bridgeheads E_b.

Before entering a further discussion about experimental findings on heavy [1.1.1]propellanes of group 14, some results from quantum chemical calculations are summarized (**Scheme 23**, **Table 9**). Quantum chemical calculations of Schleyer and Janoschek on the parent compound Si_5H_6 suggested substantial singlet biradical character and that "it would be misleading to represent the structure by drawing a line between the bridgehead atoms".[107] Schoeller et al. also predicted a long $Si_b\cdots Si_b$ separation for the Si_5 derivative.[108] Nagase has presented evidences, which support the existence of an inverted chemical bond. The biradical character of the tin derivative was found to be very small and comparable to that of the carbon homolog.[109] Gordon and coworkers[110,111] pointed out that the similarity of the $E_b\cdots E_b$ distances in **4-I** and **4-II** (for M = Ge and Sn, **Scheme 23**) and doubted the existence of a bridgehead bond in heavy [1.1.1]propellanes. They also found the $E_b\cdots E_b$ distances to decrease upon descending the group 14. For the tin derivative, there is only a little difference Δd in the $E_b\cdots E_b$ interaction in **4-I** and **4-II** (**Table 9**). The natural orbital occupation numbers given by Gordon et al. suggest fairly small biradical character in the ground-state [1.1.1]propellanes (with M = C, Si, Ge, Sn) showing a maximum of 14% for the silicon derivative, which is in accordance with Schleyer's[107] earlier assumption. Other evidence against significant $E_b\cdots E_b$ bonding is corroborated by the similarity of the distances in the singlet and triplet states of the parent systems E_5H_6 (**4-I**, **Scheme 23**) and that no bcp has been located between the bridgeheads.

Hetero[1.1.1]propellanes have also been targeted by theory (**4-III**, **Scheme 23**). Inagaki et al.[112,113] expected electropositive groups to increase the central C–C separation within $C_2(EH_2)_3$ (E = Si, Ge, Sn, Pb). Theoretical work of Nagase,[109] Gordon,[110,111] and Ottosson[114] predicted the substitution of the EH_2 groups by suitable groups L to stabilize the central bond and to shorten it. Electronegative groups L lead to significantly shortened $E_b\cdots E_b$ distances for both E_2L_3 (**4-III**) and $E_2L_3H_2$ (**4-IV**). For L = O, the metal–metal distances are much shorter than singly bonded systems such as $H_3E–EH_3$. It was

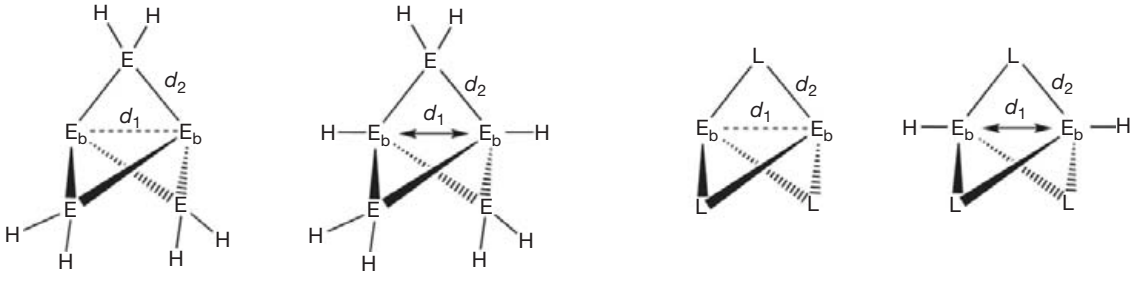

Scheme 23 [1.1.1]Propellanes E_5H_6 (**4-I**) and bicyclo[1.1.1]pentanes E_5H_8 (**4-II**) of group 14; hetero[1.1.1]propellanes E_2L_3 (**4-III**) and corresponding bicyclo[1.1.1]pentanes $H_2E_2L_3$ (**4-IV**); d_1 = distance between the central atoms E_b; d_2 = distance between the central atoms E_b and the peripheral atoms E or L. See also **Table 10**.

Table 9 Selected structural parameters for calculated group 14 [1.1.1]propellanes, bicyclopropanes, and their derivatives

E	*cf.* ***Scheme 23***	E_5H_6 (**4-I**)[110,107]	E_5H_8 (**4-II**)[110]	*Δd*	E_2O_3 (**4-III**)[111,109]	$H_2E_2O_3$ (**4-IV**)[111]	*Δd*	E_2S_3 (**4-III**)[111]	$H_2E_2S_3$ (**4-IV**)[111]	*Δd*	$E_2(CH_2)_3$ (**4-III**)[114]	$H_2E_2(CH_2)_3$ (**4-IV**)[114]	*Δd*
C	d_1	162.5	188.3	25.8	151.1	162.2	11.1	164.0	202.0	38.0	159.6	187.5	27.9
	d_2	152.3	155.5		140.8	142.7		179.2	184.6		151.7	155.0	
Si	d_1	279.3	292.5	13.2	207.6	206.0	−1.6	236.3	237.3	1.0	229.1	229.3	0.2
	d_2	235.8	236.8		170.7	170.0		218.0	218.1		192.3	191.0	
Ge	d_1	299.1	305.3	6.2	225.0	222.5	−2.5	–	–	–	247.0	247.1	0.1
	d_2	248.8	247.7		180.6	179.5		–	–		202.8	200.7	
Sn	d_1	346.9	350.9	4.0	257.7	254.6	−3.1	–	–	–	280.2	278.5	−1.7
	d_2	285.7	284.0		198.5	197.1		–	–		223.0	220.2	

Values in pm (see also **Scheme 23**); $\Delta d = d_1$(bicyclopentane) $- d_1$(propellane) (pm); details concerning the level of theory can be found in the literature citations.

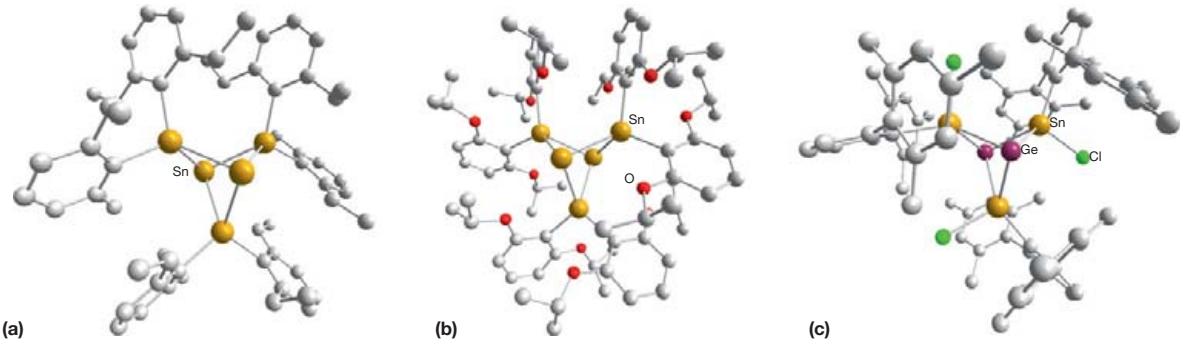

Figure 3 Molecular structures of Sn_5Dep_6 ((a), **4-14**), $Sn_5(2,6\text{-}(iPrO)_2C_6H_3)_6$ ((b), **4-15**), and $Ge_2\{Sn(Cl)(2,6\text{-}Mes_2C_6H_3)\}_3$ ((c), **4-16**).

surmised that the unusually short bridgehead distances in both E_2O_3 (or E_2S_3, **4-III**) and $E_2O_3H_2$ (or $H_2E_2S_3$, **4-IV**) do not result in significant bonding interaction. Despite the short $E_b\cdots E_b$ distances, these compounds possess a considerable degree of biradicaloid character (cf. comparable discussion for the B_2P_2 biradicaloids in Section 1.15.3).

As can be seen from this short selection, numerous quantum chemical calculations[115] have been performed on these species. However, synthetically accessible and structurally characterized species are very rare. Breakthrough discoveries have been published in the early 1990s by Sita and coworkers.[116,117] They succeeded in isolating the very first heavy [1.1.1]propellane of group 14, that is, the pentastanna[1.1.1]propellane Sn_5Dep_6 (**4-14**, Dep = 2,6-$Et_2C_6H_3$, Figure 3) by thermolysis of a cyclotristannane.[118] Sita et al. also reported a further derivative and an optimized synthetic route to **4-14**,[119] which was further improved by Breher and coworkers in later studies.[120] The best synthetic way to obtain **4-14** is to react the tristannane Sn_3Dep_6 under reducing conditions (elemental lithium) with $SnCl_2$ as additional Sn-source. X-ray structural investigations on single crystals of **4-14** revealed a large $Sn_b\cdots Sn_b$ separation of 336.7 pm (~20% longer than a regular Sn–Sn single bond, Figure 3). Although the cluster core is sufficiently shielded and kinetically stabilized by the Dep substituents, the bridgehead tin atoms are still accessible for reagents (see below).

Only a few further heavy [1.1.1]propellanes have been synthesized and structurally characterized in the following years (Figure 3). Drost et al. reported on the synthesis of the pentastanna derivative $Sn_5(2,6\text{-}(iPrO)_2C_6H_3)_6$ (**4-15**)[121] and Power and coworkers were able to isolate and characterize the heteronuclear propellane $Ge_2\{Sn(Cl)(2,6\text{-}Mes_2C_6H_3)\}_3$ (**4-16**).[122] Remarkably, the distance between the bridgehead germanium atoms in **4-16** (336.3 pm) is similar to those of the tin atoms in **4-14**. This was explained by the electronegative Cl substituents (small C–Sn–Cl angle of 103.8°).

The homonuclear germanium (**4-17**, orange crystals)[123] and silicon (**4-18**, yellow crystals)[124] propellanes have only been isolated and characterized recently (Scheme 25). The pentagerma[1.1.1]propellane **4-17** was prepared from Mes_2GeCl_2 using a freshly prepared lithium naphthalenide solution in the presence of $GeCl_2$·dioxane. This additional germanium source and/or oxidation reagent is crucial for a successful synthesis of **4-17**. The synthesis of the very sensitive silicon propellane (**4-18**) was shown to be very similar (Mes_2SiCl_2 and Si_2Cl_6 as starting materials, Scheme 25). The separation of 263.6(1) pm between the two bridgehead silicon atoms in **4-18** is ca. 30 pm (13%) longer than usually observed for a regular Si–Si single bond. A similar bond stretch was observed for the Ge_5Mes_6 derivative **4-17** ($d(Ge_b\cdots Ge_b) = 286.9(2)$ pm). NMR investigations on **4-18** revealed two resonances in the ^{29}Si NMR spectrum at $\delta = 25.5$ and −273.2 ppm for the bridging (Si_{br}) and bridgehead (Si_b) atoms, respectively ($\delta_{calcd} = 34$ and −270 ppm, BP86/def2-triple zeta valence polarization (TZVP)).[125] The Raman spectrum of **4-18** shows totally symmetric normal modes at $\nu = 479$, 370, and 340 cm^{-1} ($\nu_{calcd} = 455$, 349, and 312 cm^{-1}). However, the extraction of the contribution of the restoring $Si_b\cdots Si_b$ bond forces for the totally symmetric Raman bands could not be achieved in the desired accuracy, because too many internal coordinates are involved in each of these modes.

It is important to note that the silicon propellane **4-18** remained elusive until this recent study. Targeted by theory already more than two decades ago,[107] Masamune designated this molecule in a 1991 review article as a 'synthetic challenge.'[126] Unsurprisingly, only some closely related silicon clusters[127] containing ligand-free silicon atoms have been reported so far.[128] Related germanium and tin clusters[129] have been reported and reviewed previously.[130] Selected examples are presented in Scheme 24. The silicon cluster **4-19** bears a Si_2 dumbbell (Si–Si = 229(1) pm) with 'inverted tetrahedrally' coordinated Si atoms within its molecular core. The corresponding Ge (**4-20**) (also Sn) clusters consist of two ligand-free group 14 element atoms. While for the Si compound **4-21** another bonding model has been established ('dismutational aromaticity'),[128c,131] the germanium clusters of the general structure **4-22** ($R^1 = CH(SiMe_3)_2$ or 2,6-$Mes_2C_6H_3$) have been indicated to possibly possess some biradical character.[132] In a very recent study, a Ge_{14} polyhedron, $[(THF)_2Li]_3Ge_{14}[Si(SiMe_3)_3]_5$ (**4-23**), has been described. Quantum chemical calculations indicated that three singlet biradicaloid entities (see bicyclic substructures within **4-23** in Scheme 24) formally combine to yield the singlet hexaradicaloid.[133]

The family of heavy [1.1.1]propellanes of group 14 has been extended in recent studies. Two heteronuclear clusters of the general formula $E_2\{SiMes_2\}_3$ (E = Ge and Sn) have been synthesized and characterized in order to relate the $E_b\cdots E_b$ separation in heavy [1.1.1]propellanes with their electronic properties and reactivities.[134] These compounds consist of two ligand-free Ge (**4-24**) and Sn atoms (**4-25**), respectively (Scheme 25). As expected, the formal substitution of the bridging ER^2 entities in Sn_5Dep_6 (**4-14**) and Ge_5Mes_6 (**4-17**) with

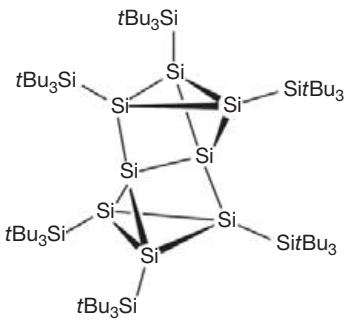

4-19

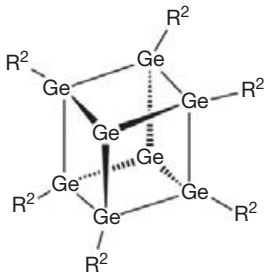

4-20

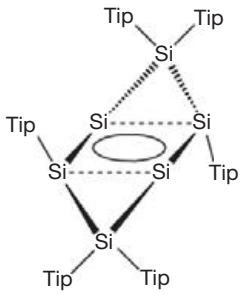

4-21

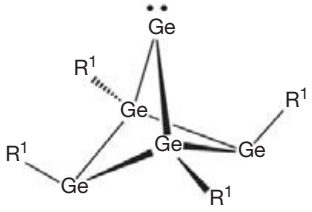

4-22

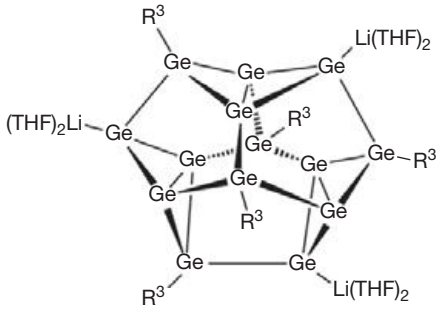

4-23

Scheme 24 Selected group 14 element clusters containing two ligand-free (or missing, **4-22**) cluster constituents; Tip = 2,4,6-*i*Pr$_3$C$_6$H$_2$; R^1 = CH(SiMe$_3$)$_2$ or 2,6-Mes$_2$C$_6$H$_3$; R^2 = N(SiMe$_3$)$_2$ or 2,6-(*i*PrO)$_2$C$_6$H$_3$; R^3 = Si(SiMe$_3$)$_3$.

the smaller SiMes$_2$ groups results in a decrease of the E$_b$···E$_b$ separation in Ge$_2${SiMes$_2$}$_3$ (Δd = 10 pm) and Sn$_2${SiMes$_2$}$_3$ (Δd = 27 pm), respectively. ^{1}H NMR spectroscopic monitoring of the crude reaction products showed that the heteronuclear [1.1.1]propellanes with two heavier group 14 elements Ge (**4-24**) or Sn (**4-25**) in the bridgehead positions and three Si atoms within the flanking units are formed in 10–15% yield. It is important to note that no other [1.1.1]propellanes with different connectivities within the molecular cores are formed under these conditions. The dihalides GeCl$_2$·dioxane and SnCl$_2$ are therefore selective sources for the bridgehead positions. The ^{29}Si NMR chemical shifts of δ = 66 (**4-24**) and 98 (**4-25**) ppm differ only slightly. The latter shows nonresolved satellites due to a one-bond coupling to the $^{117/119}$Sn isotopes (^1J = 324 Hz). The ^{119}Sn NMR chemical shift for the bridgehead tin atoms in **4-25** of δ = −1348 ppm compares very well to other tin propellanes known from the literature. The comparably large coupling of 3464 Hz (absolute value) between the bridgehead tin atoms in **4-25** was revealed to be somewhat smaller than for the pentastanna[1.1.1]propellanes (8145 and 3973 Hz) known from Sita and Drost, respectively (Figure 3).

DFT calculations (B3LYP/def2-TZVP) on these systems (slightly modified model compounds) predicted in each case the following order of the frontier MOs (Figure 4): (1) HOMO − 1: E$_b$···E$_b$ bonding orbital of a_1 symmetry; (2) HOMO: degenerate set of E$_b$–E$_{br}$ cluster bonding orbitals of *e* symmetry; and (3) LUMO: E$_b$···E$_b$ antibonding orbital of a_2 symmetry.

It was found that the relative LUMO energy of the calculated E$_5$Dmp$_6$ clusters (Dmp = 2,6-Me$_2$C$_6$H$_4$) decreases upon descending the group 14. Parallel to this, the HOMO–LUMO gap becomes significantly smaller in magnitude. Indeed, these findings were experimentally observable. Electrochemical investigations using CV studies on Sn$_5$Dep$_6$ (**4-14**)[135] as well as E$_5$Mes$_6$ (**4-17**, **4-18**)[123,124] revealed in each case two quasi-reversible reduction events furnishing the radical anions [E$_5$R$_6$]$^{\bullet-}$ and dianions [E$_5$R$_6$]$^{2-}$ (Table 10). Since the LUMO is being filled (Figure 4), these reduction processes lead to a successive decrease of the E$_b$···E$_b$ interaction (the E$_b$···E$_b$ distances are considerably longer in the reduced form, e.g., $d_{calc.}$ = 290.6 pm for Ge$_5$Dmp$_6$ → 328.9 pm for [Ge$_5$Dmp$_6$]$^{\bullet-}$, BP86/def2-TZVP). The radical anions [E$_5$R$_6$]$^{\bullet-}$ have been characterized by EPR spectroscopy (e.g., for [Ge$_5$Mes$_6$]$^{\bullet-}$ ([**4-17**]$^{\bullet-}$): $g_\perp$ = 1.980 and $g_{||}$ = 1.999, with hyperfine couplings to two equivalent germanium atoms (I(^{73}Ge) = 9/2, 7.73% n.a.) of $A_\perp \leq 20$ MHz and $A_{||}$ = 41 MHz). Furthermore, and as expected from the calculated LUMO energies, the reduction events are anodically shifted upon descending the group 14. Most notably, the stronger E$_b$···E$_b$ interactions in the heteronuclear propellanes **4-24** and **4-25** as compared to the homonuclear counterparts **4-17** and **4-14** were confirmed by these electrochemical studies. Due to the energetically destabilized LUMOs in **4-24** and **4-25** (stronger E$_b$···E$_b$ interactions), both reduction events are in each case slightly more cathodically shifted. As expected, the differences are much more pronounced for the tin-containing propellanes due to the larger difference in the E$_b$···E$_b$ separation.

A close analysis of the experimental UV/Vis spectra (in conjunction with quantum chemical calculations, TD-DFT calculations) was found to be very helpful for an interpretation of

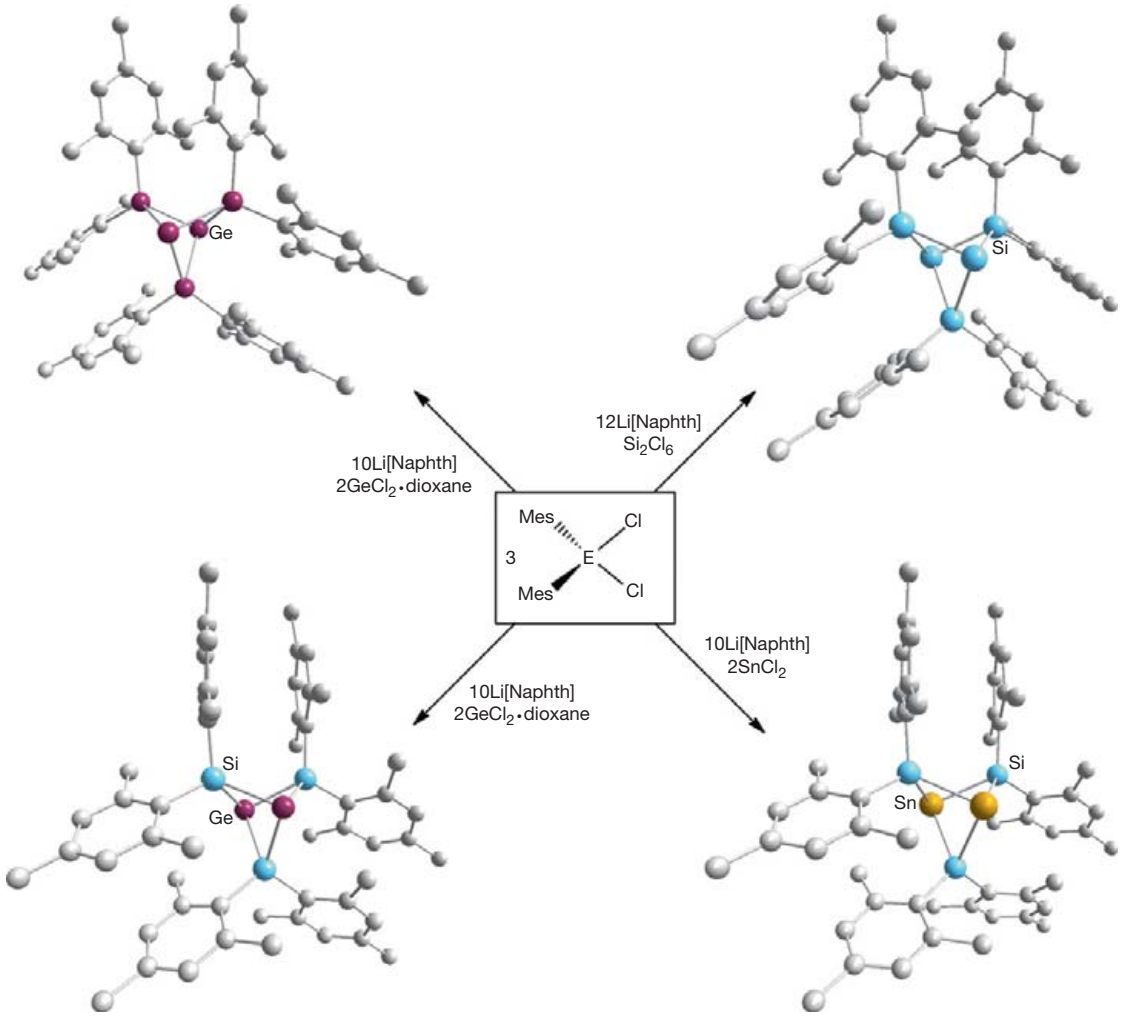

Scheme 25 Synthesis of the pentagerma- (**4-17**) and pentasila[1.1.1]propellane (**4-18**) as well as the heteronuclear [1.1.1]propellanes **4-24** and **4-25**.

the bonding in these molecules. Of particular interest are the electronic A_2 excitations from the HOMO-1 ($E_b \cdots E_b$ bonding) to the LUMO ($E_b \cdots E_b$ antibonding, Figure 4). The vertical excitation energies (or λ values from UV/Vis studies) directly correspond to the strength of the interaction between the bridgehead atoms.

In a recent comprehensive study, a linear relationship between the $^1A_2$ excitation wavelengths and the $E_b \cdots E_b$ distances was found.[134] The corresponding vertical $^3A_2$ excitations, however, showed some peculiarities without linear relationships. For instance, the heteronuclear clusters **4-24** and **4-25** showed unusually high excitation wavelengths (low excitation energies), although the $E_b \cdots E_b$ distances are much shorter and the first singlet $^1A_2$ excitation wavelengths are lower than those of its homonuclear analogs **4-17** and **4-14**. Usually, the $^3A_2$ transitions (directly related to $\Delta E_{S \rightarrow T}$) are not visible in the UV/Vis spectrum. However, the experimental spectra of a series of compounds, in particular those containing heavy tin atoms, showed characteristic absorptions at theoretically confirmed wavelengths, which belong to these triplet excitations (e.g., 546.8 nm for Si_5Mes_6 (**4-18**); 549 nm for $Sn_2Si_3Mes_6$ (**4-25**)).

It was surmised that two important factors oppositionally contribute to the $^3A_2$ excitations and, as a consequence, the ease to reach the excited triplet A_2 state of heavy propellanes. Note that – perhaps contrary to an initial guess – the biradical character of [1.1.1]propellanes (and other systems as well, see above and Section 1.15.3) is not necessarily increased by solely stretching the $E_b \cdots E_b$ bond! Higher $^3A_2$ wavelengths and thus lower $\Delta E_{S \rightarrow T}$ energies are obtained either by elongating the $E_b \cdots E_b$ distances or by arranging the involved orbitals in close spatial proximity (in this case HOMO − 1(a_1) and LUMO (a_2)). While the bond stretch leads to a smaller energy gap between the involved orbitals, a close proximity of the latter furnishes larger exchange interactions and an extra stabilization of the $^3A_2$ state.

Interestingly, LUMO occupation numbers (calculations at the (6,4)CASSCF/def2-TZVP//B3LYP/def2-TZVP level) were found to be almost invariant and fairly small (ca. 0.1 e^-) for a whole series of [1.1.1]propellane model compounds E_5Me_6.[123,124,134] Comparable occupation numbers have been reported previously.[115] Clearly, the inherent singlet ground state of [1.1.1]propellanes points toward noticeable $E_b \cdots E_b$ interactions but it appears that the $E_b \cdots E_b$ interactions in these

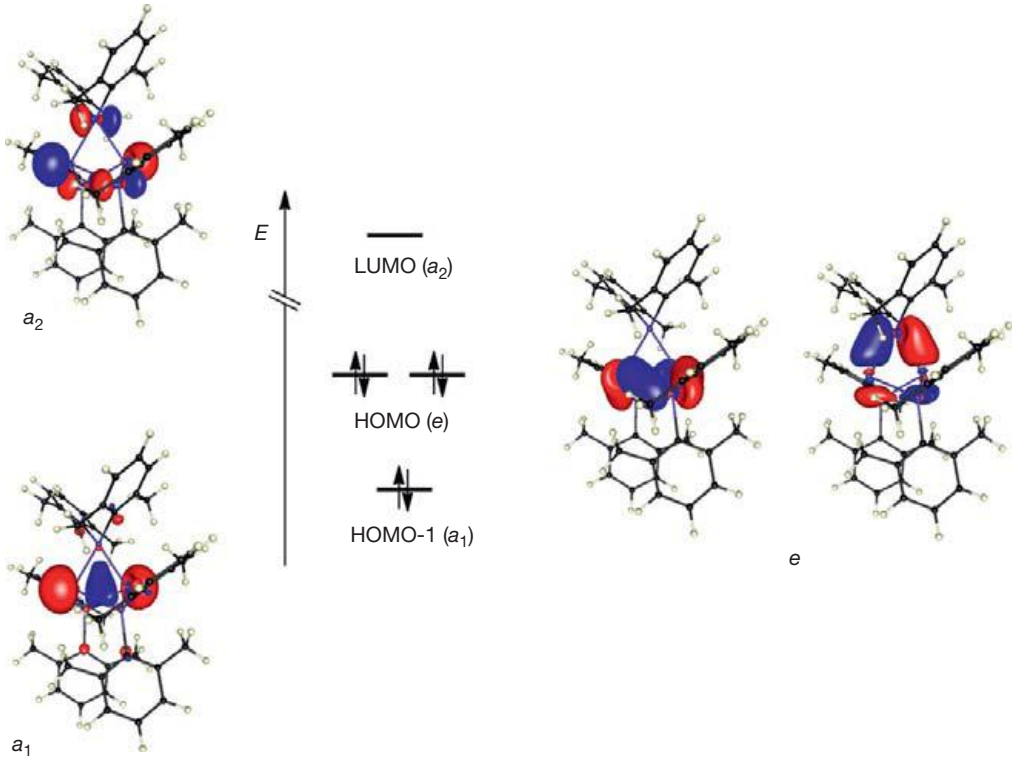

Figure 4 DFT-calculated frontier orbitals of the model compound Ge_5Dmp_6 (Dmp = 2,6-$Me_2C_6H_3$; Turbomole, RI-DFT, BP86, def2-TZVP, D_3 symmetry). The energy scale (vertical axis) is only qualitative.

Table 10 Reduction potentials of heavy [1.1.1]propellanes versus the Fc/Fc^+ couple; process 1: $E_5R_6 + e^- \rightarrow [E_5R_6]^{\bullet -}$; process 2: $[E_5R_6]^{\bullet -} + e^- \rightarrow [E_5R_6]^{2-}$

	$E^0_{1/2}(1)$ (V)	$E^0_{1/2}(2)$ (V)
Si_5Mes_6 (**4-18**)	−2.88	−3.12
$Ge_2Si_3Mes_6$ (**4-24**)	−2.29	−2.68
Ge_5Mes_6 (**4-17**)	−2.18	−2.61
$Sn_2Si_3Mes_6$ (**4-25**)	−2.13	−2.77
Sn_5Dep_6 (**4-14**)	−1.96	−2.48

species are perturbed to such a particular extent that highly correlated quantum chemical methods provide evidence for some biradicaloid character of their ground state.

Of fundamental interest in this research area is the question to what extent the reactivities of these heavy [1.1.1]propellanes are affected by the stretched bond. Note that the $Si_b \cdots Si_b$ bond strength in Si_5Mes_6 (**4-18**) was recently estimated to amount to ~174 kJ mol^{-1},[124] that is, considerably weaker than in normal disilanes (ca. 306–332 kJ mol^{-1}). The bond lengthening by 30 pm (13% compared to a regular Si–Si single bond) thus furnishes a ca. 50% weaker bond. It was further noticed that a comparably elongated Si–Si bond was found for the sterically encumbered disilane $tBu_3Si–SitBu_3$,[136] which was shown to be a convenient source for very reactive supersilyl radicals ($tBu_3Si^{\bullet}$, heating to ca. 50 °C).[137] Hence, one should *a priori* expect a radical-type reactivity for heavy [1.1.1]propellanes. It was also speculated that such radical-type reactivity could be influenced by light due to the facile accessibility of the excited singlet and triplet A_2 states in the UV/Vis region (see above). Furthermore, it was surmised that a closed-shell reactivity should also be feasible, in particular when nucleophiles are reacted with heavy [1.1.1]propellanes. In each case, either homolytic or heterolytic addition reactions of substrates to the bridgehead atoms strongly depend on the amount of interaction between the bridgehead atoms, the bond strengths within the substrates and the resulting products, and steric effects.

First experimental results on the reactivity of the pentastanna[1.1.1]propellane **4-14** were published by the Sita group. They studied sequential addition reactions of MeI and MeLi. Addition of MeLi to **4-14** quantitatively produces the adduct **4-26**, which can subsequently be reacted with MeI in a salt metathesis reaction to afford the 1,3-dimethyl-bicyclo [1.1.1]pentastannane **4-28**.[138] The latter can alternatively be synthesized by treating the l-iodo-3-methylbicyclo[1.1.1]pentastannane derivative **4-27** with MeLi (**Scheme 26**).[135] Photolysis of **4-28** furnishes **4-14** in 45% yield.

The reactivities of other [1.1.1]propellanes toward a series of simple substrates were reported later (NMR tube scale reactions).[123,124,134] Interestingly, both closed-shell and radical-type reactivities were observed for all heavy [1.1.1]propellanes.[105] It was shown that the overall reactivity strongly depends on the nature of the bridgehead atoms. Si_5Mes_6 (**4-18**) showed the highest reactivity. Compound **4-18** immediately forms the water adduct $HO–Si(SiMes_2)_3Si–H$ (**4-29**) by exposing solutions to traces of H_2O; all other [1.1.1]propellanes, however, are stable against degassed water. Phenol also reacts only with **4-18** (gentle heating), while thiophenol can readily be

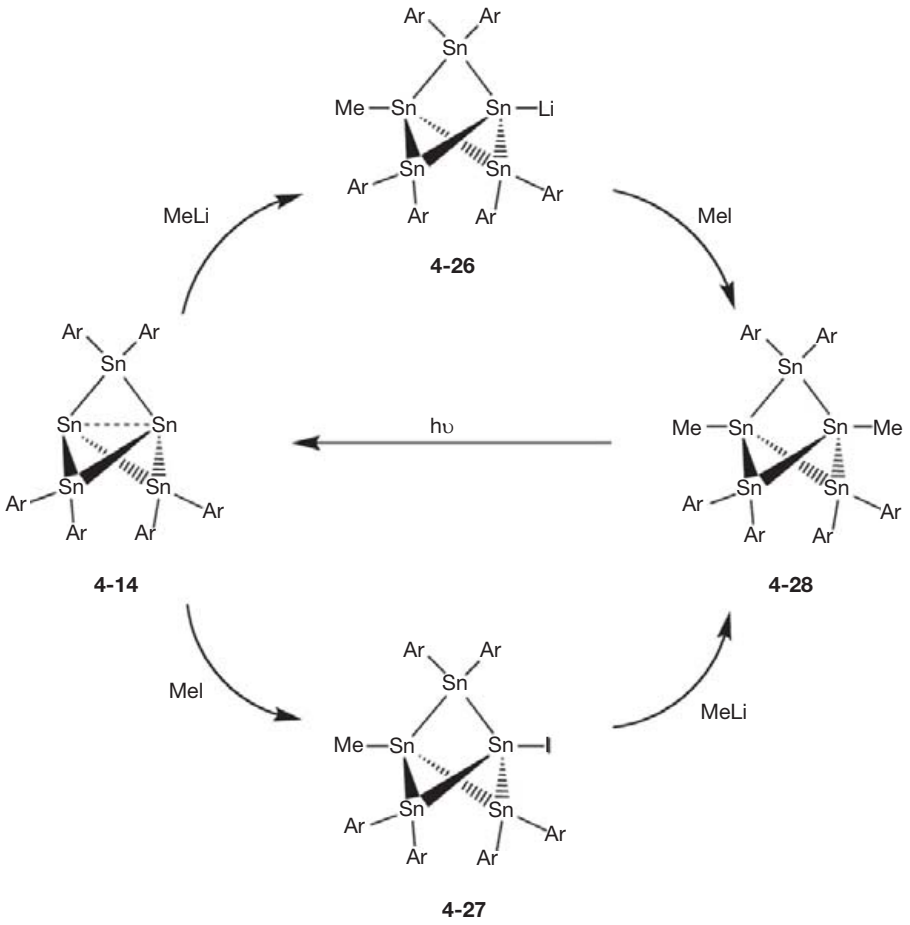

Scheme 26 Reactivity studies on **4-14** performed by Sita et al. (Ar = Dep = 2,6-$Et_2C_6H_3$).

added across the bridge of **4-17**, **4-18**, and **4-24**. The tin-containing clusters **4-14** and **4-25**, however, only gave decomposition products. Alongside this closed-shell behavior, particularly interesting radical-type reactivities were observed. First evidences came from addition reactions of Me_3SnH, which is a typical reagent for radical-type reactivity. The latter reacts quantitatively with **4-17**, **4-18**, and **4-24** furnishing the 1,3-disubstituted bicyclo[1.1.1]pentane derivatives.[139] Further evidence for biradicaloid reactivity of Si_5Mes_6 (**4-18**) came from studies using 9,10-dihydroanthracene, which gave the dihydrogen adduct **4-33** in low yield after prolonged reaction times. The general reactivity of Si_5Mes_6 is depicted in Scheme 27.

It was also found that addition reactions are not limited to substituents with small steric demand. While the homologs **4-17**, **4-18**, **4-24**, and **4-25** did not either show any reaction with $[FeCp(CO)_2]_2$ or lead to any isolable product in the case of $[RuCp(CO)_2]_2$, the tin propellane **4-14** quantitatively afforded the first transition metal-terminated bicyclo[1.1.1]pentastannanes, $[\{MCp(CO)_2\}_2\{\mu\text{-}Sn_5Dep_6\}]$ (M = Fe (**4-34**), Ru = (**4-35**)) in 68 and 66% isolated yield, respectively (Scheme 28).[120] Interestingly, the reactions only proceed in the presence of daylight. Currently, it is not clear whether this enhanced reactivity is due to excited states of triplet A_2 state of **4-14** or the photochemistry of the M–M bonded bimetallic transition metal precursors.

The products have been characterized in detail using various methods. X-ray structure analyses revealed a significant elongation of the central $Sn_b\cdots Sn_b$ distances by ca. 20 pm as compared to the starting material **4-14**. ^{119}Sn NMR spectroscopy proved to be a powerful tool in this case to determine the connectivity between the metal atoms in these clusters. Both compounds were analyzed in detail showing in each case the expected ^{119}Sn–^{119}Sn and ^{119}Sn–^{117}Sn couplings between the bridgehead (Sn_b) and bridging (Sn_{br}) tin atoms. Of particular interest in this case was a comparison of the $J(Sn_b\cdots Sn_b)$ coupling constant of **4-14** with those observed for **4-34** and **4-35**. Since both bridgehead atoms are bonded to the metal fragments and, accordingly, the formal bonding interaction between them is eliminated, couplings may still arise either through the bridging $SnDep_2$ units or *via* 'through-space interactions'[140] due to the close spatial proximity of the bridgeheads. In addition, indeed, comparably large $^{117/119}Sn$ coupling constants were observed for both systems (2908 (**4-34**) and 3896 (**4-35**) Hz; cf. 8145 Hz for **4-14**). Similar effects have already been reported for 1,3-disubstituted all-carbon bicyclo[1.1.1]pentanes.[97d]

Electrochemical studies revealed the reduction chemistry of **4-34** and **4-35** in tetrahydrofuran (THF) solutions to be very interesting. A detailed preparative and electrochemical study, including the isolation and characterization of reduction

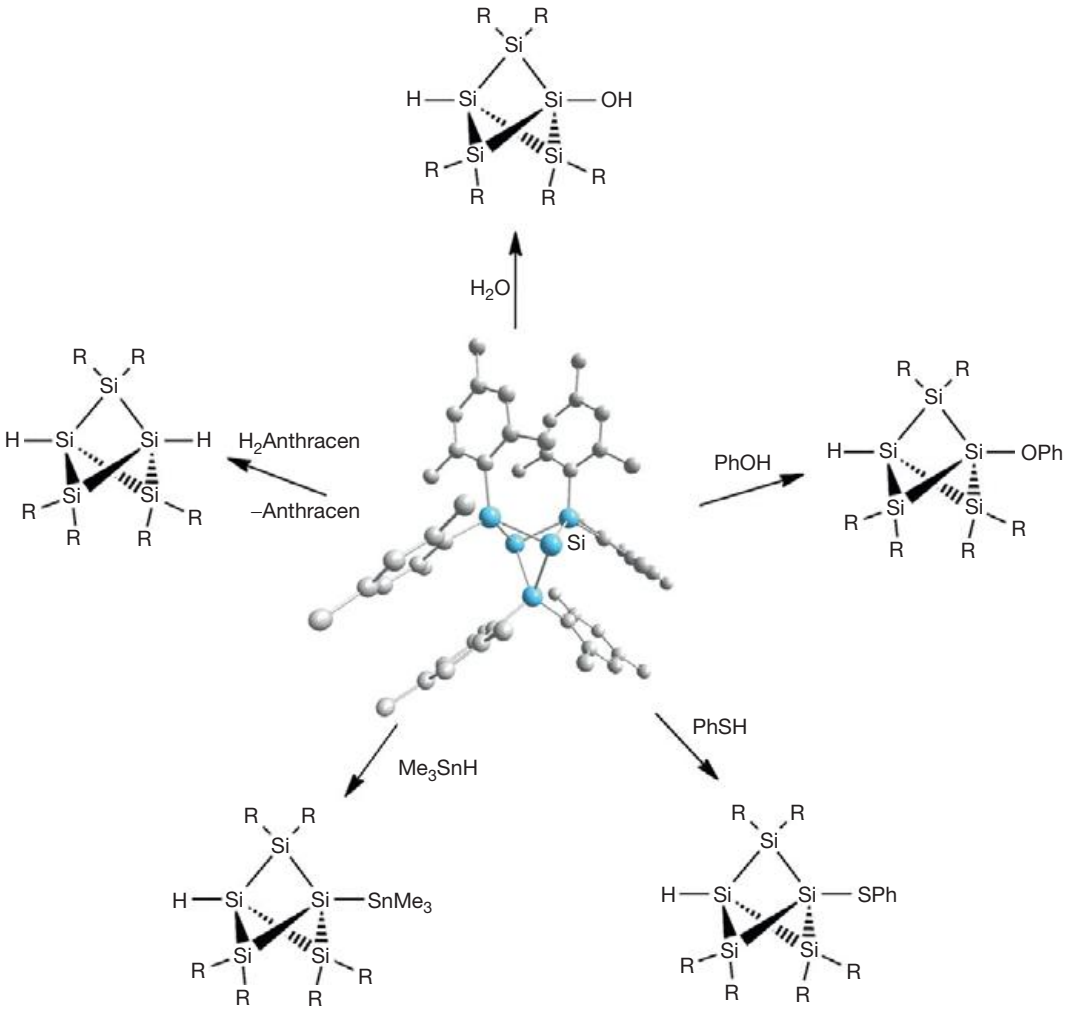

Scheme 27 Reactivity of **4-18** toward selected simple substrates (R = Mes).

products, elucidated a complex mechanism consisting of a cascade of bond-breaking and bond-making processes. The chemically reversible redox cycle consisting of electrochemical irreversible couples is shown in **Figure 5**. The corresponding equations are listed below (eqns [1]–[6]):

$$\mathbf{4\text{-}34} + e^- \rightarrow \mathbf{4\text{-}36} + \frac{1}{2}\left[FeCp(CO)_2\right]_2, \quad E_{pc} = -1.90\ V \qquad [1]$$

$$\frac{1}{2}\left[FeCp(CO)_2\right]_2 + e^- \rightarrow \left[FeCp(CO)_2\right]^-, \quad E_{pc} = -2.24\ V \qquad [2]$$

$$\mathbf{4\text{-}36} + 2e^- \rightarrow [\mathbf{4\text{-}14}]^{2-} + \left[FeCp(CO)_2\right]^-, \quad E_{pc} = -2.93\ V \qquad [3]$$

$$[\mathbf{4\text{-}14}]^{2-} + \left[FeCp(CO)_2\right]^- \rightarrow \mathbf{4\text{-}36} + 2e^-, \quad E_{pa} \approx -2.75\ V \qquad [4]$$

$$\left[FeCp(CO)_2\right]^- \rightarrow \frac{1}{2}\left[FeCp(CO)_2\right]_2 + e^-, \quad E_{pa} = -1.61\ V \qquad [5]$$

$$\mathbf{4\text{-}36} \rightarrow \frac{1}{2}\mathbf{4\text{-}14} + \frac{1}{2}\mathbf{4\text{-}34} + e^-, \quad E_{pa} = -1.0\ V \qquad [6]$$

The first electrochemically irreversible reduction event at $E_{pc} = -1.90$ V (eqn [1]) has been assigned to the splitting of one Sn–Fe bond, which results in the formation of the anionic cluster $[\{CpFe(CO)_2\}\{Sn_5Dep_6\}]^-$ (**4-36**, also isolated and characterized) and '$[FeCp(CO)_2]^{\bullet}$.' At this potential, the resulting fragment '$[FeCp(CO)_2]^{\bullet}$' immediately dimerizes to form a half of an equivalent of $[FeCp(CO)_2]_2$. The second reduction process in the CV of **4-34** ($E_{pc} = -2.24$ V) has been assigned to the reductive splitting of $[FeCp(CO)_2]_2$ into two anionic $[FeCp(CO)_2]^-$ fragments (overall a one-electron process, eqn [2]). It is reasonable to assume that the most negative reduction process at $E_{pc} = -2.93$ V again leads to a splitting of the Fe–Sn bond in $[\{CpFe(CO)_2\}\{Sn_5Dep_6\}]^-$ (**4-36**) the formation of $[\mathbf{4\text{-}34}]^{2-}$, and to a reduction of the resulting '$[FeCp(CO)_2]^{\bullet}$' fragment at this potential (eqn [3], two-electron process). The broad oxidation peak around $E_{pa} \approx -2.75$ V in the return sweep has been assigned to the re-formation of **4-36** (eqn [4]; reverse of eqn [3]). The oxidation event at $E_{pa} = -1.61$ V belongs to the re-oxidation of $[FeCp(CO)_2]^-$ as known from the literature (eqn [5]). The most positive oxidation event at $E_{pa} = -1.0$ V corresponds to a very interesting disproportionation reaction (eqn [6]), further supported by the reaction of the anionic cluster **4-36** with one equivalent of [Fc][PF] (with $[PF]^- = [Al\{OC(CF_3)_3\}_4]^-$). By summing up all equations

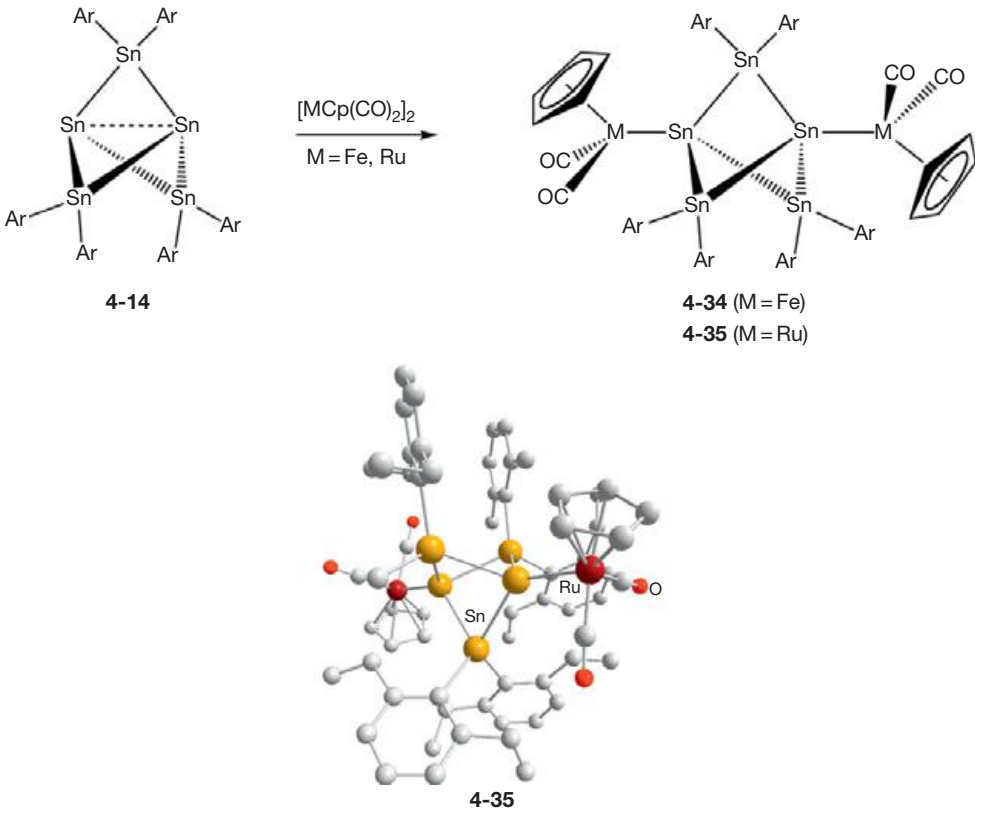

4-14

4-34 (M = Fe)
4-35 (M = Ru)

4-35

Scheme 28 Synthesis of the metal-terminated bicyclo[1.1.1]pentastannanes **4-34** and **4-35** (Ar = Dep) (top); molecular structure of **4-35** (bottom).

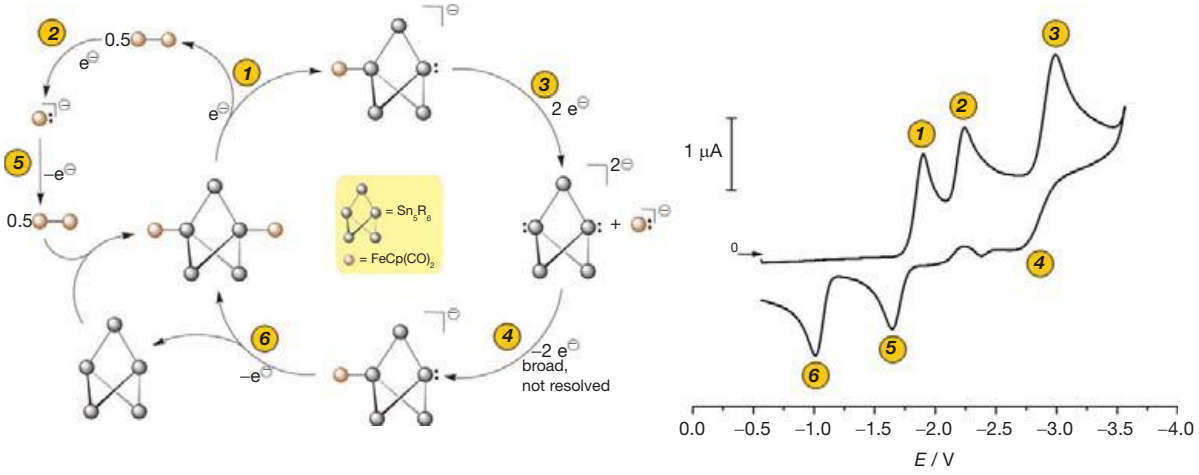

Figure 5 Proposed cascade of bond-breaking and bond-making processes during the chemically reversible but electrochemically irreversible redox cycle of **4-34**; the numbers correspond to the equations given above (potentials vs. the Fc/Fc^{+} couple). The figure was reproduced with permission of ACS (copyright 2010, Organometallics 29 (2010) 6028).

and assumptions, the authors were able to propose the mechanism depicted in Figure 5. The complicated, though very appealing, reduction chemistry of **4-34** in THF consists of a cascade of bond-breaking and bond-making processes, fully in accord with the chemically reversible redox cycle of **4-34** consisting of electrochemical irreversible couples.

The biradicaloid nature of heavy propellanes was further demonstrated by the addition of the disulfide FcS–SFc (Fc = ferrocenyl) to the bridgehead atoms of the heteronuclear propellanes **4-24** and **4-25**. The disulfide undergoes homolytic S–S bond cleavage affording the 1,3-disubstituted bicyclo[1.1.1]pentane derivatives **4-37** and **4-38** depicted in Scheme 29. X-ray structure analyses of the products revealed that the addition of the $FcS^{\bullet}$ fragments to the bridgehead atoms has only a limited geometric impact: the nonbonded Sn–Sn distance in **4-38**, for instance, is only slightly longer than

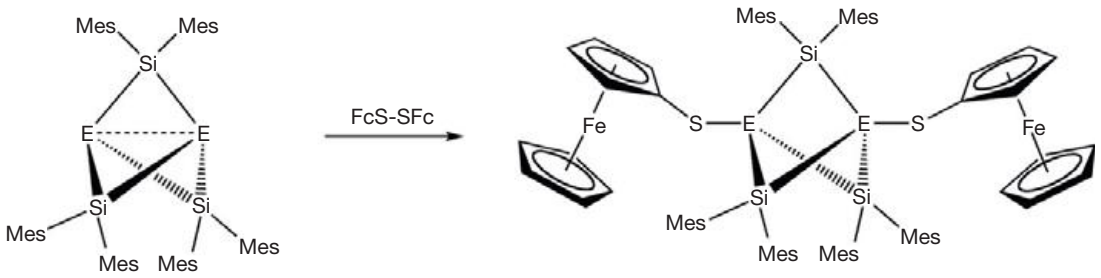

E = Ge (**4-24**), Sn (**4-25**)

E = Ge (**4-37**), Sn (**4-38**)

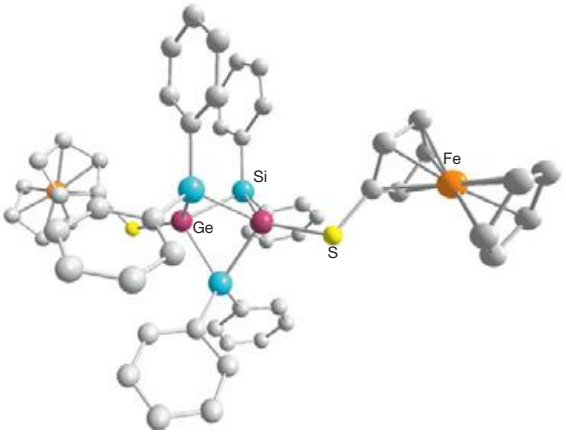

4-37

Scheme 29 Synthesis of the symmetrical bicyclo[1.1.1]pentane derivatives **4-37** and **4-38** (top); molecular structure of compound **4-37** (bottom).

$Sn_b \cdots Sn_b$ in **4-25**. Note that for other substrates even 'shorter' distances have been detected for the corresponding bicyclo[1.1.1]pentane derivatives as compared to the [1.1.1]propellane parent systems.[141] Again, similar effects are known from 1,3-disubstituted all-carbon bicyclo[1.1.1]pentanes.[97d] Most importantly, it was shown that addition reaction of FcSSFc to the heavy [1.1.1]propellanes can be drastically enhanced by daylight in the lab (NMR spectroscopic monitoring of the conversion).

1.15.4.3 Other Tin- or Germanium-Centered Biradicaloids

The first 1,3-diaza-2,4-distannacyclobutanediyl was communicated by Cox and Lappert.[142] Colorless, diamagnetic (EPR investigations for $T = 4$–298 K) crystals of $(ClSn)_2(NSiMe_3)_2$ (**4-39**) were isolated in moderate yield in an unusual (and unexpected) reaction of dimeric $[Sn(Cl)N(SiMe_3)_2]_2$ with AgOCN (Scheme 30). The authors attribute the driving force of the reaction to the oxophilicity of silicon.

An X-ray structure analysis on single crystals of **4-39** revealed a planar centrosymmetric four-membered Sn_2N_2 heterocycle with the nitrogen atoms slightly pyramidalized and the chlorine substituents arranged in a *trans* fashion. The transannular Sn···Sn separation of 339.8 pm was found to be relatively long. Interestingly, secondary *inter*molecular $(Sn \cdots Cl)_2$ contacts (329 pm) between two neighboring Sn_2N_2 rings were found in the solid state (confirmed by cross-polarization-magic angle spinning (CP-MAS) ^{119}Sn NMR spectroscopy). Furthermore, quantum chemical calculations predicted the singlet state to be favored by 57–76 kJ mol^{-1} ($-\Delta E_{S\text{-}T}$), depending on whether scalar relativistic effects were considered. Despite this relatively small singlet–triplet gap, Cox and Lappert suggested that the most appropriate description of **4-39** is a 6π-electron four-center system (pseudo-aromatic). Furthermore, a VB structure was proposed, which is in close relationship to the one proposed above for the Niecke-type biradicals (cf. Scheme 3).

A similar structural motif has been found recently by Clyburne and coworkers.[143] The carboxylate coordination within the 1,3-diaza-2,4-distannacyclobutanediyl (**4-40**) was found to be terminal monodentate (Scheme 30). The nitrogen atoms in **4-40** are almost trigonal planar and the tin atoms show trigonal pyramidal geometry. The Sn···Sn separation of 338.96 pm in **4-40** suggested no transannular bonding. DFT calculations (B3LYP/LANL2DZ) on a model compound of **4-40**, namely $[HCO_2Sn(\mu\text{-}NSiMe_3)]_2$, have provided some insight into the bonding of **4-40**, which shows some parallels to **4-39**. The singlet was found to be more stable by 54 kJ mol^{-1} than the triplet, which is consistent with the value of 76 kJ mol^{-1} reported by Lappert for compound **4-39**. The authors stated that "it is tempting to suggest that a standard four-centered six-π electron system is at play in **4-40**, but this clearly oversimplifies the situation given the well-recognized poor 5p–π 2p–π overlap that would be required between the tin and nitrogen atoms".[143] Other substituent effects have also

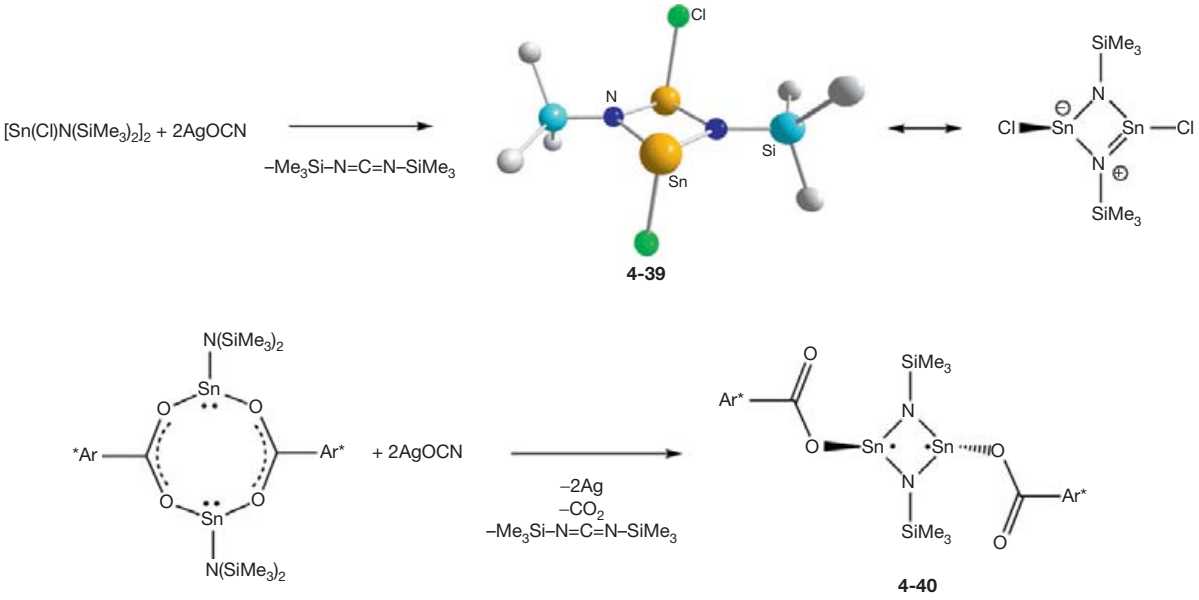

Scheme 30 Synthesis of 1,3-diaza-2,4-distannacyclobutanediyls **4-39** (top) and **4-40** (bottom) Ar* = 2,6-$Mes_2C_6H_3$.

been discussed in order to account for the planarity of the Sn_2N_2 heterocycle. Furthermore, it was also pointed out that the HOMO of **4-40** is located primarily on the N atoms (cf. Niecke-type biradicals (Scheme 3), where the HOMO is also primarily based on the more electronegative carbon instead of the phosphorus atoms).

The multiply bonded Ar′GeGeAr′ (**4-41**) species[144] also merit attention in the context of main group biradicaloids. The unusual structures of the heavy REER entities, showing *trans*-bent (C_{2h}) structures in the solid state, with increased deviation from linearity and decreased bonding interaction upon descending the group 14, have dramatic influences on their reactivities.[145] For instance, in 2005, it was shown by the Power group that the Ge and Sn alkyne analogs Ar′EEAr′ (**4-V**; Ar′=C_6H_3-2,6(C_6H_3-2,6-iPr_2)$_2$) react with H_2 under ambient conditions to give the hydrogenated products shown in Scheme 31.[146] Computational studies predicted the initial step of these reactions to involve a synergic interaction of the frontier orbitals of Ar′SnSnAr′ with H_2.[147] Comparable orbital interactions have been proposed for the reversibly ethylene activation of Ar′SnSnAr′,[148] However, it was also discussed that the H_2 activation by Ar′GeGeAr′ might also originate in part from the singlet biradical character of the ground state (see resonance structure in Scheme 31),[149–151] which has also been predicted for multiply bonded group 13 compounds.[152] In contrast, investigations of Tokitoh and coworkers[153] on a closely related digermyne (BbtGeGeBbt) (**4-42**, Bbt = 2,6-bis [bis(trimethylsilyl)methyl]-4-[tris(trimethylsilyl)methyl]phenyl) showed no biradical behavior in the reactions with H_2O, Et_3SiH, and 2,3-dimethyl-1,3-butadiene.

Nonetheless, Power and coworkers[154] used the triply bonded species as starting materials for various exciting compounds. For instance, the Ge_2N_2 heterocyclic compound, namely (Ar′Ge)$_2$(μ-$NSiMe_3$)$_2$ (**4-43**), consisting of large aryl substituents attached to germanium, has been prepared (Scheme 31). Air- and moisture-sensitive, dark-violet crystals of **4-43** were isolated in high yield upon treatment of Ar′GeGeAr′ (**4-41**) with Me_3SiN_3. In the solid state, **4-43** adopts a perfectly planar Ge_2N_2 core featuring trigonal-planar coordinated nitrogen (Σ° = 359.97(8)°) and pyramidal germanium (Σ° = 322.10(7)°) constituents. The bulky aryl substituents are situated in a *trans* fashion. The Ge···Ge separation of 275.5 pm is about 30 pm longer than a normal Ge–Ge single bond. Compound **4-43** is EPR silent between 77 and 300 K. The calculated HOMO mainly corresponds to a nonbonding combination centered on the germanium atoms with weak Ge–C (and minor nitrogen) components. The singlet–triplet separation was calculated to be $\Delta E_{S-T} = -17.5$ kcal mol^{-1}. The HOMO–LUMO gap of 58.0 kcal mol^{-1} directly corresponds to the energy difference (54.9 kcal mol^{-1}), which was extracted from UV/Vis experiments ($\lambda_{max} = 521$ nm) of **4-43**. Solutions of **4-43** in several solvents (benzene, toluene, and cyclohexane) gradually faded to pale yellow over time and it was speculated that hydrogen abstraction from the solvent was the cause. Compound **4-43** readily adds of H_2 to give a product that has been tentatively identified as Ar′(H)Ge(μ-$NSiMe_3$)$_2$Ge(H)Ar′ (**4-45**). In a further study, Power et al. reacted Ar′GeGeAr′ (**4-41**) with various other azides, which afforded an unexpected variety of products (a germanium amide, two imido derivatives, and a germanium(IV) ketimide), none of which resembles **4-43**. The results indicated that several different processes involving unusual intermediates, for example, a Ge (III) imido diradicaloid, Ge(IV) aminyl radical, C–S bond cleavage, N–H and N=C bond formation, and intra-CH-π (arene) and π(N)C-π(arene) interactions probably occur.[155]

A closely related, unsymmetric oxo/imido-bridged germanium-centered singlet biradicaloid (**4-44**) has been obtained by treatment of **4-41** with the nitrosoarene ONC_6H_4-2-CH_3 (Scheme 31)[156]. The purple-black species Ar′Ge(μ-O)(μ-NC_6H_4-2-CH_3)GeAr′ (**4-44**) was characterized by spectroscopy and X-ray crystallography. DFT calculations have also been performed. The structure of **4-44** has a planar

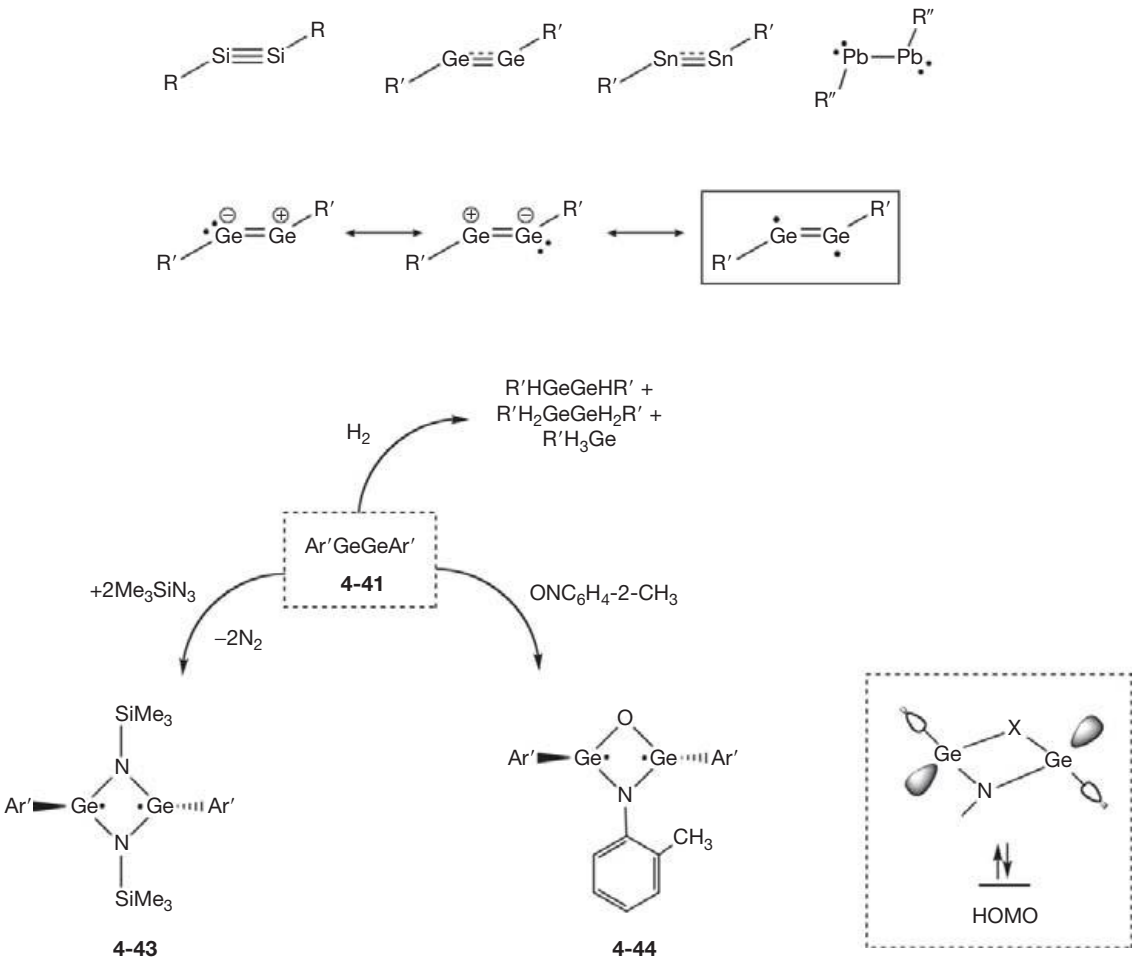

Scheme 31 Heavy REER (**4-V**) entities, showing *trans*-bent (C_{2h}) structures (top); resonance structures for Ar′GeGeAr′ (middle), and reactivity of **4-41** (bottom); HOMO of **4-44** (inset); R = Si(*i*Pr)(CH(SiMe$_3$)$_2$)$_2$, R′ = Ar′ = C$_6$H$_3$-2,6(C$_6$H$_3$-2,6-*i*Pr$_2$)$_2$, R″ = C$_6$H$_3$-2,6(C$_6$H$_3$-2,4,6-*i*Pr$_2$)$_2$.

GeNGeO core arrangement (d(Ge···Ge) = 272.8 pm) and the structural parameters are directly related to those observed for **4-43**. Typical diamagnetic ^{1}H and ^{13}C NMR spectra indicated a singlet ground state of **4-44**, which was found to be extremely air- and moisture-sensitive and, when exposed to the atmosphere, rapidly changes to a white powder that was shown to be a bisoxo-bridged germanium amide hydride. DFT calculations at the UB3LYP/6-31G* level on the model compound MeGe(μ-NH)(μ-O)GeMe (**4-46**) revealed that the HOMO is very similar to the one observed for **4-43**, for example, mainly located on the Ge atoms (calculated HOMO–LUMO gap = 55.3 kcal mol^{-1}, cf. 51.6 kcal mol^{-1} from UV/Vis).

Note that the reaction of **4-41** with the closely related ONC$_6$H$_5$ also gave Ar′Ge(μ-O)(μ-NPh)GeAr′ (**4-47**) as deduced from UV/Vis studies. However, the main reaction product was identified to be an inorganic bicyclo[2.2.0]hexane, namely Ar′Ge(η1,η1:μ$_2$-PhNO)$_2$GeAr′ (**4-48**, Scheme 32).[157] By using the related starting material 3,5-*i*Pr$_2$-Ar*GeGeAr*-3,5-*i*Pr$_2$ (3,5-*i*Pr$_2$-Ar* = C$_6$H-2,6-(C$_6$H$_2$-2,4,6-*i*Pr$_3$)$_2$-3,5-*i*Pr$_2$) (**4-49**) the analogous bicycle **4-50** was obtained. The compounds **4-48** and **4-50** feature different Ge···Ge bond distances (247.31 pm for **4-48**; and 254.03 pm for **4-50**) and represent two of the three possible conformational isomeric structures of the bicyclic biradicaloid system. Most importantly, both structures differ in the orientation of phenyl substituents: in **4-48** one Ph group is axial and the other is equatorial (*a*,*e*), whereas in **4-50** both Ph groups are in equatorial positions (*e*,*e*; denoted as Ph^a and Ph^e in Scheme 32). DFT calculations revealed that within the *e*,*e* isomer the π* orbitals of the flanking NO entities are orientated in such a way that they can interact with the antibonding orbital of the Ge–Ge bond. This leads to multicenter bonding along the OGeN ridges, which is antibonding with respect to the Ge–Ge vector, hence lengthening the Ge–Ge bond. In the case of the *a*,*a*, the above-mentioned interaction becomes unfavorable and hence a shorter Ge–Ge bond and a narrower C–Ge–Ge angle are expected.

1.15.5 Conclusion

More than two decades have passed since the first reports on the successful synthesis of main group biradicaloids appeared in the late 1980s and 1990s. Since then, several contributions to this stimulating research area have impressively extended the spectrum of these exciting molecules. This range includes

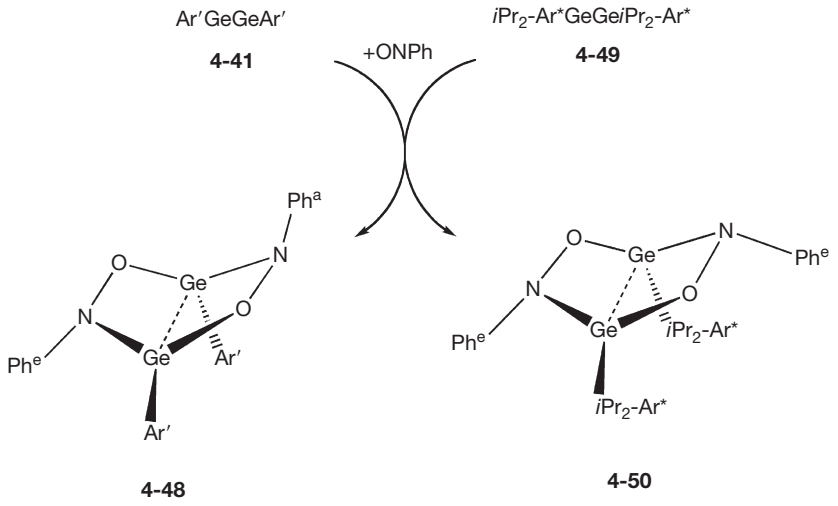

Scheme 32 Synthesis of the bicyclo[2.2.0]hexanes **4-48** and **4-50**; Ar′ = C_6H_3-2,6(C_6H_3-2,6-*i*Pr_2)$_2$; 3,5-*i*Pr_2-Ar* = C_6H-2,6-(C_6H_2-2,4,6-*i*Pr_3)$_2$-3,5-*i*Pr_2; Ph^a and Ph^e = axial and equatorial phenyl substituents.

fascinating electronic properties as well as closed-shell and radical-type reactivities. All these aspects can mainly be attributed to the inclusion of heavier main group elements into the biradicaloid scaffolds providing the essential electronic and structural flexibilities. The recent discoveries in this area will clearly draw more attention to this and other classes of main group biradicaloids. These types of molecules are poised to be further developed and extended to other systems, including those not recognized as such yet, and spectacular results are likely to occur. The catenation of biradicaloids is becoming better established and, given the importance of this field, further developments can be expected here. Although many questions regarding fundamental and applied aspects have to be answered and some classes of biradicaloids are still in its infancy, further perspectives and interesting advancements for these molecules are now emerging. Further findings will be awaited with excitement. For related chapters in this Comprehensive, we refer to Chapters 1.13 and 1.14.

1.15.6 Notes Added in the Proof

During the production of this chapter, some interesting results have been published, which are concisely summarized as follows (without any claim to completeness):

Both spectroscopic and stability studies, as well as the investigation of the electronic nature of 1,3-diphosphacyclobutane-2,4-diyls remain an area of current interest. The stability of Yoshifuji-type unsymmetrical biradicals **2-III** (cf. Section 1.15.2; R^1 = *t*Bu, R^2 = CH_2Ph (**2-8**), CH_2OMe (**6-1**), and $CH_2C{\equiv}CH$ (**6-2**)) has been investigated both experimentally and computationally. The latest studies suggest that the nature of the substituents on the phosphorus atoms has a significant effect on the air stability of the P-heterocyclic biradicals. While the cyclic biradical structure is effectively stabilized by the presence of a benzyl or an electron-withdrawing methoxymethyl group, the propargyl-substituted analog shows remarkable instability in air. This difference is supported by DFT calculations (B3LYP/6-311 G(d)) of model compounds (R^1 = Me, R^2 = CH_2OMe (**6-1a**), and $CH_2C{\equiv}CH$ (**6-2a**)), which show that the LUMO energy of the latter is considerably lowered, thus facilitating the reaction with water to destroy the cyclic biradical skeleton.[158]

In an effort to understand the electronic nature of 1,3-diphosphacyclobutane-2,4-diyls and its heavier analogs, Schoeller and co-workers employed DFT and wave-depending quantum chemical methods.[159] Calculations performed on the model compounds $(XHYH)_2$ (**6-I**) (X = N, P; Y = C, Si, Ge) show that the corresponding singlet–triplet energy separations ($-\Delta E_{S-T}$) are in the range of 10–20 kcal mol^{-1}, confirming their biradicaloid nature. Furthermore, an investigation of the influence of the substituents on the phosphorus atoms in 1,3-diphosphacyclobutane-2,4-diyls at the BP86-D/TZVP level of theory has been performed. The results highlight the strong effect of the pyramidalization of the P atoms on the ΔE_{S-T}, which concomitantly reflects on the biradicaloid nature of the species. The biradical nature is fostered by σ-attracting substituents, which cause a strong pyramidalization force at the phosphorus center, thus decreasing the singlet–triplet separation and inhibiting possible cyclic π-delocalization.

Sekiguchi and co-workers have recently succeeded in the isolation of the unprecedented and elusive 1,3-diaza-2,4-disilacyclobutanediyl $(RSi)_2(NAr)_2$ (**6-3**) (R = *i*PrSi[CH$(SiMe_3)_2$]$_2$, Ar = 3,5-$Me_2C_6H_3$) obtained from the reaction of the disilyne RSi≡SiR and *cis*-3,3′,5,5′-tetramethylazobenzene.[160] The solid-state structure of **6-3** exhibits a planar centrosymmetric Si_2N_2 ring in which no Si–Si bonding interaction is observed (263.8 pm). Spectroscopic studies suggest a singlet ground state for **6-3** and the singlet-triplet energy gap of $-\Delta E_{S-T}$ = 12.8 kcal mol^{-1} calculated for the model compound **6-3a** (R = $SiMe_3$, Ar = Ph) supported this hypothesis. However, when **6-3** was reacted with MeOH and CCl_4, it exhibited both closed-shell and radical-type reactivity, respectively, in agreement with the observations for other singlet biradicaloid molecules containing stretched Si–Si interactions (cf. **4-18** in Section 1.15.4.2).[105,124]

The study of localized singlet carbon-centered biradical species and the proper description of their electronic nature

has remained a matter of high importance, in particular due to the crucial role they play as key intermediates in chemical reactions involving homolytic cleavage and formation of covalent chemical bonds. A recent review elaborates on the concept that the ground-state spin-preference in 1,3-diradicals is a result of the balance of 'through space' (TS) and 'through bond' (TB) interactions between the two radical p orbitals, since these interactions have a contribution in determining the corresponding singlet–triplet energy gap (ΔE_{S-T}). Further substituent and heteroatom effects on the spin preference and the most stable electronic configuration of the singlet state were also analyzed. Additionally, a summary on the synthesis and characterization of long-lived carbon-centered biradicals and their intra- and intermolecular reactivity is presented.[161]

Schulz and co-workers have reported the unprecedented neutral all-pnictogen heterocycles $P_2(NR)_2$ (R = Hyp (**6-4**), Ter (**6-5**); Hyp = $Si(SiMe_3)_3$, Ter = C_6H_3-2,6-(C_6H_2-2,4,6-Me_3)$_2$), which are formally aromatic and exhibit an unusual biradicaloid bond situation.[162] Both **6-4** and **6-5** were obtained from the reduction of $(PCl)_2(NR)_2$ with the mild reducing agent $(Cp_2TiCl)_2$, but it was recognized that steric shielding plays an important role in stabilizing the biradicaloid species: While **6-5** can be isolated in large quantities and is stable up to 224°C, **6-4** decomposes readily in solution. In addition to its steric effect, the substituent has an effect on the biradical character, as observed for **6-4**, where it is increased by pushing electron density to the P_2N_2 ring when compared to **6-5** ($\Sigma q(N_2P_2) = -1.22e$ (**6-4**), $-0.41e$ (**6-5**)). Both NMR spectroscopic data ($\delta(^{31}P) = 289.8$ ppm) and quantum chemical calculations (NICS(0) = −6 ppm) indicate that **6-5** exhibits an aromatic character, where 6 π electrons are delocalized in the four-membered heterocycle. This delocalization stabilizes the biradicaloid and prevents the formation of a bicycle by hindering a transannular TS interaction (P···P 261.9 pm) in the planar N_2P_2 ring, which lies in a sterically protected pocket formed by the four mesityl rings of the Ter substituents. Computational studies (UB3LYP/6-311 + G(d,p)// 6-31 G(d,p)) yielded a ΔE_{S-T} value of −22.6 kcal mol^{-1}, while UHF and CASSCF(2,2)/6-31 G(d) calculations indicate a HOMO occupation of 1.7, which is consistent with the calculations for Niecke's biradicaloids.[21,22]

Another system exhibiting singlet biradicaloid character with extensive electronic delocalization is the novel 2,4-diimino-1,3-disilacyclobutanediyl $(RSi)_2(CNAr)_2$ (**6-6**) (R = PhC(N*t*Bu)$_2$, Ar = 2,6-*i*Pr$_2$C$_6$H$_3$), in which the amidinate ligand aids the stabilization of this main-group analog of 2,4-dimethylene-1,3-cyclobutanediyl.[163] Compound **6-6** was isolated in 26% yield from the reaction of three equivalents of RSi≡SiR with two equivalents of ArN = C = NAr. Compound **6-6** is EPR silent both at room temperature and at −100 °C, indicating a singlet ground state. Its solid-state structure contains a planar Si_2C_2 four-membered ring in which no Si...Si bonding interaction is observed (255.3(1) pm). The $-\Delta E_{S-T}$ calculated at the B3PW91/6-31 G(d) level amounts to 30.1 kcal mol^{-1}, supporting the experimental observation that the ground state is a singlet. DFT calculations (B3PW91/6-311 + G(d,p)) on the model compound $(RSi)_2(CNH)_2$ (**6-6a**) revealed that the biradical (2.028 electrons) are distributed among the Si–N σ* orbitals and the exocyclic C = N π* orbitals. Such delocalization is also supported by the value of nucleus-independent chemical shift (NICS(0) = −14.57 ppm). Finally, the biradicaloid character of **6-6a** was illustrated by CASSCF(4,6) calculations, which indicate HOMO/LUMO occupations of 1.86/0.13.

With regard to the theoretical description of the electronic structure and energetics of biradical(oid)s, Lopez and co-workers reported that PNOF (Piris natural orbital functional) is a suitable method to describe them accurately, since it offers a correct treatment of near-degeneracy effects.[164] NOF theory describes the electronic structure of a molecule in terms of the natural orbitals and their occupation numbers. The performance of the restricted functional PNOF4 in the description of biradical(oid)s was evaluated by analyzing a series of molecules with various degrees of biradical character.

A quantum chemical study (B3LYP/aug-cc-pVDZ/aug-cc-pVTZ) on 2-chalcogen-trisilabicyclo[1.1.0]butane compounds $Si_3ER_2R'_2$ (R = H, CH_3, SiH_3, *t*Bu, $SiMe_3$; R′ = SiH_3; E = S, Se) was done in order to investigate the factors controlling the bond-stretch isomerism phenomenon.[165] Besides the known short-bond (**6-7a**) and long-bond isomers (**6-7b**) for $Si_3ER_2R'_2$, a further conformer **6-7c** containing a significantly elongated central bond (Si···Si = 310–330 pm) and exhibiting an *anti* arrangement of the bridgehead substituents was found. This report suggests that while the planar **6-7c** isomer provides the most favorable ligand arrangement for bulky groups, it features the weakest Si···Si interaction and therefore lies higher (5–11 kcal mol^{-1}) in energy than the corresponding most stable short- or long-bond isomers. Additionally, the heavier analogs $Si_2GeSR_2R'_2$ (**6-8**), $SiGe_2SR_2R'_2$ (**6-9**), and $Ge_3SR_2R'_2$ (**6-10**) (R = SiH_3, R′ = H, CH_3, SiH_3, *t*Bu, $SiMe_3$) were also investigated. For Ge-containing **6-9** and **6-10**, the increased Ge···Ge distance allows a favorable arrangement of the bridgehead substituents in the long-bond isomer, thus decreasing the destabilization caused by steric repulsion. The elongated bridging bonds in **6-9** and **6-10** lead to planar isomers comparable in energy ($\Delta E < 5$ kcal mol^{-1}) to the most stable long-bond isomers when bulky bridgehead substituents are employed. Therefore, it has been suggested that such 2-thia-trimetallabicyclo[1.1.0]butanes would be promising synthetic targets.

A new main group cluster compound of the formula $Sn_4Si\{Si(SiMe_3)_3\}_4\{SiMe_3\}_2$ (**6-11**) has been reported by Schnepf and co-workers.[166] It was found that the steric demand of the bulky silyl ligands forces two threefold-coordinated tin atoms in an almost planar arrangement ($d = 382$ pm). Quantum chemical calculations on the model compound **6-11a** showed a strong dependence of the bonding situation (biradical vs. biradicaloid vs. closed-shell species) with varying arrangement of the attached ligands. Relatively sharp transitions have been detected for certain conformations.

The chemistry of [1.1.1]propellanes of group 14 (cf. Section 1.15.4.2) is further developing. In a recent study, Scheschkewitz and co-workers reported on another silicon propellane, namely Si_6Tip_6 (**6-12**),[167] which shows the typical propellane core structure (distance between the bridgehead atoms, d(Si...Si) = 270,76 pm) with two flanking $Si(Tip)_2$ entities replaced by $\{Si(Tip)\}_2SiTip_2$ moieties. All experimental results nicely correspond to those obtained for **4-18** (cf. Section 1.15.4.2). The reactivity of 5-11 has been investigated by treating the starting material with Br_2 and I_2, in each case furnishing the 1,5-dihalogenated derivatives. Compound **6-12**

has been designated as global minimum on the Si_6H_6 potential energy surface and thus the thermodynamic counterpart of benzene in the case of silicon.

In a recent study, the first alkynyl-functionalized bicyclo[1.1.1]pentanes of heavy group 14 elements, including a linked member of this new family, have been reported.[168] The novel compounds were synthesized by using the heteronuclear trisiladistanna[1.1.1]propellane **4-25** as starting material (cf. Section 1.15.4.2). NMR investigations revealed that the title compounds show significant 'through cage' communication effects, which can most likely be attributed to 'back-lobe-to-back-lobe'[169] interactions. For the alkynyl-bridged [1,1′]-bis(bicyclo[1.1.1]pentane) **6-13**, quantum chemical calculations predicted some conjugation along the rod-like scaffold.

Acknowledgments

We cordially thank Prof. H. Schnöckel for helpful and stimulating discussions and Prof. M. Yoshifuji, Prof. H. M. Tuononen, and Prof. T. Chivers for generously providing unpublished results.

References

1. (a) Gomberg, M. *Ber. Dtsch. Chem. Ges.* **1900**, *33*, 3150–3163; (b) Gomberg, M. *J. Am. Chem. Soc.* **1900**, *22*, 757–771.
2. Stable radicals can be isolated and handled as a pure compound, whereas radicals that are sufficiently long-lived to be observed using conventional spectroscopic methods but cannot be isolated are classified as persistent. Griller, D.; Ingold, K. U. *Acc. Chem. Res.* **1976**, *9*, 13–19.
3. Hicks, R. G. *Org. Biomol. Chem.* **2007**, *5*, 1321–1338.
4. Spin labeling, spin trapping, EPR imaging, radical polymerization, or catalysis, just to mention a few. The interested reader is referred to (a) Hicks, R. G., Ed.; In *Stable Radicals – Fundamentals and Applied Aspects of Odd-Electron Compounds*; Wiley: New York, 2010; (b) Berliner, L. J., Eaton, G. R., Eaton, S. S., Eds.; In Kluwer: New York, 2002; Vol. 19; (c) Lund, A., Shiotani, M., Shimada, S., Eds.; In *Principles and Applications of ESR Spectrocopy*; Dortrecht: Springer, 2011; (d) Brustolon, M., Giamello, E., Eds.; In *Electron Paramagnetic Resonance – A Practitioners Toolkit*; Wiley: New York, 2009.
5. Reviews: (a) Rajca, A. *Chem. Rev.* **1994**, *94*, 871–893; (b) Miller, J. S. *Adv. Mater.* **2002**, *14*, 1105–1110; (c) Special issue on "Molecular Conductors" *Chem. Rev.* **2004** *104*(11).
6. Monographs: (a) Lahti, P. M., Ed.; *Magnetic Properties of Organic Materials*; Marcel Dekker: New York, 1999; (b) Nalwa, H. S., Ed.; *Handbook of Organic Conductive Molecules and Polymers*; Wiley: New York, 1997; (c) Itoh, K., Kinoshita, M., Eds.; In *Molecular Magnetism, New Magnetic Materials*; Gordon and Breach: Amsterdam, 2000.
7. For selected references on interesting sulphur-nitrogen compounds see (a) Cordes, A. W.; Haddon, R. C.; Oakley, R. T. *Adv. Mater.* **1994**, *6*, 798–802; (b) Cordes, A. W.; Haddon, R. C.; Oakley, R. T. In *The Chemistry of Inorganic Ring Systems*; Steudel, R., Ed.; Elsevier: Amsterdam, 1992; (c) Rawson, J. M.; Alberola, A.; Whalley, A. *J. Mater. Chem.* **2006**, *16*, 2560–2575.
8. Power, P. P. *Nature* **2010**, *463*, 171–177.
9. Chivers, T.; Konu, J. *Comments Inorg. Chem.* **2009**, *30*, 131–176.
10. Power, P. P. *Chem. Rev.* **2003**, *103*, 789–810.
11. Lee, V. Y.; Nakamoto, M.; Sekiguchi, A. *Chem. Lett.* **2008**, *37*, 128–133.
12. Breher, F. *Coord. Chem. Rev.* **2007**, *251*, 1007–1043.
13. Selected references: (a) Borden, W. T. In *Encyclopaedia of Computational Chemistry*; von Schleyer, P. R., Ed.; Wiley: New York, 1998; pp 708–722; (b) In *Diradicals*; Borden, W. T., Ed.; Wiley: New York, 1982; (c) Moss, R. A.; Platz, M. S.; Jones, M., Jr. Eds.; *Reactive Intermediate Chemistry*. Wiley-Interscience: New York, 2004; (d) Berson, J. A. *Acc. Chem. Res.* **1997**, *30*, 238–244; (e) Berson, J. A. *Acc. Chem. Res.* **1978**, *11*, 446–453; (f) Wenthold, P. G.; Lineberger, W. C. *Acc. Chem. Res.* **1999**, *32*, 597–604; (g) Dougherty, D. A. *Acc. Chem. Res.* **1991**, *24*, 88–94.
14. For some details on the spin preferences in biradicals see Refs. [12,13], and (a) Salem, L.; Rowland, C. *Angew. Chem.* **1972**, *84*, 86–106; *Angew. Chem. Int. Ed.* **1972**, *11*, 92–111; (b) Borden, W. T.; Iwamura, H.; Berson, J. A. *Acc. Chem. Res.* **1994**, *27*, 109–116; (c) Bonačić-Koutecký, V.; Koutecký, J.; Michl, J. *Angew. Chem.* **1987**, *99*, 216–236; *Angew. Chem. Int. Ed.* **1987**, *26*, 170–189.
15. For substituent effects on the singlet ground state of localized singlet biradicals see for instance (a) Abe, M.; Ishihara, C.; Kawanami, S.; Masuyama, A. *J. Am. Chem. Soc.* **2005**, *127*, 10–11; (b) Hamaguchi, M.; Nakaishi, M.; Nagai, T.; Nakamura, T.; Abe, M. *J. Am. Chem. Soc.* **2007**, *129*, 12981–12988; (c) Zhang, D. Y.; Hrovat, D. A.; Abe, M.; Borden, W. T. *J. Am. Chem. Soc.* **2003**, *125*, 12823–12828; (d) Abe, M.; Adam, W.; Heidenfelder, T.; Nau, W. M.; Zhang, X. Y. *J. Am. Chem. Soc.* **2000**, *122*, 2019–2026; (e) Abe, M.; Adam, W.; Borden, W. T.; Hattori, M.; Hrovat, D.; Nojima, M.; Nozaki, K.; Wirz, J. *J. Am. Chem. Soc.* **2004**, *126*, 574–582; (f) Nakamura, T.; Gagliardi, L.; Abe, M. *J. Phys. Org. Chem.* **2010**, *23*, 300–307.
16. (a) Wittig, G.; Klein, A. *Ber. dtsch. Chem. Ges. A/B* **1936**, *69*, 2087–2097; (b) Seel, F. *Naturwissenschaften* **1946**, *33*, 60–61; (c) Dewar, M. J. S.; Healy, E. F. *Chem. Phys. Lett.* **1987**, *141*, 521–524.
17. Soleilhavoup, M.; Bertrand, G. *Bull. Chem. Soc. Jpn.* **2007**, *80*, 1241–1252.
18. (a) Chapter 1.17. (b) Chivers, T. *Chem. Rev.* **1985**, *85*, 341–365; (c) Chivers, T. *A Guide to Chalcogen-Nitrogen Chemistry*. World Scientific: Singapore, 2005.
19. For interesting bonding models for 1,5-$R_4P_2N_4S_2$ see (a) Chivers, T.; Hilts, R. W.; Jin, P.; Chen, Z.; Lu, X. *Inorg. Chem.* **2010**, *49*, 3810–3815; (b) Rzepa, H. S. *Nature Chem.* **2009**, *1*, 510–512; (c) Zhang, Q.; Yue, S.; Lu, X.; Chen, Z.; Huang, R.; Zheng, L.; von, R.; Schleyer, P. *J. Am. Chem. Soc.* **2009**, *131*, 9789–9799 original paper: (d) Burford, N.; Chivers, T.; Codding, P. W.; Oakley, R. T. *Inorg. Chem.* **1982**, *21*, 982–986.
20. (a) Konu, J.; Chivers, T. In *Stable Radicals – Fundamentals and Applied Aspects of Odd-Electron Compounds*; Hicks, R. G., Ed.; Wiley: New York, 2010; (b) Recent calculations revealed that the diradical character is <10% for these compounds with weak transannular S···S interactions. A maximum was found for S_4N_4 (with two such bonds) but only ca. 5% for a series of 1,5–$R_4P_2N_4S_2$ derivatives. Furthermore, a low energy triplet state was detected for S_4N_4. Tuononen, H. M.; Moilanen, J.; Chivers, T., unpublished results (personal communication).
21. Niecke, E.; Fuchs, A.; Baumeister, F.; Nieger, M.; Schoeller, W. W. *Angew. Chem.* **1995**, *107*, 640–642; *Angew. Chem. Int. Ed.* **1995**, *34*, 555–557.
22. Schmidt, O.; Fuchs, A.; Gudat, D.; Nieger, M.; Hoffbauer, W.; Niecke, E.; Schoeller, W. W. *Angew. Chem.* **1998**, *110*, 995–998; *Angew. Chem. Int. Ed.* **1998**, *37*, 949–952.
23. Sugiyama, H.; Ito, S.; Yoshifuji, M. *Angew. Chem.* **2003**, *115*, 3932–3934; *Angew. Chem. Int. Ed.* **2003**, *42*, 3802–3804.
24. Sugiyama, H.; Ito, S.; Yoshifuji, M. *Chem. Eur. J.* **2004**, *10*, 2700–2706.
25. Yoshifuji, M.; Arduengo, A. J., III; Ito, S. *Phosphorus, Sulfur Silicon Relat. Elem.* **2008**, *183*, 335–339.
26. Ito, S.; Kikuchi, M.; Sugiyama, H.; Yoshifuji, M. *J. Organomet. Chem.* **2007**, *692*, 2761–2767.
27. Ito, S.; Miura, J.; Morita, N.; Yoshifuji, M.; Arduengo, A. J., III *C. R. Chimie* **2010**, *13*, 1180–1184.
28. (a) Yoshifuji, M. private communication; (b) Yoshifuji, M.; Osborn, S. T.; Arduengo III, A. J.; Belmore, K. A.; Ito, S., *Heteroatom. Chem.* **2011**, *22*, 331–338; (c) Yoshifuji, M.; Osborn, S. T.; Arduengo III, A. J.; Belmore, K. A.; Ito, S. *Phosphorus, Sulfur Silicon Relat. Elem.* **2011**, *186*, 845–846.
29. For further information see: Schoeller, W. W.; Begemann, C.; Niecke, E.; Gudat, D. *J. Phys. Chem. A* **2001**, *105*, 10731–10738.
30. Yoshifuji, M.; Sugiyama, H.; Ito, S. *J. Organomet. Chem.* **2005**, *690*, 2515–2520.
31. Ito, S.; Miura, J.; Morita, N.; Yoshifuji, M.; Arduengo, A. J., III *Z. Anorg. Allg. Chem.* **2009**, *635*, 488–495.
32. Ito, S.; Miura, J.; Morita, N.; Yoshifuji, M.; Arduengo, A. J., III *Angew. Chem.* **2008**, *120*, 6518–6521; *Angew. Chem. Int. Ed.* **2008**, *47*, 6418–6421.
33. Ito, S.; Miura, J.; Morita, N.; Yoshifuji, M.; Arduengo, A. J., III *Heteroat. Chem.* **2010**, *21*, 404–411.
34. Niecke, E.; Fuchs, A.; Nieger, M. *Angew. Chem.* **1999**, *111*, 3213–3216 *Angew. Chem. Int. Ed.* **1999**, *38*, 3028–3031.
35. Sebastian, M.; Schmidt, O.; Fuchs, A.; Nieger, M.; Szieberth, D.; Nyulászi, L.; Niecke, E. *Phosphorus, Sulfur, and Silicon* **2004**, *179*, 779–783.
36. Sebastian, M.; Nieger, M.; Szieberth, D.; Nyulászi, L.; Niecke, E. *Angew. Chem.* **2004**, *116*, 647–651; *Angew. Chem. Int. Ed.* **2004**, *43*, 637–641.
37. Chen, Z.; Wannere, C. S.; Corminboeuf, C.; Puchta, R.; von Schleyer, P. R. *Chem. Rev.* **2005**, *105*, 3842–3888.
38. (a) Sekiguchi, A.; Matsuo, T.; Watanabe, H. *J. Am. Chem. Soc.* **2000**, *122*, 5652–5653; (b) Sekiguchi, A.; Tanaka, M.; Matsuo, T.; Watanabe, H. *Angew.*

Chem. **2001**, *113*, 1721–1723; *Angew. Chem. Int. Ed.* **2001**, *40*, 1675–1677; (c) Sekiguchi, A.; Matsuo, T.; Tanaka, M. *Organometallics* **2002**, *21*, 1072–1076.
39. Balci, M.; McLee, M. L.; von Schleyer, P. R. *J. Phys. Chem. A* **2000**, *104*, 1246–1255.
40. The open form of bis(phosphanyl)carbocations is not stable and forms cyclic, carbanionic valence isomer: (a) Kato, T.; Gornitzka, H.; Baceiredo, A.; Schoeller, W. W.; Bertrand, G. *Science* **2000**, *289*, 754–756; (b) see also Grützmacher, H. *Science* **2000**, *289*, 737–738; (c) Kato, T.; Gornitzka, H.; Baceiredo, A.; Schoeller, W. W.; Bertrand, G. *J. Am. Chem. Soc.* **2002**, *124*, 2506–2512.
41. Sebastian, M.; Hoskin, A.; Nieger, M.; Nyulászi, L.; Niecke, E. *Angew. Chem.* **2005**, *117*, 1429–1432; *Angew. Chem. Int. Ed.* **2005**, *44*, 1405–1408.
42. Niecke, E.; Fuchs, A.; Nieger, M.; Schmidt, O.; Schoeller, W. W. *Angew. Chem.* **1999**, *111*, 3216–3219; *Angew. Chem. Int. Ed.* **1999**, *38*, 3031.
43. Vignolle, J.; Cattoën, X.; Bourissou, D. *Chem. Rev.* **2009**, *109*, 3333–3384.
44. Yoshifuji, M.; Arduengo, A. J., III; Konovalova, T. A.; Kispert, L. D.; Kikuchi, M.; Ito, S. *Chem. Lett.* **2006**, *35*, 1136–1137.
45. Ito, S.; Miura, J.; Morita, N.; Yoshifuji, M.; Arduengo, A. J., III *Dalton Trans.* **2010**, *39*, 8281–8287.
46. Ito, S.; Miura, J.; Morita, N.; Yoshifuji, M.; Arduengo, A. J., III *Inorg. Chem.* **2009**, *48*, 8063–8065.
47. Scheschkewitz, D.; Amii, H.; Gornitzka, H.; Schoeller, W. W.; Bourissou, D.; Bertrand, G. *Science* **2002**, *295*, 1880–1881.
48. Bourg, J.-B.; Rodriguez, A.; Scheschkewitz, D.; Gornitzka, H.; Bourissou, D.; Bertrand, G. *Angew. Chem.* **2007**, *119*, 5843; *Angew. Chem. Int. Ed.* **2007**, *46*, 5741–5745.
49. Scheschkewitz, D.; Amii, H.; Gornitzka, H.; Schoeller, W. W.; Bourissou, D.; Bertrand, G. *Angew. Chem.* **2004**, *116*, 595–597; *Angew. Chem. Int. Ed.* **2004**, *43*, 585–587.
50. Rodriguez, A.; Olsen, R. A.; Ghaderi, N.; Scheschkewitz, D.; Tham, F. S.; Mueller, L. J.; Bertrand, G. *Angew. Chem.* **2004**, *116*, 4988–4991; *Angew. Chem. Int. Ed.* **2004**, *43*, 4880–4883.
51. Schoeller, W. W.; Rozhenko, A.; Bourissou, D.; Bertrand, G. *Chem. Eur. J.* **2003**, *9*, 3611–3617.
52. Jung, Y.; Head-Gordon, M. *Chem. Phys. Chem.* **2003**, *4*, 522–525.
53. Jung, Y.; Head-Gordon, M. *J. Phys. Chem. A* **2003**, *107*, 7475–7481.
54. (a) Head-Gordon, M.; *et al. Phys. Chem. Chem. Phys.* **2006**, *8*, 3172–3191; (b) Head-Gordon, M.; Beran, G. J. O.; Sodt, A.; Jung, Y. *J. Phys, Conf. Ser.* **2005**, *16*, 233–242.
55. Seierstad, M.; Kinsinger, C. R.; Cramer, C. J. *Angew. Chem.* **2002**, *114*, 4050–4052; *Angew. Chem. Int. Ed.* **2002**, *41*, 3894–3896.
56. Cheng, M.-J.; Hu, C.-H. *Mol. Phys.* **2003**, *101*, 1319–1323.
57. Salaneck, W. R., Lundstrom, L., Ranby, B., Eds.; In *Conjugated Polymers and Related Materials*; Oxford University Press: New York, 1993.
58. Rodriguez, A.; Tham, F. S.; Schoeller, W. W.; Bertrand, G. *Angew. Chem.* **2004**, *116*, 4984–4988; *Angew. Chem. Int. Ed.* **2004**, *43*, 4876–4880.
59. Rodriguez, A.; Fuks, G.; Bourg, J.-B.; Bourissou, D.; Tham, F. S.; Bertrand, G. *Dalton Trans.* **2008**, 4482–4487.
60. Bell, F.; Casanova, D.; Head-Gordon, M. *J. Am. Chem. Soc.* **2010**, *132*, 11314–11322.
61. Head-Gordon, M. *Chem. Phys. Lett.* **2003**, *372*, 508–511.
62. Gandon, V.; Bourg, J.-B.; Tham, F. S.; Schoeller, W. W.; Bertrand, G. *Angew. Chem.* **2008**, *120*, 161–165; *Angew. Chem. Int. Ed.* **2008**, *47*, 155–159.
63. Amii, H.; Vranicar, L.; Gornitzka, H.; Bourissou, D.; Bertrand, G. *J. Am. Chem. Soc.* **2004**, *126*, 1344–1345.
64. Fuks, G.; Saffon, N.; Maron, L.; Bertrand, G.; Bourissou, D. *J. Am. Chem. Soc.* **2010**, *131*, 13681–13689.
65. Fuks, G.; Donnadieu, B.; Sacquet, A.; Maron, L.; Bourissou, D.; Bertrand, G. *Main Group Chem.* **2010**, *9*, 101–109.
66. (a) Pankewitz, T.; Klopper, W.; Henke, P.; Schnöckel, H. *Eur. J. Inorg. Chem.* **2008**, 4879–4890; (b) Henke, P.; Pankewitz, T.; Klopper, W.; Breher, F.; Schnöckel, H. *Angew. Chem.* **2009**, *121*, 8285–8290; *Angew. Chem. Int. Ed.* **2009**, *48*, 8141–8145.
67. Uhl, W.; El-Hamdan, A. H. *Z. Anorg. Allg. Chem.* **2006**, *632*, 793–796.
68. Selected contributions to bicyclo[1.1.0]butanes chemistry: (a) Wiberg, K. B.; Ciula, R. P. *J. Am. Chem. Soc.* **1959**, *81*, 5261–5262; (b) Wiberg, K. B.; Lampman, G. M.; Ciula, R. P.; Connor, D. S.; Schertler, P.; Lavanish, J. *Tetrahedron* **1965**, *21*, 2749–2769 Theory: (c) Nguyen, K. A.; Gordon, M. S.; Boatz, J. A. *J. Am. Chem. Soc.* **1994**, *116*, 9241–9249; (d) Shevlin, P. B.; McKee, M. L. *J. Am. Chem. Soc.* **1988**, *110*, 1666–1671; (e) Hoz, S. In *The Chemistry of the Cyclopropyl Group*; Rappoport, Z., Ed.; Wiley: Chichester, 1987; Part 2, Chapter 19 Wiberg, K. B. *Adv. Alicycl. Chem.* **1968**, *2*, 185–254; (f) Koch, R.; Weidenbruch, M. *Angew. Chem.* **2002**, *114*, 1941–1943; *Angew. Chem. Int. Ed.* **2002**, *41*, 1861–1863.
69. (a) von Schleyer, P. R.; Sax, A. F.; Kalcher, J.; Janoschek, R. *Angew. Chem.* **1987**, *99*, 374–377; *Angew. Chem. Int. Ed.* **1987**, *26*, 364–366; (b) Schoeller, W. W.; Dabisch, T.; Busch, T. *Inorg. Chem.* **1987**, *26*, 4383–4389; (c) Collins, S.; Dutler, R.; Rauk, A. *J. Am. Chem. Soc.* **1987**, *109*, 2564–2569; (d) Boatz, J. A.; Gordon, M. S. *J. Phys. Chem.* **1988**, *92*, 3037–3042; (e) Dabisch, T.; Schoeller, W. W. *J. Chem. Soc., Chem. Commun.* **1986**, 896–898; (f) Nagase, S.; Kudo, T. *J. Chem. Soc., Chem. Commun.* **1988**, 54–56; (g) Boatz, J. A.; Gordon, M. S. *J. Phys. Chem.* **1989**, *93*, 2888–2891; (h) Hengge, E.; Janoschek, R. *Chem. Rev.* **1995**, *95*, 1495–1526; (i) Kudo, T.; Nagase, S. *J. Phys. Chem.* **1992**, *96*, 9189–9194; (j) Nagase, S.; Nakano, M. *Angew. Chem.* **1988**, *100*, 1098–1099; *Angew. Chem. Int. Ed.* **1988**, *27*, 1081–1083; (k) Yong Wang, Y.; Ma, J.; Inagaki, S. *J. Phys. Org. Chem.* **2007**, *20*, 649–655.
70. (a) Rohmer, M.-M.; Bénard, M. *Chem. Soc. Rev.* **2001**, *30*, 340–354; (b) Parkin, G. *Chem. Rev.* **1993**, *93*, 887–911 the concept of bond-stretch isomerism: (c) Stohrer, W.-D.; Hoffmann, R. *J. Am. Chem. Soc.* **1972**, *94*, 779–786; (d) Stohrer, W.-D.; Hoffmann, R. *J. Am. Chem. Soc.* **1972**, *94*, 1661–1668.
71. Koch, R.; Bruhn, T.; Weidenbruch, M. *J. Mol. Struc. (Theochem.)* **2004**, *680*, 91–97.
72. (a) Nagase, S. *Acc. Chem. Res.* **1995**, *28*, 469–476; (b) Zhao, M.; Gimarc, B. M. *Inorg. Chem.* **1996**, *35*, 5378–5386; (c) Kitchen, D. B.; Jackson, J. E.; Allen, L. C. *J. Am. Chem. Soc.* **1990**, *112*, 3408–3414.
73. Koch, R.; Bruhn, T.; Weidenbruch, M. *J. Mol. Struc. (Theochem.)* **2005**, *714*, 109–115.
74. Bader, R. F. W. *Atoms in Molecules: A Quantum Theory*. Oxford University Press: Oxford, UK, 1990.
75. Müller, T. In *Organosilicon Chemistry IV: From Molecules to Materials*; Auner, N., Weis, J., Eds.; Wiley-VCH: Weinheim, 2000.
76. (a) Jones, R.; Williams, D. J.; Kabe, Y.; Masamune, S. *Angew. Chem.* **1986**, *98*, 176–177; *Angew. Chem. Int. Ed.* **1986**, *25*, 173–174; (b) Masamune, S.; Kabe, Y.; Collins, S.; Williams, D. J.; Jones, R. *J. Am. Chem. Soc.* **1985**, *107*, 5552–5553.
77. Wiberg, N.; Auer, H.; Wagner, S.; Polborn, K.; Kramer, G. *J. Organomet. Chem.* **2001**, *619*, 110–131.
78. Kira, M.; Iwamoto, T.; Kabuto, C. *J. Am. Chem. Soc.* **1996**, *118*, 10303–10304.
79. Iwamoto, T.; Kira, M. *Chem. Lett.* **1998**, 277–278.
80. Ueba-Ohshima, K.; Iwamoto, T.; Kira, M. *Organometallics* **2008**, *27*, 320–323.
81. Kurosaki, K.; Kyushin, S.; Matsumoto, H.; Kyomen, T.; Hanaya, M. In 86th Annual Meeting of the Chemical Society of Japan, Chiba, Japan, 2006 March, Abstract 4F4-40.
82. In a very recent study, a structurally related, planar rhombic charge-separated tetrasilacyclobutadiene $Si_4(EMind)_4$ (EMind = 1,1,7,7-tetraethyl-3,3,5,5-tetramethyl-s-hydrindacen-4-yl) has been reported. As stated by the authors, CASSCF(4,4) calculations indicated only a low biradical character: (a) Suzuki, K.; Matsuo, T.; Hashizume, D.; Fueno, H.; Tanaka, K.; Tamao, K. *Science* **2011**, *331*, 1306–1309; (b) Apeloig, Y. *Science* **2011**, *311*, 1277–1278.
83. Iwamoto, T.; Yin, D.; Kabuto, C.; Kira, M. *J. Am. Chem. Soc.* **2001**, *123*, 12730–12731.
84. Kira, M. *J. Organomet. Chem.* **2004**, *689*, 4475–4488.
85. Iwamoto, T.; Yin, D.; Boomgaarden, S.; Kabuto, C.; Kira, M. *Chem. Lett.* **2008**, *37*, 520–521.
86. Lee, V. Y.; Yasuda, H.; Sekiguchi, A. *J. Am. Chem. Soc.* **2008**, *130*, 2758–2759.
87. Lee, V. Y.; Yasuda, H.; Sekiguchi, A. *J. Am. Chem. Soc.* **2007**, *129*, 2436–2437.
88. (a) Savin, A.; Flad, H.-J.; Flad, J.; Preuss, H.; von Schnering, H. G. *Angew. Chem.* **1992**, *104*, 185–186*Angew. Chem. Int. Ed.* **1992**, *31*, 185–187; (b) for quantum chemical calculations concerning 2,4-disilacyclobutane-1,3-diyls see: Ma, J.; Ding, Y.; Hattori, K.; Inagaki, S. *J. Org. Chem.* **2004**, *69*, 4245–4255.
89. (a) Fritz, G.; Wartenessian, S.; Matern, E.; Höhnle, W.; von Schnering, H. G. *Z. Anorg. Allg. Chem.* **1981**, *475*, 87–108; (b) for a 2-phospha-4- silabicyclo[1.1.0] butane as a reactive intermediate. see (c) Slootweg, J. C.; J. de Kanter, F. J.; Schakel, M.; Ehlers, A. W.; Gehrhus, B.; Lutz, M.; Mills, A. M.; Spek, A. L.; Lammertsma, K. *Angew. Chem.* **2004**, *116*, 3556–3559; *Angew. Chem. Int. Ed.* **2004**, *43*, 3474–3477.
90. Ando, W.; Shiba, T.; Hidaka, T.; Morihashi, K.; Kikuchi, O. *J. Am. Chem. Soc.* **1997**, *119*, 3629–3630.
91. (a) Driess, M.; Fanta, A. D.; Powell, D. R.; West, R. *Angew. Chem.* **1989**, *101*, 1087–1088; *Angew. Chem. Int. Ed.* **1989**, *28*, 1038–1040; (b) Tan, R. P.; Comerlato, N. M.; Powell, D. R.; West, R. *Angew. Chem.* **1992**, *104*, 1251–1252; *Angew. Chem. Int. Ed.* **1992**, *31*, 1217–1218; (c) Driess, M.; Janoschek, R.; Pritzkow, H. *Angew. Chem.* **1992**, *104*, 449–451; *Angew. Chem. Int. Ed.* **1992**, *31*, 460–462; (d) Fanta, A. D.; Driess, M.; Powell, D. R.; West, R. *J. Am. Chem.*

Soc. **1991**, *113*, 7806–7808; (e) Driess, M.; Pritzkow, H.; Winkler, U. *Chem. Ber.* **1992**, *125*, 1541–1546.
92. (a) Driess, M.; Pritzkow, H.; Rell, S.; Janoschek, R. *Inorg. Chem.* **1997**, *36*, 5212–5217 (and cited literature); (b) for calculations on the structurally related tetraphosphabicyclo[1.1.0]butane see Schoeller, W. W.; Lerch, C. *Inorg. Chem.* **1983**, *22*, 2992–2998.
93. Yeston, J. *Science* **2009**, *323*, 563.
94. For a review on the inverted geometries at carbon atom, see: Wiberg, K. B. *Acc. Chem. Res.* **1984**, *17*, 379–386.
95. For a very unusual 2,4-disila-1-germatricyclo-[2.1.0.$0^{2,5}$]pentane consisting of a Ge atom in an inverted tetrahedral geometry see Lee, V. Y.; Ichinohe, M.; Sekiguchi, A. *J. Am. Chem. Soc.* **2002**, *124*, 9962–9963.
96. For a closely related discussion on the presence or absence of a cross-ring sulfur–sulfur bond in a topologically analogous trinuclear Cu_3S_2 cluster see Alvarez, S.; Hoffmann, R.; Mealli, C. *Chem. Eur. J.* **2009**, *15*, 8358–8373.
97. First synthesis: (a) Wiberg, K. B.; Walker, F. H. *J. Am. Chem. Soc.* **1982**, *104*, 5239–5240; seminal preparative work (b) Semmler, K.; Szeimies, G.; Belzner, J. *J. Am. Chem. Soc.* **1985**, *107*, 6410–6411 reviews: (c) Ginsburg, D. *Acc. Chem. Res.* **1969**, *2*, 121–128; (d) Levin, M. D.; Kaszynski, P.; Michl, J. *Chem. Rev.* **2000**, *100*, 169–234; (e) Wiberg, K. B. *Chem. Rev.* **1989**, *89*, 975–983.
98. Feller, D.; Davidson, E. R. *J. Am. Chem. Soc.* **1987**, *109*, 4133–4139.
99. Kaszynski, P.; Michl, J. In: Rappoport, Z., Ed.; *The Chemistry of the Cyclopropyl Group*; Wiley: New York, 1995; Vol. 2, p 773.
100. Schafer, O.; Allan, M.; Szeimies, G.; Sanktjohanser, M. *J. Am. Chem. Soc.* **1992**, *114*, 8180–8186.
101. Messerschmidt, M.; Scheins, S.; Grubert, L.; Pätzel, M.; Szeimies, G.; Paulmann, C.; Luger, P. *Angew. Chem.* **2005**, *117*, 3993–3997; *Angew. Chem. Int. Ed.* **2005**, *44*, 3925–3928.
102. For a thorough explanation see Coppens, P. *Angew. Chem.* **2005**, *117*, 6970–6972; *Angew. Chem. Int. Ed.* **2005**, *44*, 6810–6811.
103. Polo, V.; Andres, J.; Silvi, B. *J. Comput. Chem.* **2007**, *28*, 857–864.
104. (a) Wu, W.; Gu, J.; Song, J.; Shaik, S.; Hiberty, P. C. *Angew. Chem.* **2009**, *121*, 1435–1438; *Angew. Chem. Int. Ed.* **2009**, *48*, 1407–1410; (b) Shaik, S.; Danovich, D.; Wu, W.; Hiberty, P. C. *Nature Chem.* **2009**, *1*, 443–449.
105. Nied, D.; Breher, F. *Chem. Soc. Rev.* **2011**, *40*, 3455–3466.
106. It is quite common to describe ligand-free atoms of main group element clusters as "naked". See for instance: Schnöckel, H. *Chem. Rev.* **2010**, *110*, 4125–4163.
107. von Schleyer, P. R.; Janoschek, R. *Angew. Chem.* **1987**, *99*, 1312–1313; *Angew. Chem. Int. Ed.* **1987**, *26*, 1267–1268.
108. Schoeller, W. W.; Dabisch, T.; Busch, T. *Inorg. Chem.* **1987**, *26*, 4383–4389.
109. Nagase, S. *Polyhedron* **1991**, *10*, 1299–1309.
110. Gordon, M. S.; Nguyen, K. A.; Carroll, M. T. *Polyhedron* **1991**, *10*, 1247–1264.
111. Nguyen, K. A.; Carroll, M. T.; Gordon, M. S. *J. Am. Chem. Soc.* **1991**, *113*, 7924–7929.
112. Wang, Y.; Ma, J.; Inagaki, S. *Tetrahedron Lett.* **2005**, *46*, 5567–5571.
113. See also theoretical work concerning [1.1.1]heteropropellanes: (a) Kitchen, D. B.; Jackson, J. E.; Allen, L. C. *J. Am. Chem. Soc.* **1990**, *112*, 3408–3414; (b) Ebrahimi, A.; Deyhimi, F.; Roohi, H. *J. Mol. Struc. (Theochem.)* **2003**, *626*, 223–229.
114. Sandström, N.; Ottosson, H. *Chem. Eur. J.* **2005**, *11*, 5067–5079.
115. A summary can also be found in (a) Karni, M.; Apeloig, Y.; Kapp, J.; von Schleyer, P. R. In *The Chemistry of Organic Silicon Compounds*; Rappoport, Z., Apeloig, Y., Eds.; Wiley: Chichester, 2001; Vol. 3 For further studies see for instance (b) Nagase, S.; Kudo, T. *Organometallics* **1987**, *6*, 2456–2458; (c) Nagase, S.; Kudo, T. *Organometallics* **1988**, *7*, 2534–2536; (d) Gallego-Planas, N.; Whitehead, M. A. *J. Mol. Struct. (Theochem.)* **1992**, *260*, 419–432; (e) Gallego-Planas, N.; Whitehead, M. A. *J. Mol. Struct. (Theochem.)* **1997**, *391*, 51–60; (f) Holder, A. J.; Earley, C. W. *J. Mol. Struct. (Theochem.)* **1993**, *281*, 131–139.
116. Sita, L. R. *Adv. Organomet. Chem.* **1995**, *38*, 189–243.
117. Sita, L. R. *Acc. Chem. Res.* **1994**, *27*, 191–197.
118. Sita, L. R.; Bickerstaff, R. D. *J. Am. Chem. Soc.* **1989**, *111*, 6454–6456.
119. Sita, L. R.; Kinoshita, I. *J. Am. Chem. Soc.* **1992**, *114*, 7024–7029.
120. Nied, D.; Matern, E.; Berberich, H.; Neumaier, M.; Breher, F. *Organometallics* **2010**, *29*, 6028–6037.
121. Drost, C.; Hildebrand, M.; Lönnecke, P. *Main Group Metal Chem.* **2002**, *25*, 93.
122. (a) Richards, A. F.; Brynda, M.; Power, P. P. *Organometallics* **2004**, *23*, 4009–4011; (b) For an example of a 4-**IV** heteronuclear bicyclo[1.1.1]pentane containing Group 14 and Group 15 elements: Driess, M.; Gleiter, R.; Janoschek, R.; Pritzkow, H.; Reisgys, M. *Angew. Chem.* **1994**, *106*, 1548–1551; *Angew. Chem. Int. Ed.* **1994**, *33*, 1484–1487.
123. Nied, D.; Klopper, W.; Breher, F. *Angew. Chem.* **2009**, *121*, 1439–1444; *Angew. Chem. Int. Ed.* **2009**, *48*, 1411–1416.
124. Nied, D.; Köppe, R.; Klopper, W.; Schnöckel, H.; Breher, F. *J. Am. Chem. Soc.* **2010**, *132*, 10264–10265.
125. Berger, R. J. F.; Rzepa, H. S.; Scheschkewitz, D. *Angew. Chem.* **2010**, *122*, 10203–10206; *Angew. Chem. Int. Ed.* **2010**, *49*, 10006–10009.
126. Tsumuraya, T.; Batcheller, S. A.; Masamune, S. *Angew. Chem.* **1991**, *103*, 916–944; *Angew. Chem. Int. Ed.* **1991**, *30*, 902–930.
127. For a review article concerning polyhedral silicon compounds see Sekiguchi, A.; Nagase, S. In Rappoport, Z., Apeloig, Y., Eds.; *The Chemistry of Organic Silicon Compounds*; Wiley: Chichester, 1998; Vol. 2.
128. (a) Fischer, G.; Huch, V.; Mayer, P.; Vasisht, S. K.; Veith, M.; Wiberg, N. *Angew. Chem.* **2005**, *117*, 8096–8099; *Angew. Chem. Int. Ed.* **2005**, *44*, 7884–7887; (b) Scheschkewitz, D. *Angew. Chem.* **2005**, *117*, 3014–3016; *Angew. Chem. Int. Ed.* **2005**, *44*, 2954–2956; Abersfelder, K.; White, A. J. P.; Rzepa, H. S.; Scheschkewitz, D. *Science* **2010**, *327*, 564–566; (d) Klapötke, T. M.; Vasisht, S. K.; Mayer, P. *Eur. J. Inorg. Chem.* **2010**, 3256–3260; (e) Ichinohe, M.; Toyoshima, M.; Kinjo, R.; Sekiguchi, A. *J. Am. Chem. Soc.* **2003**, *125*, 13328–13329 for recent solution studies on the polysilicides $[Si_9]^{4-}$ and $[Si_4]^{4-}$ see (f) Joseph, S.; Hamberger, M.; Mutzbauer, F.; Hartl, O.; Meier, M.; Korber, N. *Angew. Chem.* **2009**, *121*, 8926–8929; *Angew. Chem. Int. Ed.* **2009**, *48*, 8770–8772; (g) Waibel, M.; Kraus, F.; Scharfe, S.; Wahl, B.; Fässler, T. F. *Angew. Chem.* **2010**, *122*, 6761–6765; *Angew. Chem. Int. Ed.* **2010**, *49*, 6611–6615.
129. Wiberg, N.; Power, P. P. In *Molecular Clusters of the Main Group Elements*; Driess, M., Nöth, H., Eds.; Wiley-VCH: Weinheim, 2004.
130. (a) Schnepf, A. *Chem. Soc. Rev.* **2007**, *36*, 745–758; (b) Schnepf, A.; Köppe, R. *Angew. Chem.* **2003**, *115*, 940–942; *Angew. Chem. Int. Ed.* **2003**, *42*, 911–913; (b) Schnepf, A.; Drost, C. *Dalton Trans.* **2005**, 3277–3280; (c) Wiberg, N.; Lerner, H.-W.; Wagner, S.; Nöth, H.; Seifert, T. *Z. Naturforsch. B* **1999**, 877–880.
131. Gerdes, C.; Müller, T. *Angew. Chem.* **2010**, *122*, 4978–4981; *Angew. Chem. Int. Ed.* **2010**, *49*, 4860–4862.
132. Richards, A. F.; Brynda, M.; Olmstead, M. M.; Power, P. P. *Organometallics* **2004**, *23*, 2841–2844.
133. Schenk, C.; Kracke, A.; Fink, K.; Kubas, A.; Klopper, W.; Neumaier, M.; Schnöckel, H.; Schnepf, A. *J. Am. Chem. Soc.* **2011**, *133*, 2518–2524.
134. Nied, D.; Oña-Burgos, P.; Klopper, W.; Breher, F. *Organometallics* **2011**, *30*, 1419–1428.
135. Sita, L. R.; Kinoshita, I. *J. Am. Chem. Soc.* **1990**, *112*, 8839–8843.
136. Wiberg, N.; Schuster, H.; Simon, A.; Peters, K. *Angew. Chem.* **1986**, *98*, 100–101; *Angew. Chem. Int. Ed.* **1986**, *25*, 79–80.
137. Wiberg, N. *Coord. Chem. Rev.* **1997**, *163*, 217–252.
138. Sita, L. R.; Kinoshita, I. *J. Am. Chem. Soc.* **1991**, *113*, 5070–5072.
139. For a closely related bicyclo[1.1.1]pentasilane derivative see (a) Kabe, Y.; Kawase, T.; Okada, J.; Yamashita, O.; Goto, M.; Masamune, S. *Angew. Chem.* **1990**, *102*, 823–825; *Angew. Chem. Int. Ed.* **1990**, *29*, 794–796; see also for a pentasilatricyclo[2.1.0.$0^{2,5}$]pentane derivatives: (b) Lee, V. A.; Yokoyama, T.; Takanashi, K.; Sekiguchi, A. *Chem. Eur. J.* **2009**, *15*, 8401–8404.
140. Hoffmann, R. *Acc. Chem. Res.* **1971**, *4*, 1–9.
141. Nied, D. Ph.D. Thesis, Karlsruhe Institute of Technology (KIT), 2010, ISBN 978-3-8325-2729-7.
142. Cox, H.; Hitchcock, P. B.; Lappert, M. F.; Pierssens, L. J.-M. *Angew. Chem.* **2004**, *116*, 4600–4604; *Angew. Chem. Int. Ed.* **2004**, *43*, 4500–4504.
143. Dickie, D. A.; Lee, P. T. K.; Labeodan, O. A.; Schatte, G.; Weinberg, N.; Lewis, A. R.; Bernard, G. M.; Wasylishen, R. E.; Clyburne, J. A. C. *Dalton Trans.* **2007**, 2862–2869.
144. Fischer, R. C.; Power, P. P. *Chem. Rev.* **2010**, *110*, 3877–3923.
145. (a) Power, P. P. *Organometallics* **2007**, *26*, 4362–4372; (b) Power, P. P. *Chem. Commun.* **2003**, 2091–2101; (c) Wang, Y.; Robinson, G. H. *Chem. Commun.* **2009**, 5201–5213; (d) Lee, V. Y.; Sekiguchi, A. *Organic Compounds of Low Coordinate Si, Ge, Sn and Pb Compounds, from Phantom Species to Stable Compounds*. Wiley: Chichester, 2010.
146. Spikes, G. H.; Fettinger, J. C.; Power, P. P. *J. Am. Chem. Soc.* **2005**, *127*, 12232–12233.
147. Peng, Y.; Brynda, M.; Ellis, B. D.; Fettinger, J. C.; Rivard, E.; Power, P. P. *Chem. Commun.* **2008**, 6042–6044.
148. (a) Peng, Y.; Ellis, B. D.; Wang, X.; Fettinger, J. C.; Power, P. P. *Science* **2009**, *325*, 1668–1670; (b) Sita, L. R. *Science* **2009**, *325*, 1631–1632.
149. (a) Jung, Y.; Brynda, M.; Power, P. P.; Head-Gordon, M. *J. Am. Chem. Soc.* **2006**, *128*, 7185–7192; (b) Malcolm, N. O. J.; Gillespie, R. J.; Popelier, P. L. A. *J. Chem. Soc., Dalton Trans.* **2002**, 3333–3341.

150. (a) Power, P. P. *Appl. Organometal. Chem.* **2005**, *19*, 488–493; (b) Cui, C.; Olmstead, M. M.; Fettinger, J. C.; Spikes, G. H.; Power, P. P. *J. Am. Chem. Soc.* **2005**, *127*, 17530–17541.
151. Cui, C.; Olmstead, M. M.; Power, P. P. *J. Am. Chem. Soc.* **2004**, *126*, 5062–5063.
152. (a) Moilanen, J.; Power, P. P.; Tuononen, H. M. *Inorg. Chem.* **2010**, *49*, 10992–11000; (b) Schoeller, W. W. *Inorg. Chem.* **2011**, *50*, 2629–2633.
153. Sugiyama, Y.; Sasamori, T.; Hosoi, Y.; Furukawa, Y.; Takagi, N.; Nagase, S.; Tokitoh, N. *J. Am. Chem. Soc.* **2006**, *128*, 1023–1031.
154. Cui, C.; Brynda, M.; Olmstead, M. M.; Power, P. P. *J. Am. Chem. Soc.* **2004**, *126*, 6510–6511.
155. Wang, X.; Ni, C.; Zhu, Z.; Fettinger, J. C.; Power, P. P. *Inorg. Chem.* **2009**, *48*, 2464–2470.
156. Wang, X.; Peng, Y.; Olmstead, M. M.; Fettinger, J. C.; Power, P. P. *J. Am. Chem. Soc.* **2009**, *131*, 14164–14165.
157. Wang, X.; Peng, Y.; Zhu, Z.; Fettinger, J. C.; Power, P. P.; Guo, J.; Nagase, S. *Angew. Chem.* **2010**, *122*, 4697–4701; *Angew. Chem. Int. Ed.* **2010**, *49*, 4593–4597.
158. Ito, S.; Kikuchi, M.; Miura, J.; Morita, N.; Yoshifuji, M. *J. Phys. Org. Chem.* **1957**. http://dx.doi.org/10.1002/poc.
159. Schoeller, W. W.; Niecke, E. *Phys. Chem. Chem. Phys.* **2012**, *14*, 2015–2023.
160. Takeuchi, K.; Ichinohe, M.; Sekiguchi, A. *J. Am. Chem. Soc.* **2011**, *133*, 12478–12481.
161. Abe, M.; Ye, J.; Mishima, M. *Chem. Soc. Rev.* **2012**, *41*, 3808–3820.
162. Beweries, T.; Kuzora, R.; Rosenthal, U.; Schulz, A.; Villinger, A. *Angew. Chem.* **2011**, *123*, 9136–9140; *Angew.Chem. Int. Ed.* **2011**, *50*, 8974–8978.
163. Zhang, S.-H.; Wei, H.-W.; Lim, K. H.; Meng, Q.; Huang, M.-B.; So, C.-W. *Chem. Eur. J.* **2012**, *18*, 4258–4263.
164. Lopez, X.; Ruipérez, F.; Piris, M.; Matxain, J. M.; Ugalde, J. M. *Chem Phys Chem* **2011**, *12*, 1061–1065.
165. Petrov, K. T.; Pinter, B.; Veszpremi, T. *J. Organomet. Chem.* **2012**, *706–707*, 84–88.
166. Schrenk, C.; Kubas, A.; Fink, K.; Schnepf, A. *Angew. Chem.* **2011**, *123*, 7411–7415; *Angew. Chem. Int. Ed.* **2011**, *50*, 7273–7277.
167. Abersfelder, K.; White, A. J. P.; Berger, R. J. F.; Rzepa, H. S.; Scheschkewitz, D. *Angew. Chem.* **2011**, *123*, 8082–8086; *Angeu. Chem. Int. Ed.* **2011**, *50*, 7936–7939.
168. Augenstein, T.; Oña-Burgos, P.; Nied, D.; Breher, F. *Chem. Commun.* **2012**, *48*, 6803–6805.
169. (a) Schwab, P. F. H.; Levin, M. D.; Michl, J. *Chem. Rev.* **1999**, *99*, 1863–1934; (b) Levin, M. D.; Kaszynski, P.; Michl, J. *Chem. Rev.* **2000**, *100*, 169–234.

This page intentionally left blank